**School of Civil and Mechanical Engineering**

# Mine Haul Road Rolling Resistance: Influences and Impacts

**Jarrad Patrick Coffey**

**This thesis is presented for the Degree of**
**Doctor of Philosophy**
**of**
**Curtin University**

**March 2015**

**Declaration**

To the best of my knowledge and belief this thesis contains no material previously published by any other person except where due acknowledgment has been made.

This thesis contains no material which has been accepted for the award of any other degree or diploma in any university.

Signature: 

Date: 23/11/15

# Project Documentation

**Thesis Title:** Mine Haul Road Rolling Resistance: Influences and Impacts

**Author:** Jarrad P Coffey

**Date:** March, 2015

**Supervisors:** Professor Hamid Nikraz

Associate Professor Faisal Anwar

**ABSTRACT:**

Energy efficiency in mining, as with any industrial process, is now a major factor in the economic viability of any project. The rolling resistance of haul trucks is not currently well understood, and much of the literature draws recommendations from scaling of tests completed with smaller passenger vehicles. This project has investigated the impact of pavement surface and structural condition on the rolling resistance experienced by large haul trucks through completion of full-scale testing. Terrestrial laser scanning techniques were adapted to provide a quantification of the surface properties of pavements, and also to measure rebound deflection and curvature arising from tyre loading. This has revealed that pavement deflection has equal influence to pavement roughness for a loaded truck travelling at operational speeds. Shorter roughness wavelengths have been found to more significantly influence on rolling resistance, with the IRI proving to correlate well with rolling resistance at operational speeds.

Numerical modelling of the measured deflection/curvature profiles has provided insight into the applicability of available methods for haul road pavement design. Due to the ability to consider wheel load interaction in detail, three-dimensional Finite Element Analysis was shown to most accurately estimate pavement surface deflection. Two sub-grade failure theories that have been previously developed for airfield and haul road pavements present good correlation. These theories are recommended for haul road pavement design, with analysis being completed by FEA.

**Indexing Terms:** Rolling resistance, haul road, haul truck, pavement deflection, flexible pavement, unbound granular material, resilient modulus, California Bearing Ratio, pavement roughness, pavement texture.

# Table of Contents

# List of Figures

# List of Tables

# List of Equations

# List of Symbols and Abbreviations

| Abbreviation | Expansion |
|---|---|
| APSDS | Airport Pavement Structural Design System |
| ARFCOM | ARRB Road Fuel Consumption Model |
| ARRB | Australian Roads Research Board |
| CBR | California Bearing Ratio |
| CIRCLY | Mechanistic pavement design software (Mincad Systems, 2012) |
| ESWL | Equivalent Single Wheel Load |
| FEA | Finite Element Analysis |
| FWD | Falling Weight Deflectometer |
| HDM-4 | The Highway Design and Maintenance Standards Model 4 |
| HIPAVE | Heavy Industry Pavement Design (Mincad Systems, 2009) |
| IRI | International Roughness Index |
| MPD | Mean Pavement Depth |
| MRWA | Main Roads Western Australia |
| NIMPAC | NAASRA Improved Model for Project Assessment and Costing (Lloyd, 2003). |
| RLTT | Repeated Load Tri-axial Test |
| RRC | Rolling Resistance Coefficient |
| RRMIN | Minimum Rolling Resistance |
| UGM | Unbound Granular Material |
| VOC | Vehicle Operating Costs |
| WES | Waterways Engineering Station, US Army Corps (Pereira, 1977) |

# Glossary

Anisotropic:
In the context of pavement materials; a material with variation in material stiffness when measured vertically and horizontally.

Austroads:
The association of Australasian road transport and traffic agencies (austroads.com.au).

Comminution:
“The action of reducing a material, especially a mineral ore, to minute particles or fragments” (Oxford Dictionaries, 2014).

Driving resistance:
Energy required, per unit distance, for vehicle forward motion including all drivetrain and engine losses.

Encastre:
A boundary condition in geomechanical modelling allowing no displacement or curvature in any plane.

Haul truck:
Large, rigid off-the-road dump trucks commonly utilised in transport of mineral ore and waste materials within mining operations.

Isotropic:
In the context of pavement materials; a material with no variation in material stiffness when measured vertically and horizontally.

Microtexture:
Pavement surface undulations with wavelengths less than half a millimetre, primarily related to the nature of the surface of individual stone particles (Jackson et al, 2011)

Macrotexture:
Pavement surface undulations with wavelengths in the range 0.5 to 50mm (Jameson and Shackleton, 2009), typically related to the particle sizes used for the surface course (Sandberg et al, 2011).

Megatexture:
Pavement surface undulations with wavelengths of 50 to 500mm (Jackson et al, 2011).

Mesh:
The element (a discrete section of soil) structure given to a finite element analysis model that has consistent properties. Each element provides a unique calculated response to the application of the applied loads.

Non-linear:
In the context of material stress-strain response, refers to a material that does not show a perfectly elastic response.

Parasitic losses:
In the context of rolling resistance; loss of energy (or energy consumed) per unit distance travelled excluding internal tyre losses, and attributable to aerodynamic loss of the different rotating elements of the test equipment, bearing friction, and other sources of systematic loss which may occur within the wheel mechanism (Evans et al, 2009).

Poisson's ratio:
"The ratio of the proportional decrease in a lateral measurement to the proportional increase in length in a sample of material that is elastically stretched" (Oxford, Dictionaries, 2014).

Rolling resistance:
Quantity of energy consumed per unit distance travelled by a rolling wheel, often described by the Rolling Resistance Coefficient (RRC).

Rolling Resistance Coefficient (RRC):
The ratio of force arising from the rolling resistance and the vertical force applied to a rolling wheel.

Roughness:
In the context of pavements; undulation in the pavement surface with wavelengths exceeding 0.5m.

Registration:
In the context of special sciences and analysis of field-collected data, refers to the amalgamation of data taken from different positions or of adjoining areas.

Resilient modulus:

“The ratio of dynamic (resilient) stress and dynamic (resilient, recoverable) strain” (Vuong et al, 2008).

Wheel gear:

Collection of wheels spaced closely together such that they are considered as a group within the process of pavement design.

# 1 Introduction

## 1.1 Background

The optimisation of the energy consumed in any industrial process is now scrutinized by the public, regulators and law makers. However, it has always been a significant driver in the financial return earned by a commodity producer. Recent figures suggest that approximately nine percent of energy consumed in Australia is due to mining operations (Bureau of Resources and Energy Economics, 2012A). It is estimated that the load and haul process represents 25% of the total cost involved in producing and selling bulk commodities such as iron ore and coal (McIntosh Engineering, 2003). Subsequently, material transport has been noted to account for approximately 30% of total energy consumption within the production of bulk commodities (Norgate et al, 2009). To provide some context, consider that transport represents 24% of the annual national energy consumption (Bureau of Resources and Energy Economics, 2012A). The energy consumed within the transportation of mineral ores notably appears to be a significant component to the total energy consumed in Australia each year.

Rolling resistance is the term used to describe the energy required to produce horizontal motion by way of a rolling mechanism, usually a wheel. These losses occur throughout a complex system of vehicular response to pavement surface characteristics (Hammarstrom et al, 2012). Several authors have stated in recent times that the energy loss in the pavement may also be significant. Schmidt et al (2009) completed Falling Weight Deflectometer (FWD) testing on flexible and rigid (concrete) pavements, which showed a significant difference in the resulting hysteresis loops. This concept suggests that some energy is lost from the system of a moving wheel due to the pavement material's stress/strain response. Consider that Kaufman et al (1977) include values of rolling resistance on varying surfaces, with relatively higher values being suggested for 'softer' materials. This provided some early insight into the influence of pavement structural condition.

Haul road pavement design is commonly completed via a local 'recipe' or via CBR design curves that have been developed with the method detailed by the US Army Corps of Engineers (Pereira, 1977). The generation of CBR design curves utilises the same theory and test data that underpins the design of runway pavement for

large aircraft. The only full scale testing of pavement performance subject to heavy wheel loads was completed by the US Army Corps of Engineers in the 1970s, with some additional data being added in the early 2000s following further testing by the Federal Aviation Administration. Both sets of testing considered a pavement structure involving some depth of asphalt and select crushed rock, which means that some 'equivalence factor' has to be relied upon in order to transform the pavement to comprise completely of uncrushed gravel materials. The requirement for this transformation is highlighted in Figure 1.1, as it forms an integral part of pavement design. Further, the haul road pavement failure theory presented by Thompson (2009) is tested. This theory includes consideration of the pavement's serviceability and economic importance to a mine owner by considering the daily tonnes hauled along its path. In-situ and laboratory testing of pavement materials was undertaken for this project to assess the relative accuracies of employing each available design technique to haul road pavements. This investigation included methods commonly applied commercially and also more detailed analysis with FEA.

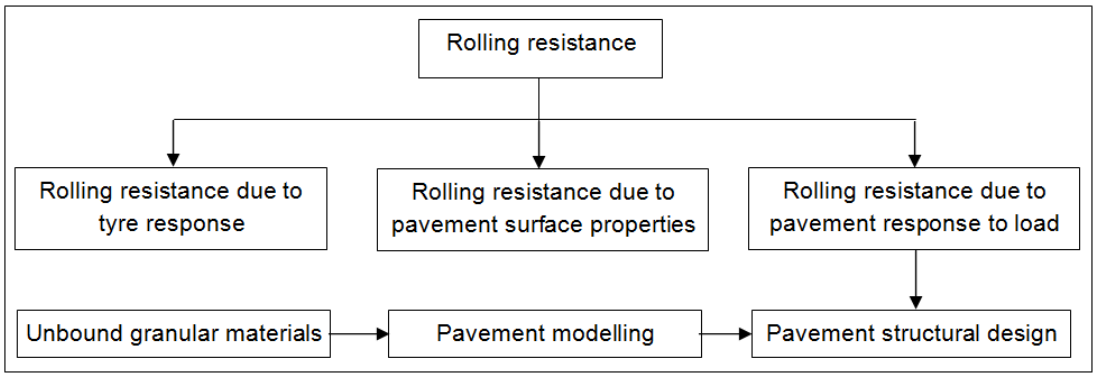


**Figure 1.1: Abbreviated project map.**

As described in Figure 1.1, this project was focussed on increasing the understanding of the performance of haul roads, which are a unique class of road in that they are privately owned and managed for the production of mineral ores. Importantly, as a result lower end-user costs may significantly outweigh any savings made at the design and construction phase of the haul road by lowering the pavement's serviceability. Currently, haul road pavements are designed to limit both rut depth and the generation of surface roughness, which is assumed to be primarily associated with shape-loss of the sub-grade. As haul roads are effectively an economic asset needed for the production of mineral ore, it is suggested that the

focus (limiting design parameter) of pavement design should be the minimisation of energy consumption for haul trucks. This suggestion is valid within the bounds of acceptable road and vehicle maintenance costs.

## 1.2 Objectives

This research will contribute to improving efficiency in mining operations utilising large haul trucks, but also relates to the fields of Civil and Geotechnical Engineering with regards to pavement design for large wheel loads. The objectives for the research are as follows:

1. Definition of the pavement surface properties that most influence the rolling resistance experienced by haul trucks.
2. Determination of the influence of pavement stiffness on the rolling resistance of haul trucks.
3. Assessment of the suitability of fuel consumption models for application with haul trucks.
4. Quantify the magnitude of pavement surface deflection due to haul truck wheel loads.
5. Characterise mine waste materials used in haul road pavement construction.
6. Compare various structural analysis methods to determine if more complex models, such as FEA, are able to better predict pavement surface deflections associated with haul trucks.
7. Compare pavement structural design techniques for large wheel loading and recommend the most appropriate.

## 1.3 Significance

There is limited understanding of haul road pavements with regard to design and efficiency in operation. Such pavements can significantly impact the cost of a mining operation, as outlined in Section 1.1.

Many studies have defined the rolling resistance due to pavement surface condition (Sandberg, 2011) for highway vehicles. However, little research has been completed to relate these findings to haul trucks operating on unsealed haul roads, some examples are Thompson et al (2003) and Widodo et al (2009). This study is intended to serve as an initiation of research in this area.

It has recently been contended that pavement stiffness may significantly influence the rolling resistance experienced by a vehicle (Lenngren, 2010). Haul roads are typically constructed from unbound mine waste or locally available materials that do not typically comply with highway pavement specifications. In addition, haul trucks now exceed gross vehicle mass values of 500 tonnes (Komatsu, 2007). Consequently, this research investigates the contribution of pavement structural stiffness to rolling resistance for large wheel loads and pavement comprising materials characterised by relatively low elastic moduli. There is no such investigation available within the literature employing full-scale testing of large haul trucks.

Flexible pavements subject to heavy wheel loads have long been designed by utilising the S77-1 curve detailed by Pereira (1977). Pavement structural design may influence rolling resistance in two primary ways. Firstly, it dictates the level of deflection, for which the influence on rolling resistance is being investigated in this study. Secondly, the failure condition considered by traditional pavement life theories is rutting/shape loss manifesting in surface roughness, which is widely accepted to significantly increase rolling resistance. Attempts have been made to relate this sub-grade failure theory to mechanistic analysis tools, such as the validation described by Wardle (2001) et al. However, to date these efforts have been focussed on airfield pavements and still include bound layers and asphaltic surfacing. This research investigates the use of various numerical structural analysis techniques in the design of haul road pavements utilising the criteria mentioned above. The investigation involves wheel loads larger than those on airfields and unbound/unsurfaced pavements.

## 1.4 Identification of Research Need

Haul road rolling resistance has been investigated previously by several authors. Regrettably, the method utilised to determine the magnitude of rolling resistance has either not been sufficiently detailed in the literature or is difficult to compare with results of similar studies. Additionally, the contribution of pavement structural stiffness has not been investigated. Considering the large expenditure involved in the construction and operation of haul roads for a typical mining operation, the magnitude of potential cost-savings is significant, even for incremental improvements in haul truck rolling resistance. This provides the basis for investigation of haul truck rolling resistance.

The design of haul road pavements is generally completed by empirical methods dating back to the development of airfield pavement design techniques in the 1970s (Pereira, 1977). Modelling of unsealed pavements, subjected to wheel loads as large as 80 tonnes, has not been validated with any readily available structural analysis technique. This research compares the ability of several analysis methods to predict pavement surface deflections, and provides insight into how best to apply sub-grade failure theories to mechanistic-empirical pavement design for haul roads. Greater understanding in this area provides the haul road designer greater control to detail a pavement that does not deteriorate past its point of failure, avoiding operation of haul trucks on a surface with a high value of rolling resistance.

Investigating the influence on pavement rolling resistance parallel to pavement design provides an opportunity to comment on the most applicable design criteria for haul roads. For example, structural performance may not be considered critical if a haul road is only to be in place for a short time. For haul roads with a short design life, optimisation of pavement construction and maintenance may be of greatest importance to limit the development of surface roughness that significantly increase rolling resistance. In this case, the functional design of the pavement, that is the provision of wearing course materials that are stable under operating conditions, may be critical. This approach may benefit the mine's operator because short design life roads typically make up a significant proportion of haul roads that are critical to production on a mine site. For roads with a longer design life, it may be important to limit the required maintenance on the pavement and so the design criteria may transition from rolling resistance to structural deformation. However, note that the latter will ultimately result in greater rolling resistance through either pavement deflection or surface roughness (as investigated in this project). An assessment of such decisions is likely to be unique for each mine site. This research is focussed on providing the technical insight to facilitate the determination of the optimum design criteria.

Currently, there is a gap in the knowledge of haul roads linking structural design and operating costs. This project serves to define which pavement properties or features most significantly influence haul truck rolling resistance, such that clear pavement design criteria may be defined. Subsequently, this project investigates the structural design tools available to a pavement designer, with a view to allowing the operating costs (as arising from haul truck rolling resistance) to be addressed at the haul road design stage.

A more detailed discussion of the knowledge gaps currently present within the literature is provided in Section 2.7.

## 1.5 Scope of the Project

This research was focussed initially on identifying the pavement characteristics that most influence haul truck rolling resistance. Measurement of pavement deflection, which in combination with laboratory testing of the pavement materials in question, facilitated an investigation of available pavement structural analysis and design techniques. Figure 1.2 presents the methodology applied, showing the primary milestones. The major steps in achieving the objectives described in Section 1.2 are detailed below.

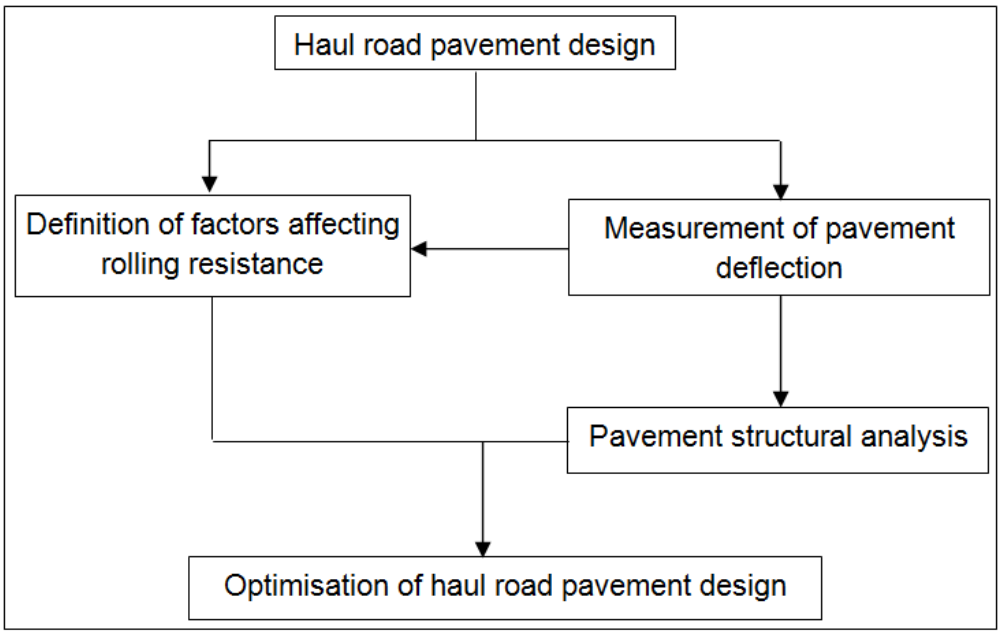


**Figure 1.2: Abbreviated Project Flow Chart.**

The haul road pavements required characterisation with respect to both texture and roughness values. There were several methods available to define these properties and a number were investigated such as walking profilometer, Australian Road Research Board roughometer and measurement of truck suspension stroke or other dynamic response. Ultimately, this data was obtained by terrestrial laser scanning

and analysis, utilising the same equipment used for measurement of pavement deflection to define the nature of the pavement surface undulations. Results for each pavement section included in the testing were analysed against continuously logged rolling resistance values to determine the influence of each respective wavelength.

Options for pavement surface deflection such as direct measurement via theodolite, precise levelling and photogrammetry were investigated. However, after completing trials, pavement surface deflection was measured with the use of terrestrial laser scanning for wheel loads arising from an unladen and laden Komatsu 830E haul truck. This technique also allowed measurement of pavement curvature, facilitating back-calculation of pavement stiffness. Comparison of the pavement surface deflection with measured rolling resistance data determined the influence of pavement structural condition on rolling resistance.

There are a few options reported in the literature for measuring rolling resistance of a given vehicle, two of which were trialled; coast-down and towing tests. Both appeared viable methodologies from initial trial test results, however complications arising from the application to haul trucks with electric wheel motors meant an alternative was required. A significant portion of the available literature utilises scaled-down tests with custom rigs, with the assumption that rolling resistance values are consistent with larger vehicle tyres and wheel loads. It was the opinion of the author that the calibration from small rigs to large haul trucks would present unacceptable unknown error and a full-scale test was further pursued. Ultimately, the personnel involved in mine operations were able to assist in utilisation of the truck performance monitoring system to log wheel motor toque and total power output. This data allowed the instantaneous rolling resistance to be calculated.

Fuel consumption of haul trucks was modelled utilising a modified version of a commonly applied mechanistic model. This was then compared to the fuel consumption estimation technique specific to haul trucks presented by the Australian Federal Department of Resources, Energy and Tourism (2010).

Pavement samples from the haul roads used for rolling resistance and deflection testing were subjected to laboratory testing. This served to define the material's index, elastic and shear strength properties for inclusion in the structural analyses modelling approaches that were undertaken. The stress state under large haul truck wheel loads meant that an extension of existing test routines was necessary, to allow for the stress dependency of unbound granular materials in the analysis discussed below.

As discussed above, pavement deflection data was available in combination with elastic properties determined from tri-axial testing with both monotonic and cyclic loading. It was therefore possible to compare the modelling capability of several techniques, including simple hand-calculation methods and software employing liner-elastic and finite element analysis methods. After determining the most appropriate methods for analysing pavement response to loading, an investigation of pavement design methods was completed by comparing pavement lifetime estimates made with each method.

The above work allowed the critical pavement properties influencing rolling resistance to be identified. Furthermore, a greater understanding of the abilities of the pavement design tools available to the practitioner has been gained. When combined, this knowledge allows the designer to identify the critical pavement design parameter and focus the design effort on optimisation. The mine owner then benefits from greater efficiency in the hauling of ore and waste materials.

# 2 Background

This section details the available literature, to explain how each topic relates to the current project, as depicted in Figure 2.1. The primary goal of this project is optimisation of energy consumption in the haulage process required for the production of mineral ores, which is reflected at the top of Figure 2.1. Pavement structural analysis and design relevant to haul roads is then detailed, as shown below.

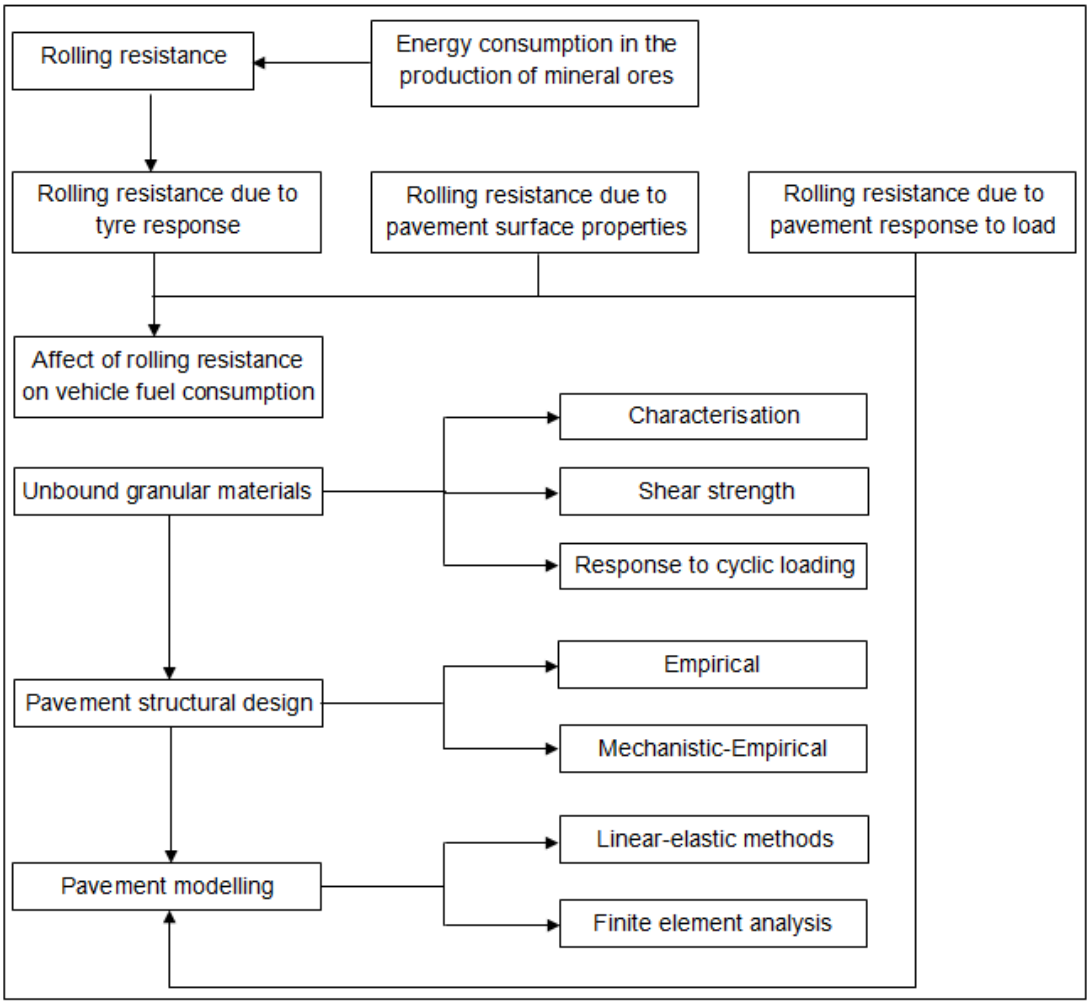


**Figure 2.1: Project background map.**

## 2.1 Energy Consumption in the Production of Ore

For the discussion below the energy produced in the mining and processing of mineral ores and in the transport of ores is separated. This has been done to provide a broad context for the issue of haulage fuel efficiency and then further define the potential benefits of improvements.

### 2.1.1 Energy Consumption in Mining

The energy consumption inherent in any commercial activity has become increasingly present in the public conscience. Mining and mineral processing are two industry sectors widely accepted as large energy consumers. However, in total only 9% of Australia's energy consumption was due to mining operations in 2012 (Bureau of Resources and Energy Economics, 2012A), compared with 24% in transport and 30% in electricity generation (Bureau of Resources and Energy Economics, 2012A). In the mineral rich state of Western Australia, the relative consumption by industry is vastly different with mining which accounting for 29.5% of the state's energy consumption in 2009-10. The most telling statistic of the size of Western Australia's mining sector may be that the iron ore industry alone is approximated to consume in excess of three million litres of diesel per day (Shastri et al, 2012). To give greater perspective, consider that Western Australia's energy consumption was 17.3% of the national total in 2009-10 (Australian Bureau of Statistics, 2013). The steady growth in global commodity prices in recent decades has seen consumption in mining grow from 65 PJ (2.4% of gross domestic consumption) in 1974-1975 to 509 PJ (8.6%) in 2009-2010. Although this figure is statistically significant, consider that over the same time period consumption in transport has remained relatively steady at approximately 25% (Bureau of Resources and Energy Economics, 2012).

It is difficult to distinguish between the energy consumption of various processes employed in the production of any commodity. For example it is commonly accepted that 70% of energy consumed in conventional mining and processing circuits is consumed in the comminution of ore, however coal and iron ore commodities require vast amounts of bulk transport, which (including mining extraction) represent up to 30% of total energy consumption (Norgate et al, 2011). From a global point of view, steel production accounts for significantly more energy consumption than production of any other metal (Norgate et al, 2011). Figure 2.2 shows the origin of

carbon-dioxide emissions from the activities constituting the production of iron ore. Although the breakdown presented here is specific to each mining process (the energy consumed in hauling alone is discussed in Section 2.1.2) the results present an overall view of the industry in Australia. One consideration of the energy consumption in iron ore operations in the study reported by Norgate et al (2009) is the proportion of operations requiring wet processing of ores, which represents a significantly lengthened processing circuit when compared to dry crushing and screening.

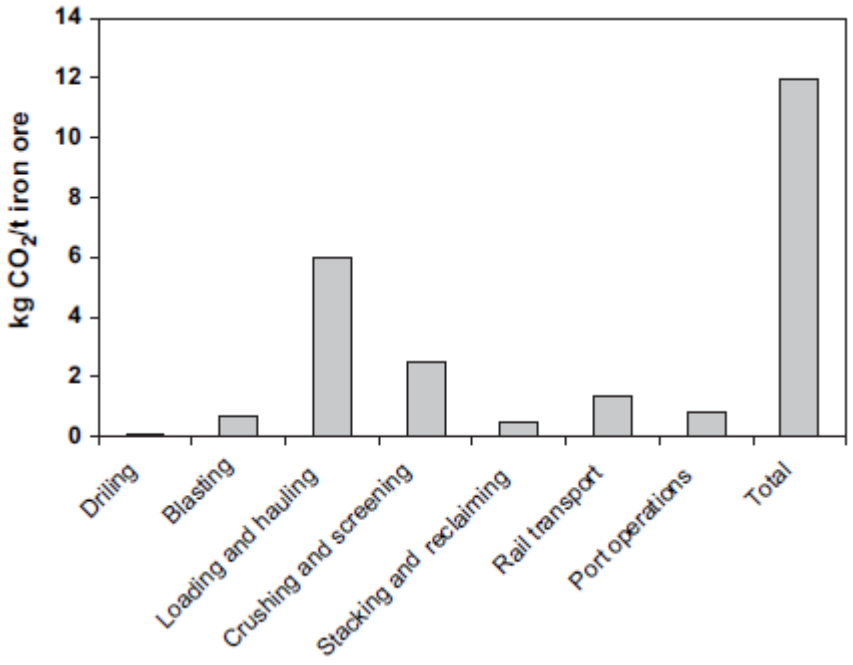


**Figure 2.2: Contributions of net carbon-dioxide emissions for each stage of iron ore production (Norgate et al, 2009).**

The energy consumption in the mining industry is expected to increase further in the future as additional amounts of waste are required to be removed as a result of increased over-burden removal arising from deeper deposits of lower grade becoming economically viable (Norgate et al, 2011). This effect may be so profound that the absolute prices of metals are expected to adjust to reflect the intensities of production, as carbon footprints are progressively built in to the cost structure (Norgate et al, 2009). Hence, the energy consumption and intensity of a unit of saleable product is likely to be an area of increasing focus for miners.

### 2.1.2 Energy Consumption in the Load and Haul Process

Transport of ore and waste material within a mine site is generally completed either by overland conveyor or haulage via trucking. Other methods such as slurry pipeline, hoists (especially in underground mining) or rail are also relatively common for commodities involving a smaller quantity of material extraction. However intra-site transport in bulk commodities such as coal and iron ore are dominated by haulage via truck (Li et al, 2011). Note that the transported volume of precious metals is relatively insignificant in comparison to bulk commodities when considering the total tonnages transported in Australia due to lower mined volume and a higher degree of processing near extraction (Li et al, 2011). Energy consumption of conveyor systems is relatively well understood and accurately estimated whereas that in a haulage process completed by large off-the-highway rigid dump trucks is not as well defined. The less processing that occurs close to the mine site results in a higher volume of product that must be transported (Li et al 2011). Haulage costs in an open pit environment may represent up to 50% of the mining cost and 25% of the total costs (including processing, marketing and overheads) in hard rock mining (de la Vergne, 2003). Similarly, a value of 50% of total operating costs is stated in reference to the South African coal mining industry by Thompson et al (2003). The exact cost of haulage (due to energy consumption equipment and road associated costs) will be unique to each site and is dependent on the geology of the site, load density, road surface and gradients (Department of Resources, Energy and Tourism, 2010).

Measuring fuel consumption rates for haulage vehicles is a complex task. Kecojevic et al (2010) contend the most accurate method is from observation at the mine site. This view is expanded upon by the Department of Resources, Energy and Tourism (2010) who include comment that observation needs to occur over a sufficient time period to account for any natural variations in fuel use when determining the baseline energy used in haulage. If such a program to capture fuel use data is not possible then estimation of fuel use from manufacturer data may be possible. Most equipment manufacturers describe operating conditions in estimating fuel consumption of vehicles, with the operating class generally including comment on the condition of haul roads (Kecojevic et al, 2010). The judgement of the class of road is a subjective one that must often be made with limited direction as to the definition or guidance being provided.

One study has attempted to define energy use through analysis of published data for various mine sites and determined that on average loading and haulage account for the consumption of diesel at a rate of 2.2 kg/t of iron ore produced in Australia (Norgate et al, 2009). If a net calorific value of 42.91 (MJ/kg) is considered (Staffell, 2011) then approximately 94.4 MJ/t of energy is consumed in the process. Therefore approximately 60% of energy consumed for a tonne of iron ore is spent in the load and haul process (Norgate et al, 2009). This amount of diesel use is undoubtedly significant and thus means that for the 393.9 million tonnes of iron ore produced in Australia in 2009 (Geoscience Australia, 2013) a total of approximately 37 Gigajoules were consumed in loading and intra-site haulage. This equates with approximately 2.8 million litres used per day. It is for this reason that load and haul is identified as the second greatest area for potential energy savings in the production of ore, after crushing and grinding (Norgate et al, 2009). Possible improvements (outside of technological advance and monitoring of diesel-powered haul trucks) focus on reduction in haulage requirements through pit design and adoption of in-pit crushing and conveying (Department of Resources, Energy and Tourism, 2012).

Mine contractors and operators have attempted to increase energy efficiency with initiatives such as reducing the stopping of haulage vehicles and optimising engine controls (Britton et al, 2012). An example of the effect of stopping is presented in Figure 2.3, where it is evident that the fuel saved in the process of stopping the vehicle is far out-weighed by that consumed in returning the vehicle to the original speed. Stopping a haulage vehicle also results in reduced production, thus some mine operators have attempted to optimise the vehicle flow of their sites (Department of Resources, Energy and Tourism, 2012). Although such initiatives will provide benefit, many studies also note that the road surface is a major contributor (see Section 2.2.5), yet do not investigate a means to improve efficiency. In the study presenting the findings reproduced in Figure 2.3 it is also noted that a dry and hard-packed haul road keep fuel costs and tyre wear to a minimum whereas wet conditions can increase rolling resistance (Department of Resources, Energy and Tourism, 2012). No substantiation of this statement is provided and therefore it can only be assumed it is derived through observation and experience.

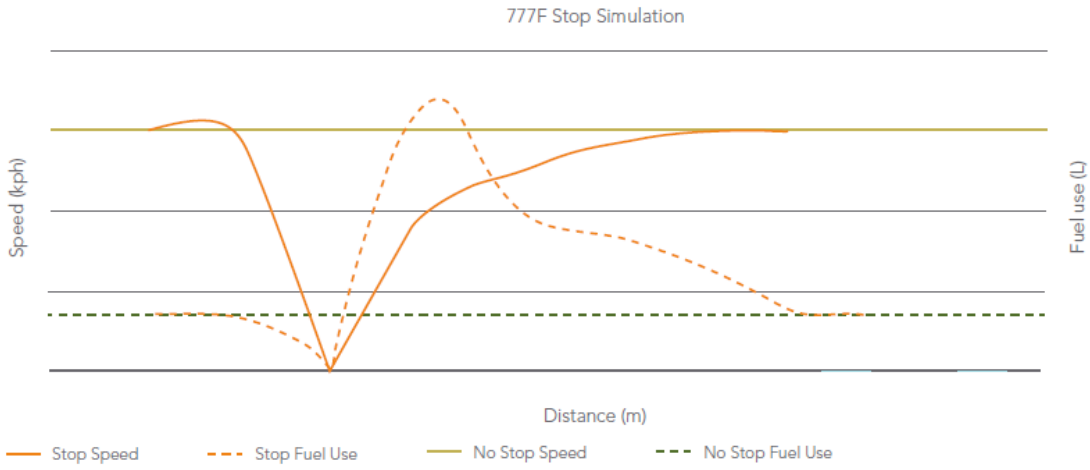


**Figure 2.3: Stop simulation impact of fuel consumption for a Caterpillar 777F (Department of Resources, Energy and Tourism).**

A method for estimating the fuel (and therefore energy) consumption of haul trucks is presented by the Department of Resources, Energy and Tourism (2010) in Appendix A. This is a first pass approach requiring assumptions for fuel to wheel energy efficiency, load density and transmission efficiency. While it is a simple model it does allow for some optimisation of the energy balance within the bounds of the assumptions made (Department of Resources, Energy and Tourism, 2010). The method considers many inputs and includes a subjective estimate of the rolling resistance and traction coefficient. If the final result of 6.84 L/100km/t is considered and converted to the unit of MJ/t.km with net calorific value of 40 MJ/L for diesel (Staffell, 2011) a final value of 2.74 MJ/t.km is calculated. One study of note that also attempts to describe and optimise haulage efficiency (although not applying the model discussed above) is reported by Britton et al (2012). The key aspects affecting fuel efficiency were considered to be the directness (ratio of total haulage distance to the direct distance to the dumping point) and energy balances. These theories alone with a simple fuel consumption model allow one to complete some degree of optimisation for any haulage route.

If the energy consumption values of the haulage system assumed above are compared against the average energy consumption for general road freight, 2 MJ/tonne km (Bureau of Resources and Energy Economics, 2012), it can be seen that off-highway transport is indeed more energy intensive that normal road transport. This is despite the economies of scale at play with regard to the large

payload sizes employed in mine haulage. However, also consider that the final value noted above for the haul truck scenario includes a climbing gradient of 4.5%, which most definitely would exceed the average value experienced by all freight vehicles on Australian roads.

The approach for estimating the energy consumption of haulage operations described above may be supplemented by a method for estimation of fuel consumption due to pavement roughness. Such a model, derived specifically for haul trucks has been derived by Thompson et al (2003). This set of functions was derived through development of an engine-speed model and computer modelling for various haul trucks, including mechanical and electric drivetrains. Ultimately, it was found that fuel consumption was most affected by speed as with heavy commercial vehicles (Thompson et al, 2003), which was supported through a monitoring program. The model derived by Thompson et al (2003) quantifies fuel consumption for trucks experiencing unfavourable total grades, thus either travelling on a positive grade or downhill on a pavement of exceptionally high rolling resistance. The model was found to have an R-squared value of 64% and thus was deemed a reasonable fit to the observed data. Not surprisingly, this model includes vehicle mass and speed as key input parameters, however does not include any term for engine or drivetrain efficiencies. Despite this, the inclusion of total resistance means that it is a neat approach in estimating fuel use in conjunction with the method noted above, while taking into consideration road geometry. This model is considered the most relevant model of its type available.

## 2.2 Rolling Resistance

### 2.2.1 Theory of Rolling Resistance

The theory of rolling resistance has been researched with a view to improving the performance of self-propelled vehicles for approximately a century. In simple terms the notion refers to the effort required to move a wheel over a given terrain via the motion of rotation or rolling, see Figure 2.4. ISO 28580:2009 utilises the rolling resistance coefficient, which is the most commonly adopted for quantification. In its most basic form this can be expressed as:

**Equation 2.1: ISO 28250 definition of the rolling resistance coefficient.**

$$R_c = \frac{Tyre\ Load\ (kN)}{Rolling\ Resistance\ Force\ (N)}$$

Where:

$R_c$= Rolling Resistance Coefficient (dimensionless)

Although there is no universally accepted measure at the current time, the majority of literature adopts Equation 2.1 for the definition of the rolling resistance coefficient (RRC). There is no general relation available that links tyre inflation pressure, speed, rolling resistance and the coefficient of rolling resistance. Therefore Equation 2.1 can be used to describe only unique situations and should not be applied for estimation of tyre load or rolling resistance (Evans et al, 2009). Rolling resistance can be thought of as the force producing a torque in the direction opposing travel in the desired direction and hence is essentially the sum of all the energy losses within the vehicle, tyre and pavement systems (Sandberg et al, 2011). ISO 28250:2009 (International Organisation for Standardisation, 2009) discusses this method of quantification in terms of ‘parasitic losses’. Although the above description is useful in describing the net effect of rolling resistance, it is important to remember that the resistance is the result of a complex system involving many parameters. Further the rolling resistance is not a force (despite being often expressed in J/m or N), but rather is the scalar quantity of energy lost per meter travelled (Evans et al, 2009).

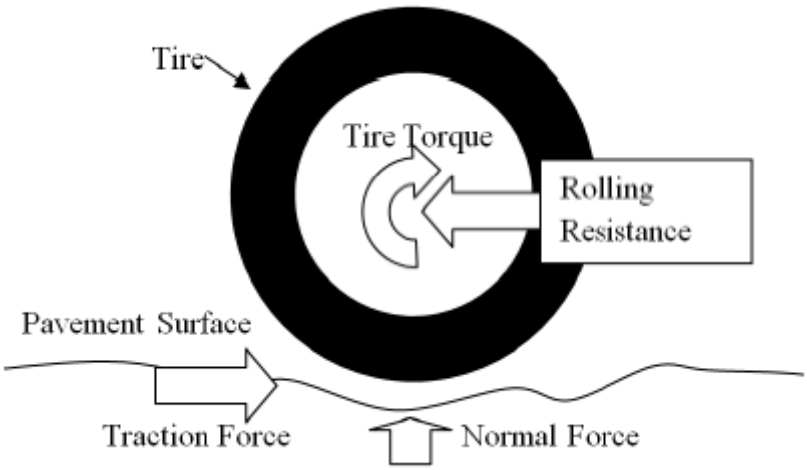


**Figure 2.4: Forces acting on a rolling tyre (Jackson et al, 2011).**

Careful distinction of the different quantities often referred to simply as ‘rolling resistance’ is required for clarity. In most literature the driving resistance is actually measured and discussed, which refers to the sum of rolling resistances of each wheel in contact with the ground and any associated losses in the tyres, vehicle suspension, bearings or transmission (Hammarstrom et al, 2012). Note that there are many other smaller influences, which are detailed in the ensuing chapter. Driving resistance is often applied due to the difficulties of measuring the resistance to motion experienced by a single tyre and also the practicality of defining such a value in isolation. Most investigations are interested in the energy consumption of the whole driving system and so it is prudent to consider the entire system together. Such an approach allows for significant learning in experimental research, however the problem remains in making use of the results for pavement design. This issue is magnified when it is considered that other losses such as bearing losses can be studied effectively in a laboratory (Sandberg et al, 2011) and empirical relations developed based on extensive data. Thus the study of pavement/tyre interaction in isolation is important but the results are difficult to apply.

The early twentieth century saw modern studies of rolling resistance commence with Bernstein (1913) developing empirical theories taking account of a deformable terrain (Wong, 2010). These authors believed that rolling resistance was due primarily to the effort required to compress the soil (Komandi, 1999). Over the past century there have been many extensions of this work derived and several other noteworthy theories reported. This research is associated closely with the field of

terramechanics, which is discussed in Section 2.2.3. The advent of modern pavement analysis methods has resulted in similar studies generally considering a perfectly elastic surface or a rigid surface depending if the author was primarily interested in pavement or tyre response. The original investigations considering tyre sinkage have also continued, mainly by those with interests in agriculture or military applications where off-the-road travel is common.

A great number of investigations have explored the effects of individual variables on rolling or driving resistance for a specific vehicle. These provide the basis for critique of any theory suggested in the literature, but what makes such comparisons particularly difficult is the presence of pneumatic tyres. Most functions derived with observation of mechanics consider a rigid wheel, and thus the interaction of soil/pneumatic tyres needs to be understood in great detail in order to draw significant conclusions from such work. Jackson et al (2011) provide one such summary, from which it is clear that a universally accepted definition and measure for rolling resistance would help to simplify and increase the impact of each author's contribution. An example of potential harmonisation is to consider the aerodynamic resistance of the rotating tyre. ISO 28250:2009 and other accepted industry standards do not take this into account, which is undoubtedly not negligible at higher speeds (Sandberg et al, 2011). It is evident in almost all studies that this effect has been neglected and as a result may have been included in the rolling resistance values presented. One common definition could potentially allow for all such losses to be considered and therefore create a more consistent research basis. Such an approach would enhance correlation of future research.

The following sections describe groupings of investigations on the topic of rolling resistance. A distinction is made to isolate tyre derived losses from those inherent in various components of the vehicle (suspension, engine and drivetrain). Similarly, discussion relating to pavement/terrain interaction is separated into discussion of response due to surficial ('functional') features and structural support. A further distinction is made with regards to the structural support whereby deformable terrain is considered distinct from the loading response of designated pavements, as the former relates to the study of terramechanics and the latter to pavement engineering.

### 2.2.2 Rolling Resistance due to Tyre Response

Tyres play a crucial role in the driving resistance experienced by any vehicle. They are indeed the only part of the vehicle that contacts the ground and the interaction that occurs at this interface is immensely complex. Essentially the energy losses experienced by tyres in the rolling motion can be separated into three categories; friction between tyre and road (2-10%), air resistance in and outside of tyre (1.5-3.5%) and internal tyre hysteresis (90-95%) (Clark, 1981). Tyre manufacturers attempt to balance three elements; rolling resistance, traction and tread wear which are mutually inclusive and complexly interdependent (Evans et al, 2009. These goals complicate the aim of simply minimising tyre rolling resistance, as the latter two focus on the frictional and durability characteristics of the tread section of the tyre. To simplify the actions acting at the interface of tyre and pavement, consider that two types of interactions occur, which can be described as ‘stick-slip’ and ‘stick-snap’ (Sandberg et al, 2011). ‘Stick-slip’ refers to situations where the coefficient of friction is not sufficient to prevent any longitudinal movement. ‘Stick-snap’ describes a situation where friction is sufficient to prevent longitudinal movement and the rubber material is strained, resulting in the adhesion between the two faces being broken. These actions in combination with the bending and dynamic actions of the tread section and side-walls encompass the majority of reactions exhibited by pneumatic tyres. A visual summary is provided in Figure 2.5.

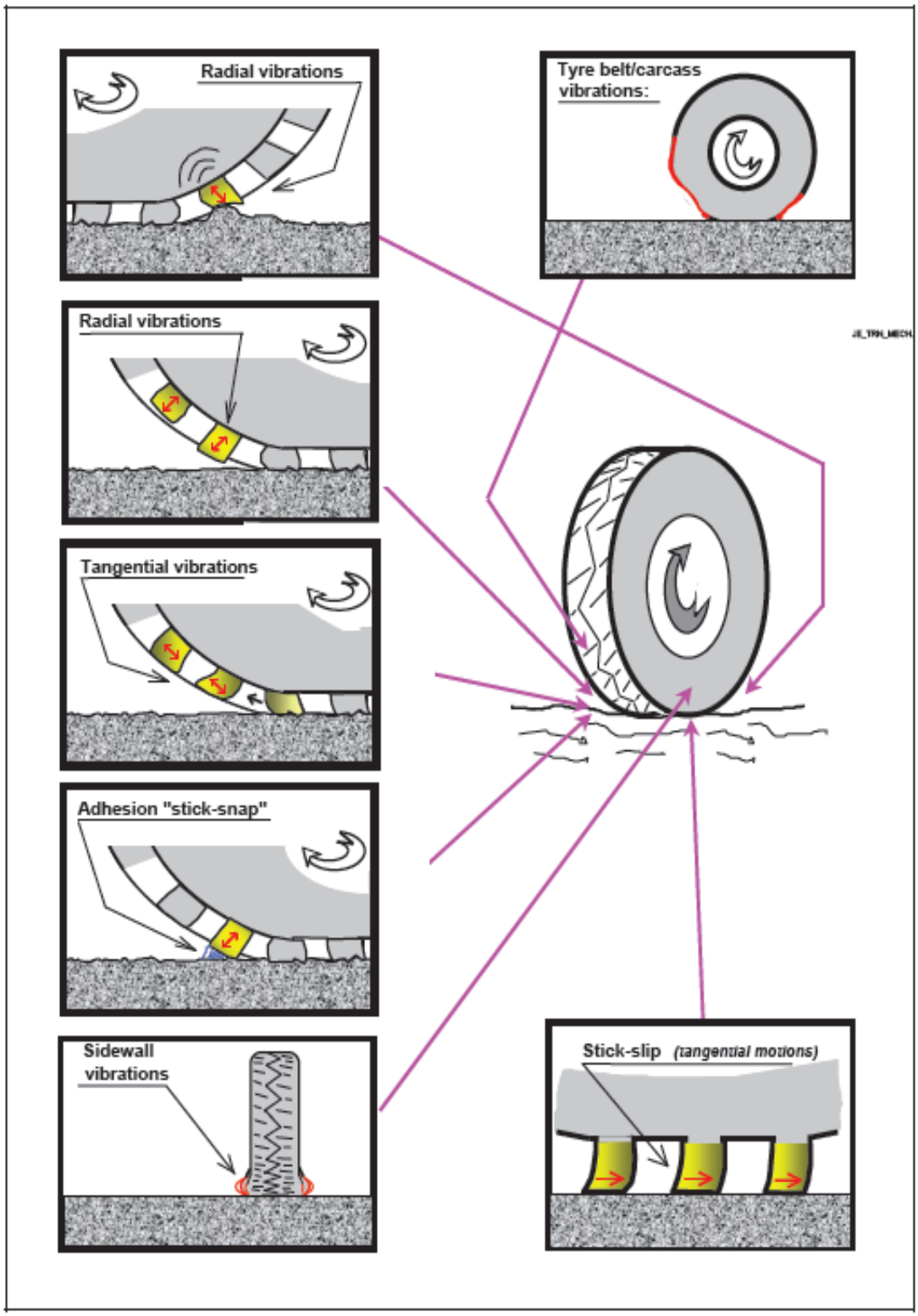


**Figure 2.5: Rolling loss generation mechanisms due to tyre deflection (Sandberg et al, 2011).**

To explain the energy loss through the mechanism of a rolling pneumatic tyre one should observe the theory of thermodynamics, where energy transfer occurs either due to work being completed or alternatively transferred as heat (LaClair, 2006). There is no net displacement between the tyre outer tread and the wheel's rim, hence all losses must result from the loss of heat. Generation of heat occurs primarily through hysteresis of rubber and also through friction between tyre tread and the pavement surface, tyre bead and wheel rim. The induced stresses are highest at the front of the contact patch, which is where the majority of heat originates and then concentrates in the tyre's steel belts which are included in the structure of the tyre to increase stiffness (Li et al, 2012). The contact patch deflects and results in bulging of the adjacent side-walls, these are the two main areas in which the tyre rubber is strained. Most rubber compounds are viscoelastic; viscous materials resist shear flow and strain linearly with time as stress is applied. Elastic materials strain instantaneously when stress is applied and return to their original orientation as quickly as possible after the release of the applied stress (Brancatti et al, 2011). The hysteresis in the tyre rubber occurs with strain leading stress due to the deformation being greatest in the rubber component of the tyre. This results in strain energy potential being stored in a significant lag phase between strain and stress, which is lost as heat energy (Lin et al, 2004). Although the greatest build-up of heat occurs in the steel belts it is indeed the least stiff component of the tyre, the rubber, that dissipates heat the most. Hence rubber deformation is the predominant element within the mechanism of a rolling tyre that causes rolling resistance. Further, it is worth noting that tyres cool while stationary much slower than they heat up (Venkataraman, 2007), thus the effect of stopping in traffic is minimal.

The potential for improvements in tyre technology is evident from the relatively recent past. It is estimated that rolling losses have been reduced by up to 70% due to the implementation of radial tyre construction in the past couple of decades (Pillai, 2004). Figure 2.6 describes the variance in performance between cross-ply and radial-ply tyres. The evolution of radial tyres has occurred due to superior rubber compounds being developed, this means the tyre is not as stiff and conforms to the road surface better (Venkataraman, 2007). Flexibility is achieved by the steel belts within a radial tyre running perpendicular to the bead and not continuing through the sidewalls as illustrated in Figure 2.6. This difference in the contact patch means the tyre can better traverse pavement texture. Subsequently, hysteresis is reduced due to the larger contact patch resulting in less flex in the tyre side walls being required to conform to the road surface, which results in less heat build-up and energy loss

(Venkataraman, 2007). Furthermore, any heat generated is more easily dissipated through the thinner tyre side walls of radial tyres, which is significant due to the low diffusivity of rubber compounds used in tyre construction (Brancatti et al, 2011). Therefore a radial tyre of equal size generally improves rolling resistance and traction, however this is dependent on the utilisation of the correct operating pressure (Michelin, 2000).

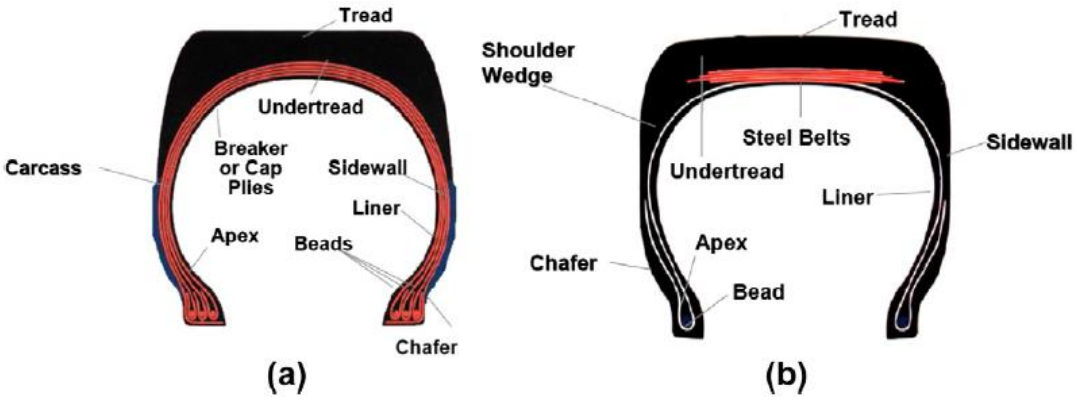


**Figure 2.6: Illustration of the differences in construction of (a) Bias and (b) radial tyres (Tonkovich et al, 2012).**

It has long been acknowledged that tyre temperature and inflation pressure impact on performance. The inflation pressure is critical as it largely determines the strain and therefore hysteresis experienced by a tyre, the faster a tyre is driven when under-inflated the higher the rolling resistance it experiences (Nielsen et al, 2002). A study completed by Pillai (2004) found rolling loss to be inversely proportional to inflation pressure. The modelling completed by Venkataraman (2007) describes stress being highest at the front of the contact patch, which results in the front of the contact area being larger than the rear. This disparity is reduced with a higher inflation pressure which in turn results in lower rolling resistance (Venkataraman, 2007). Tyre temperature obviously impacts the strain rate experienced by rubber, so much so that Li et al (2012) suggest that higher ambient temperatures lead to shorter lifetimes for large dump truck tyres. Yong et al (1990) report that tyre inflation pressure has a more profound effect as road roughness increased, with a higher efficiency associated with higher inflation pressures.

### 2.2.3 Terramechanics and Rolling Resistance

The study of 'terramechanics' has yielded many functions for the prediction of rolling resistance by employing the available mechanical relations applicable to each individual component of the rolling wheel mechanism. Of particular interest is the study of traction forces developed between a rolling tyre and a deformable terrain. Although such and understanding is useful, it must be noted that many of the relations were developed by applying classical soil mechanics, which relate to static loads. Consequently it must be remembered that the load applied by a rolling tyre varies significantly in application rate and duration (Schuring, 1963). Modern attempts have been made to model the problem with advanced software such as finite element analyses such as that detailed in Grujicic et al (2010). However, material response (such as the non-linear soil behaviour) may not currently be understood well enough to utilise such tools to utilise the results in practice, as was suggested some decades ago by Plackett (1985).

The theoretical study of terramechanics is undoubtedly useful to the study of off-road rolling resistance. One important point is the difference in the application of applied force for towed and driven wheels. Consider Figure 2.7 below, where it is shown in diagram (a) that a force ($F_t$) acts at the centroid of the wheel. This is effectively equivalent to (b) where a couple is shown to be applied (again $F_t$), which is resolved to a moment and linear force ($F_k$) in (c). Note that the force is applied at the base of the wheel. The former is the case for a towed and the latter for a driven wheel (Komandi, 1999). Thus the moment required to overcome rolling resistance in each case is equivalent ($F_t.R=F_k.R$), only applied differently. It is for this reason that when considering the factors affecting the rolling resistance moment the study does not need to be separated to consider driven and towed wheels (Komandi, 1999).

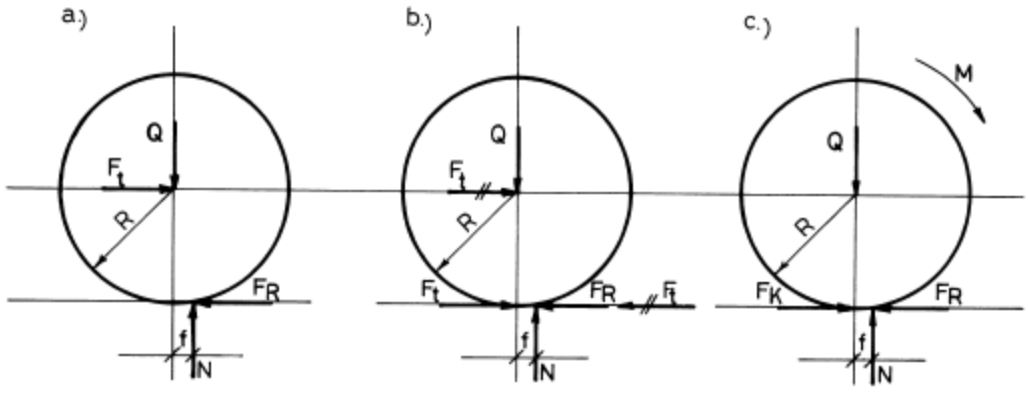


**Figure 2.7: Mechanical relationship between (a) towed and (b) driven wheels, and the shifting of forces (c) (Komandi, 1999).**

Another limitation of utilising basic mechanics to describe the rolling motion relates to the rotation of the wheels due to moment F.Q in Figure 2.7. In all cases this actually only relates to a rotation and not a forward translation (Komandi, 1999). Thus the resistance experienced is against rotation and not a rolling mechanism. This limitation should be kept in mind when considering any theoretical description of rolling mechanics.

A concept from the field of off-road vehicle mechanics worth noting here is the notion of slip. At the wheel/terrain interface there is undoubtedly shear forces acting tangentially to the direction of tyre motion and hence some displacement must occur (Wong, 2010). The wheel must ‘slip’ to some degree when a thrust is applied or generated by a wheel gear. It is common for the performance of off-road vehicles to be described with consideration of 20% slip, which is considered to provide satisfactory working conditions (Wong, 2010). This topic is discussed further in Section 2.2.3.3.

For estimating the traction (and therefore rolling resistance) in a deformable terrain, two distinct methods have been researched. One was popularized by Bekker (1956) who considered the stress at a point under a rigid plate with given sinkage analogous to the corresponding point under a rolling rigid wheel. This assumption is known to be incorrect (Gee-Clough, 1977) and assumes there to be no shear stress (tangential or normal) at the wheel-terrain interface (Wong, 2010). A practical issue associated with the theories developed from the work of Bekker is that they often apply soil properties that are not utilised in conventional soil mechanics and thus are

often difficult to define (Plackett, 1985). Ultimately it is contended that rolling resistance and sinkage (depth of tyre penetration into supporting medium) are an interdependent system of variables (Grahn, 1991) and hence such theories must be used with caution. The second method originated with sand and clay 'mobility numbers' derived by Freitag. This method utilises the soil cone index to describe soil strength, which is not a comprehensive measure and for which data may be difficult to obtain for use in practice (Plackett, 1985). Both models are empirical in nature, which raises doubt that they can be applied in the evaluation of environments not represented within their development (Wong, 2010). Both are discussed further in the following.

#### 2.2.3.1 Pressure Sinkage

Pressure-sinkage relationships were extensively researched and extended by Bekker (1956). It was this work that provides perhaps the neatest function explaining the additional resistance experienced by a tyre rolling on a deformable terrain in comparison to a tyre running on a compacted pavement. It considers tyre losses separately to soil effects, which distinguishes it from the theories noted in the discussion above.

Equation 2.2 helps describe the difference in rolling resistance on a deformable terrain and a compacted pavement. The additional terms due to the deformation of the supporting terrain represent resistance due to compaction and 'bulldozing'. It has been understood for well over a century that rolling resistance is reduced more by an increase in wheel diameter, creating a long contact patch, than by an increase in wheel width (Gee-Clough, 1976) which increases resistance with significant sinkage and bulldozing soil in front of the tyre (Gee-Clough, 1979). Note that bulldozing is noted to occur when the sinkage/wheel diameter ratio exceeds 0.06 (Sitkei, 1966).

**Equation 2.2: Bekker's equation describing the three components of off-road rolling resistance (Gee-Clough, 1979).**

$$R = R_c + R_b + R_t$$

Where:

$R$ is the rolling resistance

$R_c$ is the rolling resistance due to soil compaction

$R_b$ is the rolling resistance due to bulldozing

$R_t$ is the rolling resistance due to tyre flexing

To understand the compaction term, Bernstein (1913) proposed that the deformation caused by a wheel to create a rut was analogous to the pressure sinkage relationship under a rectangular plate (Plackett, 1985). Bekker extended this theory to consider both frictional and cohesive components of the soil, as he contended that compaction resistance was derived from both (Plackett, 1985). Other authors such as Schuring (1963) support the theory concluding that rolling resistance was closely related to the bearing capacity of the soil and sinkage of the wheel. Grahn (1991) furthered this work to take account of dynamic effects and vehicle speed to calculate maximum shrinkage. Grahn (1991) also noted that sinkage decreases with driving speed despite maximum pressure increasing due to a decreased contact patch area. Additional research into the prediction of sinkage has continued by authors such as Reece, who utilised classical soil mechanics to describe soil failure beneath a strip footing with respect to a pressure/sinkage relationship (Plackett, 1985).

Resistance due to soil compaction can be calculated by taking account of the effective stiffness of the tyre due to inflation pressure and tyre carcass stiffness (Plackett, 1985). The resistance to bulldozing has also been described by Bekker in two parts separating global and localized shear failure (Gee-Clough, 1979).

#### 2.2.3.2 Mobility Numbers

An alternative method to the reliance on pressure/sinkage relationships was derived by Freitag, who utilised dimensional analysis to determine ‘mobility numbers’ for friction and cohesive soils (Plackett, 1985). This research showed that the main traction parameters could be correlated with a dimensionless number, termed either the ‘sand’ or ‘clay’ number (Gee-Clough, 1979). Both mobility numbers are used to estimate sinkage and therefore rolling resistance. Attempts were made to extend

these (Crossley et al, (2001) in soil-bin experiments, but ultimately the correlations were found to be quite poor due to the extrapolation of the testing conditions that were implicated. Gee-Clough (1980) utilised a deflection factor of the tyre to calculate the mobility number, however noted limited practical application of the relation. Other attempts have been made to expand the method, but ultimately it has been shown to have little practical use due to the difficulties alluded to above in extrapolating from the original conditions (Plackett, 1985).

Finally it is worth noting that numerical approaches to modelling rolling resistance, such as mobility numbers, are problematic in that the mechanics utilised is not necessarily well understood in terms of critical state soil mechanics and plasticity theory. These issues need to be addressed before computer methods should be relied upon (Plackett, 1985).

#### 2.2.3.3 Wheel Slip

The rolling resistance theories derived from Bernstein and later Bekker do not take into account wheel slip (Plackett, 1985). Due to this omission it was realised that rolling resistance would be overestimated (Gee-Clough, 1976). Prior to this it was also noted that sinkage could not be related to an infinitesimal element under a rigid plate with the same sinkage and pressure as a tyre (Onafeko, 1969). Another issue with the theories derived from the work of Bekker was that the shear stress between the soil and tyre was either omitted or considered constant. Gee-Clough (1976) states that this is the reason skid and slip was not included originally, as it is the unbalanced moment created by the shear stress acting in opposing directions during the passing of a wheel that explains the presence of slip. Figure 2.8 describes the nature of the shear stresses and also presents differences between the normal stress distribution between a wheel and a plate. Plackett (1985) also contends that it is very difficult to discriminate between soil compaction and sinkage as well as horizontal movement due to bulldozing within a soft soil environment. The culmination of these issues meant more traditional soil mechanics methods were needed to describe the problem. An attempt to apply such was made by Hetherington et al (1978), where the contact area was idealised as a series horizontal strip footings to allow the application of Terzaghi's theory, but ultimately considers failure only perpendicular to the plane of the wheel (Placket, 1985).

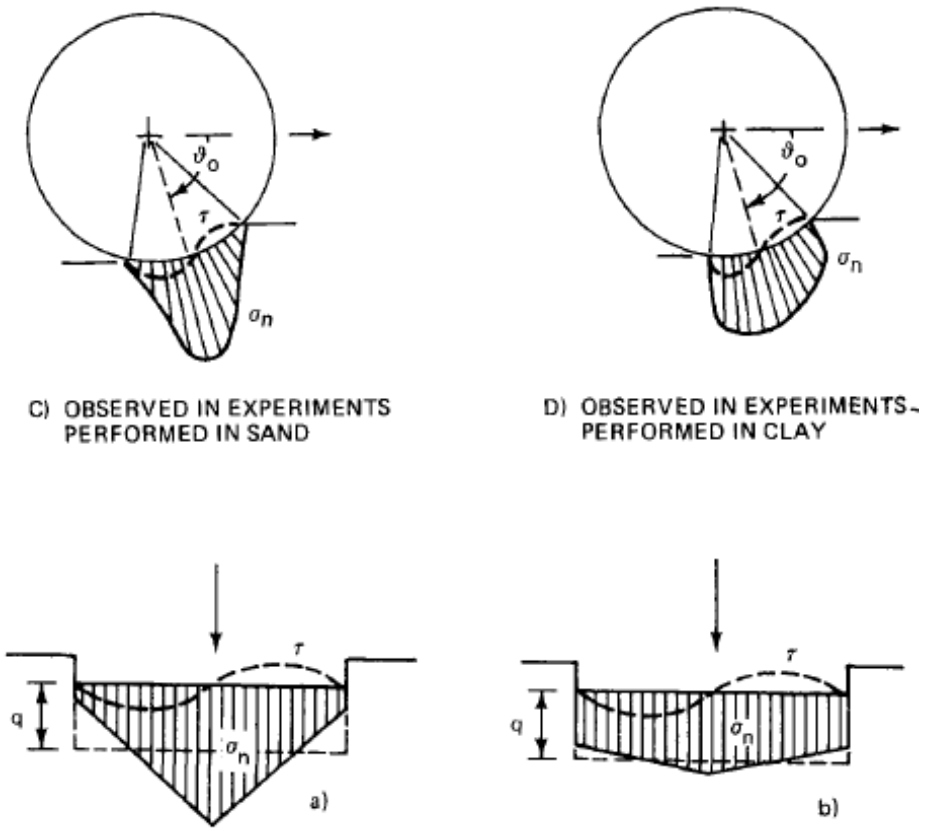


**Figure 2.8: Normal and shear stresses beneath a tyre in relation to the same soil beneath a rigid plate (Gee-Clough, 1976).**

#### 2.2.3.4 Numerical Modelling

In recent years, an advance in the capacity of personal computers has seen an effort to utilise numerical modelling to describe the motion of off-road pneumatic tyres. This is a very complex process requiring a three-dimensional model to account for soil moving laterally as it is displaced by the wheel and inclusion carcass stiffness in modelling of the tyre (providing bearing support between the tread/belts and the rim) (Fervers, 2004). Hambleton et al (2008) derived a model very similar to that proposed by previously noted authors. Ultimately it was concluded that the complexity of considering all out-of-plane effects presents potential errors. One exception to this is when considering cohesive soils where three-dimensional effects appear to have little effect on the sinkage/indentation per unit width (Hambleton et al, 2008). Furthermore, analytical models tend to oversimplify the dynamic tyre contact, which can result in surface settlements being defined in terms of wheel sinkage instead of changes in soil density through compaction (Xia, 2011).

Advanced numerical modelling has been able to provide findings in line with that discussed above. For example, it has been shown that rolling resistance is improved with multiple narrow wheels, rather than a single, wide wheel (Hambleton et al, 2009). Xia (2011) notes that the energy used by a rolling tyre can be reduced through increased stiffness of tyres and/or terrain. Fervers (2004) also found through three-dimensional modelling of tyres and soil that decreased inflation pressure can significantly reduce rolling resistance. An increase in tyre translation speed (vehicle speed) is also noted to produce a reduction in rolling resistance, as the soil is contacted for a shorter duration and is therefore subject to less compaction (Xia, 2011). These results describe the power of numerical modelling to improve the efficiency of off-the-road transport.

### 2.2.4 Rolling Resistance due to Structural Support of Engineered Pavements

The ‘structural contribution’ to rolling resistance is a term used herein to denote the relative bearing strength effects of a pavement. In effect, it is the rolling resistance experienced due to energy loss through the stress/strain response (hysteresis) of pavement materials. In many texts such as Jackson et al (2011) it is noted to be a very small effect, accounting for as little as approximately 1% of total rolling resistance or even being negligible. Testing carried out in Europe suggests that pavement deflection contributes very little (Hammarstrom et al, 2008). Coast-down tests were used to define rolling resistance, where a vehicle is allowed to coast from a known speed and the deceleration is measured to define the total resistance experienced. This research is likely the most detailed study completed, however it considers vehicles only as large as goods trucks on asphaltic and rigid (concrete) pavements. A similar study has been conducted in New Zealand considering a similar sized vehicle on flexible pavements, both sealed and unsealed where a very significant portion of rolling resistance measured is attributed to pavement deformation effects (Jamieson et al, 2002). Figure 2.9 shows the raw data from this study. Although there is a limited number of roads tested, one was unsealed (top right corner of Figure 2.7), and hence was found to have limited stiffness and moderate roughness which resulted in a fuel consumption 2-4% higher than stiffer pavements of a similar roughness. This study resulted in the conclusion that pavement stiffness was the most significant contributor to the static rolling resistance coefficient. Research effort into the effect of pavement rigidity has

increased significantly in recent years, however it is still not certain in what conditions pavement deflection significantly impacts rolling resistance.

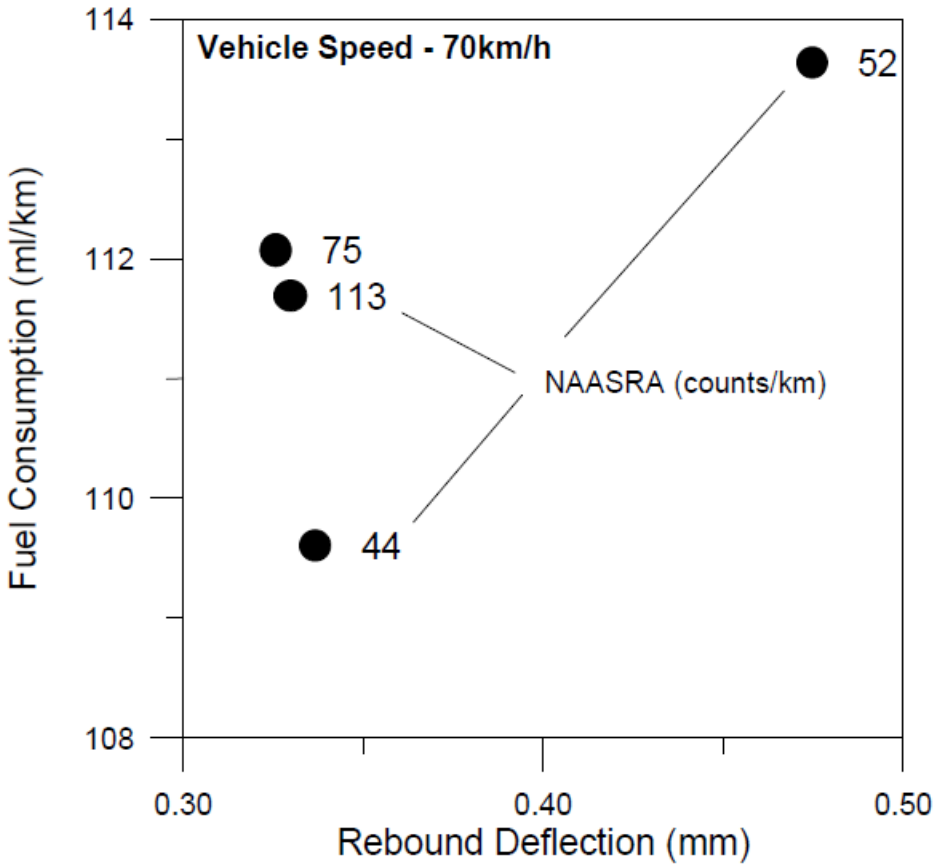


**Figure 2.9: Relation between fuel consumption, pavement rebound deflection and roughness (Jamieson and Cenek, 2002).**

If one is to consider the relative stiffness of both tyre and pavement, some insight can be gained into the relative hysteresis in each. Jackson et al (2011) describes a typical truck tyre as having a stiffness of approximately 1000 N/mm and pavement a value of approximately 28,000 N/mm, thus it would be reasonable to expect in the most simplistic of analyses that more energy would be lost through heat generation within the tyre by a factor of around 28. In this case, of the total energy loss in the system (rolling resistance), approximately 3.5% would be attributable to pavement response (Jackson et al, 2011).

Although the above discussion refers to a relatively crude estimation, it does appear to have some basis when compared to the available literature reporting empirical studies. One suggestion is that the sensitivity to pavement deflection may have been wrongly attributed to surface roughness (Jamieson et al, 1999). This may well be plausible since the pavement considered in the studies consisted of widely different wearing courses. For example, the most common comparison was between rigid concrete pavements against asphalt of varying grades. This effect was discussed at length in a report commissioned by the Australian Roads Research Board (Mclean et al, 1998), who ascertained that the idealisation of a wheel constantly climbing out of a deflection bowl is not consistent with the mechanism at play but rather there exists energy losses through pavement hysteresis.

Research dating as far back as the 1950's, reports findings of lower rolling resistance with improved support conditions, as can be observed in Table 2.1. The method employed is similar to that adopted in studies conducted since, in that the rolling resistance coefficient was determined for a range of vehicles on a range of surfaces. However, this study is of particular note due to the fact that an off-the-road tyre was utilised in conjunction with passenger car and truck tyres. Thus it can be seen that the high lugs of the 'agricultural tyre' (an off-the-road tyre) have resulted in a higher rolling resistance on the rigid concrete and the lowest value on the soft sand (Taborek, 1957). Firstly, as the agricultural tyre is likely to also have a high profile and almost certainly would have been of bias construction it is fair to assume that hysteresis would have been significant in the tread and sidewalls on the rigid surface. Conversely, it is highly likely that this tyre would have had an increased width and diameter compared to the other two tyres involved and therefore could be expected to have a lower rolling resistance coefficient than the road tyres. Secondly, note that between the concrete and the 'medium hard soil' rolling resistance is observed to increase significantly. Of particular interest here would be a detailed description of the nature of surface condition for the 'medium hard soil'. If a significant amount of sinkage had occurred, the increase in rolling resistance could be attributed to this effect. However if no such effect was noted the result could serve as a pre-cursor to the increased resistance effect of pronounced pavement deflection.

**Table 2.1: Rolling resistance coefficients for various tyres and surfaces (Taborek, 1957).**

| Tyre Type | Surface | | |
|---|---|---|---|
| | Concrete | Medium Hard Soil | Sand |
| Passenger Car | 0.015 | 0.08 | 0.30 |
| Truck | 0.011 | 0.06 | 0.25 |
| Tractor | 0.020 | 0.04 | 0.20 |

A similar relationship has been reported in recent years, specifically for the prediction of tractive forces available to earthmoving equipment, as derived by machine manufacturer Caterpillar (Holman, 2006). A definition is made between tracked and tyred vehicles with more categories of ground support supplied than above. Softer soils are distinguished as those presenting some degree of rutting (considered as penetration of the tyre into the soil surface), which is often referred to as sinkage to describe the mechanism of bulldozing soil around a tyre. It would therefore be useful to add the effect of tread pattern and/or the presence of tyre lugs to better define the likely level of slippage (see Section 2.2.4). Despite this omission the data presented by Holman (2009) does show a four-fold increase in rolling resistance between a condition of no visible flexing of the pavement surface to sinkage of 50mm. From the above discussion, it is clear that this data is relevant to theories relating to both terramechnics and pavement engineering. Thus presentation of empirical findings is likely the most prudent way to present such data in the absence of standardised testing methods or universally accepted theories for describing rolling resistance in each field of study.

A study completed by Cenek et al (1996) resulted in Equation 2.3 being derived, in which Benkelman beam rebound deflection is the most significant variable when considering the coefficient of static rolling resistance. It is contended that there are losses associated with pavement deflection due to hysteresis. Note that this study was completed utilising a light truck as the reference vehicle. Table 2.2 presents a summary of the raw data from which this relation was developed. The relation presented here relates deflection linearly with the static rolling resistance coefficient. Hysteresis is a function of stress/strain response whereby a stiffer material could indeed exhibit larger losses depending on its strain rate and plastic behaviour. Therefore linearly relating deflection and static rolling resistance is an over-simplification. Of course the relative stiffness values of tyre and pavement are also likely significant in such a theoretical discussion of rolling resistance due to

pavement deflection. Although this is a somewhat preliminary investigation it does allude to such effects being significant.

**Equation 2.3: Static rolling resistance according to Cenek et al (1996).**

$$C_0 = 0.011 + 0.0033D - 0.00044M$$

Where:

$C_0$ is static coefficient of rolling resistance

$D$ is Benkelman beam rebound deflection (mm)

$M$ is truck mass (tonnes)

**Table 2.2: Typical values of deflection for calculation of rolling resistance and the relative effect of Portland cement concrete (PCC) pavements (Mclean et al, 1998).**

| Pavement Type | Typical Deflection (mm) | $C_o$ | % Diff. from PCC Pavement | |
|---|---|---|---|---|
| | | | $C_o$ | Fuel |
| PCC | 0.1 | 0.053 | - | - |
| Deep strength AC | 0.5 | 0.067 | 26 | 5 |
| AC Surfaced | 1.0 | 0.083 | 57 | 11 |
| Strong granular | 0.8 | 0.076 | 43 | 9 |
| Weak granular | 1.5 | 0.100 | 89 | 18 |

A comprehensive model for vehicle fuel consumption, observing the significant effect of rolling resistance has been derived for use within the Worldbank's HDM-4 model (Zaabar et al, 2010a). This model is likely the most widely applied globally. Note that Benkelman beam rebound deflection is only considered for vehicles over 2500kg on bituminous (flexible) pavements. The constant applied to the measured deflection is significant. For example, on a bituminous road an equal effect would arise from a 1mm deflection, IRI of 33.5 (pavement could be considered impassable

at such a level) or a texture depth of 2.35mm. Thus the data this relation was derived from either showed minimal deflection, or rolling resistance showed a very strong relation to deflection. Interestingly, the same factor is not applied to unsealed roads, which may have provided some greater insight in to the influence of deflection. Unfortunately this was not completed due to the lack of a standard test method for rebound deflection on an unsealed surface. This relation shows just how little is understood regarding the hysteresis generated in pavements due to trafficking and the respective operational costs.

The mechanics involved in the energy loss associated with the loading/unloading of a pavement from a wheel undergoing a longitudinal translation is undoubtedly complex. It has been suggested it is best visualised as a 'bow wave' formed in front of the wheel within the sub-structure of the pavement or predominantly within weaker layers (Sandberg et al, 2011). Hereby, the materials in front of the wheel are stiffer than behind the wheel and thus some energy must be lost in the passing of such a 'wave'. This energy maybe lost as heat, re-orientation of the particles constituting the pavement materials or through cracking or compaction depending on the properties of the materials of interest and the relative magnitude of the stresses induced (Sandberg et al, 2011).

Some estimation of the energy lost through a load/unload cycle occurring within the pavement structure may be estimated by observation of the hysteresis under FWD testing (Schmidt et al, 2009). This effect can be observed in Figure 2.10, where the total energy lost can be determined by summing the area contained within subsequent curves, which are induced by the pulsed dynamic loading utilised within FWD testing. Note that Schmidt et al (2010) estimate that the energy lost due to a rolling tyre would be 70-80% of the maximum energy found to be lost through FWD testing, when the same vertical load is applied. However, this effect may be complicated by the pavement material's load response due to variations in loading rate. For example, asphalt (which made up the composition of the pavement tested in generating Figure 2.10) stiffness increases with the rate of loading (Jameson, 2008A). Analysis of Figure 2.10 reveals that the energy lost within an asphalt pavement is far more significant than within a rigid concrete pavement. In fact Schmidt et al (2010) estimate that within pavements with low structural capacities a greater proportion of rolling resistance is attributable to pavement hysteresis and could ultimately add up to an additional 20%. A study similarly focussed on FWD testing of pavements has been completed by Lenngren et al (2010). Within this study it was found that fuel consumption of a truck travelling at 80 km/h was

increased 5-10% when driving on an asphalt pavement, showing an energy loss approximately 4 times greater than that of Portland cement concrete pavement. The link between total rolling resistance and fuel consumption is immensely complex (see Section 2.3), however this does present clear evidence that increased pavement hysteresis could lead to a greater energy loss and therefore a greater cost to the end-user (Lenngren et al, 2010). Zaabar (2010) reports a similar effect, where heavy trucks experience greater fuel consumption on asphalt pavements compared to concrete pavements, an effect attributed to the viscoelasticity of asphalt. However, in this particular study no physical tests were carried out in an attempt to determine the hysteresis properties of the pavement. This method of testing pavement related losses requires further research but does provide an understanding of the potential inefficiencies of pavements with lower structural stiffness.

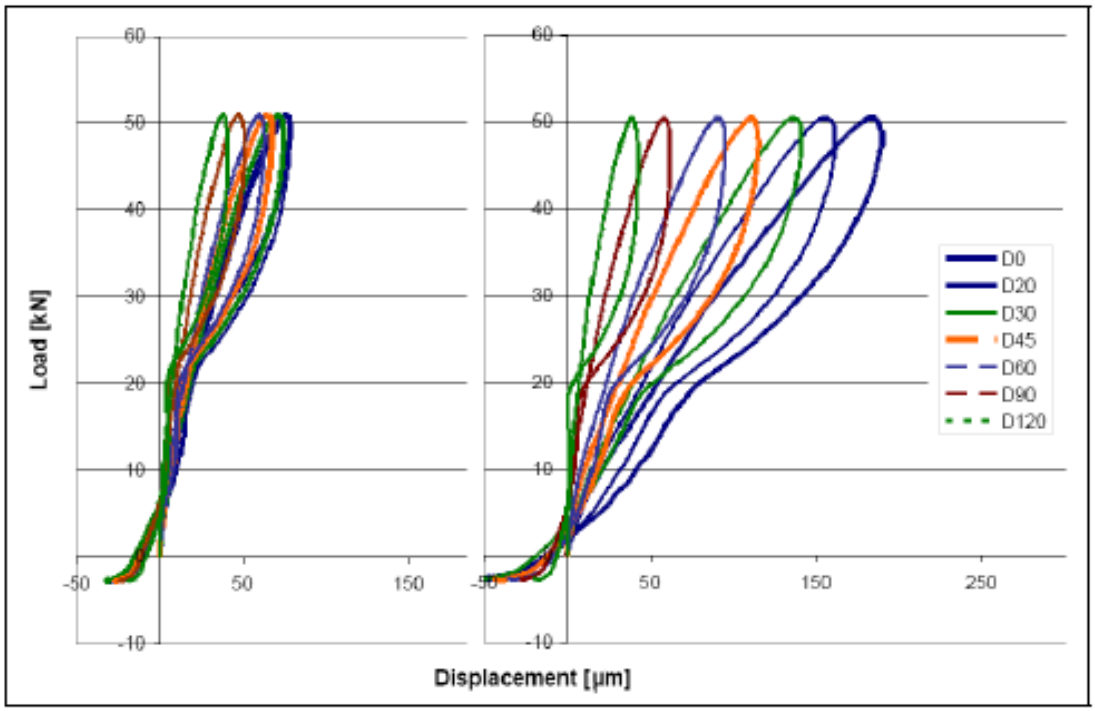


**Figure 2.10: Hysteresis of rigid concrete pavement (left) and an asphaltic pavement (right) materials undergoing FWD testing (Schmidt et al, 2009).**

Douglas et al (1992) completed a study of pavement stiffness for haul roads within the Canadian forestry industry. The contention was that on very low stiffness roads

(roads with sub-grade CBR values less than 1% were considered) the hysteresis of the pavement and sub-grade was found to provide a significant rolling resistance. Furthermore, it is noted that designing unsealed pavements using design criteria for low volume sealed roads is inappropriate, as ruts can be repaired (Douglas et al, 1992). For example, 40% of trucking in Canada is for haulage of forestry products at low speed on unsealed roads, which are often founded on poor sub-grade materials. Therefore, pavement design with a focus on optimising pavement stiffness may be more appropriate than design to limit rut depth if rolling resistance was found to be significantly influenced by the flexibility (inverse of stiffness) of a pavement (Douglas, 1992). It was concluded that design should be focussed primarily on the operating costs of vehicles (Douglas, 1991), implying that stiffness could be adopted as the key design criteria.

### 2.2.5 Rolling Resistance due to Surface Condition of Engineered Pavements

Rolling resistance derived from surface condition refers to the resistance experienced by a tyre due to undulations in the pavement surface. In most cases it invokes a particular tyre response and hence the following discussion links directly with Section 2.2.2. To understand the effects of roughness and texture it is first necessary to understand the definitions and specific actions of each. Although roughness is sometimes used to describe all surface irregularities (Santero et al, 2011), it actually refers to those with a wavelength greater than 0.5m and often restricted at a maximum of 50m, to avoid confusion with road vertical geometry (Mclean et al, 1998) and thus describes ride quality. Shorter wavelength surface deviations are referred to as texture. Figure 2.11 provides a visualisation of the different classes of texture. Microtexture relates to wavelengths less than half a millimetre and is primarily related to the nature of the surface of individual stone particles (Jackson et al, 2011). Tyre adhesion and skid resistance is chiefly controlled by microtexure (Jameson et al, 2009). In relation to Section 2.2.2 it affects stick, slip and snap actions both positively and negatively in terms of rolling resistance (Sandberg et al, 2011). Macrotexture considers wavelengths in the range 0.5 to 50mm (Jameson and Shackleton, 2009). This typically relates to the particle sizes used for the surface course and affects localised tyre deflections and shearing leading to energy loss (Sandberg et al, 2011). Often this value is confused with megatexture, which describes wavelengths of 50 to 500mm. Jackson et al (2011)

note this has a significant effect on rolling resistance by inducing vibration into the tyre. All three categories of texture are defined by the Mean Profile Depth (MPD), although in practice it is the two larger wavelength groupings that are counted (Jackson et al, 2011).

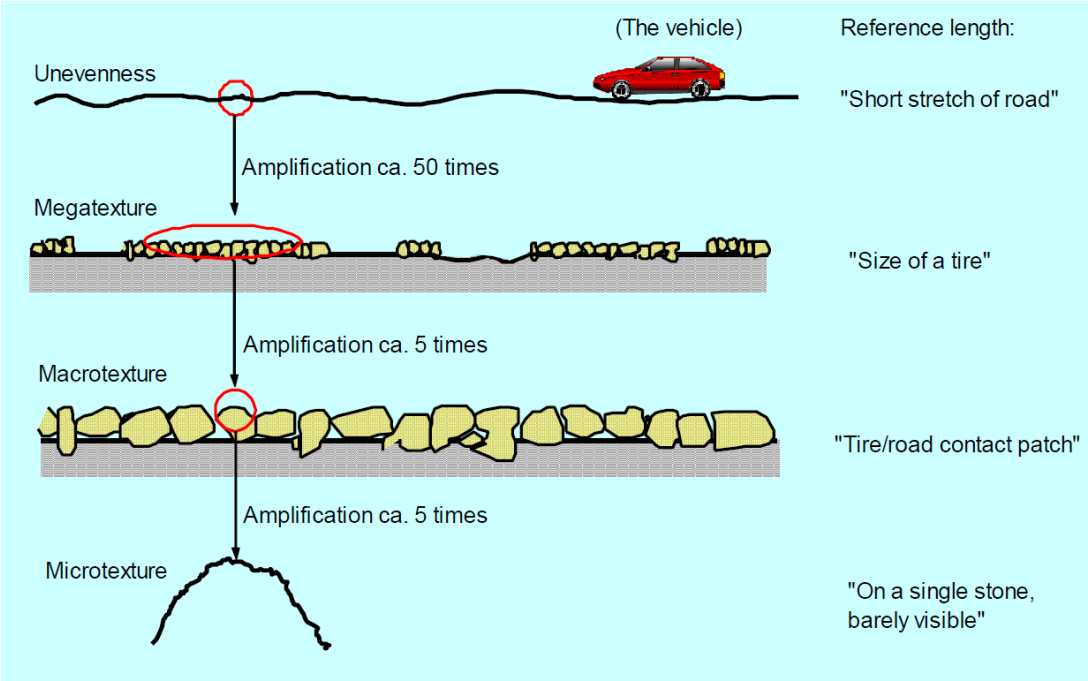


**Figure 2.11: The ranges in wavelength for varying types of roughness (Sandberg, 2010).**

Nielsen et al (2010) contends that the impact of texture on rolling resistance is speed dependent with an increase of 1mm in macrotexture resulting in a 17% increase at 54km/h and a 30% increase at 90km/h. Furthermore Sandberg et al (2011) states the majority of functional rolling resistance is generated by macro and megatexture, due to the wavelength of these types of surface undulation being similar to the dimensions of the contact patch for most tyres and therefore induces undesirable tyre-surface interaction mechanisms (Mclean et al, 1998). Descornett (1990) estimated that megatexture can increase fuel consumption by up to 9% alone due to the vibrations created in the tyre/suspension system. Therefore it is very important to define macro and megatexture.

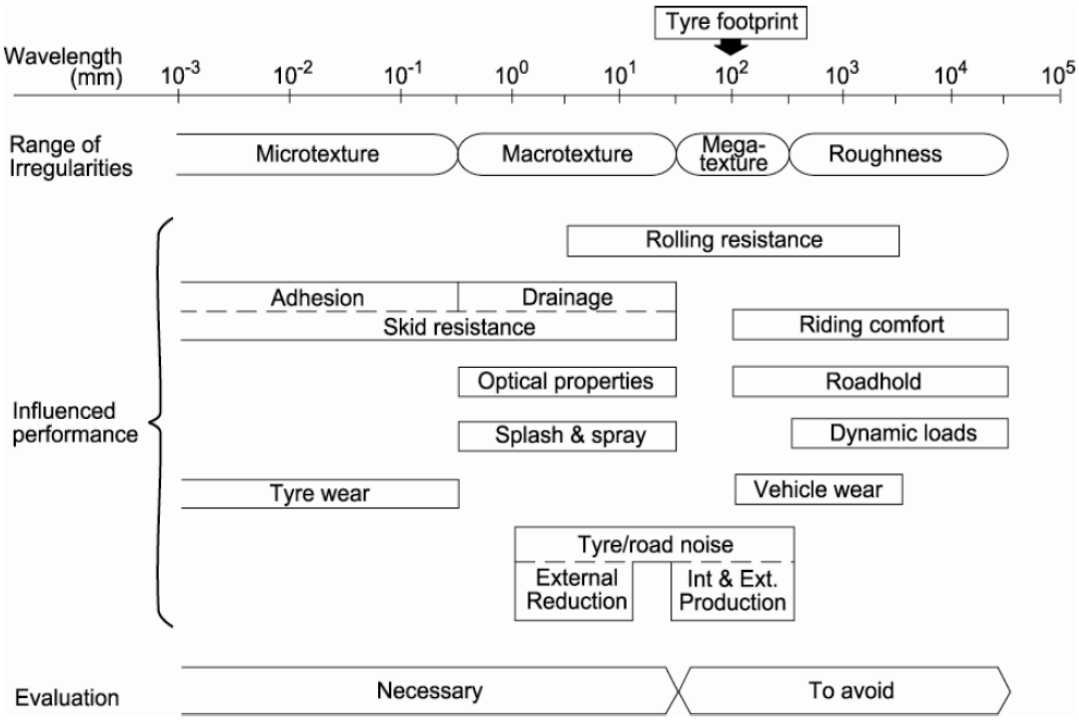


**Figure 2.12: Pavement Texture and Roughness wavelengths and their relation to vehicle performance (Jameson et al, 2009).**

Roughness is generally described by either of two measures; International Roughness Index (IRI) or NAASRA roughness counts (Jameson and Shackleton, 2009). The former represents the utilisation of more advanced technology for measurement, whilst applying the quarter-car model developed for the latter (Gillespie, 1992). A close relation has been defined for the two and is described in Equation 2.4.

**Equation 2.4: Transformation between NAASRA Counts/km to IRI (m/km) (Jameson and Shackleton, 2009).**

$$NAASRA\ \ Counts/km = 26.5 * (lane\ IRI) - 1.27$$

Figure 2.13 presents typical ranges for different pavement conditions experienced by Austroads. This provides some insight into the raw IRI scoring commonly found

for unsealed pavements in comparison with sealed pavements, which provides some indication of the potential increase in VOC when utilising models such as those discussed in Section 2.3.

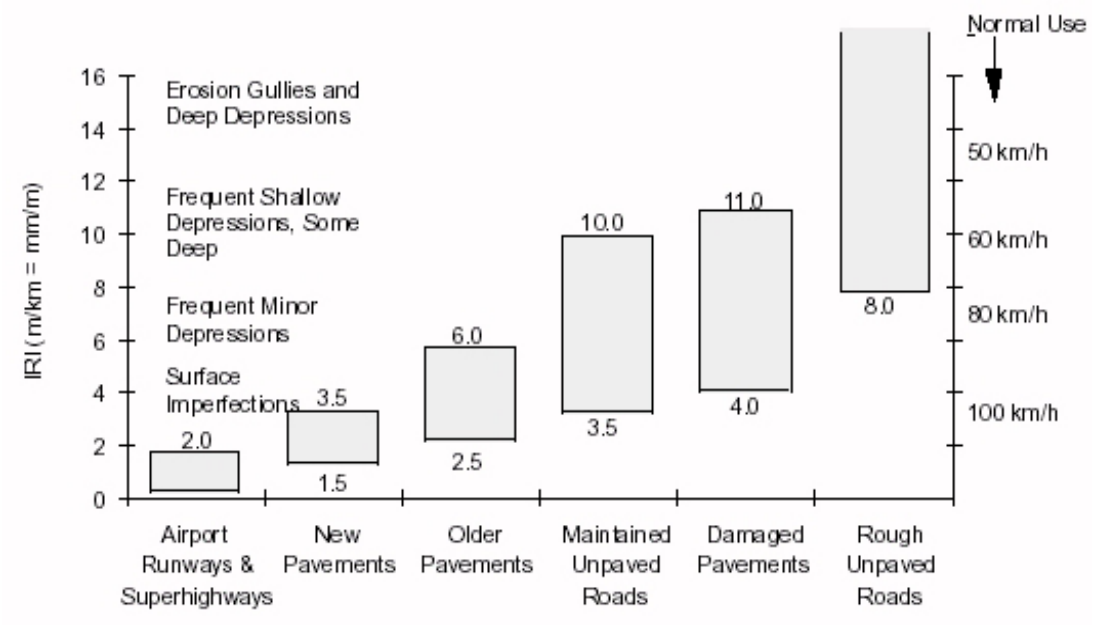


**Figure 2.13: Typical IRI range for different pavement type (Tan et al, 2011).**

The World Bank provides some guidance on subjective judgement of IRI for unpaved roads, reproduced in Table 2.3. Such guidance can be used for the purpose of estimating IRI, but ultimately roughness depends on the response of each individual vehicle and its travelling speed (Gillespie, 1992).

**Table 2.3: Guidance on subjective assessment of IRI for unpaved roads (The World Bank, 1999).**

| *Roughness Range (IRI)* | *Road Description* |
|---|---|
| *1.5 to 2.5* | *Recently bladed surface of fine gravel or soil surface with excellent longitudinal and transverse profile (usually found only in short lengths).* |
| *3.5 to 4.5* | *Ride comfortable up to 80-100 km/h, aware of gentle undulations or swaying. Negligible depressions (e.g. < 5mm/3m) and no potholes.* |
| *7.5 to 9.0* | *Ride comfortable up to 70-80 km/h but aware of sharp movements and some wheel bounce. Frequent shallow-moderate depressions or shallow potholes (e.g. 6-30mm/3m with frequency 5-10 per 50m). Moderate corrugations (e.g. 6-20mm/0.7-1.5m).* |
| *11.5 to 13.0* | *Ride comfortable at 50km/h (or 40-70 km/h on specific sections). Frequent moderate transverse depressions (e.g. 20-40mm/3m-5m at frequency 10-20 per 50m) or occasional deep depressions or potholes (e.g. 40-80mm/3m with frequency less than 5 per 50m). Strong corrugations (e.g. > 20mm/0.7-1.5m).* |
| *16.0 to 17.5* | *Ride comfortable at 30-40 km/h. Frequent deep transverse depressions and/or potholes (e.g. 40-80mm/1.5m at frequency 5-10 per 50m); or occasional very deep depressions (e.g. 80mm/1-5m with frequency less than 5 per 50m) with other shallow depressions. Not possible to avoid all the depressions except the worst.* |
| *20.0 to 22.0* | *Ride comfortable at 20-30 km/h. Speeds higher that 40-50 km/h would cause extreme discomfort, and possible damage to the car. On a good general profile: frequent deep depressions and/or potholes (e.g. 40-80mm/1.5m at frequency 10-15 per 50m) and occasional very deep depressions (e.g. > 80mm/0.6-2m). On a poor general profile: frequent moderate defects and depressions (e.g. poor earth surface).* |

Roughness is generally expected to affect more than just losses in the tyre. Mclean et al (1996) contend that roughness less than 3m in wavelength induce wheel hop (wheel movement relative to vehicle body) and wavelengths of 7m to 28m are associated with the vehicle body bouncing on the suspension. In terms of rolling resistance, Nielsen et al (2010) reports that like texture the effect is speed dependent with an increase of 1.8% at 54km/h and an increase of 6% at 90km/h for an increase in IRI of 1m/km. Note that these increases are far less than that for a unit increase of texture. A great deal of empirical research is available presenting similar results to that contained in Table 2.4. Rolling resistance and therefore fuel consumption are sensitive to unit changes in IRI, however the relationship is highly variable. Which is testament to the effect of pavement texture (consider the dependence on macro and megatexture in Figure 2.12) and other sources of energy loss.

One study which is relevant but difficult to compare with any other was completed by Jamieson et al (2002), who found an increase in loose material present at the surface of an unsealed road increased rolling resistance by 25%. This study was completed with a light truck at steady state speeds ranging from 20 to 75 km/h. Unfortunately, the degree of slip (as per Section 2.2.3) and texture of the pavement were not defined.

**Table 2.4: Results of selected studies showing the sensitivity of rolling resistance and roughness (Mclean et al, 1998).**

| Source | Method | IRI* Range | Vehicle Type | % Change per Unit of IRI | |
|---|---|---|---|---|---|
| | | | | Rolling Resist. | Fuel Cons. |
| Young (1988) | Coast down - artificial roughness | 1.3 to 4.0 | Truck | | 4.1 |
| | Direct fuel measurement - artificial roughness | 3.3 to 5.6 | Car | | 3.1 |
| | Direct fuel measurement - vehicles side by side | 2.3 to 4.4 | Car | | 3.6 |
| | Direct fuel measurement - range of surfaces | 1.7 to 5.4 | Car | | 0.8 |
| Ross (1982) | Direct fuel measurement - range of surfaces | 0.5 to 3.7 | Car | | 0.4 |
| Bester (1984) | Rolling resistance - range of surfaces | 1.4 to 5.5 | Car | 2.6 | 0.5 |
| Descornet (1990) | Rolling resistance - range of surfaces | 0.8 to 7.7 | Car | 4.0 | 0.8 |
| Laganier and Lucas (1990) | Rolling resistance - range of surfaces | 1 to 6** | Car | 6.0 | 1.2 |
| Sandberg (1990) | Direct fuel measurement - range of surfaces | 1 to 6* | Car | | 1.7 |
| du Plessis et al (1990) | Rolling resistance - range of surfaces | 1.2 to 15 | Car | 3.4 | 0.7 |
| | | | Truck | 4.4 | 1.1 |
| Watanatada et al (1987) | Rolling resistance - range of surfaces | 2 to 14 | Car | 2.5 | 0.5 |
| | | | Truck | 1.8 | 0.5 |

* 1 unit of IRI = 26 NRC
** Estimated range

One additional factor that must be noted when considering functional performance is the relative weight of the vehicle and tyre size (contact patch area). Many other vehicle characteristics are likely significant, however these are the two that are addressed within the literature. Firstly, Sandberg et al (2011) notes that IRI seems more significant for a truck and MPD more so for a passenger vehicle. To some extent this could be attributed to the relative tyre sizes employed; for example, a truck tyre may be influenced by short wavelength roughness in the same way a passenger car tyre is influenced by megatexture.

Furthermore, Lenngren (2010) states that rolling resistance appears more dependent on pavement hysteresis, which further confuses the relation between any single pavement parameter and rolling resistance. Although some conclusions can be drawn from the logic described in the literature the overall system of pavement, tyre and vehicle is immensely complex and relative vehicle size appears to cause differing vehicle response.

#### 2.2.5.1 Rolling Resistance Models

There exist many models relating pavement functional characteristics to the rolling resistance experienced by a passing vehicle. Those discussed below are considered the more comprehensive examples within the literature. It must be highlighted that many relationships have been developed utilising differing rolling resistance measuring methodologies due to the lack of a standardised test method. Some relations are derived via regression from coast-down rolling resistance tests and others from steady-state torque methods. It must be assumed each method produces results equivalent to the other, in order to make comparisons of the conclusions derived from each in the literature. Currently there has not been a study completed to comment on the equivalency of the two methods.

A general equation for rolling resistance with cognisance of functional pavement effects was developed by Hammarstrom et al (2008). It considers the separate effects of texture (MPD) and roughness (IRI), with both being influenced by vehicle mass. Interestingly, the resistance due to texture is influenced by velocity, an effect disputed in some literature as discussed above. The general equation can be used to develop specific functions for a given vehicle with regression from a matrix of testing. Such work was completed for a couple of vehicles, one for passenger vehicles and one for trucks (27 tonne truck utilised in the testing). Within these two

relationships velocity only influences the roughness component. With the constant applied for trucks being approximately 50% greater than that for a passenger vehicle. This type of relation is not well suited to extrapolation and ideally should be developed for discrete vehicles and pavement conditions.

Also worth consideration is the structure of the rolling resistance surface factor included within the HDM-4 rolling resistance model (Zaabar et al, 2010). The vehicle mass and velocity are considered independently meaning the pavement condition is considered in isolation. The other main factor included is tyre derived rolling resistance, which is directly affected by velocity and mass, which appears appropriate if one considers the discussion included in Section 2.2.2. The rolling resistance surface factor in HDM-4 considers texture, roughness and rebound deflection independently. However, it considers a larger vehicle to be influenced more by texture and an equivalent amount or less by roughness, this is of course at odds with the discussion contained within Sandberg et al (2011) and the discussion above. Considering pavement types separately makes the HDM-4 model more detailed than many other relations reported in the literature. However, it may also result in some effects not being fully captured for certain pavements, a prime example being the lack of influence of structural capacity for unsealed pavements. More general relations may capture such effects within the data used for derivation. Thus the approach employed within the HDM-4 model does appear more comprehensive than the other relations discussed. Conversely, it may produce erroneous results through assumptions of the relative influence of texture, roughness and deflection for a given pavement as there is some disagreement within the literature.

A model developed by Jamieson et al (2002) is similar, although it considers the static rolling resistance coefficient (Equation 2.6) to be influenced by varying texture categories and rebound deflection. Conversely the speed dependent coefficient (Equation 2.7) considers velocity in conjunction with tyre size and vehicle mass. This model appears to be the most complex general model available when considering functional pavement effects while also incorporating the structural capacity as part of the static coefficient. Thus it has additional modelling capacity compared to the HDM-4 model. Similar to the HDM-4 model it has been derived considering unsealed and highway pavements, however one shortcoming is that although it includes a term for pavement rigidity (Jamieson et al, 2002), it has not been developed with consideration of rigid concrete pavements.

**Equation 2.5: Rolling resistance force equation (Jamieson and Cenek, 2002).**

$$F_R = M.g(C_0 + C_v.V^2)$$

Where:

$F_R$ is the rolling resistance force (N)

M is the vehicle mass (kg)

$g$ is gravitational acceleration

V is vehicle speed (m/s)

$C_0$ is the static coefficient of rolling resistance

**Equation 2.6: Static coefficient of rolling resistance (Jamieson and Cenek, 2002).**

$$C_0 = 0.0131 * RD + 0.015 * SWR - 0.004 * MWR + 0.000075 * LWR - 0.003 * SR - 0.000042$$

Where:

$C_v$ is the speed dependant coefficient of rolling resistance

**Equation 2.7: Speed dependant coefficient of rolling resistance (Jamieson and Cenek, 2002).**

$$C_v = 0.00032 * Rad - 1.64 \times 10^{-9} TM + 2.73 \times 10^{-5} MR - 0.00012$$

Where:

$RD$ is Average Rebound Deflection (mm) from Benkelman Beam Tests

$SWR$ is Root Mean Square short wavelength roughness (microtexture - mm)

$MWR$ is Root Mean Square medium wavelength roughness (macrotexture - mm)

$LWR$ is Root Mean Square long wavelength roughness (megatexure - mm)

$SR$ is Site Roughness (NAASRA counts/km)

$MR$ is ratio of front to rear axle mass

$TM$ is total vehicle mass (kg)

$Rad$ is tyre radius (m)

### 2.2.6 Rolling Resistance of Haul Roads

Limited literature is available explaining the rolling resistance of haul roads due to pavement surface characteristics. One study has been completed by Thompson et al (2003) that not only considers roughness, modelled specifically by a 'Roughness Defect Score' to be a factor in rolling resistance, but considers it to be directly proportional. Coast-down testing was completed to define the rolling resistance and then compared with defect data, to show a progression in Defect Score (roughness) produces an increase in rolling resistance. Figure 2.14 details the data obtained from the testing and the values predicted by the model.

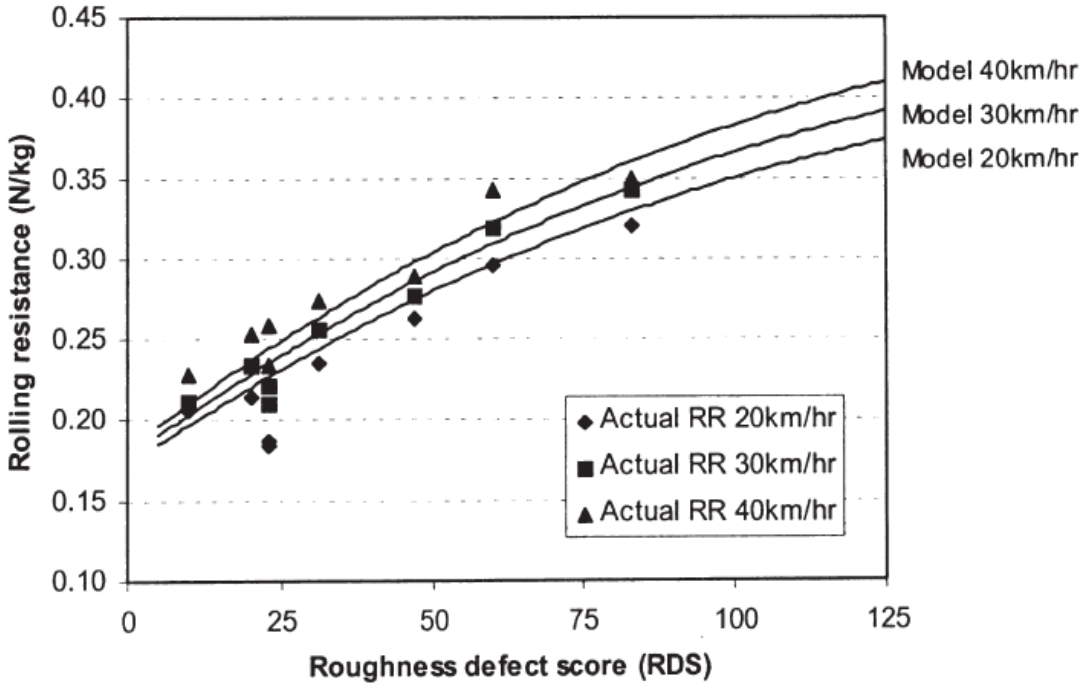


**Figure 2.14: Actual and predicted rolling resistance (Thompson et al, 2003).**

From this data Thompson et al (2003) were able to develop a model for rolling resistance with the roughness defect score being the dependent variable, which was expected to vary as described in Figure 2.15. For details on the Roughness Defect Score (RDS) utilised, the original paper by Thompson et al (2003) should be consulted. Equation 2.8 describes the method for calculating the rolling resistance from RDS. Essentially, rolling resistance is considered to increase exponentially as a function of maintenance interval. A minimum value of rolling resistance is applied and is calculated as a function of speed, as detailed in Equation 2.9.

**Equation 2.8: Rolling resistance function considering roughness defect score (Thompson et al, 2003).**

$$RR = RRMIN + RDS * e^{(RRI)}$$

Where:

$RR$ is the rolling resistance

$RRMIN$ is minimum rolling resistance at RDS=0

$RDS$ is the roughness defect score

$RRI$ is a regression function describing rate of change of RDS, defined by Equation 2.10.

**Equation 2.9: Minimum rolling resistance (Thompson et al, 2003).**

$$RRMIN = e^{(-1.8166+0.0028*V)}$$

Where:

$RRMIN$ is the minimum rolling resistance for a given road pavement

$V$ is the vehicle speed in km/h

**Equation 2.10: Rolling resistance regression function (Thompson, 2011).**

$$RRI = -6.068 - 0.00385RDS + 0.0061V$$

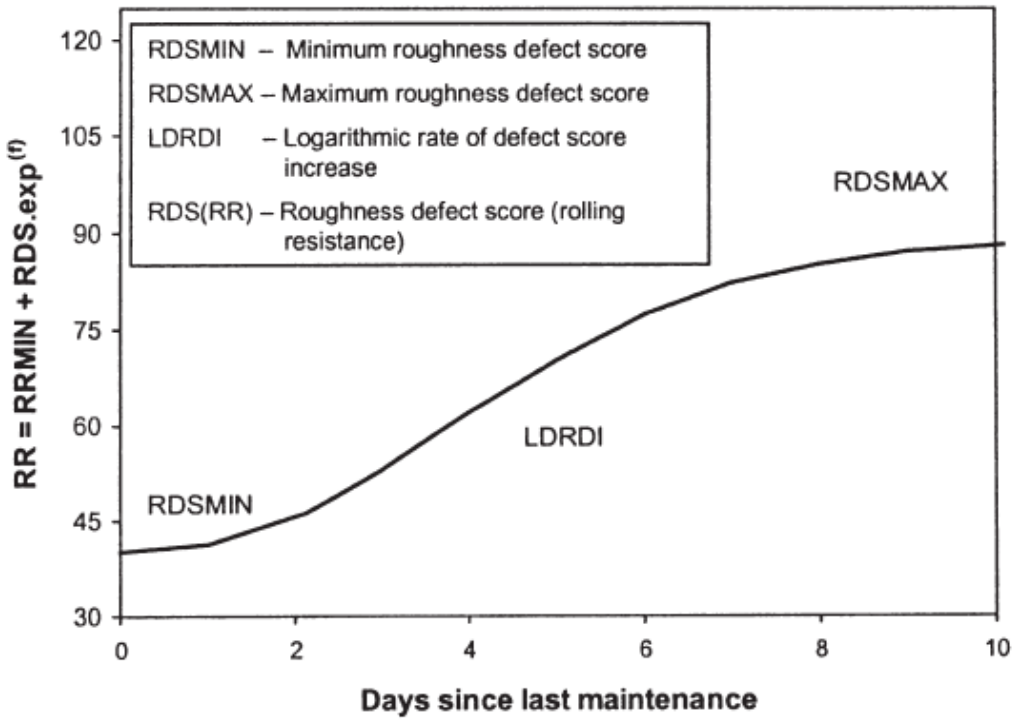


**Figure 2.15: Defect score (rolling resistance) progression against maintenance interval (Thompson and Visser, 2003).**

This model does not explain the pavement condition in great detail, nor does it allow for variation of vehicle parameters. However, it does relate the pavement condition and maintenance intervals, which was predicated toward providing a solution to industry without the requirement for a great deal of testing. From this point of view the model serves its purpose, but does not relate rolling resistance to common pavement condition measures as are utilised in elsewhere in the literature.

There have been several studies completed that consider off-road type tyre/soil interaction effects in considering the rolling resistance of haul roads. The earliest of which was completed in the 1970's when it was noted that haulage efficiency is largely dictated by rolling resistance of the road surface (Kaufman et al, 1977). This research compiled a study of the rolling resistance experienced by haul trucks encompassing gravel and stabilized earth materials as well as asphalt and concrete. The results of this can be seen in Table 2.5, which also includes the results of several other empirical studies. Equation 2.11 should also be considered, which allows for more general solutions to be obtained. Tannant et al (2001) state that for lightly loaded wheels, Equation 2.11 may produce underestimates of rolling

resistance. Although this data provides some general guidance, it should not be considered to be comprehensive. For example, it does not allow estimations of energy losses due to effects of pavement deformation, which are noted to affect the resistance encountered (Tannant et al, 2001).

**Equation 2.11: Rolling resistance function relating to weight and penetration depth (Caterpillar, 2006).**

$$RR = 2\%\ of\ GMW + 0.6\%\ of\ GMW\ per\ cm\ of\ tyre\ penetration$$

$RR$ is the rolling resistance coefficient

$GMW$ is the Gross Machine Weight

**Table 2.5: Rolling resistance factors for haul roads determined via various studies (Tannant et al, 2001).**

| Type of surface | Rolling resistance (%) | Reference |
|---|---|---|
| Cement, asphalt, soil cement | 2 | Kaufman & Ault (1977) |
| Hard-packed gravel, cinders, or crushed rock | 3 | Kaufman & Ault (1977) |
| Moderately packed gravel, cinders, or crushed rock | 5 | Kaufman & Ault (1977) |
| Unmaintained loose earth | 7.5 | Kaufman & Ault (1977) |
| Loose gravel and muddy rutted material | 10-20 | Kaufman & Ault (1977) |
| Asphalt | 0.8-1.5 | Johnson (1989) |
| Crushed limestone | 3.4-4.2 | Dionne (1987) |
| In-situ benonitic clay shale | 7-13 | Dionne (1987) |
| Loose snow | 4.5 | Caterpillar (1988) |
| Packed snow | 2.5 | Caterpillar (1988) |
| Concrete and asphalt | 1.5* | Euclid (undated) |
| Smooth, hard, dry dirt and gravel, well maintained | 2* | Euclid (undated) |
| Soft unplowed dirt, poorly maintained | 4* | Euclid (undated) |
| Wet, muddy surface on firm base | 4* | Euclid (undated) |
| Soft, plowed dirt or unpacked dirt fills | 8* | Euclid (undated) |
| Loose sand and gravel | 10* | Euclid (undated) |
| Deeply rutted or soft spongy base | 16* | Euclid (undated) |
| * add 1.5% for every inch of tire penetration | | |

Research completed in Indonesia in recent years has resulted in the derivation of Equation 2.12 and Equation 2.13 (Widodo et al, 2009). These are based on equations originally generated by Bernstein (1913) as have many of the relations discussed within Section 2.2.3. One significant advantage of these relations is the consideration of rolling resistance on a vertical grade, which is relevant for mining due to many haul roads being constructed on ramps providing egress from pits. Both equations have been derived through soil bin testing in which compacted gravelly sand and silt were used as the pavement material, to mirror what is experienced within local mines (Widodo, 2009A).

**Equation 2.12: Rolling resistance function of grades less than 8% (Widodo et al, 2009).**

$$RR = 0.115\left[\frac{W^{6.96}}{P.A}\right]^{0.17}$$

**Equation 2.13: Rolling resistance function of grades of 8% and greater (Widodo et al, 2009).**

$$RR = 0.116\left[\frac{W^{4.67}}{P^{0.5}.G}\right]^{0.24}$$

Where:

$RR$ is the rolling resistance force (N)

$W$ is the total load (N)

$P$ is the tyre inflation pressure (Pa)

$A$ is the soil/tyre contact area ($m^2$)

$G$ is the road alignment vertical grade (%)

There have been several studies completed quantifying the rolling resistance of haul road surfaces through empirical data. Table 2.6 details the experience at a Canadian mine, considering the variation of road surface and ambient conditions. The data within Table 2.5 explains rolling resistance due to material type and surface condition to some extent, although 'good', 'average' and 'poor' are not defined in detail.

**Table 2.6: Haul road rolling resistance values with seasonal variation (Tannant et al, 2001).**

| Location | Winter (Good) | Summer (Average) | Spring / Fall (Poor) |
|---|---|---|---|
| Sub-Grade – oilsand | 4 – 6% | 6 – 9% | 9 – 12% |
| Sub-Grade – Clearwater | 4 – 6% | 6 – 8% | 8 – 10% |
| Sub-Grade – dump material | 7 – 9% | 10 – 12% | 12 – 16% |
| Road Surface – temporary | 3 – 5% | 4 – 6% | 4 – 6% |
| Road Surface – permanent | 3 – 5% | 3 – 5% | 3 – 5% |

## 2.3 Vehicle Operating Costs

The following discussion with regards to Vehicle Operating Costs (VOC) relates only to fuel consumption. Several models exist for vehicle maintenance and tyre wear, however it is unclear how these relate to large rigid haul trucks.

### 2.3.1 Fuel Consumption Models

The study of rolling resistance in relation to pavement properties ultimately manifests itself most significantly within the impact it has on vehicle fuel consumption. Various Austroads Panels have recommended further research of the roughness/VOC relationship (Tan et al, 2011). Fuel consumption is a function of driving resistance and engine efficiency, whereby an increase in engine speed will reduce efficiency, while an increase in torque will increase engine efficiency (Hammarstrom et al, 2012). To expand upon this idea it is also important to note that driving resistance is a function of road conditions and driver behaviour, whilst engine

speed is a function of vehicle speed and gear position (Hammarstrom et al, 2012). Thus it is clear that the model for fuel consumption for any given vehicle is very complex, with interdependent variables and potential variances between seemingly similar vehicles. It is therefore difficult to estimate the isolated effect of pavement condition on the fuel economy of a vehicle, however there are some empirical study results available that provide a probable range.

Nielson et al (2010) note there have been several studies completed to empirically relate rolling resistance and VOC, and ultimately conservatively recommend use of a ratio of a 3% change in fuel consumption for a 10% change in rolling resistance. The Transport Research Board (2006) completed a similar literature review and estimated that a range of 1-2% change in fuel consumption results from a 10% change in rolling resistance, the higher values relating to highway driving and the lower values with urban environments. Interestingly the 'factor of four' ratio (1% change in fuel consumption per 4% change in rolling resistance) is often noted for trucks and used for estimation purposes (Tan et al, 2011).

It is often considered that rolling resistance due to pavement condition is derived most significantly from pavement surface properties to the extent that other influences are considered negligible. It is for this reason that many studies focus on the effect of roughness (IRI) and texture (MPD) in isolation. Unsealed pavements are not considered in many studies. Jamieson et al (2002) was one such study which did consider unsealed pavements and ultimately expressed support of a 4:1 ratio of change in rolling resistance to fuel consumption. Unfortunately this finding was not extensively detailed and further research is required.

There are some specific complications in relating rolling resistance and fuel economy worth noting. Firstly, the approach of relating percentage change in rolling resistance to fuel consumption can be problematic, as a given percentage change in fuel consumption is related to an absolute change in rolling resistance (Transport Research Board, 2006). Thus the effect is lesser at lower speeds. Secondly, recent Australian-based research has shown that the roughness/fuel consumption relationship is indeterminate under variable speed conditions (Tan et al, 2011). Therefore the data and models presented in this Section can only serve as an estimate of fuel consumption in steady-state operating conditions or perhaps at the network level considering average values.

Also available for estimation are mechanistic approaches, which are vastly superior to empirical methods, as they consider fuel consumption as a function of individual

vehicle characteristics and factors influencing the resistance to motion (Greenwood et al, 2003). Mechanistic model development employs the principals of physics and in many cases the inefficiencies of the mechanical operation (derived empirically) of an internal combustion engine to describe the amount of energy required to move a given load.

The most common of the fuel consumption models derived from direct fuel measurement in Australia is the NIMPAC (NAASRA Improved Model for Project Assessment and Costing) model, originally developed by NAASRA (The National Association of Australian State Road Authorities) in the 1970's (Lloyd, 2003). The basic fuel speed relationship predicts average fuel consumption for a section of road (combining sections of positive and negative total grade) at approximate steady speeds between 8 and 104 km/h (Thoresen et al, 1996). Direct fuel measurement models (such as NIMPAC) provide a quantification of variables through measurement in full-scale tests, rather than measuring rolling resistance and then relating this to fuel consumption (Tan et al, 2011). Furthermore, NIMPAC does not allow for variations in the vehicles specifications (Thoresen et al, 1996), certainly a shortcoming when considering very large vehicles. This can be described by the lack of any vehicle-specific terms included in the general fuel consumption function within the model. The model does not isolate rolling resistance to a degree where its influence can be examined explicitly (Tan et al, 2011). Therefore it does not provide instantaneous fuel consumption values as are present within other mechanistic fuel consumption models below.

One mechanistic model has been developed by VTI (National Road and Transport Research Institute, Sweden). It has been adopted by the MIRIAM project (Models for Rolling Resistance in Road Infrastructure Asset Management Systems), a collaboration between 12 partners from Europe and the USA. The VETO model (note that VETO is not an acronym) is used to define fuel consumption for a range of vehicles for pavement surfaces of varying MPD and IRI. It is a mechanistic model based on physical relationships and is able to estimate fuel consumption for specific road segments with high precision, involving a great deal of variables that define the road and vehicle of interest (Karlsson et al, 2012). The model includes dependence between pavement roughness and vehicle speed, whereas texture is considered to have an influence independent of speed.

The Australian Roads Research Board (ARRB) Road Fuel Consumption Model (ARFCOM) was developed following the completion of a number of studies on fuel

consumption being completed in Australia in the early 1980's (Greenwood et al, 2003). It was developed to predict fuel consumption as a function of engine input and output power, where engine accessory power is considered as a function of engine speed (Zaabar, 2010), shown in Figure 2.16. Engine maps were utilised in the models development to quantify the fuel consumption required for a given power demand. The final form of the model requires a significant amount of simplified input data but was judged suitable for application to all vehicle classes (Greenwood et al, 2003).

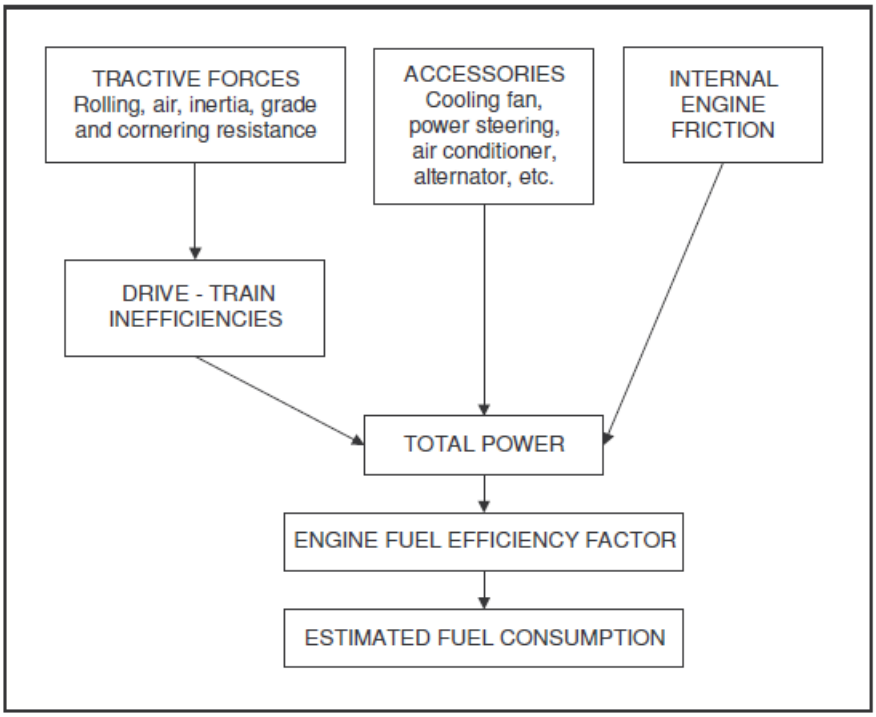


**Figure 2.16: ARFCOM approach for fuel consumption modelling (Greenwood et al, 2003).**

The instantaneous fuel consumption is the steady state product of engine efficiency factor and net power required. The ARFCOM model was adapted for use in HDM-4, with changes to the prediction of engine speed, accessories power and engine drag (Zaabar, 2010). However, rolling resistance is treated the same in both models. The total power is the sum of requirements for the generation of tractive force, the running of vehicle accessories and the power to run the engine. Note that drivetrain inefficiencies can serve to both increase power requirement even on a pavement

with a negative gradient (Zaabar, 2010). The traction function includes a term for the rolling resistance, which has a significant weighting that considers the Benkelman beam deflection and pavement surface condition, with the relative influence of each varying with pavement type.

Chatti et al (2012) includes an analysis of fuel consumption variation with changes in roughness (IRI) and texture (MPD). Roughness has a greater effect on smaller vehicles and texture has a greater effect on heavier vehicles. Texture is also shown to have a lesser effect at higher speeds (Chatti et al, 2012). However note that analysis also showed the HDM-4 model to overestimate fuel consumption from roughness.

A fuel consumption model for haul trucks was developed by Thompson et al (2003) in line with models utilised in the public domain through vehicle simulations and observation of torque/speed maps. For validation this model was then tested against results from fleet fuel consumption and journey data. The results were found to largely mirror that of heavy commercial vehicles with a slight increase in fuel consumption with vehicle speed due to dynamic rolling resistance effects (Thompson et al, 2003). The model is broken down to consider sections of unfavourable (positive) total grade and favourable (negative) total grade, as is done in the HDM-4 model. Difficulty in validation is reported due to the lack of an inclusion for queuing times (truck stationary while waiting to be loaded or dump) and other time losses, however the model was found to be in-line with the original simulation that was completed for the mine circuit (Thompson et al, 2003).

## 2.4 Haul Roads

Structural design of haul road pavements involves a significantly more uncertainty than that of highway pavement design. This is due to the lack of significant full-scale tests to derive sub-grade failure theories and complexity surrounding the use of non-standard road building materials. The following discussion provides a background to the available design methodologies.

### 2.4.1 Empirical Pavement Design

Empirical pavement design is recommended for use in the absence of more rigorous material testing, analysis and design methodologies within the structural pavement design section of Austroads Guide to Pavement Technology (Jameson, 2008). The recommended process utilises the same inputs for design as with mechanistic methods, with regards to traffic data, pavement cross-section geometry and material stability parameters. Within the methodology recommended by Austroads, an assumption is made that regardless of material stiffness a finite cover is able to be defined that affords suitable sub-grade protection. Subsequent to this a definition of required base thickness is made to explain the composition of pavement layers. In addition, Main Roads Western Australia (MRWA) currently specify that the minimum thickness to be adopted shall be defined by the empirical design procedure, which has been optimised for Western Australian conditions through many years of anecdotal evidence (MRWA, 2012).

Austroads current CBR cover curves for sub-grade materials is noted to yield similar results to the mechanistic-empirical method, with a maximum granular vertical moduli of 350MPa and an SAR7/ESA (Standard Axle Repetitions with number 7 relating to rutting and shape loss/Equivalent Standard Axles) ratio of 1.2 (Jameson, 2008). Thus the empirical design is slightly more conservative when assuming the use of sound gravel for the base-course layer of the pavement. Therefore, for general highway pavements, specifically those ‘capped’ with either sprayed bituminous or asphaltic layers, modern empirical design methodologies have been aligned with more involved analysis and design techniques.

Empirical design for haul roads can be traced back to the manual derived by Kaufman and Ault (1978). Since publishing, this text has been utilised and referenced throughout the global mining industry and is still relevant in today’s environment of advanced computerised engineering design tools.

Figure 2.17 presents the CBR cover curves included in the guidelines produced by Kaufman et al (1977). Some critical points to note for use of the cover curves (Figure 2.17) for the purposes of haul road pavement design are listed below (Kaufman et al, 1978):

1. The highest wheel loading present should always be used for design and increase by 20% if tandem axle.

2. When the recommended thickness to the pavement surface fail to consume the open dimension (Figure 2.17), the residual space must be filled with a sub-base of at least CBR 80%.
3. Proper compaction equipment should be used, usually heavy rollers, however few surface mine operators have access to such equipment.
4. If proper sub-base and base are established prior to placing wearing course, it need not exceed 6 inches.

Additionally, note that the indicative material properties and associated CBR values presented in Figure 2.17 should be employed as an initial guide only. Ideally subsequent testing should be completed for detailed design with due consideration of soaked or unsoaked CBR testing (Atkinson, 1992).

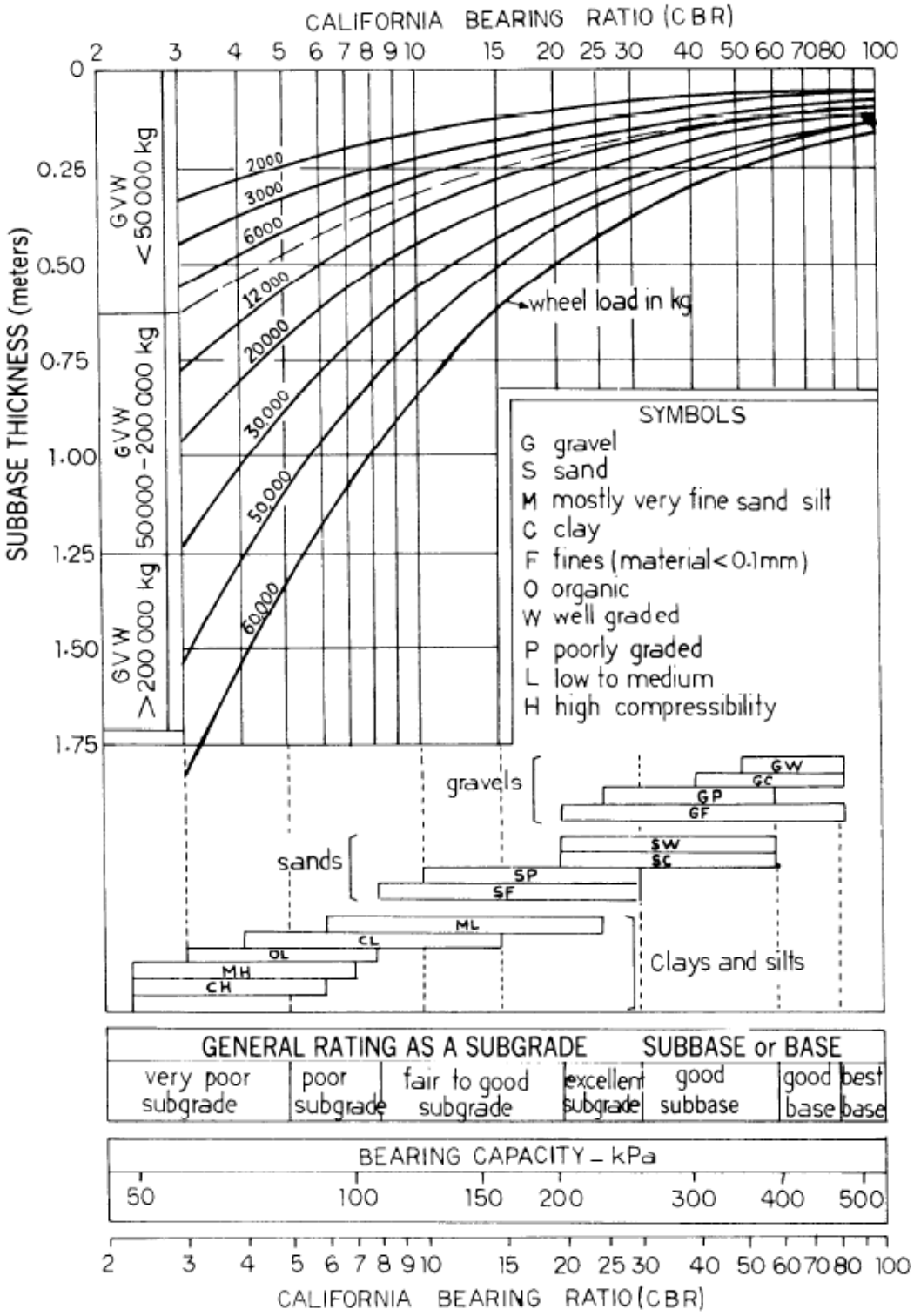


**Figure 2.17: Material classification and CBR cover curves (Kaufman et al, 1977).**

The first note above is concerned with the treatment of multiple wheels adjacent to one another in the design vehicle's wheel-base assembly. The recommendation made in Kaufman et al (1978) is simplified compared to more detailed methodologies developed around the same time period for heavy wheel loading observed in airfield pavements. Pereira (1977) suggests the use of the Equivalent Standard Wheel Load (ESWL), which originated in the 1950's as proposed by Foster and Ahlvin (1954). An ESWL is a fictitious wheel load, which produces the same deflection as all wheels present in a wheel-gear at a given point on a pavement. In applying the ESWL, pavement deflection is calculated with consideration of a semi-infinite, homogenous, isotropic and elastic medium through Boussinesq's theorem (Pereira, 1977) for a combination of wheel loads. This approach may lead to increased stress levels in certain layers of the pavement (Tannant et al, 2001). Design is complicated by the fact that ESWL varies with depth and is effectively a function of the maximum deflection factor arising from consideration of multiple wheels to the maximum deflection factor for a single wheel (Pereira, 1977).

Use of the ESWL was adopted for development of CBR design curves in conjunction with full-scale tests to define the cover requirements for a given sub-grade CBR and design traffic volume. These tests considered single and multiple wheel gears that were present on a range of aircraft used at the time (Pereira, 1977). Observation of the results lead to derivation of a pavement thickness/CBR equation that can then be used to plot cover requirement curves, commonly referred to as the S77-1 method. Alternatively the S77-1 curve can be utilised to avoid iterative design. Figure 2.18 presents the S77-1 curve, which is an update of the S77-1 with inclusion of additional scale test data. Note that this method utilises sub-grade deflection instead of strain, which results in greater wheel load divergence as deflections attenuate much more slowly than strains (Wardle et al, 2010). This leads to difficulty associated with selection of which wheels to include in determination of ESWL and the subsequent derivation of a design thickness. Another limitation of the method is the limited range of CBR to wheel load ratios for which it can be applied (White, 2007). This is due to the limited range of sub-grades present within the full-scale testing from which the method was derived. In an effort to increase practical application, subsequent multiple-wheel heavy gear trafficking tests were completed to derive a more general equation, however the results applicability are not readily discussed in the literature.

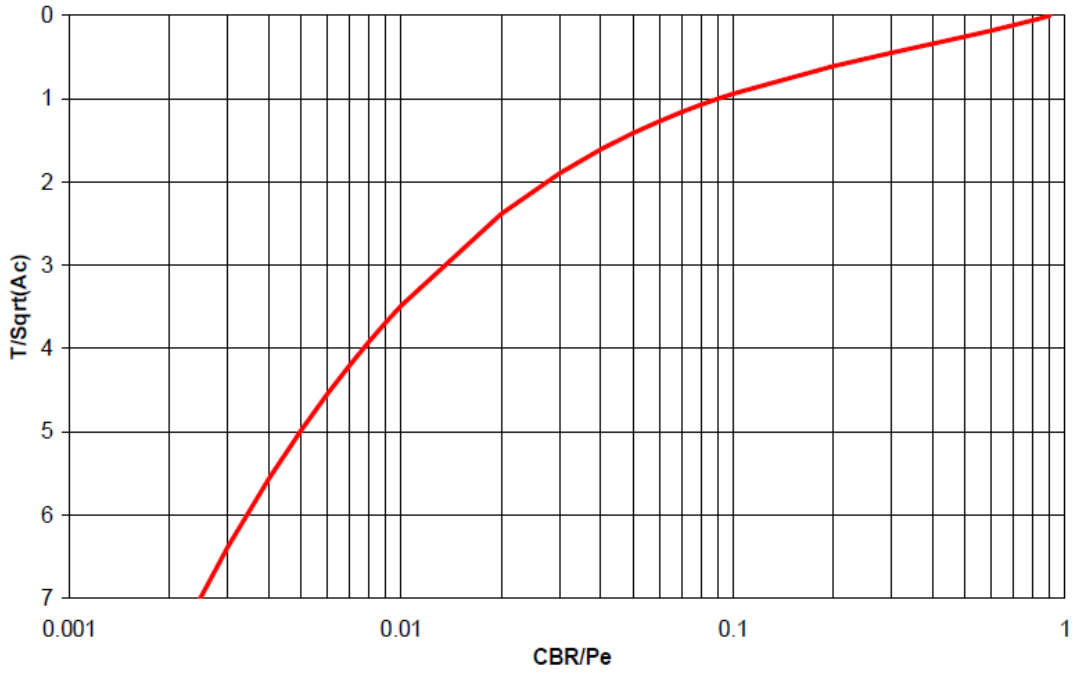


**Figure 2.18: US Corps of Engineers CBR curve (Pereira, 1977).**

It is worth noting that the pavements included in the full-scale tests associated with development of the S77-1 method had a fixed structure of asphalt, fine crushed rock, underlain by varying thicknesses of natural uncrushed gravel on the sub-grade (White, 2007). To transform a 'non-standard' pavement structure such as that of a mine haul road, material equivalences must be utilised to account for the absence of asphalt and crushed rock layers, this poses perhaps the greatest source of error in extrapolating from the original model (White, 2007). Although this may be the case, the method remains the only basis for development of design theories/methods for the heavy wheel loading experienced on haul roads.

### 2.4.2 Mechanistic Pavement Design

Mechanistic/empirical design refers to methods where pavement stress/strain response is defined through appropriate structural analysis, with failure then being defined by an adopted 'failure criterion' or 'transfer function' (Jameson, 2008a), see Section 2.5. The most common failure mode considered is an accumulation of permanent vertical strains at the top of the sub-grade (considered to be the locality of the majority of rut depth generation). The proceeding section discusses available

theories for design via mechanistic means. Note that the failure theories discussed below are more simplistic than that described in Section 2.6.5.2, as yet these are not available for design purposes in any commercial software.

Mechanistic design techniques utilise elastic moduli values instead of CBR percentages to describe the stiffness of each layer within a pavement. As with determination of CBR values for empirical design; such estimates should only be used in preliminary designs prior to an appropriate regime of testing or in the absence of access to such testing (Jamieson, 2008). Tannant et al (2001) note use of the American Association of State Highway and Transportation Officials (AASHTO) Falling Weight Deflectometer (FWD) testing methodology to determine layer moduli, although this can only be completed post-construction. Some literature, such as Thompson (2009), recommend estimation of resilient modulus from CBR or as suggested by Thompson et al (1997), through comparison with Dynamic Cone Penetration (DCP) tests results. Such an approach is not supported by several studies, as outlined by de Carteret et al (2009), which conclude there is no physical relation between CBR and resilient modulus results. Austroads recommend that a range of values (150-400 MPa) be applied for sub-base quality gravels placed in a layer underlying a thin surfacing (Jamieson, 2008). Materials used in mine haul road construction likely differ from a typical 'sub-base gravel', however it should be noted that it is recommended that the maximum value in the range above are not exceeded design models for UGM layers (MRWA, 2013). A more detailed discussion of unbound granular material response to cyclic loading can be found in Section 2.6.5.1.

Thompson (2009) suggests inclusion of a crushed rock layer for the attenuation of induced stresses. A resilient modulus of 3000 MPa is adopted for this 'Run of Mine' material as it is described as being considered analogous to a pre-cracked cement stabilized layer. This figure is the lower bound of the range noted by Austroads for pre-cracked cemented base-course materials, however note that a value of only 500 MPa is recommended for the post-fatigue cracking phase (Jamieson, 2008). This estimate is utilised due to the relative difficulty in measuring the resilient modulus of such coarse materials, however it is not clear if large coarse rock layers exhibit resilient properties similar to that of a cemented layer. This note has been included to provide some guidance on the inclusion of large coarse rock fills within haul road pavements, as the practice is common within the mining industry.

There exists many transfer functions that describe pavement sub-grade failure and therefore define pavement lifetime. Figure 2.19 describes the variation in various failure theories that are available. Note that the two bottom rows represent design methodologies for heavier than standard highway traffic and therefore should be expected to present some differences. However it is undoubtedly significant that such marked disparity should exist between various methodologies used in practice (Wardle et al, 2003).

| | | Subgrade Strain ($*10^{-6}$) | | | | |
|---|---|---|---|---|---|---|
| | | 500 | 800 | 1000 | 1500 | 2000 |
| Design Method | Austroads (1992) | $616*10^6$ | $22*10^6$ | $4.4*10^6$ | $240*10^3$ | 30,000 |
| | Shell (1985), 50% reliability | $9.8*10^6$ | $1.5*10^6$ | $620*10^3$ | $120*10^3$ | 38,000 |
| | Shell (1985), 95% reliability | $1.7*10^6$ | $260*10^3$ | $105*10^3$ | 21,000 | 6,500 |
| | Brown and Brunton (1984) | $620*10^3$ | $130*10^3$ | 58,000 | 14,000 | 5,000 |
| | British Airports Authority (Woodman, 1992) | $1.3*10^6$ | 90,000 | 25,000 | 2,400 | 460 |
| | Wardle and Rodway (1998) | $1.5*10^6$ | 68,000 | 15,000 | 1,000 | 160 |

**Figure 2.19: Comparison pavement lifetime for given strain level from common transfer functions (Wardle et al, 2003).**

Through observation of common pavement failure theories and measurement of pavement deflections, Thompson et al (1997) asserted that restricting vertical strain at any level in the pavement to a maximum of 2000 microstrain resulted in pavements exhibiting ‘good’ performance. This was achieved through comparison of condition monitoring of pavements with deflection data obtained from multi-depth deflectometer stacks placed within the pavements. Although simple to use and related specifically to empirical data from operating haul roads it is difficult to make comparisons with other methods. As a result of the fixed ‘critical’ strain it is likely most other common sub-grade failure theories will provide both thicker and thinner pavement designs, as they provide variation in the critical strain value with changes in sub-grade resilient modulus. Thompson et al (1997) include only one case study which includes a waste rock layer with an assumed elastic modulus of 3000 MPa (as discussed above), making comparisons with empirical methods difficult.

Thompson (2009) further developed a more detailed pavement strain criterion relating pavement performance directly to operating intensity and maintenance

requirements. Figure 2.20 details the method, whereby each category of haul road has been defined as (Thompson, 2009):

1. Adequate but fairly maintenance intensive.
2. Good with normal maintenance interventions.
3. Outstanding with low maintenance requirements.

This methodology is logical in scope, as the method has been developed specifically for haul roads through observation of operating pavements. Describing maintenance requirements from definition of traffic and the desired level of performance also presents an opportunity for some understanding of potential maintenance costs during the pavement design. Such a definition would allow comparison of the capital and maintenance costs for different options. The range of sub-grade/pavement material strength/stiffness parameters for which the model is applicable is not clear, as testing outside of the bounds of its development has not been reported.

| Haul Road Category | Typical Description | Range of maximum permissible vertical elastic strains (μstrains) | |
|---|---|---|---|
| | | Traffic volumes ^ 100kt/day | Traffic volumes v 100kt/day |
| CATEGORY I | Permanent life-of-mine high traffic volume main hauling roads and ramps in- and ex-pit. Operating life >20 years | 900 | 1500 |
| CATEGORY II | Semi-permanent medium- to high traffic volume ramp roads in- and ex-pit. Operating life >10 years | 1500 | 2000 |
| CATEGORY III | Shorter-term medium- to low-volume in-pit bench access, ex-pit dump, or ramp roads. Operating life <5 years (@ > 50kt/day) or <10 years (@ <50kt/day) | 2000 | 2500 |

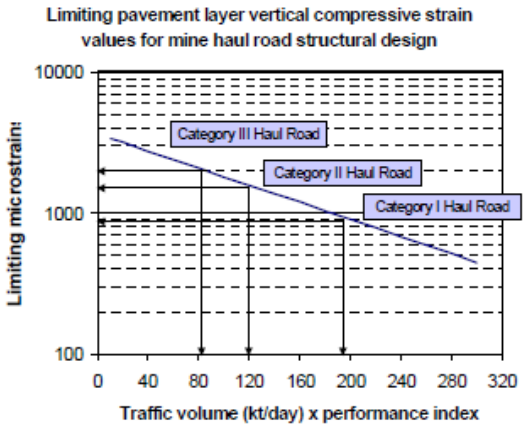


Maximum permissible vertical strains can also be determined from (*kt/day x performance index*) where performance index is defined as;

1 Adequate but fairly maintenance intensive
2 Good with normal maintenance interventions
3 Outstanding with low maintenance requirements

**Figure 2.20: Pavement strain theory relating operational intensity and maintenance requirements (Thompson, 2009).**

An alternate method of defining critical strain is a modification of the Austroads adopted method, derived by Wardle et al (2005). This theory considers strain induced, stress repetitions (vehicle passes) and sub-grade modulus as variables, with the latter being an addition to the method adopted by Austroads for design of flexible pavements. Development was completed through regression of results generated through Airport Pavement Structural Design System (APSDS) software (Mincad Systems) and validation with the empirical method described by Pereira (1977) in Section 2.4.1. The empirical method was developed by the US Army Corps of Engineers through observation of pavements being trafficked by aircraft ranging in mass from 40 to 397 tonnes. The most notable advantage over the empirical method is the flexibility afforded the designer through inclusion of layer moduli instead of the use of empirical material equivalency factors (Wardle et al, 2010). Ultimately, the functions governing sub-grade failure were developed for

variables dependent on sub-grade resilient modulus, applicable to pavements with sub-grade CBR values ranging from 3% to 15% (Wardle et al, 2010).

This methodology has been applied within the layered elastic pavement design software HIPAVE (Wardle et al, 2005). Wardle et al (2010) have also developed a general set of equations that are applicable to all sub-grade CBR values, landing gears with up to six wheels and aircraft weights up to 560 tonnes. The applicability of the set of design equations derived through use of these functions for haul road pavement design has not been commented upon in the literature, aside from descriptions of the HIPAVE software's development by its authors (Mincad Systems). It is the only method relating sub-grade strains whilst taking account of varying sub-grade properties and a large range of wheel loads representing the largest commercial planes in operation. Shortcomings of the method relate to the fact the sub-grade strains were not measured in a physical test, but were predicted by a numerical model in validation of estimated pavement lifetimes. Thus it must be assumed the material equivalencies employed in the model were correct and are applicable to materials employed for pavements subsequently designed by the method. However, it does offer the pavement designer a higher level of understanding and flexibility than alternative methods. The reader is referred to Section 2.5.3 for additional discussion of this sub-grade failure theory.

#### 2.4.2.1 Interaction between Adjacent Wheels

At current, there are short-comings in the knowledge pertaining to interaction of closely spaced axle groups (Wardle et al, 1999). Since this conclusion was drawn 15 years ago, little knowledge has been gained in this area which has resulted in some confusion and debate regarding the modelling of heavy-industry pavements. Note that the following discussion relates to airfield pavements that are commonly constructed of select materials and surfaced in asphalt. How this discussion relates to haul roads constituted of mine waste materials is not clear.

The original design method (sub-grade failure theory) for heavy wheel loading was developed by the US Army Corps at the Waterways Experiment Station, where single wheel gears were used to complete full-scale pavement tests (Pereira, 1977). No tests were carried out to investigate the increased damage due to wheel interaction (White, 2007). The derived method includes the use of Equivalent Single-Wheel Load (ESWL), a fictitious load that takes into account the interaction between the wheels present within a gear (Pereira, 1977). To calculate the ESWL, the theory

of superposition and deflection factors that have been calculated for the depth and radial distance from load centre are used. The resulting ESWL, which is variable with depth, was then used to calculate the required thickness of the pavement using the S77-1 equation (see Section 2.4.1). The use of ESWL suggests that there was an allowance for interaction between wheel loads (White, 2007). However as strain attenuates much more rapidly with radial distance than deflection (see Figure 2.21) it was considered that the method over estimated pavement thickness; which resulted in alpha factors being introduced to take account of the number of wheels in a landing gear (White, 2007). Note that Figure 2.21 presents results from a linear-elastic modelling of deflection and vertical strain resulting from a tyre load at the top of the pavement sub-grade.

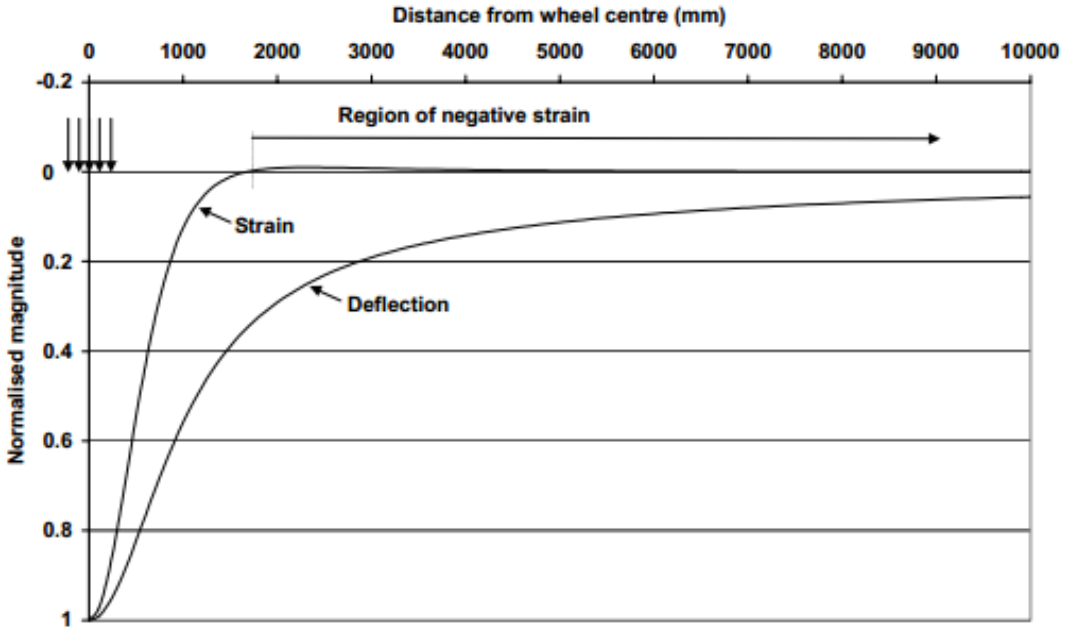


**Figure 2.21: Attenuation of sub-grade strain and deflection with distance from load centre (Rodway et al, 1999).**

There have been many views expressed about how to best allow for wheel interaction, due to the realisation that currently it is not able to be properly included. Wardle et al (2007) state that it is generally necessary to model only one half of the axle, after modelling the whole axle and checking for interaction of the strain induced by adjacent wheel loads (and presence of negative strains, as discussed

later). The introduction of large aircraft, such as the Boeing 777 and Airbus A380 have caused a rethink within recent design software packages considering entire wheel gears instead of isolated tyres, however there is currently no justification for this (White, 2007). Rodway et al (1999) note that common software (APSDS, Mincad Systems and Layered Elastic Design Federal Aviation Administration, United States Federal Aviation Administration) used for the design of airfield pavements utilise single gear loadings and so critical strains should occur in the region beneath the gear. The accuracy of these calculated strains removed radially from the load centre are described as being suspect. Yet it is often these doubtful values that are used to predict gear interactions.

In some cases, the configuration of wheel gears or relative proximity to other gears is such that anomalous negative strains are calculated under adjacent load centres (Wardle et al, 2003). As noted previously strains attenuate slower than deflections and thus negative strains can be calculated at radial distances where other wheels are placed. This can result in improved predicted life due to inclusion of adjacent wheels or gears in the model (Wardle et al, 1999). It is most certainly counter-intuitive that an increase in wheel loads should increase predicted pavement life. Another significant issue which is discussed at length within Section 2.5 and Section 2.6 is the lack of an ability to properly model the elasto-plastic and stress dependent nature of unbound materials (Wardle et al, 1999). This further compounds the issue of adequately accounting for wheel load interactions, resulting in greater uncertainty with regards to current design methods.

## 2.5 Pavement Modelling

Pavement design has evolved significantly over the past century. Initial designs were based on past experience and available resources (Hamory, 2015) and were therefore largely analytical. In 1885, Boussinesq provided an elastic solution for a half-space (Kim, 2007), allowing structural analysis of geotechnical structures including pavements. This method has been extended and the modelling of pavements for structural design is becoming increasingly complex. In recent decades, FEA has been researched with a view to incorporating complex material constitutive relations, such as those discussed in Section 2.5. Well accepted linear-elastic methods and Finite Element Methods, which are the subject of increasing research effort, are outlined in the following.

Some inherent differences between modelling of pavements with each approach are noted below:

- linear-elastic models consider the stress state for nominal pavement layers (or sub-layers in some cases) and radius from load centre, where FEA considers the stress state for discrete elements due to external loading
- linear-elastic models are axisymmetric, FEA models can be plane-strain, axisymmetric or three-dimensional
- linear-elastic solutions use the theory of superposition to model load interaction, FEA considers all specified external loads in the generation of each element's stress state within each iteration of load application
- loads are most commonly circular in linear-elastic models, whereas load geometry can generally be applied via any shape chosen by the designer in FEA
- sub-layered linear-elastic models assign moduli values based on some external input (for example moduli of supporting layer in HIPAVE). FEA models with nonlinear material subroutines consider convergence of stress state and the defined constitutive material model, within a specified tolerance.

These differences are discussed in greater detail in the following sections.

### 2.5.1 Linear-Elastic

Linear-elastic analysis has been prevalent in pavement design for many years. Following Boussinesq's theorem, Burmister considered the problem of an elastic layered medium as a half-space and subsequently applied this theory to the design and construction of airfield pavements in the mid twentieth century (Chen, 1971). Further work, to introduce a second layer to the pavement system was completed by Burmister, who eventually generated three layer solution tables (Kim, 2007). This work was extended by many authors but often considering a Poisson's ratio of 0.5. Pereira (1977) also describes the use of Boussinesq's one-layer theory for the calculation of deflections to define the Equivalent Standard Wheel Load at varying depths in the US Army Corps procedure for development of CBR design curves for airfields. Within this method, the pavement and sub-grade are considered together as a semi-infinite, homogenous, isotropic and elastic medium (Pereira, 1977). The Burmister solution is considered an improvement due to the ability to model multiple layers, however the interface between the layers is still treated as continuous (Kim et al, 2007A). Note that as a legacy of these early developments, the majority of

linear-elastic solutions continue to be axisymmetric. Further, this means that loads can only be imposed on a circular area (Gonzalez et al, 2012).

A scheme of axisymmetric loading is presented in Figure 2.22. Note that only two directional components are required. As symmetry is assumed, any lateral position with equal radius and depth will have the same induced stress. It is also important to note that in this configuration the line load represents a circular loaded area with radius ‘a’.

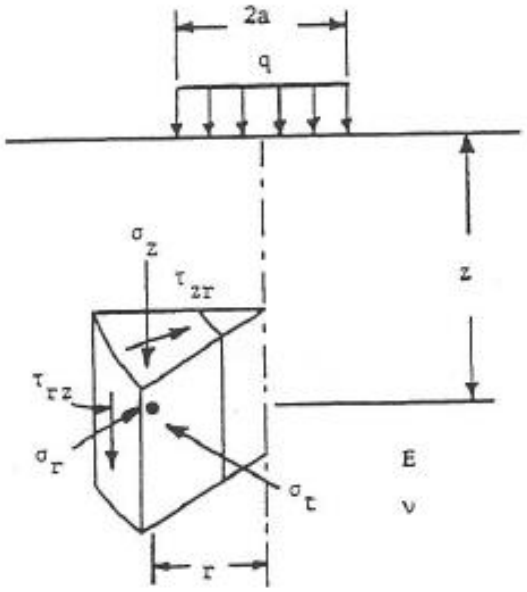


**Figure 2.22: Component of tresses under axisymmetric loading (Nikraz, 1998).**

With observation of Figure 2.22, the vertical and radial stress and strain may be calculated via Equation 2.14 through Equation 2.18. Note that these equations can be extended to calculate deflections throughout the system. Functions for shear stress are not included here as they are not typically used for pavement analysis and design.

**Equation 2.14: Vertical stress in an axisymmetric loaded pavement (Nikraz, 1998).**

$$\sigma_Z = q\left[1 - \frac{z^3}{(a^2 + z^2)^{1.5}}\right]$$

**Equation 2.15: Radial stress in an axisymmetric loaded pavement (Nikraz, 1998).**

$$\sigma_r = \frac{q}{2}\left[1 + 2v - \frac{2z(1+v)}{(a^2 + z^2)^{0.5}} + \frac{z^3}{(a^2 + z^2)^{1.5}}\right]$$

**Equation 2.16: Vertical strain in an axisymmetric loaded pavement (Nikraz, 1998).**

$$\varepsilon_z = \frac{q(1+z)}{E}\left[1 - 2v + \frac{2vz}{(a^2 + z^2)^{0.5}} - \frac{z^3}{(a^2 + z^2)^{1.5}}\right]$$

**Equation 2.17: Radial strain in an axisymmetric loaded pavement (Nikraz, 1998).**

$$\varepsilon_r = \frac{q(1+z)}{E}\left[1 - 2v - \frac{2z(1-v)}{(a^2 + z^2)^{0.5}} + \frac{z^3}{(a^2 + z^2)^{1.5}}\right]$$

Where (shown in Figure 2.22):

$\sigma_Z$ is vertical stress

$\sigma_r$ is radial stress

$\varepsilon_z$ is vertical strain.

$\varepsilon_r$ is radial strain

$q$ is the pressure intensity

$z$ is the depth from pavement surface

$a$ is the radius of the circular loaded area

$v$ is Poisson's ratio.

Foster and Ahlvin (1954) derived charts to simplify the analysis presented above, which have been widely applied since. More recently a considerable number of linear-elastic solution based software have been developed to perform the repetitive and complex computations required by classical multi-layer theory and in the pursuit of mechanistic design solutions (Kim, 2007). In Austroad's technical basis for their structural design procedure, it is noted that the pavement is assumed infinite in all directions and the moduli independent of stress (Jameson, 2008b). This approach is commonly adopted in design, which is in direct contrast to authors such as Kim et al (2007A) that note Boussinesq's equations to be inappropriate for calculating pavement response due to variation in layer elastic moduli and Poisson's ratio. Despite these complications, the relatively short computational time and in some cases inclusion of specific models to mimic stress dependency, means that linear-elastic analysis is still widely used today. To further this statement, linear-elastic analysis is used in several studies (for example Gonzalez et al, 2012; Kim, 2007; Sahoo et al 1997; Ghadimi, 2015) as a means of validating the numerical solving capabilities of newly developed FEA software. Due to the linear-elastic method employing a closed-form solution, it provides confidence in the accuracy achieved with an FEA method, which only approximates the exact solution. Following validation, the researcher's focus often turns to increasing complexity in the FEA model. Indirectly there is still a reliance on linear-elastic solutions due to the lack of physical testing being completed for validation of FEA models.

It is important to note that all elastic layered programs consider each individual layer as a plate in bending (Dawson et al, 2008). This results in negative strains being calculated at a radial distance from the load. When multiple wheel gears are considered this can lead to less damage being predicted under adjacent wheels and thus longer pavement lifetimes being erroneously predicted (Wardle et al, 2003). Ultimately, to avoid this issue it is recommended that only single wheel gear loads are applied for the purpose of design (Wardle et al, 2003).

Axisymmetric models cannot consider multiple wheel loads without use of the theory of superposition of strains (Gonzalez et al, 2012). Kim (2007) states that this approach is valid for linear-elastic models as the alteration in stress state due to multiple loads does not influence the predicted response. Further consideration of the modelling of wheel load interaction is discussed in Section 2.4.2.1.

An important consideration with regard to linear-elastic modelling, is the assignment of the elastic modulus of granular pavement layers independent of stress state. Essentially, all pavement layers are modelled as homogenous, and linear in response, after Burmister's development of a two-layer analysis. Realistically, this approach is invalid as pavement layers exhibit elastic deformation in combination with other responses (Hadi et al, 2003). CIRCLY (Mincad Systems 2012) adopts the Austroads sub-layering method to mimic a nonlinear response which is based upon the selection of the resilient modulus of the top sublayer. HIPAVE (Mincad Systems, 2012B) and APSDS (Mincad Systems, 2009) apply the Barker-Brabston method of sub-layering (Barker et al, 1975) developed by the US Army Corps of Engineers for design of airfield pavements. This method considers larger wheel loads than the Austroads method, and is therefore considered more appropriate for design of heavy-industry flexible pavements. Sahoo et al (2010) conclude that, from a study of the effect of nonlinear modelling of granular layers, linear-elastic analysis may result in under-design for roads where granular material forms the only structural layer. Further discussion of the treatment of nonlinearity within unbound granular pavement layers is contained within Section 2.6.1.

Linear-elastic models also typically suffer from characterisation of unbound granular pavement layers as being isotropic. Tutumluer et al (1997) note that such a characterisation is unrealistic for most geomaterials. Austroads advise that the horizontal component of stress dependency cannot be directly modelled via a linear-elastic model (Jameson, 2012). CIRCLY addresses this issue by including an option to complete modelling of UGM layers with an anisotropic ratio of two (vertical to horizontal modulus) (Mincad Systems 2012A). A detailed discussion of anisotropy of pavement materials is provided in Section 2.6.3.

From the above discussion it is clear that there are many issues with the use of linear-elastic analyses for flexible pavements, mainly associated with characterisation of materials as isotropic, stress independent (which is unrealistic for most geomaterials) and subject to axisymmetric loads (Kim et al, 2007A). Such shortcomings can largely be overcome by more detailed techniques, such as the

Finite Element Method discussed in Section 2.5.2. Alternatively, to retain favourable calculation times whilst attempting to address the above issues, the following modifications could be made:

- adoption of the sub-layering method to take account of the stress-dependency of granular materials (see Section 2.6.1), such as applied in KENLAYER, CICRLY and associated software
- approximation of anisotropy for granular materials, as applied in CIRCLY via an assumption of vertical to horizontal modulus ratio of two. Shear moduli being calculated from the vertical moduli and Poisson's ratio using elastic theory (Mincad Systems, 2012)
- in-built non-linear material models, such as that adopted in KENLAYER (Dawson et al, 2008)
- inclusion of boundary frictional characteristics, to allow consideration of layer interaction, such as combinations of smooth and rough (continuous) boundaries included as a design input in CIRCLY (Mincad Systems, 2012).

Finally, linear-elastic design software such as CIRCLY (Mincad Systems) and HIPAVE (Mincad Systems, 2012B) consider pavement failure mechanisms associated with vertical strain repetitions at the top of the sub-grade layer. In reality, there is no physical link between resilient and plastic strains, especially considering that rutting is often a function of shear failure. The damage models employed by CIRCLY and HIPAVE is discussed further in Section 2.5.3.

### 2.5.2 Finite Element Analysis

Computations with FEA are much more complex than those completed with the linear-elastic approach. A closed form solution may no longer be possible once it becomes evident that the assumptions of homogenous, linear-elastic pavement materials have become invalid within the modelling of real situations (Hadi et al, 2003). One major advantage is that FEA can incorporate stress-dependency, allowing the models discussed in Section 2.6.5.1 to be applied. A specific benefit of this approach is that the modulus can vary radially from the load (which may be critical for modelling of wheel interaction). Other advancements are possible, such as the inclusion of the constitutive models that apply the failure envelopes discussed in Section 2.6.4. This allows permanent deformation analyses to be addressed,

possibly with the application of the theories presented in Section 2.6.5.2. Ultimately, truly mechanistic design may be possible. Although the calculations are complex in FEA, it must be remembered that a pre-requisite to any analysis, is a model that can effectively describe the material's behaviour due to induced stresses (Siripun et al, 2011).

The fundamental workings of FEA are explained in the following. This is a general description of pavement numerical analysis and is not intended as an exhaustive description of the method's derivation. It is important to keep in mind that FEA is simply a mathematical method for solving a differential equation (through partial differentiation without a closed form solution) under specific boundary conditions (Ghadimi, 2015). Therefore, FEA provides only approximate solutions.

Firstly, the body being analysed is discretised into a user-defined number of elements. The geometry and orientation of elements in analysis completed by general solution software, such as ABAQUS, is reliant on the meshing strategy selected. Figure 2.23 presents triangular elements during the discretisation of the body, this was not the element type used throughout the pavement analysis for this project but is included here for descriptive purposes. This procedure results in meshing of the body, an example of which is presented in Figure 2.23. Where each element intersects with another element or the boundary of the body is referred to as a node.

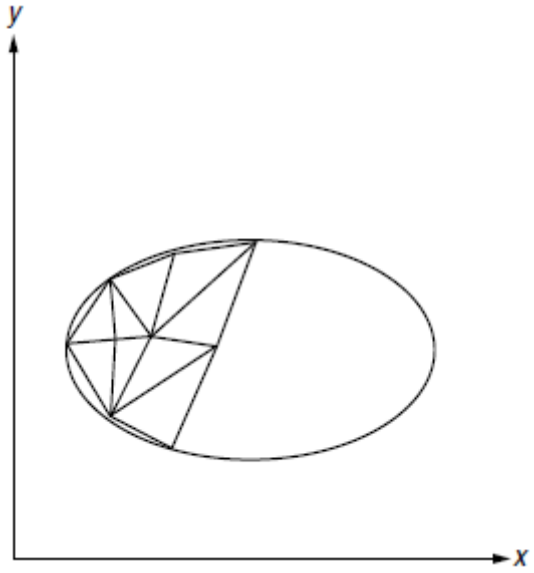


**Figure 2.23: Meshing of a membrane model (Komzsik, 2009).**

Internal displacements within an element may be related to nodal displacements (strains within the body) through the application of an assumed shape function through Equation 2.18.

**Equation 2.18: Nodal displacements from strain and shape functions (Chen et al, 2011).**

$$\{u\} = [N].\{q\}$$

Where:

$\{u\}$ is the elemental displacement matrix

$[N]$ is the assumed shape function matrix

$\{q\}$ is the nodal displacement matrix.

Development of the shape function matrix is dependent on the type of elements chosen. Generally, assembly utilises local element displacements ($u$ and $v$) in the form of polynomials of local (element) coordinate variables ($s$, $r$ and $t$ within Figure 2.24) (Chen et al, 2011). The derivation of the shape function matrix then varies due

to local geometry and nodes per element, however note that the terms within the B matrix are constants, which implies that the strain is constant throughout an element (Chen et al, 2011). Examples of element types with nodes and local coordinate systems, are presented in Figure 2.24. Note the additional complexity and computational effort required when introducing three-dimensional modelling.

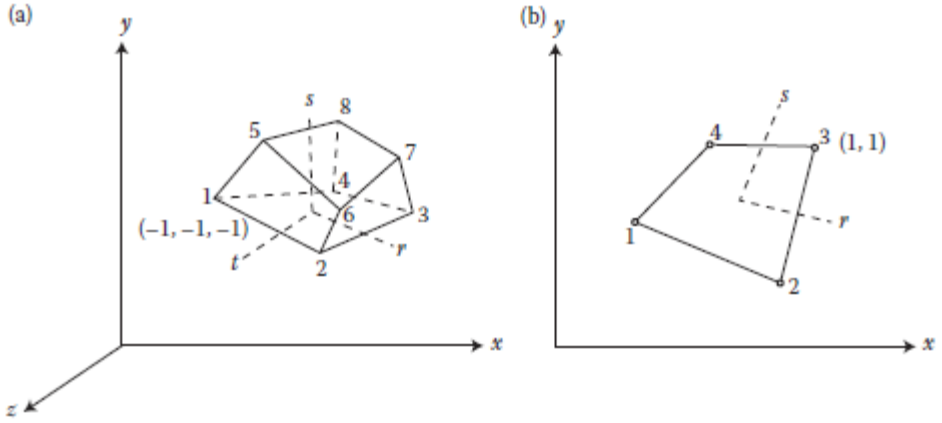


**Figure 2.24: Examples of isoparametric elements. (a) three-dimensional brick element and (b) two-dimensional quadrilateral element (Desai et al, 2014).**

There is full derivation and details of different shape functions for different element types within the literature. None have been included here as the focus is on presenting the general framework of the FEA method only.

From the description above, the strain vector can be determined through differentiation of elemental displacements, via Equation 2.19.

**Equation 2.19: Calculation of strain vector (Chen et al, 2011).**

$$\{\varepsilon\} = [B].\{q\}$$

Where:

$\{\varepsilon\}$ is the strain vector matrix

$[B]$ is a matrix derived from a derivative of $[N]$.

In order to calculate the stress field within the body from the calculated strains, a function is required to describe the material elastic properties. Equation 2.20 details a general form for orthotropic materials.

**Equation 2.20: General elasticity matrix for determination of elemental stresses in a two-dimensional, orthotropic material (Cheung et al, 2002).**

$$[C] = \frac{1}{1 - \upsilon_x \upsilon_y} \begin{bmatrix} E_x & \upsilon_y E_x & 0 \\ \upsilon_x E_y & E_y & 0 \\ 0 & 0 & (1 - \upsilon_x \upsilon_y) G \end{bmatrix}$$

Where:

$[C]$ is the elastic moduli matrix

$\upsilon_x$ is Poisson's ratio in the x-direction

$\upsilon_y$ is Poisson's ratio in the y-direction

$E_x$ is the elastic modulus in the x-direction

$E_y$ is the elastic modulus in the y-direction

$G$ is the shear modulus.

Once the material elastic properties are defined, stresses may be calculated via Equation 2.21.

**Equation 2.21: Calculation of elemental stresses (Cheung et al, 2002).**

$$\{\sigma\} = [C].\{\varepsilon\}$$

Where:

$\{\sigma\}$ is the stress vector.

Where an orthotropic material is not being considered it is necessary to utilise a more complex constitutive model than depicted in Equation 2.20 to describe the relation between stress and strain tensors (Ghadimi, 2015). Inclusion of such models requires an incremental solution technique, which is discussed in more detail later.

Now that the response of each element can be calculated through application of equilibrium, the principle of virtual work is utilised to relate the node displacements to the system of external loads (Equation 2.22).

**Equation 2.22: External work done (Chen et al, 2011).**

$$dW^* = \{dq\}^T\{P\}$$

Where:

$dW^*$ is the matrix of external work done

$\{dq\}^T$ is the virtual node displacements

$\{P\}$ is the system of loads to which the body is subjected.

Logically, the virtual strain may be expressed as a function of elemental displacement and some description of element geometry, which is achieved with Equation 2.23 and is termed the virtual strain.

**Equation 2.23: Virtual strain (Chen et al, 2011).**

$$\{d\varepsilon\} = [B]\{dq\}$$

Where:

$\{d\varepsilon\}$ is the virtual strain

$\{dq\}$ is the virtual displacements.

If the virtual strain energy density is $\{d\varepsilon\}^T\{\sigma\}$ (where $T$ denotes the transpose of a matrix) and external work done is assumed equal to virtual strain energy, then after reduction the virtual strain energy may be expressed by Equation 2.24.

**Equation 2.24:Virtual strain energy (Chen et al, 2011).**

$$dU^* = \int_v \{a\varepsilon\}^T\{\sigma\}dV = \int_v \{aq\}^T[B]^T\{\sigma\}dV = \{aq\}^T \int_v [B]^T\{\sigma\}dV$$

Where:

$dU^*$ is the virtual strain energy.

According to the principle of virtual work, external work done is equal to virtual strain energy. Application of this principle results in the derivation of Equation 2.25, which describes the relation between element stress and nodal loads (Chen et al, 2011).

**Equation 2.25: System of loads from the principle of virtual work (Chen et al, 2011).**

$$\{P\} = \int_v [B]^T\{\sigma\}dV$$

Where:

$\{P\}$ is the system of loads.

The final step to achieve equilibrium is to apply the constitutive relations. This process results in the derivation of the stiffness matrix (which relates external loads to displacements) through the approach described below. External loads are often applied incrementally within FEA, such that an approximation of material behaviour can be included (Cheung et al, 2002). Such an approach is required when a nonlinear constitutive material model is adopted, as depicted in Figure 2.25 and noted in Figure 2.26 for integration of each element. Alternatively, all of the external loads may be applied and an iterative procedure repeated in accordance with the constitutive law until equilibrium is attained (Cheung et al, 2002). In reality a mix of the two approaches is generally utilised, whereby the external load is applied incrementally with the iterations continued until convergence is reached for each increment. Convergence can be considered to have occurred when the unbalanced element forces are negligible (Ghadimi, 2015). This approach is represented within Figure 2.25. In the case of ABAQUS, the Newton-Raphson approach is often utilised (NCHRP, 2004). A single iteration is suitable for the linear-elastic case, which is applicable to the current study. Since only a linear-elastic solution is required, the following details this simplified analysis.

Constitutive relations for a two-dimensional linear-elastic system can be expressed by Equation 2.25.

Substituting Equation 2.19 and Equation 2.25 into Equation 2.26 results in an expression for the external loads, Equation 2.26.

**Equation 2.26: External loads (Chen et al, 2011).**

$$\{P\} = [k]\{q\}$$

Where:

$\{k\}$ is the stiffness matrix.

The stiffness matrix can be determined from Equation 2.27. As seen above, three factors are addressed in determining the stiffness matrix; geometry of elements, degrees of freedom for nodal displacement and material properties (Hadi et al, 2003).

**Equation 2.27: Stiffness matrix (Chen et al, 2011).**

$$[k] = \int [B]^T [C][B] dV$$

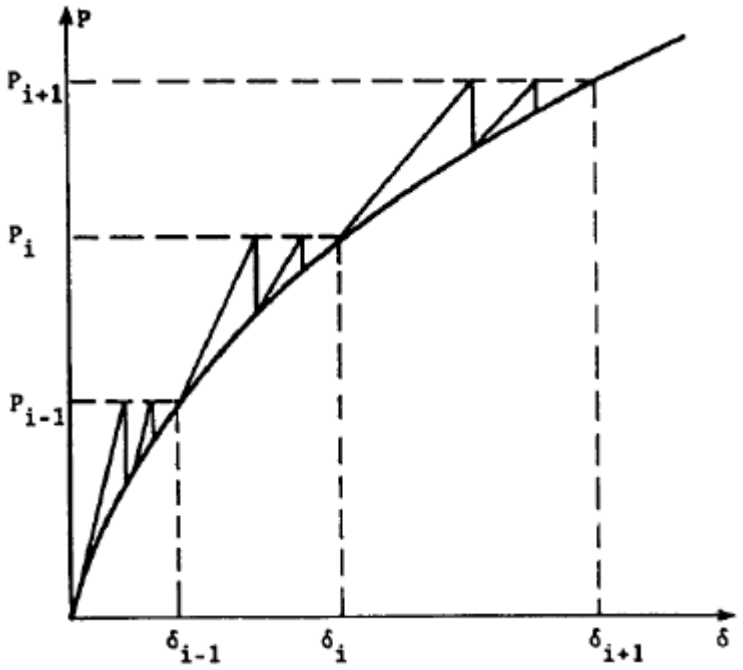


**Figure 2.25: Representation of incremental and iterative procedure of analysis being applied together (Cheung et al, 2002).**

From the above formulation, the internal response to external loads on a body may be determined. This represents a basic explanation of the FEA method. Far greater complexity can be applied to the derivation of the shape function matrix for different element types and the constitutive model, linking stress and strain response. The reader is referred to the literature for a more detailed explanation of these components of FEA. Some constitutive models for unbound granular materials are described within Section 2.6.4.

The application of the above FEA formulation can then applied as per Figure 2.26.

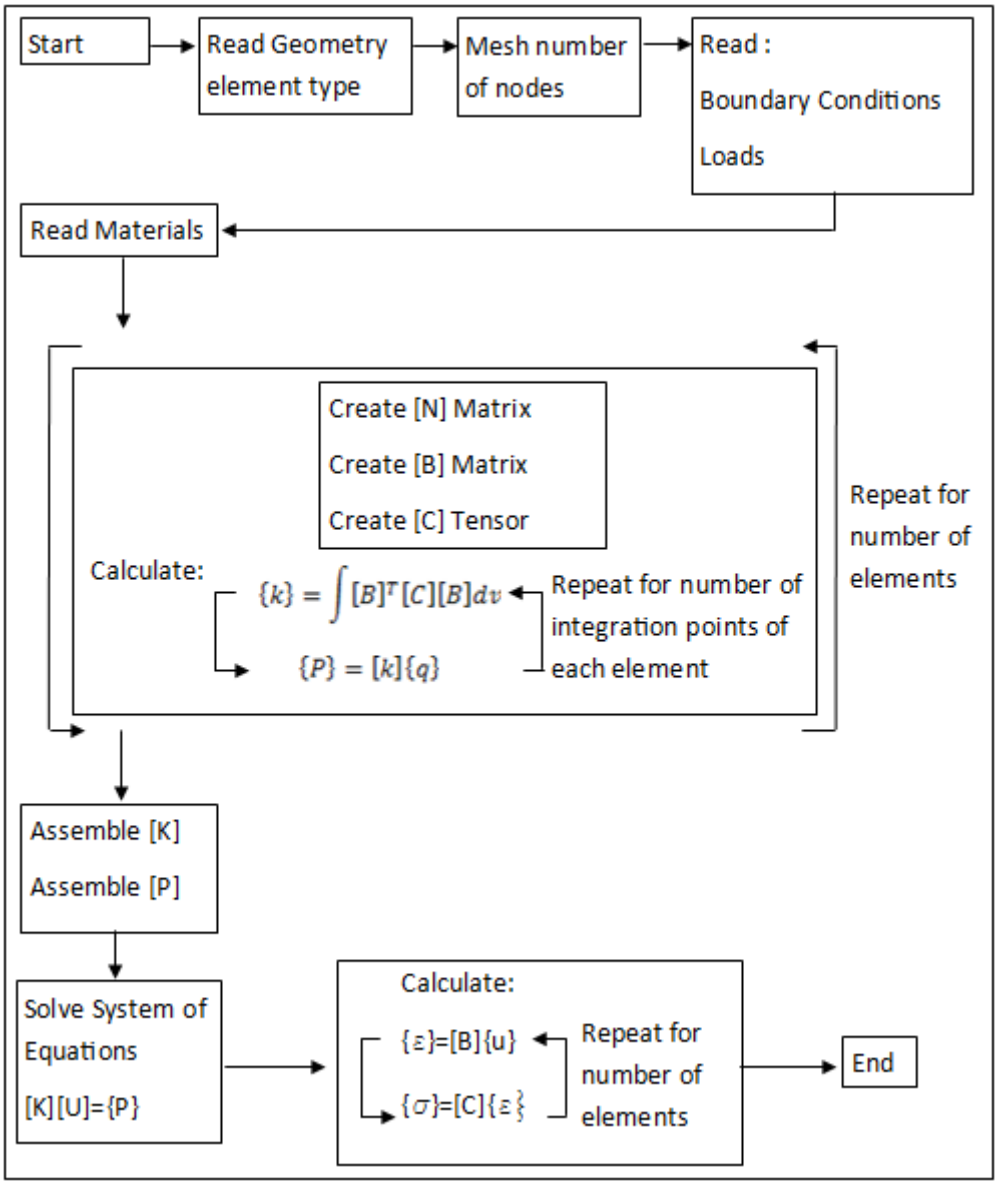


**Figure 2.26: FEA calculation procedure (adapted from Ghadimi, 2015).**

There are a number of FEA coded software available commercially, some with features such as tensile strain cut-offs (Dawson et al, 2008), one such code utilised in many fields is ABAQUS (Dassault Systemes). With reference to a broader context than pavement analysis, some benefits of FEA include (Sukumaran, 2004):

- linear and non-linear-elastic, viscoelastic and elastoplastic material modelling
- two and three-dimensional calculation
- static, harmonic and transient dynamic simulated loading
- interface modelling with friction
- thermal gradient analysis.

Incorporation of such advanced features has been found to provide benefit to pavement design. Based on a preliminary study, Hadi et al (2003) conclude that a moving load and nonlinear material characterisation will result in higher than expected deflection values at the top of the sub-grade when compared to static loading and linear materials. However, these estimated deflections matched closest with the field measured values. Sahoo et al (2010) found that nonlinear characterisation of pavement materials resulted in increases in vertical strain and surface deflection with a maximum difference of 35% and 44%, respectively. Note however that a linear-elastic sub-grade was adopted in the study.

Finite element analysis is now often carried out three-dimensionally, with most researchers preferring this approach, due to the consideration of the complex behaviour of composite pavement materials and the effect of differing traffic loads (Sahoo et al, 2010). As alluded to in Section 2.5.1, FEA is often validated against axisymmetric linear-elastic solutions. In the case of three-dimensional FEA being applied, it is common that the model is segmented to include only a quarter of the wheel load and pavement. Where multiple wheel loads and nonlinear material models are incorporated (as discussed below), the theory of superposition is no longer valid when applied to axisymmetric modelling. The response of a nonlinear system is dependent on the response of the incremental loading scheme (Kim, 2007). Alternate geometries, such as plane-strain models have been tested by Ghadimi et al (2013) and found to produce significantly higher pavement deflection estimates than axisymmetric or three-dimensional models. Consequently, it was

recommended that the simplification of the pavement response to the plane-strain condition be completed with extreme caution.

It is worth noting that the issue of fictitious tensile strains calculated by most linear-elastic methods is not automatically overcome through the use of FEA, with some programs applying tension cut-off functions, as alluded to above (Dawson et al, 2008). Application of a tension cut-off is generally quite simple, where the strength of any element found to exceed a tensile limit (typically zero) is set as having no strength in subsequent load increments or iterations. This approach is common within recent research and development of FEA software published by Austroads (Gonzalez et al, 2012). The idea is also extended to shear failure, where any point with a shear stress calculated in excess of the chosen shear strength envelope, is corrected through redistribution to adjacent elements in the mesh. Any point that has been found to exceed the shear envelope has its modulus reduced to zero in subsequent load increment calculations (Gonzalez et al, 2012). In the same discussion, it is explained that the Drucker-Prager model is preferred to the Mohr-Coulomb model for definition of shear failure, due to the former projecting on principal stress space as a circle, as opposed to a hexagon for the latter, which presents computational benefits (Jameson, 2012). This is just one approach taken, however a comprehensive literature review was completed for the Austroads project in question and the reader is referred to the report.

The issue of plasticity within pavement modelling is introduced with the inclusion of plastic models, such as the Mohr-Coloumb and Drucker-Prager. Although this may serve to increase the accuracy of modelling, it is not applied to determine the pavement service life at this time. Sub-grade failure theories currently utilised are reliant on the magnitude of vertical sub-grade compressive strain. Further discussion of such models is contained in Section 2.5.3. In recent years a significant amount of research has focussed on more realistic representation of unbound granular material deformation behaviour under repeated load applications. Such theories have applied the shakedown theory and are discussed further in Section 2.6.5.2.

The selection of mesh type has a significant effect on the results generated by FEA. Sukumaran (2004) states that the same mesh used to complete drastically different tasks can lead to a highly impractical model. Essentially, each element represents a discrete portion of the physical structure, with accuracy dependent on mesh refinement and construction (Kim et al, 2007A). As mentioned above, many different

mesh options exist, with geometry affecting the element stiffness matrix generated, along with the degrees of freedom allowed for the nodes and material properties assigned (Hadi et al, 2003). Generally, a fine mesh is applied nearer to the wheel load to take account of steeper stress and strain gradients, with size increasing as vertical and radial distance increases. There is a significant body of literature available on the development and impact of various meshing strategies and required geometry/aspect ratios for FEA, which is beyond the scope of this study. Ghadimi et al (2013) have investigated the effect of mesh element type by comparing the deflection and strain outputs of an FEA model completed in ABAQUS (Dessault Systemes, 2011) to that of a linear-elastic model. It is noted that a four-node brick element is inappropriate for estimating pavement deflection and the use of eight-node axisymmetric elements is recommended.

Model geometry has also been noted to have a significant effect on the calculated pavement response in FEA. Kim (2007) compared axisymmetric and three-dimensional model outputs with linear-elastic model outputs and reported that it was advantageous to reduce the number of nodes in both cases. Furthermore, the three-dimensional model was able to produce accurate results with a smaller horizontal and vertical extent being included. Ultimately, Kim (2007) adopted a three-dimensional model extending 10 times the load radius horizontally and 60 times the load radius vertically, on the basis that it produced pavement response similar to the axisymmetric model in a reduced computational time.

For the case of flexible pavements with little or no bituminous surfacing, there is not a great deal of specific literature available. Certainly, it is suggested that stress dependency of granular materials and strain based subgrade soil models is considered essential for accurate pavement analyses (Sukumaran, 2004). Such inclusions (and those discussed above) allow for the avoidance of calculating non-existent tensile stresses (Gonzalez et al, 2007; Sahoo et al, 2010), thus providing a better understanding of the pavement. Dawson et al (2008) recommend that analysis of flexible pavements largely composed of UGMs would be optimised through consideration of non-linear plastic analysis with an appropriate FEA platform. Studies such as Hadi et al (2003) have shown calculated deflections in granular layers to be comparable to those found in similar situations in accelerated loading facilities. In the same study the use of FEA was further supported, where it was found the accuracy of calculated deflections were increased when considering non-linear granular materials and cyclic loading.

When considering material models for analysis, it is worth noting that deviations from the common idealisation of isotropic elasticity may be appropriate due to the soil being either inelastic or anisotropic (Muir Wood, 1991). Further to this, in an anisotropic material a change in mean normal stress affects a change in shear strain, as well as volumetric strain (Arnold et al, 2004). Thus modelling is made considerably more complex than when linear-elastic theory is applied. Austroads state that the use of finite element models allow for stress dependency and anisotropy in both directions, facilitating analysis that cannot be directly modelled using linear-elastic theory (Jameson, 2008a). One anomaly of linear-elastic analysis is that significant horizontal stresses are calculated in unbound layers, which Tutumluer (1995) noted decreased by 75% when considering materials as cross-anisotropic compared to isotropic. The inclusion of cross-anisotropy appears to have a significant impact in the stress distribution of FEA analyses. This is significant to note for flexible pavements with a thin (non-structural) surfacing. Youdale (1984) noted increased sub-grade vertical strain as a result of modelling pavement materials as anisotropic-elastic when compared to isotropic elastic characterisation.

A further application of FEA common in the literature, are detailed studies of tyre/pavement and soil interaction. Dual tyre assemblies with lower tyre inflation pressures are particularly effective in reducing the stresses imposed on unbound layers. The effect is most notable when in combination with low stiffness unbound granular material (Dawson et al, 2008). One such study relevant to the current research is that completed by Fervers (2004). A tyre modelled with a representative structural stiffness and loaded to 30kN was modelled over two soils as described, with consideration of variable tyre pressure. Lower inflation pressure (750 kPa to 150 kPa) resulted in a decrease in rolling resistance from 8.2kN to 3.9kN on a cohesive material with low internal angle of friction and compaction resistance. The result was different on a dry sand material (low cohesion, high angle of internal friction and high compaction resistance), where the rolling resistance was decreased from 8kN (7.5 bar) to 2.9kN (1.5 bar). Despite the fact the sinkage values were similar, the higher inflation pressure tyre accumulated a ‘bulldozing’ wave in front, leading to higher resistance to forward motion. The potential benefits of studying tyre inflation pressure through FEA analysis are further explained by Douglas (1997). It was found through an empirical study considering a 44kN wheel load with an 800mm diameter truck tyre on an unsealed granular pavement over a clay sub-grade, a decrease in rut depth of 44% was noted after 10,000 passes when tyre pressure was halved. These results, when combined with those relating to tyre

inflation pressure in Section 2.2.3, provide an example (although not validated) of the potential practical benefits arising from the computational power of FEA.

### 2.5.3 Damage Models

Damage models describe the number of pavement strain repetitions prior to the accumulation of an unacceptable level of permanent deformation (plastic strains). Figure 2.17 is one example where the curves have been derived from the theory most commonly used for large wheel loads. The field testing was carried out by the United States Army Corps of Engineers and is reported, along with the procedure for derivation of the curves, in Pereira (1977). Failure of the pavement was considered to have occurred once unacceptable rutting was observed. This failure theory is commonly referred to as the S77-1. It was adapted to computerised linear-elastic analysis (mechanistic-empirical pavement design) in the development of APSDS (Wardle et al, 2001). Equation 3.34 through Equation 3.36 detail this failure theory. Figure 2.27 provides a comparison of the failure theory and that adopted by Austroads for design of highway pavements (Jameson, 2012). Note that the number of allowable repetitions of a large wheel load are less than that of a commercial vehicle for a given sub-grade strain. The theory also benefits from consideration of sub-grade elastic modulus (‘Esg’, in unit of MPa, within Figure 2.27). Intuitively, it can be seen that a ‘softer’ sub-grade is considered to deform quicker for a set sub-grade strain value. Modelling similar to that described in Section 2.5.1 is used by APSDS and HIPAVE software programs in order to calculate the maximum sub-grade strain, which is then used to estimate the pavement life of the given pavement configuration. Note that it is within this calculation step that the interaction of wheel loads must be considered (see Section 2.4.2.1). Therefore, it is critical to accurately model the pavement response, which may be assisted by the adoption of FEA, as discussed in Section 2.5.2.

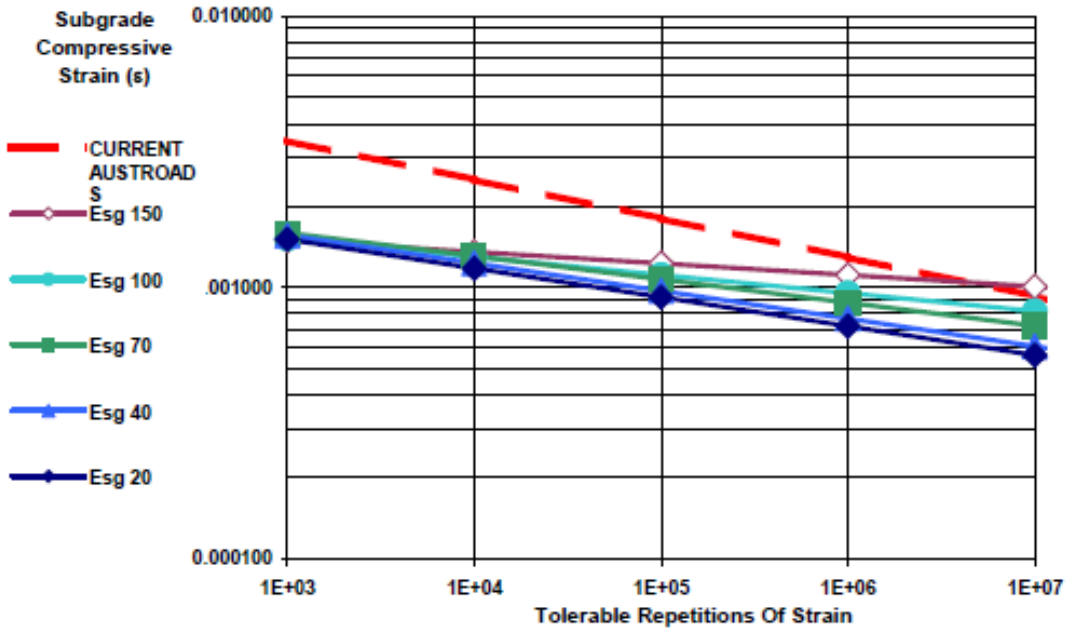


**Figure 2.27: Comparison of Austroads and HIPAVE damage models (Wardle et al, 2005).**

There are some limitations inherent in the design method discussed above that must currently be accepted for pavement design. Firstly, modelling via specialist pavement software packages employing a linear-elastic closed-form solution effectively consider the soil making up the pavement to have infinite strength. Subsequently, the use of sub-grade resilient strain to predict the accumulation of plastic shear and volumetric strain is surely questionable. With regards to rutting, this approach actually constitutes an analytical method of design (Dawson et al, 2008). Further, the consideration of sub-grade strain only ignores the damage that may accumulate within unbound pavement layers. This is despite the large body of research (discussed in Section 2.6.5.2) supporting the validity of this mode of failure. This issue is yet to be addressed in commercial software, likely due to the complexities of modelling permanent deformation of UGMs explained in Section 2.6.5.2. Presently, true mechanistic solutions are being sought by researchers through application of FEA (Section 2.5.2) with the incorporation of advanced material constitutive and failure models (Section 2.6).

For the discussion of the more advanced permanent deformation theories, the reader is referred to Section 2.6.5.2.

## 2.6 Unbound Granular Materials

Unbound granular materials are just as the name suggests, granular in composition and not subjected to any internal binding action. Austroads (Vuong et al, 2008) describe three generic materials that fit into this classification; naturally occurring granular materials (natural gravels, sand/clay and fissile rock), crushed rock and crushed recycled materials. Although differing in origin, their behaviour is generally considered consistent, which means they are modelled similarly in assessing the performance of pavements.

In the case of unbound granular materials there is strong evidence to suggest variation exists between vertical and horizontal modulus and hence they are anisotropic (Jameson, 2008). Granular materials also present a degree of strain-hardening and an increase of resilient modulus with increasing bulk stress (Sahoo et al, 2010). In reality, the materials considered herein are non-linear and anisotropic.

### 2.6.1 Stress Dependency

A critical effect that requires inclusion in analysis of a pavement is the fact that stiffness varies with the applied stress state (Rodway et al, 2007). It has been noted by many authors that the mobilised resilient modulus will be higher when subject to larger stresses (Brown, 2004). This is well represented by the often applied Uzan model (Tan et al, 2011). Further discussion of such models is provided in Section 2.6.5.1. Other available methods consider linear-elastic theory whereby the granular materials are partitioned and assigned decreasing modulus values with depth to approximate effect of dissipation of stresses. Note that material composition and properties play a significant role in the determination of stress dependency (Jameson, 2008). For example it is noted that the majority of fine-grained cohesive subgrade soils exhibit stress-softening type behaviour (modulus decreases in proportion to the stress level), whereas coarse-grained materials have been observed to strain harden (Kim et al, 2010).

The theory of sub-layering is often applied to approximate the effect of stress dependency. Two theories are considered, Austroads, developed for stress levels consistent with highway loads and the method developed by the US Army Corps of Engineers (Barker et al, 1975), which takes into account the heavy axle loads

common to airfields. Both of these theories consider the relative stiffness of the support layer (Jameson, 2008a). Figure 2.28 shows the basis of the sub-layering methodology developed by the US Army Corps of Engineers (Barker et al, 1975). Note that there are a few complications with this model that a user should be aware of. For example to ensure the mobilisation of the base layer moduli the material should be compacted to greater than 100% modified maximum dry density and have dried back to less than 70% degree of saturation (Wardle et al, 2007).

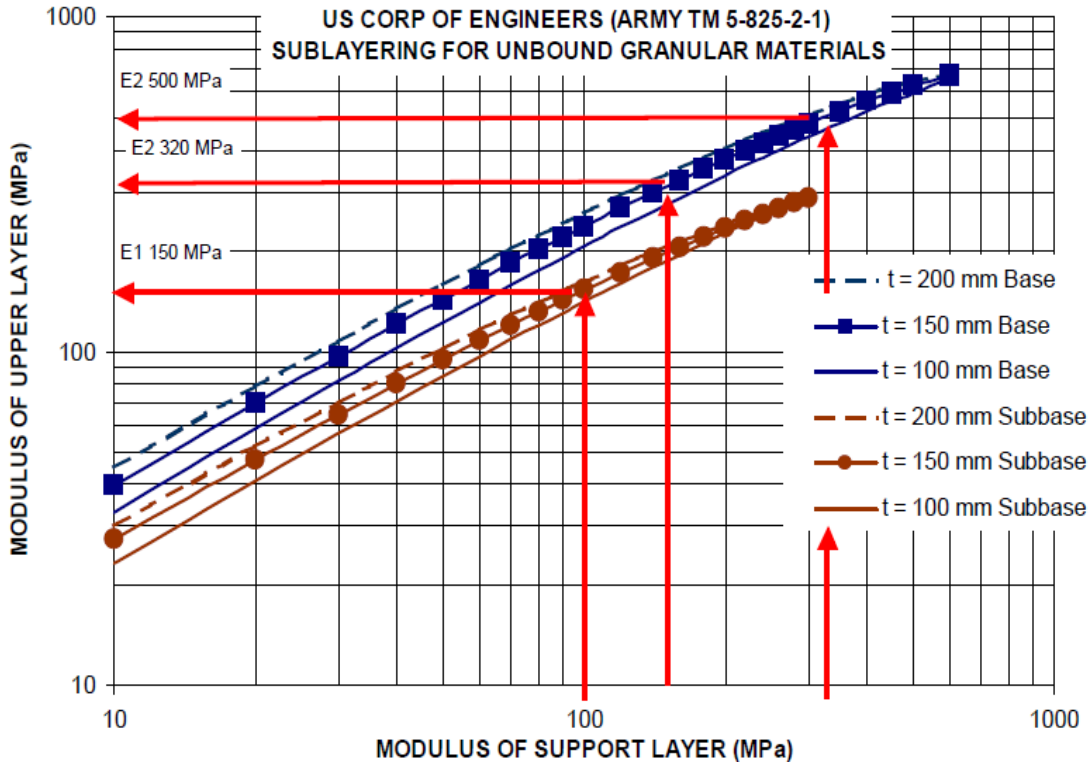


**Figure 2.28: Sub-layering of unbound granular layers (Wardle et al, 2007).**

Stress dependency can be accounted for through utilisation of Finite Element Method (FEM) for pavement analysis, however the effect of relative support is not considered (Jameson, 2008). Austroads include a method for sub-layering of asphalt surfaced cement-bound pavements that considers the modulus of the overlying layer for selection of the top sub-layer modulus. The modulus of the top granular sub-layer is determined from the minimum of presumptive values (which only consider bound or high quality material cover) or from an exponential relation for the sub-grade modulus and the total granular thickness. The ratio between top

and bottom layers is then calculated as the fifth root of the top granular sub-layer and the sub-grade moduli (Jameson, 2008a). Hence the US Army Corps of Engineers (Barker et al, 1975) method appears more appropriate for consideration of haul roads, due to the exclusion of bound surface layers.

### 2.6.2 Non-Linearity

The unbound granular materials utilised in flexible pavement layers are more complex in their behaviour than other common construction materials such as steel or concrete (Rao, 1991). In order to simplify analysis and design utilising unbound granular materials, they are often idealised as a homogenous isotropic elastic material whereby bulk stress is considered the sum of the three principal stresses (Karg et al, 2009). Most analytical models use elastic layered theory and hence consider unbound granular materials to be linear-elastic (Sahoo et al, 2010). Brown (1996) notes that the origins of such simplified analyses lie with Burmister's stress solution for layered media, which was derived in the 1950's. Although widely utilised, very little detailed reasoning exists for the use of the approximation. In the case of rationalising UGM performance via the resilient modulus, it is commonly stated that any permanent deformations under a single load application is small compared to the resilient component, such that it may be considered negligible (Brown, 1996). The point of difference for heavily loaded unbound pavements may be the fact that stiffness is known to decay with strain (Atkinson, 2000), so where the deformations in highway pavements may be small compared to elastic effects the same may not hold true for layers composed of unbound granular material not protected by asphalt layers. Figure 2.29 provides an indication of such an effect. Note that for sub-grades under highway pavements the small-strain '$E_o$' may be applicable, however in base layers of haul roads a move to the right is probable with significant reductions in stiffness. Many studies, such as Rao (1991), have been conducted to compare in-service deflections to those estimated from linear-elastic analyses. Such models may provide suitable insight for pavements fitting within the research experience, however extrapolations are difficult. It is noted by Brown (1996) that this approach is likely inappropriate for thinly surfaced pavements unless account is taken of non-linear effects. Rodway et al (2007), the creators of the HIPAVE (Mincad Systems, 2012B) industrial pavement design software also advise caution when using such linear-elastic models for off-road situations due to non-linearity of sub-grade behaviour.

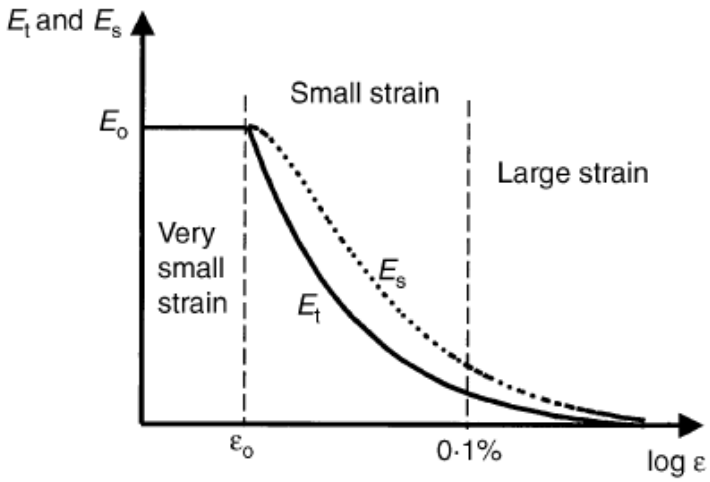


**Figure 2.29: Simple illustration of the decay of stiffness with strain level (Atkinson, 2000).**

It is likely non-elastic deformations occur within granular pavements subjected to an induced stress, such as viscous, plastic and visco-elastic deformations. All of these are stress dependent and thus the materials behave in a non-linear manner (Hadi et al, 2003). On a finer scale, it is ultimately the inter-particle movements (dilations) as a result of loading that govern the non-linear stress/strain behaviour, which is also inherently accompanied by permanent deformations (Vuong et al, 2008). The two statements above succinctly describe the internal response to the application of stress to an unbound granular material and the mechanism that provides for non-linear and plastic behaviour.

A note should also be given to the effects of soil damping. Generally, soil foundations are represented by a spring-dashpot mechanism and assumed to be viscous or linear-hysteretic (Beskou et al, 2011). This adds complexity to modelling, but also allows for energy dissipation within the sub-grade, a lack of which may be a shortcoming of some of the models in the literature or commercially available.

Research studies, such as that of Picoux et al (2009), have been completed that attempt to quantify the effect of non-linearity in pavement modelling. The most relevant to haul roads is the study completed by Sahoo et al (2010), which showed non-linear analysis resulted in a 44% increase in surface deflection and a 35%

increase in vertical stain at the top of the sub-grade. Modelling considered a typical granular pavement (varying thickness with vertical modulus of 250 MPa, over 50 MPa sub-grade) subjected to dual tyres of width 190-200mm and a 560kPa inflation pressure. It was ultimately concluded that linear-elastic analysis could lead to unsafe designs (Sahoo et al, 2010). Of course this is just one isolated comparison considering two specific modelling techniques, however it does serve as an example of how important non-linearity of pavement layers may be to low stiffness roads under significantly large loading.

### 2.6.3 Anisotropy

There is strong evidence that unbound granular materials exhibit a variation of modulus in different orientations, or anisotropy (Jameson, 2008b). In recent decades much research has characterised UGMs as non-linear and anisotropic (Kim, 2004). A complete general description of a soil includes 21 elastic constants (for an anisotropic elastic material considering strain energy conservation), which is quite prohibitive when it is considered that generally only three constants can be deduced from a normal tri-axial laboratory test. A special form of anisotropy, referred to as cross anisotropy is often adopted to describe aggregate and soil behaviour (Muir-Wood, 1991). Cross anisotropic behaviour requires five resilient properties; resilient moduli in vertical and horizontal direction, Poisson's ratio in vertical and horizontal directions and shear modulus in the vertical-horizontal plane (Kim, 2004). This idealisation aids the pavement engineer in more adeptly modelling the unbound layers included within any pavement.

The cause of anisotropy within pavements structures is not clear. Within soil deposits one common theory is that soils are often deposited or 'bedded' over time at a slow rate of deposition and hence consolidate in the vertical direction (Muir Wood, 1991). In the case of pavements it may originate due to compaction of relatively thin layers through mechanical means, although occurring over a short period of time, the particles may take on a preferred orientation leading to the difference in directional stiffness (Jameson, 2008b). Interestingly, it was found by Kim (2004) that anisotropy increased when material gradations became finer and poorly graded, which may be a significant finding when considering that sub-grade properties may change significantly along a road alignment.

Definition of the anisotropic modular ratio (ratio of vertical to horizontal elastic modulus) is quite difficult, as outlined in a recent Austroads report focussed on the

development of a non-linear anisotropic Finite Element Model (Gonzalez et al, 2012):

- degree of anisotropy is very difficult to measure in the laboratory,
- in FEA, anisotropy may not be required to accurately predict deflection bowl shapes,
- most models in the literature are isotropic.

In the literature search for the above report it was found that the anisotropic modular ratio ranged from 1 to 4 for granular materials and from less to greater than 1 for sub-grade materials (Gonzalez et al, 2012). In the current Austroads pavement design guide it is recommended that modular ratio be taken as two (Jameson, 2008a), a value that has been included in all Mincad Software packages for unbound pavement layers as well as for sub-grades (White, 2007).

### 2.6.4 Shear Strength and Yield Criteria

The discussion relating to yield criterion's for UGMs here is brief, as inclusion of such theories into pavement design is still relatively in its infancy. The most commonly applied failure theory is likely the Drucker-Prager model, which is a three-dimensional projection of the Mohr-Coloumb failure envelope, whereby the yield surface forms a cone (Arnold, 2004). The reason for considering a failure criterion is explained by Figure 2.30, where the material exhibits strain hardening (Brito, 2011). This effect is potentially significant due to the fact that when it is combined with non-linear and anisotropic effects the performance of a given pavement could vary significantly over time. Lastly, note that the models mentioned above consider monotonic loading (Brito, 2011) and not cyclic loading as applied to a pavement.

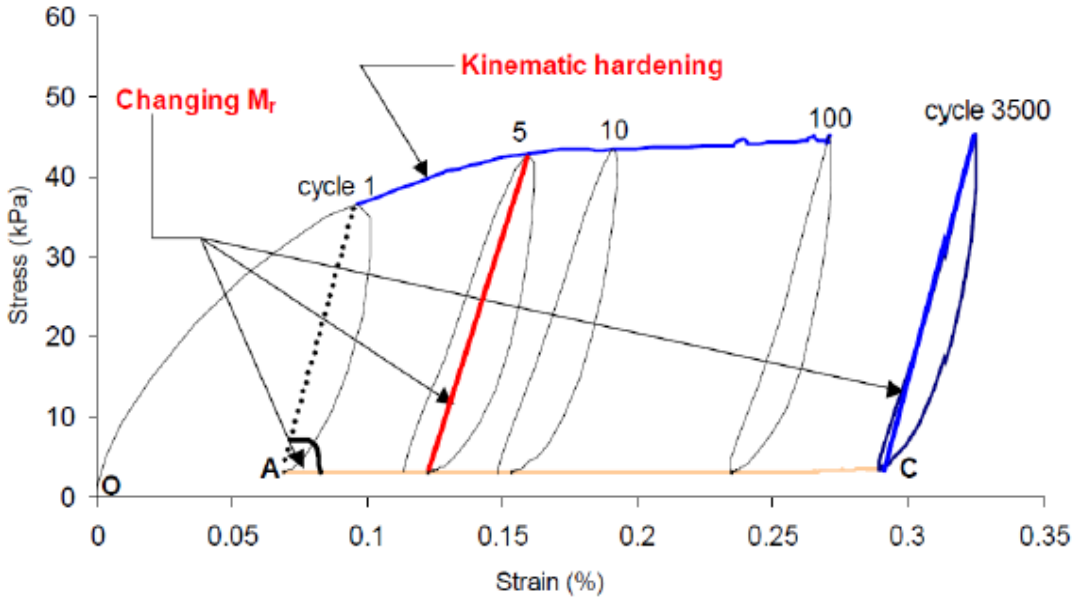


**Figure 2.30: Illustration of kinematic hardening and associated changes in resilient response with loading cycles (Brtio et al, 2011).**

### 2.6.5 Response to Cyclic Loading

Pavement materials experience cyclic actions due to the application of passing traffic, the response of UGMs, both instantaneous and time-dependant is described in the proceeding sections.

#### 2.6.5.1 Resilient Modulus

The most commonly utilised parameter for describing pavement material response to cyclic loading is the resilient modulus. This is defined as the ratio of recoverable (resilient) strain to applied deviator stress (Brown, 2004). It is used within pavement design as Young's modulus is utilised within conventional liner-elastic soil analyses involving the application of a monotonic loading (Lekarp et al, 2000). However, recoverable instead of total strain is utilised to represent the cyclic loading condition of a pavement under wheel loading. Within a single cycle of loading the pavement experiences resilient and permanent strain responses, as presented in Figure 2.31. The stress path here describes the hysteretic loop experienced by the material, whereby the open end represents the permanent deformation (strain) induced. This is discussed further in Section 2.6.5.2.

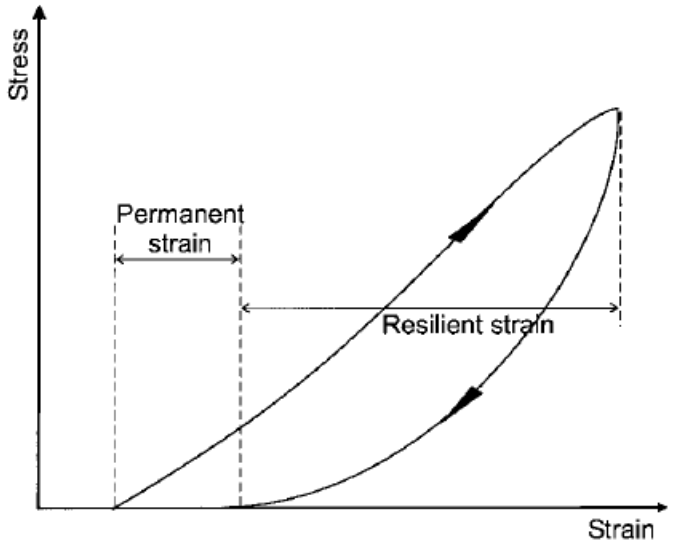


**Figure 2.31: Stress path showing the resilient and permanent strains experienced by a granular material within one loading cycle (Lekarp et al, 2000).**

Much of the research effort to date has been focussed on quantifying the factors that influence resilient behaviour. Rodway et al (2007) provide a list of the variables most affecting changes in resilient modulus of a granular layer:

1. Quality of aggregate: soundness, durability, particle size distribution, angularity.
2. Thickness of the layer.
3. Stiffness of the supporting layer.
4. Moisture content.
5. Stress-state.
6. Relative density.

The stress state is considered by the majority of authors to have the greatest influence, with confining stress being found to have a much more profound effect than variances in deviator stress (Lekarp et al, 2000). Therefore the ratio between mean normal stress increase and resilient modulus is significant and shows far greater sensitivity than for other factors. Poisson's ratio is commonly utilised in conjunction with resilient modulus and is also believed to be influenced by stress state, however more research is currently needed on this topic (Lekarp et al, 2000).

The effect of strain on resilient modulus is not clear within the literature. However, Frost et al (2004) note a high sensitivity to small differences in strain, when low deviator stress is applied. However the strain accumulated during testing is not taken into account by most test methods, and hence the undeformed specimen height is utilised in calculations of resilient modulus (Kim et al, 2007). It is likely greater accuracy could be achieved if the deformed lengths were utilised.

It may be most prudent to consider the effect of strain in conjunction with the stress history of the material. But as with strain level, there is little agreement on the effect of stress history, however it appears the effect is minimal unless the loading was significant enough to cause large permanent deformations (Lekarp et al, 2000).

Density is known to affect the shear strength of granular materials (Jameson, 2008a), however when considering the resilient modulus there has been little agreement between researchers to date (Lekarp et al, 2000). Uncertainty may be due to the difficulty to mobilise stress within a poorly compacted material, as may occur in the situation of poor support being provided by an inferior sub-grade. It is worth noting that the accumulation of permanent strain is likely of greater concern for poorly compacted materials and thus control must be exerted for this property, eliminating concern related to resilient modulus.

The effect of water content on modulus has been investigated by several researchers. Lenngren (2009) conducted repeated FWD testing of a highway section over its first year in service. It was found that the resilient strain induced under similar load pulses was far more severe in wetter time periods and especially within sections of the roadway susceptible to moisture ingress (see Figure 2.32). Exact measurements of moisture content were not made and so the marked difference presented in Figure 2.32 should only be taken as an indication of the potential effect of elevated moisture contents within a granular pavement layer.

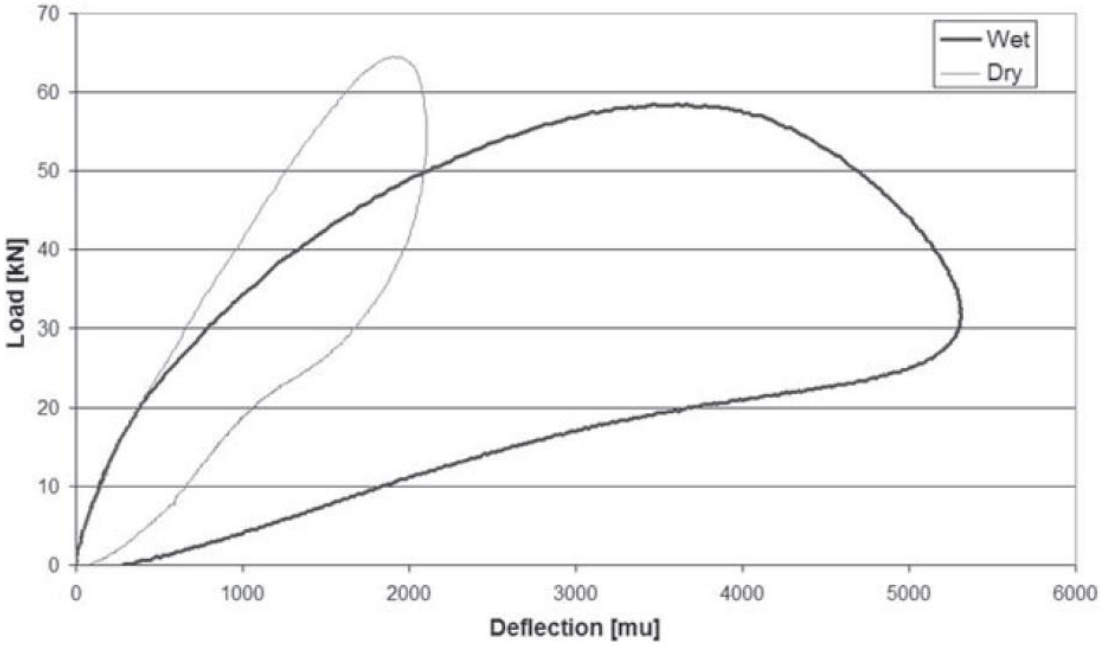


**Figure 2.32: Pavement layer response under FWD test, comparing wet and dry state (Lenngren, 2009).**

Kim et al (2007) note that the resilient modulus was found to be highest when sandy-silty or clayey soil samples were tested in the dry state. This result was attributed to the capillary suction arising from the cohesive properties of the soils as they dried out. These samples were not compared to coarser soil samples (see discussion of particle grading below). Most literature reports that moisture content does not significantly impact resilient response for dry and partially saturated materials (Lekarp et al, 2000). However high pore pressures could occur in the case of a high degree of saturation, poor drainage or low permeability (Vuong et al, 2008), and result in a lower effective stress and consequently a low modulus value.

The particle grading of granular materials is also stated to have an effect to some degree on modulus (Lekarp et al, 2000). Perhaps most notable has been research focussed on the effect of the maximum (top) sized particles. Lindly et al (1995) undertook RLT tests with an up-scaled apparatus, which resulted in the magnitude of the top-size having little effect on modulus. The tests did however show less repeatability with an increase in maximum particle size. A study by Lekarp et al (1999) showed a 25% increase in resilient modulus when a similar material's top-size was increased from 16mm to 90mm. This finding is supported by Lambert et al

(2008), where resilient modulus is shown to increase significantly with a coarse gravel material; when layer thickness increased from equal to maximum particle size to twice layer thickness.

A considerable number of resilient modulus models are available within the literature. The simplest of the commonly employed models is the 'k- θ' (Seed et al, 1967) which considers bulk stress as the only variable, which means the model is widely used but does have several drawbacks (Lekarp et al, 2000). Caution should be exercised with this model as detailed stress conditions are not well represented by the use of mean normal stress, which can yield significant errors (Brown, 2004). The model can be modified to take account of deviator/shear stress (although noted to have a minimal effect on modulus in isolation) and failure (Gonzalez et al, 2012), after which re-orientation of particles obviously means a significant change to material behaviour. However, such models should be carefully applied as the effect of failure zones in the pavement could have a profound effect on predicted performance in other layers/adjacent areas (Lekarp et al, 2000). Despite this, such models are commonly employed to model resilient modulus, for example the Uzan model was adjudged the most suitable model for UGMs by Austroads (Gonzalez et al, 2012). This recommendation was based on the contention that the model fitted stress states anticipated within in-service pavements and not just in the states included in a repeated load tri-axial test. The Uzan model is known to show an increased post-failure modulus, which contradicts observations from other research (Lekarp et al, 2000). Finally, for modelling purposes, Ekblad (2008) states superior performance is only experienced when a stress dependent Poisson's ratio is also utilised.

An alternative method for defining the elastic behaviour of granular materials is the Boyce model. Stresses and strains are separated into volumetric and shear components; resilient modulus and Poisson's ratio are then replaced by bulk and shear moduli (Lekarp et al, 2000). Thus the model is based upon three variables; bulk modulus, shear modulus and Poisson's ratio. A fourth parameter is ideally required, which is dependent on the others, so that the strains are derived from an elastic potential (Bouzidi, 2003). To explain the benefits of such a technique, observe Figure 2.33. Here it is apparent that this approach may be advantageous, as there is a reversal of the shear strains induced once the wheel has passed the point of interest in the pavement.

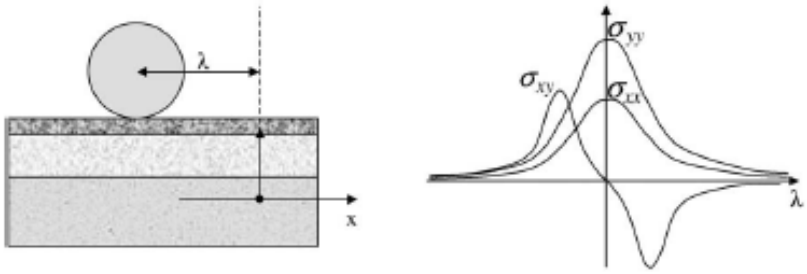


**Figure 2.33: Normal and shear stress against relative position of a passing wheel load (Bouzidi, 2003).**

Finally, note should be given to the resilient Poisson's ratio of unbound granular pavement materials. This property has not been studied in nearly as much detail as the modulus. To date it has been shown to increase with decreasing confining pressure and increasing deviator stress (Lekarp et al, 2000). Further research is required for this parameter to be better applied in pavement design..

#### 2.6.5.2 Permanent Deformation

Under cyclic loading, UGMs exhibit elastoplastic behaviour, characterised by permanent deformation with an increasing number of load repetitions (Gidel et al, 2001). Definition of permanent deformation is important and ultimately the main outcome modelled by structural analysis of pavements. Research effort in this area undoubtedly lags behind that of resilient modulus (Lekarp et al, 2000A). Deformation is, of course, strongly related to the strength and stiffness of a pavement material (Frost et al, 2004). It is perhaps often over-looked that accumulation of strains (permanent deformation) is the result of rearrangement of grains, shear deformation, abrasion of soil particles and non-recoverable drainage of pore water during cyclic loading (Karg et al, 2009). These responses to the application of stress result in the behaviour discussed herein, which can be categorised into two major reactions; frictional sliding (shear strain) or volumetric compaction (Karg et al, 2009). This is described by the three modes shown in Figure 2.34. Mode 0 is associated with compaction of the base layer, Mode 1 with shear deformation of base materials and Mode 2 representing shear deformation initiating in the sub-grade with the base subsequently deforming in shear (Dawson et al, 2004). For consideration of unsealed pavements it is particularly noteworthy that a Mode 3 is also considered by

Dawson et al (2004) which is associated with particle damage (attrition or abrasion). Several methodologies for describing the deformation of unbound granular pavement layers are described below. It is prudent to make note that although monitoring rut depth through direct measurement is quite simple, the prediction of such deformation is extremely complex (Lekarp et al, 2000A).

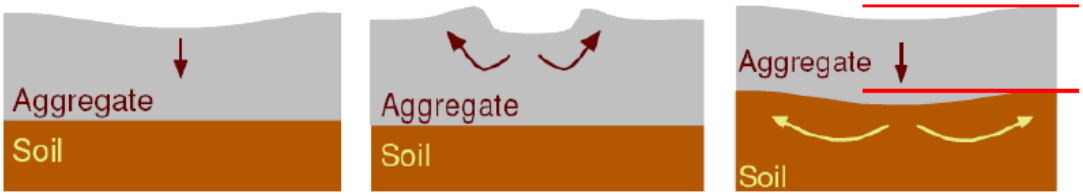


**Figure 2.34: Modes 0, 1 and 2 (respectively) of rutting (after Dawson et al, 2004).**

Permanent deformation due to repetitions of vertical sub-grade strain is the criteria by which pavement life is estimated by Austroads and design software CIRCLY and HIPAVE (Mincad Systems, 2012B). Two variables are involved, both calculated from the sub-grade vertical modulus. This design model has been verified against the results of testing from which common CBR design curves were developed in the 1970's (and discussed in Section 2.4.1). The empirical data from which the theory was developed considers a set layer structure for the pavement which, as discussed previously, is transformed through material equivalency factors. Another shortcoming is the fact that development completed by Us Army Corps of Engineers (Pereira, 1977) considered CBR values for characterising the sub-grade, which has been transformed through use of the design software, APSDS (Mincad Systems) to make use of the sub-grade stiffness. There is no relation that has been shown to allow accurate modulus approximations from CBR values (Sukumaran et al, 2004).

Like elastic response to loading, accumulations of plastic strains within unbound pavement layers is a highly complex system. Figure 2.35 explains the basic theory used in most deformation models, whereby stress level and number of loading repetitions are the primary factors.

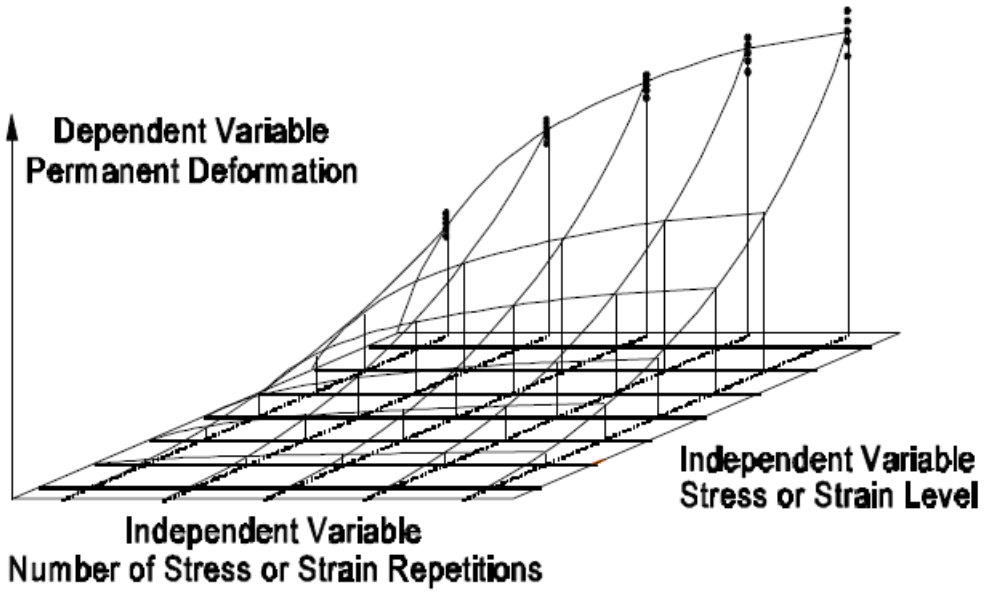


**Figure 2.35: Explanation of permanent deformation due to number of strain repetitions and stress/strain state (Theyse, 1997).**

There exist many theories of permanent deformation, of varying complexity. Perhaps the most widely accepted model for unbound granular materials is termed ‘shakedown’.

As alluded to above, the use of stress to model permanent deformation has become a research focus in recent times. This has resulted from observations that low stress ratios ultimately result in equilibrium and high stress ratios result in gradual failure. This leads to the postulate that a threshold stress must exist which defines this change in behaviour, termed the ‘shakedown’ limit (Lekarp et al, 1998). An elastic response alone cannot cause failure, rather it is irrecoverable plastic or viscous strains that accumulate with repeated load to produce failure in the form of surface slip, rutting or surface cracking (Collins et al, 2000). The typical response of unbound granular materials is shown in Figure 2.36, further explanation is provided by Arnold et al (2002):

- Range 1 – Plastic Shakedown Range: A high strain rate per load cycle for a finite number of load repetitions (compaction). Strain rate then decreases per load cycle until response is entirely resilient. Stability in Range A is strongly dependent on the moisture content of the material (Dawson et al, 2004).

- Range 2 – Plastic Creep Shakedown Range: Initial behaviour similar to that of Range A while the material is compacted. Permanent strain is then either constant or slightly increasing or decreasing, however this rate is acceptable. Perhaps after as many as two million cycles, response may change to Range 1 or Range 3.
- Range 3 – Incremental Collapse Shakedown Range: initial compaction may be observed, after which the permanent strain rate increases and remains constant with increasing number of load cycles.

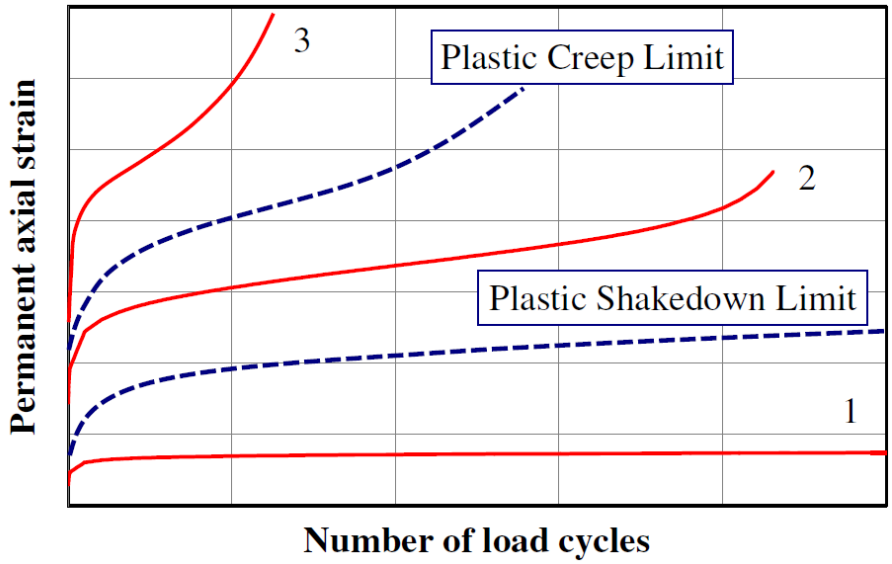


**Figure 2.36: Shakedown ranges and limits (Cerni et al, 2011).**

Definition of each range of shakedown response is possible by examining the permanent strain against the rate at which it occurs (Siripun et al, 2011). If such development is plotted, areas of consistent strain rate per loading cycle can be used to characterise each range of behaviour.

To simplify the theory a little, Frost et al (2004) describe a stiffness asymptote occurring at around 50% of deviator stress at failure. This is an example of a simple practical limit that may provide acceptable performance for a defined material and application. Lekarp et al (1998) argues that failure in granular layers is a gradual process rather than a sudden collapse, thus the use of static shear strength may be of limited value. It is contended that the permanent deformation behaviour is related

to the maximum shear stress ratio and length of the stress path of the induced loading in p-q stress space (Lekarp et al, 1998). Such an approach can be extended by inclusion of the Drucker-Prager yield line, the proximity this limit and the stress ratio would then assist in determining the response type (Arnold et al, 2002) and therefore safe use for design of any pavement layer.

Observation of the hysteresis loops reveals the nature of the response for a single load repetition and also longer term response. Where a loop is observed to grow in size represents an increase in accumulated plastic strain (Figure 2.37). This explanation is somewhat over-simplified; rather the area contained within a hysteresis loop represents the deformation work per volume element (Werkmeister et al, 2004). Note that as tension cannot develop in UGMs, diagrams such as Figure 2.37 should be carefully interpreted, where cyclic plasticity is being represented (Nguyen, 2007) and not a tension portion of the loop. Beyond Range A responses, the dissipated energy per cycle relates to a stationary value, so that vertical strain decreases to a constant rate depending on loading characteristics, and frictional and stiffness characteristics of the grain contacts (Siripun et al, 2011). It is interesting to note that the elastic unloading section is a similar shape over all ranges and loading magnitudes (Werkmeister et al, 2004).

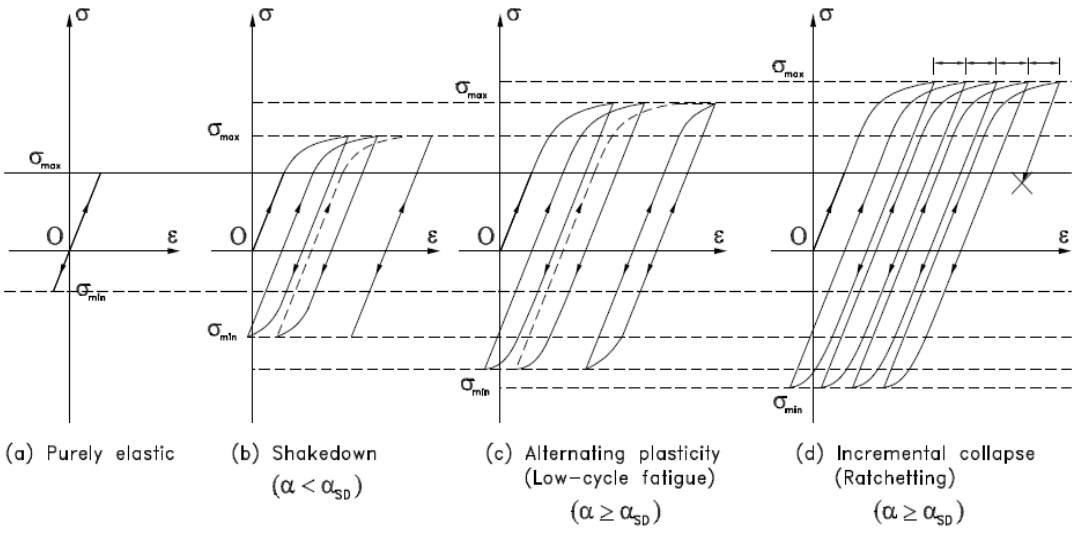


**Figure 2.37: Characterisation of shakedown ranges via hysteresis loops and accumulation of plastic strains (Nguyen, 2007).**

The majority of the work completed through a UGM hysteresis loop is transmitted to heat and partly to a change of material properties leading to damage. A small part is dissipated through cumulative work on the material (Werkmeister et al, 2004). However note that the total amount of plastic energy dissipated on any load path must be finite (Nguyen, 2007).

The direct application of the shakedown ranges with respect to pavement layer design remains somewhat in its infancy. Dawson et al (2004) suggest that for (well designed and constructed) unsealed or thinly sealed pavements, Range A response is only possible within the best quality unbound granular materials. Thus the objective, in most cases, is to design granular layers to ensure Range B behaviour, with as small a slope as possible (see Figure 2.36) to limit plastic strains.

Linear-elasticlinear-elasticlinear-elasticlinear-elasticlinear-elasticlinear-elasticlinear-elasticlinear-elastic

## 2.7 Identification of Issues Requiring Further Research

The following discussion identifies specific components of this research that are not directly addressed by the literature, and requires further development. Several of the identified deficiencies require tests to be developed, due to a lack of published or accepted testing methodologies being available in the literature.

### 2.7.1 Rolling Resistance of Haul Trucks

It has long been recognised that the nature of the haul road pavement significantly impacts the efficiency of a haulage operation, as evidenced by a similar comment in Kaufman et al (1977). Empirical tables for RRC values are available and have been updated by various researchers (Atkinson, 1992; Tannant et al, 2001; Holman, 2006). The data in such tables alludes to an influence of pavement stiffness on rolling resistance. Holman (2006) presents an equation that considers plastic rutting (such as occurs in a soft sand) of the pavement surface as the sole independent variable, with a RRC of 2% resulting for no wheel penetration. Thompson et al (2001) successfully relates a Roughness Defect Score to RRC. This is a practical measure for monitoring the deterioration of the pavement surface with time and traffic, but attempts to describe all modes of pavement distress within a single value. Furthermore, it is not easily related to common pavement texture and roughness values used in general pavement rolling resistance research. For example,

Sandberg et al (2011) note that truck rolling resistance is most affected by roughness, whereas texture is more significant for cars. If the classifications of texture and roughness in Section 2.2.5 were applied to haul road research, this trend could be extended. Utilising such measures would allow the framework for the investigation of various pavement properties in general pavement research to be applied to haul roads, allowing a greater understanding of haul truck rolling resistance.

The literature presents case studies (Jamieson and Cenek, 2002; Schmidt et al, 2009) where pavement stiffness is suggested to have a significant impact on rolling resistance. To date there has not been a study of haul road pavements considering pavement stiffness through either deflection measurement or any other technique. Combined with the lack of haul truck rolling resistance measurements including detailed consideration of pavement surface condition, this provides the basis for the research objectives identified in Section 1.2. To achieve these objectives it is considered that full-scale tests should be utilised throughout, defining truck performance and pavement response to truck loading and motion.

### 2.7.2 Method for Rolling Resistance Testing of Large Vehicles

As noted in Section 2.2.5.1, a variety of methods have been used to measure rolling resistance in previous research. To date, there has not been an attempt to harmonise these methods, such that a universally accepted method for definition of RRC is possible. This issue is further compounded by confusion with regard to the definition of rolling resistance. Some research actually measures the driving resistance of a whole vehicle, such as those applying coast-down test methods (Thompson et al, 2001; Hammarstrom et al, 2008) or the steady state torque method (Jamieson and Cenek, 2002). Alternate approaches define rolling resistance as stated by ISO 28580:2009 (the horizontal force for wheel motion divided by vertical load on the wheel, see Equation 2.1), but used scaled-down towed cart methods to measure rolling resistance (for example Widodo et al, 2009; Lee 2010). The latter approach often employs considerably smaller tyres than that fitted to haul trucks, with no examples of such testing being described in the literature.

The need for a rolling resistance test method that considers the large wheel loads applied to a pavement by rigid dump trucks used in mining is desirable, in order to properly investigate the impact of pavement deflection.

### 2.7.3 Method for Full-Scale Pavement Deflection Testing with Large Vehicles

The structural stiffness of pavements, when being related to rolling resistance, is often quantified by a description of the constituent material (see Table 2.5). Although such a descriptive method can supply practical guidance for field use, it does not include sufficient detail for investigation of the influence of pavement structural condition of rolling resistance. This is exacerbated by the fact that this contribution is generally contended to be relatively small in comparison to pavement texture or roughness.

Some pavement rolling resistance research has included direct measurement of pavement deflection, for example Jamieson and Cenek (2002), with use of a standard Benkelman Beam apparatus. In fact, the Worldbank includes a term for Benkelmen Beam rebound deflection in the adopted function for rolling resistance within the widely adopted HDM-4 model (Zaabar, 2010a). Other studies relating rolling resistance to pavement stiffness have made use of Falling Weight Deflectometer (FWD) testing to define likely energy loss under a passing wheel load (Lenngren et al, 2010). Such an approach may be inappropriate for haul roads due to the unsealed surface and variable moisture regime within the pavement.

There is no method for measuring deflection under haul truck wheel loads currently available within the literature. One difficulty that must be addressed by the any method that is investigated, is to ensure the measurement apparatus is placed clear of the induced deflection bowl.

### 2.7.4 Measurement of Pavement Texture and Roughness

The measurement of pavement texture and roughness is required to define the surface condition of the pavement. A method providing greater detail than the RDS reported by Thompson et al (2001) or the IRI (Gillespie, 1992) would be preferable for this research. Correlation of roughness with different pavement longitudinal wavelength allows recommendations to be developed with regard to material selection and construction methodology, if a specific wavelength range is shown to significantly influence rolling resistance.

Pavement texture is generally related to the surfacing aggregate size and method of pavement construction (see Figure 2.11). It is noted in Section 2.2.5, that it is the single greatest determinant of rolling resistance experienced by passenger-car vehicles (Sandberg et al, 2011). Mclean et al (1998) contends that such

wavelengths of surface undulation induce an undesirable tyre response, as they are contained within the pavement contact patch. Therefore, definition of surface roughness at a high resolution is required, such that this effect can be investigated for haul trucks.

Research relating measured haul road pavement roughness and rolling resistance is confined to Thompson et al (2001). The method of pavement roughness measurement in this instance does not consider a distinction of pavement roughness wavelength, but is defined by subjective assessment of pavement surface defects. It is recognised in Section 2.2.2 and Section 2.2.5, that rolling resistance can be a unique function of pavement roughness and vehicle characteristics. Consequently, a test allowing post-processing of data and segregation into texture and roughness categories, defined by mean wavelength, is required for a full understanding of haul road rolling resistance.

### 2.7.5 Analysis of Pavements Subjected to Large Wheel Loads

An ability to predict pavement response to load is central to conventional pavement design techniques. Generally, the pavement model is used to calculate the vertical compressive strain induced at the top of the sub-grade layer, which is used to predict pavement lifetime (Jameson, 2008). The influence of pavement stiffness on rolling resistance is investigated in this study. If shown to be a significant contributor, the importance of an ability to compare the relative stiffness of two alternate pavement layer configurations would be increased (see Section 2.7.6).

Thompson (2011) suggests that both linear-elastic and FEA analysis can be used successfully for haul road pavements. However, there is no comparison of the two methods for haul roads available in the literature. Furthermore, there is not any comparison of measured pavement response to that predicted by either method. Wardle et al (2001) have back-analysed pavement configurations included in the trial sections tested to develop the S77-1 curve reported by Pereira (1977). This allows the pavement designer to predict pavement lifetime (prior to the development of unacceptable rut depth) from calculated sub-grade vertical compressive strain. Subsequently, variable pavement layer configurations can be considered through application of material equivalence factors, which effectively transforms the standard pavement structure utilised in the original field trials (Pereira, 1977). The pavements included in the field trials, and subsequent analysis, included significant asphaltic concrete and bound layers applied for the surfacing course and base-course (White, 2007). Since unbound granular layers were not physically tested as base-course,

and without a surfacing course of at least 40mm, design of such pavements is considered inappropriate and caution is advised (Jameson, 2008). At current, such assumptions are necessary for haul road pavement design. Furthermore, Austroads (Jameson, 2008) and MRWA (2013) suggest an upper limit for resilient modulus of unbound materials based on a maximum mean normal stress of 240kPa. This serves as an example of the dangers of utilising published 'range' values for material parameters instead of considering their in-service condition. Therefore, some means of investigating the ability of each calculation method to predict measured pavement response is required, in an effort to provide insight into the suitability of each method.

Advanced numerical modelling in the form of FEA has become commonplace in pavement research. It provides benefits such as those listed in Section 2.5. However, it has not been tested in the literature for modelling of haul road pavements or compared to closed-form methods provided by analysis applying elastic theory. In order to apply this technique to haul road research it should first be shown to be superior to less time-intensive linear-elastic methods in predicting measured pavement response.

### 2.7.6 Definition of Critical Design Criteria for Haul Road Pavements

Haul road pavements are commonly designed based on local experience or the CBR cover curves based on the field trials completed by the U.S Army Corps of Engineers and reported by Pereira (1977). The latter has been extended by Wardle et al (2001) to allow more flexible application of the failure theory to linear-elastic modelling in the software platforms APSDS and HIPAVE. These failure theories are based on airfield pavement design theories, where aircraft stability and surface properties for safety at high speeds govern (Civil Aviation Safety Authority, 2013). However, haul roads are part of the commercial production process of surface mining, and therefore the impact to the mine operator should be considered in defining the critical pavement design parameter. Thompson (2009) presents a system wherein haul roads are categorised with consideration of the acceptable operating condition, volume of material hauled daily and pavement lifetime. In turn, these parameters are used to define the limiting pavement compressive strain for design. It is important to note that both failure theories discussed above relate elastic response (sub-grade strain) to plastic failure (rutting). Aside from any

technical argument of the appropriateness of relating these two responses, the approach must be questioned for application to unsealed pavements where environmental factors are likely to have a significant influence on material performance. Despite such complications, the method reported by Thompson (2011) provides the impetus for further investigation of the pavement condition in conjunction with rolling resistance, as it indirectly considers rolling resistance due to including a performance index in the determination of the road category. Thompson (2013) considers that only the functional performance of the haul road influences rolling resistance. Therefore, it is considered prudent that an extension be pursued to allow measurement techniques to replace subjective assessment of surface defects, and include the influence of structural capacity. A mine owner or operator would benefit from being able to estimate the cost associated with use of a haul road during the design phase. This can then be used with the best available analysis techniques, as discussed in Section 2.7.5, to optimise the costs associated with material haulage considering pavement design, construction and haul truck operations.

# 3 Procedure

## 3.1 Project Overview

The process taken to define haul road rolling resistance and explore the adequacy of current structural analysis techniques is presented in Figure 3.1. Within the project were two distinct processes. To the left of Figure 3.1 the primary focus of the project is represented, to define the factors affecting haul road rolling resistance. This is broken into two streams; functional or surficial pavement characteristics and pavement structural capacity. Definition was made by pavement roughness and texture for the former and pavement deflection for the latter. In turn, measurement of pavement deflection allowed investigation of various pavement structural analysis techniques, represented on the right side of Figure 3.1. In order to allow a definitive comparison of analysis methods, laboratory testing of the materials sampled on-site at the deflection test locations was completed for input into structural analysis. Deflection and soil modulus values were then used to test the accuracy of commercially available software in order for recommendations to be made as to the most appropriate for use in haul road pavement design, with a view to optimising haul truck rolling resistance.

The following section details each step of testing and analysis completed as part of the project.

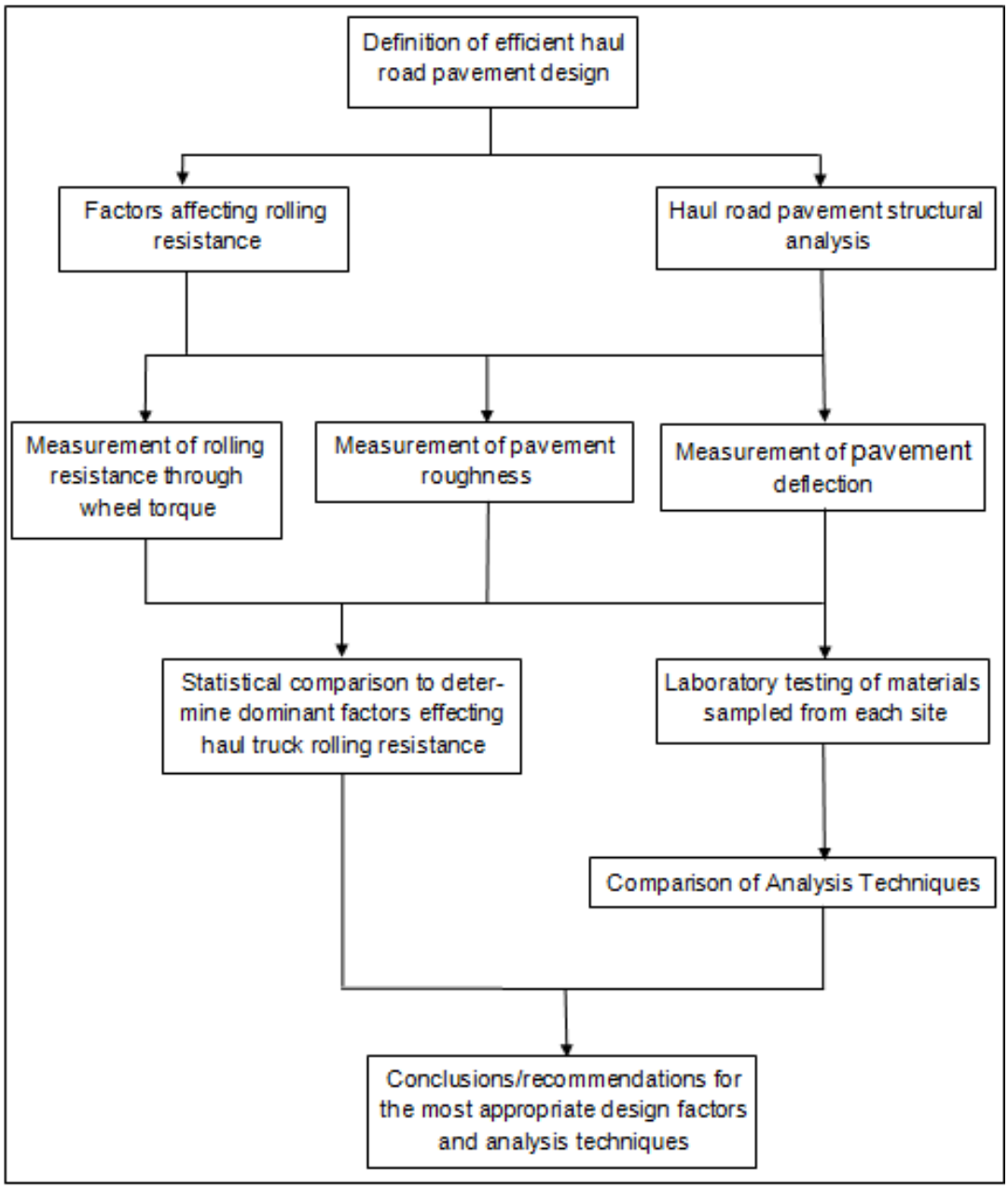


**Figure 3.1: Project Flow Chart.**

## 3.2 Experimental Design

The experimental method adopted for this project was motivated by the research needs arising from the lack of targeted investigations, as identified in Section 2.7. In general, there was a focus on utilising accepted pavement parameters in the investigation of haul truck rolling resistance. This approach has not been taken in

previous research, which meant that extending the findings from the study of highway pavements to haul roads is difficult. The following discussion explains the approach taken for the in-situ and laboratory testing of haul road pavements.

As stated in Section 2.7.1, full-scale testing was considered the optimal means to investigate the influence of pavement properties on haul truck rolling resistance. Firstly, this was to address the lack of such testing completed to date, but also avoided the difficulty of relating the results of smaller, scaled testing to in-service haul trucks. As the influence of pavement deflection was a key parameter being investigated, it was considered critical that actual wheel loads and a 'typical' pavement structure and materials be utilised in the testing. Similar to the lack of full-scale testing for rolling resistance in the literature, quantitative means of describing pavement texture, roughness and deflection for haul roads were found to be rare. This has meant that some inference or extrapolation of results must be made to compare the available research findings. Secondly, simplified testing introduces the risk of experimental error, where subjective assessment is required (for example the RDS detailed by Thompson, 2011) or where idealised tests must be calibrated to estimate a specific physical response. An example of an idealised test is the use of FWD to estimate potential rolling resistance through pavement hysteresis (Lenngren et al, 2010). In an attempt to avoid such complications, every effort was made to utilise full-scale testing, which meant that no standard test methods were available and resulted in the development of the in-situ tests detailed in Section 3.3.

The pursuit of full-scale testing presented challenges, as a single haul truck can transport in the order of 8,000 tonnes of iron ore in a single shift, which at the time of testing was valued at approximately $128AUS per tonne (ycharts.com). As a result, the mine operator imposed strict time restrictions on the availability of a fully functioning truck and driver. For this reason the development of tests included a focus on rapid repeatability and utilising a minimal amount of equipment. Section 3.3 details the process undertaken to determine the most appropriate means of testing, and the development of each test, culminating in Section 3.5 which details the test and analysis method used for in-situ testing.

The goal of in-situ testing was primarily to determine which pavement or operational parameters most impact haul truck rolling resistance. From the literature, it was evident that pavement structural and surface properties needed to be measured, but also truck speed and load should be varied. Air drag was also a significant issue that needed to be addressed, despite the relatively slow operating speeds of haul trucks,

their substantial frontal surface area means that a significant degree of drag can be generated in times of high wind speed. For this reason, wind speed was monitored regularly throughout rolling resistance testing. The deflection test results presented an opportunity for an investigation of numerical modelling methods for haul roads, This was aided by the fact that the entire deflection bowl was able to be measured via the test method developed (see Section3.5.7). With the aid of sampling and laboratory testing of haul road pavement materials (which was used to determine material parameters) key inputs for modelling were obtained.

Laboratory testing was planned to define the elastic modulus and shear parameters of the samples taken from each pavement section, with a similar stress state as that experienced when loaded by a haul truck. To achieve this, the confining and deviatoric stresses within accepted test methods for triaxial testing with monotonic and repeated load tests were extended up to a maximum deviatoric stress of 1000kPa. The data from the monotonic load testing allowed the Mohr-Coloumb shear parameters for an unconsolidated undrained sample to be determined, which provides a key understanding of the physical properties of the material. The definition of these parameters then allowed various pavement modelling techniques to be trialled.

As noted in Section 2.7.5, there are a number of software programs available that could be applied for the purpose of haul road pavement analysis. Although linear-elastic and FEA solutions should in theory produce similar outputs under identical inputs and assumptions, this situation does not necessarily arise when utilising commercial pavement design software. For example linear-elastic analyses, such as the solution employed by CIRCLY, assumes loading to be applied over a circular area of an axisymmetric pavement. From interrogation of terrestrial laser scans taken to measure pavement deflection under haul truck wheel loads in this project, it is shown that contact areas are not circular. Furthermore, the question of pavement geometry for modelling has significant practical implications. Ghadimi et al (2013) have reported erroneous calculated pavement strains when utilising a plane-strain assumption. This result should be tested for haul road pavements and extended to consider three-dimensional modelling. It was considered valuable to define which analysis techniques can accurately predict surface deflections. To further this, the most appropriate modelling technique was to be recommended through comparison of observed and predicted surface deflection and curvature. Such knowledge is aimed at informing future researchers and practitioners currently undertaking mechanistic-empirical haul road pavement design.

There are only a limited number of pavement failure criteria that are reported in the literature that can be applied to haul road design. The earliest example is the CBR curves reported by Kaufman et al (1977), which apply the expressions reported by Turnbull et al (1957). This approach has since been updated by authors such as Thompson (2013), utilising failure criteria developed from various iterations of testing at the U.S Army Corps of Engineers Waterways Experiment Station. The most recent failure criteria developed from testing at this location was that reported in Pereira (1977). Further testing was completed in both the USA and France in preparation for larger commercial aircraft wheel loads that were planned to come into service in the early 2000s. However, to date there have not been any changes recommended for the failure criteria. Wardle et al (2001) completed a validation of the criteria for the development of the APSDS software. This program calculates the pavement life by considering the sub-grade compressive strain calculated for a given wheel load and pavement layer structure. Some validation is required for use on haul roads, as caution has been advised using such analysis methods for pavements that do not have at least a 40mm surfacing (Jameson, 2008). The pavements included in the field trials from which the failure criterion was developed all had such a surface treatment. Therefore, it is considered necessary to trial the linear-elastic solution method for haul roads, prior to proceeding with more detailed research on the design of such pavements. This project benefits from having in-situ loading/deflection data and pavement elastic modulus values that have been defined in a variety of ways. As such, predicted deflections can be compared to those measured, providing an opportunity to comment on the accuracy of different analysis approaches and recommend the most suitable for haul road design.

Thompson (2011) considers the limiting pavement lifetime criterion to be pavement layer strain, although the criterion for limiting strain is determined from the daily haulage mass and desired level of serviceability. This has been developed through the back analysis of in-service haul road pavements. All design criteria for haul roads the structural design of haul road pavements refer to the generation of pavement surface rutting and roughness as the mechanism representing the end of the pavement's serviceable life. If either pavement stiffness or roughness was found to significantly impact rolling resistance, the design criterion for haul roads should be revisited to include some consideration of operating costs, which would be represented by the estimated rolling resistance.

An examination of the combination of analysis technique and failure theory is also required. The critical pavement response should be calculated via a method that

applies a validated pavement model. Therefore, if rolling resistance was found to be dominated by surface roughness, the current methods employed could be retained but with a greater understanding of the most appropriate method for pavement analysis. This ability would be perhaps even more crucial if pavement stiffness was found to significantly influence rolling resistance. In this instance, an understanding of the layer structure that produces the greatest net stiffness under the loading of the design vehicle would be an important element of the pavement design process.

## 3.3 Development of In-situ Test Methods

The testing identified above was further investigated in line with the findings of the literature review (Section 2.7). A key requirement for each in-situ test was that it had to be quick and repeatable. Komatsu 830E haul trucks can nominally transport up to 8,000 tonnes of iron ore in a working shift, and so the potential economic impact of taking a single truck out of service for even a single, 12 hour shift is significant. For this reason, the amount of time allocated for testing was expected to be limited, providing the impetus for tests that were repeatable and able to be completed in a methodical manner quickly. To aid in this goal, repeated use of similar equipment was pursued.

### 3.3.1 Pavement Deflection

As discussed in Section 3.2, it was considered advantageous to complete in-situ measurements of pavement deflection. Firstly, it allows direct comparison to rolling resistance testing and secondly, it facilitates a targeted investigation of various pavement modelling techniques. In both instances, this alleviates uncertainties of the in-situ pavement response when utilising either scaled or idealised deflection tests or measurements of pavement stiffness, with the assumption of purely elastic response. For example, it is widely accepted in geotechnical practice that the zone of influence of a loaded footing is proportional to its width. Since haul truck tyre contact patches are vastly larger than that of a typical commercial vehicle, it was considered that any other test method would not be entirely representative. This is based on the fact that the same volume of pavement material would not be equivalently stressed within the test.

The mine's operating procedures dictate that no person shall approach closer than 50m to a running haul truck. Therefore, scaled tests (i.e. testing with a smaller vehicle) were an attractive alternative, as full access to the vehicle would be possible. However, the magnitude of deflection was likely to be much smaller,

meaning a much more sensitive measurement method would be required, and any extrapolation of the results would have to be based on the assumption of pure elastic pavement response. The latter is perhaps not inappropriate, but consider the discussion above, in conjunction with the fact that the effective pavement base-course depth was two metres thick. It was considered unlikely that a wheel load of a utility or small earthmoving plant would necessarily penetrate (induce elastic strains) to the sub-grade layer. Lastly, there is not an established method for measuring pavement surface deflection under a single wheel load. Benkelman beam tests (see MRWA WA_326.1) utilise a commercial vehicle with a dual-wheeled rear axle. For these reasons, a scaled test was not considered appropriate.

The second alternative for testing of pavement deflection was to utilise an accepted test of pavement stiffness. Two viable options were identified; falling weight deflectometer (FWD) and plate load tests (PLT). Typically, for use of the former, a reference contact stress (Jameson et al, 2009) is utilised in order to allow back-calculation of pavement stiffness with commercially available software. The net load applied during the test is 40kN, with an alternative being the Heavy Weight Deflectometer, which can typically apply a maximum 320 kN load (dynatest.com). It is evident that both methods apply significantly smaller loads than that of a Komatsu 830E (maximum wheel load 634kN; Komatsu, 2006). There were also uncertainties related to the use of this technology on an unsealed surface. PLT were an attractive option, as the plate size could be increased from the typical 152mm to 762mm ( ASTM, 2009) to represent the tyre contact area of a haul truck, alleviating concerns about a limited load penetration depth. The test could also be completed with repeated load applications (see test method D1195/D1195M-09, ASTM, 2009), providing some insight into the degree of elastic to plastic response of the pavement, and also providing an indication of any strain-hardening behaviour. However, if such a plate was utilised for the test, a load equal to that of the maximum wheel loads of a Komatsu 830E haul truck would need to be provided as a reaction force. The only way to provide such a large, mobile force would be to utilise a haul truck itself. Furthermore, geomechanics texts such as Knappett et al (2012), suggest the stress distribution under a rigid and flexible contact medium are not consistent, when applied to an unbound granular material. Thus, it was considered more appropriate to pursue a method that could measure the in-situ deflections under a haul truck tyre, rather than the deflection of an idealised loading via a steel plate. Some insight into the impact of modelling uniform contact stresses, as should be present under a rigid plate, could be gained by completing this test in

conjunction with measured deflection under a haul truck tyre. Safety concerns, with effectively jacking a haul truck in the field, and the financial cost of fabricating a suitable apparatus mean that unfortunately, PLT was not able to be completed.

As a result of the above investigative process, it was decided a method that could measure the deflection induced by a haul truck tyre should be developed. Firstly, it is important to note that the mine site had a rule in place that no person shall encroach closer than 50m to a running haul truck. This meant that the test method would benefit greatly from being able to be operated remotely, such that the test equipment could be set up away from the haul truck. An alternative was to have a procedure for mechanically isolating the truck in place (including having to place large wheel chocks), which would allow work close to the vehicle for test setup. This option was considered to be prohibitive from a timing point of view. Another issue that would need to be addressed is the fact that the diameter of the deflection bowl induced by a haul truck is unknown, and is also likely to be large and variable. Consequently, the equipment used to measure deflection needed to be placed outside the deflection bowl. This is a known complication of both deflectograph and Benkelman Beam testing (Jameson and Shackleton, 2009). As a result, a scaled-up version of the Benkelman Beam was considered possible, but the size would be such (initial linear-elastic FEA modelling indicated that a length up to 20m may be appropriate) that moving the device in the field would be difficult. As a result, the development of less labour intensive methods were pursued.

Adaptation of common surveying techniques appeared promising. For example, the precise levelling technique was considered. However, this would require a person to access between the truck's rear axle dual tyres and survey control/datum points to be set up on the site. The latter was not considered prohibitive as the mine site had a survey team working full-time at the mine. Conversely, personnel access between two haul truck tyres was physically difficult and not favoured from a personnel safety point of view. However, two more advanced surveying techniques were evident after considering the available survey technology.

Terrestrial laser scanning and photogrammetric methods are being rapidly developed for spatial monitoring of structures. Photogrammetric methods involve taking a series of photographs from several varied positions (generally at least eight), each with a reference scale within view (typically accurate to a micrometre). Post-processing algorithms can then be used to define the geometry of the structure. One short coming of the method in the context of this project was that

small targets (typically 32mm diameter circles of contrasting colour to their background) must be placed and captured in each photo. The relative position, and therefore distance between, these points is the output of the software's algorithm. The placement of targets was anticipated to be difficult. To overcome this issue, temporary raised pavement markers were constructed, where the reflective strip used to provide delineation of a traffic lane edge for a driver was removed and replaced with a 32mm diameter black adhesive tape (see Figure B.1, Appendix B). A large number of these targets were then planned to be placed in an array over the pavement, such that they could be placed before the truck reverses back over the array. This process was developed in preference to the procedure outlined above for isolating the truck to allow close access. Although this method was plausible, it suffered from two short-comings. Firstly, trials of fixing the pavement markers to an unsealed surface proved difficult, without having to nail each to the surface. Secondly, the accuracy able to be achieved with photographing from a range of even 10m appeared questionable after initial trials. Post-processing was completed with the iWitnessPRO software (iwitnessphoto.com). However, it was difficult to accurately define the centre of the targets using this software. The centre is automatically selected and can be manually relocated, but due many of the photos having been taken from low incident angle (less than 45 degrees), the targets appeared quite pixelated. As such, the selection of centre points for each target from visual inspection was considered a likely source of error. Considering the accuracy of pavement deflection would need to be determined to at least an accuracy of 1mm, it appeared the use of photogrammetric methods may not be suitable.

Lastly, the use of terrestrial laser scanning utilising the time of flight technique was investigated. The basis of this method is that a laser beam travels at a constant speed within a known medium, thus measuring the time for receipt of the reflected beam allows the relative distance between scanner and the object to be defined (Vosselman et al, 2010). When repeated a large number of times, the relative distance at discrete points between the scanner and an entire structure can be defined. This technology is able to be used in its simplest form when the laser scanner is placed in a fixed position, and the surrounding environment adapted. It involves placing targets (typically a minimum of four) at any point within the scanned view, these are then used as control points during registration of two or more scans. This principle was able to be combined with the theory of superposition, as applied in Benkelman Beam testing, for the measurement of pavement deflections. This process involved scanning the pavement area of interest with the truck in place and

repeated after the truck was removed from the area. The two scans were then combined (registered) and the difference in geometry of the two surfaces defined through post-processing with the Leica Cyclone 8.1.3 software (Leica Geosystems, 2014).

The utilisation of terrestrial laser scanning had several benefits over the other techniques discussed above. The scanner was able to be remotely operated via a 50m long Ethernet cable, meaning the truck could be moved into the desired location after the scanner was placed. Measurements could also be completed with use of the full-scale haul truck wheel loads. Scanning times were typically 10 minutes at a resolution of 10mm (i.e. the defined points within the scanned area were spaced on an orthogonal grid at 10mm intervals), which meant the test was quick and repeatable. The test also presented the best means to measure pavement curvature, as it would be coincidentally captured simply by extending the scan area to a sufficient offset from the wheel loads. An understanding of pavement curvature provides greater insight into the structural response of the haul road pavement and supporting sub-grade. In similar fashion, the interaction between adjacent wheel assemblies and axles was able to be estimated by mapping deflection between load locations. Load interaction is subject to significant debate with regards to pavement modelling and thus this data is valuable for testing the adequacy of various modelling methods (See Section 5.4.2). The scan data also allows one to measure the tyre contact patch geometry, providing insight into a critical modelling input commonly estimated for large off-the-highway radial tyres. Lastly, as discussed in proceeding sections, the technology also provided an effective means of acquiring a pavement alignment survey, including the quantification of roughness and texture.

Terrestrial laser scanning was trialled and developed prior to commencement of measurement on the mine site. Details of validation testing of laser scanning for the desired accuracy (0.5mm) is presented in Appendix B.

Further detail of the method, as applied within the testing phase of the project, along with details of the post-processing, is contained within Section 3.5.7.1.

### 3.3.2 Pavement Roughness

Pavement roughness is known to significantly influence the rolling resistance of highway vehicles, as discussed in Section 2.2.5. For this reason, it needed to be well defined for this project. Further, a single value quantifying roughness, such as

the IRI, was not preferable, as it may not provide sufficient insight into the nature of pavement surface defects that result in changes of rolling resistance. Each of the methods discussed below were considered with a view to simplifying the testing, with the benefit of applying an established and accepted test method. However, the majority of the methods suffer from an inability to distinguish between short and long wavelength roughness. The measure of roughness (specifically NAASRA counts or IRI) was developed with rider comfort in mind, and consequently may not be the best representation of vehicle response for a large, rigid haul truck.

The most simplistic means to define haul road roughness, with the added benefit of being directly related to a published rolling resistance function, is the RDS (Thompson et al, 2003). Such a measure is highly practical for the road owner, but suffers from subjectivity of the assessor. However, a visual inspection procedure does present an opportunity for the assessor to note the nature of surface defect, which may provide insight into how the design, construction or maintenance system may be optimised. Therefore, the RDS was adopted for the project. However, a more detailed method was also required to provide greater understanding of the rolling resistance generated from pavement response.

A conventional method for measuring roughness, which could be applied to capture the relative dynamic response of the haul truck, was an adaptation of the quarter-car model (Figure 3.2). Examples of this approach that may be adaptable to haul trucks include the Response-Type Road Roughness Measurement Systems (RTTMS) such as the NAASRA meter (Mclean et al, 1996). With such measures, the roughness is estimated from the measurement of relative movement between the rear axle and body of a vehicle, or from the response of the components shown in Figure 3.2. Although such a measure is somewhat attractive, it is predicated on the dynamic response of the vehicle, and thus was expected to be difficult to implement with a haul truck. It may have been possible to utilise a smaller vehicle such as a utility, as more advanced methods are now available employing systems installed on utility vehicles, as a result these were preferentially investigated.

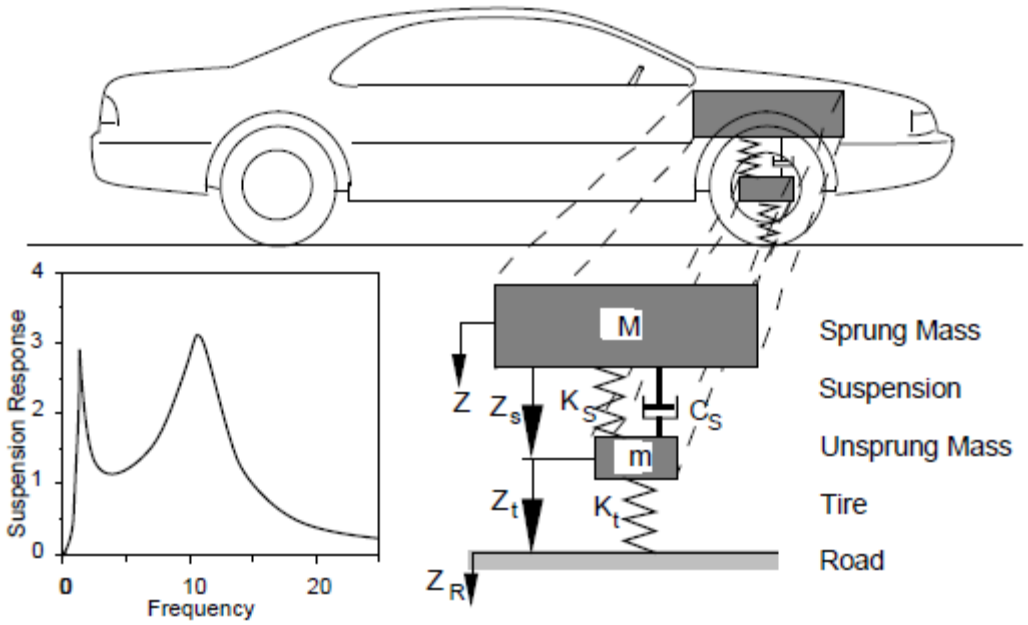


**Figure 3.2: The quarter-car model (Gillespie, 1992).**

One system that is fitted to a utility type vehicle for defining pavement roughness is the ARRB roughometer. As discussed above, this device is of the vehicle response type, however it utilises accelerometer measurement of axle movement to remove the uncertainties associated with individual vehicle response (ARRB Group, 2011). It was considered that this device could adequately define the pavement roughness of the haul road. Ultimately, it was not utilised due to development of the technique applying terrestrial laser scanning described below and in Section 3.5.6, but also due to limitations for utilising it to measure pavement texture (see Section 3.3.3).

Laser profilometer methods, such as that detailed in Austroads test method AG:AM/T001 (Austroads, 2007), are commonly used to define long sections of road pavement condition, whereby the output is IRI per unit measure (100m in the case of the test method referenced). As it was planned to utilise laser scanning to survey the pavement alignment, it was also investigated for the definition of pavement roughness. If a high resolution scan could be obtained, it would also provide the benefit of being subjected to detailed analysis after testing. The registration procedure available within the Leica Cyclone 8.1.3 software also meant that long sections of pavement could be scanned from multiple locations and the scans joined together for analysis.

Ultimately, the method of terrestrial laser scanning was adopted. A detailed description of the test and analysis method is contained within Section 3.5.6.

### 3.3.3 Pavement Texture

In much of the literature, pavement texture is contended to significantly impact rolling resistance, through generation of tyre hysteresis (see Section 2.2.5), although it is unclear if this relation extends to haul trucks. Further, haul truck tyres are vastly larger than those fitted to common commercial vehicles. Subsequently it is contended that a short-wavelength roughness could induce tyre and vehicle response in a haul truck analogous to that experienced by a commercial passenger vehicle in response to pavement megatexture. For this reason, it was considered advantageous to adopt a method of texture measurement that can be related directly to that of roughness from terrestrial laser scanning (see Section 3.3.2 and Section 3.5.6).

Pavement texture is most commonly measured via laser profilometer. However, concerns were raised by owners of such equipment when approached to complete testing for the unsealed pavements examined within this project. Feedback received indicated that measuring texture with sensitive equipment on rough pavements ultimately presents a risk to the integrity of the laser equipment, and thus it is generally avoided. For this reason, the measurement of pavement texture was trialled with the sand patch method, utilising Austroads test methodology AG:PT/T250. Attempts trialling this method proved troublesome, as the texture of the sections considered were (in the case of Section 2 and 3) very high, in contrast the AG:PT/T250 method only considers texture depth up to 6mm. It is possible an extrapolation from the method could be made, however it is not clear how much additional sand should be used for a given texture depth greater than 6mm, or if the standard cylinder used for spreading the sand would be appropriate for this task.

To overcome these issues the pavement texture was estimated from measurements taken from the alignment scans with a terrestrial laser scanner, as discussed in Section 3.3.2 and detailed in Section 3.5.6.

### 3.3.4 Rolling Resistance

An ability to accurately define the rolling resistance experienced by a haul truck was critical to the project. Several methods are available for defining rolling resistance

generally, however only the towed and coast down method have been applied to haul trucks previously and neither have a published test method.

The measurement of rolling resistance is often complicated by misinterpretation of rolling and driving resistance (see Section 2.2.1). The methods below generally relate to the measurement of driving resistance (except for cart methods), which in keeping with this report is also referred to as rolling resistance.

#### 3.3.4.1 Available Methods

Tannant et al (2001) describe a method for towing a haul truck with suitably powerful mine equipment in order to provide accurate results. The rolling resistance is calculated from the measurement of drawbar pull required to sustain constant motion of the truck. This is a novel way of measuring rolling resistance and is the basis for the initial scaled-down trials described in Section 3.3.4.2. Some shortcomings do exist for this method. The first is that a continuous monitoring of the load cell tension is required, which can be overcome with the use of a digital data logger. Further, the method assumes the tension in the sling used to pull the truck is consistent. For this to be valid the pavement rolling resistance must be assumed constant across the section, otherwise the truck would accelerate and decelerate, modifying the tension in the sling. Ideally the sling would be made of a relatively stiff material, which is at odds with commonly accepted methods of towing large vehicles, whereby a brittle material is avoided due to the release of significant stored energy should the sling fail. Although not insurmountable, these issues would need to be addressed for the use of this method for testing on-site.

Perhaps the most commonly used method to measure rolling resistance is the coast-down method. In this instance, the vehicle's deceleration is measured after the gearbox is disengaged at a defined vehicle speed (Hammarstrom et al, 2008). In simplistic versions, the distance travelled by the vehicle is measured and the back-calculated deceleration rate used to estimate the rolling resistance experienced by the vehicle. For this method to be applied, the test must be completed on a flat surface to remove uncertainty with acceleration or decelerations associated with road gradient. This method was pursued through trial testing described within Section 3.3.4.2, where the introduction of an accelerometer to log the deceleration rate was introduced in the second round of tests, in an attempt to increase accuracy and shorten the duration required to complete the test. This method also requires accurate measurement of vehicle's velocity at the commencement of coasting. Developing such a test method was an attractive option as there is a relatively large

amount of literature describing the implementation and analysis of such testing, as well as regression results relating pavement properties and rolling resistance for different sized vehicles. A comprehensive summary is provided in Sandberg (2011) and the reader is referred to this paper and Section 2.2 for further background.

Both methods discussed above require the vehicle in question to be able to be placed in neutral (in the case of coast-down tests, at speed) and safely towed. Unfortunately, many modern haul trucks, including the Komatsu 830E haul trucks available for use within this study, employ electronic drivetrain systems. A main diesel generator feeds a central inverter, which in turn powers the wheel hub motors fitted to the rear axle. The basis of such a system is efficiency and fewer mechanical components requiring regular maintenance (komatsu.com.au). However, it also means that the trucks cannot be placed into neutral at speed. They can be towed, however the mine operator only does so when all other options have been exhausted, for fear of causing damage to the wheel motors. This meant that the towed method was considered only a ‘last resort’ and the coast-down method would not be possible.

As discussed previously, in Section 3.2, cart methods were not considered appropriate for rolling resistance testing. It is the author’s opinion that for similar applications to this project, such methods require thorough validation for specific vehicles, which in turn requires full scale testing. That is not to say such methods cannot provide benefit as a monitoring and asset management tool for haul roads, as described in Tannant et al (2001).

Although applied in a limited number of studies, and not with electric wheel motors, the steady state torque method appeared to present an opportunity to overcome the issues discussed above. Jamieson et al (2002) present the case of a small commercial truck being used for testing over various surfaces, where the driving torque is continuously measured. In conjunction with measurement of the wind speed and direction, this allows the rolling resistance (more specifically the driving resistance) to be calculated at each point of the test. The Komatsu 830E haul trucks available for this study are fitted with on-board monitoring software in-built to the GE Invertex electric drive system. This system can monitor a large number of truck sensors and data loggers at any time, which includes main inverter power output and also individual wheel motor torque output. Both can be utilised to calculate the rolling resistance. However, the former will include accessory and mechanical losses, whereas the latter is the direct torque applied to the rear axle dual wheel

assemblies to produce truck motion. Therefore, with the appropriate parameters being logged by the GE Invertex software, the rolling resistance could be determined when the truck is driven in a steady state. Of course, this method suffers from the possibility of the truck being driven inconsistently in the form of throttle or steering changes. For this reason, the data was to be closely analysed with several layers of screening to remove perceived inconsistencies, as detailed in Section 3.5.8.

#### 3.3.4.2 Trials

As a result of the literature search and desktop study of different rolling resistance test methods, trials were undertaken. All trials in the proceeding section were undertaken prior to it being known that a haul truck with a suitable mechanical gearbox would not be available for testing. Both trials focussed on the testing of rolling resistance (more accurately driving resistance) of a Nissan Navara utility, with a net weight of 2060kg (including driver).

An agricultural tractor was used to tow the utility in the initial trial. The general test setup for the second trial (identical set up to the first, only a car instead of a tractor was used as the towing vehicle) can be seen in Figure 3.3. A tension load cell was fabricated and calibrated for the purpose of this test, which can be seen in operating condition in Figure 3.4. Data was logged by a P3 strain indicator and recorder (Vishay Precision Group). Tension measurements were taken at a frequency of one second. The standard deviation of the between sample group's recorded mean tension is reported, along with the mean in Table 3.1. This is included to provide an indication of test accuracy. The coast-down tests were conducted with the distance and time to stopping measured, in order to estimate the net deceleration rate of the utility via Newton's second equation of motion. Note that a multi-link chain was used as the sling in the initial trial and an elastic nylon recovery strap was used to tow the utility for the second trial. The unsealed track used for the initial trial tests is shown in Figure 3.5 and was composed of dense sand, which had been compacted by decades of trafficking by farm equipment.

**Figure 3.3: Photo of towed rolling resistance measurement trial test setup.**

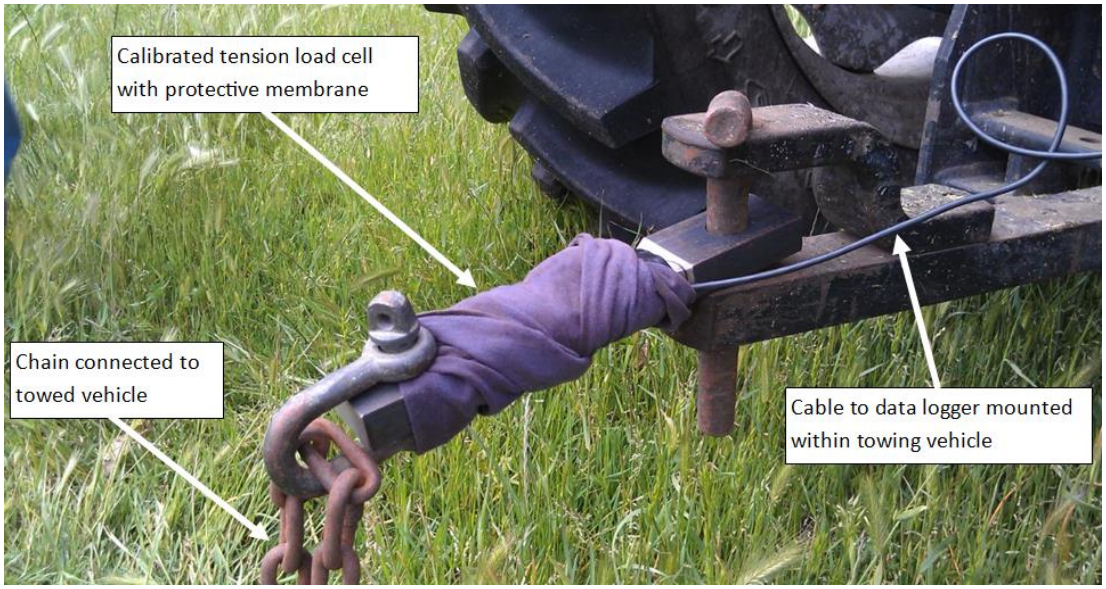


**Figure 3.4: Annotated photo of load cell setup used in towed rolling resistance measurement trials.**

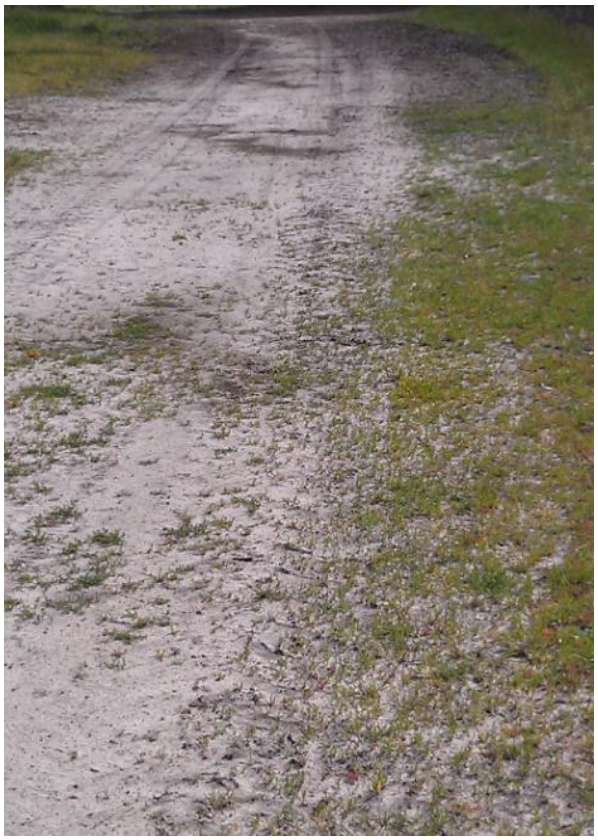

**Figure 3.5: Track used for initial towed and coast-down rolling resistance testing trials.**

Table 3.1 presents the results for the average rolling resistance of towed and coast-down tests from the initial trial. Note that the utility had a 780kg weight applied for the final two coast down tests included at the bottom of the table. A reasonable level of correlation can be seen between the respective test methods. However, the towing trial presented an increase in rolling resistance with speed, whereas the cost-down test showed the opposite trend, for unloaded and loaded conditions. The addition of a load results in an increase in rolling resistance at both 10 and 20km/h. These initial results were encouraging. As a coast-down test was observed to be much easier to execute, a second trial was planned, with accelerometer logging of the vehicle deceleration instead of measuring the distance for the vehicle to stop from a designated speed. The track used for the second trial was composed of dense lateritic sandy gravel, as presented in Figure 3.6.

**Table 3.1: Rolling resistance test method trial results – towed and coast-down with distance measurement.**

| Speed | Method | Weight | RR (%) | St. Dev |
|---|---|---|---|---|
| 10 | Tow | 2060 | 3.5 | 0.29 |
| 20 | Tow | 2060 | 3.9 | 0.13 |
| 10 | Coast | 2060 | 4.6 | 0.29 |
| 20 | Coast | 2060 | 4.3 | 0.40 |
| 10 | Coast | 2840 | 5.7 | 0.36 |
| 20 | Coast | 2840 | 4.7 | 0.19 |

The test results from the second trial are presented in Table 3.2. Once again, this test showed some encouraging results at a test speed of 10km/h. However, correlation was poor at 20km/h. Further, it appeared that the accelerometers in-built to the HTC cellular mobile phone and Asus tablet were rather insensitive to the rate of deceleration. The results between 10 and 20km/h tests are very similar. This issue may have been due to the software application used (which was sourced at no cost from the 'Google Play' application store), or the accelerometers themselves may have been inappropriate for the task.

Overall, the rolling resistance was found to be lower than that found during the initial trial. This may be attributed to having been completed on a dense, very even gravel surface as opposed to the sandy track used in the initial trials. The standard deviation of the towed test results were similar to the initial trial, suggesting some repeatability of the method. Both trials presented a relatively low rolling resistance if compared to Table 2.5.

**Figure 3.6: Track used for second rolling resistance test trial.**

**Table 3.2: Rolling resistance results from second test trial (coast-down with accelerometer and towed).**

| | RRC (%) | | | |
|---|---|---|---|---|
| Vehicle Speed (km/h) | 10 | | 20 | |
| | Mean | Standard Deviation | Mean | Standard Deviation |
| Coast-down Accelerometer - HTC | 2.32 | 0.11 | 2.33 | 0.07 |
| Coast-down Accelerometer - Asus | 2.99 | 0.21 | 3.00 | 0.04 |
| Towed | 2.87 | 0.21 | 1.27 | 0.17 |

Note, the coast-down method (distance measurement instead of logging of deceleration rate) was also used, as above, to complete rolling resistance testing on a soft soil. The condition of the soil, before and after coast-down testing can be seen in Figure 3.7. The average rolling resistance in this soil, when tested at 10, 20 and 30km/h was 12.5% with a standard deviation of 0.5%. This finding was in keeping with the results reported in Table 2.5 for muddy rutted material.

**Figure 3.7: Coast-down test site, muddy rutted material (prior to testing, left and after testing, right).**

Both the towed and coast-down method for testing rolling resistance appeared potential solutions for testing haul truck rolling resistance. Each method had been reported in the literature for testing with haul trucks, Tannant et al (2001) for towed testing and Thompson et al (2003) for the coast-down test. This data would present a point of reference and comparison for the results of the testing completed for this project. Despite this fact, a simpler test was still pursued and ultimately adopted. It is the author's opinion that the logging of wheel motor torque provides an opportunity for monitoring of rolling resistance of haul roads during operation (especially with the advent of autonomous haul trucks). Therefore, the need to move away from the methods trialled above was viewed as a positive development for the project and for mining practice in the future.

## 3.4 Statistical Analysis Techniques

Some common statistical analysis techniques have been applied within the interpretation and analysis of in-situ and numerical test data. Each utilised method is detailed in the following, to provide the arithmetic form of the test and key

assumptions. For ease of calculations, all statistical analyses were completed utilising the Microsoft Excel 2010 software.

### 3.4.1 Chi-Square Test

The chi-square test can be used to indicate the goodness-of-fit between an observed sample and a defined cumulative distribution function (Dickinson Gibbons et al, 2003).

The chi-square test has been applied in this project to determine if a sample follows a normal distribution. In order to commence the test, the sample is divided into 'bins' of equal magnitude and the frequency of results within each bin tallied. The null hypothesis is that the expected frequencies are similar to those observed, thus the distribution closely approximates normality. Within this project the expected frequencies are calculated via a normal distribution, with upper and lower limits given by the upper and lower bound of each bin, and utilising the observed sample's mean and standard deviation. Therefore if the chi-square statistic, calculated by Equation 3.2, is less than the critical chi-square value (calculated via Equation 3.1, at a level of significance of 0.05), the observed data is considered to follow a normal distribution. Note that the degrees of freedom ($\upsilon$) involved in the test are equal to $N$-1, where population parameters are to be estimated from the observed sample.

**Equation 3.1: Chi-square distribution (Spiegel, 2011).**

$$\chi^2 = \frac{N.s^2}{\sigma^2} = \frac{(X_1 - \bar{X})^2 + (X_2 - \bar{X})^2 + \cdots + (X_N - \bar{X})^2}{\sigma^2}$$

Where:

$\chi^2$ is the chi-square statistic

$N$ is the sample size

$s$ is the sample standard deviation

$\sigma$ is the population's standard deviation

$X_N$ is the sample mean

$\bar{X}$ is the mean of sample size $N$

**Equation 3.2: Chi-square statistic for goodness-of-fit tests (Spiegel, 2011).**

$$\chi^2 = \sum_j \frac{(o_j - e_j)^2}{e_j}$$

Where:

$\chi^2$ is the chi-square statistic

$o_j$ is the observed frequency

$e_j$ is the expected frequency

### 3.4.2 One-Way ANOVA

Analysis of variance (ANOVA) tests determine if the means of multiple samples vary significantly (Stamatis, 2012). ANOVA compares the variation within and between samples (often referred to as 'treatments') to calculate the F-statistic (Spiegel, 2011), which in turn can be compared to a critical value to make a judgement on the null hypothesis. The null hypothesis is that the mean of all groups in the analysis are equal. The alternate hypothesis is that they are not equal. This test is used in the current project to consider if two or more test samples have originated from the same test case, and therefore should be considered as a single population. Where this is shown to be true for two or more samples, they are used to calculate the mean rolling resistance for a given pavement section and test case.

The assumptions applied within an ANOVA analysis are provided by Stamatis (2012):

1. the population is normally distributed
2. variances are equal between samples
3. three or more independent groups are applied in the analysis

4. samples are drawn randomly from the population
5. measurement should be at least at the interval level.

**Table 3.3: Computational procedure for one-way ANOVA (Stamatis, 2012.**

| Source of Variation | Sum of Squares (SS) | Degrees of Freedom (df) | Mean Square (MS) | *F* |
|---|---|---|---|---|
| Between groups | $\frac{(\sum x_1)^2}{n_1}+\frac{(\sum x_2)^2}{n_2}+\ldots$ $+\frac{(\sum x_k)^2}{n_k}-\frac{(\sum x)^2}{N}$ | $K-1$ | $\frac{\text{Between SS}}{\text{Between df}}$ | $\frac{\text{MS Between}}{\text{MS Within}}$ |
| Within groups | (Total SS) – Between SS | (Total df) – (Between df) or $N-k$ | $\frac{\text{SS Within}}{\text{df Within}}$ | |
| Total | $\sum x^2-\frac{(\sum x)^2}{N}$ | $N-1$ | | |

The following notation is applicable to Table 3.3:

$x_1$, $x_2$… are the sample mean values

$n_1$, $n_2$… are the sample sizes

$K$ is the number of samples

$N$ is the population size

Note that in this project, ANOVA has been applied to two groups in several cases. In these cases, a t-test (see Section 3.4.3) has been subsequently completed to confirm the result.

### 3.4.3 T-test

The t-test (often referred to as ‘Student’s t-test’) may be applied for testing of equal means when the distribution of a random sample is not normally distributed (Czaplicki, 2014). Student’s probability distribution, like a normal distribution, is symmetrical about a statistic of zero, with the density function and therefore the

shape of the curve varying with degrees of freedom (r in Figure 3.8). If the t-statistic is found to be less than the probability calculated for a given level of significance and degrees of freedom (area under relevant curve in Figure 3.8 or calculated via Equation 3.9), then the null hypothesis may be accepted.

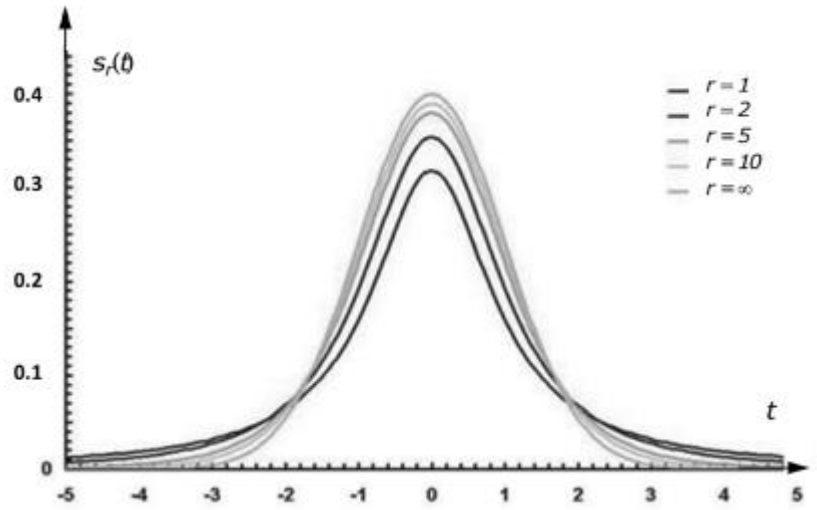


**Figure 3.8: Student's t probability distribution (Czaplicki, 2014).**

The t-test is used in the current study to confirm the result of hypothesis testing with one-way ANOVA (see Section 3.4.2), when only two samples are found to have equal means.

The t-test, assuming unequal variance, is detailed below (Equation 3.3 to Equation 3.8). Note that when using this form of analysis, it is preferable for the sample sizes to be equal (Stamatis, 2012). Many authors provide more detailed functions for the calculations of the t statistic, which have not been reproduced here.

Firstly, the sample and population means must be calculated via Equation 3.3 and Equation 3.4.

**Equation 3.3: Sample mean for calculation of the t statistic (Stamatis, 2012)**

$$u_i = x_{1i} - x_{2i}\left(\frac{n_1}{n_2}\right)^{1/2}$$

Where:

$u_i$ is the mean of sample i

$x_{1i}$ is a point from sample 1

$x_{2i}$ is a point from sample 2

$n_1$ is the size of sample 1

$n_2$ is the size of sample 2

**Equation 3.4: Population mean for calculation of the t statistic (Stamatis, 2012).**

$$\bar{u} = \frac{1}{n_1}\sum_{i=1}^{n_1} u_i$$

Where:

$\bar{u}$ is the population mean

$i$ = 1,2,3,… $n_1$

Now, the t statistic can be calculated from Equation 3.5:

**Equation 3.5: The t statistic (Stamatis, 2012).**

$$t = \frac{\bar{x}_1 - \bar{x}_2}{\sqrt{\frac{Q}{n_1^2(n_1 - 1)}}}$$

Where:

$t$ is the t statistic

$Q$ is defined in Equation 3.6

$\bar{x}_1$ is defined in Equation 3.7

$\bar{x}_2$ is defined in Equation 3.8

**Equation 3.6: Factor Q, for calculation of the t statistic (Stamatis, 2012).**

$$Q = n_1 \sum_{i=1}^{n_1} (u_i - \bar{u})^2 = n_1 \sum_{i=1}^{n_1} u_i^2 - \left( \sum_{i=1}^{n_i} u_i \right)^2$$

**Equation 3.7 (Stamatis, 2012).**

$$\bar{x}_1 = \frac{1}{n_1} \sum_{i=1}^{n_1} x_{1i}$$

**Equation 3.8 (Stamatis, 2012).**

$$\bar{x}_2 = \frac{1}{n_2}\sum_{i=1}^{n_2} x_{2i}$$

For use in hypothesis testing (equality of two sample means for this project) the critical t value is calculated from Student's t-distribution (Equation 3.9). It is worth noting that this distribution closely approximates a normal distribution for large samples (>30) (Spiegel, 2011). The degrees of freedom ($\nu$) for this distribution is given by $N$-1.

**Equation 3.9: t distribution (Spiegel, 2011).**

$$t = \frac{\bar{X} - u}{\left(\frac{\hat{s}}{\sqrt{N}}\right)}$$

Where:

$t$ is the t statistic

$\bar{X}$ is the sample mean

$u$ is the population mean

$\hat{s}$ is the sample standard deviation

$N$ is the sample size

### 3.4.4 Kruskal-Wallis

The Kruskal-Wallis is a nonparametric test for analysis of variance, which can test the equality of medians (null hypothesis) among groups, based on the sum of ranks (Czaplicki, 2014). Results of the Kruskal-Wallis test closely resemble a chi-square distribution for sample sizes larger than five (Spiegel, 2011). It requires the data within all samples to be ranked in ascending order, such that if adjacent ranks are well distributed between samples, the sum of ranks would be divided proportionately (Dickson Gibbons et al, 2003). This is the basis of the calculation of the H statistic, shown in Equation 3.10. Nonparametric tests do not rely upon assumptions of data

complying with any specific distribution or equal variances between samples, and therefore provide an alternative for hypothesis testing, where assumptions of ANOVA fail to be met. Where the null hypothesis of the Kruskal-Wallis test is found to be acceptable, the sample data can be considered to have originated from the same population (Czaplicki, 2014). In the context of the current study, this means the samples inputted to a successful test may be used together to calculate the mean rolling resistance value for a given pavement section and test case.

**Equation 3.10: H statistic for the Kruskal-Wallis test (Spiegel, 2011).**

$$H = \frac{12}{N(N+1)} \sum_{j=1}^{k} \frac{R_j^2}{N_j} - 3(N+1)$$

Where:

$H$ is the H statistic

$N$ is sum of ranks (sum of size of k samples)

$k$ is the number of samples

$R_j$ is the sum of ranks for sample j

$N_j$ is the size of sample j

### 3.4.5 Pearson Product-Moment Correlation Coefficient

The product-moment correlation coefficient is commonly used to test the linear correlation between two samples (Spiegel, 2011). It is based upon how far the samples lay from a regression line of best-fit. It ranges from negative one (a strong inverse correlation) to one (a strong positive correlation) (Graham, 2013). Correlation coefficient, r, may be calculated via Equation 3.11. The issue of sample size is critical for the correlation coefficient and for this reason reporting of its value

should be accompanied by a level of significance. This can be sourced from Table 3.4, with the degrees of freedom being equal to the sample size minus one.

**Equation 3.11: Pearson's sample coefficient of correlation (Stamatis, 2012).**

$$r = \frac{\sum XY - n\overline{XY}}{\sqrt{(\sum X^2 - n\bar{X}^2)(\sum Y^2 - n\bar{Y}^2)}}$$

Where:

$r$ is Pearson's sample coefficient of correlation (dimensionless)

$X$ are observed values of the first independent variable

$Y$ are observed values of the second independent variable

$n$ is the sample size

$\bar{X}$ is the mean of the first independent variable

$\bar{Y}$ is the mean of the second independent variable

**Table 3.4: Pearson correlation coefficient levels of significance (adapted from the University of New England, 2015).**

| | Level of Significance for two-tailed test | | | |
|---|---|---|---|---|
| Degrees of Freedom | 0.1 | 0.05 | 0.02 | 0.01 |
| 1 | 0.988 | 0.997 | 0.9995 | 0.9999 |
| 2 | 0.9 | 0.95 | 0.98 | 0.99 |
| 3 | 0.805 | 0.878 | 0.934 | 0.959 |
| 4 | 0.729 | 0.811 | 0.882 | 0.917 |
| 5 | 0.669 | 0.754 | 0.833 | 0.874 |

### 3.4.6 Method of Least Squares Regression

The method of least squares derives a linear equation of best-fit for a dependent variable, given a sample of corresponding independent variables. The general equation of the regression line is given by Equation 3.12, with the gradient conveniently calculated by Equation 3.13.

**Equation 3.12: Linear form of equation produced by least-squares regression (Graham, 2013).**

$$\bar{Y} = a + b\bar{X}$$

**Equation 3.13: Regression equation for 'b', least squares method (Graham, 2013).**

$$b = \frac{n\sum \bar{X}\bar{Y} - \sum \bar{X}\sum \bar{Y}}{n\sum \bar{X}^2 - (\sum \bar{X})^2}$$

Where:

$n$ is the sample size

$a$ is the regression line gradient

$b$ is the regression line intercept

$\bar{Y}$ is the dependent variable

$\bar{X}$ is the independent variable

The coefficient of determination for the regression is then commonly calculated through analysis of the regression equation and original data, via Equation 3.14.

This is effectively the ratio of explained variation to unexplained variation (Spiegel, 2011) and will vary from zero (all variation unexplained) to one (all variation explained).

**Equation 3.14: Coefficient of determination (Spiegel, 2011).**

$$r^2 = \frac{\sum(Y_{est} - \bar{Y})^2}{\sum(Y - \bar{Y})^2}$$

Where:

$r^2$ is the coefficient of determination

$Y_{est}$ is the dependent variable estimated by the regression equation

$\bar{Y}$ is the sample mean

$Y$ is the sample data

The level of significance can then be determined taking the square root of the calculated coefficient of determination to determine the correlation coefficient, and comparing with the values stated in Table 3.4.

## 3.5 In-Situ Testing Method and Analysis

In-situ testing was completed at a Rio Tinto operated mine site in Western Australia's Pilbara region over three days between the 24th and 26th of January, 2014.

### 3.5.1 Site Selection

A site representative of common haul roads was sought for in-situ testing. A mine waste dump was ultimately selected as some control over the stratigraphy of the site was possible, due to knowledge of the material placed in subsequent lifts forming the dump. This was considered valuable, as it was not anticipated any invasive test

for definition of substructure layers, such as borehole or Cone Penetration Test (CPT), would be possible due to financial constraints. From discussion with mine planners, it was evident that the material present at the surface of the dump was representative of that placed below it to a significant depth. In total the waste dump was approximately 40m thick at the time of testing. It was composed of coarse clayey or silty gravels with large cobbles consisting of boulders and broken blasted fragments of Banded Iron Formation (BIF). This structure is typical of waste dumps throughout iron ore mines of the Pilbara region in Western Australia.

With regard to rolling resistance testing, this provided confidence that variation of results along a pavement section was not due to significant changes in sub-surface stiffness. Therefore, it is effectively assumed that pavement deflection was equal along each pavement section.

For pavement modelling, this meant that the characterisation of the sub-grade could be made with relative confidence. The parameter that would have provided the greatest additional benefit was the in-situ density of the waste dump material. From the author's experience, it was known that density was a highly variable parameter for truck-dumped soil, with compaction by means of trafficking by haul truck and bull-dozer. The completion of large-scale density tests was not pursued, as it was not considered that it would provide significant benefit in estimating the elastic properties of the sub-grade for modelling purposes. This assumption was somewhat validated by the consistency of deflections between the two deflection test sites on Sections 1 and 2 (see Section 4.4).

### 3.5.2 Site Layout

There was constraint placed by mine operations on access to many areas of the mine site and availability of haul trucks for testing. Therefore it was decided to select a site that would allow for an efficient circuit to be followed for testing. This was set atop a very large waste dump that was essentially flat and comprised a total of 38-41 metres of mine waste fill, placed in approximately 2m thick layers and compacted by means of trafficking by haul trucks and bulldozers. This methodology is common industry practice for construction of waste dumps, haul roads and land bridges and thus was considered a suitably representative site. Three sections were investigated in detail, including testing for deflection and roughness. Figure 2.2 shows the layout of the site, including notes for the location of deflection tests, the aerial photograph was taken approximately two months prior to the testing date. Note that the

abbreviation ‘St.’ refers to station numbers where deflection tests were completed. The abbreviation ‘Ch.’ designates the chainage of each section (m) with the zero chainage was chosen as the starting point of testing completed in an anti-clockwise circuit.

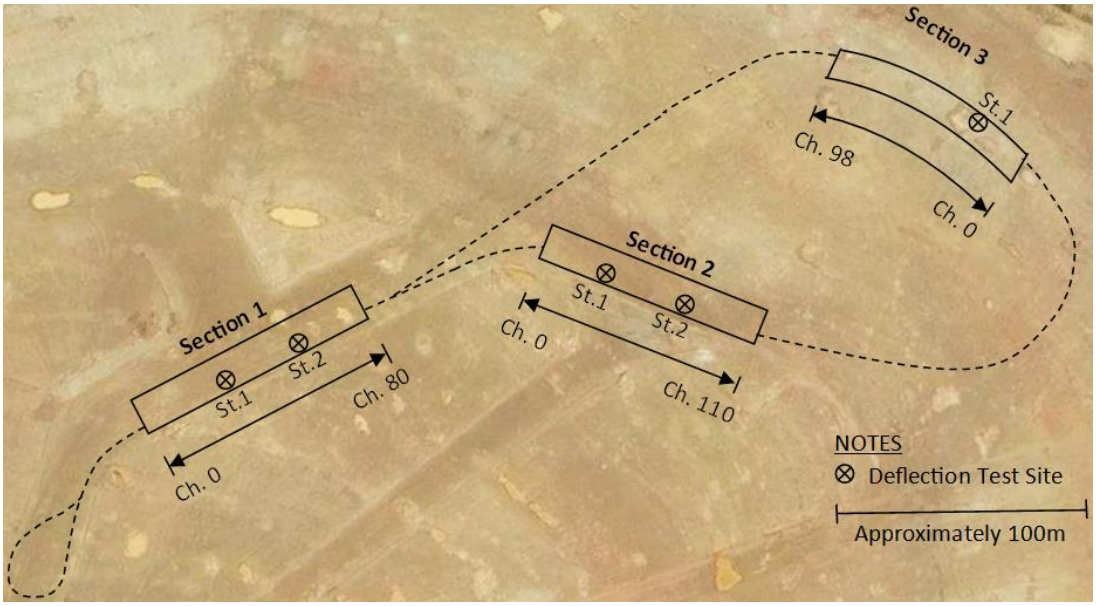


**Figure 3.9: Site layout and test sites (aerial photograph not taken at date of testing).**

Photos of each of the three sections are presented in Figure 3.10, Figure 3.11 and Figure 3.12.

**Figure 3.10: Section 1, looking from chainage 80m back to zero.**

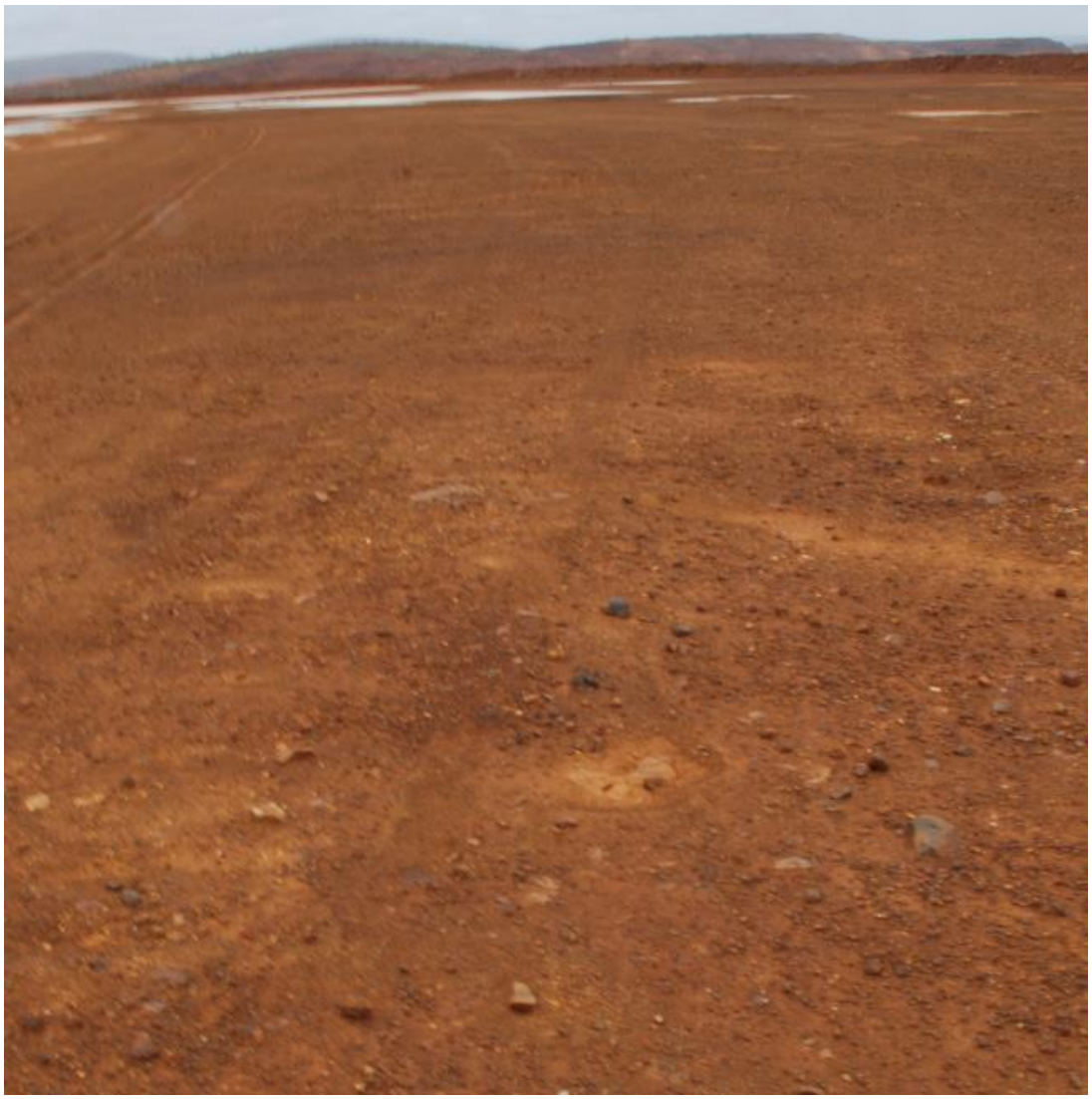

**Figure 3.11: Section 2, looking from chainage 110m towards zero.**

**Figure 3.12: Section 3, looking from chainage 98m back to zero.**

### 3.5.3 Ambient Conditions

Ambient conditions were taken from the Bureau of Meteorology website for the region over the dates of testing. It was advised by the mine operator, based on previous continuous on-board monitoring of a sensor fitted within a tyre on the majority of the haul trucks on the site, that tyre temperature did not show very significant variation with ambient temperature and hence this was not considered a critical parameter.

#### 3.5.3.1 Wind Speed

Wind speed was measured with a VelociCalc Rotating Vane Anemometer. The accuracy of this instrument is 0.01 m/s and thus more than exceeds the requirements of wind velocity for this project. This wind speeds were taken before

and after each set of testing (comprising three completed circuits) from the access platform to the haul truck, which means the measurements were taken near to the maximum height of the vehicle.

### 3.5.4 Haul Truck Description

The haul truck utilised for testing was a Komatsu 830E AC electric drive, fitted with 40.00R57 tyres. The precise unladen weight it not known, but only minor additions (including the two passengers on-board during rolling resistance testing) had been made and the published value of 164.2 tonne (Komatsu, 2006) was utilised for this project. The payload was measured by on-board load cells to be 220 tonne, with the accuracy of this equipment known to be relatively high as it is used to monitor mine production, which is weighed at multiple other points between dumping and loading onto ships at the export port. As is common with off-the-highway earthmoving haulage equipment the truck was fitted with dual-wheel assemblies on the rear axle. Weight distribution is shown in Table 3.5, for an unloaded and loaded Komatsu 830E haul truck.

#### 3.5.4.1 Tyre Pressure

Tyre pressures were electronically monitored by the mine operator using a continuous on-board monitoring system. This facility was utilised for this project to confirm tyre pressures during testing, which were observed to remain very consistent once warmed through the driving of the truck to the mine waste dump location for testing.

### 3.5.5 Pavement Texture

Pavement texture testing was completed by means of terrestrial laser scanning, as detailed in Section 3.3.4. To define texture from this testing, 1m radius circular sections were chosen at three random locations along each pavement section (within the wheel paths). Generally these locations were nearer the centre of the section as the scans are of higher resolution in these locations due to being in closer proximity to the position of the laser scanner. A 1m radius circle was chosen to replicate the gross contact area of a dual wheel assembly of a Komatsu 830 haul truck with 40.00R57 tyres fitted (as utilised in testing), which resulted in each test

location being represented by an average of 315 scanned points. The selected point cloud data generated from the scans was then exported to Microsoft Excel, where texture was estimated as twice the standard deviation of measured elevations for each section. This value was selected to capture the deviations above and below the 'average' plane of elevations within the selected sections obtained for the test. All results for each pavement section were then averaged to define an estimated texture depth.

This method for definition of pavement texture is considered to interface well with the low sensitivity of the method used to define pavement roughness, with the shortest moving average wavelength being 0.5m long. The basis for this decision is Figure 2.12, where 0.5m is presented as the boundary between the two surface properties. Therefore in simple terms there is some overlap of the two measures. However this was deemed necessary, as it was considered appropriate to consider texture within the extent of a tyre contact patch to truly represent surface features that could affect losses within a tyre. The selection of pavement roughness wavelength was based upon existing measures and thus it was considered appropriate to maintain these bounds. It is not considered that there is significant duplication of results between the 0.5m wavelength roughness and texture results. Lastly, note that both measures are not at any point utilised concurrently for modelling purposes and consequently it is not possible the effect of texture roughness within the 0.5-1.0m wavelength range can be over-stated in any larger effects such as rolling resistance estimates.

Although this test method is non-standard and cannot consider microtexture or even potentially shorter wavelength macrotexture it is considered a suitable estimation of pavement texture for an unsealed pavement being trafficked by large vehicles. Difficulty with defining texture of unsealed pavement surfaces is known to be problematic and hence models such at the HDM-4 omit it from VOC estimations on such pavement surfaces. Utilising data from the adopted method for estimation of magnitudes of rolling resistance and ultimately VOC has inherent inaccuracies, as no empirical method has been developed with texture definition in this way. The intent of defining texture was primarily to allow subjective assessment of whether it has a significant effect on rolling resistance, when compared to levels of pavement roughness and deflection. Therefore the method adopted for defining pavement texture is considered adequate for this purpose.

### 3.5.6 Pavement Roughness

The following describes how pavement roughness was defined for the study.

#### 3.5.6.1 Site Data Collection - Terrestrial Laser Scanning

Pavement roughness was measured by means of a Leica C10 terrestrial laser scanning of each pavement section.. The laser scanner was placed at the centre of the pavement section and set to scan the entire section from one fixed location. To achieve a sufficient point-cloud density (scan resolution) at the extremities of each pavement section, the tri-pod supporting the scanner was extended to its full height, approximately 2.4m from ground level to the laser level. The resolution of the scan (orthogonal distance between data points) was set to 10mm, which resulted in a 1-2 hour scan time for each pavement section.

Recorded scan data was then exported to Microsoft Excel to determine the variance of pavement surface elevation within each wheel track  Following the data analysis detailed in Section, 3.5.6.2, roughness was expressed in terms of average standard deviation, calculated from moving averages of varying lengths in parallel with the pavement centreline. The benefit of this approach is that it allows a thorough analysis to be made, whereby roughness of differing wavelength can be evaluated for impacts on rolling resistance.

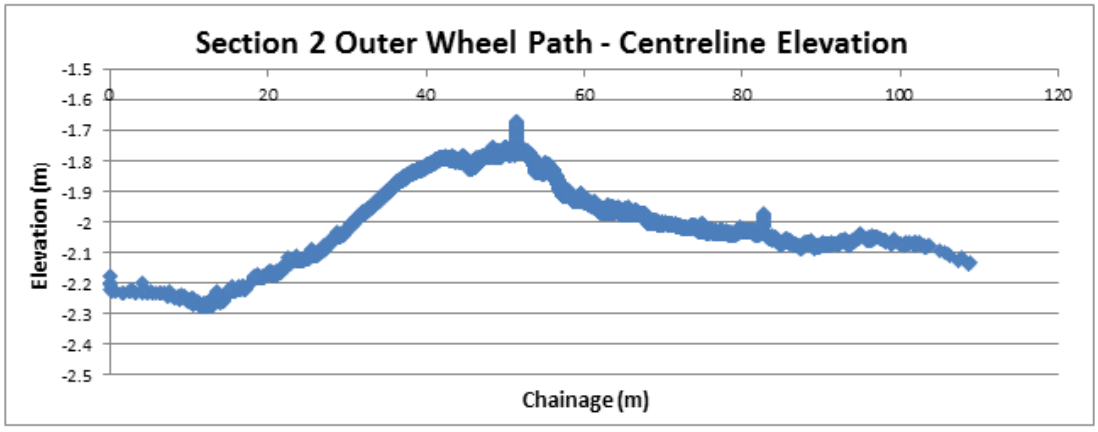


**Figure 3.13: Example result for wheel path elevation data.**

Despite the shortcomings alluded to above, the International Roughness Index (IRI) was also approximated from the scan data. This allowed input into existing rolling resistance models that allowed comparison of various factors.

#### 3.5.6.2 Analysis of Data

Registration (joining) of pavement scans was not required, as a single scan was able to capture the entire section in all instances. Leica Cyclone 8.1.3 software was then used to select the points comprising each wheel path, with this data then being exported to Microsoft Excel for statistical analysis. Wheel paths for a 40.00R57 tyre are approximately 1.1m wide (goodyearotr.com), however a section of 100mm width was selected at the centre of the wheel paths. This was a necessary refinement due to limitations in the volume of data that can be accommodated by a single Microsoft Excel spread sheet.

To define pavement roughness the surface elevation standard deviation was calculated over differing moving averages (longitudinally along the wheel path centreline). This allowed comparison with instantaneous rolling resistance results to define the nature/wavelength roughness that impacts haul truck performance. The moving averages selected were 0.5m, generally considered the boundary between wavelengths constituting megatexture and roughness (Mclean et al, 1996), 1m, 5m, 10m and 20m. Longer wavelengths were not considered reliable due to the nature of some sets of approximate steady-state rolling resistance data being only 50m in length (see Section 3.5.8.2). Each wheel path was investigated separately for each wavelength moving average, the average of both wheel paths was then calculated to define the mean standard deviation for each moving average. However the difference of elevation/roughness between wheel paths at equivalent chainages was also recorded and presented graphically as it was suspected it could be a source of rolling resistance.

The pavement IRI was able to be approximated by means of Equation 3.15. This model has been developed for roughness with a spatial frequency of 0.01 to 5 cycles per metre and has been found to correlate well with IRI and counts measured with the UK high-speed road monitor reasonably well (Mclean et al, 1996). Utilising a single wheel path to measure and define roughness is common practice (Gillespie, 1992). However it was decided to utilise an averaging of the two wheel paths in this study to account for inconsistency of the road surface that likely arises from

construction with large equipment only and the absence of any quality assurance survey.

**Equation 3.15: Approximate calculation of IRI from variance from three meter moving average (Mclean et al, 1996).**

$$IRI = 0.4 + 1.9(VAR_3)^{0.5}$$

Where:

$VAR_3$ is the variance of pavement surface elevation, over a 3m moving average wavelength.

Note that the measure of IRI in Equation 3.15 considers the quarter-car model, discussed in Section 2.2.5 and thus does not describe the vehicle response or rider comfort experienced by an occupant in a large rigid dump truck. However its inclusion was considered beneficial to allow comparison with pavements described in the literature, as this is the accepted 'standard' measure for pavement roughness.

#### 3.5.6.3 Roughness Defect Score

Each section of road was also assessed using the Roughness Defect Score described in Section 2.2.5. This methodology has been developed specifically for haul roads and thus all scoring was carried out in adherence to the guidance supplied by Thompson (2011). As with IRI, this was incorporated as it allows a better understanding of both similar pavements reported in the literature and also is used as a dependant variable within a relevant rolling resistance model (see Section 3.5.8.3).

### 3.5.7 Pavement Deflection

The process undertaken to measure and analyse pavement deflection under static wheel loads of a Komatsu 830E haul truck is presented below.

#### 3.5.7.1 Site Deflection Testing

The measurement of pavement deflection was completed using a Leica C10 terrestrial laser scanner. There is no precedent for this application of the technology, thus the procedure used was itself subject to development and testing. A test report of assurance testing is contained within Appendix B – Terrestrial Laser Scanner Assurance Test Report. Measurement involved defining of surface displacement between two scans taken around the area of pavement contained in between and around the dual-wheel assembly, with and without the truck parked in the area of interest. The physical setup of the test is presented in Figure 3.14. Note that the distance between the truck and scanner setup is somewhat deceiving in this photo, as the scanner is offset from the longitudinal axis of the truck, making the two objects appear closer than they actually are.

**Figure 3.14: Setup of pavement deflection testing.**

The procedure for testing is outlined below:

1. Leica C10 Scanstation is setup with appropriate targets (minimum 5) on the pavement surface, to be remotely operated to allow for compliance with the mine operators vicinity restrictions to heavy mobile equipment.
2. The haul truck is reversed to within 15m of the Scanstation and parked.
3. The targets are individually scanned to a horizontal resolution of 1mm and vertical resolution of 1mm.
4. The area of pavement under the rear axle (variable distances to each side and behind the axle) is scanned at a horizontal resolution of 10mm and vertical resolution of 0.5mm. This is to allow reduce required scan times and is not considered to impact accuracy in the determination of the maximum surface deflection.
5. Steps 3 and 4 are repeated after the truck is removed from the scanned area.

#### 3.5.7.2 Data Analysis

The scans of the pavement surface with and without the truck in place were registered together using Leica Cyclone 8.1.3 software. As the targets and the scanner used at each location do not move between the two scans, this process is relatively simple. Leica Cyclone 8.1.3 software was then used to complete registration of the two scans and subsequently to provide measurements of displacement.

The procedure for measurement of displacement using the Leica Cyclone 8.1.3 software is outlined below. The surface in between and surrounding the dual wheel assembly is examined to detect the area over which the maximum deflection occurs. This should not be an isolated area but rather confirmed as the part of the deflection bowl showing the greatest difference between the two scans, to avoid the recording of analogous results. Deflection is reported as a maximum value stated to nearest 0.1 of a millimetre. Observation of the testing report in Appendix B suggests an accuracy of 0.5mm may be more appropriate, however 0.1mm is retained to allow estimation of curvature for input to software for the back-calculation of pavement modulus and is thus carried through reporting of all deflection results. If a deflection bowl is able to be detected the deflection at each radial distance to a maximum radius of 2.5m was reported. For consistency, the curvature bowl has been defined from along the centreline of the right hand dual wheel assembly for all tests.

The process utilised for determining deflection in an area of interest was:

1. A TIN mesh was applied to both point clouds for the area of interest (between and immediately surrounding dual wheel assembly).
2. The mesh was exported to Microsoft Excel such that the displacement between the data points constituting the two meshes can be calculated.
3. The average displacement was calculated, if the deflection showed inconsistency near the edges of the chosen area, a smaller area was chosen to remove curvature effects. However, generally the area observed for calculation of deflection spanned the distance between tyres in the dual wheel assembly, and was nominally 300mm long.

#### 3.5.7.3 Pavement Curvature

Pavement curvature was also defined to allow back-calculation of pavement elastic modulus (see Section 3.9.1). The scan data used to define pavement deflection was used following registration of the scans taken with and without the truck present. From the registered scans, a strip of approximately 100mm wide was taken, commencing at approximately the end of the tyre contact patch between the right hand rear dual tyre assembly and continued backwards for approximately 3.5m. This area of interest then had a TIN mesh applied (essentially applying a smoothed surface to the point cloud), as per the procedure within Section 3.5.7.2 to allow the 'surface deviation' feature to be utilised within Cyclone. The resulting point cloud had a resolution of 10mm and details the elevation difference between the loaded and unloaded scans, which was then exported to Microsoft Excel for analysis. Once the raw surface deviation data was tabled in Microsoft Excel the distance from the edge of the tyre contact patch was calculated for each point generated. After plotting the distance from the extremity of the contact path against deviation and trialling several different types of trend-line it was apparent that the correlation was poor, with $R^2$ less than 0.5 in most cases. This appeared to result from the unevenness of the pavement surface, especially in locations where an isolated stone was observed. In an effort to smooth the data a 100mm moving average was calculated for the raw deviation data, which produced greater consistency. The moving averages were then plotted against distance from the extremity of the tyre contact patches, with a logarithmic trend-line fitted. Using the equation for the resulting trend-line, the deflection for 0.2m to 2.5m was defined. For the purpose of back-

calculation of soil modulus it is also necessary to define the deflection at the load point, for this the maximum deflection as per the results in Section 4.4 were used.

Note that the edge of the tyre contact path was used as the 'zero radius' point, as the contact patch itself is approximately 1.0m long (see Section 4.4.3). Due to geometric constraints of placing the scanner directly behind the wheel assembly, and occlusion effects (interference of the scans due to proximity to the tyres) scanning of the surface between the tyres was problematic. Typically, the scan extended only 0.5m from extent of the contact path nearest the scanner. In some cases where the scanner was further offset from the centre of the truck the angle was such that far less than 0.5m was able to be scanned between the dual tyres. For these reasons it was not possible to determine accurately the deflection at the very centre of the loaded area and instead the maximum recorded value was used.

This method varies from that of the Benkelman beam test, in that the curvature is defined by measuring the deflection at varying radii from the tyre contact, rather than monitoring the reduction of deflection as the truck moves away from the testing location as in MRWA Test Method WA 326.1 (MRWA, 2001). Secondly the curvature is not defined by a ratio of maximum deflection and deflection at a chosen radii, as is done by Austroads (Jameson et al, 2009). Rather, the data acquired has been chosen to allow back-calculation of modulus via software generally utilised for analysing Falling Weight Deflectometer (FWD) test data.

#### 3.5.7.4 Interaction of Deflection between Tyres

Various pavement design methods discussed in Section 2.4 describe the use or exclusion of interaction of deflections or strains between wheel gears. From the scans described above, with the addition of two scans taken from the side of the truck at Station 1 for Section 1 and Section 2, it is able to determine the amount of deflection interaction between the rear wheel gears and also front and rear axle. The same method for registration of the data from loaded and unloaded scans was utilised as is detailed in Section 3.5.7. Strips between wheels of approximately 100mm were then 'TIN' meshed and the deviation point cloud determined. This data was then exported to Microsoft Excel to define the deflection profile of the surface between adjacent tyres.

#### 3.5.7.5 Geometry of Tyre Contact Patches

The geometry of the tyre contact patch is a critical input within pavement modelling and design. For that reason the geometry of contact patches was measured from the registered scans used to define maximum deflection. Data was incomplete in some circumstances, due to the line of sight able to be achieved by the scanner from its position relative to the truck. Where possible the maximum outline of tyre/pavement contact was recorded for dual tyre assemblies, as this is used for some design techniques. Examples of various contact geometry being measured in Leica Cyclone 8.1.3 software are presented in Figure 3.15 through Figure 3.17.

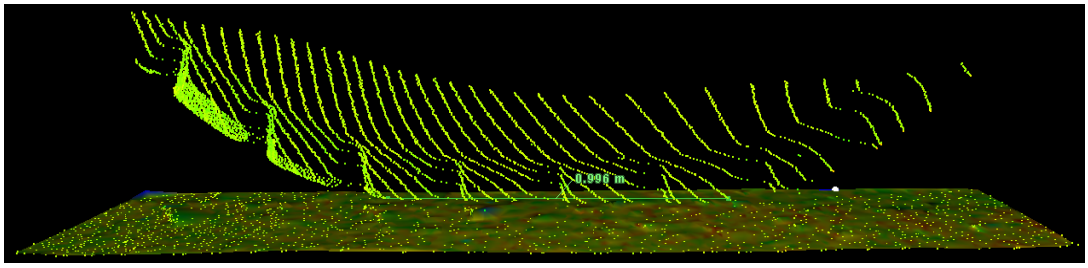

**Figure 3.15: Example of measurement for tyre contact patch length (elevation side view of the lower section of tyre on a pavement surface).**

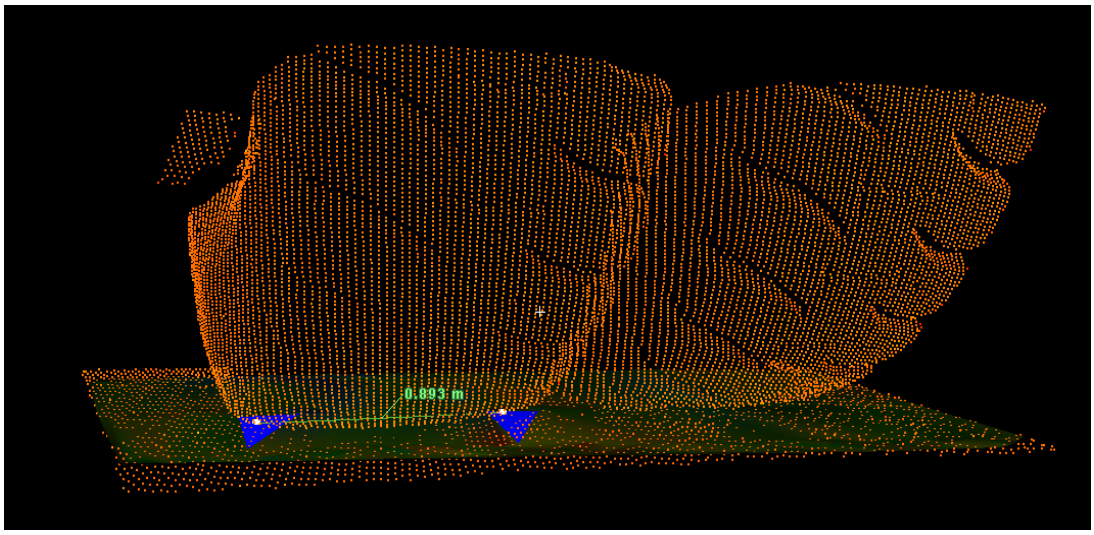


**Figure 3.16: Example of measurement for tyre contact patch width (elevation view of dual tyre assembly on a pavement surface).**

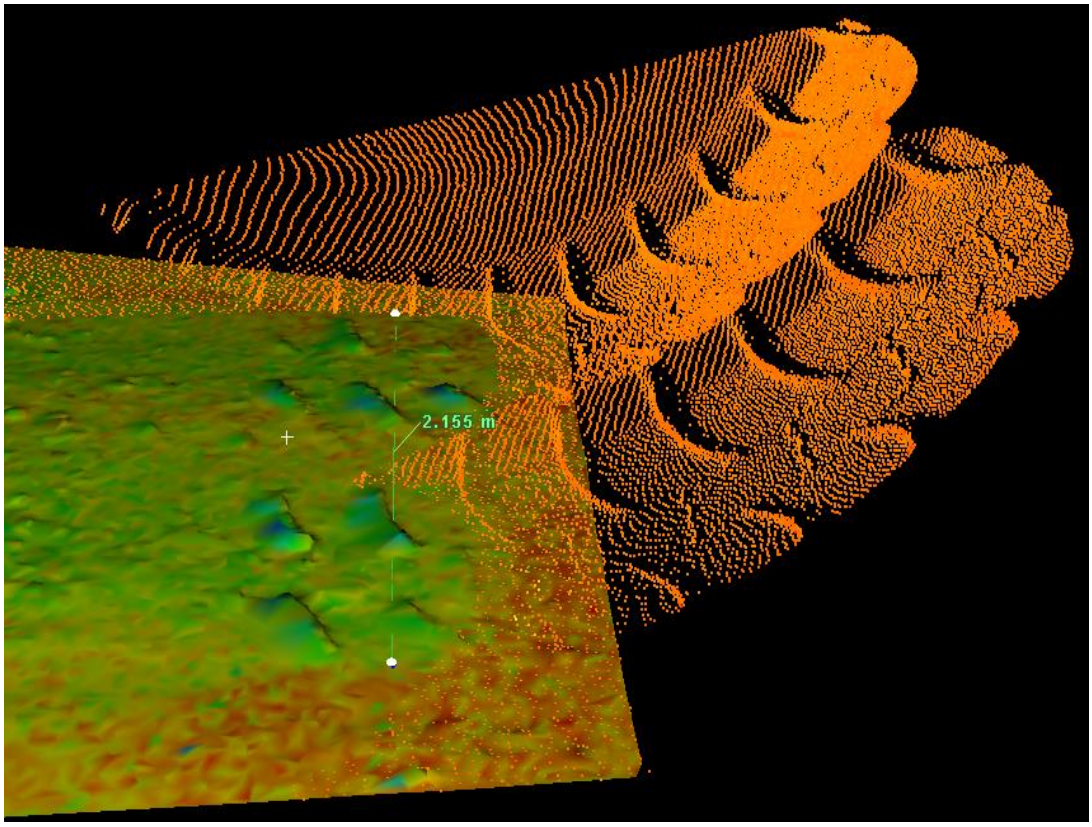


**Figure 3.17: Example of measurement for dual tyre assembly contact patch width (elevation side view of dual tyre assembly on a pavement surface).**

The contact patch geometry results were averaged and then used to estimate the total truck weight with weight distributions taken from Komatsu (2006), see Table 3.5, to transform a rear or front tyre load into the total truck weight. The results present an opportunity to comment upon the relative stiffness of the tyre carcass with respect to the total contact stress also considering inflation pressure.

**Table 3.5: Weight distribution for a Komatsu 830 haul truck (Komatsu, 2006).**

| | Total Load (%) | |
|---|---|---|
| Load Condition | Front Axle | Rear Axle |
| Unloaded | 50 | 50 |
| Loaded | 33 | 67 |

Further the total calculated tyre contact area was utilised to estimate the total truck weight via the relation presented by Hadi et al (2003) and reproduced in Figure 3.18. This estimation is often utilised for modelling purposes and therefore comparison with the known truck weight assists in commenting on the contact patch pressure distribution.

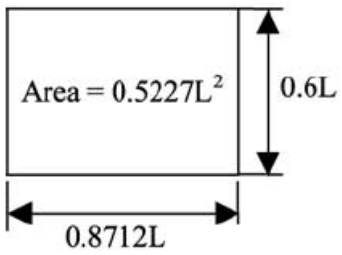


**Figure 3.18: Estimated tyre contact patch geometry from contact area (Hadi et al, 2003).**

### 3.5.8 Rolling Resistance

#### 3.5.8.1 Site Data Collection

Rolling resistance was measured through standard on-board power monitoring and logging equipment. Parameters logged included power and torque output, as well as the vehicle speed at a frequency of 20 milliseconds. The equipment necessary to complete such logging was simply a laptop computer connected with the GE Invertex software, which is the engine monitoring and management system supplied as standard with the GE motors utilised on Komatsu 830E-AC haul trucks. There was no means to automatically and accurately activate logging at the start of a test section, nor was the truck able to log its GPS location. In the absence of such capabilities, manual logging of the time the truck entered the test section was completed, this is accurate to only a second. However, the raw data was moderated to remove any anomalies within the first and last second of any logged test data.

#### 3.5.8.2 Analysis of Data

To allow analysis of the data captured from on-board logging, all data was exported to Microsoft Excel. The process for calculation of instantaneous rolling resistance for each data point recorded (0.04 second intervals) is outlined in the steps below:

1. Relative wind effects (see Section 3.5.3.1) were calculated considering the speed and direction in relation to the truck for each section that rolling resistance was tested. The equation used for the calculation of the power required to overcome air resistance is presented in Equation 3.16. The wind vector was calculated for each section from the wind speed/direction test results taken at the conclusion of each circuit driven (see Section 3.5.3.1).

**Equation 3.16: Power required to overcome wind effects.**

$$P_a(HP) = \frac{FA * C_d * MPH^3}{156{,}000}$$

Where:

$P_a$ is the power due to air resistance (HP)

$FA$ is the frontal area of the truck (542.07 square feet).

$C_d$ is the aerodynamic drag coefficient (0.9 as per Caterpillar, 2007)

$MPH$ is the truck speed in Miles Per Hour (MPH)

2. Rolling resistance force was calculated from the results of wheel torque measured by the GE Invertex software at each of the rear wheel assemblies, with the use of Equation 3.17.

**Equation 3.17: Driving force from wheel motor torque and wind effects.**

$$F_{TOTAL} = Gear\ Ratio \frac{Wheel\ Motor\ Torque\ (kNm)}{Rolling\ Radius\ (m)} - F_{WIND}(kN)$$

Where:

$Gear\ Ratio$ is taken as 31.875:1 (Komatsu, 2006)

$Rolling\ Radius$ is considered to be 1.03*Static Wheel Radius (Jamieson et al, 1999)

$F_{WIND}$ is a vector with the scalar value calculated by Equation 3.16.

The total force was then used to calculate the instantaneous rolling resistance coefficient (RRC) by way of Equation 3.18.

**Equation 3.18: Rolling resistance coefficient.**

$$RRC\ (\%) = 100 * \frac{F_{TOTAL}}{Truck\ Weight\ (Unladen) + Payload}$$

Where:

$F_{TOTAL}$ was calculated via Equation 3.17;

$Truck\ Weight\ (Unladen)$ was 1610.8 kN; and

$Payload$ was measured via inbuilt on-board load monitoring.

3. Rolling resistance tests were completed for a total of three runs with all combinations of the following considered:
    - driving direction;

- unladen and full payload; and
- 15 km/h and 30km/h driving speed.

Following acquisition of data from rolling resistance testing, as described above, analysis of data proceeded as below. There were two primary steps involved in this process:

a) analysis of recorded torque data to determine the RRC attributed to each section and truck condition
b) analysis of the correlation of pavement properties, pavement section and truck load condition against RRC, culminating in regression of functions predicting RRC from pavement parameters. This process is depicted in Figure 3.19.

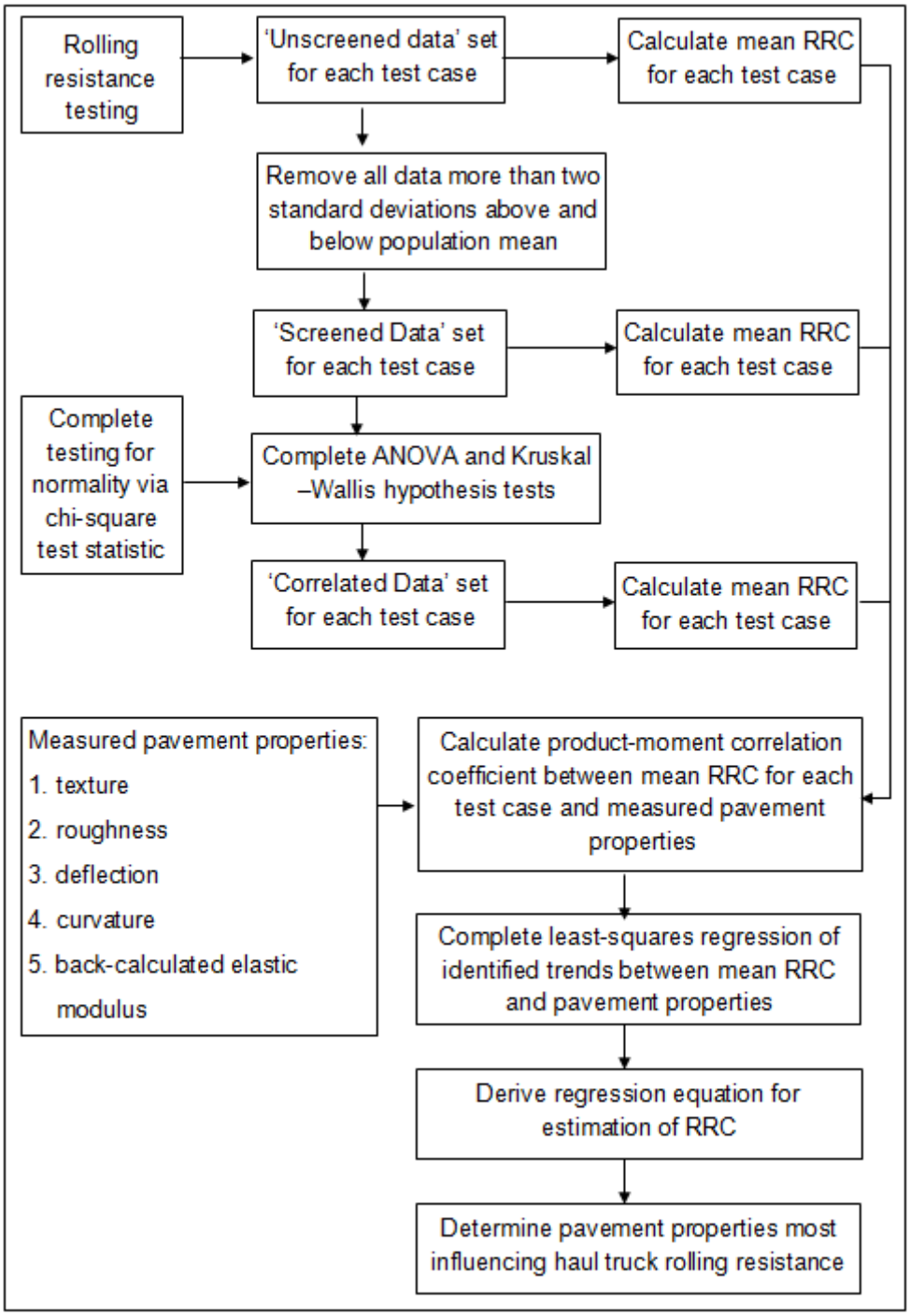


**Figure 3.19: Flow chart of analysis for rolling resistance test data.**

The process alluded to in a) resulted in three sets of data being derived for each pavement section and truck payload/speed combination. Each subsequent step resulted from greater detail within the analysis. This approach was taken to account for the uncertainty associated with the refinement (reduction) of data removing

indications of truck response to pavement properties. For example, due to the lack of previous haul truck rolling resistance testing in the literature, it was impossible to state with certainty that a 'spike' in torque was due to a particular isolated pavement property or pressure being momentarily applied to the truck's throttle. Therefore, the analysis would search for trends within the data, after each set was calculated through the steps of analysis detailed below.

Within the following discussion, a 'test case', shall denote a specific combination of truck speed and payload for the three pavement sections.

Initially all raw data, with removal of data from the first and final second of testing from each pavement section (as described in Section 3.5.8.1), was collated for truck payload and driving speed. Each test case was made up of six individual tests, resulting from three traverses of the pavement section in each direction. The mean and standard deviation RRC was determined for each pavement section and test case. As a result of this process, the set of results denoted the 'unscreened data' was derived, as presented in Section 4.5.

Subsequently, the 'screened data' was derived (results presented in Section 4.5).This involved discarding RRC resulting from torque readings failing either of the criteria listed below. Note that both criteria are nominal in nature, but have been selected qualitatively from observation of all test data and the truck driver's behaviour within the testing. As a result, it was considered that the driving speed and throttle applied was very consistent throughout the testing, hence changes in torque due to driver action should be relatively minimal. Further, observation of the unscreened data suggested that there was inherent variation within the RRC results, however it was clear that it was unlikely RRC would exceed a certain level (selected as the upper limit noted in 2. below) and should also not approach zero (resulting in the lower limit in 2. below).

The criteria applied to derive the screened data involved removal of:

1. any torque readings changing greater than 10kNm from the previous reading (with readings taken at a frequency of 0.04 seconds)
2. any RRC reading less than 1 population standard deviation under lowest mean RRC from any of the tests, or greater than 1 population mean above highest mean RRC, was removed.

Following the process above, the mean and standard deviation was calculated for each test case, resulting in the screened data, as presented in Section 4.5.

There was some consistency evident between the two sets of data derived above. However, it was considered appropriate to test the correlation of the remaining data of the six sets making up each test case. The adopted test method had not been attempted prior to this project and involved a human element. Furthermore, some variation would be expected between tests, due to slight differences in wheel path resulting in potential differences in the pavement characteristics traversed in each test. As highlighted in Section 3.2, it is not well defined in the literature which pavement characteristics most significantly influence haul truck rolling resistance. Therefore, it was not possible to give any precedence to any data set over another through subjective assessment. However, the variation in the mean RRC of each test suggests that the data should also be refined to consider only the data arising from tests where a statistical relation could be established. The basis and process for this decision is discussed below, drawing heavily on the techniques detailed in Section 3.4.

Firstly, the data from each test underwent a chi-square goodness of fit test for normality, as per Section 3.4.1. The Microsoft Excel Data Analysis tool was utilised to determine the frequency of RRC data that fell into bins spanning 0.2% RRC, from 0 to 4%. The calculated sample size, mean and standard deviation were then used to calculate the expected frequency within each bin, assuming a normal distribution. Note that bins below the minimum recorded RRC value and above the maximum, were excluded from the calculation of expected frequency. The recorded and estimated frequency for each bin was then used to estimate the chi-square test statistic. This value was then compared to the critical chi-square score for a level of significance (alpha) of 0.05. A typical distribution of the frequency of data is shown in Figure 3.20.

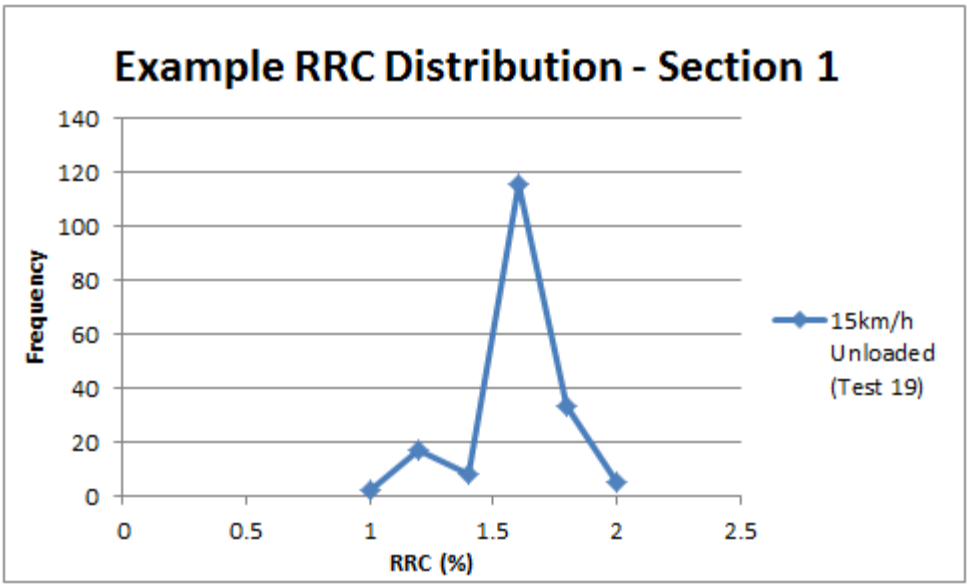


**Figure 3.20: Example distribution of RRC, when distributed into bins.**

The outcome of the chi-square test was that typically, the data from the majority of rolling resistance tests was not normally distributed, see Section 4.5.2.

Since many samples were found to not be normally distributed, it was also considered necessary to complete a nonparametric analysis. This approach was taken in an effort to avoid type two errors (incorrectly accepting a null hypothesis). As such, nonparametric analysis was completed for each test case considering the six original samples. The nonparametric test employed was the Kruskal-Walls, as per Section 3.4.4. This test is often utilised as a nonparametric alternative to one-way ANOVA, and therefore was expected to be well suited for this application. The level of significance was once again adopted as 0.05 for nonparametric hypothesis testing.

The following discussion provides an overview of the robustness of the ANOVA and non-parametric (Kruskal-Wallis) hypothesis tests. Robustness refers to the relative consequence of failure to comply with one of the test's assumptions. This discussion is not exhaustive, as this is the subject of much literature, to which the reader is referred for further detailed discussion. The null hypothesis being tested for both tests is one of equal means (ANOVA) and of being selected from the same population (Kruskal-Wallis). The relevance of both hypotheses must be questioned, as some variance in measured wheel motor torque is expected due to changes in pavement properties and driver behaviour. This third step of analysis aims to find correlation in two or more sets of test data, under the assumption the resulting

population best represents the true steady state operating conditions of the haul truck on the pavement sections. In doing so, it must be remembered that useful data on the response to a given pavement property may be lost. This is the basis of giving the unscreened and screened data sets equal weight to that resulting from the following analysis (producing the 'correlated data set').

It is often reported in the literature that violation of normality should be of little concern when completing ANOVA tests (Glass et al, 1972). Other authors report that the ANOVA f-test is known to be quite robust to the assumption of normality, when the number of factors is small and the sample size large (Akritas and Papadatos, 2001). The Kruskal-Wallis has been noted to have questionable ability when the number of samples is small (<5). Furthermore, from the same study it is concluded that even for non-normal data, ANOVA appears to outperform in this case (Khan et al, 2003). This view is further supported by Feir et al (1974), who state that when normality or homogeneity of variance is doubtful, ANOVA is recommended in preference of Kruskal-Wallis, with the latter becoming competitive for large sample sizes. The idea of noncompliance with base assumptions for hypothesis tests is extended with consideration of kurtosis (a measure of peakedness or flatness compared to a normal distribution) and skewness (a measure of the symmetry of the distribution) (Stamatis, 2012). It has been found that both ANOVA and Kruskal-Wallis are influenced significantly more by kurtosis of the error distribution than skewness, irrespective of its direction (Khan et al, 2003). Some caution is recommended, as literature such as Micceri (1989) warn against the potential bias of some investigators to find parametric techniques to be robust.

Despite the above discussion relating to robustness, it should be noted that the level of significance has often been noted to generally be exceeded when sample sizes or variance is unequal (Glass et al 1972). The practical implication is that the probability of a type one error is greater than stated (by the tests' alpha value). This results in conservative findings in the context of this project, where a correlation between two test samples is being sought.

Type one errors (incorrectly rejecting a null hypothesis) were attempted to be controlled through observation of each tests p-value. This value represents the probability of mistakenly rejecting the null hypothesis (Stamatis, 2012). In all cases, the null hypothesis was accepted when the p-value was less than the level of significance adopted for the test (0.05).

Ultimately, the approach applied for this project, was to proceed with the mean values of samples found to have equal variances via ANOVA testing. This test showed the greatest correlation between samples, with 10 of the 12 tests cases having two or more samples being found to have equal mean values. This result was replicated for four of the 10 test cases through Kruskal-Wallis testing. A further two test cases were also shown to have samples from the same population.

As noted in Section 3.4.2, ANOVA assumes equal variances between samples (as highlighted in Section 3.4). In an effort to provide further assurance against incorrectly accepting a null hypothesis of a relation between any two samples, a t-test assuming unequal variances was completed for the two best correlated data samples from the ANOVA analysis. This test was completed in accordance with the procedure contained in Section 3.4.3. For both the ANOVA and t-tests a level of significance of 0.05 was adopted throughout. The null hypothesis was accepted if the test statistic (the F-value in ANOVA and t statistic in the t-test) was found to be less than the critical value, determined in accordance with the relevant distribution in Section 3.4.

Where two or more samples were found to be related from acceptance of the null hypothesis through the test procedure above, the mean RRC was calculated. Data samples that were found to be from a common population were retained and carried through the remainder of the analysis. This data set shall be referred to as the ‘correlated data’. These values were then utilised to test if the RRC data for each section and test case correlated with any of the pavement properties defined through the testing described in Section 3.5. Table 3.6 shows all potential correlations that are to be tested for each set of test data. Note that the greyed cells represent irrational combinations. For example, a deflection/curvature/modulus cannot be listed for the first two columns, as this combines average RRC values relating to an unloaded and loaded truck. This process was completed with use of Pearson’s product-moment correlation (r). The mean RRC values for each section and test case meant that the sample size being used to test the correlation was three. Therefore, as per Table 3.4, a statistically significant correlation was considered to have been identified when the product-moment correlation exceeded 0.997 (single degree of freedom).

The above procedure for correlation testing was completed for all three sets of data; the unscreened, the screened and the correlated data.

**Table 3.6: Example table used for correlation testing of pavement properties and RRC.**

| | | Correlation (r) | | | | | | | |
|---|---|---|---|---|---|---|---|---|---|
| | Truck Speed (km/h) | 15 | 30 | 15 & 30 | | 15km/h | | 30km/h | |
| | Payload (Tonnes) | 0 & 220 | | 0 | 220 | 0 | 220 | 0 | 220 |
| | Property | | | | | | | | |
| Average Standard Deviation | 0.1m moving average | | | | | | | | |
| | 0.2m moving average | | | | | | | | |
| | 0.5m moving average | | | | | | | | |
| | 1m moving average | | | | | | | | |
| | 5m moving average | | | | | | | | |
| | 10m moving average | | | | | | | | |
| | 20m moving average | | | | | | | | |
| | IRI | | | | | | | | |
| | MPD | | | | | | | | |
| | Deflection (no payload) | | | | | | | | |
| | Deflection (220 tonne) | | | | | | | | |
| | Curvature (no payload) | | | | | | | | |
| | Curvature (220 tonne) | | | | | | | | |
| | Modulus (no payload) | | | | | | | | |
| | Modulus (220 tonne) | | | | | | | | |

In an attempt to determine the percentage of induced rolling resistance arising from each pavement property, multiple variable regression was completed. An equation of the form shown by Equation 3.19 was pursued. Note it was considered that each pavement property should have a positive coefficient in order for the relationships to be rational. That is the function takes a form where the contribution of each pavement parameter to the total rolling resistance is added. Initially, this focussed on all measured pavement properties, however it soon became clear that rational relationships (those with no negative constants applied to any independent variable) only resulted for all test cases when only deflection and IRI were applied. As a result a regression equation was derived utilising these pavement properties for each set of data, considering all vehicle speeds. More significant correlations were observed between pavement properties and RRC for testing conducted at 30km/h, therefore regression was also completed considering data collected from testing at 30km/h only. The coefficient of determination was observed and noted to provide an indication of the significance of each result. The level of significance for each derived regression equation was controlled by observation of the significance associated with the derived F-value for each test. This is the probability that the resulting regression equation does not explain the variation in the independent variable (RRC). It is the calculated probability that regression F-value (regression

mean squares/residual mean squares) is less than that determined for the level of significance chosen for the test and the degrees of freedom in the regression. For this study it is considered necessary for this value to be less than 0.05 for the regression equation to be considered significant.

**Equation 3.19: Form of regression equation for RRC.**

$$RRC = a.Deflection + b.IRI + c.MPD + d.0.1m\ Roughness \dots\dots i.20m\ Roughness$$

Where:

$a, b, c, d.....i$ are regression coefficients

$Deflection$ is the measured pavement rebound deflection

$IRI$ is the estimated International Roughness Index (Equation 3.15)

$MPD$ is the estimated Mean Pavement Depth

$0.1m\ Roughness$ is the average standard deviation of the pavement surface elevation for a moving average wavelength of 0.1m

$20m\ Roughness$ is the average standard deviation of the pavement surface elevation for a moving average wavelength of 20m.

To further apply the regression equations derived through the above process, it was attempted to determine the relative impact of each pavement property in terms of the proportion of RRC resulting from each. By calculating the amount of RRC predicted by both pavement deflection and IRI with the regression equation for each data set, it was possible to examine which property was more significant. This process was completed twice, for all test speeds and again for only the data arising from testing at 30km/h. From observation of the resulting data it was evident that a significant difference occurred between testing with and without a payload applied to the truck. This result should be somewhat expected as a linear regression has been applied and deflection increases for the loaded case, but IRI remains constant for each section. It was evident from the results, that the proportions were very consistent for the screened and correlated data sets. However, the unscreened data

set showed much less influence of deflection for the analysis considering all test speeds. This is intuitive, due to the poor correlation between RRC and pavement deflection resulting from the correlations predicted by the process discussed above. Consequently, mean values were taken for the screened and correlated data sets, and the results arising from all test speeds and only 30km/h compared.

The process described above, whereby a sequential analysis of RRC data is undertaken was considered necessary. It is uncertain exactly which changes in recorded wheel motor torque is related to driver behaviour, and which in response to some pavement feature. Therefore, to immediately discard test data due to some nominal rule or qualitative interpretation of the test data could restrict any correlation being found. Testing of correlation between rolling resistance and pavement properties at each level of data analysis was considered the best means to identify correlations. Where a consistent trends in correlation were observed between the three sets of data, it is considered a statistically significant influence of rolling resistance has been identified.

Lastly, it should be remembered that the values of RRC presented in this dissertation in fact represent driving resistance. Due to the relative distribution of weight between an unloaded and loaded condition for a Komatsu 830E, the RRC values reported here should be doubled for the unloaded case and increased by 50% for the loaded case. As discussed previously, it is considered appropriate to consider driving resistance when undertaking the procedure outlined above to determine the pavement properties most influencing RRC. However, the modification should be made in order to compare the data to findings of many of the other studies reported in the literature.

#### 3.5.8.3 Comparison with Available Models

Although there are many models available for the estimation of the rolling resistance experienced by a rolling wheel, only a few have been considered appropriate for comparison to the physical tests completed in this project. Primarily this is due to the large vehicle mass of the haul trucks considered being vastly larger than that considered in the development of any models described below. One model that is investigated is that reported by Thompson (2011) and reproduced within Equation 2.8 through Equation 2.10, which was developed though coast-down tests of haul trucks. Another model that has been developed (see Equation 2.11 and Equation 2.12) for use with haul trucks but not yet validated is reported by Widodo et al

(2009). Caterpillar (2006) have also published an equation for estimation of rolling resistance, which is reproduced in Equation 2.11. This function is not included in the analysis for this project as tyre penetration is not visible on the tested pavements and deflections are far less than a centimetre (see Section 4.4). All of these models have been developed for haul trucks specifically, although the model reported by Widodo et al (2009) was developed with use of a towed trailer and had not been verified against full-scale test data for haul trucks at this time.

As will be discussed in more detail in Section 3.6.1 with regards to fuel consumption modelling, the screened data set has been used for comparison purposes. This set has had uncertainty due to driver and truck response removed and therefore best represents the rolling resistance experienced by the truck. As the values measured in this study relate to driving resistance an adjusted set of rolling resistance results have been generated, considering the vertical load applied to each wheel in the testing. Further discussion of this process is supplied in Section 4.5.7.

Several commonly applied models reported in the literature for passenger vehicles were also considered. This was completed despite the lack of understanding in the applicability of applying models derived for sealed highway pavements that have been trafficked by relatively light vehicles in deriving such models. However the basis of such models are pavement parameters that are focussed primarily on roughness and texture, with Benkelman beam rebound deflection included in some. Investigation of such functions therefore facilitates discussion of the potential relative impacts for haul trucks.

During the 1990's and early 2000's considerable research was completed in New Zealand to define the effect of pavement surface on vehicle (specifically light truck) rolling resistance. Equation 2.5 presents the general equation to which these functions are applied. Note that the factors $C_0$ and $C_v$ have been expanded in Equation 2.3 and Equation 3.20. The first model considered was reported by Cenek (1994) and appears in an adapted form in Equation 3.20. This function utilises only IRI and vehicle speed as dependant variables. A similar function, taking account of rebound deflection and truck mass was then developed (Jamieson et al, 1996) and is presented in Equation 2.3. The two relationships were ultimately synthesised and the definition of pavement roughness further detailed to separate relative wavelengths, with the relation presented by Equation 2.6 and Equation 2.7. However this last modification is not able to be tested as it is not clear what wavelengths apply to short, medium and long wavelength roughness. A potential

issue with these functions is the inclusion of vehicle mass within the function. Development was completed with small to medium sized trucks whose Gross Vehicle Mass (GVM) did not exceed 13.01 tonnes during testing. However one potential advantage of this context is that the trucks were rigid and had similar load distribution to that of a large haul truck and were tested while empty and fully laden.

**Equation 3.20: Rolling resistance force as per Cenek, 1994 (via Greenwood et al, 2003).**

$$RRC = 0.0041 + 0.00043.IRI + 0.0000025.v$$

Where:

$RRC$ is the rolling resistance coefficient.

$v$ is the vehicle speed (m/s).

$IRI$ is the international roughness index (m/km).

A modified version of the ARRB (Australian Roads Research Board) Road Fuel Consumption Model utilised within the HDM-4 VOC model was also considered. Equation 3.21 presents the rolling resistance factor due to pavement surface properties included within the model. As with the relations originating in New Zealand, this includes a term for Benkelman beam rebound deflection which provides the basis for consideration of this model. However the validity of utilising these functions is unclear considering the extreme wheel loading presented by the haul truck utilised during testing. Tyre response due to roughness and texture is also undoubtedly largely extrapolated, as the radius and thus contact patch is relatively much larger than would have been considered in the models development. Therefore the constants supplied in Table 3.7 may require modification. Despite this fact these models are tested in the absence of any alternative as the ability to better predict rolling resistance with a model that also allows estimation of fuel consumption (see Section 3.6) would prove a valuable input to mine planning.

**Equation 3.21: HDM-4 rolling resistance surface factor (Worldbank via Zaabar, 2010).**

$$CR2 = Kcr2[a0 + a1 \times Tdsp + a2 \times IRI + a3 \times DEF]$$

Where:

$Kcr2$ is a calibration factor.

$a0$ to $a3$ are model coefficients, see Table 3.7.

$Tdsp$ is the Texture Depth using sand patch method (mm).

$IRI$ is the International Roughness Index (m/km).

$DEF$ is the Benkelman Beam rebound Deflection (mm).

**Table 3.7: HDM-4 rolling resistance surface factor coefficients (Worldbank via Zaabar, 2010).**

| Surface class | surface type | <=2500kg | | | | >2500Kg | | | |
|---|---|---|---|---|---|---|---|---|---|
| | | a0 | a1 | a2 | a3 | a0 | a1 | a2 | a3 |
| Bituminous | AM or ST | 0.5 | 0.02 | 0.1 | 0 | 0.57 | 0.04 | 0.04 | 1.34 |
| Concrete | JC or GR | 0.5 | 0.02 | 0.1 | 0 | 0.57 | 0.04 | 0.04 | 0 |
| unsealed | GR | 1 | 0 | 0.075 | 0 | 1 | 0 | 0.075 | 0 |
| unsealed | - | 0.8 | 0 | 0.1 | 0 | 0.8 | 0 | 0.1 | 0 |
| block | CB, BR or SS | 2 | 0 | 0 | 0 | 2 | 0 | 0 | 0 |
| unsealed | SA | 7.5 | 0 | 0 | 0 | 7.5 | 0 | 0 | 0 |

A couple of models resulting from recent research being conducted as part of the MIRIAM (Models for Rolling Resistance in Road Infrastructure Asset Management Systems) project are also trialled. Like the relations described above, these have been developed for light passenger vehicles with the consideration of a vast data set. One potential shortcoming is the fact that neither of the equations below considered unsealed pavements in their derivation. The first (Equation 3.22) was

developed as part of the ECRPD (Energy Conservation in Road Pavement Design, Maintenance and Utilisation) project and includes speed independent and dependent terms for the roughness (IRI), as well as pavement texture. Due to the large dataset it is considered a comprehensive comparison of pavement surface properties and rolling resistance and the further adaption made by the VTI (Swedish national roads authority) has been reproduced in Equation 3.23 and tested against rolling resistance data in this project.

**Equation 3.22: Rolling resistance coefficient derived in the ECRPD project (Sandberg et al, 2011).**

$$RRC = 0.0061 + 0.0014.MPD + 0.00095.IRI + 0.000076.IRI.(V - 20)$$

Where:

$RRC$ is the rolling resistance coefficient.

$MPD$ is the mean pavement depth (mm).

$IRI$ is the international roughness index (m/km).

$V$ is the vehicle speed (m/s).

**Equation 3.23: Rolling resistance coefficient within the VETO model (Hammarstrom et al, 2012).**

$$RRC = 0.00414 + 0.00102.MPD + 0.0000158.IRI.V$$

Where all variables are as per Equation 3.22.

In instances where the RRC values estimated by an model are observed to closely match those measured, the Pearson correlation coefficient, as per Section 3.4.5, is analysed to provide greater insight.

Lastly an attempt is made to compare the test results found in this project with the empirical data reported in the literature, mainly that contained within Table 2.5 and Table 2.6. There has been no specific methodology applied to assessing these relations as it is not being attempted to recommend any one for estimation purposes. Rather the predicted and measured values are to be subjectively compared to allow further comment on the impact of the various input variables.

## 3.6 Potential Impacts on Vehicle Operating Costs

The impact of pavement on Vehicle Operatic Costs (VOC) is a critical for defining road user costs, which holds significant potential benefits when the road in question is a (self-owned) critical piece of infrastructure for generation of revenue. In the case of mine haul roads an understanding of the relationship could assist in assigning haulage equipment maintenance and of course present opportunities to reduce operating costs. Within the literature there is an extremely limited number of models defining user costs for haul trucks and none that utilise pavement based inputs similar to those utilised within this study. Therefore only an attempt to define fuel consumption is made, through use of the HDM-4 model.

### 3.6.1 Fuel Consumption

Fuel consumption has been modelled through use and modification, where required, of the HDM-4 model as described in Section 2.3.1. ARFCOM, which was developed by the Australian Roads Research Board, is the basis of this model and hence the discussion above regarding use of the rolling resistance prediction function. The only variable considered here is the power required to overcome rolling resistance, in order to assess what percentage change in fuel consumption is probable from driving on the three pavement sections considered in the testing for this project. The factor for total tractive power is considered and analysed for sensitivity to pavement inputs including rolling resistance estimated from IRI results through use of the model derived by Cenek (1994), as proposed by Greenwood et al (2003) against rolling resistance coefficient results from this project (see Section 0). The ‘screened data’ set was used for input to fuel consumption estimates. This data set was

utilised as both models make allowances for accessory power and mechanical inefficiency. The HDM-4 model includes estimates for both based upon engine speed and maximum power output and the Department of resources model factors the power required to overcome the total of grade, air and rolling resistances. In order to consider the true magnitude of fuel consumption changes due to differing rolling resistance values, the total power requirement must be estimated. Such estimations are difficult as the ARFCOM model is predicated on a traditional mechanical transmission and drive-train vehicle. This is a shortcoming of the method proposed, however note that the model is mechanistic in nature and hence the estimation of fuel consumption for the power required to overcome rolling resistance for a given load is valid, but the estimation of transmission and drive-train efficiency may be somewhat inaccurate. Furthermore, the accessory power consumption is estimated from the data included within Greenwood et al (2003), but it is possible that a haul truck operating on a modern mine will have considerably more instrumentation installed than that of a long-haul highway truck, which is used as the basis of estimation. Also note that accessory power is estimated through consideration of the ratio of maximum power drag with the vehicle travelling at 100 km/h. This speed is not achieved in the current project and it is likely that the ratio of total power, when applied to operating speeds of 15 and 30km/h result in underestimates.

The inputs for the fuel consumption modelling are presented in Table 3.8, with chosen values indicated in Table 3.9. Some modifications are made to the traditional model in the interests of simplicity and applying the measured RRC instead of estimating the power to overcome rolling resistance using the term provided in the model, which includes the CR2 term detailed in Equation 3.21. ARFCOM also includes a term for minimum fuel consumption for the vehicle (Equation 3.24), which defines the power demand when pavement properties are favourable such that the vehicles engine is essentially idling and not under load. Despite being unlikely, fuel consumption could potentially be governed by this estimation and therefore it has been excluded from the modelling. This is to alleviate the potential complications that could arise should this value be calculated to exceed those due to the measured rolling resistance. This is considered appropriate, as the rolling resistance has been measured, whereas the minimum fuel consumption would be an estimate based on the maximum power output.

**Equation 3.24: Idling fuel consumption as per HDM-4 (Greenwood et al, 2003).**

$$FCMIN = \beta(\text{Paccs} + \text{Peng})$$

Horizontal curvature and longitudinal gradients are considered negligible in the modelling. This results in a simplification of the model presented in Table 3.8 and Table 3.9. Data required for inclusion of these effects is available within the literature.

**Table 3.8: Definition of constants and variables within the HDM-4 fuel consumption model (Greenwood et al, 2003).**

| Parameter | Description | Function |
|---|---|---|
| ceng | speed independent engine drag parameter | 0.017*Pmax |
| beng | speed dependent engine drag parameter | 0.7+0.026*Pmax |
| α | Engine idle fuel consumption (mL/s) | β*(Peng+Paccs) |
| RPM | operating engine speed | $a0+a1*v+a2*v^2$ |
| Pa | power to overcome air resistance (kW) | $0.7331*C*D*AF*v^3$ |
| Pr | power to overcome rolling resistance (kW) | $M*g*v*(RRC_{measured})$ |
| Pi | power to overcome inertial effects (kW) | M'*a |
| Ptr | Power to overcome tractive resistance | Pa+Pr+Pg+Pc+Pi |
| Paccs | Power to run accessories | $EALC*(RPM/TRPM)+ECFLC*Pmax*(RPM/TRPM)^{2.5}$ |
| Peng | Power to overcome internal engine drag | $ceng+beng*(RPM/1000)^2$ |
| Ptot | Total power requirements (kW) | Ptr/edt+Paccs+Peng |
| IFC | Instantaneous Fuel Consumption (mL/s) | β*Ptot |
| TRPM | load governed maximum engine speed (rev/min) | 1900 (Komatsu, 2006) |

**Table 3.9: Values used for constants and variables within the HDM-4 fuel consumption model.**

| Input Variable | Description | Modelling Value | Reference |
|---|---|---|---|
| a | acceleration ($ms^{-2}$) | 0 | NA |
| IRI | Roughness (m/km) | Varies for each Section | NA |
| **Constant Variables** | | | |
| Cd | Aerodynamic drag coefficient | 0.9 | Zaabar, 2010 |
| AF | Projected frontal area ($m^2$) | 40.992 | Komatsu, 2006 |
| g | acceleration due to gravity ($m/s^2$) | 9.81 | NA |
| M | Vehicle Mass (kg) | 164,200 and 384,200 | NA |
| v | Velocity (m/s) | 4.17 and 8.33 | NA |
| M' | Effective Vehicle Mass (EMRAT*M) (kg) | 422,620 (EMRAT=1.1) | Greenwood et al, 2003 |
| β | fuel to power efficiency factor (mL/kW/s) | 0.07 | Greenwood et al, 2003 |
| EALC | accessory load constant (kW) | 10 | Greenwood et al, 2003 |
| ECFLC | cooling fan constant | 0.05 | Greenwood et al, 2003 |
| Pmax | maximum rated engine power (kW) | 1865 | Komatsu, 2006 |
| RPM | operating engine speed (RPM) | 1097 (15km/h) and 1089 (30km/h) | Zaabar, 2010 |
| edt | drive-train efficiency factor | 0.95 | Greenwood et al, 2003 |

In order to provide a point of comparison to the IFC results derived from the ARFCOM model described above, the model presented by the Department of Resources, Energy and Tourism (2010) was also utilised to estimate IFC. A full example calculation is shown in Appendix A, however as wheel torque was measured in the current project only a small portion of the full model was required for estimation of fuel consumption, as reproduced in Table 3.10. Note that estimations for the transmission efficiency (0.95) and efficiency at the wheels (25%) have been selected to be in-line with the inputs to the ARFCOM modelling and also the values suggested within Appendix A. Further the estimated calorific values of 38.6MJ/L of diesel fuel, as suggested in Appendix A, has been applied.

**Table 3.10: Input parameters for IFC modelling via Department of Resources, Energy and Tourism (2010).**

| Parameter | Function |
|---|---|
| Wheel rotations/second (radians/second) | ω=Vehicle velocity/(π.Wheel outside Diameter) |
| Power from wheel torque (kW) | Power=2πω.Wheel Torque |
| Engine output power (kW) | Power from wheel torque/0.95 |
| Fuel input power (kW) | Engine output power/0.25 |
| Fuel input per second (ml/s) | $IFC = \frac{Fuel\ input\ power}{38.6 * 1000}$ |

Thompson et al (2003) report a fuel consumption model, derived as part of a VOC model for haul trucks. However this model only utilised truck speed as a dependant variable and hence it is not able to be tested with the inclusion of pavement roughness or measured RRC found through the testing of this project.

## 3.7 Material Sampling

Sampling of materials was made from windrows from recent maintenance grading of the alignments in question. The collection of material was completed in compliance with Main Roads Western Australia Test Method 100.1 from windrows adjacent the road alignments and therefore employing the principles for sample collection from a stockpile.

## 3.8 Laboratory Testing

The objective of the laboratory testing carried out for this project was to define the shear and elastic properties of the soils sampled from the deflection test sites. These parameters provide insight into the applicability of the laboratory testing employed through comparison of modelling results, which was completed using the elastic parameters derived through both from laboratory testing and back-analysis of deflection data (see Section 3.9.1). Additionally, Particle Size Distribution (PSD) tests were completed to help describe the nature of the materials sampled from the deflection test sites. Atterberg testing was not completed due to a shortage of material sampled, arising from restrictions on transportation within financial constraints. Instead precedence was given to Repeated Load Tri-axial Tests (RLTT) to define resilient modulus and multi-stage unconsolidated-undrained (UU) tests to define shear strength parameters, as both provide direct input parameters to pavement modelling techniques. Classification of materials in accordance with AS 1726 (Standards Australia, 1993) and MRWA (2003) guidance on selection of natural materials as pavement courses was completed to provide an understanding of the nature of materials encountered.

### 3.8.1 Particle Size Distribution

The PSD of each sample was determined in accordance with AS 1289.3.6.1 (Standards Australia, 2009). Hydrometer testing for particles finer than 75 micron was not considered necessary for the scope of this project.

PSD test results were utilised for classification of the materials as per AS 1726. This considers the factors Coefficient of Uniformity ($C_u$) and Coefficient of Curvature ($C_c$), which are defined in Equation 3.25 and Equation 3.26 respectively. Additionally, the percentage of the material passing a 0.075mm aperture is required for classification of material in accordance with AS 1726. To provide some broad guidance, well graded gravels have a $C_u$ greater than 4 and a $C_c$ between 1 and 3, with percentage finer than 0.075mm being less than 5 (AS 1726). Detailed guidance on the classification of materials utilising these factors and the PSD results is contained within AS 1726.

**Equation 3.25: Cu factor as per AS 1726 (Standards Australia, 1993).**

$$C_u = \frac{D_{60}}{D_{10}}$$

**Equation 3.26: Cc factor as per AS 1726 (Standards Australia, 1993).**

$$C_c = \frac{(D_{30})^2}{D_{10}.D_{60}}$$

Where:

$C_u$ is a factor defined in AS 1726 (Standards Australia, 1993)

$C_c$ is a factor defined in AS 1726 (Standards Australia, 1993)

$D_{10}$ is the aperture opening that 10% (by weight) of the sample passes

$D_{30}$ is the aperture opening that 30% (by weight) of the sample passes

$D_{60}$ is the aperture opening that 60% (by weight) of the sample passes

Assessment of the sampled materials was also completed in accordance with MRWA guidance for the selection of natural gravels for use in unbound granular pavements (MRWA, 2003). For this assessment the Dust Ratio (DR) and Grading Modulus (GM) were calculated via Equation 3.27 and Equation 3.28 respectively. For selection of gravels for base-course, the DR should be within the range of 0.3 to 0.7 and the grading modulus should exceed 1.5. Additionally, the PSD results were compared with the 'Lt10' selection criteria within MRWA (2003). These limits relate to material selection for lateritic gravels in semi-arid and arid regions of Western Australia. Many of the mines in Western Australia are located within such climatic regions.

**Equation 3.27: Dust Ratio as per MRWA (2003).**

$$DR = \frac{P_{0.075}}{P_{0.425}}$$

**Equation 3.28: Grading Modulus as per MRWA (2003).**

$$GM = \frac{[300(P_{2.36} + P_{0.425} + P_{0.075})]}{100}$$

Where:

$DR$ is the dust ratio

$GM$ is the grading modulus

$P_{0.075}$ is the percentage of the sample by weight passing a 0.075mm aperture

$P_{0.425}$ is the percentage of the sample by weight passing a 0.425mm aperture

$P_{2.36}$ is the percentage of the sample by weight passing a 2.36mm aperture

### 3.8.1 Optimum Moisture Content/Maximum Dry Density

Optimum Moisture Content/Maximum Dry Density (OMC/MDD) testing was completed in accordance with AS 1289.5.1.1 (Standards Australia, 2003). Standard compactive effort (596 kJ/m$^3$) was selected in preference to modified compactive effort (2703 kJ/m$^3$). This decision was made due to the haul road pavements in question being compacted by wheel actions, without the use of dynamic/vibratory means on an approximate two meter lift thickness and without moisture conditioning. This approach may have been better supported via in-situ density testing, however this was not possible due to the coarse nature of the material excluding the use of a nuclear densometer via the method described by AS 1289.5.8.1 (Standards Australia, 2007A). In-situ density testing by the water replacement method, as described by AS 1289.5.3.5 (Standards Australia, 1997) was considered but was ultimately judged as being too time-consuming for the limited time available for on-site testing.

### 3.8.2 Shear Parameters

Shear parameters were determined through a modified test method, based on AS 1289.6.4.1 (Standards Australia, 1998). A Controls Triax100 tri-axial testing machine was utilised to complete this test, with manual logging of data from dial gauges and automatic control of pore pressure via an automated displacement pump. It was not practical to apply the method in the above Australian Standard with a 67mm diameter sample. An adequate sample could not be produced due to the angular nature of coarse particles within the sampled soils, resulting in the impermeable membrane being pierced during compaction through tamping. Furthermore, it was found that the sample could not be effectively removed from the tamping mould. Ultimately it was decided to follow the same procedure with a 100mm diameter sample size (200mm height), with the sample preparation described in Austroad's test methodology AG:PT/T05 (Austroads, 2007) being utilised (as used for RLTT testing, see Section 3.8.3). Multi-stage testing was applied due to testing requiring the 100mm diameter samples, after being originally planned to be completed using 67mm diameter samples. As a 67mm diameter sample weighs approximately a third the weight of a 100mm diameter sample it was possible to apply multi-stage testing with a 100mm diameter sample to obtain the data required with the limited quantity of material available. Samples were not allowed to consolidate, however the sample for Section 1 did remain sealed in a mould for approximately 4 weeks as repairs to the tri-axial apparatus were occurring. Drainage during the test was also not allowed, as it was considered more representative of the transient loading of a passing wheel. As deflection tests were completed over periods of less than an hour (see Section 3.5.7) this condition was also considered more appropriate than the sample being fully drained.

Stress states for testing were selected such that they were located on a similar stress path to that utilised for RLTT testing. These stress states were selected to extend the critical stress path for the stages of testing within the AG:PT/T05 (Austroads, 2007) test method, to replicate the higher deviatoric stress present under a haul truck tyre (see 'Modified Stress States' in Figure 3.22). Therefore, testing was completed with confining stresses of 30, 100, 200 and 300 kPa. Section 1 was not tested at a confining stress of 30 kPa, as it was anticipated that the stress history may have had too large an effect (the 300 kPa stage had been completed first prior to repairs to the apparatus). A fixed strain rate of 1mm/minute was utilised throughout, which represents an axial strain rate of only 0.5% per minute which is

significantly less than the 1-2% suggested within AS 1289.6.4.1 (Standards Australia, 1998). This rate was selected to ensure adequate time was available to cease testing once the commencement of plastic yield was observed, representing the end of each stage.

#### 3.8.2.1 Elastic Modulus

The elastic modulus was required to facilitate modelling of the deflections measured on-site, as the loading was not cyclic in nature as would be represented by the resilient modulus. This value was selected from the deviator stress/axial strain plots of the multi-stage tri-axial testing. Tangent moduli were selected from the elastic loading portion of the curve. For this reason, tri-axial testing was completed with a confining stress range of 30-300 kPa. The ensuing stress states were considered to likely encompass the typical deviator and confining stresses induced during on-site deflection testing and thus representative estimates of elastic modulus can be calculated from the results of tri-axial testing. This approach assumes that the material acts elastically when subjected to the loading considered.

### 3.8.3 Resilient Modulus

Repeated loading tri-axial testing was completed using a GCTS STX-300 Dynamic Stress-Path Soil Tri-axial System, run through a PCP Pressure Control Panel connected to a SCON-1500 Digital System Controller. This equipment, with a sample in testing configuration, is shown in Figure 3.21.

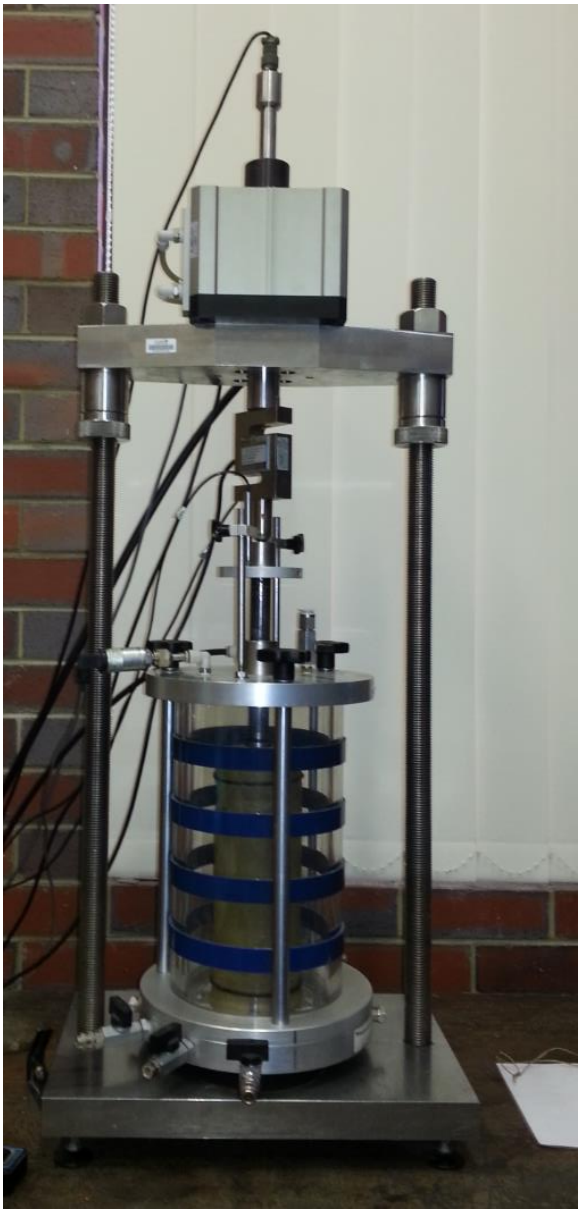

**Figure 3.21: RLTT test setup.**

Resilient modulus tests were completed in accordance with Austroads' test methodology AG:PT/T053 (Austroads, 2007). This test comprises 66 stages of testing with a maximum confining pressure of 150 kPa and a maximum deviator stress of 600 kPa. This was not considered representative of the loading experienced by haul road pavements, with the inflation pressure of the tyres considered in this project 890 kPa. For this reason, several stages were added to the testing regime, with the maximum deviator stress being 900 kPa, with confining stresses of 40 to 150 kPa. Resultant resilient modulus/bulk stress plots were then

observed for selection of the resilient modulus for respective stages of modelling. Figure 3.22 presents the additional stress stages. Initially the 'Modified Stress States 1' was applied. If the sample was still intact the 'Modified Stress States 2' was then completed. From observation of tri-axial test results, the relevant confining stress (and therefore mean normal stress) that corresponds to a deviatoric stress of 890 kPa was determined. Utilising this value, relevant resilient modulus values were selected for use in modelling with the assumption that material behaviour remains elastic.

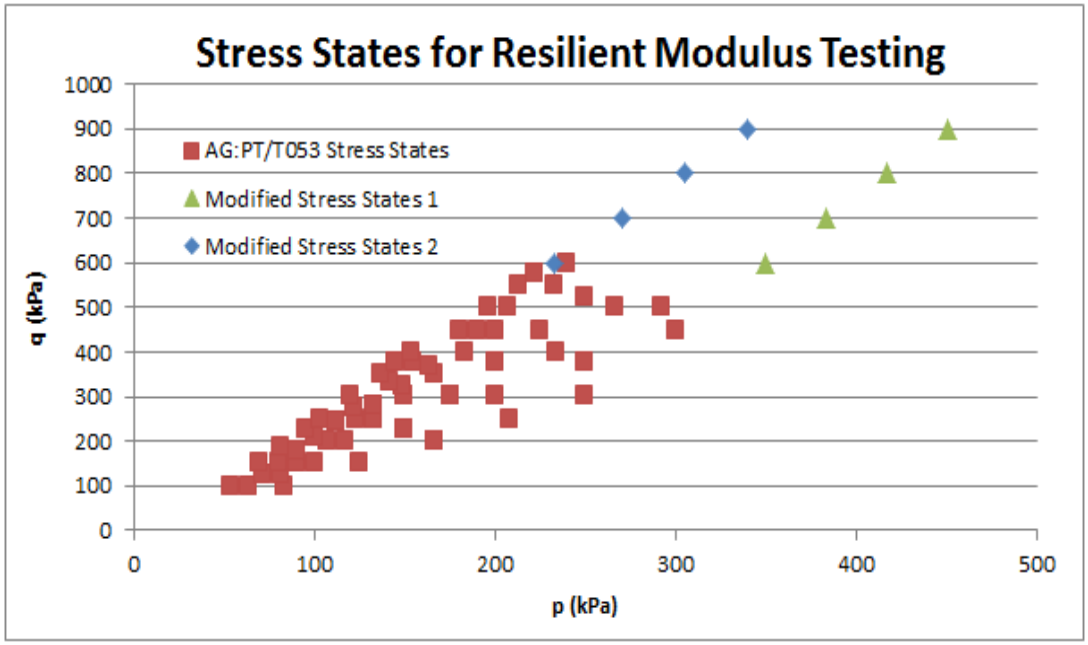


**Figure 3.22: Stress states (in p-q space) for resilient modulus testing.**

To assist in analysis and account for the non-linear response of the unbound materials encountered within the project, a trend-line relating to the 'k-Θ' theory, first published by Seed et al (1967) was derived for the set of results for each section. This relation was then used to estimate the resilient modulus at deviatoric stress levels relating to the 890kPa inflation pressure present on the truck utilised in testing. The resilient modulus was also calculated at a mean normal stress of 240kPa, as advised for calculation of resilient modulus by Main Roads Western Australia (MRWA, 2013).

## 3.9 Numerical Modelling

Several methods of numerical analysis have been considered within this project. The uses range from back-calculation of soil modulus with simple hand-calculation methods, to three-dimensional Finite Element Analysis (FEA) with complex software. Each is described in detail within the proceeding sections. An overview of the approach taken to address the objectives relating to pavement structural analysis, as stated in Section 1.2, is presented in Figure 3.23.

As stated in Section 3.2, there is very limited literature available relating observed haul road pavement response and the ability of structural analysis methods. Currently, there is only very broad direction available with state-of-the-art guidance documents (such as Thompson, 2013), stating that approach taken does not significantly influence the outcome. Consequently, it is considered valuable to investigate this statement, considering the level of data that may be available to a haul road pavement designer. The primary goal of the analysis detailed in the following, is to investigate whether the available linear-elastic and finite element approaches can accurately predict the deflected pavement surface profile, including deflection values and curvature profiles as depicted in Figure 3.23. As stated in Section 2.5.1, linear-elastic modelling is often utilised to validate finite element analysis models, prior to the complexity of the model being increased beyond the capabilities of the linear-elastic method. A similar approach is taken here. If possible, the most appropriate means of structural analysis is to be recommended. Consideration is then to be given to whether the best-performed approach can be considered to have been validated from the modelling completed for this project. This should incorporate consideration of the most appropriate material characterisations from laboratory testing.

The modelling in this project was completed subsequent to the in-situ and laboratory testing. It is anticipated that this level of information is likely to exceed that typically available to a practitioner. Furthermore, the investigation is aimed at making use of the available information to make recommendations that can best benefit the haul road pavement designer, utilising approaches that can realistically be implemented in practice.

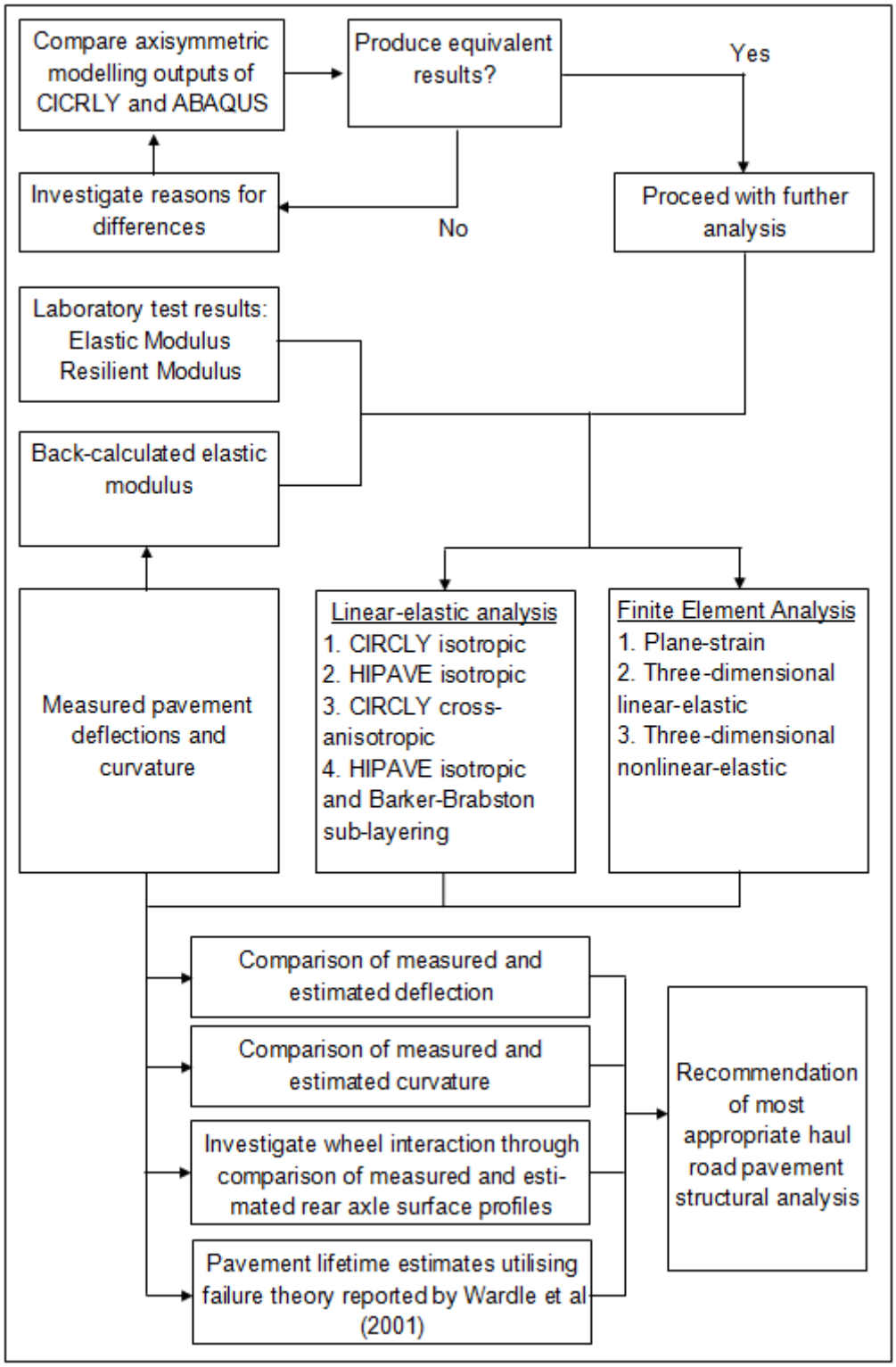


**Figure 3.23: Flow chart of approach taken for investigation of haul road pavement structural analysis methods.**

### 3.9.1 Back-calculation of Soil Modulus

#### 3.9.1.1 Calculation Methods

Back-calculation of soil modulus was completed by application of elastic theory, presented for the estimation of elastic settlements in several texts, including Knappett et al (2012). The measured contact patch (see Section 3.5.7.5 and Table 3.12) was modelled as a flexible footing, with the maximum deflection assumed to occur at the centre of the footing. Initially, the known tyre inflation pressure of 890kPa was utilised. However it was apparent that the uncertainty relating to contact stress distribution as discussed in Section 5.4.3 influenced the calculation significantly, with the soil moduli results estimated higher for the tyre load excluding truck payload. Therefore, the known tyre loads (Table 3.11) and measured contact patches were used to estimate the average contact pressure of the contact area (see Table 3.12). Influence factors (*Is* in Table 3.12) were calculated considering contact area geometry and with the assumption that maximum deflection occurs at the centre of the contact area. These values were estimated through interpolation of the values considered in Knappett et al (2012). Equation 3.29 was then used to back-calculate soil modulus from the maximum measured deflection for each section and load condition.

**Equation 3.29: Estimation of soil modulus from elastic theory (Knappett et al, 2012).**

$$E = \frac{q.B(1-\upsilon^2)I_S}{s}$$

Where:

$E$ is the soil modulus (Pa)

$q$ is the contact stress (Pa)

$B$ is the footing breadth (m)

$\upsilon$ is Poisson's ratio

$I_S$ is the Influence Factor as per Knappett et al (2012)

$s$ is the measured surface deflection (m)

**Table 3.11: Tyre load used for back-calculation of soil modulus.**

| | Tyre Load (kN) |
|---|---|
| Unloaded | 402.70 |
| Loaded | 1256.33 |

**Table 3.12: Geometry and pressure characteristics used in back-calculation.**

| Section 1 | Unloaded | Loaded |
|---|---|---|
| L (m) | 2.155 | 2.381 |
| B (m) | 0.739 | 0.996 |
| a ($m^2$) | 1.59 | 2.37 |
| L/b | 2.92 | 2.39 |
| Is | 1.70 | 1.60 |
| p (kPa) | 252.87 | 529.77 |
| **Section 2** | **Unloaded** | **Loaded** |
| L (m) | 2.107 | 2.281 |
| B (m) | 0.761 | 1.125 |
| a ($m^2$) | 1.60 | 2.57 |
| L/b | 2.77 | 2.03 |
| Is | 1.67 | 1.53 |
| p (kPa) | 251.15 | 489.58 |
| **Section 3** | **Unloaded** | **Loaded** |
| L (m) | 2.181 | 2.302 |
| B (m) | 0.709 | 1.045 |
| a ($m^2$) | 1.55 | 2.41 |
| L/b | 3.08 | 2.20 |
| Is | 1.73 | 1.56 |
| p (kPa) | 260.42 | 522.26 |

#### 3.9.1.2 Evercalc

Evercalc is a software package developed and published by the Washington State Department of Transport (USA). It is a back-analysis package for use with data arising from Falling Weight Deflectometer testing, although it also allows manual data input. This meant that the software was able to be used to back-analyse the

curvature data collected within this project. The following describes the modelling for the determination of pavement modulus.

Within Evercalc, tyre contact patches are considered to be circular. Therefore it was decided to utilise the average measured tyre contact geometry for the unloaded and loaded cases (see Table 4.17) to calculate an equivalent radius to allow input to Evercalc. The total area encompassed the entire dual-wheel rear axle assembly and thus included the approximately 300mm wide separation area between tyres. This was considered a necessary idealisation, as a dual-wheel assembly was present on the truck used for measurement of deflection, with wheel load being a required input. Contact area radii are presented with the back-analysis results in Table 4.64. Wheel loads are given in Table 3.11.

An option for the inclusion of a 'stiff' layer of user-defined elastic modulus is included within Evercalc. This feature was disabled for the back-analysis, as it was not able to be applied at a user defined depth, which results in variable depths for the uppermost layer in the analysis. As this layer represented the pavement in question, which was known to be approximately 2.0m thick, the feature was omitted from the back-analysis. The structure utilised in the analysis is presented in Figure 3.24. The elastic moduli of the three supporting layers are fixed at the values indicated. These were selected from an estimation of the stress state and consideration of the tri-axial elastic modulus test results presented in Section 4.7.5.3Stress state was estimated via Boussinesq's theorem (see Bowles, 1997) and superposition of the wheel load, considering the area of influence to increase at a radius to depth ratio of 0.5, and overburden pressure (estimated using an average unit weight of 24 $kN/m^3$, see Section 4.7.3). Although it is somewhat unusual to consider elastic modulus to increase with depth in pavement design, consider that this structure is relatively deep and represents quite a stiff foundation. This is representative of the supporting structure on the mine waste dump, where fill was as deep as 40m (see Section 3.5.2). The moduli values were considered to occur at mid-depth for all layers except the bottom layer, for which stresses can only be considered at the top of the layer as it is assumed to have infinite depth. Further, Evercalc includes an allowance for temperature correction of the pavement. This relates to asphalt surfaced pavements and is therefore not applicable to this study.

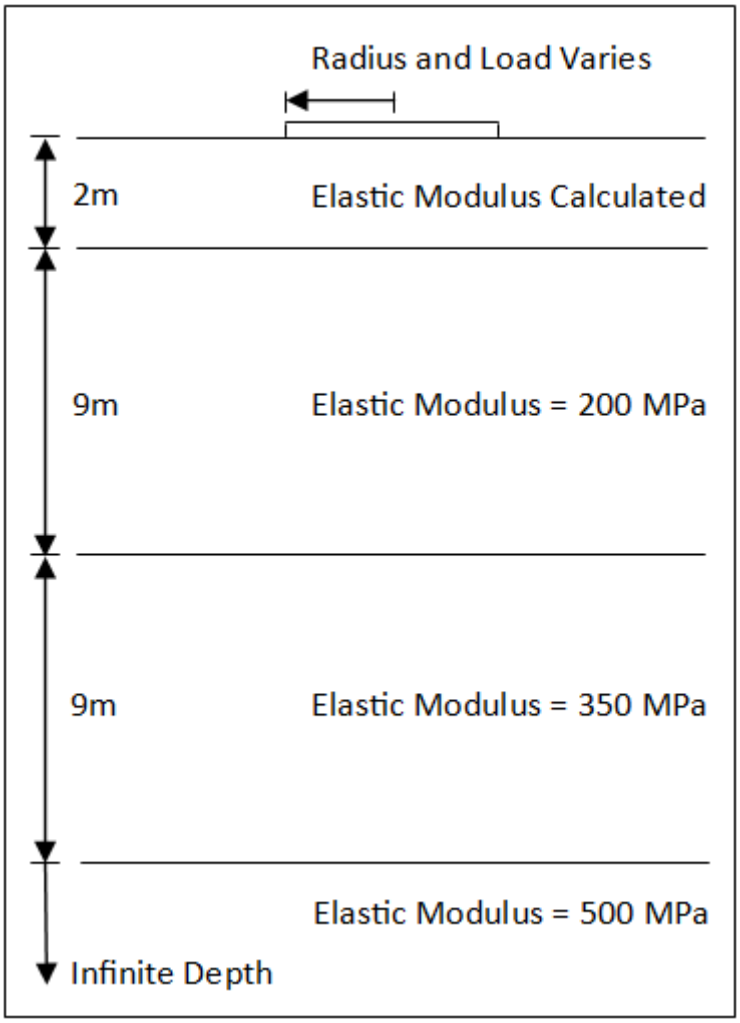


**Figure 3.24: Pavement and supporting structure used in Evercalc back-calculation of pavement elastic modulus.**

To perform the back-calculation, curvature data (see Section 4.4.1) was directly entered for each pavement section. The back-calculation was performed twice; once with curvature data extending from the centre of the loaded area and secondly with curvature extending from the edge of the loaded area. The former is likely more appropriate as it is similar to common FWD tests where geophones recording strain data commence from a small radial distance removed from the edge of the loaded plate. However, consider that the radius of the loaded area is actually a fictitious value that was estimated from the contact geometry presented in Section 4.4.3 and has subsequently been adopted to allow back-calculation using the Evercalc software. It is anticipated the 'true' value of pavement elastic modulus lies at a point between the two results. Although this is a source of error, the approach was

adopted in the absence of more advanced methods being available for such large tyre contact geometry and loading.

Root Mean Square (RMS) results are reported for each back-calculation. In completing the back-calculation process, Evercalc iteratively predicts curvature for varied soil elastic moduli within the user-specified range for each pavement layer. This data is then compared with the curvature data that was derived from direct measurement from the scans taken during on-site deflection testing (see Section 3.5.7). The RMS in turn describes the percentage relative error between the calculated and measured curvature data.

### 3.9.2 WES Method

Design of heavily loaded unbound granular pavements has often been completed using CBR curves described in Section 2.4.1. Pavement deflection was the pavement response that was considered to govern permanent deformation in the original derivation of the S77-1 method (Pereira, 1977), from experiments carried out at the Waterways Experiment Station (WES). This method was subsequently used to derive CBR design curves (Wardle et al, 2003). However the deflection is not actually calculated nor inputted within the method when deriving a design curve for a specific vehicle, but is used in calculating the Equivalent Single Wheel Load (ESWL). This method is based on Boussinesq's single-layer theorem and considers the pavement to be a single, isotropic mass (Wardle et al, 2010). Calculation of pavement deflection first requires determination of the ESWL, a fictitious wheel load with the same contact geometry as one of the wheels in the design gear. However, the inflation pressure is calculated such that it produces a pavement deflection equal to that produced by the entire group. ESWL varies with depth and therefore calculation is an iterative process involving calculation of the deflection profiles with depth at multiple points (Pereira, 1977).

Equation 3.30 was used to calculate deflection at the mid-point of the tyres on a rear-axle dual wheel gear present on the Komatsu 830E, as utilised during on-site testing. Because the pavement surface deflection is considered in the present study, the calculation of ESWL is simplified with the use of Equation 3.31. When estimating the deflection due to the multiple wheels on a haul truck, the ESWL pressure is used in place of tyre inflation pressure, to account for the effects of multiple wheel loads. Deflection factors were selected via linear interpolation between the tables

presented in Pereira (1977), the reader is referred to the original reference for further information.

**Equation 3.30: Pavement deflection, as per Pereira (1977).**

$$\Delta_m = \frac{p.r}{E} \sum F_M$$

Where:

$\Delta_m$ is the calculated deflection (mm)

$p$ is the tyre contact pressure (kPa)

$r$ is the tyre contact area radius (m)

$E$ is the elastic modulus of the material (MPa)

$F_M$ is the deflection factor for each wheel considered (unit-less)

**Equation 3.31: Calculation of ESWL from known wheel load.**

$$P_e = P \frac{F_M}{F_e}$$

Where:

$P_e$ is the ESWL

$P$ is the load on one wheel in the group

$F_e$ is the maximum deflection factor for a single wheel

**Equation 3.32: Maximum deflection due to ESWL (Pereira, 1977).**

$$\Delta_e = \frac{p_e r}{E} F_e$$

Where:

$\Delta_e$ is the maximum deflection due to ESWL

$p_e$ is the ESWL contact pressure

$F_e$ is the maximum deflection factor due to the ESWL

Once the characteristics of the ESWL were calculated via Equation 3.31, the maximum deflection due to ESWL was calculated using Equation 3.32. The point considered was at the pavement surface at the centre of a rear wheel assembly of the Komatsu 830E. The methodology is as described above, except the maximum deflection factor due to a single wheel load ($F_e$) was utilised instead of the maximum deflection factor ($F_M$). For the case of a Poisson's ratio of 0.35, the maximum deflection factor due to a single wheel was 1.75. This value was utilised for all calculations involving Equation 3.32.

Finally, it was attempted to gain some understanding of the inflation pressure that is best to utilise in pavement modelling via calculation of the average contact pressure from measured pavement deflections. For this purpose the contact radii matching the measured contact area were utilised, along with the static elastic moduli values derived through tri-axial testing. The resulting contact pressure was then used to calculate the corresponding wheel load. Subsequently, this value was compared to wheel loads published by a tyre manufacturer for various inflation pressures (goodyearotr.com). The known wheel load and calculated ESWL is also presented for comparison in Section 4.8.2. The published data is an example of the data typically used in mechanistic design and the latter in empirical designs with the S77-1 curve presented by Pereira (1977). This analysis provides some insight into the adequacy of available pavement design methods, through comparison of published wheel load and pavement/tyre contact data and the corresponding values that are estimated in completing designs via commonly accepted pavement design techniques.

### 3.9.3 Linear-Elastic Software

There are many software programs available that allow analysis of layered pavements using linear materials and elastic theory. The pre-cursor to CIRCLY was developed at the CSIRO (Commonwealth Scientific and Industrial Research Organisation), prior to the program becoming commercially available in 1977 (Mincad Systems, 2012). Since its release CIRCLY (Mincad Systems, 2012) has been updated several times and Mincad Systems have also released an off-shoot, HIPAVE (Mincad Systems, 2012B), which is optimised for mechanistic design of flexible pavements subjected to heavy wheel loads arising from freight handling vehicles (Mincad Systems, 2009). These programs allow significant variation of loading and material modelling to be considered, which forms the basis for their use within this project. The modelling completed with each is explained in the following sections. Note that HIPAVE is discussed first as it has been used more extensively for this project, with CIRCLY being used to test different load inputs and allowances for material stress-dependency with the Austroads sub-layering methodology.

The following assumptions are held constant throughout all linear-elastic modelling completed within the software packages discussed below:

1. all materials are considered to be linear-elastic
2. wheel loads are applied to a circular contact area with constant imposed contact pressure
3. all materials have a Poisson's ratio of 0.35.

#### 3.9.3.2 HIPAVE

HIPAVE 5 is a linear-elastic pavement design software program produced by Mincad Systems (2012B). It is a customisation of the CIRCLY software that was developed to provide a tool for pavement design in accordance with the method originally selected by Austroads (Jameson, 2008A). The focus of HIPAVE is the design of heavy industrial pavements, particularly those of port facilities and container terminals (Wardle et al, 2006). This means that the program includes a material model for UGMs commonly referred to as the Barker-Brabston sub-layering model (see Section 2.6.2), which approximates non-linear material effects. Note that the maximum elastic modulus considered within the Barker-Brabston method for unbound material is 275 MPa (Wardle et al, 2010). When including this

characterisation of a UGM, the material modulus is calculated from the modulus of the sub-grade layer upwards. Therefore the base-course layer was also characterised as isotropic, with the various elastic modulus values discussed in Section 3.8 (these values are also included in Section 4.8.5.1). Modelling generally excluded the use of the Barker-Brabston characterisation of pavement and sub-grade materials. The pavement structure of the modelling remains constant throughout, as illustrated in Figure 3.25. This figure presents the loading regime along the rear axle of a Komatsu 830E haul truck. Response due to the front axle was generally not included within the analysis. Although not all wheel loads are included in every modelled case, the geometry of loads considered is shown in Figure 3.26. Contact pressures were calculated from known axle loads and the contact areas presented in Section 4.4.3. Geometry was selected as per Komatsu (2006).

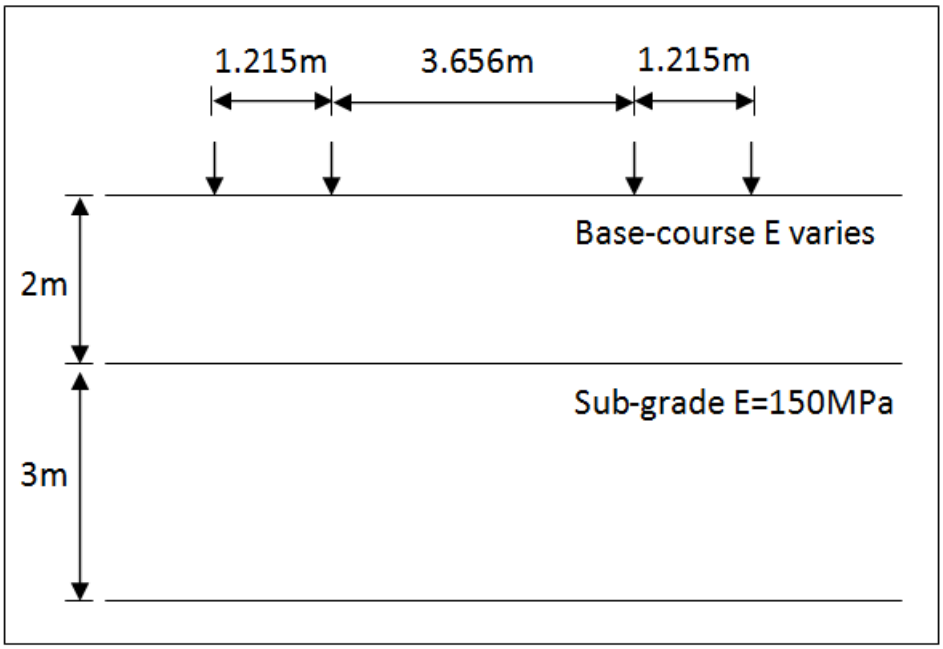


**Figure 3.25: HIPAVE model geometry and material inputs, along the rear axle of Komatsu 830E haul truck.**

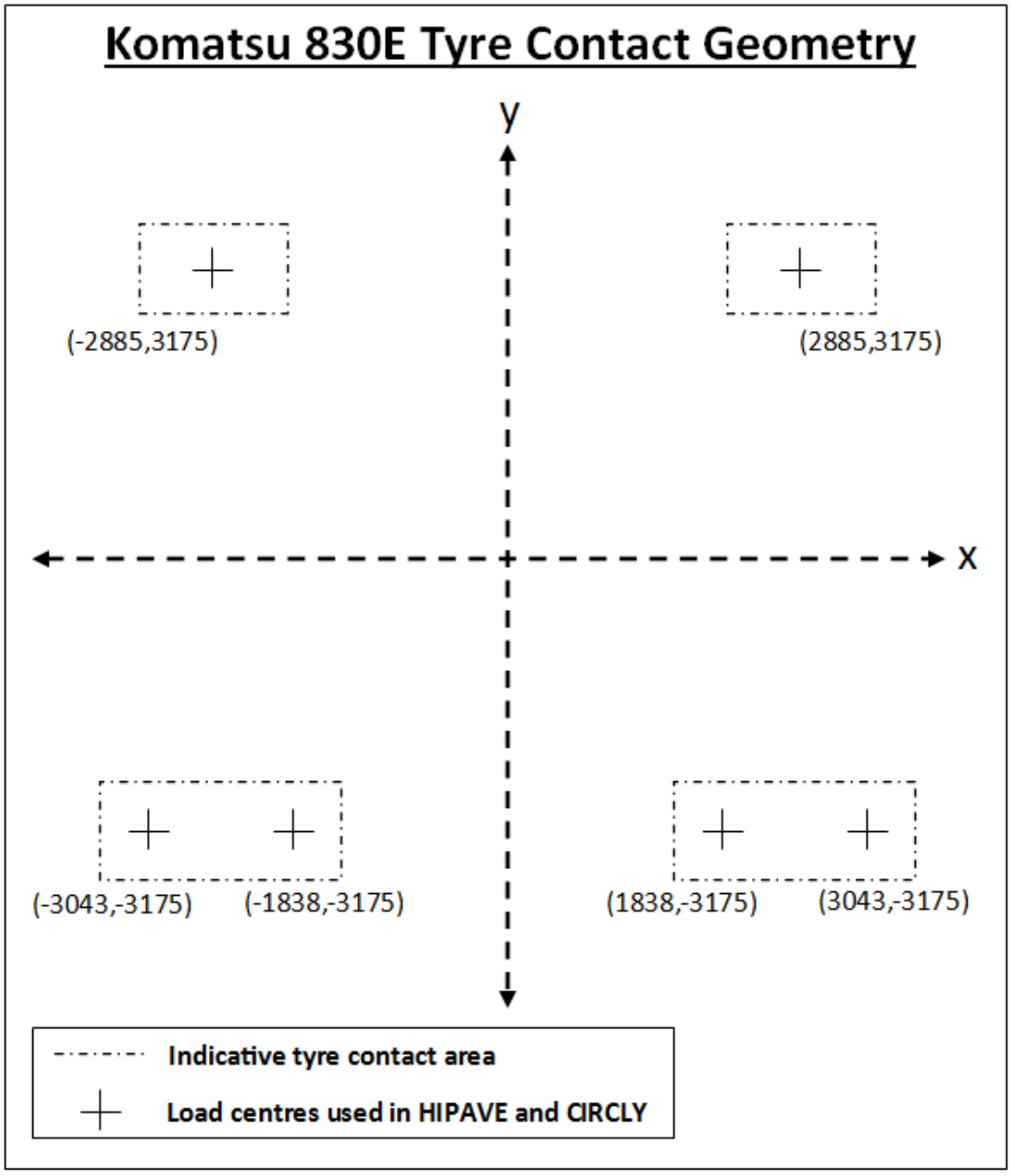


**Figure 3.26: Geometry used for HIPAVE and CIRCLY modelling of Komatsu 830E contact geometry.**

Initially, a sub-grade elastic modulus of 150 MPa (analogous to a CBR of 15%) was selected. This decision was based on the tri-axial testing completed (see Section 3.8.2.1). A significant depth of influence should be expected from the relatively large loaded area of the haul truck tyres. High confining pressures could therefore be expected to be induced within the sub-grade layer, when compared to general flexible pavements, thus resulting in relatively high elastic modulus values being

mobilised. The modelling was repeated, with a select foundation as shown in Table 3.13 and Table 3.14, utilising isotropic base-course characterisation. The elastic moduli values for layer A, B and C relate to two metre deep layers from the under-side of a two meter deep base-course layer. Elastic modulus values were selected from calculation of the vertical stress state on a sub-grade soil element via Boussinesq's theory, with consideration of additional surcharge at-depth due to the presence of the truck tyres. Lateral soil pressure at rest was then estimated using a 40 degree internal angle of friction. Modulus values were then selected from interpolation of tri-axial testing.

**Table 3.13: Foundation layer elastic moduli values for unloaded truck – Select foundation.**

| Section | Layer | a (m) | P | v | z (m) | $\sigma_1$ - due to surcharge | $\sigma_{1,TOTAL}$ | $\sigma_3$ | E (Mpa) |
|---|---|---|---|---|---|---|---|---|---|
| 1 | A | 0.712 | 253.80 | 0.35 | 3 | 21.44 | 97.37 | 34.76 | 60 |
| | B | 0.712 | 253.80 | 0.35 | 5 | 7.72 | 134.27 | 47.93 | 80 |
| | C | 0.712 | 253.80 | 0.35 | 7 | 3.94 | 181.11 | 64.66 | 100 |
| 2 | A | 0.819 | 191.82 | 0.35 | 3 | 21.44 | 94.14 | 33.61 | 148 |
| | B | 0.819 | 191.82 | 0.35 | 5 | 7.72 | 128.87 | 46.01 | 182 |
| | C | 0.819 | 191.82 | 0.35 | 7 | 3.94 | 173.55 | 61.96 | 227 |
| 3 | A | 0.702 | 261.08 | 0.35 | 3 | 21.44 | 92.08 | 32.87 | 142 |
| | B | 0.702 | 261.08 | 0.35 | 5 | 7.72 | 125.44 | 44.78 | 160 |
| | C | 0.702 | 261.08 | 0.35 | 7 | 3.94 | 168.75 | 60.24 | 184 |

**Table 3.14: Foundation layer elastic moduli values for loaded truck – Select foundation.**

| Section | Layer | a (m) | P | v | z | $\sigma_1$ - due to surcharge | $\sigma_{1,TOTAL}$ | $\sigma_3$ | E (Mpa) |
|---|---|---|---|---|---|---|---|---|---|
| 1 | A | 0.869 | 529.69 | 0.35 | 3 | 66.67 | 142.60 | 50.91 | 80 |
| | B | 0.869 | 529.69 | 0.35 | 5 | 24.00 | 150.55 | 53.75 | 90 |
| | C | 0.869 | 529.69 | 0.35 | 7 | 12.24 | 189.41 | 67.62 | 100 |
| 2 | A | 0.904 | 489.47 | 0.35 | 3 | 66.67 | 139.36 | 49.75 | 193 |
| | B | 0.904 | 489.47 | 0.35 | 5 | 24.00 | 145.15 | 51.82 | 198 |
| | C | 0.904 | 489.47 | 0.35 | 7 | 12.24 | 181.86 | 64.92 | 235 |
| 3 | A | 0.864 | 535.84 | 0.35 | 3 | 66.67 | 137.30 | 49.02 | 167 |
| | B | 0.864 | 535.84 | 0.35 | 5 | 24.00 | 141.72 | 50.59 | 169 |
| | C | 0.864 | 535.84 | 0.35 | 7 | 12.24 | 177.05 | 63.21 | 188 |

Following the above characterisation of the support structure, it was decided to trial including a Barker-Brabston sub-base layer to produce a similar approximation of material stress-dependency. This layer was considered two metres thick and was placed between the two metre thick base-course (with moduli values as measured through the various methods described in Section 3.8) and three metre thick sub-grade with an elastic modulus of 150MPa. The pavement was also modelled twice more, with idealisation as a single layer of Barker-Brabston base and sub-base with the top of the layer in contact with the wheel load. Barker-Brabston sub-layer moduli (for both base and sub-base materials) are assigned with consideration of the stiffness of the support layer. Therefore significantly different deviatoric stress is applied when the material is placed at depth compared to being in direct contact with the tyre load. Such an arrangement allows for some consideration of stress-dependency while maintaining control over the maximum modulus mobilised at the pavement surface (which as stated above is 275 MPa for a UGM).

Interaction of tyre loads were tested by comparing the surface deflection profile and vertical strain at the top of the sub-grade arising firstly from analysis with inclusion of the whole rear axle of the Komatsu 830E and secondly with only a single dual-wheel assembly. It is contended that strains attenuate closer to the applied load than deflections (see Section 2.4.2.1). Examination of these two responses was considered adequate for comment on the likelihood of interaction of load response from adjacent wheel gears. If deflection was not observed to interact at the surface, or if the vertical strain level was not found to be higher at the mid-point of the rear axle when both wheel gears are considered then it was concluded that wheel interaction does not occur. See Section 3.9.7 for further discussion of the examination of wheel load interaction.

#### 3.9.3.3 CIRCLY

Modelling within CIRCLY was completed to test the suitability of differing material models, and load characteristics, in predicting the measured pavement deflections with linear-elastic theory based software. Its origins extend back to the development of what is commonly referred to as the Austroads mechanistic design procedure, where CIRCLY was recommended for use in estimating pavement deflection (Jameson, 2008A). The geometry and loading characteristics were the same as for HIPAVE modelling as shown within Figure 3.25 and Figure 3.26, with one exception. Sub-grade depth was also trialled as continuing to infinite depth. Initially, sub-

layering of unbound granular base-course materials was considered with the Austroads (2004) method (Jameson, 2008). This was completed to compare the impact of changing the sub-layering methodology from that applied within HIPAVE. Additionally a non-uniform distribution of contact pressure was trialled, with a significantly higher contact stress at the edges of the tyre as advised in Jameson (2008). Thus the loading applied in CIRCLY was applied with a load exponent of -0.5, see Mincad Systems (2014) for further explanation. Non-uniform load distributions were found to significantly over estimate pavement deflections and were therefore not completed within the analysis for this project. Note that the Austroads sub-layering method involves input of the elastic modulus of the top sub-layer, whereas the Barker-Brabston method utilised by the HIPAVE software is dependent on the supporting layer's elastic moduli. The modulus of the top sub-layer was then selected as the minimum of the inputted base-course modulus value and that calculated from the sub-grade modulus. The base-course layer was also considered without sub-layering, thus characterising it with a single modulus value.

There exists two major differences between HIPAVE and CIRCLY, beyond sub-layering. These are the characterisation of unbound materials as cross-anisotropic and load input involving definition of contact area and pressure (in place of wheel load). Cross-anisotropic characterisation involves five inputs. Firstly elastic modulus in the vertical ($E_V$) and horizontal ($E_H$) direction are required. To simplify definition of the horizontal modulus, Austroads (Jameson, 2008) advises that a degree of anisotropy ($E_V$/ $E_H$) equal to two is appropriate in all cases of unbound pavement materials. Also required is Poisson's ratio in each direction, which was selected to be 0.35 in all cases, as suggested by Austroads (Jameson, 2008). The fifth input is the shear modulus and is calculated via Equation 3.33. The relative effects of cross-anisotropy are discussed within Section 2.6.3. Note that despite the CIRCLY User Manual suggesting that the tyre inflation pressure is generally used as the contact pressure, it was decided to use the average contact pressure, calculated from measured contact geometry and known tyre loads. Contact areas within CIRCLY are considered as circular, and therefore a radius producing an equivalent area to the measured rectangular contact areas was inputted.

**Equation 3.33: Shear modulus function used within CIRCLY (Mincad Systems, 2009).**

$$f = \frac{E_v}{(1+v)}$$

Where:

$f$ is the shear modulus (MPa)

$E_v$ is the vertical elastic modulus (MPa)

$v$ is Poisson's ratio in the vertical direction

### 3.9.4 Finite Element Analysis

Finite Element Analysis (FEA) was completed with use of the Dessault Systemes ABAQUS Standard 6.10 software. This is a general FEA package allowing detailed input of materials, boundary conditions and loading. However, an effort was made to maintain some simplicity in the modelling, so as to allow a test of the capabilities of the model in comparison with those discussed in the preceding sections. One benefit of FEA is that soil anisotropy is considered to be allowed for by the redistribution of stresses carried out during iterations of the calculation, as noted in Section 2.5.2. The effect of such complexity is that computing time is increased exponentially over a simple layered-elastic analysis and therefore it may be that at the current point in time FEA is not be practical for use as a design tool for haul road pavements. Despite this, an ability to closely model pavement deflections would present opportunities to investigate structural response through numerical modelling, which could guide future research efforts towards increasing the understanding and definition of the model's inputs.

Note that the only characteristics of FEA modelling that is held constant for all analysis are outlined below:

1. all materials are considered to be isotropic
2. Poisson's ratio is 0.35 for all materials
3. the contact pressure between wheel and pavement surface is constant.

At first modelling comprised of a simplified sub-grade structure, where all sub-grade layers shown in Figure 3.27 and Figure 3.28 had a resilient modulus of 150MPa. This was done to replicate the modelling completed within CIRCLY and HIPAVE, however it is worth noting that only the resilient modulus was utilised within FEA. This was completed so that the 'k-Θ' model could be applied, as detailed in Gonzalez et al (2012). All other geometry and model inputs were as described below and applied to models resulting from the iterative process to better define sub-grade layer structure.

Following the initial, simplified analysis, FEA modelling comprised of two discreet steps. Firstly, two-dimensional models were utilised to complete the iterative procedure described below to determine an appropriate layer structure. The resulting structure was subsequently used for three-dimensional modelling, from which pavement surface deflection and sub-grade vertical strains were taken. This procedure was selected based on the recommendation of Ghadimi et al (2013) whereby a plane strain approximation was found to produce poor predictions of pavement response, as discussed in Section 2.5.2. However, the non-linear effects of UGMs in flexible pavements is widely accepted (see Section 2.6.1), and thus the iterative procedure was carried out with a two dimensional (plane strain) model to reduce computational time.

An annotated sketch of the two-dimensional model used is presented in Figure 3.27. The base-course is 2m thick throughout the modelling and is supported on 18m of sub-grade. A fixed encastre boundary condition was selected for the base of the model. The horizontal extent of the model are 15m from the outside of wheel loads in both directions, with the mid-point of the rear axle at the centre. Measured tyre contact area geometry (Section 3.5.7.5) was utilised, with the total contact area arising from the dual wheel gears included together in the modelling. Average pressure arising from the known wheel loads was then applied as a uniform contact pressure (as adopted in CIRCLY and HIPAVE modelling). This approach includes the small strip of separation between the tyres, found to be approximately 350mm wide, within the loaded area (see Section 4.4.3). At this time it is considered necessary to make this simplification, as an extremely high resolution mesh (requiring a long computation time) would otherwise be required to effectively model the area. It is anticipated that this approach does not introduce significant error into the results, as the known total wheel load is applied and consequently the net effect is a slightly lower contact pressure being applied over a marginally larger contact area than occurs in reality.

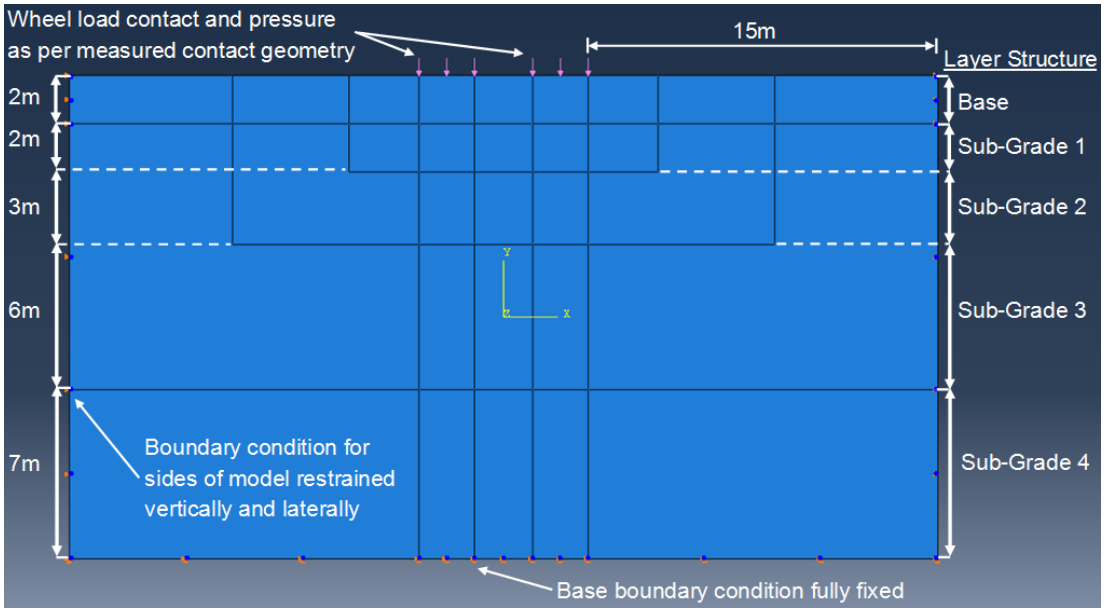


**Figure 3.27: Annotated sketch of plane-strain FEA model.**

A fine mesh was utilised throughout the modelling with a higher resolution employed around the loaded area (0.1m element size) and directly below the loaded area to a considerable depth. A structured mesh was used to ensure the shape of mesh elements was consistent throughout modelling.

Loading applied to the model included gravity initially and the wheel loads secondly. The effect of gravity was to apply stress due to over-burden pressure to the soil at-depth. This stress state was used in the iterative procedure described below, to estimate non-linear effects in each sub-grade layer (see Figure 3.27) due to the stress-dependant nature of UGMs. The gravity action was not applied during the tests producing the deflection estimates presented in Section 4.8.6.

The boundary conditions for the model are relatively simple. Lateral deflections are dis-allowed at the edge of the model, with vertical deflections allowed. The base of the model is fully fixed. Due to the considerable size of the model, it is not anticipated that these boundary conditions have a significant effect on the results.

In order to replicate the non-linear effects of the pavement and sub-grade, multiple iterations, balancing mean normal stress at the middle of each layer and resilient modulus, were made for all pavement sections. This approach applied the resilient

modulus models discussed in Section 3.8.3, by utilising the resultant mean normal stress at the centre of each layer and re-calculating the layer's resilient modulus to be applied in the subsequent step. The point considered was typically taken directly under one of the wheel loads. However, it was found that higher stress states occurred at the mid-point of both wheel loads from the 'Sub-Grade 2' layer downwards, when modelling a full rear axle. The iterations were terminated once each layer resilient moduli was within 5% of the previous step.

The above method effectively prioritises the relationship derived from the data for laboratory resilient modulus testing over modulus results arising from measured pavement surface deflection data. This approach was adopted due to the fact that the iterations discussed above to mimic non-linear soil effects are not able to be completed automatically in the ABAQUS software. Furthermore, as discussed in Section 3.9.1.2, there has not been an accepted method developed for wheel loads as large as that present on haul trucks. However, the derived resilient modulus values are in fitting with the range stated in the literature for gravel materials (Jameson, 2008), as discussed in Section 5.7.3. Also, the focus of this project with regards to pavement modelling was to test each method's ability to model haul road pavements. Therefore, it would be a considerable extrapolation to attempt a back-calculation of pavement layer modulus and support structure with the use of FEA.

Three-dimensional modelling was then completed with geometry and material properties replicated from the two-dimensional models derived via the procedure above, in order to test the effect of additional geometric detail. Figure 3.28 presents the geometry, load and boundary conditions utilised for the three-dimensional modelling. Note that the geometry was held constant for all modelling of all sections, other than that of the wheel load contact area, which was varied to match the measured geometry (see Section 3.5.7.5). This approach is consistent with the two-dimensional modelling described above. The model geometry was smaller than recommended in much of the literature in terms of the ratio of overall modelled area and depth to tyre contact radius. However, the total size of the model was similar to many of the models presented in the literature in terms of the number of elements. Subsequently, the model was constructed to restrain the number of elements in order to achieve a workable calculation time. After observing initial results with this geometry, it appeared the calculated pavement response was not significantly affected by this simplification. An eight-noded axisymmetric mesh was selected for three-dimensional modelling, as recommended by Ghadimi et al (2013), due to their noted ability in producing accurate pavement response outputs. The element sizes

were 0.25m near the load centres, linearly increasing to a 0.8m maximum element size adjacent the model boundaries. The pavement surface deflection and sub-grade vertical strain were then compared with that from the two-dimensional models.

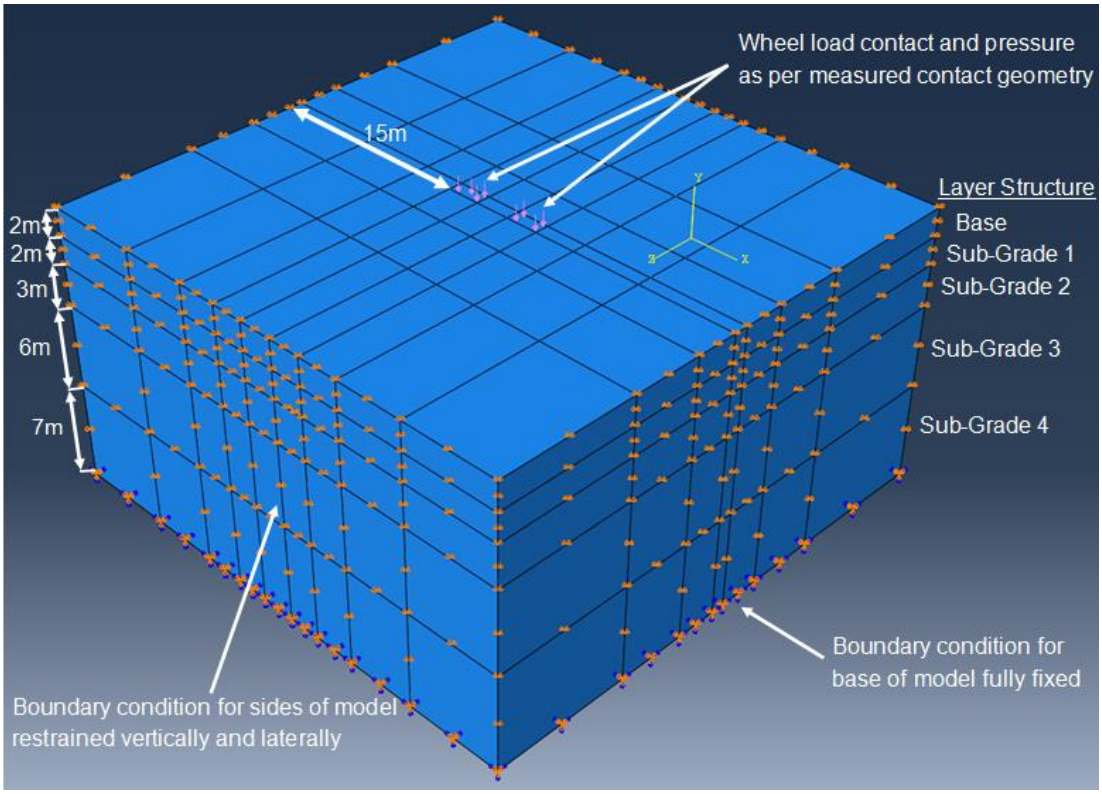


**Figure 3.28: Annotated sketch of three-dimensional FEA model.**

Once the above iteration was completed the model output was interrogated to define the deflection and sub-grade strain outputs required. The interaction of wheel loads, as described in Section 3.9.7, was also investigated.

### 3.9.5 Comparison of Linear-Elastic and FEA Axisymmetric Modelling

In order to complete a comprehensive comparison of two modelling techniques, linear-elastic and FEA in this project, it is necessary to describe any variation in modelling outputs that occur under conditions of equal input parameters. For the current study, linear-elastic modelling (CIRCLY) and FEA (ABAQUS) have been

compared with an axisymmetric model. For this purpose the sub-grade modulus was set at 150MPa, with the base-course modulus varying. It was decided to select the base-course modulus from the values measured in the laboratory for this project. Consequently, the modulus values arising from the monotonic triaxial test (static elastic modulus) and repeated load triaxial test (resilient modulus) have been applied. The base-course was maintained as 2m deep throughout. For CIRCLY analysis, the sub-grade was set as 3m deep. Based on the geometry recommended in the literature (Kim, 2007; Gonzalez et al, 2012; Ghadimi, 2015), the ABAQUS model extended 10m laterally and 100m vertically. This represents approximately 178 loaded tyre radii vertically and 18 radii laterally. Figure 3.29 shows the FEA model used for this purpose. Note that roller supports were applied to the boundaries extending in either lateral direction. The outer faces were not allowed to displace but had no constraint against rotation, while the base of the model was fixed against displacement and rotation.

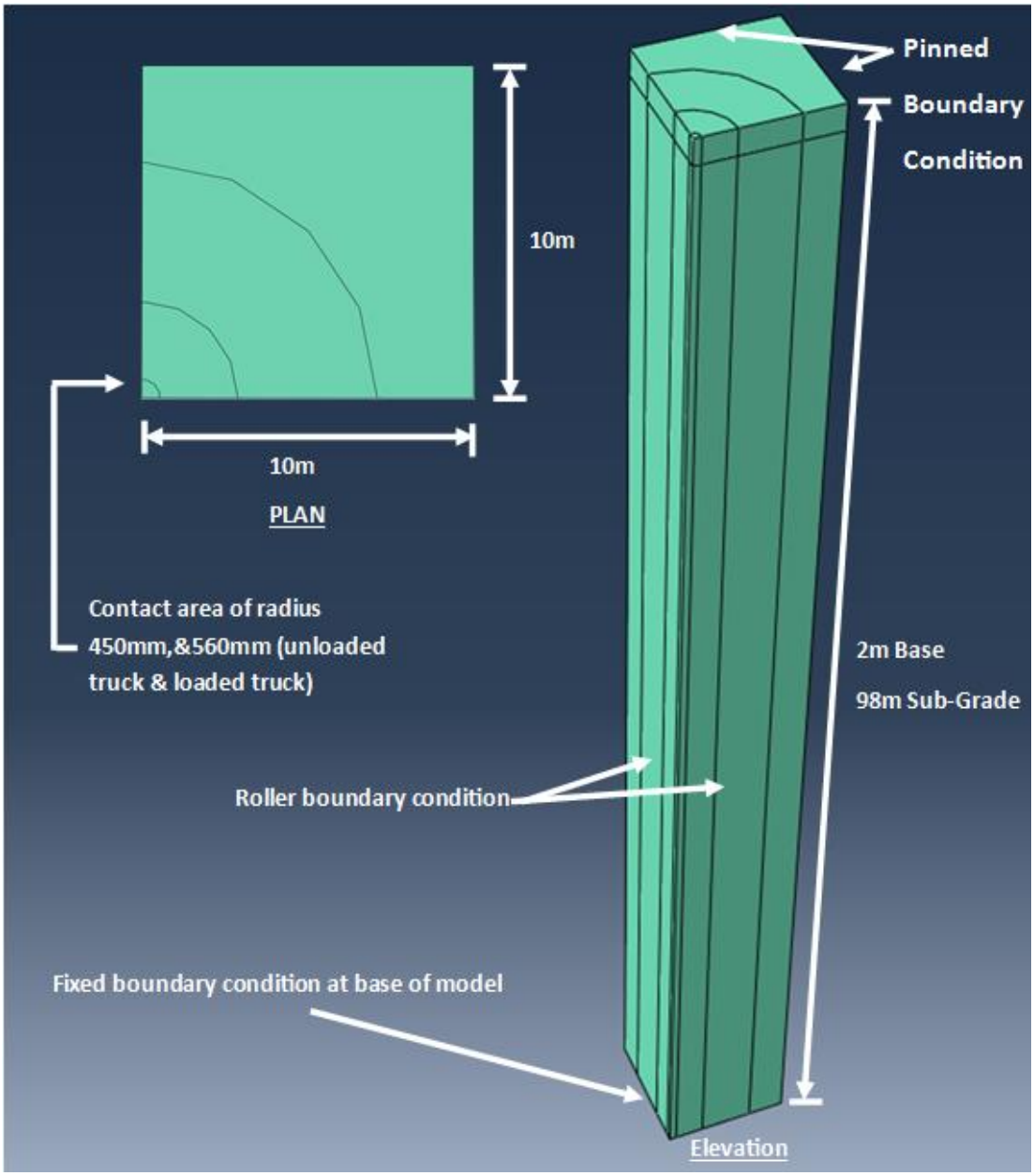


**Figure 3.29: Annotated sketch of axisymmetric FEA model.**

### 3.9.6 Comparison of Isotropic and Anisotropic Base-Course Characterisation

Following the above comparison relating to isotropic linear-elastic half-spaces, the relative effect of cross-anisotropic base-course material was investigated. This is a common practice and is recommended by Austroads (Jameson et al, 2008) for characterisation of UGM pavement layers. For this reason it has been included as a

material input within CIRCLY. The anisotropic ratio (vertical modulus:horizontal modulus) was selected as two, in line with Austroads recommendations.

Comparison was made by utilising CIRCLY to repeat the modelling discussed in Section 3.9.5 with the base-course modified to be cross-anisotropic. The results are then able to be compared to provide insight into the relative effect of anisotropy of pavement materials. To provide more detailed understand, sub-grade horizontal strain was also calculated for two situation considered a relatively 'soft' sub-grade with light loading (section 1 with base-course modelled with static elastic modulus and an unloaded truck) and a relatively stiff base-course with heavy load (section one base-course modelled with resilient modulus and a loaded truck). The results of this modelling are of importance as it provides an insight in to the degree of load that is transferred radially away from the load with the introduction of base-course anisotropy. A practical indication of the impact of including anisotropic materials in pavement modelling is provided by observing the different estimated pavement calculated by HIPAVE (isotropic) and CIRCLY (cross-anisotropic), see Section 3.9.9 for further discussion on this topic.

### 3.9.7 Modelling of Wheel Load Interaction

Wheel interaction could potentially impact pavement lifetime estimates, primarily with use of mechanistic-empirical design techniques. Two parameters are investigated within the modelled pavement below the mid-point of the rear axle of the Komatsu 830E haul truck. This has been considered the most critical location for potential wheel load interaction as it represents the mid-point between wheel gear loads that each account for one third of total truck weight when loaded. The two parameters investigated were:

1. Deflection at the pavement surface.
2. Vertical compressive strain at the top of the sub-grade.

In both instances analysis was initially completed applying only half of the rear axle and then repeated with the full rear axle. This procedure was repeated with both CIRCLY and HIPAVE, with investigation of the strain level completed at this location within the analysis outputs from ABAQUS Standard 6.10. Plots of the deflection outputs arising from modelling with half and full axles were then compared to investigate tyre interaction predicted by the various modelling methods.

### 3.9.8 Comparison of Pavement Curvature

Comparison of pavement deflection does not provide much understanding into the sensitivity of the analysis technique. For example, there are simple equations such as Equation 3.29 that can estimate the deflection for simple elastic soil structures for a given loading intensity and geometry. An investigation of the pavement curvature predicted by each analysis method is considered necessary to provide some insight into the accuracy of the soil response to load at depth. As is explained in the preceding section, this is critical to accurately predict pavement lifetime with the currently available pavement failure theories.

The predicted pavement deflection profile (curvature) along the rear axle of the Komatsu 830E was compared to measured deflection profiles attained through the process detailed in Section 3.5.7. To provide further understanding of the ability of each modelling method, the curvature from the centre of the dual-wheel assembly in a direction directly back from the truck has also been investigated. The latter is essentially similar to the curvature function commonly utilised in pavement engineering for back-calculation of pavement stiffness values.

FEA (ABAQUS) modelling adopted the resilient modulus values for the characterisation of the base-course, as these values produced the best agreement with measured deflection values. For the same reason, the static elastic modulus values have been adopted for the CIRCLY modelling. Although a point of difference in the two methods, objective six and seven of the study (Section 1.2) relate to investigation of the most appropriate methods for the analysis of haul roads. This includes selection of the most appropriate testing methods to characterise pavement materials. If the resilient modulus had been adopted for the CIRCLY analysis, as with ABAQUS, the curvature values would have been found to be even further from that measured during deflection testing.

### 3.9.9 Comparison of Pavement Lifetime Estimates

Following the above linear-elastic analyses, predictions of pavement life were then made with utilisation of both CIRCLY and HIPAVE, to allow comparison to the CBR design curves discussed in Section 3.9.9.1. Note that lifetime estimates generated via CIRCLY made use of the same sub-grade failure theory utilised by HIPAVE. Therefore, the focus of the investigation was the different methodologies adopted in each software package to calculate critical sub-grade strains. Comparison of lifetime

estimates were made by selecting various points on the S77-1 derived CBR design curves for a Komatsu 830E haul truck, and then modelling the resulting pavements (thickness and CBR values) in both HIPAVE, CIRCLY and ABAQUS Standard 6.10.

As stated in Section 3.9, current practice for mechanistic-empirical haul road pavement design does not consider the sensitivity of different structural analysis methods. Therefore, this comparison is intended to present the differences in sub-grade vertical compressive strain, and the resulting pavement lifetime estimates that result from the use of different analysis techniques. A comparison of surface deflection profiles is described above. For the purpose of design, such analysis must be applied with a defined pavement failure theory. There is little benefit in providing recommendation of a given modelling approach based on predicted pavement surface deflected profiles, if the same approach provides poor estimates of sub-grade strain resulting in unrealistic estimated pavement lifetimes.

To further the discussion above, it is imperative that, if shown to have a significant effect on haul truck rolling resistance, pavement design is completed in such a way to present opportunities to optimise road user cost. Therefore, limiting elastic strain may address rolling resistance arising from hysteresis best represented by pavement deflection. However, the time-dependent effect of pavement rutting may still require addressing to limit rolling resistance due to pavement roughness. It is understood that the failure theory considered throughout the estimation of pavement lifetime considers a failure to have occurred when a 20mm rut has developed. This is considered to be associated with a high level of pavement roughness, and consequently it may be that the pavement lifetime (or time to maintenance) is actually shorter than that found from the procedures below. Although this is dependent on the outcome of the interrogation of the generation of haul truck rolling resistance completed for this project.

To consider the deterioration of the haul road pavement surfaces, the theory presented by Thompson (2009) is also considered to provide some insight into the serviceability of the pavement considered due to the calculated sub-grade strain. The basis of this theory is shown in Figure 2.20. This theory also considers the pavement rolling resistance indirectly, by consideration of the performance index. Therefore, if it is shown to align somewhat with the theory reported by Wardle et al (2001), it may be extended by further including the understanding of how haul road rolling resistance is generated and how this could be optimised in design.

#### 3.9.9.1 Generation of CBR Design Curves with S77-1

Design curves were generated via the method described by the U.S. Army Corps of Engineers in Pereira (1977) with use of the S77-1 curve presented in Figure 2.18 (White, 2007). A detailed explanation of the method utilised for the generation of curves is not presented here, as it was completed in accordance with the methodology detailed by Pereira (1977). The inputs utilised were as per published values for a 40.00R57 off-the-road tyre (goodyearotr.com), which was fitted to the Komatsu 830E haul truck during in-situ testing. The contact area radius was 575mm (goodyearotr.com). A single wheel load was considered to be 64,037kg as was utilised during in-situ deflection testing. Finally, Poisson's ratio for the pavement material was 0.35 as advised by Austroads for unbound granular materials (Jameson, 2008).

Selection of 'alpha factors' are required to account for multiple wheels within a group for the purpose of CBR curve generation. As noted in Wardle et al (2010), it is considered appropriate to model only a single wheel gear in mechanistic design. The basis of this recommendation is that strain (considered the controlling factor for mechanistic design) attenuates much more rapidly in the radial direction from the load centre than deflection (Wardle et al, 2010). This issue creates some conflict, as deflection was the limiting design criteria applied within modelling completed in the derivation of the S77-1 method. Accordingly it was decided to stay with the recommended approach for each respective design method. Subsequently, the CBR design curves generated within this study have considered variable alpha factors to take account of all six wheels on a Komatsu 830E and varying load repetitions, as advised by Pereira (1977).

Design curves have been calculated considering all wheel loads separately, as per the method presented by Pereira (1977) and also with dual-wheel gears being represented by a single contact area. The latter was found to produce the most accurate surface deflection predictions and as such it is considered valuable to consider the effect on resulting design pavement thickness. Although an extrapolation from the original pavement model this could represent a simplification that better represents wheel load interaction for haul trucks.

Finally, the pavement thickness calculated by the method described by Pereira (1977) includes a 75mm layer of asphalt and 150mm of crushed rock over variable uncrushed gravel sub-bases. Consequently, some equivalence of these two upper materials must be made. This was completed via the equivalency factors stated by

White (2007), meaning the thickness of uncrushed gravel layers were scaled by 1.6 when replacing asphalt and 1.2 when replacing crushed rock. Consequently, 75mm of unbound granular material (minimum CBR 20%, as per the P154 material described in Section 3.9.9.2) has been added to each calculated design thickness.

#### 3.9.9.2 HIPAVE/CIRCLY Pavement Lifetime Estimates

Pavement lifetime estimates made within HIPAVE and CIRCLY utilised similar pavement models and an identical sub-grade failure theory. The pavement model employed was composed of Barker-Brabston sub-base materials overlaying an isotropic sub-grade of varying elastic moduli. The natural granular material considered in designs derived via the S77-1 curve, as described by Pereira (1977), is considered a P-154 material as specified by the Federal Aviation Administration (FAA, 1995) and has a minimum CBR value of 20% (White, 2007). For this reason the base-course material was selected as a cross-anisotropic material with an elastic moduli of 200 MPa for modelling with CIRCLY and HIPAVE. Note that this is despite the P154 material nominally having a resilient modulus of approximately 150MPa, as this would have suggested it was only of sub-grade quality. From the discussion within Section 5.7.3 this was considered inappropriate for UGMs subjected to high stress states. The sub-grade was also modelled with cross-anisotropic characterisation and varying elastic moduli to provide some comparison with the design arising from use of the S77-1 curve (White, 2007). No sub-layering was applied to either base or sub-grade materials within CIRCLY or HIPAVE.

Contact pressures within both CIRCLY and HIPAVE were those of the published maximum value for a 40.00R57 tyre, which is 700 kPa (goodyearotr.com). This is commensurate with the recommendations arising from the investigation of pavement deflection estimates within this project (refer to Section 5.8.2). Tyre contact area (represented by radius for the assumed circular contact area in both programs) was a constant 575mm throughout modelling, as published for a 40.00R57 tyre (goodyearotr.com).

As stated above, the sub-grade failure theory utilised for both software packages was identical. Critical strains were calculated as required and then pavement lifetime values were estimated as per Equation 3.34, Equation 3.35 and Equation 3.36. This is the method inbuilt within HIPAVE and is described by Wardle et al (2005). The ‘k’ and ‘b’ constants vary with sub-grade modulus and are presented for the respective materials considered within the modelling in Table 3.15. Note that the sub-grade

failure theory has been extrapolated for a sub-grade CBR value of 20% (elastic modulus of 200MPa). Although generally considered inappropriate for design by MRWA (MRWA, 2013) and Austroads (Jameson, 2008) this has been included to test the suitability of such a measure. Equation 3.35 and Equation 3.36 have been extended to allow consideration of the number of wheels in a gear. However, the increased accuracy noted in the validation of these equations is only 2.2% for a two wheel configuration (Wardle et al, 2010). Due to the uncertainty of the interaction of wheel loads occurring under a haul truck, the updated 'k' and 'b' factors have not been adopted in the analysis. Further, consider that there is conjecture as to the suitability of using a factor of 10 when transforming sub-grade CBR values to resilient modulus values (see Section 2.6.5.2), which further complicates the prediction of lifetime estimates utilising this method.

**Equation 3.34: Pavement life as per Wardle et al (2005).**

$$N = \left(\frac{k}{\varepsilon}\right)^{b}$$

Where:

$N$ is the number of allowable strain repetitions (number of $\varepsilon$ repetitions in pavement life)

$\varepsilon$ is the induced sub-grade vertical compressive strain (unit-less strain)

$k$ is a parameter, as per Equation 3.35

$b$ is a parameter, as per Equation 3.36

**Equation 3.35: 'k' parameter for use in estimating pavement life.**

$$k = 1.64 * 10^{-9}E^3 - 4.31 * 10^{-7}E^2 + 2.18 * 10^{-5}E + 0.00289$$

**Equation 3.36: 'b' parameter for use in estimating pavement life.**

$$b = -2.12 * 10^{-7}E^3 + 8.38 * 10^2 - 0.0274E + 9.57$$

Where:

$E$ is the sub-grade elastic modulus (MPa)

The resulting failure criteria are described below in Table 3.15.

**Table 3.15: Sub-grade failure criterion as per Wardle et al (2005).**

| Sub-Grade E (Mpa) | k | b |
|---|---|---|
| 30 | 0.0032 | 9.496476 |
| 50 | 0.003108 | 10.2685 |
| 100 | 0.0024 | 14.998 |
| 150 | 0.001998 | 23.5995 |
| 200 | 0.00313 | 35.914 |

Finally, it is stated by Austroads (Jameson, 2008) that modelling with a thin surfacing (nominally asphalt less than 40mm thick) involves a low level of confidence. The impact of modelling with relatively high elastic modulus materials is potentially a significant source of error. This area requires significant further research, but is considered outside the scope of this investigation.

#### 3.9.9.3 FEA Modelling – Pavement Lifetime Estimates

Pavement lifetime estimates completed with FEA were initially made with an effort to mirror the models employed in linear-elastic modelling. This involved utilising the average tyre contact geometry found through terrestrial laser scanning described in Section 3.5.7.5. The iterative process of balancing pavement layer moduli with estimated stress from plane strain FEA models, as discussed ins Section 3.9.4 resulted in a relatively consistent foundation structure ('Sub-Grade 2' to Sub-Grade

4' in Figure 3.27 and Figure 3.28). It is contended that these relatively high elastic moduli values are plausible due to the high confining stress resulting from the significant overburden pressure. Subsequently, these layers were designated elastic modulus values of 250MPa, 300 MPa and 350MPa within modelling for pavement lifetime estimates for comparison with CBR design curve predictions. The pavement layer thickness and moduli values were then selected as with CIRCLY and HIPAVE modelling, to allow for direct comparison of pavement lifetime estimates utilising the sub-grade failure theory detailed in Section 3.9.9.2.

Secondly, pavement lifetime estimates were made for the pavements involved in on-site deflection testing. The maximum assumed sub-grade modulus of 150MPa was used for calculation, in line with the maximum value in the validation completed by Wardle et al (2001). This involved selecting the critical sub-grade strain values that occurred in the results of the modelling described in Section 3.9.4. This allows further comparison with estimates made via the other methods discussed above.

# 4 Results

The following section presents the results for the testing and modelling detailed in Section 3.

## 4.1 Ambient Conditions

The maximum temperature on the day of rolling resistance testing (25 January 2014) was 36.9 degrees Celsius. However testing was completed from 8:30 AM to 10:30 AM and thus the ambient temperature was approximately 30 degrees Celsius over the duration of testing.

### 4.1.1 Wind Speed Data

Wind speed and direction was measured at the beginning and end of each set of testing (note the time elapsed between each test set was approximately 3 minutes), the results are presented in Table 4.1.

**Table 4.1: Wind speed data relating to rolling resistance tests.**

| Test Set Description | Wind Speeds (m/s) | Wind Direction |
|---|---|---|
| Prior 15km/h Anti-Clockwise Loaded | 0.4 | Westerly |
| Prior 30km/h Anti-Clockwise Loaded | 0.4 | Westerly |
| Prior 30km/h Clockwise Loaded | 0.7 | Westerly |
| Prior 15km/h Clockwise Loaded | 1.1 | Westerly |
| Prior 15km/h Anti-Clockwise Unloaded | 1.3 | Westerly |
| Prior 30 km/h Anti-Clockwise Unloaded | 1.4 | Westerly |
| Prior 15km/h Clockwise Unloaded | 2.1 | Westerly |
| Prior 30km/h Clockwise Unloaded | 2.2 | Westerly |

### 4.2 Pavement Texture

Pavement texture results are shown in Table 4.2. The standard deviation referred to below relates to the differences between test locations for each pavement section.

**Table 4.2: Pavement texture results for each section.**

| Section | Average Texture (mm) | Standard Deviation (mm) |
|---|---|---|
| 1 | 8.4 | 3.2 |
| 2 | 19.9 | 4.5 |
| 3 | 22.4 | 2.4 |

### 4.3 Pavement Roughness

A summary of pavement roughness results is presented in Table 4.3, where roughness is presented as the standard deviation to moving averages over varying wavelengths. Table 4.4 attempts to present roughness in a standardised form, through use of an approximation for IRI employing the average variance of pavement surface undulations, calculated over a 3m moving average.

**Table 4.3: Summary of average standard deviation from various moving averages for each section.**

| Section | Average Standard Deviation (0.5m Moving Average) | Average Standard Deviation (1m Moving Average) | Average Standard Deviation (5m Moving Average) | Average Standard Deviation (10m Moving Average) | Average Standard Deviation (20m Moving Average) |
|---|---|---|---|---|---|
| 1 Inner | 0.0025 | 0.0034 | 0.0110 | 0.0191 | 0.031 |
| 1 Outer | 0.0026 | 0.0032 | 0.0082 | 0.0132 | 0.0206 |
| 1 Average | 0.0026 | 0.0033 | 0.0096 | 0.0162 | 0.0258 |
| 2 Inner | 0.0032 | 0.0043 | 0.0134 | 0.0236 | 0.0383 |
| 2 Outer | 0.0049 | 0.0075 | 0.0249 | 0.0413 | 0.0599 |
| 2 Average | 0.0041 | 0.0059 | 0.0191 | 0.0325 | 0.0491 |
| 3 Inner | 0.0206 | 0.0209 | 0.0239 | 0.0290 | 0.0394 |
| 3 Outer | 0.0072 | 0.0086 | 0.0173 | 0.0268 | 0.0451 |
| 3 Average | 0.0139 | 0.0147 | 0.0206 | 0.0279 | 0.0423 |

**Table 4.4: Estimated IRI for each section, as per Mclean et al (1996).**

| Section | Mean Variance from 3m Moving Average ($mm^2$) | Estimate IRI (m/km) |
|---|---|---|
| 1 Inner | 74.1 | 6.5 |
| 1 Outer | 41.5 | 4.9 |
| 1 Average | 57.8 | 5.8 |
| 2 Inner | 96.1 | 7.5 |
| 2 Outer | 353.5 | 14.3 |
| 2 Average | 224.8 | 11.4 |
| 3 Inner | 566.7 | 18.1 |
| 3 Outer | 210.1 | 11.0 |
| 3 Average | 388.4 | 15.0 |

### 4.3.1 Pavement Roughness Plots – Section 1

Graphical results for Section 1 comparing road chainage against each parameter listed below, are presented in the proceeding:

- Elevation (m);
- Standard deviation (0.5m moving average);
- Standard deviation (1m moving average);
- Standard deviation (5m moving average);

- Standard deviation (10m moving average);
- Standard deviation (20m moving average).

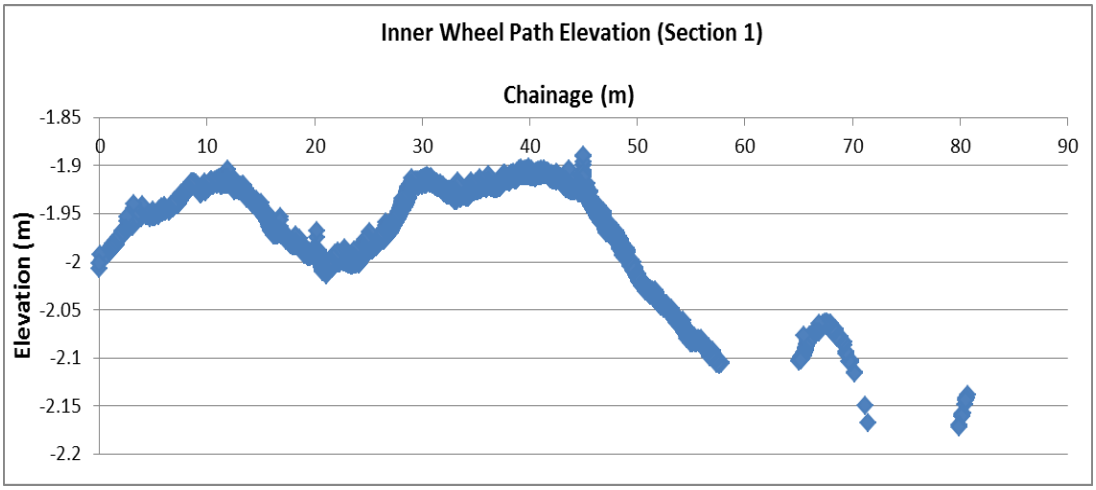


**Figure 4.1: Section 1 inner wheel path elevation.**

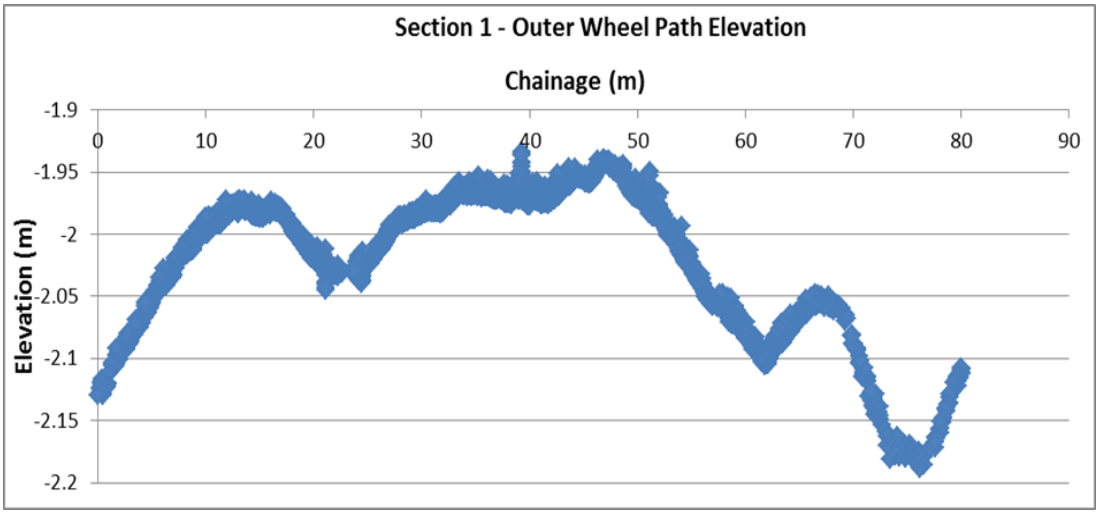


**Figure 4.2: Section 1 outer wheel path elevation.**

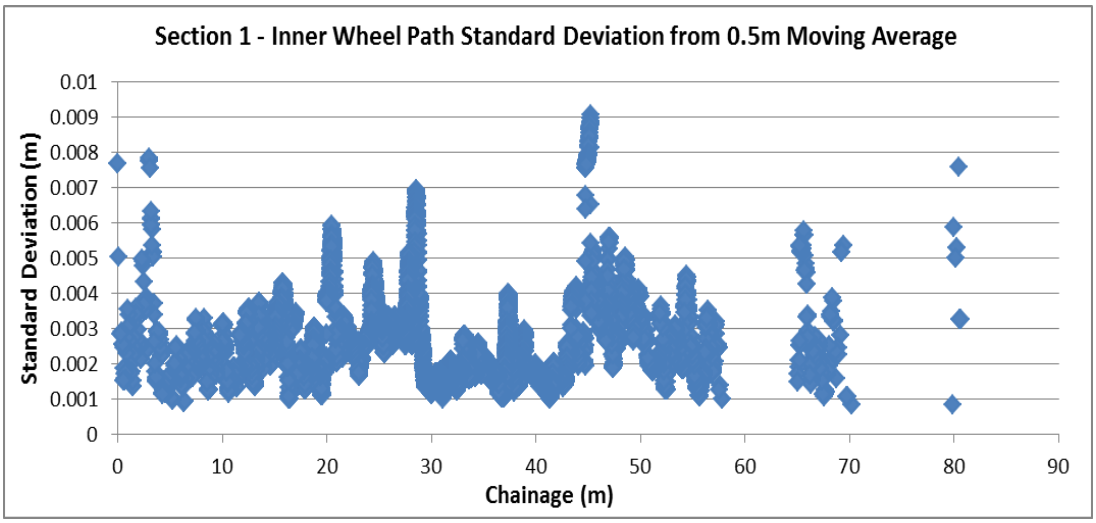


**Figure 4.3: Section 1 inner wheel path, standard deviation (0.5m moving average).**

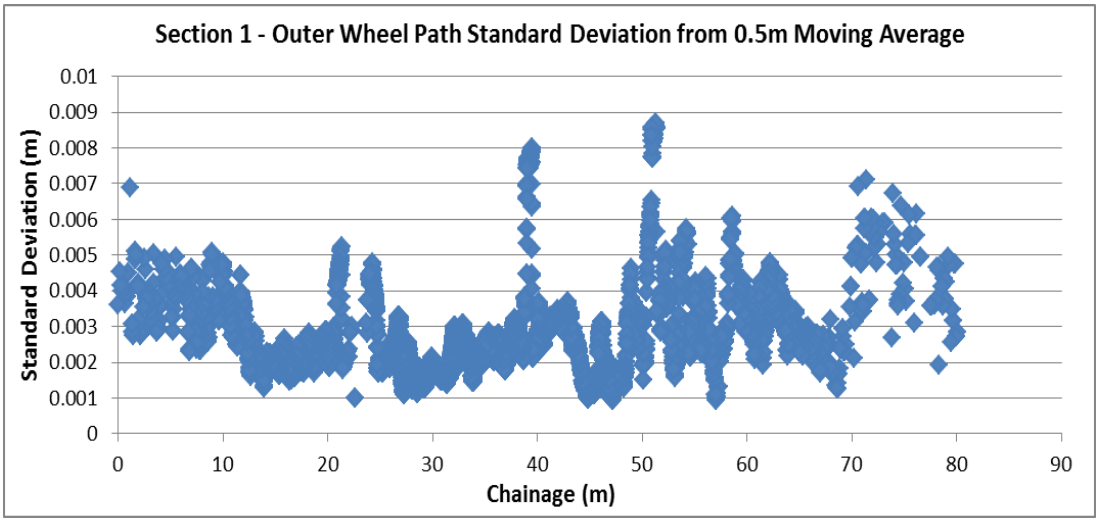


**Figure 4.4: Section 1 outer wheel path, standard deviation (0.5m moving average).**

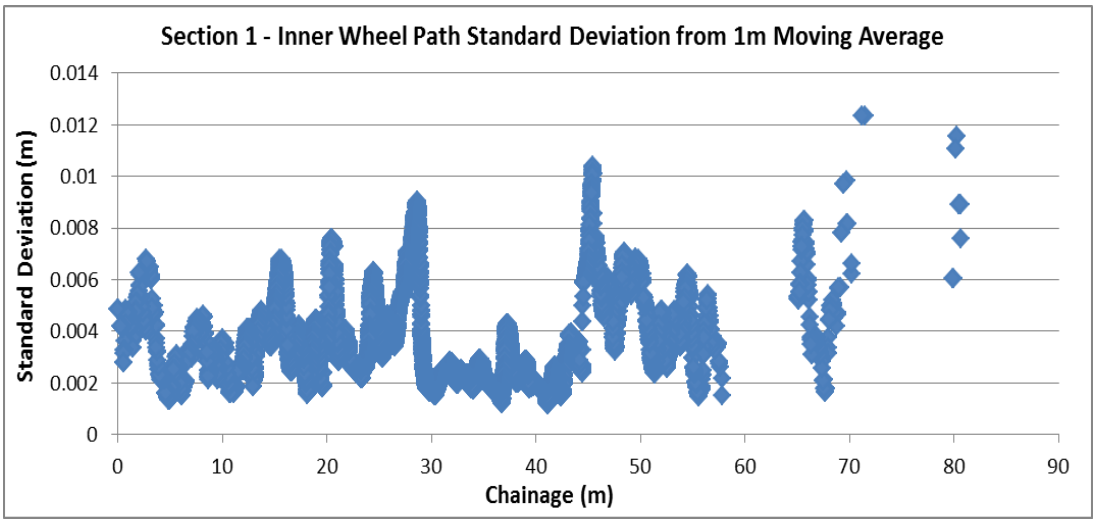


**Figure 4.5: Section 1 inner wheel path, standard deviation (1m moving average).**

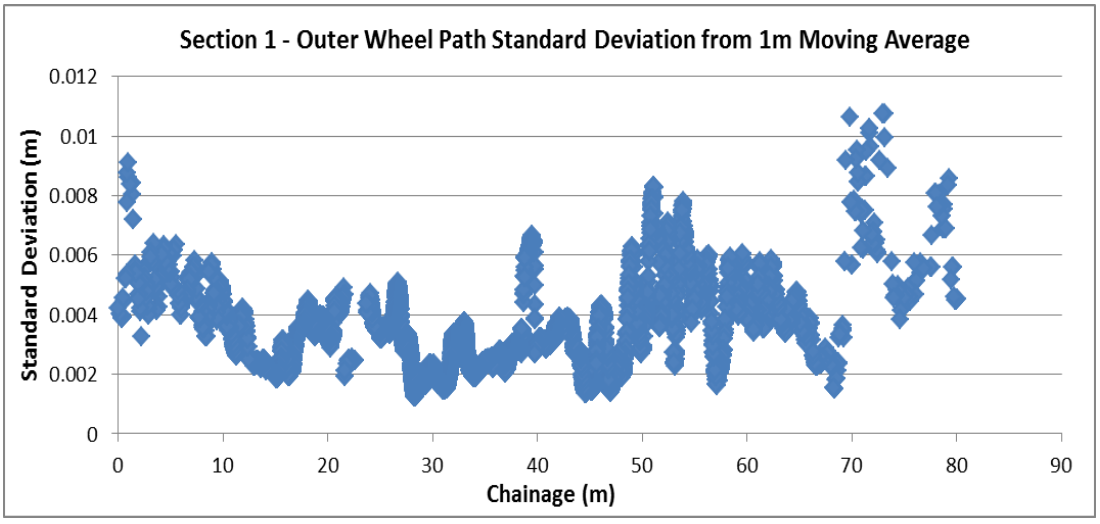


**Figure 4.6: Section 1 outer wheel path, standard deviation (1m moving average).**

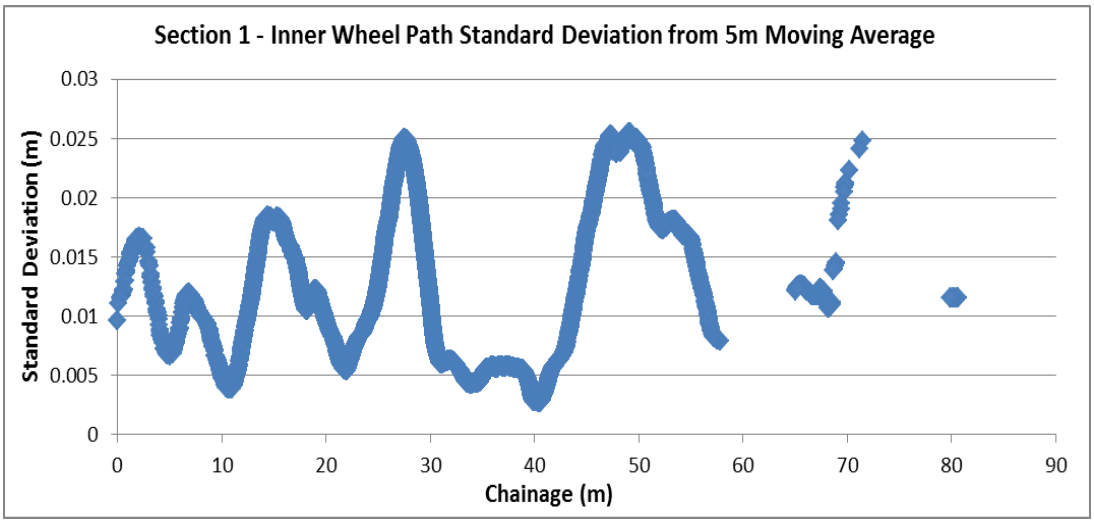


**Figure 4.7: Section 1 inner wheel path, standard deviation (5m moving average).**

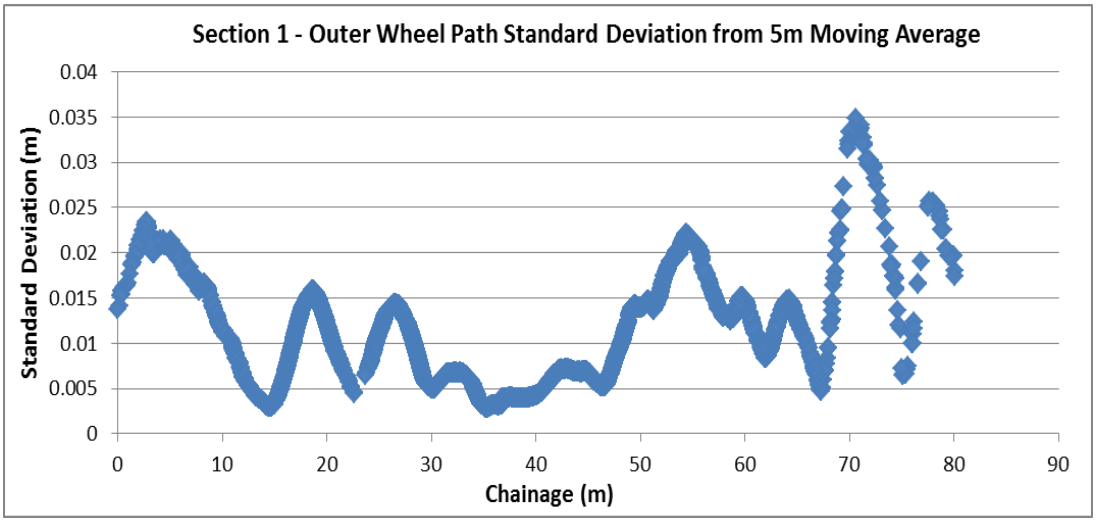


**Figure 4.8: Section 1 outer wheel path, standard deviation (5m moving average).**

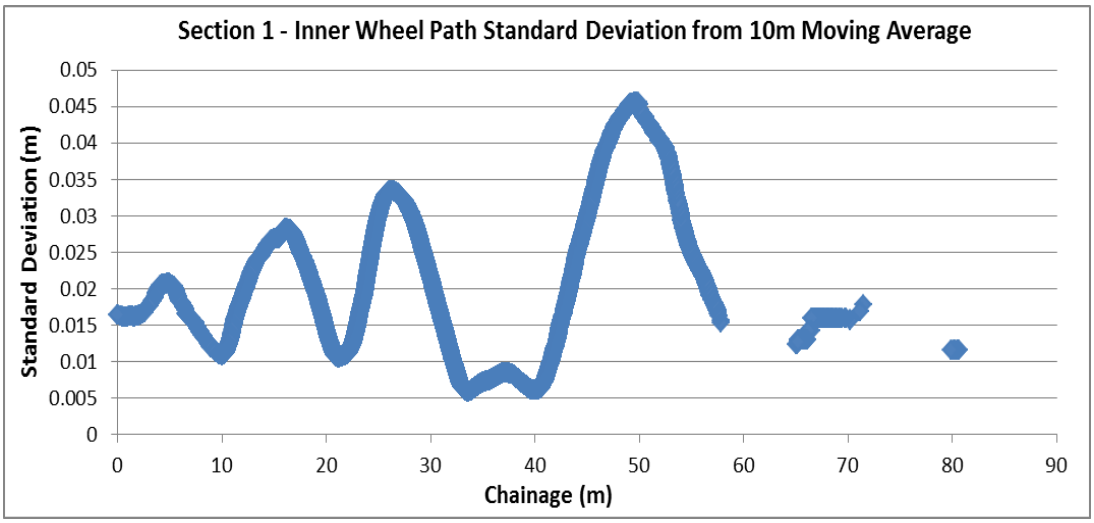


**Figure 4.9: Section 1 inner wheel path, standard deviation (10m moving average).**

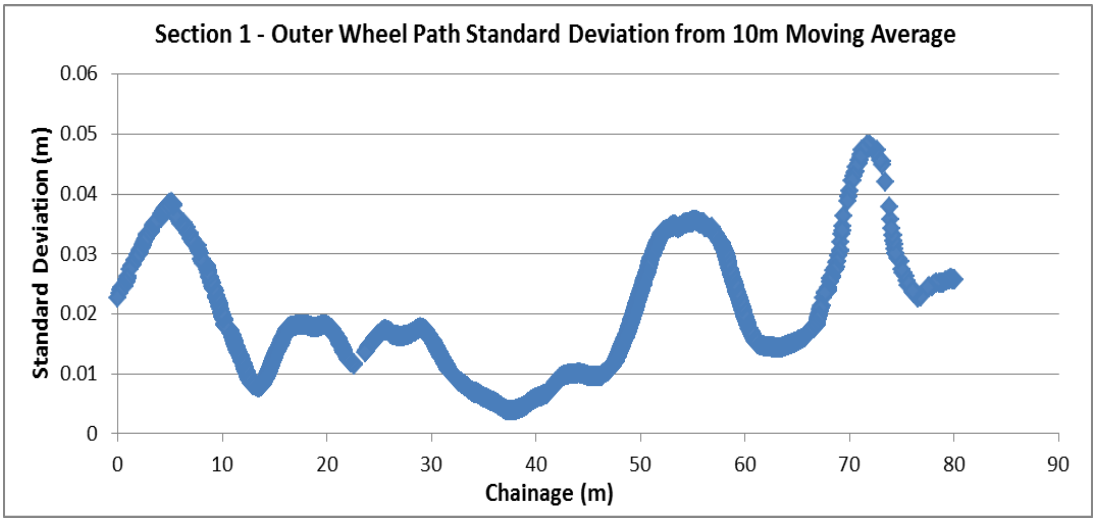


**Figure 4.10: Section 1 outer wheel path, standard deviation (10m moving average).**

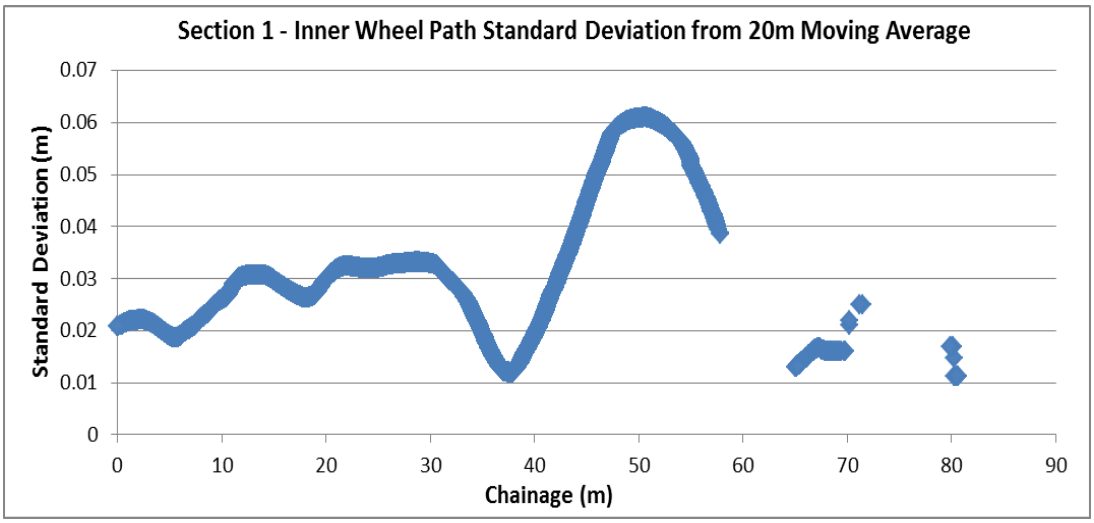


**Figure 4.11: Section 1 inner wheel path, standard deviation (20m moving average).**

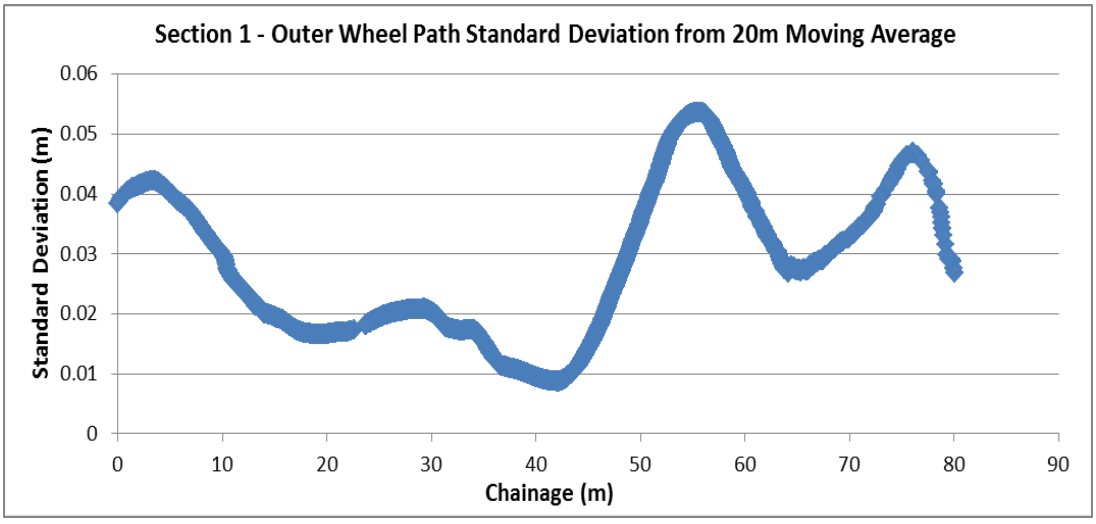


**Figure 4.12: Section 1 outer wheel path, standard deviation (20m moving average).**

### 4.3.2 Pavement Roughness Plots – Section 2

Graphical results for Section 2 comparing road chainage against each parameter listed below, are presented in the proceeding:

- Elevation (m);
- Standard deviation (0.5m moving average);

- Standard deviation (1m moving average);
- Standard deviation (5m moving average);
- Standard deviation (10m moving average);
- Standard deviation (20m moving average).

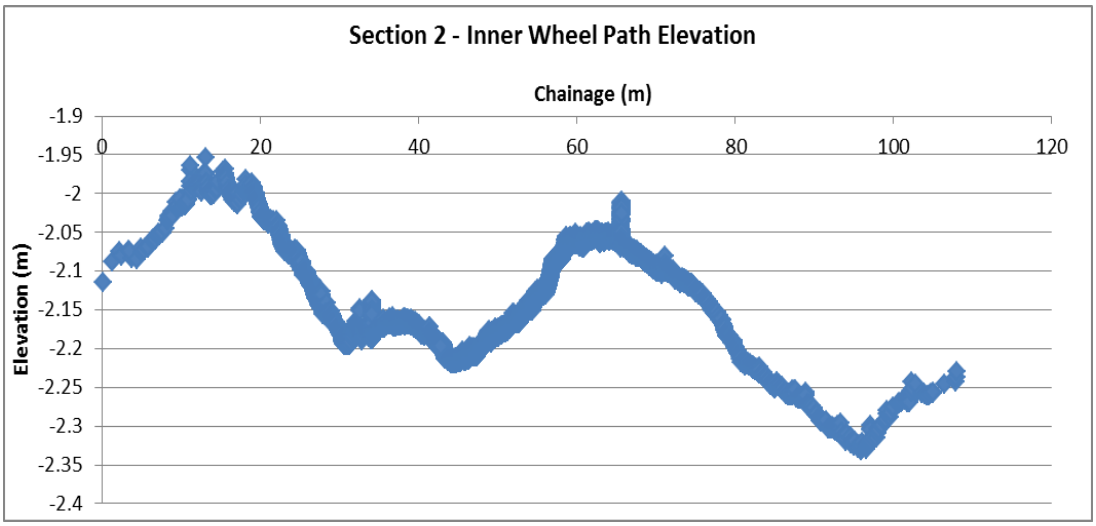


**Figure 4.13: Section 2 inner wheel path elevation.**

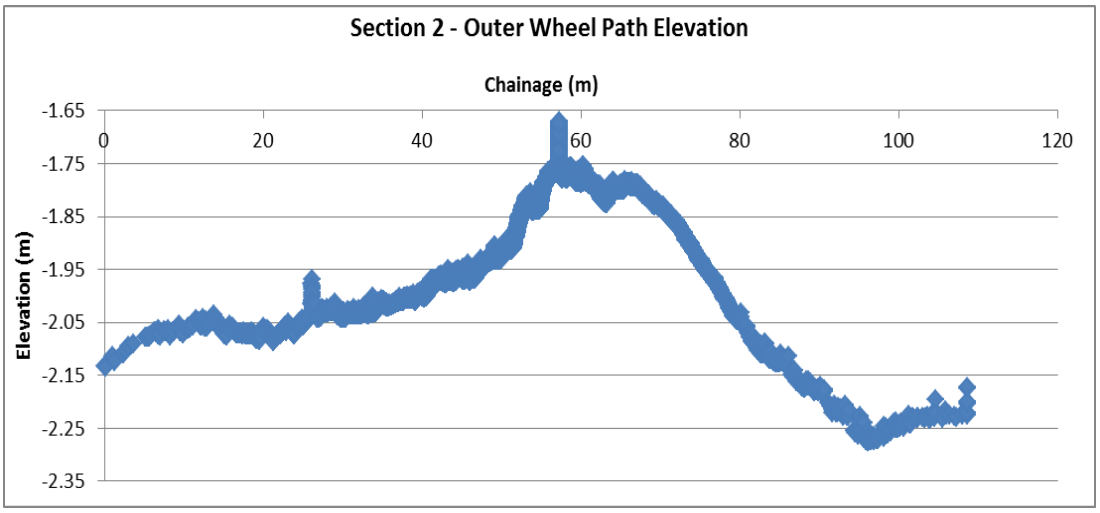


**Figure 4.14: Section 2 outer wheel path elevation.**

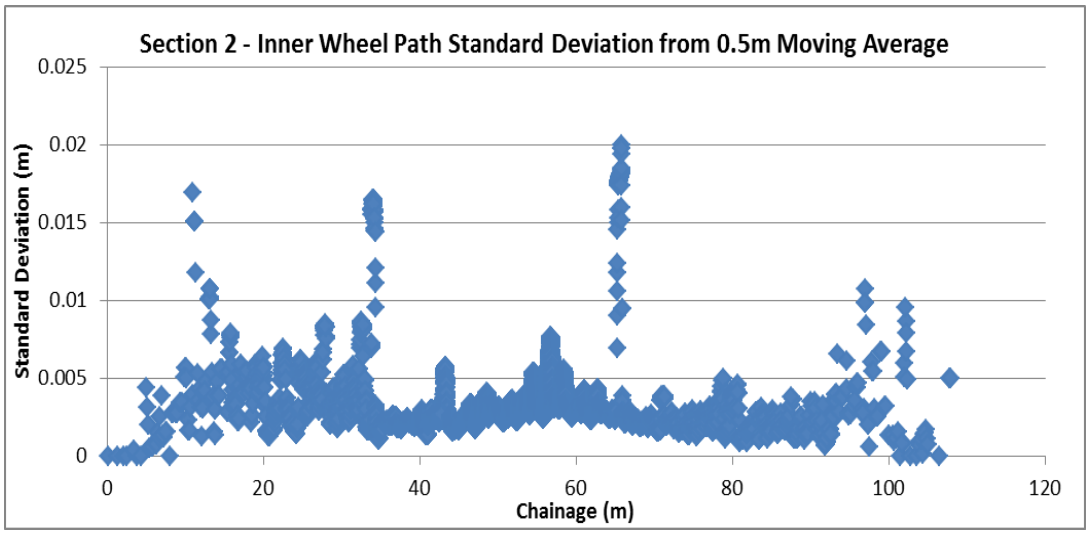


**Figure 4.15: Section 2 inner wheel path, standard deviation (0.5m moving average).**

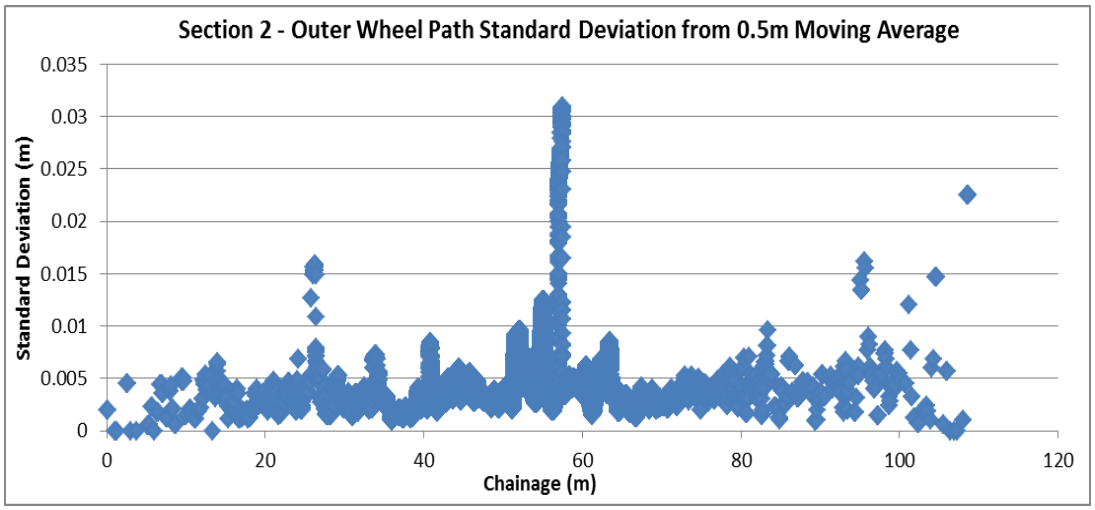


**Figure 4.16: Section 2 outer wheel path, standard deviation (0.5m moving average).**

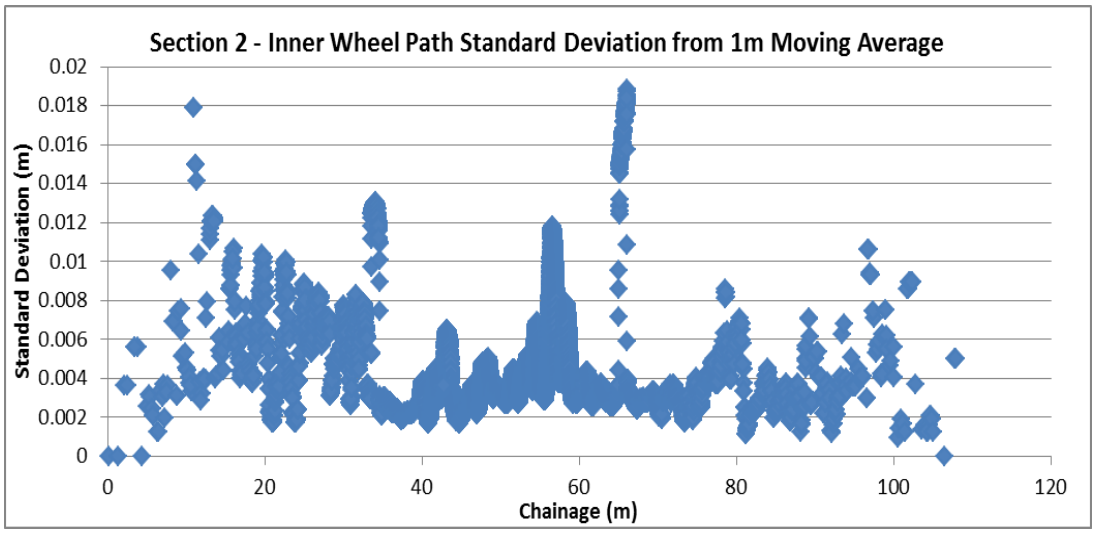


**Figure 4.17: Section 2 inner wheel path, standard deviation (1m moving average).**

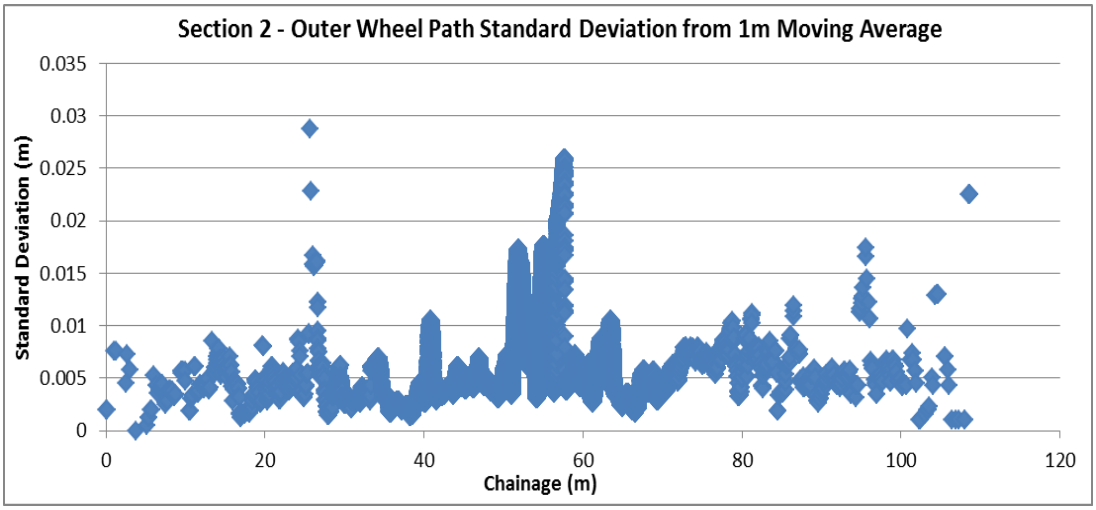


**Figure 4.18: Section 2 outer wheel path, standard deviation (1m moving average).**

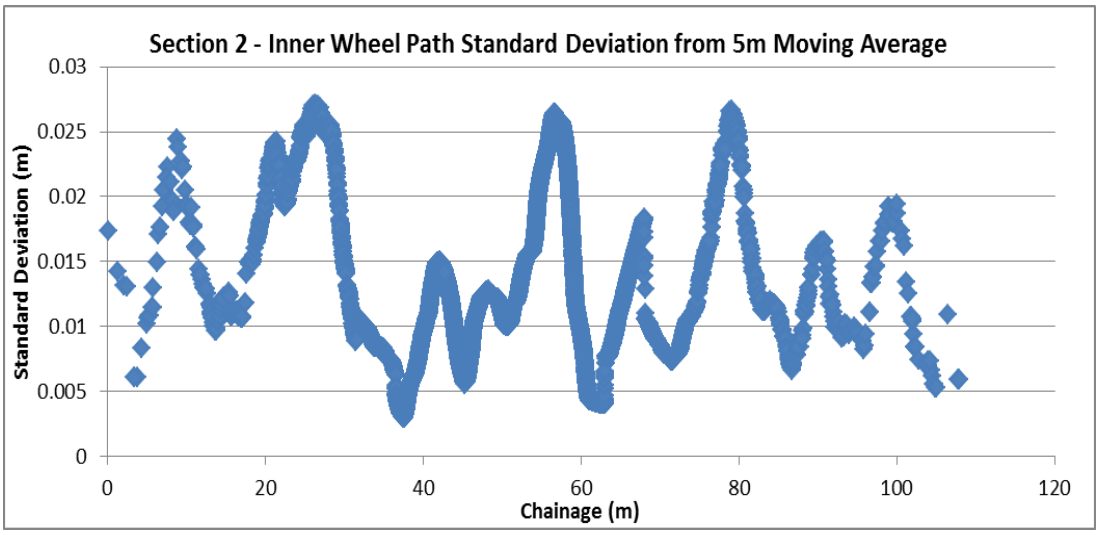


**Figure 4.19: Section 2 inner wheel path, standard deviation (5m moving average).**

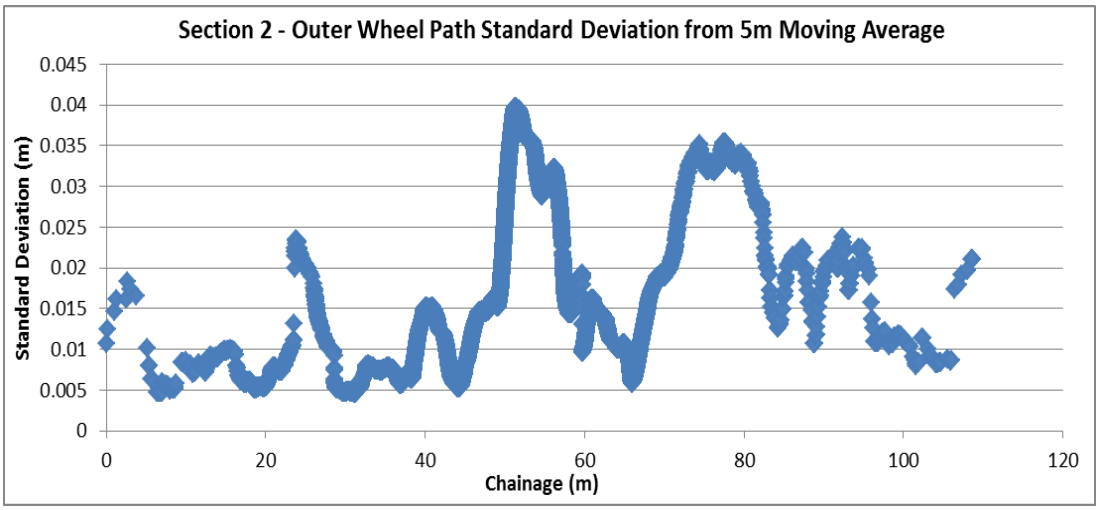


**Figure 4.20: Section 2 outer wheel path, standard deviation (5m moving average).**

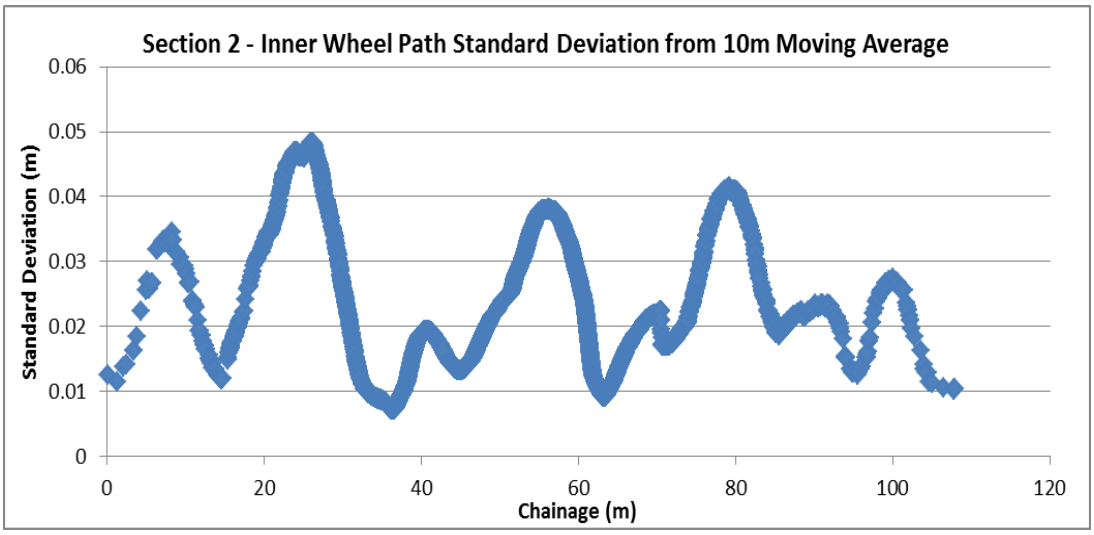


**Figure 4.21: Section 2 inner wheel path, standard deviation (10m moving average).**

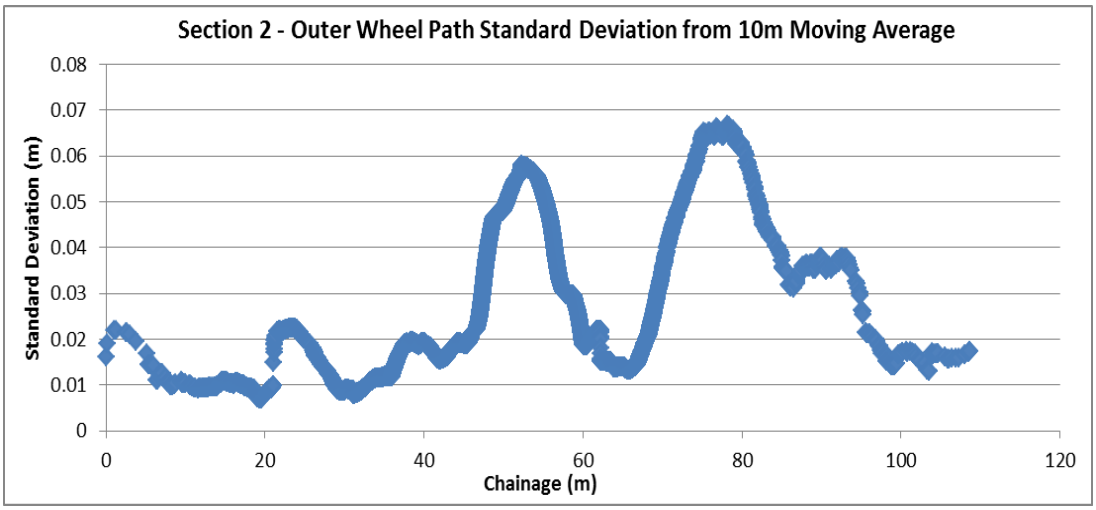


**Figure 4.22: Section 2 outer wheel path, standard deviation (10m moving average).**

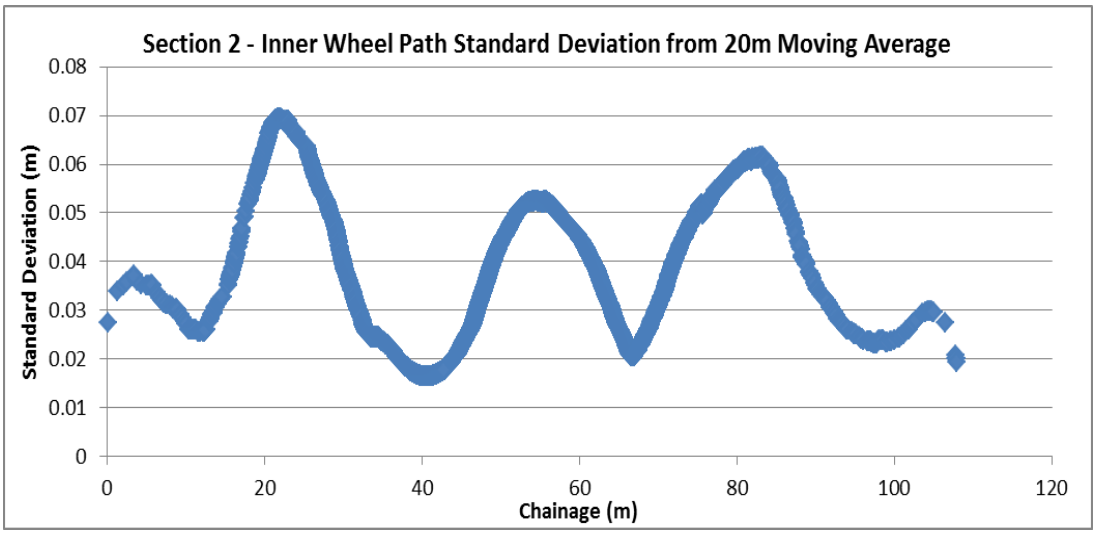


**Figure 4.23: Section 2 inner wheel path, standard deviation (20m moving average).**

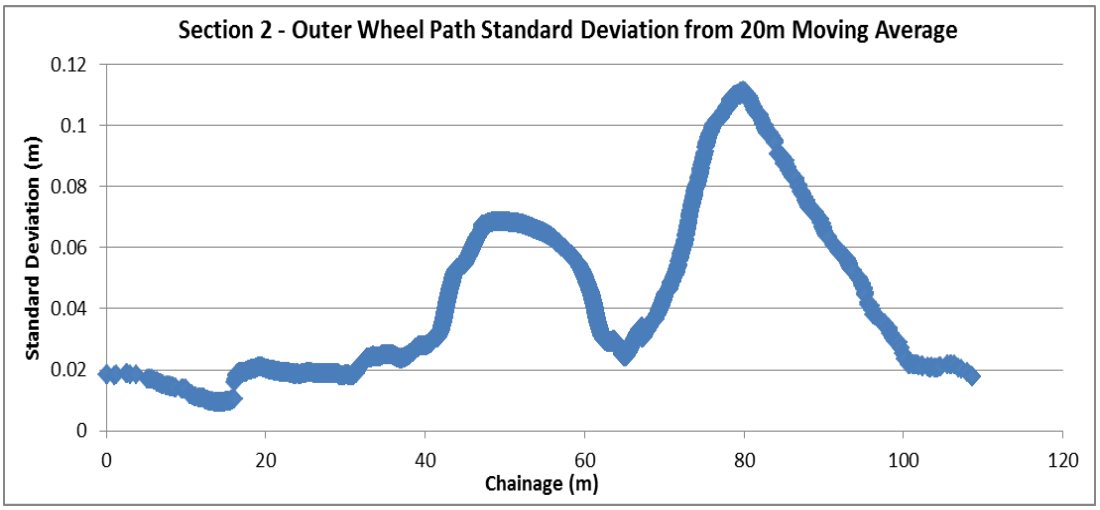


**Figure 4.24: Section 2 outer wheel path, standard deviation (20m moving average).**

### 4.3.3 Pavement Roughness Plots – Section 3

Graphical results for Section 3 comparing road chainage against each parameter listed below, are presented in the proceeding:

- Elevation (m);

- Standard deviation (0.5m moving average);
- Standard deviation (1m moving average);
- Standard deviation (5m moving average);
- Standard deviation (10m moving average);
- Standard deviation (20m moving average).

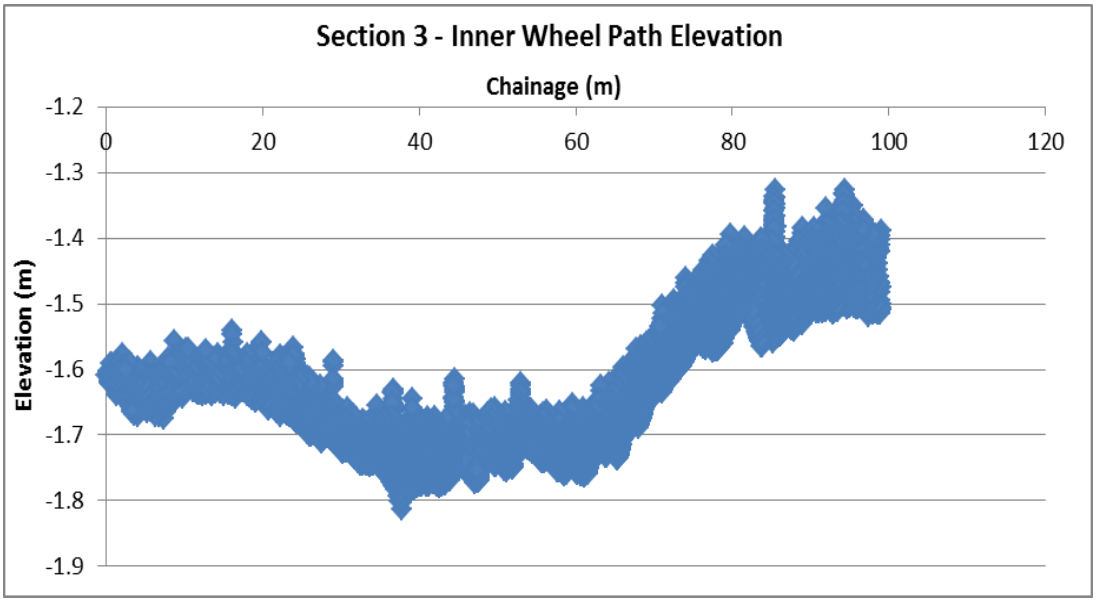


**Figure 4.25: Section 3 inner wheel path elevation.**

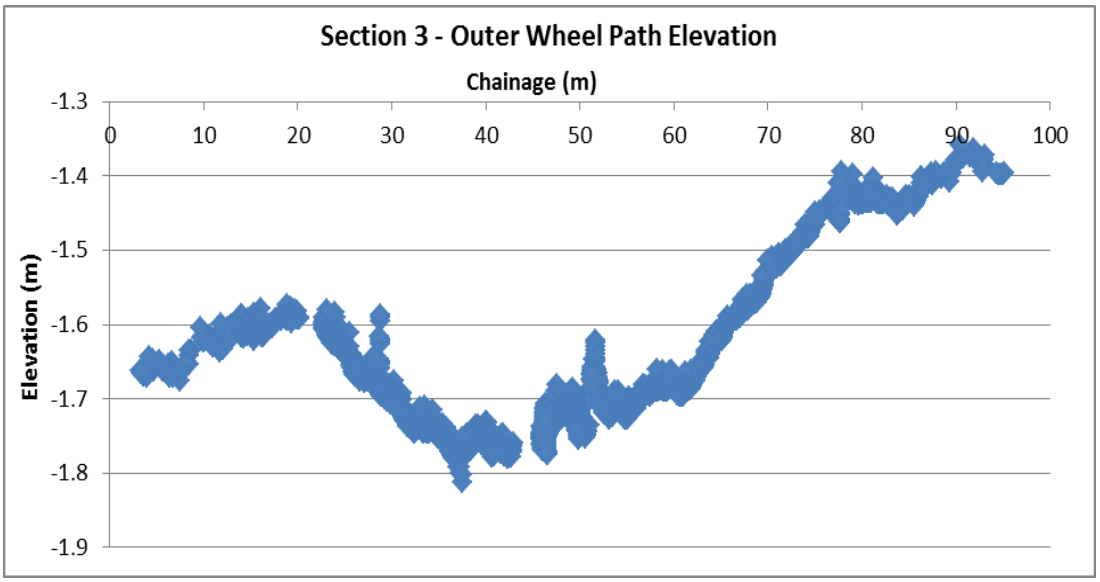


**Figure 4.26: Section 3 outer wheel path elevation.**

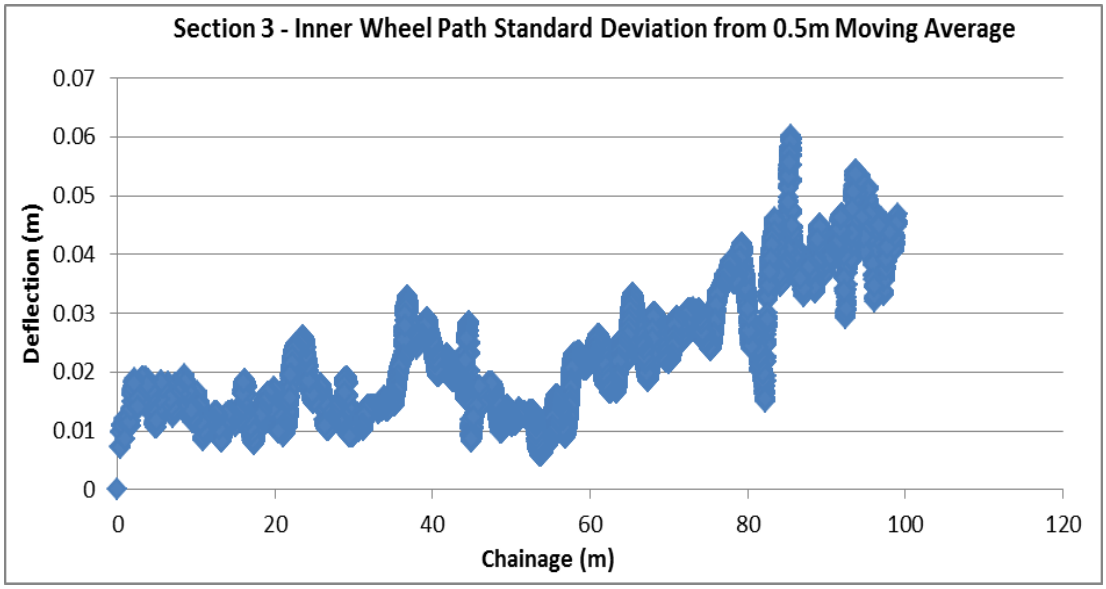


**Figure 4.27: Section 3 inner wheel path, standard deviation (0.5m moving average).**

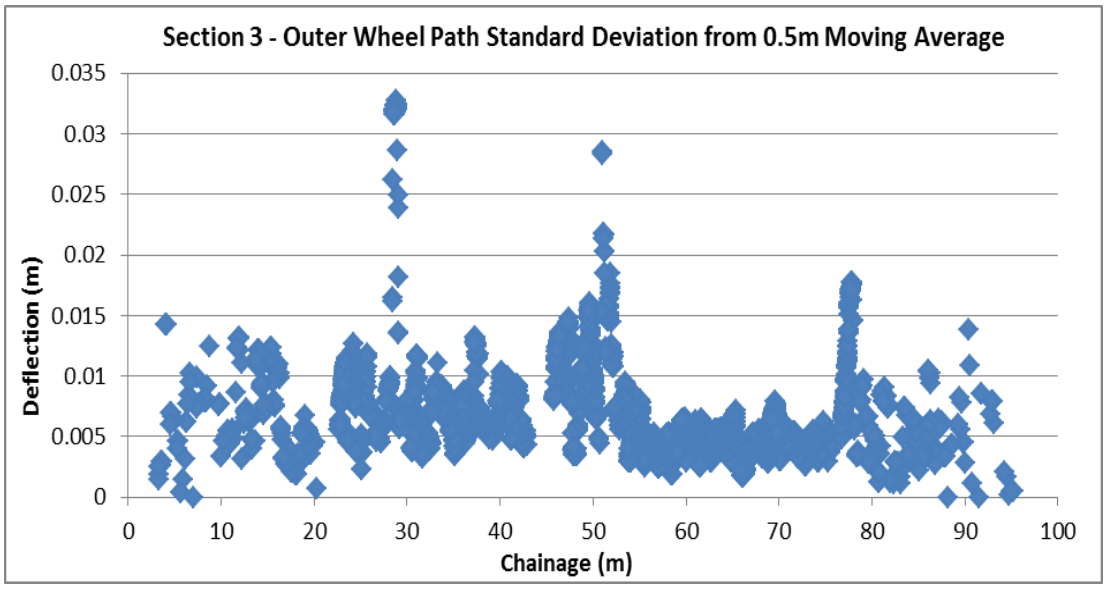


**Figure 4.28: Section 3 outer wheel path, standard deviation (0.5m moving average).**

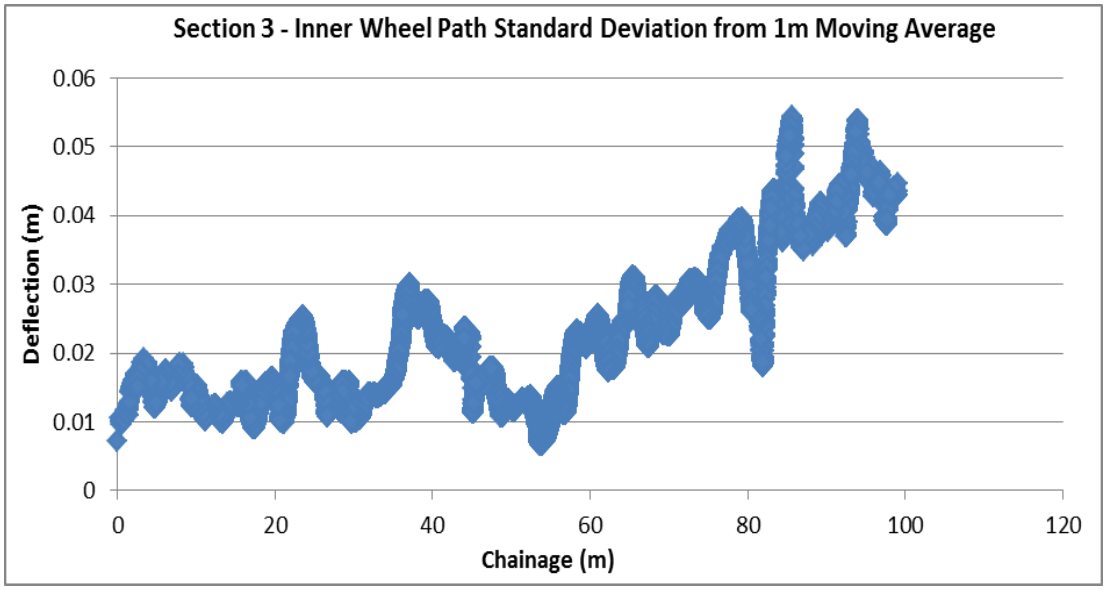


**Figure 4.29: Section 3 inner wheel path, standard deviation (1m moving average).**

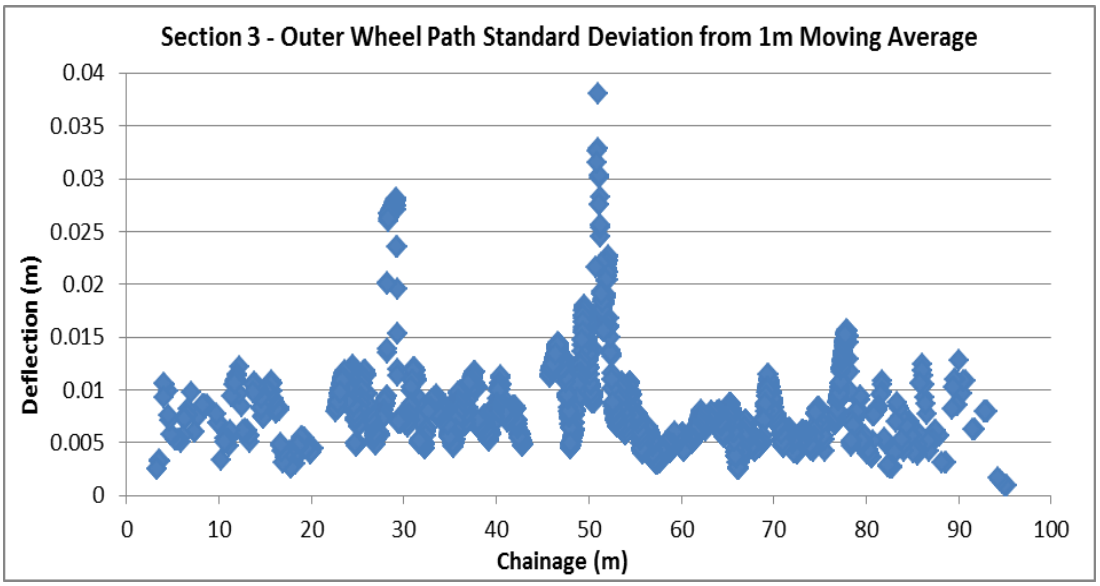


**Figure 4.30: Section 3 outer wheel path, standard deviation (1m moving average).**

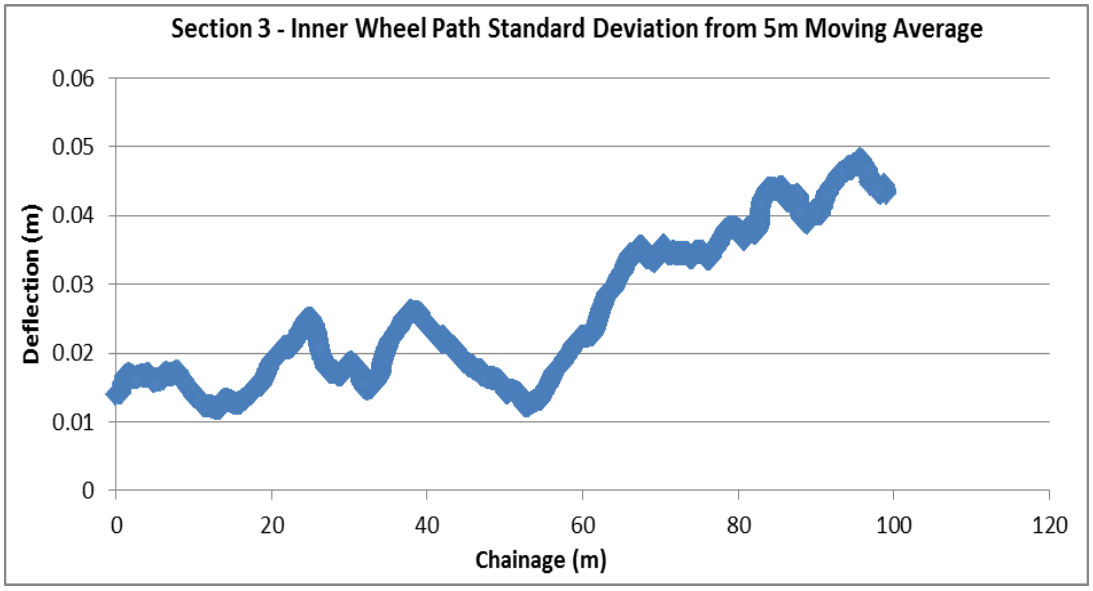


**Figure 4.31: Section 3 inner wheel path, standard deviation (5m moving average).**

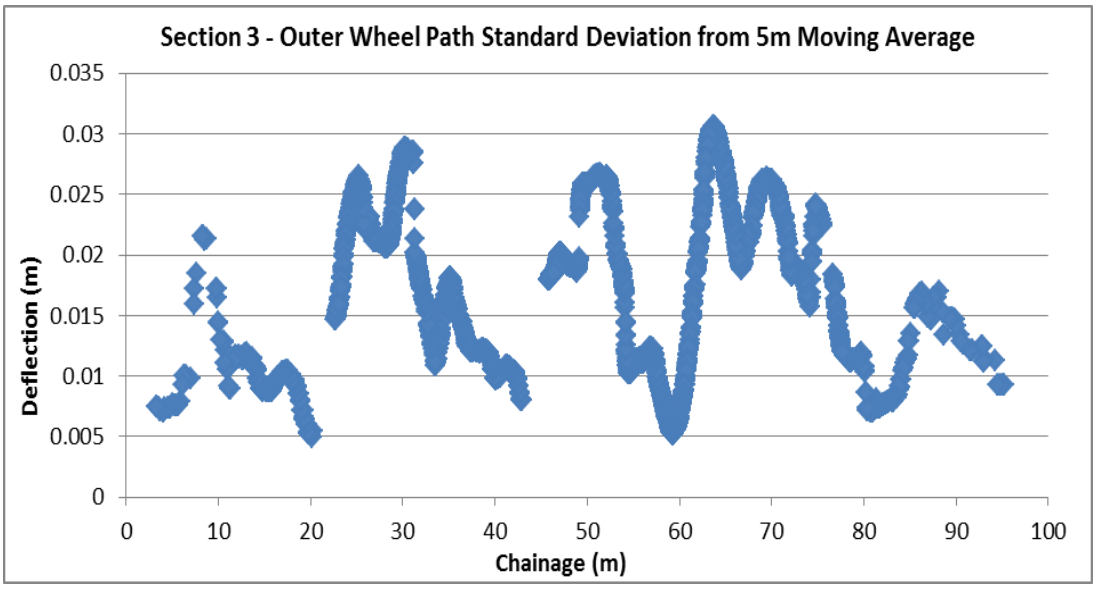


**Figure 4.32: Section 3 outer wheel path, standard deviation (5m moving average).**

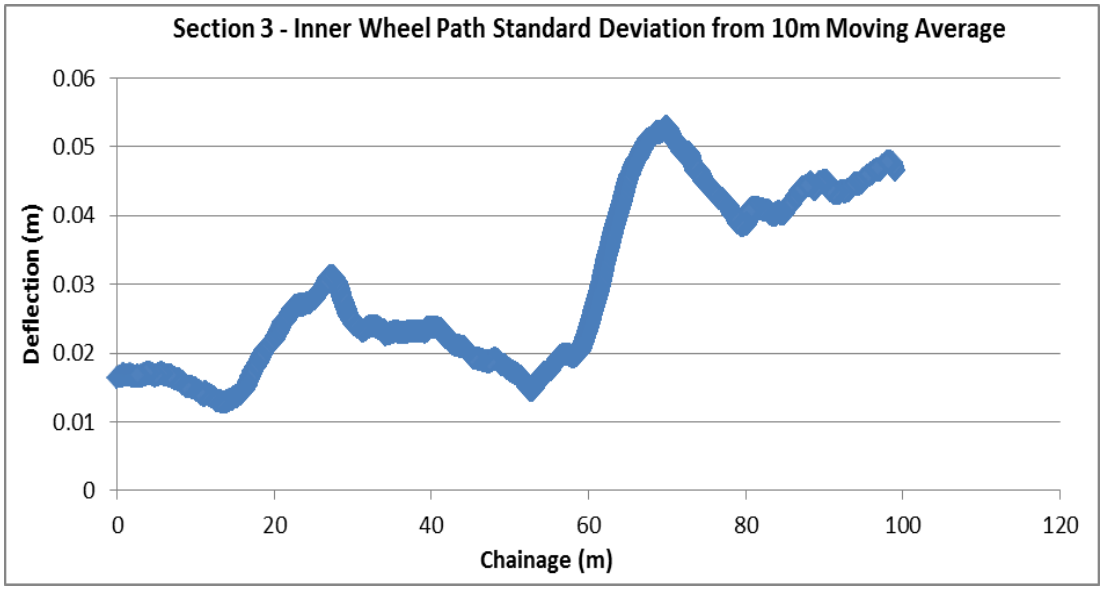


**Figure 4.33: Section 3 inner wheel path, standard deviation (10m moving average).**

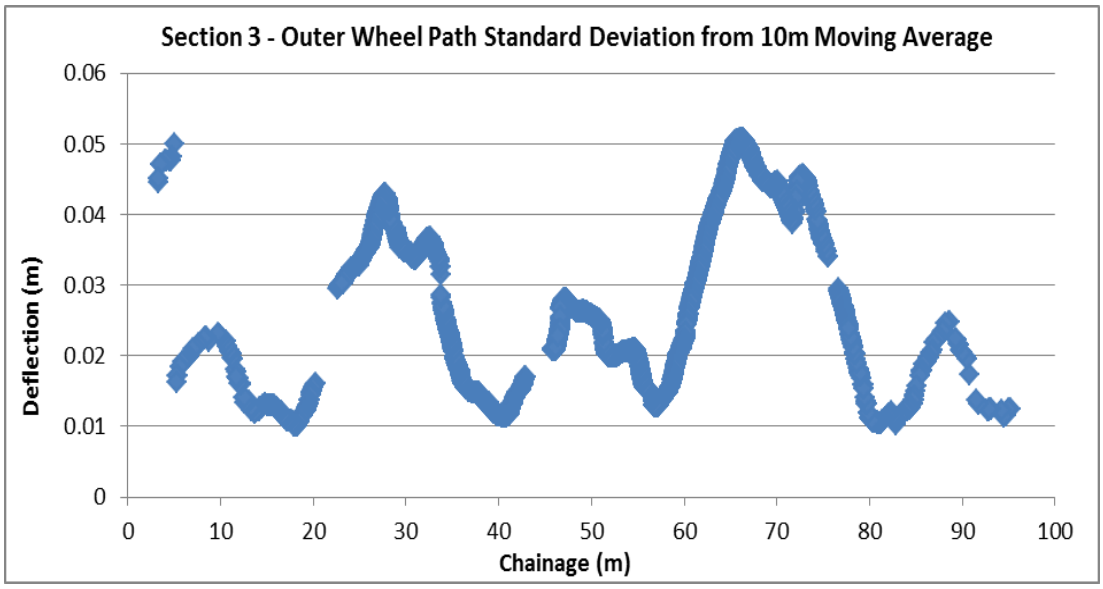


**Figure 4.34: Section 3 outer wheel path, standard deviation (10m moving average).**

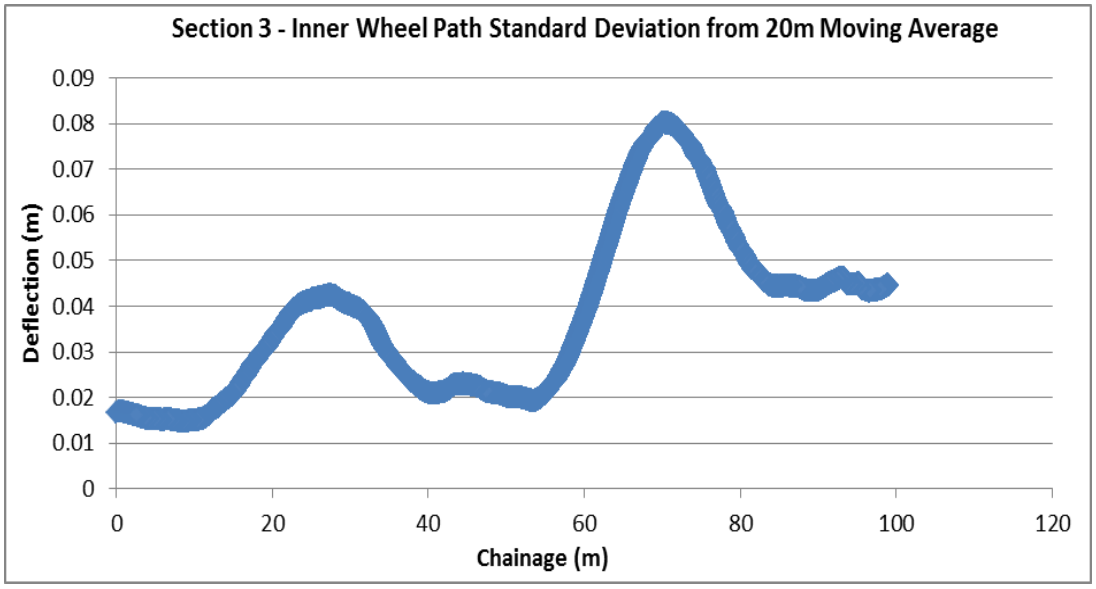


**Figure 4.35: Section 3 inner wheel path, standard deviation (20m moving average).**

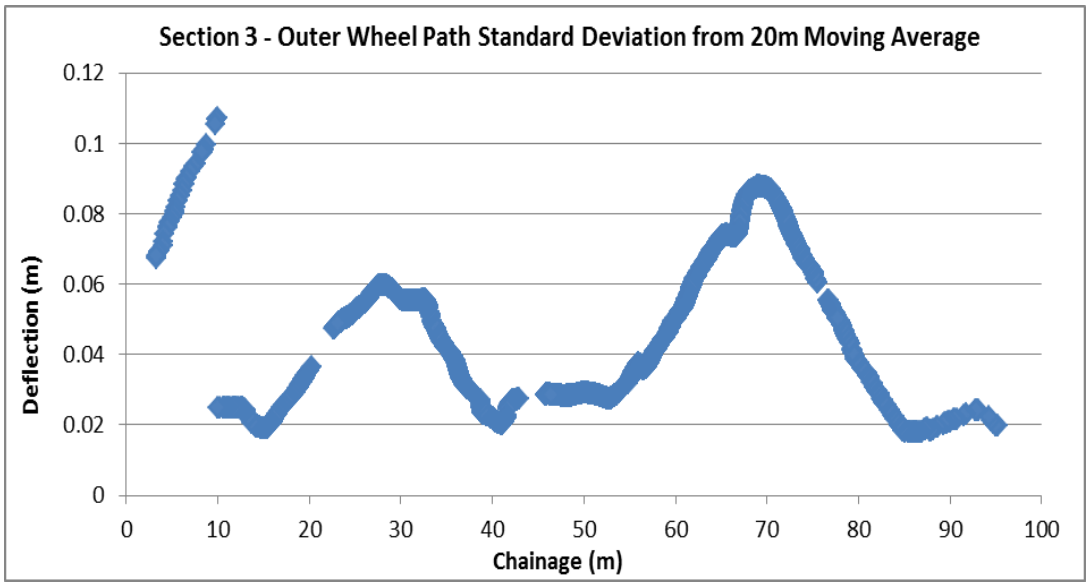


**Figure 4.36: Section 3 outer wheel path, standard deviation (20m moving average).**

### 4.3.4 Roughness Defect Score

The Roughness Defect Score for each pavement section is presented below.

**Table 4.5: Section 1 Roughness Defect Scoring sheet.**

| Mine Haul Road RDS Evaluation Sheet | | | |
|---|---|---|---|
| Date: | 24/01/2014 | | |
| Site: | Emu Section 1 | | |
| Chainage: | 0-80 | | |
| **Defect** | **Degree** | **Extent** | **Defect Score** |
| **Potholes** | 1 | 1 | 1 |
| **Corrugations** | 1 | 2 | 2 |
| **Rutting** | 1 | 1 | 1 |
| **Loose Material** | 1 | 1 | 1 |
| **Stoniness** | 1 | 4 | 4 |
| | | **RDS** | 9 |

**Table 4.6: Section 2 Roughness Defect Scoring sheet.**

| Mine Haul Road RDS Evaluation Sheet | | | |
|---|---|---|---|
| Date: | 24/01/2014 | | |
| Site: | Emu Section 2 | | |
| Chainage: | 0-110 | | |
| **Defect** | **Degree** | **Extent** | **Defect Score** |
| **Potholes** | 1 | 1 | 1 |
| **Corrugations** | 4 | 5 | 20 |
| **Rutting** | 1 | 1 | 1 |
| **Loose Material** | 2 | 5 | 10 |
| **Stoniness** | 4 | 5 | 20 |
| | | **RDS** | 52 |

**Table 4.7: Section 3 Roughness Defect Scoring sheet.**

| Mine Haul Road RDS Evaluation Sheet | | | |
|---|---|---|---|
| Date: | 24/01/2014 | | |
| Site: | Emu Section 3 | | |
| Chainage: | 0-90 | | |
| **Defect** | **Degree** | **Extent** | **Defect Score** |
| **Potholes** | 1 | 1 | 1 |
| **Corrugations** | 3 | 5 | 15 |
| **Rutting** | 1 | 1 | 1 |
| **Loose Material** | 2 | 5 | 10 |
| **Stoniness** | 5 | 5 | 25 |
| | | **RDS** | 52 |

## 4.4 Pavement Deflection

Pavement deflection results are presented below. Note that where deflection data is shown for the loaded condition with the wheel gear ‘side-on’, these figures are not included in the average values shown at the bottom of each table.

**Table 4.8: Pavement deflection results for Section 1.**

| Section 1 | Maximum Deflection (mm) |
|---|---|
| Station 1 | |
| Unloaded | 1.0 |
| Loaded | 2.5 |
| Loaded - Side | 1.5 (just in front of tyre) 2.0 (beside side wall of tyre) |
| Average | 2.0 |
| Station 2 | |
| Unloaded | 1.5 |
| Loaded | - |
| Average | 1.5 |
| Both Stations | |
| Average | **1.7** |

**Table 4.9: Pavement deflection results for Section 2.**

| Section 2 | Maximum Deflection (mm) |
|---|---|
| Station 1 | |
| Unloaded | 2.0 |
| Loaded | 4.0 |
| Loaded - Side | 1.7 (in front of contact patch) 1.9 (along side of contact patch) |
| Average | 3.0 |
| Station 2 | |
| Unloaded | 2.0 |
| Loaded | - |
| Average | 2.0 |
| Both Stations | |
| Average | **2.7** |

**Table 4.10: Pavement deflection results for Section 3.**

| Section 3 | Maximum Deflection (mm) |
|---|---|
| Station 1 | |
| Unloaded | 2.0 |
| Loaded | 5.0 |
| Average | **3.5** |

### 4.4.1 Pavement Curvature

Pavement curvature data for each pavement deflection test are presented in the following. Each result includes a graphical plot of the measured deflection and a table defining deflection values calculated using the equation shown for the trend line, for pre-defined values of radial distance from the centre of the dual wheel gear assembly. The curves are replicated in Section 4.8.7, where an assessment of various pavement structural analysis are tested. Data within tables in this section were utilised for back-calculation of pavement elastic modulus via the Evercalc software, see Section 4.8.1.2.

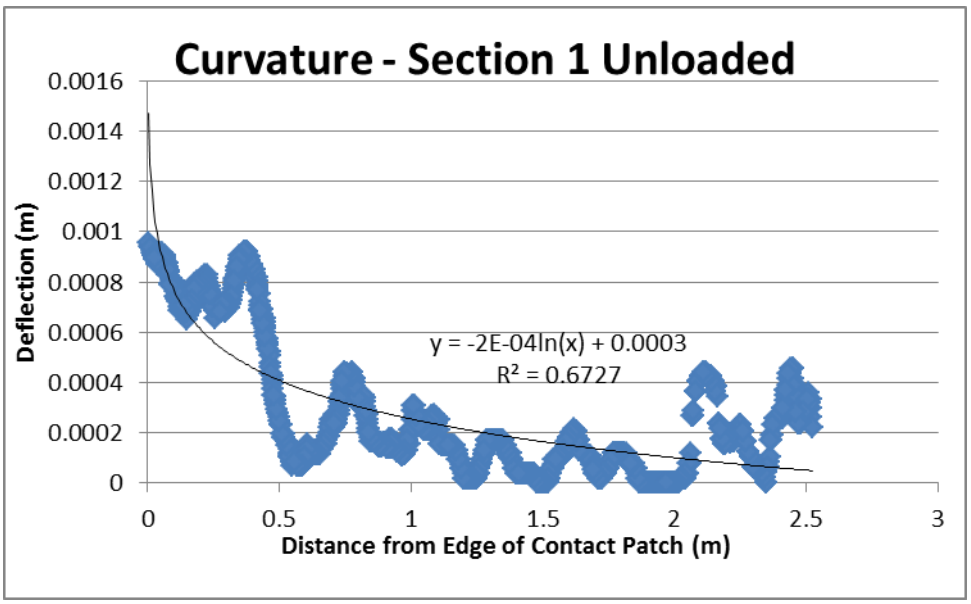


**Figure 4.37: Curvature, Section 1 unloaded (0.1m moving average and logarithmic trend-line).**

**Table 4.11: Calculated deflection to define curvature, Section 1 Unloaded.**

| Radius (m) | Deflection (m) |
|---|---|
| 0 | 0.00120 |
| 0.2 | 0.00062 |
| 0.3 | 0.00054 |
| 0.4 | 0.00048 |
| 0.5 | 0.00044 |
| 0.6 | 0.00040 |
| 0.75 | 0.00036 |
| 0.9 | 0.00032 |
| 1.5 | 0.00022 |
| 2.5 | 0.00012 |

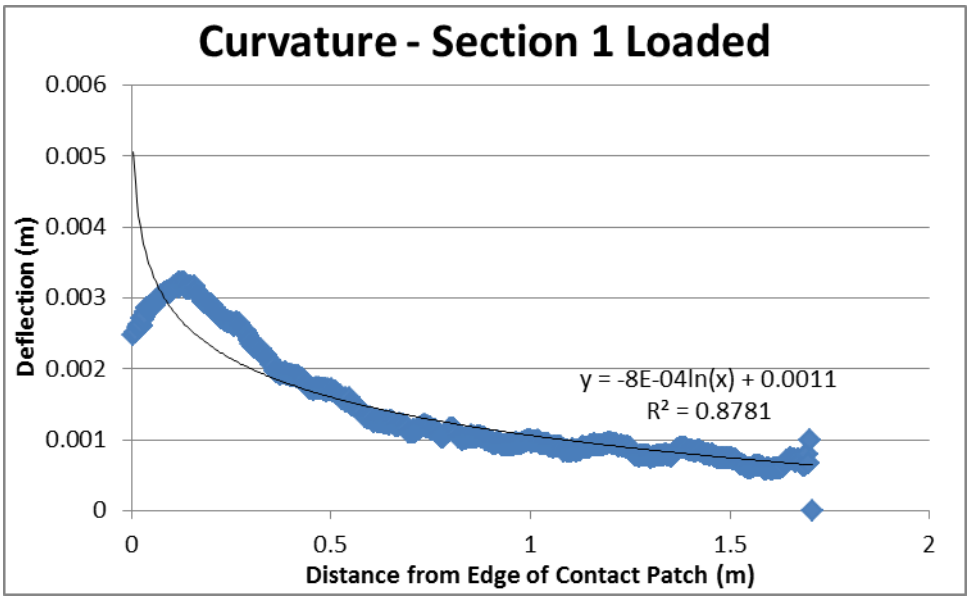


**Figure 4.38: Curvature, Section 1 loaded (0.1m moving average and logarithmic trend-line).**

**Table 4.12: Calculated deflection to define curvature, Section 1 loaded.**

| Radius (m) | Deflection (m) |
|---|---|
| 0 | 0.00260 |
| 0.2 | 0.00239 |
| 0.3 | 0.00206 |
| 0.4 | 0.00183 |
| 0.5 | 0.00165 |
| 0.6 | 0.00151 |
| 0.75 | 0.00133 |
| 0.9 | 0.00118 |
| 1.5 | 0.00078 |
| 2.5 | 0.00037 |

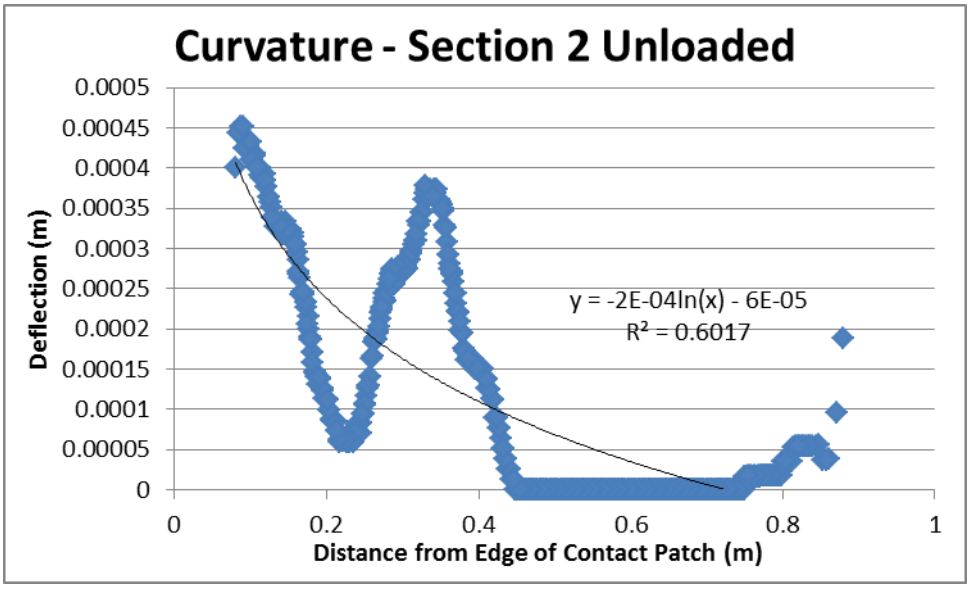


**Figure 4.39: Curvature, Section 2 unloaded (0.1m moving average and logarithmic trend-line).**

**Table 4.13: Calculated deflection to define curvature, Section 2 unloaded.**

| Radius (m) | Deflection (m) |
|---|---|
| 0 | 0.00200 |
| 0.2 | 0.00200 |
| 0.3 | 0.00100 |
| 0.4 | 0.00050 |
| 0.5 | 0.00000 |
| 0.6 | 0.00000 |
| 0.75 | 0.00000 |
| 0.9 | 0.00000 |
| 1.5 | 0.00000 |
| 2.5 | 0.00000 |

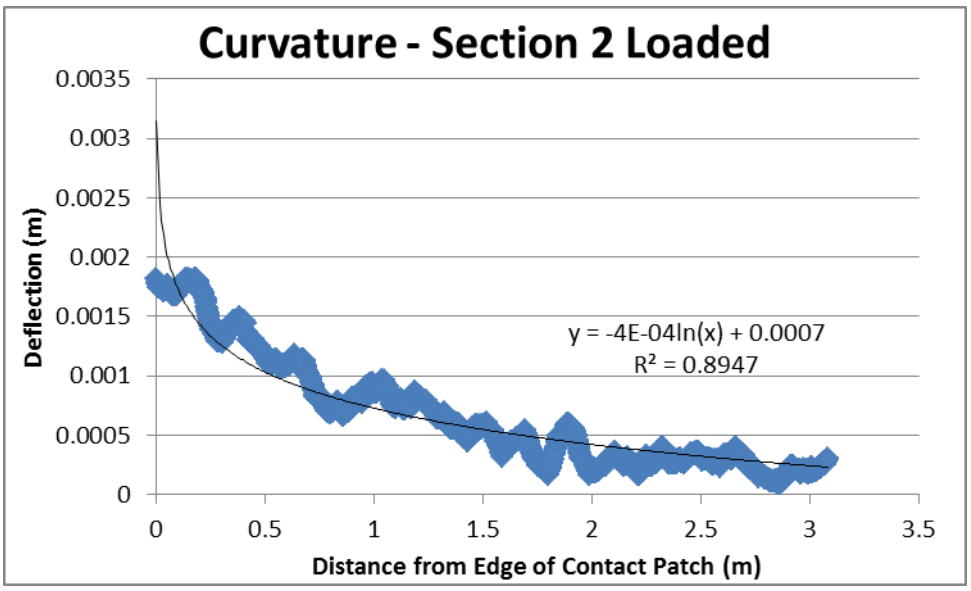


**Figure 4.40: Curvature, Section 2 loaded (0.1m moving average and logarithmic trend-line).**

**Table 4.14: Calculated deflection to define curvature, Section 2 loaded.**

| Radius (m) | Deflection (m) |
|---|---|
| 0 | 0.00380 |
| 0.2 | 0.00134 |
| 0.3 | 0.00118 |
| 0.4 | 0.00107 |
| 0.5 | 0.00098 |
| 0.6 | 0.00090 |
| 0.75 | 0.00082 |
| 0.9 | 0.00074 |
| 1.5 | 0.00054 |
| 2.5 | 0.00033 |

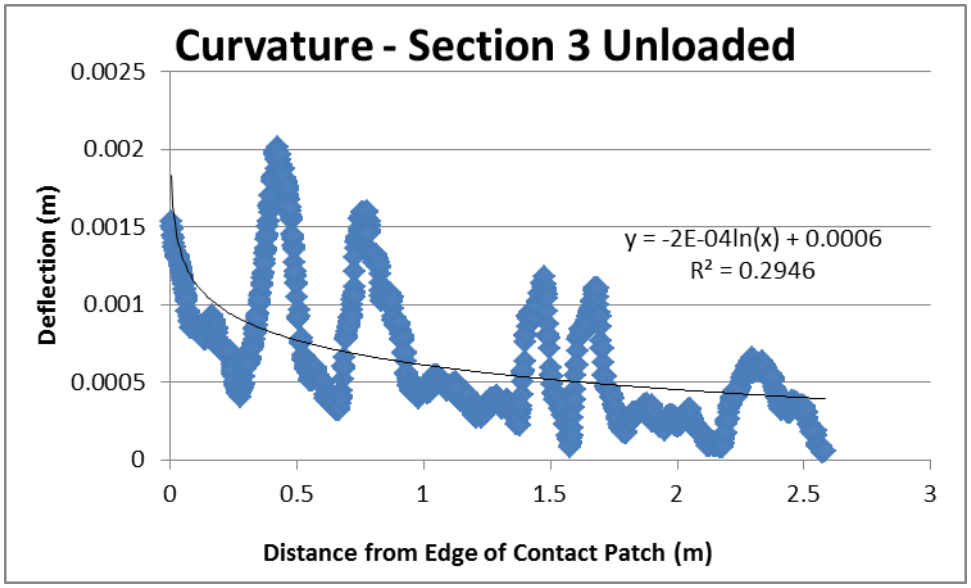


**Figure 4.41: Curvature, Section 3 unloaded (0.1m moving average and logarithmic trend-line).**

**Table 4.15: Calculated deflection to define curvature, Section 3 unloaded.**

| Radius (m) | Deflection (m) |
|---|---|
| 0 | 0.00190 |
| 0.2 | 0.00092 |
| 0.3 | 0.00084 |
| 0.4 | 0.00078 |
| 0.5 | 0.00074 |
| 0.6 | 0.00070 |
| 0.75 | 0.00066 |
| 0.9 | 0.00062 |
| 1.5 | 0.00052 |
| 2.5 | 0.00042 |

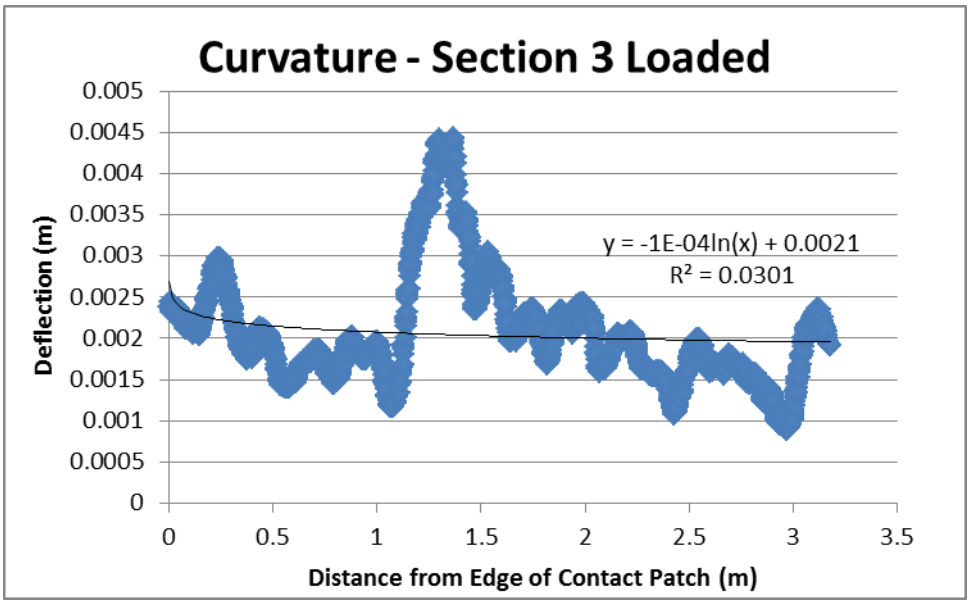


**Figure 4.42: Curvature, Section 3 loaded (0.1m moving average and logarithmic trend-line).**

**Table 4.16: Calculated deflection to define curvature, Section 3 loaded.**

| Radius (m) | Deflection (m) |
|---|---|
| 0 | 0.00520 |
| 0.2 | 0.00216 |
| 0.3 | 0.00212 |
| 0.4 | 0.00209 |
| 0.5 | 0.00207 |
| 0.6 | 0.00205 |
| 0.75 | 0.00203 |
| 0.9 | 0.00201 |
| 1.5 | 0.00196 |
| 2.5 | 0.00191 |

### 4.4.2 Interaction of Deflection between Tyres

The following presents plots of the pavement surface deflection profile directly under the rear axle of the haul truck utilised in the testing. Polynomial curves have been fitted using the least-squares regression technique in order to provide remove the variation observed at the surface, such that they can be compared to profiles modelled by various software in Section 4.8.7. Note that a polynomial curve has not been fitted to Figure 4.43, due to a concave profile resulting. It is expected that either some unforeseen error has affected the measurement of the curvature profile. Ultimately it should be expected to be minimal from observation of the magnitudes of deflection in Figure 4.44. The deflection values for the truck in the unloaded condition can also be observed as being significantly smaller than the loaded condition for Sections two and three in the following.

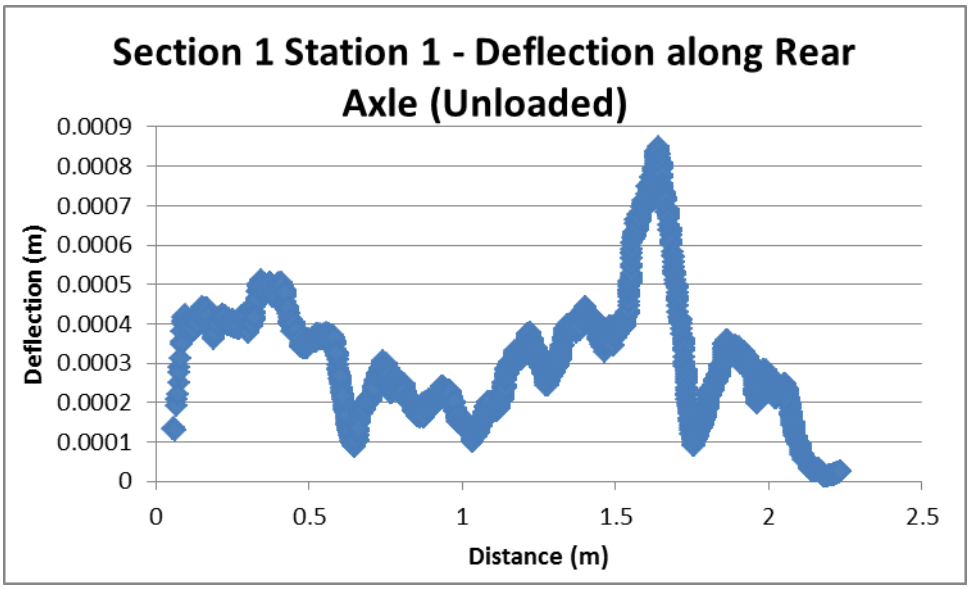


**Figure 4.43: Section 1, Station 1 (unloaded truck) deflection along rear axle from inside of left hand wheel assembly to inside of right hand wheel assembly.**

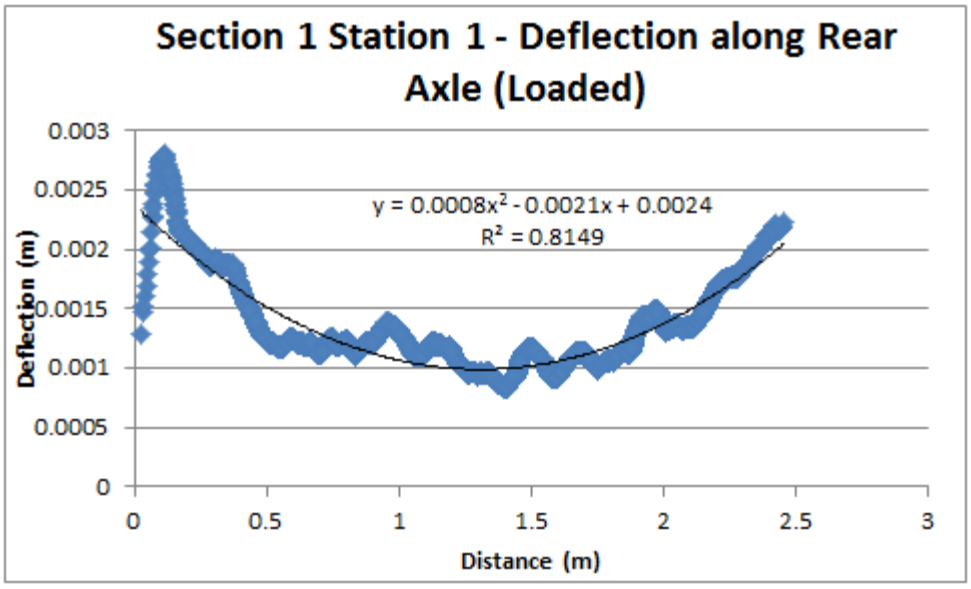


**Figure 4.44: Section 1, Station 1 (loaded truck) deflection along rear axle from inside of left hand wheel assembly to inside of right hand wheel assembly.**

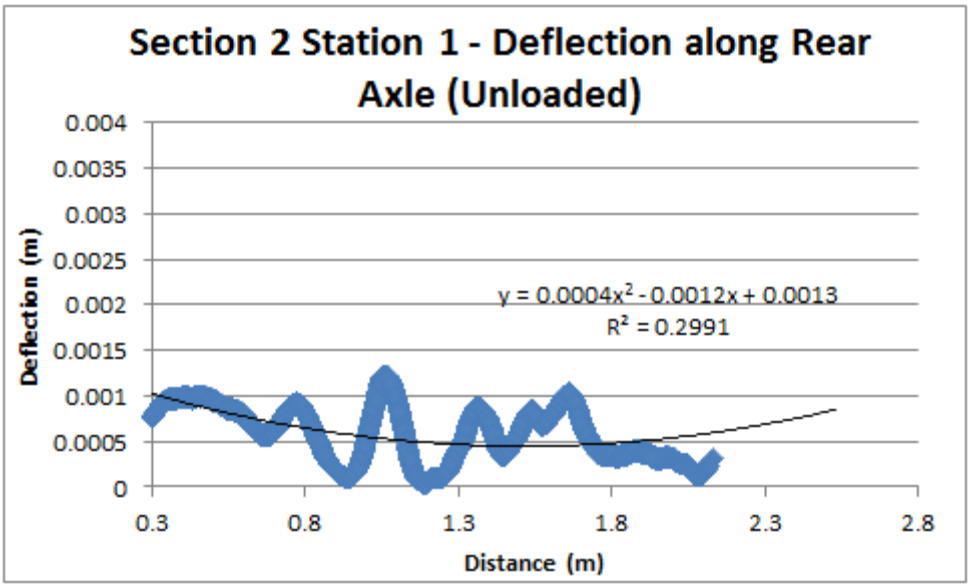


**Figure 4.45: Section 2, Station 1 (unloaded truck) deflection along rear axle from inside of left hand wheel assembly to inside of right hand wheel assembly.**

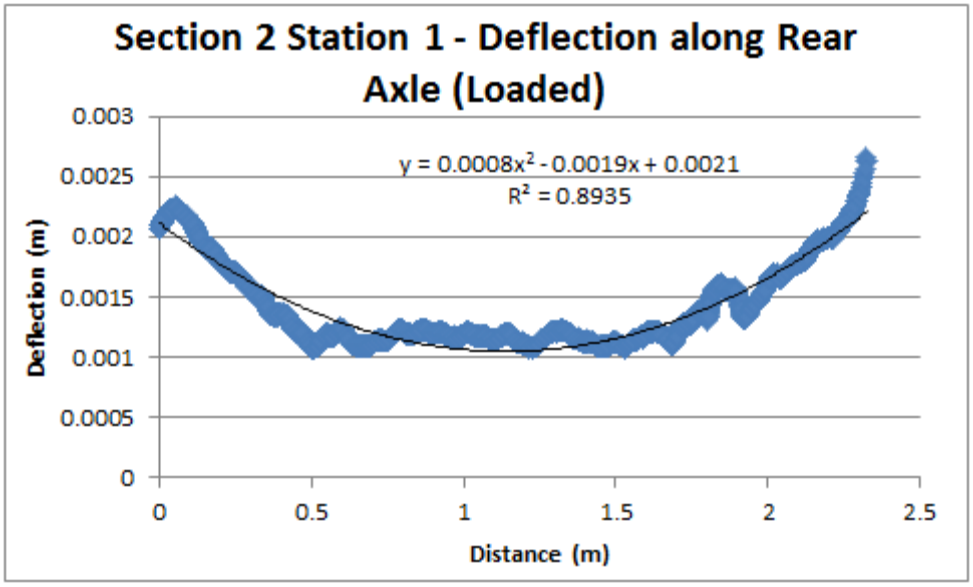


**Figure 4.46: Section 2, Station 1 (loaded truck) deflection along rear axle from inside of left hand wheel assembly to inside of right hand wheel assembly.**

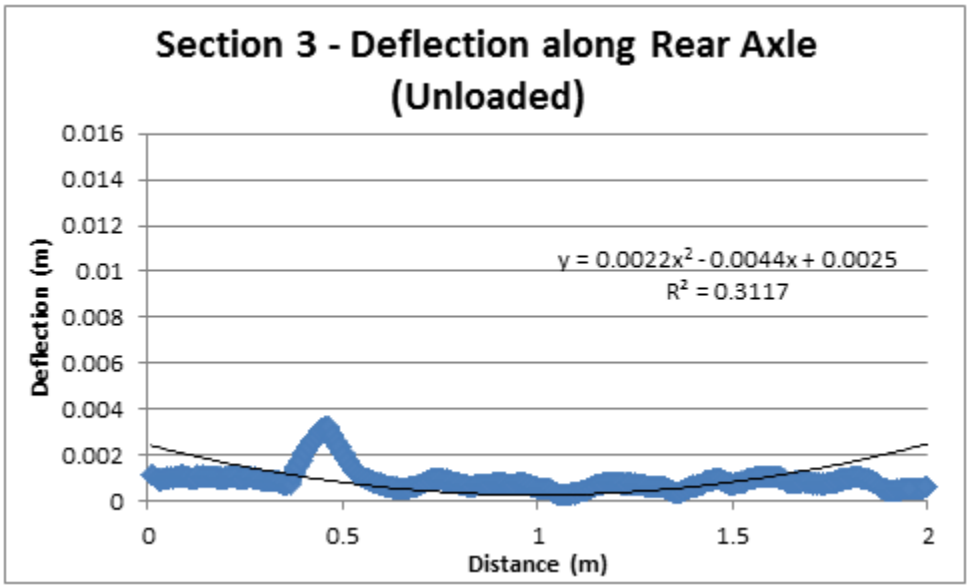


**Figure 4.47: Section 3 (unloaded truck) deflection along rear axle from inside of left hand wheel assembly to inside of right hand wheel assembly.**

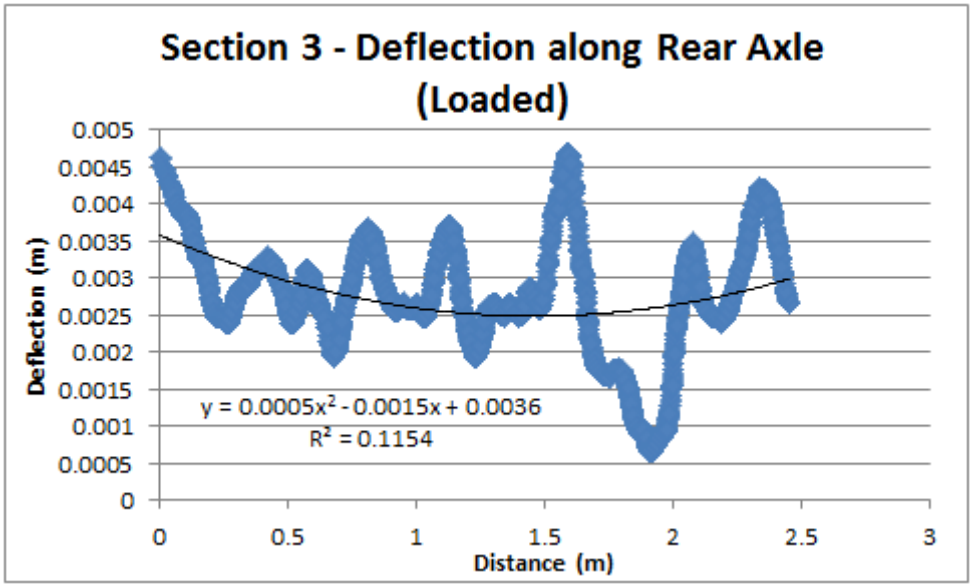


**Figure 4.48: Section 3 (loaded truck) deflection along rear axle from inside of left hand wheel assembly to inside of right hand wheel assembly.**

### 4.4.3 Geometry of Tyre Contact Patches

Average measured tyre contact patch geometry (Table 4.17) and estimates of total truck weight (Table 4.18) made from these results are presented below. The latter is included to provide an indication of the accuracy of assuming the average tyre/pavement contact patch has the tyre inflation pressure. All results relate to rear axle tyre, unless note otherwise.

**Table 4.17: Tyre contact patch geometry results**

| **Section 1** | Width - Single Tyre (mm) | Width - Dual Tyre (mm) | Separation - Dual Tyre (mm) | Length (mm) |
|---|---|---|---|---|
| Station 1 | | | | |
| Unloaded | 877 | 2155 | 371 | 739 |
| Loaded | 1019 | 2381 | 289 | 996 |
| Loaded - Side | - | - | - | 1038 |
| Station 2 | | | | |
| Unloaded | 866 | 2140 | 401 | 725 |
| Unloaded - Front | 910 | - | - | 902 |

| **Section 2** | Width - Single Tyre (mm) | Width - Dual Tyre (mm) | Separation - Dual Tyre (mm) | Length (mm) |
|---|---|---|---|---|
| Station 1 | | | | |
| Unloaded | 893 | 2107 | 346 | 761 |
| Loaded | 920 | 2281 | 344 | 1125 |
| Loaded - Side | - | - | - | 1207 |
| Station 2 | | | | |
| Unloaded | 895 | 2196 | 374 | 810 |

| **Section 3** | Width - Single Tyre (mm) | Width - Dual Tyre (mm) | Separation - Dual Tyre (mm) | Length (mm) |
|---|---|---|---|---|
| Station 1 | | | | |
| Unloaded | 898 | 2181 | 397 | 709 |
| Unloaded - Front | 1008 | - | - | 926 |
| Loaded | 963 | 2244 | 319 | 1045 |

| **Averages** | Width - Single Tyre (mm) | Width - Dual Tyre (mm) | Separation - Dual Tyre (mm) | Length (mm) |
|---|---|---|---|---|
| Unloaded | 886 | 2156 | 378 | 749 |
| Unloaded - Front | 959 | - | - | 914 |
| Loaded | 967 | 2302 | 317 | 1082 |

**Table 4.18: Estimated truck weights from average tyre geometry and tyre inflation pressure.**

| | Area ($m^2$) | Tyre Load (kN) | Tyre Load (Tonnes) | Total Truck Mass (Tonnes) |
|---|---|---|---|---|
| Unloaded | 0.663 | 590 | 60.18 | 481.41 |
| Unloaded - Front | 0.877 | 780 | 79.52 | 318.09 |
| Loaded | 1.047 | 932 | 94.97 | 569.84 |

Table 4.19 presents the constant pavement/tyre contact pressure, which have been estimated from the measured contact area and known tyre loads in the unloaded and loaded condition (Komatsu, 2006).

**Table 4.19: Estimated uniform tyre contact pressure from measured tyre contact geometry.**

| | Area ($m^2$) | Tyre Load (kN) | Constant Contact Pressure (kPa) |
|---|---|---|---|
| Unloaded | 0.663 | 201.35 | 303.56 |
| Unloaded - Front | 0.877 | 402.7 | 459.43 |
| Loaded | 1.047 | 628.17 | 600.06 |

### 4.4.4 Summary of Pavement Structural Condition

To provide a succinct summary of the structural condition of each respective pavement section, Table 4.20 is provided.

**Table 4.20: Summary of pavement section structural condition.**

| | | Deflection (D0) (mm) | | Curvature ($D_0$-$D_{0.9}$) (mm) | | Modulus (Mpa) | |
|---|---|---|---|---|---|---|---|
| | Payload (Tonnes) | 0 | 220 | 0 | 220 | 0 | 220 |
| Section | 1 | 1 | 2.5 | 0.88 | 1.42 | 126 | 595 |
| | 2 | 2 | 4 | 2 | 3.06 | 246 | 1000 |
| | 3 | 2 | 5 | 1.28 | 3.19 | 104 | 382 |

## 4.5 Rolling Resistance

The following results correspond to the testing completed within Section 3.5 through Section 3.5.8. This presents the raw data collected during testing and the respective steps taken for data analysis. Ultimately a regression of the statistically significant correlations identified in the data was undertaken to determine the ability of using a limited number of pavement parameters to predict the rolling resistance experienced by the haul truck for a given set of operating conditions.

### 4.5.1 Summary of Truck Speed During Tests

The following summarises the truck speed for each test case. Ass there is no accepted correlation between vehicle speed and RRC, the variability evident in Table 4.21 is not expected to impact the results of rolling resistance testing sufficiently to require any additional screening of the data.

**Table 4.21: Average truck speed during rolling resistance testing.**

| | Mean Truck Speed (km/h) | | | |
|---|---|---|---|---|
| Section | 15 unloaded | 15 loaded | 30 unloaded | 30 loaded |
| 1 | 17.1 | 18.0 | 30.8 | 32.2 |
| 2 | 16.3 | 17.6 | 29.6 | 31.7 |
| 3 | 16.5 | 17.2 | 29.8 | 31.2 |

### 4.5.2 Chi-square Test for Normality

The following summarises the results of the chi-square test for normality. Note that at a level of significance of 0.05 only one test per section was found to follow a normal distribution. Only the tests used found to have equal means/have originated form the same population in the ANOVA or Kruskal-Wallis tests respectively, have been included in the normality testing. Consequently, the number of tests included in the following chi-square results for each pavement section are not equal.

**Table 4.22: Section 1 chi-square test for normality results.**

| Test | Speed | Payload (Tonnes) | Chi-Square | Chi-critical |
|---|---|---|---|---|
| 22 | 15 | 0 | 298.2 | 19.7 |
| 28 | 15 | 0 | 133.9 | 9.5 |
| 8 | 15 | 220 | 63.7 | 15.5 |
| 9 | 15 | 220 | 163.1 | 11.1 |
| 18 | 15 | 220 | 17 | 9.5 |
| 19 | 15 | 220 | 73.8 | 7.8 |
| 25 | 30 | 0 | 424 | 12.6 |
| 26 | 30 | 0 | 74.9 | 9.5 |
| 12 | 30 | 220 | 444.7 | 9.5 |
| 13 | 30 | 220 | 2.49 | 11.05 |
| 15 | 30 | 220 | 18.7 | 12.6 |

**Table 4.23: Section 2 chi-square test for normality results.**

| Test | Speed | Payload (Tonnes) | Chi-Square | Chi-critical |
|---|---|---|---|---|
| 22 | 15 | 0 | 5.75 | 7.8 |
| 28 | 15 | 0 | 1445.8 | 18.3 |
| 10 | 15 | 220 | 29.5 | 7.8 |
| 19 | 15 | 220 | 93 | 16.9 |
| 30 | 30 | 0 | 643.2 | 21 |
| 31 | 30 | 0 | 76.9 | 18.3 |
| 12 | 30 | 220 | 102.1 | 19.7 |
| 15 | 30 | 220 | 99.1 | 19.7 |

**Table 4.24: Section 3 chi-square test for normality results.**

| Test | Speed | Payload (Tonnes) | Chi-Square | Chi-critical |
|---|---|---|---|---|
| 22 | 15 | 0 | 227.2 | 16.9 |
| 28 | 15 | 220 | 399.1 | 16.9 |
| 29 | 15 | 220 | 379.8 | 18.3 |
| 9 | 15 | 220 | 55.9 | 14.1 |
| 10 | 15 | 220 | 264.2 | 14.1 |
| 25 | 30 | 0 | 67.9 | 18.3 |
| 31 | 30 | 0 | 239.5 | 16.7 |
| 11 | 30 | 220 | 94.8 | 25 |
| 12 | 30 | 220 | 86.7 | 26.3 |
| 13 | 30 | 220 | 205.6 | 18.3 |
| 15 | 30 | 220 | 113.2 | 16.9 |
| 16 | 30 | 220 | 2.35 | 9.5 |

### 4.5.3 Summary of Tests per Section, Speed and Direction

The following presents the results for the average RRC for each test case and level of data analysis. Following the 'screened data' results is a summary of the statistical analysis completed on this set of data in order to produce the 'correlated data'.

**Table 4.25: Summary of 'unscreened data' mean RRC.**

| | | Rolling Resistance Coefficient (RRC) | | | | | | | |
|---|---|---|---|---|---|---|---|---|---|
| | Truck Speed (km/h) | 15 | 30 | 15 & 30 | | 15km/h | | 30km/h | |
| | Payload (Tonnes) | 0 & 220 | | 0 | 220 | 0 | 220 | 0 | 220 |
| Section | 1 | 1.34 | 1.08 | 1.14 | 1.28 | 1.3 | 1.38 | 0.98 | 1.17 |
| | 2 | 1.34 | 1.31 | 1.32 | 1.32 | 1.41 | 1.26 | 1.23 | 1.38 |
| | 3 | 1.34 | 1.40 | 1.31 | 1.43 | 1.44 | 1.24 | 1.18 | 1.61 |

**Table 4.26: Summary of 'screened data' mean RRC.**

| | | Rolling Resistance Coefficient (RRC) | | | | | | | |
|---|---|---|---|---|---|---|---|---|---|
| | Truck Speed (km/h) | 15 | 30 | 15 & 30 | | 15km/h | | 30km/h | |
| | Payload (Tonnes) | 0 & 220 | | 0 | 220 | 0 | 220 | 0 | 220 |
| Section | 1 | 1.27 | 0.69 | 0.77 | 1.19 | 1.08 | 1.45 | 0.46 | 0.92 |
| | 2 | 1.18 | 1.07 | 0.99 | 1.26 | 1.06 | 1.29 | 0.92 | 1.22 |
| | 3 | 1.27 | 1.42 | 1.24 | 1.45 | 1.23 | 1.31 | 1.25 | 1.58 |

Hypothesis testing, as per Section 3.5.8.2, was undertaken on the screened data set to further remove potential sources of error in the correlation testing between pavement properties and RRC. The results of non-parametric (Table 4.27) and parametric (Table 4.28) hypothesis testing are presented below.

**Table 4.27: Kruskal-Wallis hypothesis test results of screened data.**

| Section | Truck Speed | Payload (Tonnes) | Tests Referenced | H | H-critical | P-value | Mean RRC |
|---|---|---|---|---|---|---|---|
| 1 | 15 | 0 | 21,29 | 17.92 | 3.84 | - | 1.08* |
| 1 | 15 | 220 | 18,19 | 0.04 | 3.84 | 0.84 | 1.5 |
| 1 | 30 | 0 | 24,26 | 9.90 | 3.84 | - | 0.27* |
| 1 | 30 | 220 | 12,13 | 3.23 | 3.84 | 0.07 | 0.95 |
| 2 | 15 | 0 | 21,27 | 2.45 | 3.84 | 0.12 | 1.23 |
| 2 | 15 | 220 | 10,19 | 0.11 | 3.84 | 0.74 | 1.2 |
| 2 | 30 | 0 | 26,30 | 16.11 | 3.84 | - | 0.77* |
| 2 | 30 | 220 | 12,15 | 0.98 | 3.84 | 0.32 | 1.22 |
| 3 | 15 | 0 | 28,29 | 13.73 | 3.84 | - | 1.09* |
| 3 | 15 | 220 | 9,10 | 1.23 | 3.84 | 0.27 | 1.41 |
| 3 | 30 | 0 | 25,31 | 7.85 | 3.84 | 0.01 | 1.29* |
| 3 | 30 | 220 | 11,12,13,15,16 | 158.20 | 9.89 | - | 1.58* |

* Denotes that null hypothesis rejected
- Denotes that P-value too small to report at 2 significant figures

**Table 4.28: ANOVA hypothesis test results of screened data.**

| | | | | One-way ANOVA | | | t-test | | |
|---|---|---|---|---|---|---|---|---|---|
| Section | Truck Speed | Payload (Tonnes) | Tests Referenced | F | F-critical | P-value | t-stat | t-critical | Mean RRC |
| 1 | 15 | 0 | 21,27 | 0.21 | 3.85 | 0.64 | 0.11 | 1.97 | 0.88 |
| 1 | 15 | 220 | 8,9,18,19 | 0.35 | 2.62 | 0.79 | NA | NA | 1.51 |
| 1 | 30 | 0 | 25,26 | 1.65 | 3.89 | 0.20 | 1.25 | 1.97 | 0.34 |
| 1 | 30 | 220 | 12,13,15 | 0.67 | 3.05 | 0.51 | NA | NA | 0.96 |
| 2 | 15 | 0 | 22,28 | 5.61 | 3.86 | 0.02 | 2.06 | 1.97 | 0.98* |
| 2 | 15 | 220 | 10,19 | 0.61 | 3.85 | 0.43 | 0.74 | 1.97 | 1.2 |
| 2 | 30 | 0 | 30,31 | 3.06 | 3.86 | 0.08 | 1.71 | 1.97 | 0.98 |
| 2 | 30 | 220 | 12,13 | 0.38 | 3.89 | 0.54 | 0.62 | 1.97 | 1.22 |
| 3 | 15 | 0 | 22,28,29 | 0.03 | 3.01 | 0.97 | NA | NA | 1.08 |
| 3 | 15 | 220 | 9,10 | 0.01 | 3.85 | 0.92 | 0.11 | 1.97 | 1.41 |
| 3 | 30 | 0 | 25,31 | 2.83 | 3.86 | 0.09 | 1.64 | 1.97 | 1.29 |
| 3 | 30 | 220 | 11,12,13,15,16 | 96.87 | 2.40 | - | NA | NA | 1.58* |

* Denotes that null hypothesis rejected
- Denotes that P-value too small to report at 2 significant figures

The results from the ANOVA hypothesis testing (the correlated data set) was applied to derive mean RRC values for the different test cases.

**Table 4.29: Summary of 'correlated data' mean RRC.**

| | | Rolling Resistance Coefficient (RRC) | | | | | | | |
|---|---|---|---|---|---|---|---|---|---|
| | Truck Speed (km/h) | 15 | 30 | 15 & 30 | | 15km/h | | 30km/h | |
| | Payload (Tonnes) | 0 & 220 | | 0 | 220 | 0 | 220 | 0 | 220 |
| Section | 1 | 1.20 | 0.65 | 0.61 | 1.24 | 0.88 | 1.51 | 0.34 | 0.96 |
| | 2 | 1.13 | 1.10 | 1.02 | 1.21 | 1.06 | 1.2 | 0.98 | 1.22 |
| | 3 | 1.25 | 1.44 | 1.19 | 1.50 | 1.08 | 1.41 | 1.29 | 1.58 |

### 4.5.4 Correlation between RRC and Pavement Properties

Pearson's correlation coefficient was applied to identify correlations between any of the measure pavement properties and RRC. Firstly, a summary of pavement structural properties is presented (Table 4.30). This is a culmination of test results presented in Section 4.4 and Section 4.8.1. It is provided here, as it presents the pavement deflection, curvature and elastic modulus values utilised for correlation analysis presented in Table 4.31 through Table 4.33. Note that statistical significance is highlighted for a level of significance of 0.05, in accordance with Table 3.4.

**Table 4.30: Summary of pavement structural stiffness measures.**

| | | Deflection (D0) (mm) | | Curvature ($D_0$-$D_{0.9}$) (mm) | | Modulus (Mpa) | |
|---|---|---|---|---|---|---|---|
| | Payload (Tonnes) | 0 | 220 | 0 | 220 | 0 | 220 |
| Section | 1 | 1.2 | 2.6 | 0.88 | 1.42 | 126 | 595 |
| | 2 | 2 | 3.8 | 2 | 3.06 | 246 | 1000 |
| | 3 | 1.9 | 5.2 | 1.28 | 3.19 | 104 | 382 |

**Table 4.31: Pearson correlation coefficient for 'unscreened data' between pavement properties and mean RRC values.**

| | | Correlation (r) | | | | | | | |
|---|---|---|---|---|---|---|---|---|---|
| | Truck Speed (km/h) | 15 | 30 | 15 & 30 | | 15km/h | | 30km/h | |
| | Payload (Tonnes) | 0 & 220 | | 0 | 220 | 0 | 220 | 0 | 220 |
| | Property | | | | | | | | |
| Average Standard Deviation | 0.1m moving average | 0.457 | 0.751 | 0.500 | 0.970 | 0.702 | -0.648 | 0.374 | 0.901 |
| | 0.2m moving average | 0.443 | 0.761 | 0.513 | 0.973 | 0.713 | -0.660 | 0.388 | 0.908 |
| | 0.5m moving average | 0.390 | 0.797 | 0.562 | 0.985 | 0.752 | -0.702 | 0.441 | 0.931 |
| | 1m moving average | 0.299 | 0.852 | 0.640 | 0.997 | 0.812 | -0.768 | 0.525 | 0.962 |
| | 5m moving average | -0.387 | 0.989 | 0.985 | 0.812 | 0.997* | -0.999 | 0.950 | 0.912 |
| | 10m moving average | -0.716 | 0.852 | 0.975 | 0.519 | 0.887 | -0.918 | 0.996 | 0.679 |
| | 20m moving average | -0.726 | 0.845 | 0.972 | 0.507 | 0.881 | -0.913 | 0.995 | 0.669 |
| | IRI | -0.125 | 0.992 | 0.901 | 0.939 | 0.981 | -0.965 | 0.832 | 0.989 |
| | MPD | -0.347 | 0.994 | 0.976 | 0.836 | 0.999* | -0.999 | 0.936 | 0.928 |
| | Deflection (no payload) | | | 0.999 | | 0.979 | | 0.982 | |
| | Deflection (220 tonne) | | | | 0.942 | | -0.962 | | 0.990 |
| | Curvature (no payload) | | | 0.804 | | 0.628 | | 0.879 | |
| | Curvature (220 tonne) | | | | 0.775 | | -0.998 | | 0.885 |
| | Modulus (no payload) | | | 0.416 | | 0.173 | | 0.539 | |
| | Modulus (220 tonne) | | | | -0.542 | | -0.045 | | -0.364 |

* Denotes statistically significant positive correlation at 0.05 level of significance

**Table 4.32: Pearson correlation coefficient for 'screened data' between pavement properties and mean RRC values.**

| | | Correlation (r) | | | | | | | |
|---|---|---|---|---|---|---|---|---|---|
| | Truck Speed (km/h) | 15 | 30 | 15 & 30 | | 15km/h | | 30km/h | |
| | Payload (Tonnes) | 0 & 220 | | 0 | 220 | 0 | 220 | 0 | 220 |
| | Property | | | | | | | | |
| Average Standard Deviation | 0.1m moving average | 0.498 | 0.877 | 0.906 | 0.977 | 0.988 | -0.442 | 0.842 | 0.912 |
| | 0.2m moving average | 0.484 | 0.884 | 0.912 | 0.980 | 0.985 | -0.456 | 0.851 | 0.919 |
| | 0.5m moving average | 0.433 | 0.909 | 0.934 | 0.990 | 0.974 | -0.507 | 0.880 | 0.940 |
| | 1m moving average | 0.344 | 0.945 | 0.965 | 0.999* | 0.947 | -0.588 | 0.922 | 0.969 |
| | 5m moving average | -0.343 | 0.933 | 0.907 | 0.792 | 0.516 | -0.971 | 0.955 | 0.901 |
| | 10m moving average | -0.683 | 0.717 | 0.671 | 0.490 | 0.140 | -0.987 | 0.762 | 0.659 |
| | 20m moving average | -0.693 | 0.708 | 0.661 | 0.478 | 0.127 | -0.985 | 0.754 | 0.649 |
| | IRI | -0.078 | 0.995 | 0.987 | 0.927 | 0.727 | -0.871 | 0.999* | 0.984 |
| | MPD | -0.303 | 0.947 | 0.924 | 0.817 | 0.552 | -0.960 | 0.966 | 0.918 |
| | Deflection (no payload) | | | 0.847 | | 0.404 | | 0.909 | |
| | Deflection (220 tonne) | | | | 0.930 | | -0.866 | | 0.986 |
| | Curvature (no payload) | | | 0.318 | | -0.268 | | 0.439 | |
| | Curvature (220 tonne) | | | | 0.753 | | -0.984 | | 0.873 |
| | Modulus (no payload) | | | -0.180 | | -0.700 | | -0.050 | |
| | Modulus (220 tonne) | | | | -0.570 | | -0.288 | | -0.388 |

* Denotes statistically significant positive correlation at 0.05 level of significance

**Table 4.33: Pearson correlation coefficient for 'correlated data' between pavement properties and mean RRC values.**

| | | Correlation (r) | | | | | | | |
|---|---|---|---|---|---|---|---|---|---|
| | Truck Speed (km/h) | 15 | 30 | 15 & 30 | | 15km/h | | 30km/h | |
| | Payload (Tonnes) | 0 & 220 | | 0 | 220 | 0 | 220 | 0 | 220 |
| | Property | | | | | | | | |
| Average Standard Deviation | 0.1m moving average | 0.797 | 0.848 | 0.755 | 0.992 | 0.616 | 0.152 | 0.782 | 0.928 |
| | 0.2m moving average | 0.788 | 0.856 | 0.765 | 0.990 | 0.628 | 0.137 | 0.792 | 0.934 |
| | 0.5m moving average | 0.751 | 0.885 | 0.801 | 0.980 | 0.672 | 0.079 | 0.826 | 0.953 |
| | 1m moving average | 0.683 | 0.926 | 0.855 | 0.956 | 0.741 | -0.018 | 0.877 | 0.978 |
| | 5m moving average | 0.051 | 0.952 | 0.988 | 0.540 | 0.999* | -0.658 | 0.980 | 0.882 |
| | 10m moving average | -0.343 | 0.756 | 0.849 | 0.169 | 0.934 | -0.900 | 0.825 | 0.628 |
| | 20m moving average | -0.355 | 0.747 | 0.842 | 0.155 | 0.929 | -0.906 | 0.817 | 0.618 |
| | IRI | 0.318 | 0.999 | 0.993 | 0.747 | 0.953 | -0.432 | 0.997* | 0.976 |
| | MPD | 0.094 | 0.964 | 0.994 | 0.576 | 0.997 | -0.626 | 0.988 | 0.902 |
| | Deflection (no payload) | | | 0.960 | | 0.996 | | 0.947 | |
| | Deflection (220 tonne) | | | | 0.753 | | -0.423 | | 0.978 |
| | Curvature (no payload) | | | 0.566 | | 0.712 | | 0.530 | |
| | Curvature (220 tonne) | | | | 0.488 | | -0.703 | | 0.852 |
| | Modulus (no payload) | | | 0.097 | | 0.284 | | 0.053 | |
| | Modulus (220 tonne) | | | | -0.813 | | -0.785 | | -0.425 |

* Denotes statistically significant positive correlation at 0.05 level of significance

Note that the correlation coefficient between the measured pavement deflection (when expressed to 0.1mm accuracy from testing) and RRC for a loaded truck travelling at 30km/h has been found to be 0.999 for each of the unscreened, screened and correlated data sets. Although this level of accuracy is beyond that confirmed for the laser scanning method of pavement deflection, this result does further confirm the trend that can be seen between the deflection and RRC for loaded trucks throughout the data.

If the unloaded and loaded RRC for testing at 30km/h are considered, the correlation with pavement deflection was found to be 0.820. This is statistically significant at the 0.05 level of significance (requiring a correlation coefficient in excess of 0.811).

The above results are considered evidence that a positive linear correlation has been confirmed between the pavement deflection and RRC for a loaded truck travelling at 30km/h.

### 4.5.5 RRC Regression Analysis

Initially multiple linear regression was completed between each the 12 tests cases for each data set. This regression included texture in addition to deflection and IRI initially, but was later removed after negative coefficients resulted. As a result the regression focussed on only the pavement properties found to consistently correlate with RRC above. Note that the constant term was set to zero in all regression analysis, as a result of a minimum RRC value not being apparent in earlier analysis to screen the data. Further, it was anticipated that the constant term would be influenced by the fact that any data more than two standard deviations from each test case mean RRC had been removed from the data in the derivation of the screened data set. Table 4.34 presents a summary of the linear regression equations.

**Table 4.34: Linear regression equations for RRC considering all tests.**

| Data Set | Regression Equation | $r^2$ | Significance of F-value |
|---|---|---|---|
| Unscreened | $RRC=0.0973*Deflection+0.0853*IRI$ | 0.913 | 0.000009 |
| Screened | $RRC=0.1499*Deflection+0.062*IRI$ | 0.939 | 0.000002 |

| | | | |
|---|---|---|---|
| Correlated | *RRC=0.1756*Deflection+0.0544*IRI* | 0.942 | 0.000002 |

As a result of the findings in Section 4.5.4, it was evident that superior correlation between pavement properties and RRC occurred for tests conducted at 30km/h. Therefore, regression was completed utilising the six test cases relating to these tests, with the results presented in Table 4.35.

**Table 4.35: Linear regression equations for RRC considering 30km/h tests only.**

| Data Set | Regression Equation | $r^2$ | Significance of F-value |
|---|---|---|---|
| Unscreened | *RRC=0.1682*Deflection+0.0663*IRI* | 0.958 | 0.0057 |
| Screened | *RRC=0.1537*Deflection+0.058*IRI* | 0.993 | 0.0004 |
| Correlated | *RRC=0.1506*Deflection+0.0598*IRI* | 0.987 | 0.0009 |

### 4.5.6 Relative Influence of Pavement Properties on RRC

The regression equations presented above provide an opportunity for an analysis of the relative influence of each pavement property on the generation of rolling resistance. For each data set, the portion of the estimated RRC arising from both deflation and IRI was calculated. First this focussed on the regression equation resulting from all test data. The results for each data set are presented in Table 4.36 though Table 4.37. A summary of the results is presented in Table 4.39.

**Table 4.36: Percentage of predicted RRC attributed to each pavement property, all truck speeds (unscreened data).**

| | | | | | | Percent RRC derived from: | |
|---|---|---|---|---|---|---|---|
| Section | Load | Speed | Deflection (mm) | IRI (m/km) | RRC (%) | Deflection (mm) | IRI (m/km) |
| 1 | 0 | 15 | 1 | 5.8 | 1.3 | 7 | 38 |
| 2 | 0 | 15 | 2 | 11.4 | 1.41 | 14 | 69 |
| 3 | 0 | 15 | 2 | 15.0 | 1.44 | 14 | 89 |
| 1 | 220 | 15 | 2.5 | 5.8 | 1.38 | 18 | 36 |
| 2 | 220 | 15 | 4 | 11.4 | 1.26 | 31 | 77 |
| 3 | 220 | 15 | 5 | 15.0 | 1.24 | 39 | 103 |
| 1 | 0 | 30 | 1 | 5.8 | 0.98 | 10 | 50 |
| 2 | 0 | 30 | 2 | 11.4 | 1.23 | 16 | 79 |
| 3 | 0 | 30 | 2 | 15.0 | 1.18 | 16 | 108 |
| 1 | 220 | 30 | 2.5 | 5.8 | 1.17 | 21 | 42 |
| 2 | 220 | 30 | 4 | 11.4 | 1.38 | 28 | 70 |
| 3 | 220 | 30 | 5 | 15.0 | 1.61 | 30 | 79 |
| | | | | Mean Unloaded | | 13 | 72 |
| | | | | Mean Loaded | | 28 | 68 |

**Table 4.37: Percentage of predicted RRC attributed to each pavement property, all truck speeds (screened data).**

| | | | | | | Percent RRC derived from: | |
|---|---|---|---|---|---|---|---|
| Section | Load | Speed | Deflection (mm) | IRI (m/km) | RRC (%) | Deflection (mm) | IRI (m/km) |
| 1 | 0 | 15 | 1 | 5.8 | 1.08 | 14 | 33 |
| 2 | 0 | 15 | 2 | 11.4 | 1.06 | 28 | 67 |
| 3 | 0 | 15 | 2 | 15.0 | 1.23 | 24 | 76 |
| 1 | 220 | 15 | 2.5 | 5.8 | 1.45 | 26 | 25 |
| 2 | 220 | 15 | 4 | 11.4 | 1.29 | 46 | 55 |
| 3 | 220 | 15 | 5 | 15.0 | 1.31 | 57 | 71 |
| 1 | 0 | 30 | 1 | 5.8 | 0.46 | 33 | 78 |
| 2 | 0 | 30 | 2 | 11.4 | 0.92 | 33 | 77 |
| 3 | 0 | 30 | 2 | 15.0 | 1.25 | 24 | 74 |
| 1 | 220 | 30 | 2.5 | 5.8 | 0.92 | 41 | 39 |
| 2 | 220 | 30 | 4 | 11.4 | 1.22 | 49 | 58 |
| 3 | 220 | 30 | 5 | 15.0 | 1.58 | 47 | 59 |
| | | | | Mean Unloaded | | 26 | 67 |
| | | | | Mean Loaded | | 44 | 51 |

**Table 4.38: Percentage of predicted RRC attributed to each pavement property, all truck speeds (correlated data).**

| | | | | | | Percent RRC derived from: | |
|---|---|---|---|---|---|---|---|
| Section | Load | Speed | Deflection (mm) | IRI (m/km) | RRC (%) | Deflection (mm) | IRI (m/km) |
| 1 | 0 | 15 | 1 | 5.8 | 0.88 | 20 | 36 |
| 2 | 0 | 15 | 2 | 11.4 | 1.06 | 33 | 59 |
| 3 | 0 | 15 | 2 | 15.0 | 1.08 | 33 | 76 |
| 1 | 220 | 15 | 2.5 | 5.8 | 1.51 | 29 | 21 |
| 2 | 220 | 15 | 4 | 11.4 | 1.2 | 59 | 52 |
| 3 | 220 | 15 | 5 | 15.0 | 1.41 | 62 | 58 |
| 1 | 0 | 30 | 1 | 5.8 | 0.34 | 52 | 93 |
| 2 | 0 | 30 | 2 | 11.4 | 0.98 | 36 | 63 |
| 3 | 0 | 30 | 2 | 15.0 | 1.29 | 27 | 63 |
| 1 | 220 | 30 | 2.5 | 5.8 | 0.96 | 46 | 33 |
| 2 | 220 | 30 | 4 | 11.4 | 1.22 | 58 | 51 |
| 3 | 220 | 30 | 5 | 15.0 | 1.58 | 56 | 52 |
| | | | | Mean Unloaded | | 33 | 65 |
| | | | | Mean Loaded | | 51 | 44 |

**Table 4.39: Summary (screened data and correlated data) of RRC derived from each pavement property, all truck speeds.**

| | Percent RRC derived from: | |
|---|---|---|
| | Deflection (mm) | IRI (m/km) |
| Mean Unloaded | 30 | 66 |
| Mean Loaded | 48 | 48 |

Note the approximate ratio of RRC derived from deflection to IRI in Table 4.39, is one third (deflection) to two-thirds (IRI) for the unloaded case and half for each deflection and IRI in the loaded case.

As noted previously, the correlations observed within the test data suggest that better correlation occurred between RRC and pavement properties for the testing conducted at 30km/h. For this reason the exercise above was repeated with only the 30km/h test data considered. Table 4.40 through Table 4.42 present the proportions for each 30km/h test case for each data set, with a summary provided in Table 4.43.

**Table 4.40: Percentage of predicted RRC attributed to each pavement property, 30km/t test data (unscreened data).**

| | | | | | | Percent RRC derived from: | |
|---|---|---|---|---|---|---|---|
| Section | Load | Speed | Deflection (mm) | IRI (m/km) | RRC (%) | Deflection (mm) | IRI (m/km) |
| 1 | 0 | 30 | 1 | 5.8 | 0.98 | 17 | 39 |
| 2 | 0 | 30 | 2 | 11.4 | 1.23 | 27 | 61 |
| 3 | 0 | 30 | 2 | 15.0 | 1.18 | 29 | 84 |
| 1 | 220 | 30 | 2.5 | 5.8 | 1.17 | 36 | 33 |
| 2 | 220 | 30 | 4 | 11.4 | 1.38 | 49 | 55 |
| 3 | 220 | 30 | 5 | 15.0 | 1.61 | 52 | 62 |
| | | | | Mean Unloaded | | 18 | 46 |
| | | | | Mean Loaded | | 46 | 50 |

**Table 4.41: Percentage of predicted RRC attributed to each pavement property, 30km/t test data (screened data).**

| | | | | | | Percent RRC derived from: | |
|---|---|---|---|---|---|---|---|
| Section | Load | Speed | Deflection (mm) | IRI (m/km) | RRC (%) | Deflection (mm) | IRI (m/km) |
| 1 | 0 | 30 | 1 | 5.8 | 0.46 | 33 | 73 |
| 2 | 0 | 30 | 2 | 11.4 | 0.92 | 33 | 72 |
| 3 | 0 | 30 | 2 | 15.0 | 1.25 | 25 | 70 |
| 1 | 220 | 30 | 2.5 | 5.8 | 0.92 | 42 | 37 |
| 2 | 220 | 30 | 4 | 11.4 | 1.22 | 50 | 54 |
| 3 | 220 | 30 | 5 | 15.0 | 1.58 | 49 | 55 |
| | | | | Mean Unloaded | | 23 | 54 |
| | | | | Mean Loaded | | 47 | 49 |

**Table 4.42: Percentage of predicted RRC attributed to each pavement property, 30km/t test data (correlated data).**

| | | | | | | Percent RRC derived from: | |
|---|---|---|---|---|---|---|---|
| Section | Load | Speed | Deflection (mm) | IRI (m/km) | RRC (%) | Deflection (mm) | IRI (m/km) |
| 1 | 0 | 30 | 1 | 5.8 | 0.34 | 44 | 100 |
| 2 | 0 | 30 | 2 | 11.4 | 0.98 | 31 | 69 |
| 3 | 0 | 30 | 2 | 15.0 | 1.29 | 23 | 68 |
| 1 | 220 | 30 | 2.5 | 5.8 | 0.96 | 39 | 36 |
| 2 | 220 | 30 | 4 | 11.4 | 1.22 | 49 | 55 |
| 3 | 220 | 30 | 5 | 15.0 | 1.58 | 48 | 56 |
| | | | | Mean Unloaded | | 25 | 59 |
| | | | | Mean Loaded | | 45 | 49 |

**Table 4.43: Summary (screened data and correlated data) of RRC derived from each pavement property 30km/h truck data.**

| | Percent RRC derived from: | |
|---|---|---|
| | Deflection (mm) | IRI (m/km) |
| Mean Unloaded | 24 | 57 |
| Mean Loaded | 46 | 49 |

Again note the approximate ratios noted above for testing at all truck speeds (Table 4.39) has been replicated for the test data for testing at 30km/h (Table 4.43).

### 4.5.7 Comparison with Available Models

For comparison purposes, the RRC values resulting from the screened data set are applied. This is to allow some removal of uncertainty related to truck and driver response. Further discussion behind this decision is provided in Section 5.5.2. The RRC values found through testing in the current study actually related to driving resistance, as the power generated at the rear axle must also propel the non-driving front axle. The models below are similar in that they apply coast-down tests, with the exception of that reported by Widodo et al (2009). For comparison with this model a true rolling resistance (relating to a single wheel) should be considered. For this purpose Table 4.44 has been developed, whereby RRC values are increased by

100% for an unloaded truck and 50% for the loaded case, as per the weight distributions in Komatsu (2006).

**Table 4.44: Adjusted RRC relating to a single wheel (screened data set).**

| | | Rolling Resistance Coefficient (RRC) | | | | | |
|---|---|---|---|---|---|---|---|
| | Truck Speed (km/h) | 15 & 30 | | 15km/h | | 30km/h | |
| | Payload (Tonnes) | 0 | 220 | 0 | 220 | 0 | 220 |
| Section | 1 | 1.54 | 1.78 | 2.16 | 2.18 | 0.92 | 1.38 |
| | 2 | 1.98 | 1.88 | 2.12 | 1.94 | 1.84 | 1.83 |
| | 3 | 2.48 | 2.17 | 2.46 | 1.97 | 2.50 | 2.37 |

Results for estimation of rolling resistance with models developed specifically for haul roads are presented in Table 4.45 (Thompson et al, 2003) and Table 4.46 (Widodo et al, 2009).

**Table 4.45: Predicted rolling resistance values as per Thompson et al (2003).**

| Section | Speed (km/h) | RRMIN (%) | RDS | RR (%) |
|---|---|---|---|---|
| 1 | 15 | 1.73 | 9.00 | 1.95 |
| 1 | 30 | 1.80 | 9.00 | 2.05 |
| 2 | 15 | 1.73 | 52.00 | 2.83 |
| 2 | 30 | 1.80 | 52.00 | 3.01 |
| 3 | 15 | 1.73 | 52.00 | 2.83 |
| 3 | 30 | 1.80 | 52.00 | 3.01 |

**Table 4.46: Typical rolling resistance values for a Komatsu 830 as per Widodo et al (2009).**

| | RR (N) | RRC (%) |
|---|---|---|
| Unloaded | 44777 | 11.12 |
| Loaded | 160263 | 12.74 |

Predictions based on the models derived through research in New Zealand (Cenek et al, 1996) with a commercial truck are presented in Table 4.47, Table 4.48 and Table 4.49. The first two primarily consider pavement roughness and the latter rebound deflection.

**Table 4.47: Comparison of estimated RRC via Cenek et al (1996), utilising IRI results and measured RRC values (15km/h).**

| Section | IRI | RRC (%) |
|---|---|---|
| 1 | 5.8 | 0.67 |
| 2 | 11.4 | 0.91 |
| 3 | 15 | 1.07 |

Note that the RRC values noted in Table 4.47 have a calculated Person correlation coefficient (see Section 3.4.5) of 0.7 with the measured unloaded RRC from the current study.

**Table 4.48: Comparison of estimated RRC via Cenek et al (1996), utilising IRI results and measured RRC values (30km/h).**

| Section | IRI | RRC (%) |
|---|---|---|
| 1 | 5.8 | 0.68 |
| 2 | 11.4 | 0.92 |
| 3 | 15 | 1.08 |

Note that RRC noted in Table 4.48 correlate well with those measured within the current study (applying the screened data results). The correlation coefficient exceeds 0.997 (limit of statistical significance of 0.05) when both the unloaded and loaded truck condition is considered. In the case of the loaded case the model under estimated the RRC by a range of 25-32%, with correlation with unloaded measured RRC being less consistent with a range from a 46% over estimate to a 14% under estimate.

**Table 4.49: Predicted static RRC ($C_o$) as per Jamieson et al (1999).**

| | Rebound Deflection (mm) | $C_o$ |
|---|---|---|
| Section 1 - Unloaded | 1.2 | -0.154 |
| Section 1 - Loaded | 2.6 | -0.149 |
| Section 2 - Unloaded | 2 | -0.151 |
| Section 2 - Loaded | 3.8 | -0.146 |
| Section 3 - Unloaded | 1.9 | -0.152 |
| Section 3 - Loaded | 5.2 | -0.141 |

Estimations using the HDM-4 (ARFCOM) model are presented in Table 4.50, taking account of pavement roughness and vehicle speed.

**Table 4.50: Rolling resistance estimates using the HDM-4 model.**

| | | | | Unloaded | | Loaded | |
|---|---|---|---|---|---|---|---|
| Section | IRI (m/km) | CR1 | CR2 | Fr (N) | RRC (%) | Fr (N) | RRC (%) |
| 1 | 5.8 | 1.3 | 0.638 | 2948 | 0.18 | 6220 | 0.17 |
| 2 | 11.4 | 1.3 | 1.254 | 5794 | 0.36 | 12226 | 0.32 |
| 3 | 15 | 1.3 | 1.65 | 7624 | 0.47 | 16086 | 0.43 |

Lastly, results of predictions via research as part of the MIRIAM project are presented (Table 4.51 and Table 4.52). These models consider velocity, texture and roughness in estimating RRC.

**Table 4.51: Estimated RRC from equation derived in ECRPD project for trucks.**

| | Velocity (km/h) | | | RRC (%) |
|---|---|---|---|---|
| Section 1 | 15 | Texture (mm) | 8.4 | 0.62 |
| | | $IRI_{Estimate}$ (m/km) | 5.8 | |
| | 30 | Texture (mm) | 8.4 | 0.62 |
| | | $IRI_{Estimate}$ (m/km) | 5.8 | |
| Section 2 | 15 | Texture (mm) | 19.9 | 0.63 |
| | | $IRI_{Estimate}$ (m/km) | 11.4 | |
| | 30 | Texture (mm) | 19.9 | 0.64 |
| | | $IRI_{Estimate}$ (m/km) | 11.4 | |
| Section 3 | 15 | Texture (mm) | 22.4 | 0.64 |
| | | $IRI_{Estimate}$ (m/km) | 15 | |
| | 30 | Texture (mm) | 22.4 | 0.64 |
| | | $IRI_{Estimate}$ (m/km) | 15 | |

**Table 4.52: Predicted RRC from the VETO model (Hammarstrom et al, 2012).**

| | Velocity (km/h) | | | RRC (%) |
|---|---|---|---|---|
| Section 1 | 15 | Texture (mm) | 8.4 | 0.42 |
| | | $IRI_{Estimate}$ (m/km) | 5.8 | |
| | 30 | Texture (mm) | 8.4 | 0.42 |
| | | $IRI_{Estimate}$ (m/km) | 5.8 | |
| Section 2 | 15 | Texture (mm) | 19.9 | 0.44 |
| | | $IRI_{Estimate}$ (m/km) | 11.4 | |
| | 30 | Texture (mm) | 19.9 | 0.44 |
| | | $IRI_{Estimate}$ (m/km) | 11.4 | |
| Section 3 | 15 | Texture (mm) | 22.4 | 0.44 |
| | | $IRI_{Estimate}$ (m/km) | 15 | |
| | 30 | Texture (mm) | 22.4 | 0.44 |
| | | $IRI_{Estimate}$ (m/km) | 15 | |

## 4.6 Potential Impacts on VOC

### 4.6.1 Fuel Consumption

The estimates of instantaneous fuel consumption (IFC) for measured rolling resistance values, via the HDM-4 model are presented in Table 4.53. For

comparison, estimates have also been generated utilising the Department of Resources model, shown in Table 4.54. The correlation between the two models is presented in Figure 4.49.

**Table 4.53: Results of modelling IFC with HDM-4 fuel consumption model.**

| Section | Speed (km/h) | Load Condition | AVG RRC (%) | Pr (kW) | IFC (mL/s) |
|---|---|---|---|---|---|
| 1 | 15 | Unloaded | 1.08 | 72.49 | 14.76 |
| | 15 | Loaded | 1.45 | 227.73 | 26.20 |
| | 30 | Unloaded | 0.46 | 61.72 | 13.96 |
| | 30 | Loaded | 0.92 | 288.84 | 30.70 |
| 2 | 15 | Unloaded | 1.06 | 71.15 | 14.66 |
| | 15 | Loaded | 1.29 | 202.60 | 24.35 |
| | 30 | Unloaded | 0.92 | 123.45 | 18.52 |
| | 30 | Loaded | 1.22 | 383.03 | 37.64 |
| 3 | 15 | Unloaded | 1.23 | 82.56 | 15.50 |
| | 15 | Loaded | 1.31 | 205.74 | 24.60 |
| | 30 | Unloaded | 1.25 | 167.72 | 21.77 |
| | 30 | Loaded | 1.58 | 496.05 | 45.97 |

**Table 4.54: Fuel Consumption estimates for each section as per Department of Resources, Energy and Tourism (2010).**

| Section | Speed (km/h) | Load Condition | AVG RRC (%) | Total Force (kN) | Wheel Torque (kNm) | Wheel Rotations /Second | Power from Wheel Torque (kW) | Engine Output Power (kW) | Fuel input Power (kW) | Fuel Input per Second (ml/s) |
|---|---|---|---|---|---|---|---|---|---|---|
| 1 | 15 | Unloaded | 1.08 | 17.40 | 31.98 | 0.4167 | 83.68 | 88.08 | 352.32 | 9.13 |
| | 15 | Loaded | 1.45 | 54.65 | 100.45 | 0.4167 | 262.86 | 276.70 | 1106.80 | 28.67 |
| | 30 | Unloaded | 0.46 | 7.41 | 13.62 | 0.7433 | 63.57 | 66.92 | 267.68 | 6.93 |
| | 30 | Loaded | 0.92 | 34.67 | 63.73 | 0.7433 | 297.50 | 313.16 | 1252.65 | 32.45 |
| 2 | 15 | Unloaded | 1.06 | 17.07 | 31.38 | 0.4167 | 82.13 | 86.45 | 345.80 | 8.96 |
| | 15 | Loaded | 1.29 | 48.62 | 89.37 | 0.4167 | 233.86 | 246.17 | 984.67 | 25.51 |
| | 30 | Unloaded | 0.92 | 14.82 | 27.24 | 0.7433 | 127.15 | 133.84 | 535.36 | 13.87 |
| | 30 | Loaded | 1.22 | 45.98 | 84.52 | 0.7433 | 394.52 | 415.28 | 1661.12 | 43.03 |
| 3 | 15 | Unloaded | 1.23 | 19.81 | 36.42 | 0.4167 | 95.30 | 100.31 | 401.26 | 10.40 |
| | 15 | Loaded | 1.31 | 49.37 | 90.75 | 0.4167 | 237.48 | 249.98 | 999.93 | 25.91 |
| | 30 | Unloaded | 1.25 | 20.14 | 37.01 | 0.7433 | 172.75 | 181.85 | 727.39 | 18.84 |
| | 30 | Loaded | 1.58 | 59.55 | 109.46 | 0.7433 | 510.93 | 537.82 | 2151.28 | 55.73 |

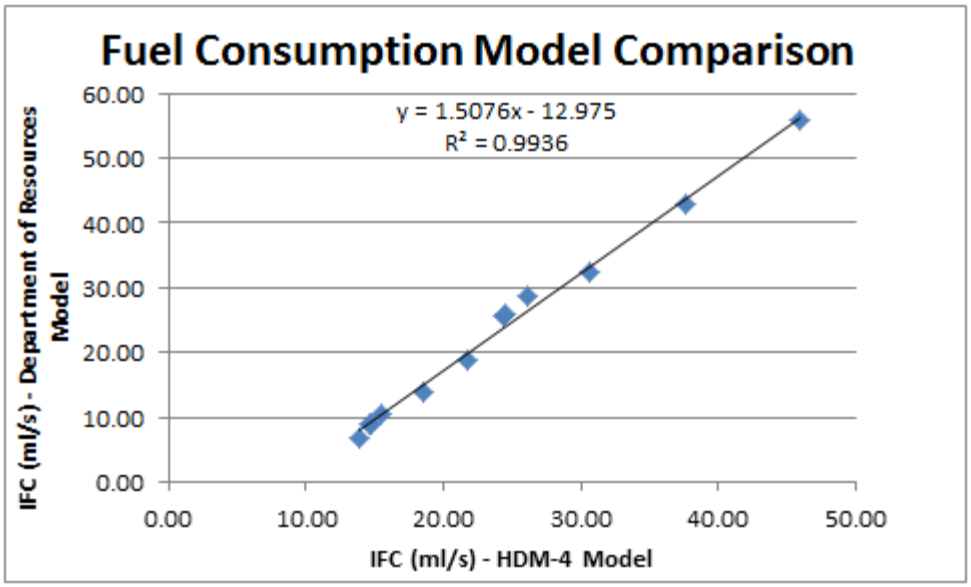


**Figure 4.49: Comparison of fuel consumption models.**

## 4.7 Laboratory Testing

The proceeding section presents the details of laboratory testing completed for the project. Note that some additional data is presented in this section (for example, photographs of in-situ soil conditions), as it has been interpreted with the data from laboratory testing.

### 4.7.1 In-situ Photographs

Photographs of in-situ material for each pavement section are presented below.

**Figure 4.50: In-situ material of Section 1.**

**Figure 4.51: In-situ material of Section 2.**

**Figure 4.52: In-situ material of Section 3.**

### 4.7.2 Particle Size Distribution

Particle Size Distributions (PSD) for materials samples taken from each pavement section are shown in Figure 4.53, with the Main Roads Western Australia (MRWA) 'Lt10' grading envelope (MRWA et al, 2003).

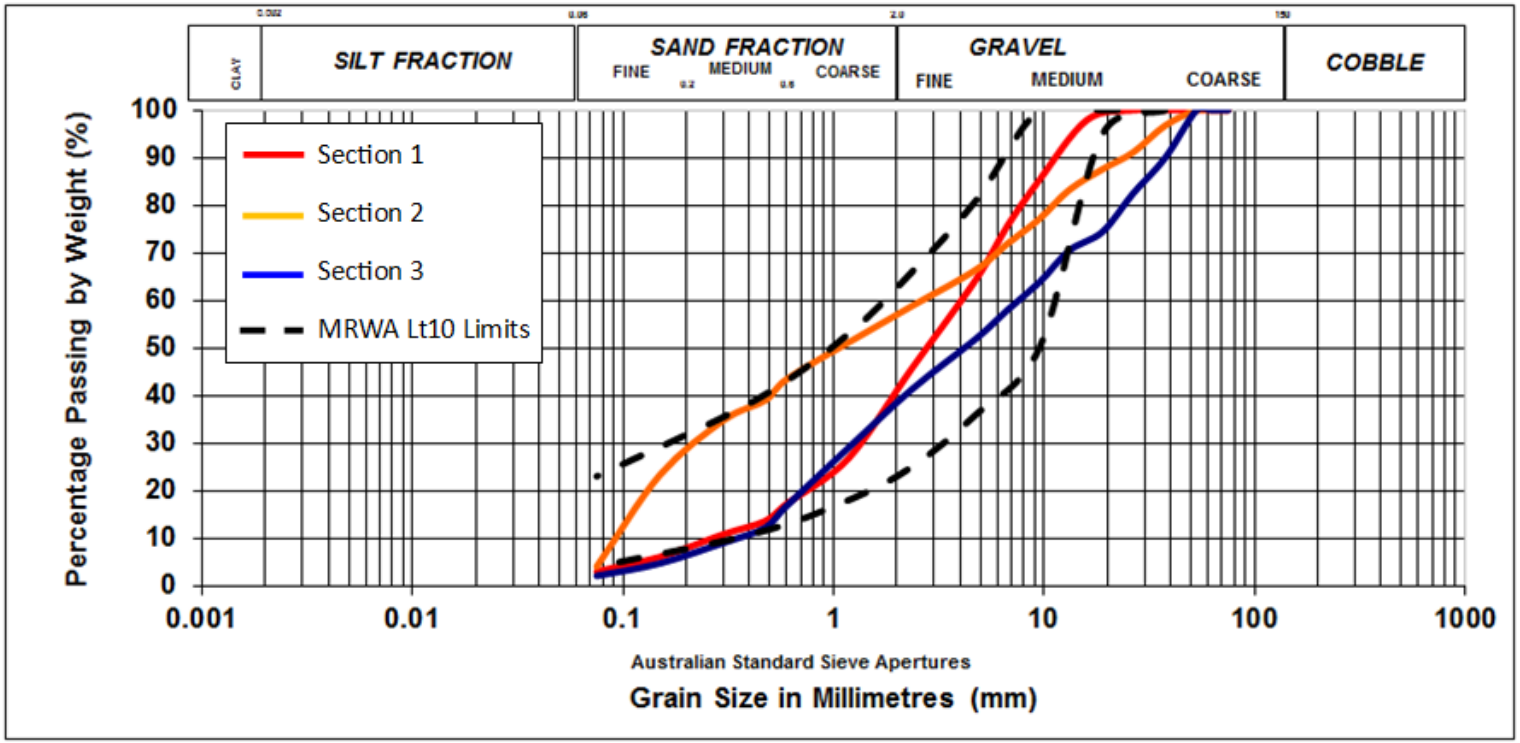


**Figure 4.53: PSD results, with MRWA 'Lt10' envelope for lateritic gravels in semi-arid regions (MRWA, 2003).**

In addition to PSD results, Table 4.55 presents results from interpretation of grading results. Table 4.55 classifies each material according to the Unified Soil Classification system, which is contained with AS 1726.

**Table 4.55: Assessment of materials as per AS 1726 and MRWA selection criteria.**

| | AS 1726 | | | | MRWA Selection | |
|---|---|---|---|---|---|---|
| **Section** | **Percentage <0.075mm** | **Cu** | **Cc** | **Classification** | **DR** | **GM** |
| **1** | 3.00 | 14.17 | 2.01 | GW | 0.22 | 2.38 |
| **2** | 4.01 | 24.00 | 0.24 | GP | 0.10 | 1.98 |
| **3** | 2.07 | 23.14 | 0.50 | GP | 0.17 | 2.44 |

### 4.7.3 Optimum Moisture Content/Maximum Dry Density

The results for the optimum moisture content (OMC) and maximum dry density (MDD) for each section are presented below.

**Table 4.56: OMC/MDD results summary.**

| Section | OMC (%) | MDD ($t/m^3$) |
|---|---|---|
| 1 | 8 | 2.8 |
| 2 | 9 | 2.47 |
| 3 | 11 | 2.4 |

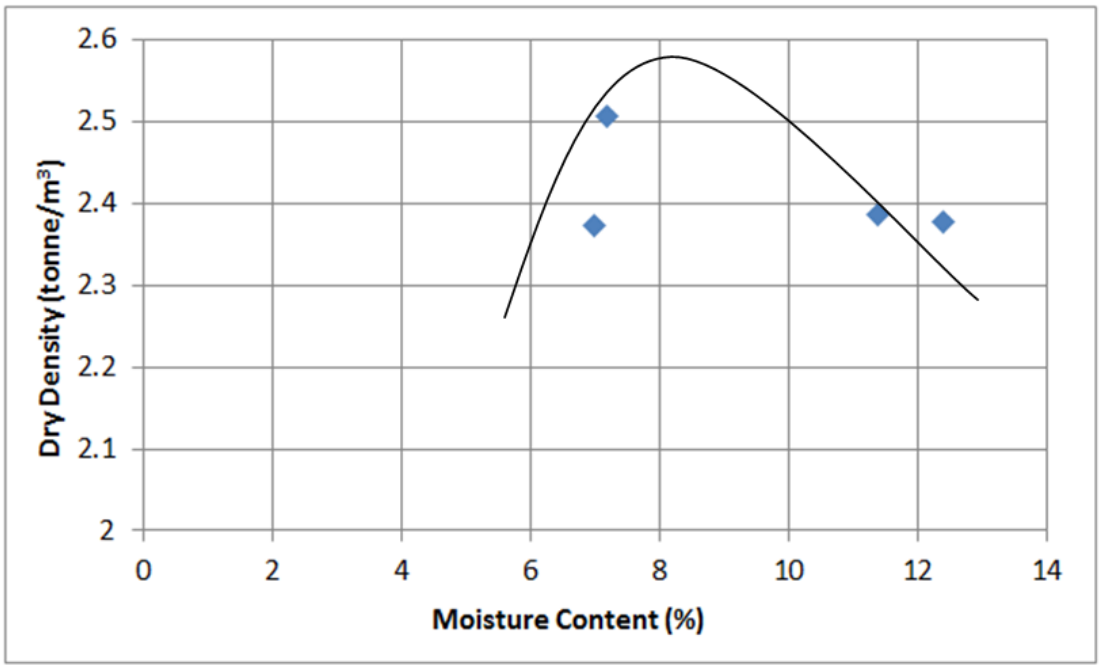


**Figure 4.54: Section 1 OMC/MDD results with plotted trend line.**

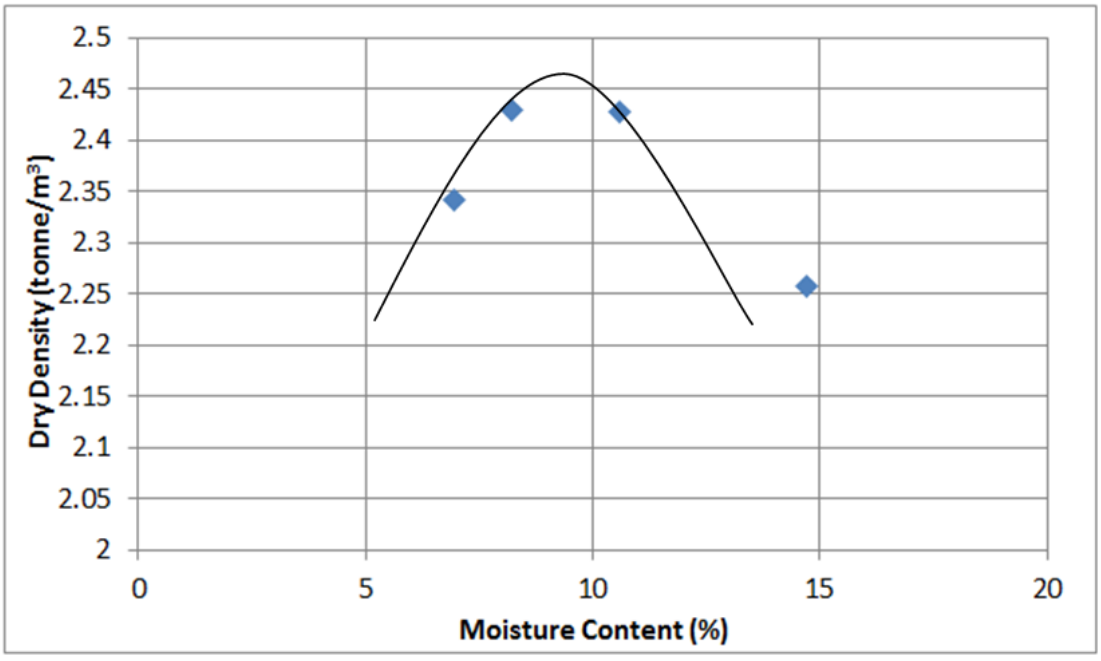


**Figure 4.55: Section 2 OMC/MDD results with plotted trend line.**

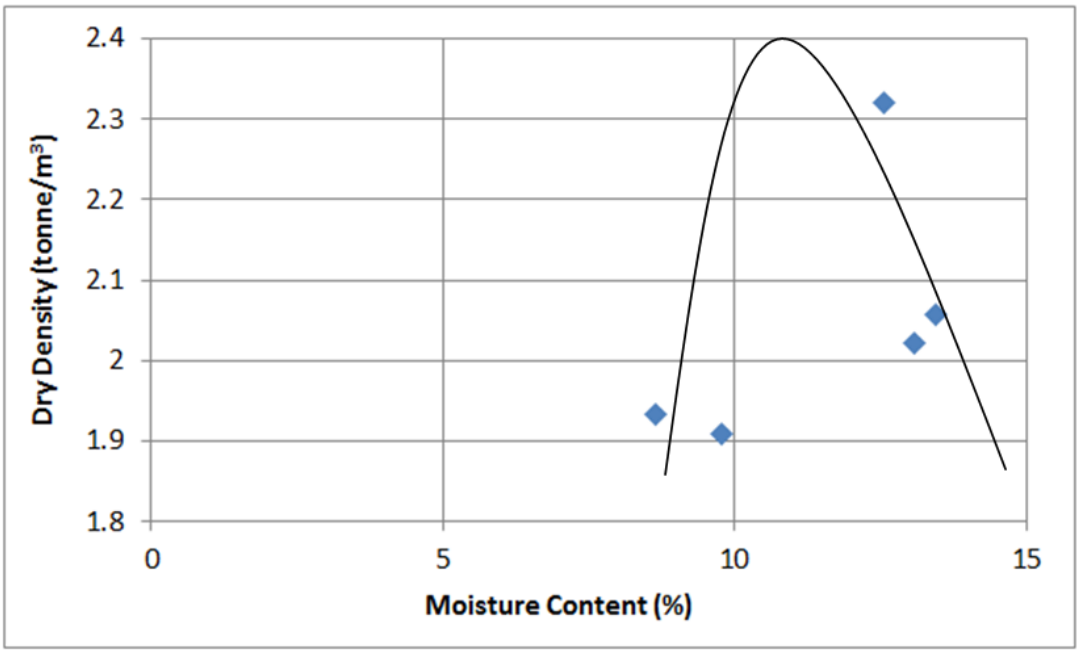


**Figure 4.56: Section 3 OMC/MDD results with plotted trend line.**

### 4.7.4 Repeated Load Tri-axial Test (RLTT)

The following details the repeated load tri-axial testing undertaken for the project. This includes a description of the condition of the soil during testing.

#### 4.7.4.1 Resilient Modulus

Plots of resilient modulus against mean normal stress for each section are presented below. The first graph for each section relates to the results from Austroads AG:PT/T053 test method, with Sections 2 and 3 also including a second plot , which relates to the additional stress states described in Section 3.8.3. The power function relating to the trend-line drawn on each graph, along with the coefficient of determination ($R^2$) is included on each graph. This equation is the 'k-Θ' relation to describe non-linear soil modulus response to differing levels of mean normal stress. A summary of the results, indicating resilient modulus values at a deviatoric stress of 890kPa is included in Table 4.57.

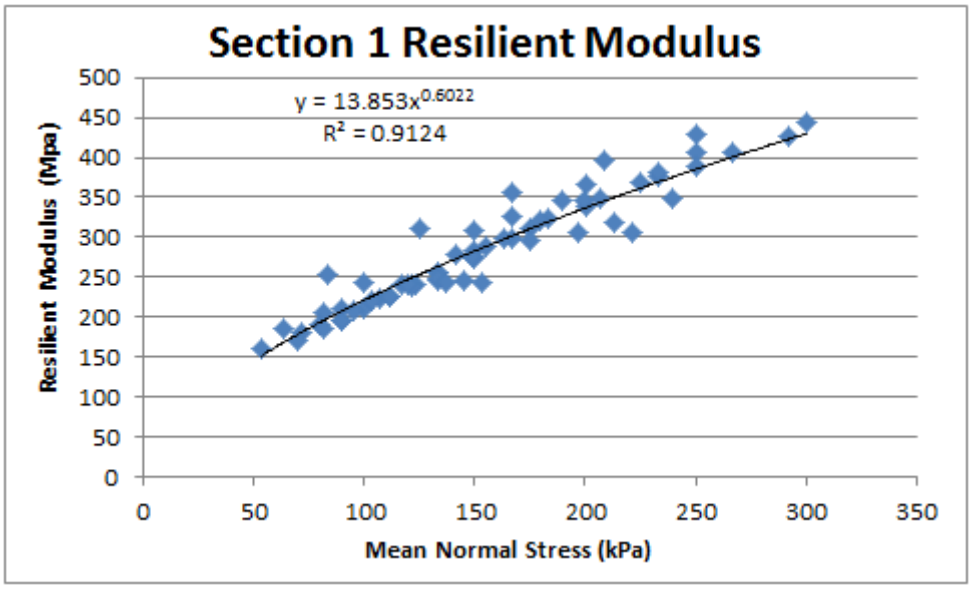


**Figure 4.57: Section 1 resilient modulus plot (Austroads test stress regime).**

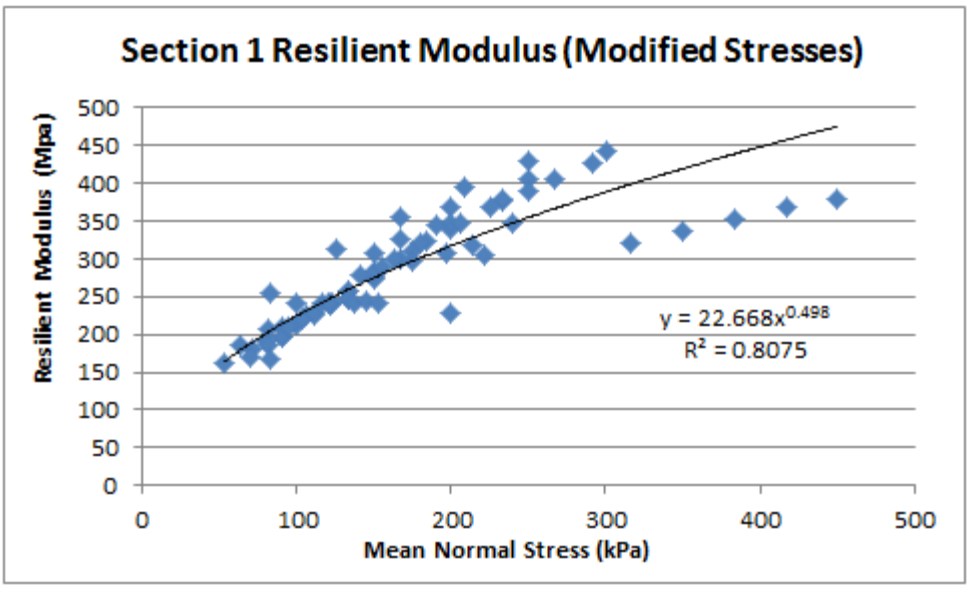


**Figure 4.58: Section 1 resilient modulus plot (modified stress regime).**

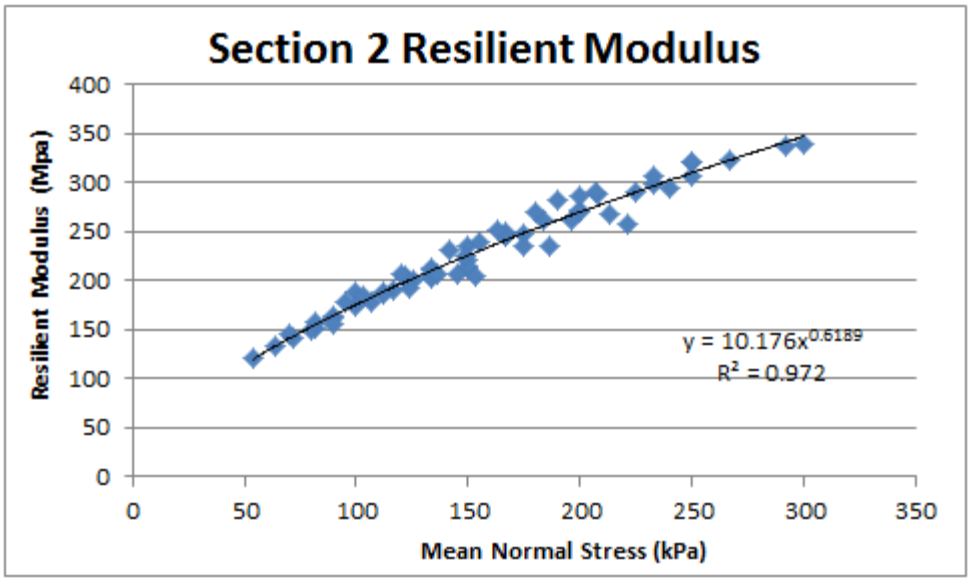


**Figure 4.59: Section 2 resilient modulus plot (Austroads test stress regime).**

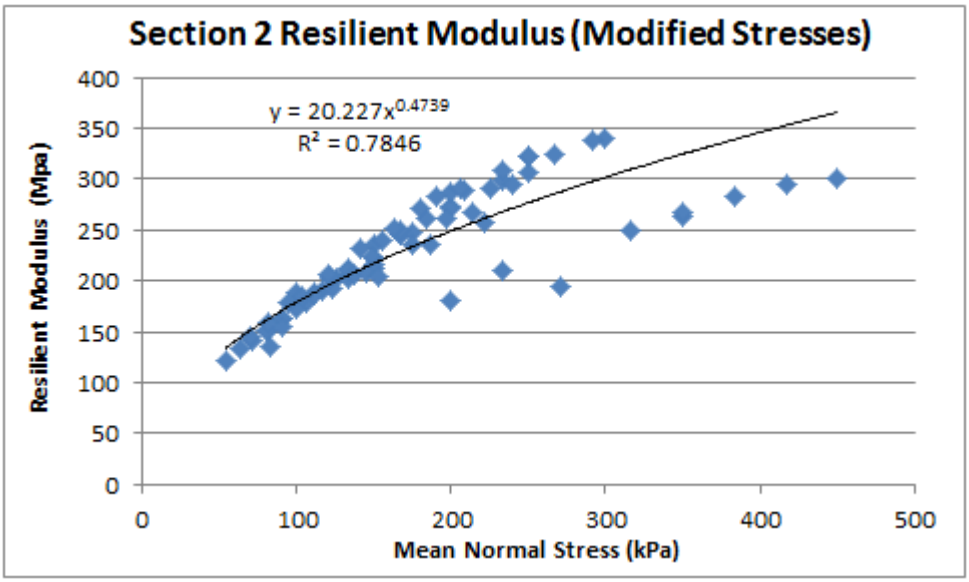


**Figure 4.60: Section 2 resilient modulus plot (modified stress regime).**

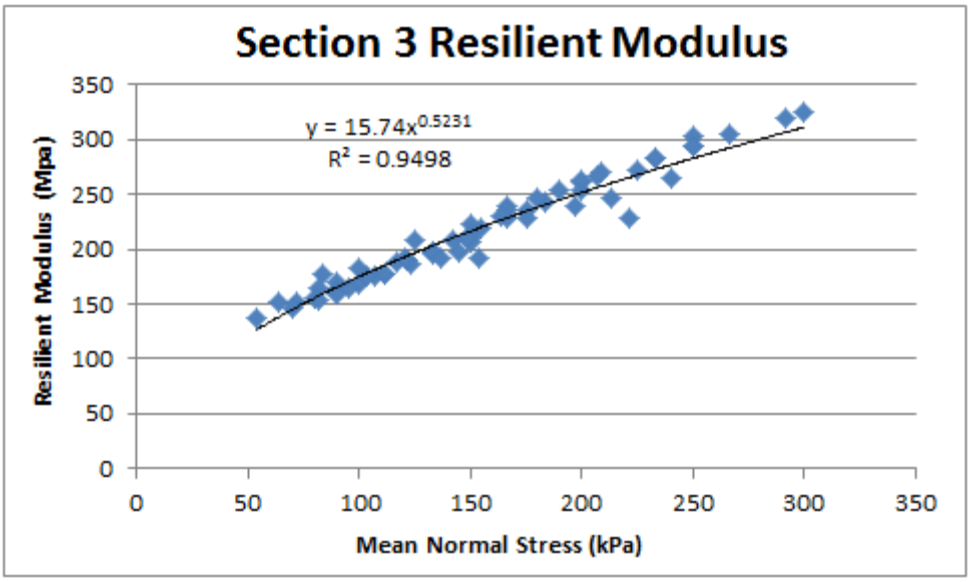


**Figure 4.61: Section 3 resilient modulus plot (Austroads test stress regime).**

A summary of the calculated resilient modulus, from the RLT results presented above, is provided in Table 4.57, which relate to a deviatoric stress of 890kPa. Note that the mean normal stress exceeds the maximum of 240kPa stated by MRWA (2013). The values of mean normal stress in Table 4.57 are considered acceptable due to the significantly larger tyre loads and pressures experienced by haul roads.

**Table 4.57: Interpreted resilient modulus results for stress state from tri-axial testing.**

| Section | Confining Stress (kPa) | Mean Normal Stress (kPa) | Interpreted Resilient Modulus for 890 kPa Deviatoric Stress (MPa) |
|---|---|---|---|
| 1 | 91 | 388 | 441 |
| 2 | 83 | 380 | 338 |
| 3 | 107 | 404 | 363 |

#### 4.7.4.2 Permanent Deformation

The measured permanent deformation accumulated during the repeated load tri-axial tests are presented below. Note that sequence 65 to 70 relate to the additional stress states which relate to the higher mean normal stresses in Figure 4.57 to Figure 4.61. This represents the operating stresses likely under a haul truck. The exaggerated deformation occurring from sequence 55 onwards is related to the low confining stresses applied, resulting in high stress ratios (deviatoric:confining stress).

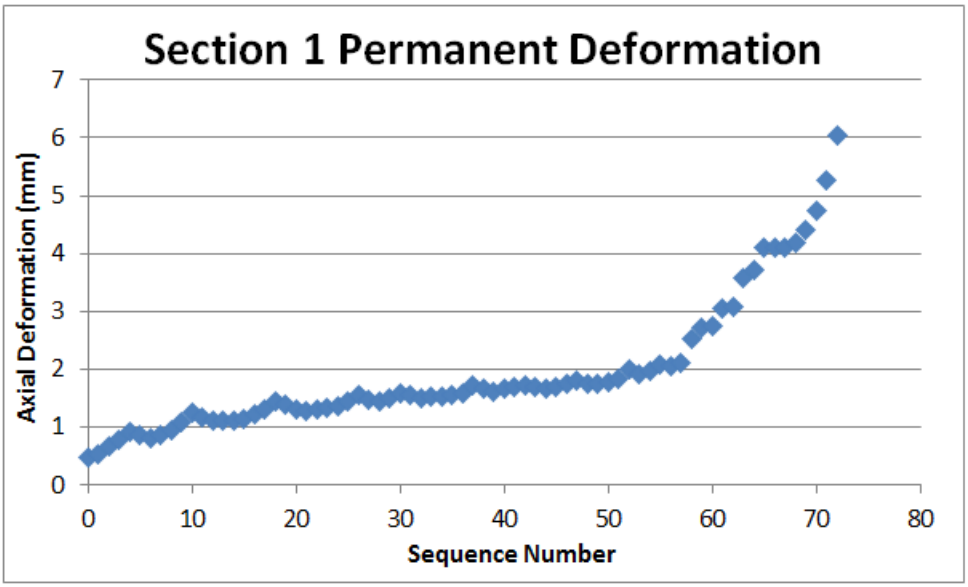


**Figure 4.62: Section 1 permanent deformation against test sequence number.**

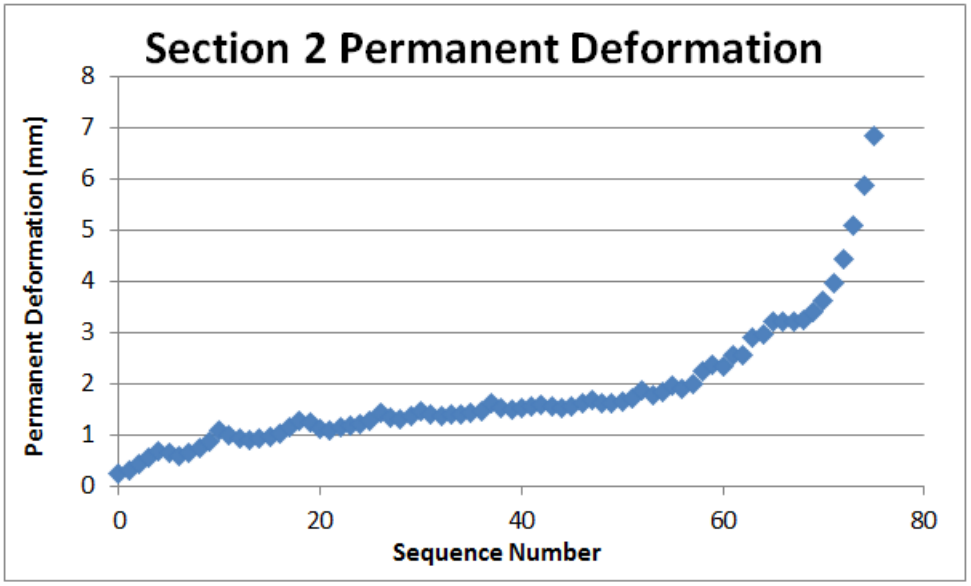


**Figure 4.63: Section 2 permanent deformation against test sequence number.**

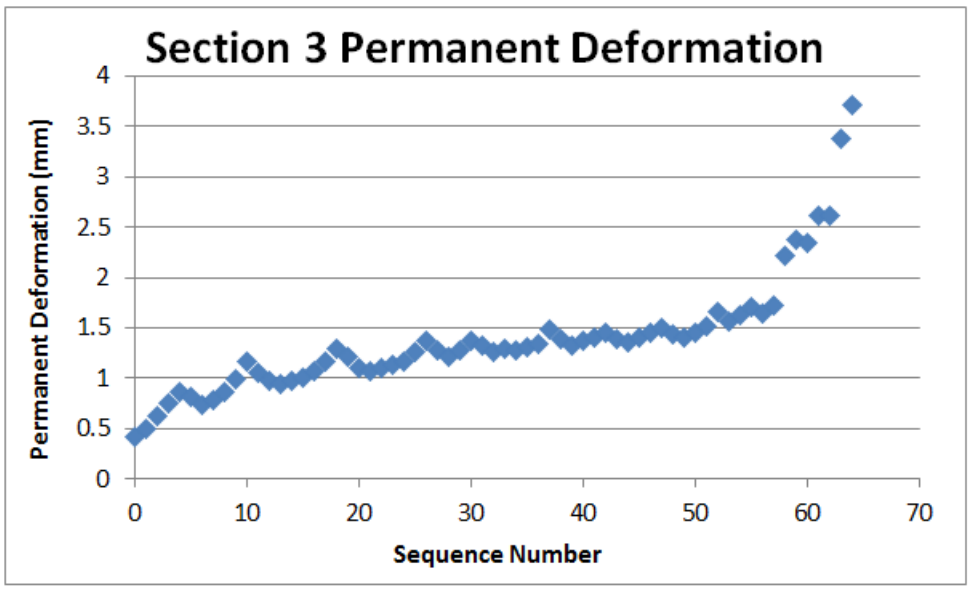


**Figure 4.64: Section 3 permanent deformation against test sequence number.**

#### 4.7.4.3 Test Density/Moisture Conditions

Table 4.58 details the soil conditions present during repeated load tri-axial testing.

**Table 4.58: Sample density and moisture ratios, RLTT testing.**

| Section | Sample Weight (kg) | Wet Density (tonne/m3) | Dry Density (tonne/m$^3$) | Density Ratio (% MDD) | Moisture Content (%) | Moisture Ratio (% OMC) |
|---|---|---|---|---|---|---|
| 1 | 4.0227 | 2.56 | 2.39 | 93 | 7.1 | 89 |
| 2 | 3.5092 | 2.24 | 2.12 | 86 | 5.2 | 58 |
| 3 | 4.072 | 2.59 | 2.33 | 97 | 11.5 | 105 |

### 4.7.5 Tri-axial Testing

The following details the tri-axial testing undertaken with monotonic loading conditions.

#### 4.7.5.1 Stress/Strain Plots

Stress/strain plots are presented for triaxial testing of each sample in the following. The inconsistency of the testing for section 1 (Figure 4.65) is considered to be related to the stress history of the sample, and is discussed in detail in Section 5.7.3.

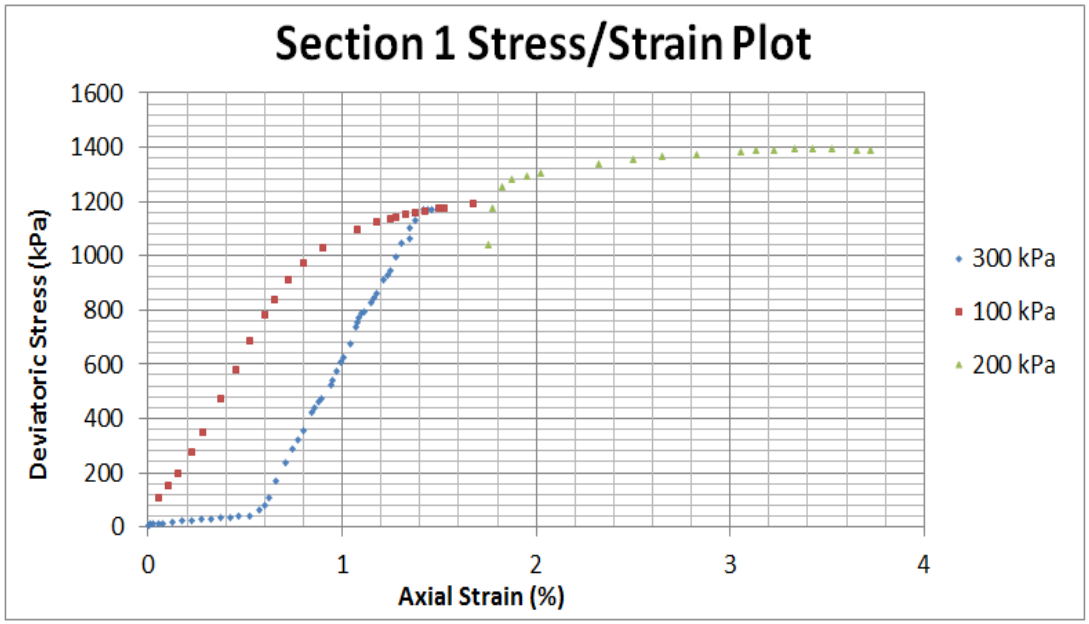


**Figure 4.65: Section 1 stress/strain plot (legend showing confining stress).**

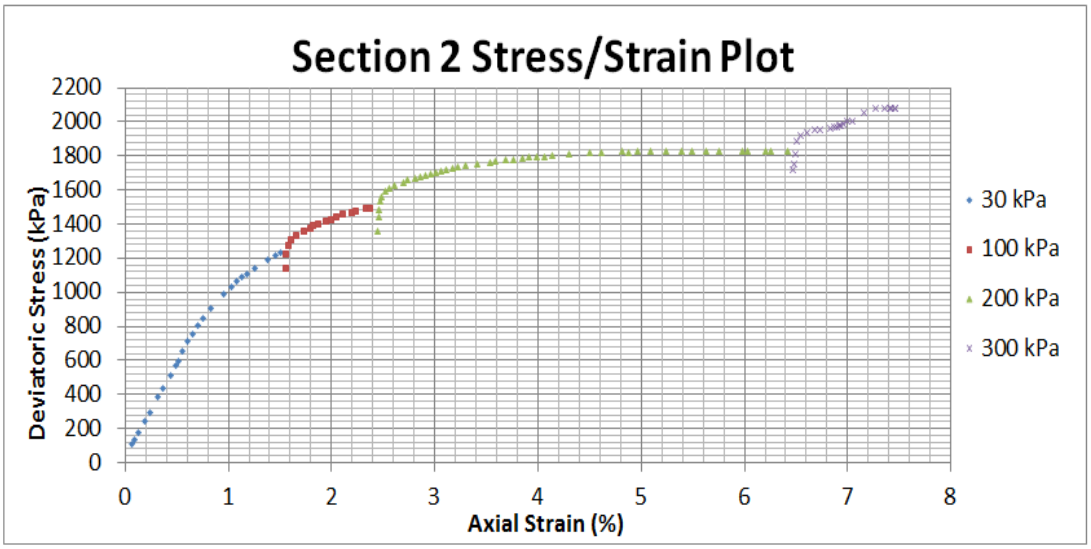


**Figure 4.66: Section 2 stress/strain plot (legend showing confining stress).**

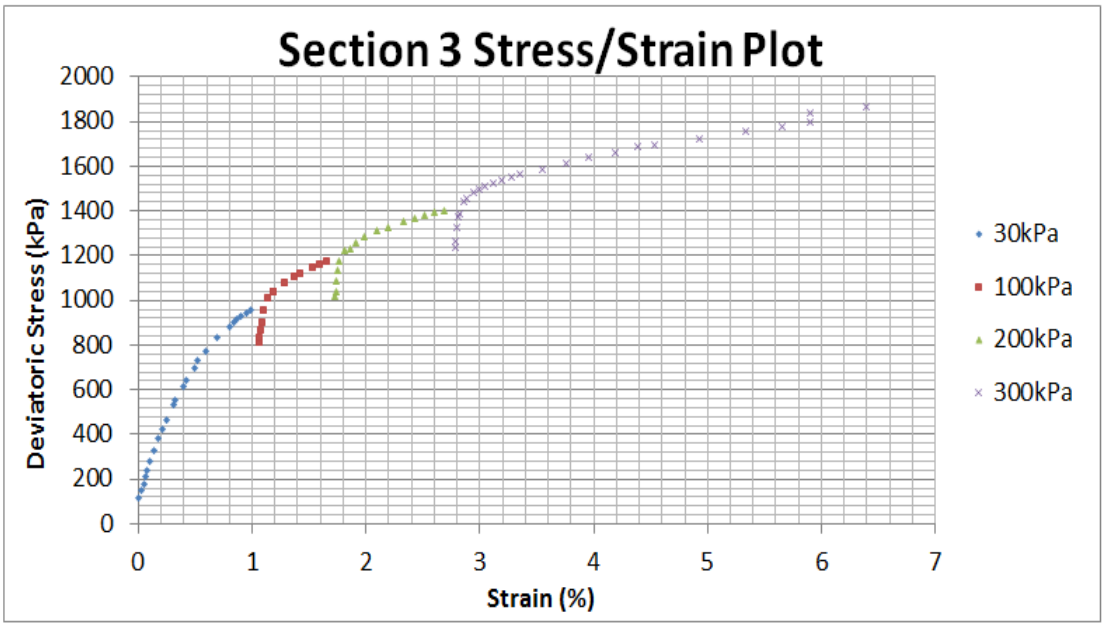


**Figure 4.67: Section 3 stress/strain plot (legend showing confining stress).**

#### 4.7.5.2 Mohr-Coloumb Strength Envelope

Mohr-Coloumb strength envelopes, relating to the test results detailed above, are presented in the following. A summary of the Mohr-Coloumb strength parameters is also presented in Table 4.59.

**Table 4.59: Mohr-Coloumb failure envelope summary.**

| | c (kPa) | ϕ (degrees) |
|---|---|---|
| Section 1 | 290 | 39 |
| Section 2 | 280 | 39 |
| Section 3 | 230 | 40 |

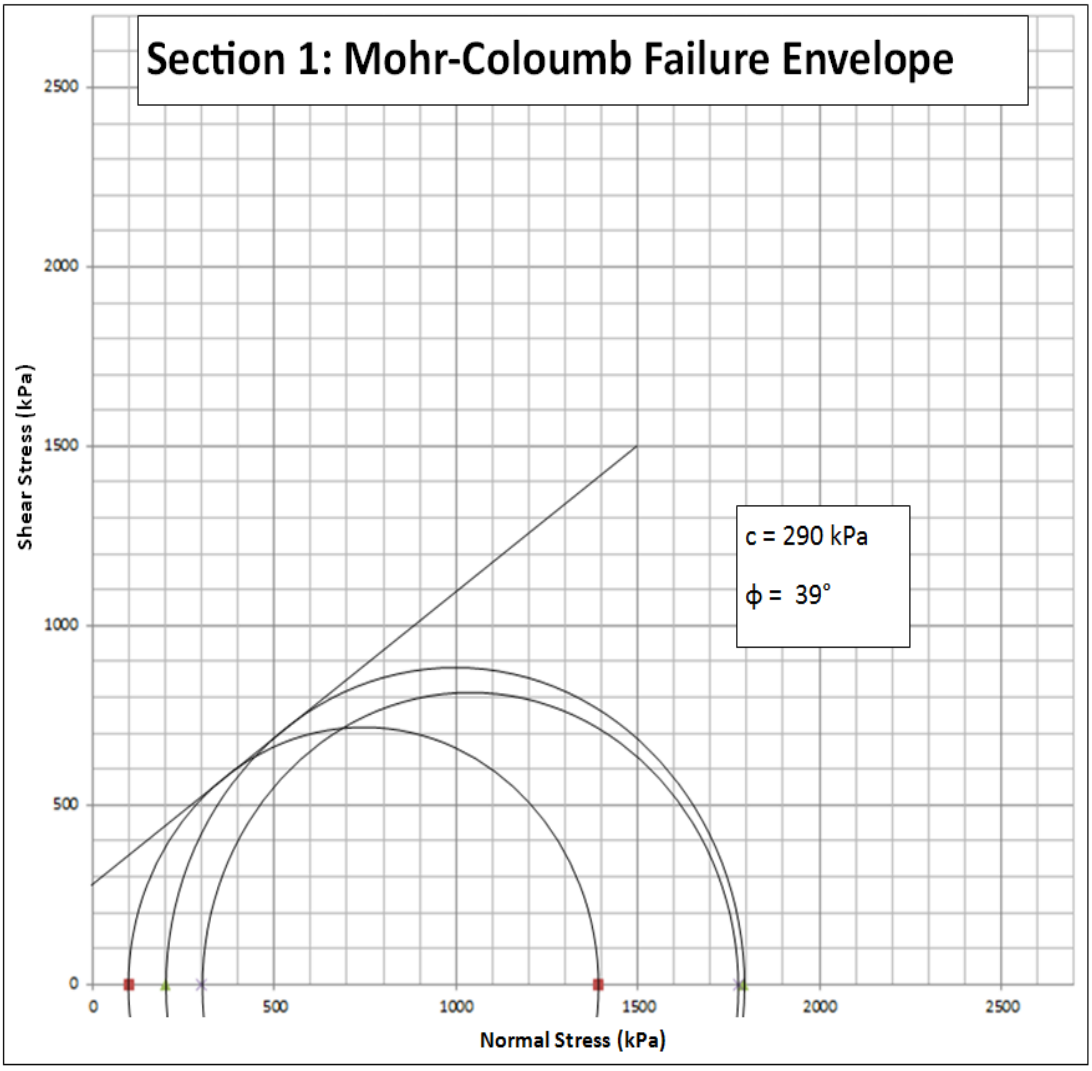


**Figure 4.68: Section 1 Mohr's circle, showing Mohr-Coloumb failure envelope (incomplete).**

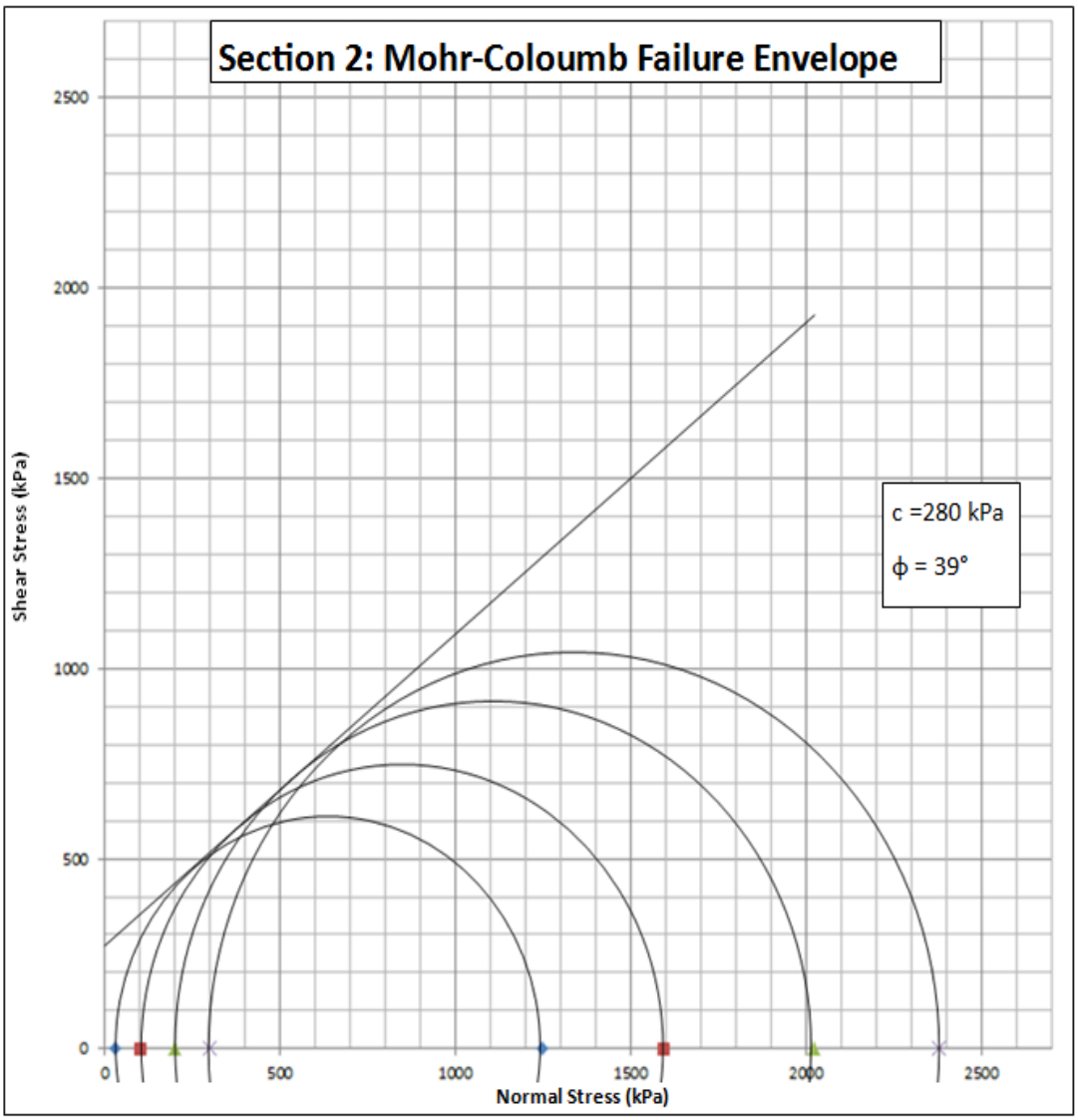


**Figure 4.69: Section 2 Mohr's circle, showing Mohr-Coloumb failure envelope.**

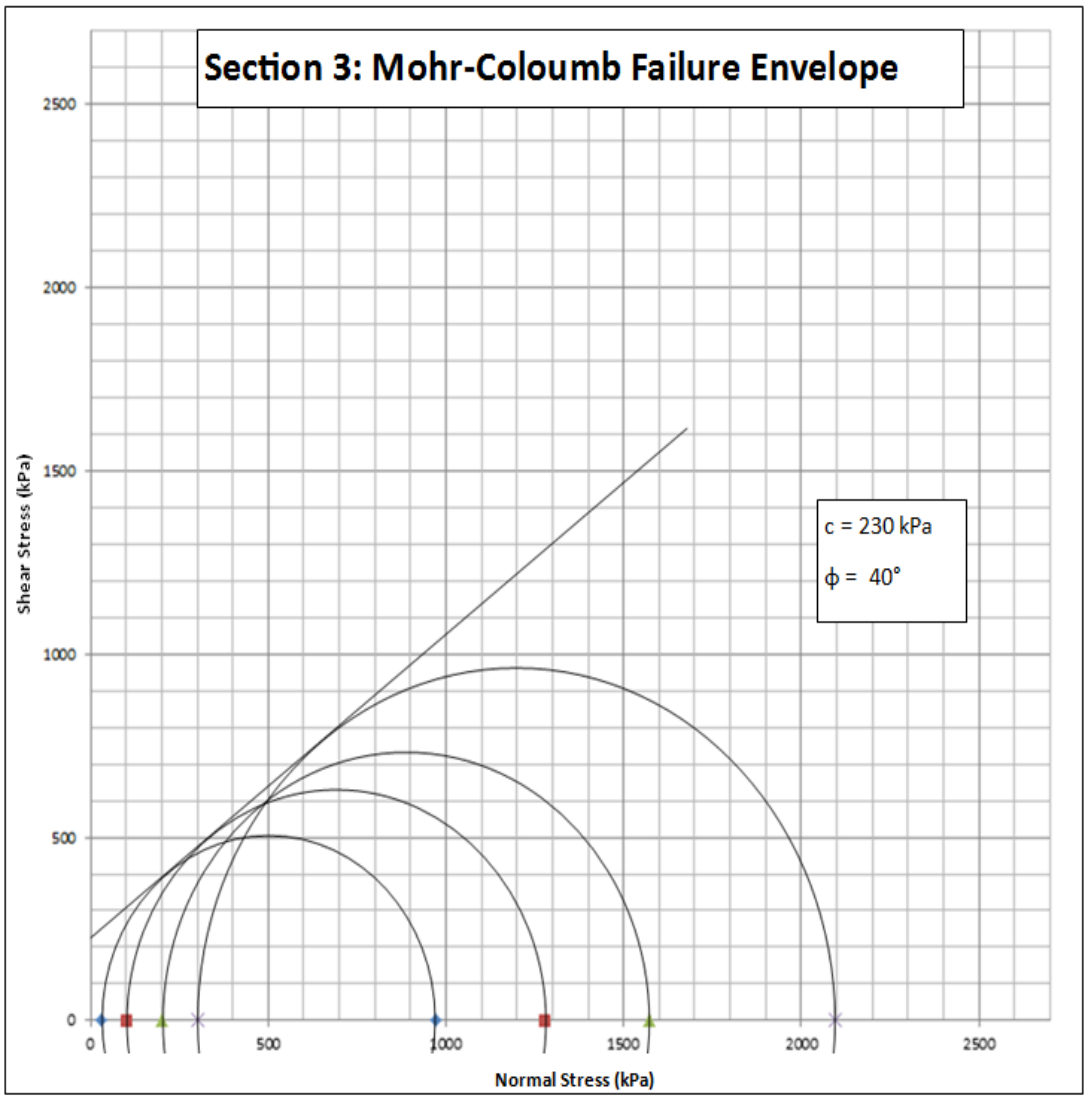


**Figure 4.70: Section 3 Mohr's circle, showing Mohr-Coloumb failure envelope.**

#### 4.7.5.3 Elastic Modulus

Tangent elastic moduli results are shown in Table 4.60. Secant elastic moduli (relating to the elastic yield point) are presented in Table 4.61. The tangent elastic modulus and confining stress are included for a deviatoric stress of 890kPa to provide insight into the material properties that were considered to have occurred during site testing.

**Table 4.60: Tangent elastic modulus values from tri-axial testing.**

| | Initial | | | Yield | | | | |
|---|---|---|---|---|---|---|---|---|
| Section | Confining Stress (kPa) | Deviator Stress (kPa) | Strain (%) | Deviator Stress (kPa) | Strain(%) | Tangent Elastic Modulus (MPa) | Elastic Modulus at 890kPa Deviatoric | Confining at 890kPa Deviatoric |
| 1 | 100 | 294 | 0.15 | 1014 | 0.725 | 125 | 271 | 91 |
| | 200 | 1247 | 1.755 | 1460 | 1.825 | 304 | | |
| | 300 | 473 | 0.66 | 1452 | 1.325 | 147 | | |
| 2 | 30 | 137.8 | 0.07 | 878 | 0.76 | 107 | 254 | 83 |
| | 100 | 1240.7 | 1.555 | 1406 | 1.61 | 301 | | |
| | 200 | 1559.8 | 2.45 | 1763 | 2.49 | 508 | | |
| | 300 | 2016.4 | 6.47 | 2183.97 | 6.51 | 419 | | |
| 3 | 30 | 143.7 | 0.005 | 586 | 0.325 | 138 | 255 | 107 |
| | 100 | 916.2 | 1.06 | 1111 | 1.14 | 244 | | |
| | 200 | 1221.8 | 1.73 | 1332.8 | 1.75 | 555 | | |
| | 300 | 1539.3 | 2.79 | 1674.4 | 2.815 | 540 | | |

**Table 4.61: Failure secant elastic modulus values from tri-axial testing.**

| | Initial | | | Failure | | |
|---|---|---|---|---|---|---|
| Section | Confining (kPa) | Deviator (kPa) | Strain (%) | Deviator (kPa) | Strain(%) | Failure Secant Elastic Modulus (MPa) |
| 1 | 100 | 194 | 0.15 | 1191 | 1.675 | 65 |
| | 200 | 1047 | 1.755 | 1362 | 2.5 | 42 |
| | 300 | 173 | 0.66 | 1165 | 1.425 | 130 |
| 2 | 30 | 107.8 | 0.07 | 1220 | 1.56 | 75 |
| | 100 | 1140.7 | 1.555 | 1494 | 2.335 | 45 |
| | 200 | 1359.8 | 2.45 | 1824 | 5.09 | 18 |
| | 300 | 1716.4 | 6.47 | 2079 | 7.355 | 41 |
| 3 | 30 | 113.7 | 0.005 | 941 | 1.08 | 77 |
| | 100 | 816.2 | 1.06 | 1177 | 1.765 | 51 |
| | 200 | 1021.8 | 1.73 | 1374 | 2.815 | 32 |
| | 300 | 1239.3 | 2.79 | 1795 | 5.905 | 18 |

#### 4.7.5.4 Test Density/Moisture Conditions

The soil moisture and density conditions present during tri-axial testing are presented in Table 4.62.

**Table 4.62: Sample density and moisture ratios, tri-axial testing.**

| Section | Sample Weight (kg) | Wet Density (tonne/m3) | Dry Density (tonne/$m^3$) | Density Ratio (% MDD) | Moisture Content (%) | Moisture Ratio (% OMC) |
|---|---|---|---|---|---|---|
| 1 | 4.137 | 2.64 | 2.45 | 95 | 7.5 | 94 |
| 2 | 4.225 | 2.69 | 2.47 | 100 | 9 | 100 |
| 3 | 3.659 | 2.33 | 2.11 | 85 | 10.5 | 95 |

## 4.8 Numerical Modelling

Numerical modelling of various pavement responses via several methods has been undertaken. The modelling follows the regime discussed in Section 3.9. Initial results relate to back-analysis of measured deflection and curvature data. The focus then turns to applying the material parameters defined above, and through back-analysis techniques in Section 4.8.1 to test the ability of a variety of modelling approaches to predict the measured pavement surface deflection and curvature.

Note that the inflation pressure is considered to be 890kPa in all cases noted below. The 'estimated tyre pressures' relate to the average pavement/tyre contact pressure inferred from the measured tyre contact areas and known wheel loads, as presented in Table 4.19.

### 4.8.1 Back-Calculation of Pavement Modulus

#### 4.8.1.1 Calculation Methods

Table 4.63 presents the soil modulus values, back-calculated as described in Section 3.9.1.

**Table 4.63: Back-calculated soil modulus results.**

| | Unloaded | | Loaded | |
|---|---|---|---|---|
| Section | Deflection (mm) | Elastic Modulus (MPa) | Deflection (mm) | Elastic Modulus (MPa) |
| 1 | 1.2 | 90 | 2.6 | 117 |
| 2 | 2 | 55 | 3.8 | 84 |
| 3 | 1.9 | 56 | 5.2 | 61 |

#### 4.8.1.2 Evercalc

Back-calculated pavement modulus results, derived through the Evercalc software are presented in the following. Table 4.64 presents the base modulus and relative error, for back-calculation of base course elastic modulus considering the curvature to initiate at the centre of the observed contact area, whereas Table 4.65 considers curvature commencing at the edge of the loaded area (observed wheel contact area). The sub-grade structure was constant for all back-calculations, the reader is referred to Section 3.9.1.2 for explanation.

**Table 4.64: Pavement modulus back-calculated from curvature data with Evercalc software (from centre of contact area).**

| Section | Axle | Load Condition | Load (kN) | Plate Radius (m) | Modulus (MPa) | %RMS |
|---|---|---|---|---|---|---|
| 1 | Rear | Unloaded | 402.7 | 0.717 | 126 | 25.05 |
| | Rear | Loaded | 1256.3 | 0.89 | 595 | 22.47 |
| 2 | Rear | Unloaded | 402.7 | 0.717 | 246 | 29.47 |
| | Rear | Loaded | 1256.3 | 0.89 | >1000 | 40.33 |
| 3 | Rear | Unloaded | 402.7 | 0.717 | 104 | 46.07 |
| | Rear | Loaded | 1256.3 | 0.89 | 382 | 33.49 |

**Table 4.65: Pavement modulus back-calculated from curvature data with Evercalc software (from edge of contact area).**

| Section | Axle | Load Condition | Load (kN) | Plate Radius (m) | Modulus (MPa) | %RMS |
|---|---|---|---|---|---|---|
| 1 | Rear | Unloaded | 402.7 | 0.712 | 1000 | 41.37 |
| | Rear | Loaded | 1256.3 | 0.869 | 1000 | 50.2 |
| 2 | Rear | Unloaded | 402.7 | 0.819 | - | - |
| | Rear | Loaded | 1256.3 | 0.904 | 1000 | 85.55 |
| 3 | Rear | Unloaded | 402.7 | 0.702 | 519 | 23.93 |
| | Rear | Loaded | 1256.3 | 0.864 | 454 | 29.41 |

### 4.8.2 Pavement Deflection – WES Method

Pavement deflection estimates ($\Delta_m$), calculated via the method presented by Pereira (1977) are detailed in the following. The first set of results apply a tyre inflation pressure of 890 kPa, considering all wheel loads present for a Komatsu 830E and with only half of the rear axle (single dual-tyre assembly).

**Table 4.66: Deflection calculated via Pereira (1977). All wheels considered and contact pressure equal to inflation pressure.**

| Section | Payload (tonnes) | A ($m^2$) | r (m) | p (kPa) | E (Mpa) | $\Sigma F_M$ | $\Delta_m$ (mm) | $\Delta_{ACTUAL}$ (mm) |
|---|---|---|---|---|---|---|---|---|
| 1 | 0 | 0.65 | 0.45 | 890 | 271 | 1.73 | 2.59 | 1.20 |
| 2 | 0 | 0.68 | 0.47 | 890 | 254 | 1.72 | 2.80 | 2.00 |
| 3 | 0 | 0.64 | 0.45 | 890 | 255 | 1.75 | 2.75 | 1.90 |
| 1 | 220 | 1.01 | 0.57 | 890 | 271 | 2.59 | 4.83 | 2.60 |
| 2 | 220 | 1.04 | 0.57 | 890 | 254 | 2.55 | 5.13 | 3.80 |
| 3 | 220 | 1.01 | 0.57 | 890 | 255 | 2.60 | 5.14 | 5.20 |

**Table 4.67: Deflection calculated via Pereira (1977). Single wheel gear and contact equal to inflation pressure.**

| Section | Payload (tonnes) | A ($m^2$) | r (m) | p (kPa) | E (Mpa) | $\Sigma F_M$ | $\Delta_m$ (mm) | $\Delta_{ACTUAL}$ (mm) |
|---|---|---|---|---|---|---|---|---|
| 1 | 0 | 0.65 | 0.45 | 890 | 271 | 1.56 | 2.33 | 1.20 |
| 2 | 0 | 0.68 | 0.47 | 890 | 254 | 1.53 | 2.49 | 2.00 |
| 3 | 0 | 0.64 | 0.45 | 890 | 255 | 1.57 | 2.47 | 1.90 |
| 1 | 220 | 1.01 | 0.57 | 890 | 271 | 2.37 | 4.43 | 2.60 |
| 2 | 220 | 1.04 | 0.57 | 890 | 254 | 2.34 | 4.71 | 3.80 |
| 3 | 220 | 1.01 | 0.57 | 890 | 255 | 2.39 | 4.71 | 5.20 |

The modelling undertaken to produce the results above, was then repeated with the estimated tyre pressure (from tyre contact geometry and known wheel loads) applied. Modelling was completed with all wheel loads present for a Komatsu 830E and with only half of the rear axle (single dual-tyre assembly).

**Table 4.68: Deflection calculated via Pereira (1977). All wheels considered and contact pressure estimated from contact area and wheel load.**

| Section | Payload (tonnes) | A ($m^2$) | r (m) | p (kPa) | E (Mpa) | $\Sigma F_M$ | $\Delta_m$ (mm) | $\Delta_{ACTUAL}$ (mm) |
|---|---|---|---|---|---|---|---|---|
| 1 | 0 | 0.65 | 0.45 | 311 | 271 | 1.73 | 0.74 | 1.20 |
| 2 | 0 | 0.68 | 0.47 | 297 | 254 | 1.72 | 0.60 | 2.00 |
| 3 | 0 | 0.64 | 0.45 | 317 | 255 | 1.75 | 0.80 | 1.90 |
| 1 | 220 | 1.01 | 0.57 | 620 | 271 | 2.59 | 2.87 | 2.60 |
| 2 | 220 | 1.04 | 0.57 | 607 | 254 | 2.55 | 2.80 | 3.80 |
| 3 | 220 | 1.01 | 0.57 | 624 | 255 | 2.60 | 3.09 | 5.20 |

**Table 4.69: Deflection calculated via Pereira (1977). Single wheel gear and contact pressure estimated from contact area and wheel load.**

| Section | Payload (tonnes) | A ($m^2$) | r (m) | p (kPa) | E (Mpa) | $\Sigma F_M$ | $\Delta_m$ (mm) | $\Delta_{ACTUAL}$ (mm) |
|---|---|---|---|---|---|---|---|---|
| 1 | 0 | 0.65 | 0.45 | 311 | 271 | 1.56 | 0.66 | 1.20 |
| 2 | 0 | 0.68 | 0.47 | 297 | 254 | 1.53 | 0.53 | 2.00 |
| 3 | 0 | 0.64 | 0.45 | 317 | 255 | 1.57 | 0.72 | 1.90 |
| 1 | 220 | 1.01 | 0.57 | 620 | 271 | 2.37 | 2.63 | 2.60 |
| 2 | 220 | 1.04 | 0.57 | 607 | 254 | 2.34 | 2.56 | 3.80 |
| 3 | 220 | 1.01 | 0.57 | 624 | 255 | 2.39 | 2.83 | 5.20 |

The analysis of deflection was again repeated, with the dual-wheel assembly modelled as a single contact area (as was applied in the FEA analysis detailed in Section 3.9.4).

**Table 4.70: Deflection calculated via Pereira (1977). Dual-wheel gear modelled as a single tyre, with influence of all wheel considered and contact pressure estimated from contact area and wheel load.**

| Section | Payload (tonnes) | A ($m^2$) | r (m) | p (kPa) | E (Mpa) | $\Sigma F_M$ | $\Delta_m$ (mm) | $\Delta_{ACTUAL}$ (mm) |
|---|---|---|---|---|---|---|---|---|
| 1 | 0 | 0.65 | 0.64 | 311 | 271 | 1.88 | 1.37 | 1.20 |
| 2 | 0 | 0.68 | 0.65 | 297 | 254 | 1.89 | 1.45 | 2.00 |
| 3 | 0 | 0.64 | 0.63 | 317 | 255 | 1.88 | 1.48 | 1.90 |
| 1 | 220 | 1.01 | 0.80 | 620 | 271 | 1.91 | 3.50 | 2.60 |
| 2 | 220 | 1.04 | 0.81 | 607 | 254 | 1.91 | 3.69 | 3.80 |
| 3 | 220 | 1.01 | 0.79 | 624 | 255 | 1.91 | 3.73 | 5.20 |

Table 4.71 provides a summary of the above deflection estimates, calculated with the method detailed n Pereira (1977).

**Table 4.71: Summary of deflection estimate accuracy using WES method with varying input parameters.**

| Wheels Considered | Wheel Modelling | Modulus Value | Contact Stress | Average Variance (%) |
|---|---|---|---|---|
| All | Single | Static | Inflation | 54 |
| All | Single | Static | Average | 41 |
| Dual Assembly Only | Single | Static | Inflation | 42 |
| Dual Assembly Only | Single | Static | Average | 43 |
| All | Dual as Single | Static | Average | 30 |
| Dual Assembly Only | Dual as Single | Static | Average | 22 |

### 4.8.3 Comparison of linear-elastic and FEA Axisymmetric Modelling

The results below show the correlation between linear-elastic and FEA modelling with equivalent input parameters. These results relate to axisymmetric modelling of a 2m deep base-course with the variable modulus values as indicated, supported by a 150MPa sub-grade. Figure 4.71 and Figure 4.72 show graphically the similarity in the curvature results estimated by the two modelling techniques. Further, note that with equal analysis inputs and assumptions, HIPAVE and CIRCLY have been confirmed to produce the same output.

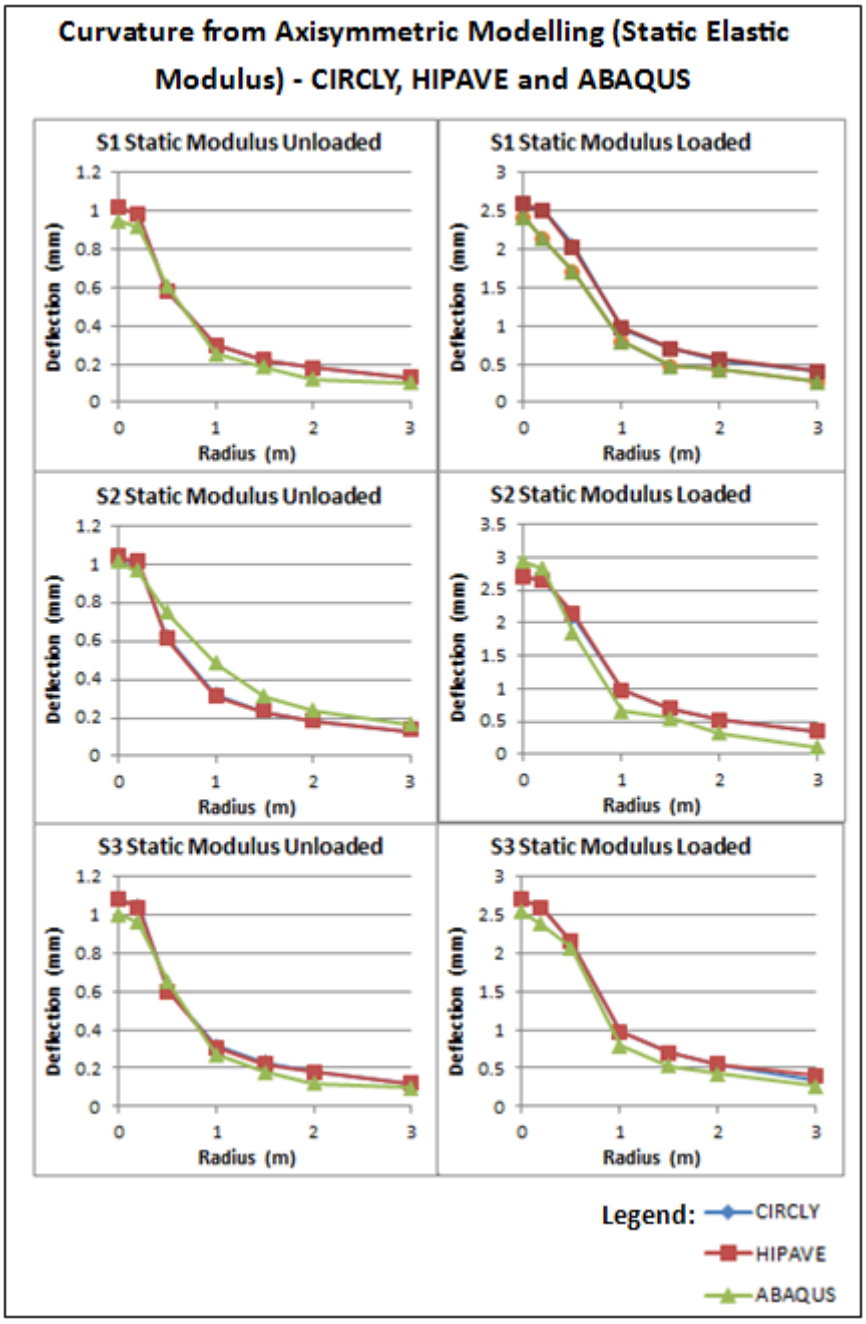


**Figure 4.71: Comparison of CIRCLY and ABAQUS modelled curvature using static elastic modulus values for base-course (Note CIRCLY results are obscured by the HIPAVE results).**

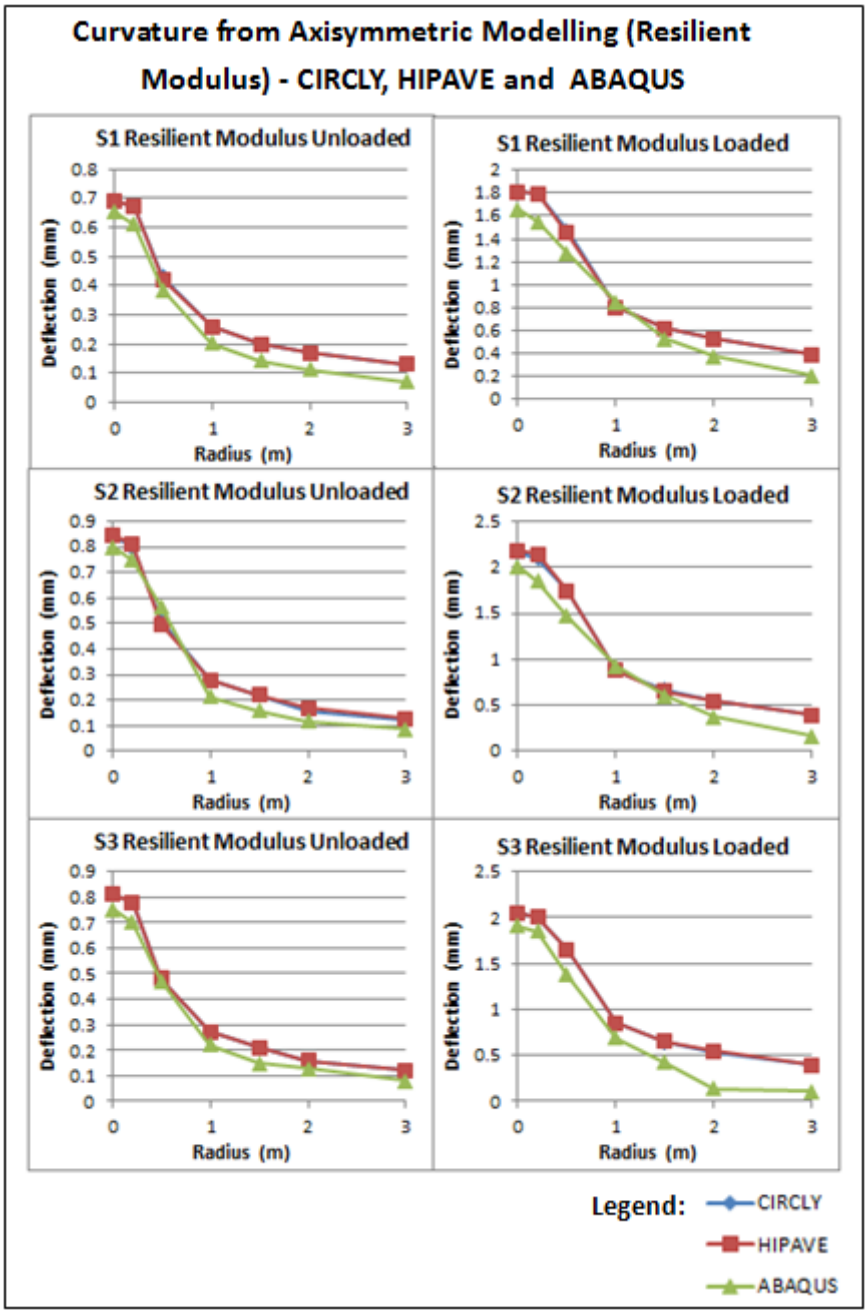


**Figure 4.72: Comparison of CIRCLY and ABAQUS modelled curvature using resilient modulus values for base-course (Note CIRCLY results are obscured by the HIPAVE results).**

### 4.8.4 Comparison of Isotropic and Anisotropic Base-Course Characterisation

The following outlines the comparison of modelling with only a change in the base material being characterised as isotropic and anisotropic. As in Section 4.8.3, the

model is axisymmetric with a base-course depth of 2m over an infinite sub-grade. From observation of Figure 4.73 and Figure 4.74, it is clear that modelling with an anisotropic ratio of two (vertical:horizontal elastic modulus) increases the deflection near the load centre, but has a negligible effect beyond a one meter radius.

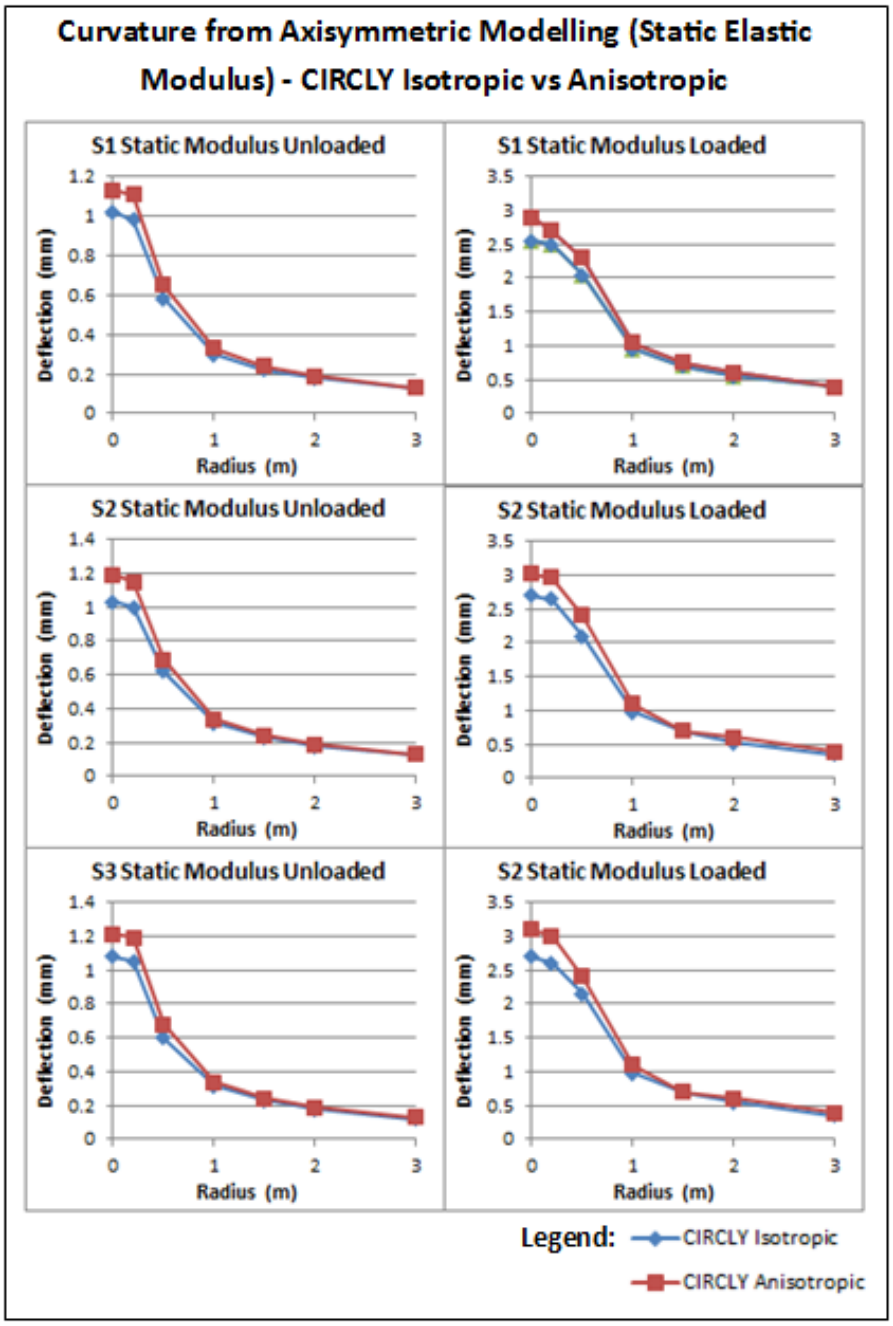


**Figure 4.73: Comparison of isotropic and anisotropic base-course characterisation of predicted curvature, applying static elastic modulus values.**

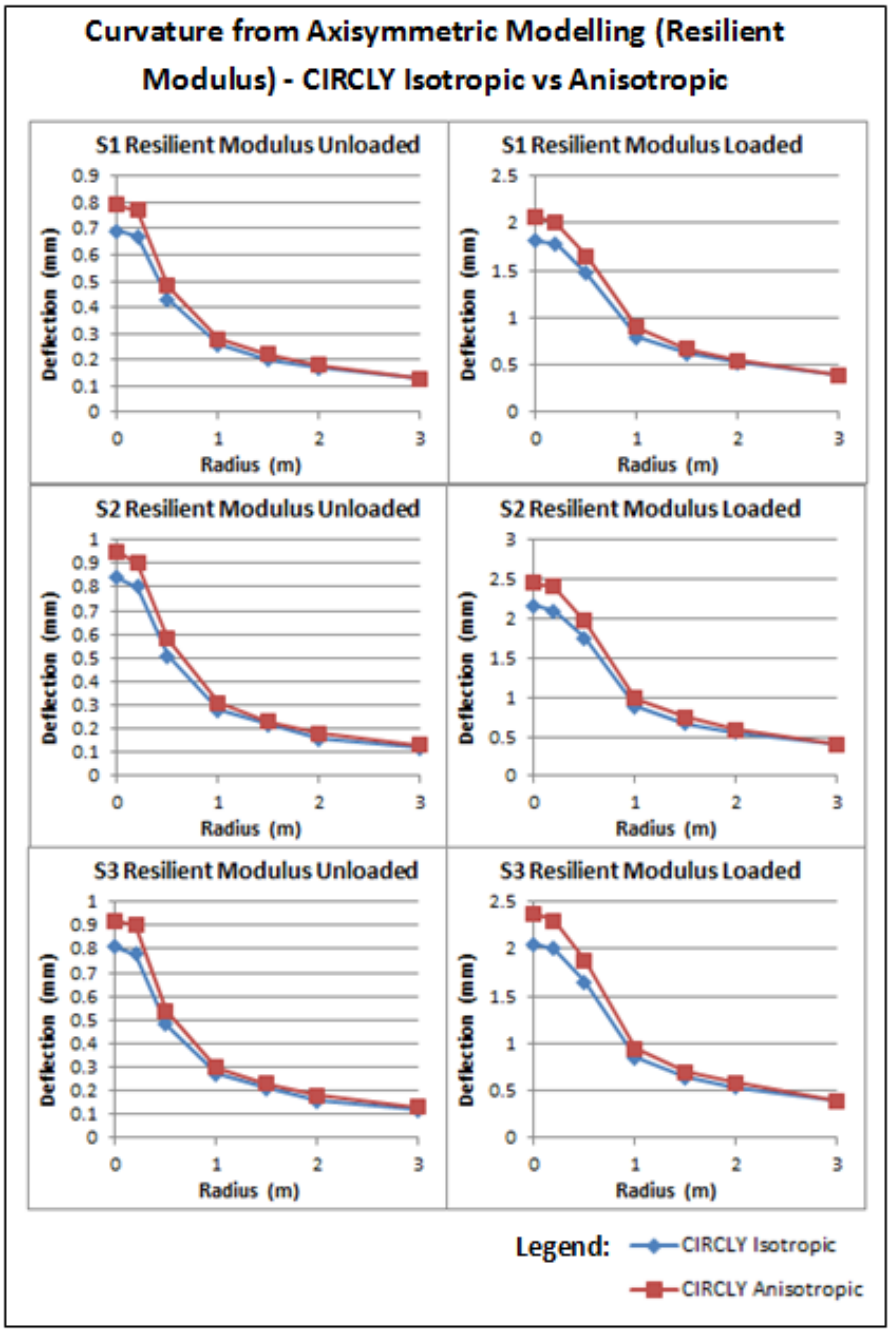


**Figure 4.74: Comparison of isotropic and anisotropic base-course characterisation of predicted curvature, applying resilient modulus values.**

In addition to the comparison of pavement surface curvature, the horizontal stress has been investigated at the top of the sub-grade. Two situations have been investigated. Figure 4.75 relates to a relatively low base-course modulus (section

one static elastic modulus) and an unloaded truck. Figure 4.76 relates to a relatively high base-course modulus (section one resilient modulus) and a loaded truck.

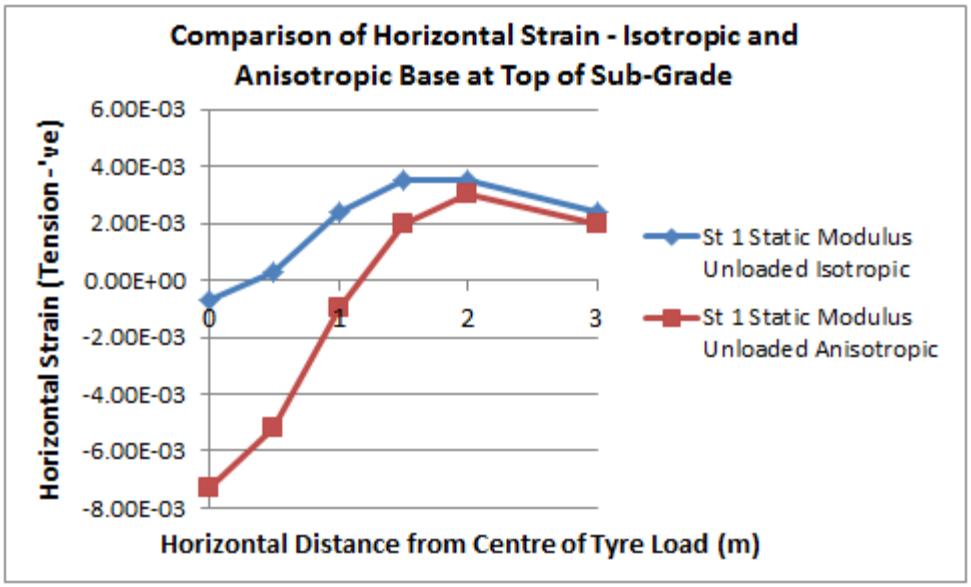


**Figure 4.75: Comparison of horizontal strain at top of sub-grade for section one unloaded truck with static elastic modulus to characterise the base-course.**

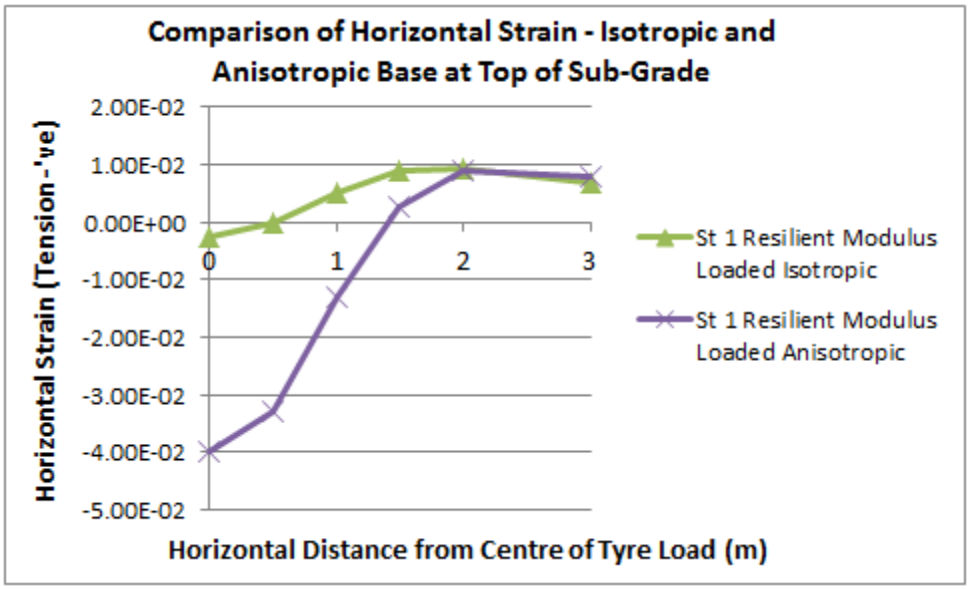


**Figure 4.76: Comparison of horizontal strain at top of sub-grade for section one unloaded truck with resilient modulus to characterise the base-course.**

### 4.8.5 Linear-Elastic Modelling

Table 4.72 presents a summary of HIPAVE and CIRCLY estimated pavement surface deflections. Note that only the full results for each program with the modelling setup providing the best results are presented in full below. Comparison can be made via Table 4.72.

**Table 4.72: Summary of HIPAVE and CIRCLY estimations of pavement surface deflection.**

| Program | Modulus Value | Contact Stress | Base Characterisation | Foundation Structure | Average Variance | Correlation |
|---|---|---|---|---|---|---|
| HIPAVE | Static | Estimated from Load | Istropic | CBR=15% | 0.22 | 0.84 |
| | Resilient | Estimated from Load | Istropic | CBR=15% | 0.33 | 0.88 |
| | Back-Calculated | Estimated from Load | Istropic | CBR=15% | 0.59 | 0.11 |
| | Barker-Brabston Base | Estimated from Load | Istropic | CBR=15% | 0.47 | 0.81 |
| | Barker-Brabston Sub-Base | Estimated from Load | Istropic | CBR=15% | 0.26 | 0.81 |
| | Static | Inflation Pressure | Istropic | CBR=15% | 0.23 | 0.84 |
| | Resilient | Inflation Pressure | Istropic | CBR=15% | 0.33 | 0.88 |
| | Back-Calculated | Inflation Pressure | Istropic | CBR=15% | 0.62 | -0.35 |
| | Barker-Brabston Base | Inflation Pressure | Istropic | CBR=15% | 0.40 | 0.81 |
| | Barker-Brabston Sub-Base | Inflation Pressure | Istropic | CBR=15% | 0.37 | 0.81 |
| | Static | Estimated from Load | Istropic | Select Foundation | 0.36 | 0.64 |
| | Resilient | Estimated from Load | Istropic | Select Foundation | 0.31 | 0.70 |
| | Back-Calculated | Estimated from Load | Istropic | Select Foundation | 0.63 | 0.05 |
| | Static | Estimated from Load | Istropic | Barker-Brabston Sub-Base | 0.25 | 0.25 |
| | Resilient | Estimated from Load | Istropic | Barker-Brabston Sub-Base | 0.35 | 0.35 |
| | Back-Calculated | Estimated from Load | Istropic | Barker-Brabston Sub-Base | 0.60 | 0.60 |
| HIPAVE Single Gear | Static | Estimated from Load | Istropic | CBR=15% | 0.23 | 0.84 |
| | Resilient | Estimated from Load | Istropic | CBR=15% | 0.40 | 0.88 |
| | Back-Calculated | Estimated from Load | Istropic | CBR=15% | 0.65 | -0.21 |
| CIRCLY | Static | Estimated from Load | Cross-Anisotropic | Isotropic Sub-Grade (CBR=15%) | 0.23 | 0.82 |
| | Resilient | Estimated from Load | Cross-Anisotropic | Isotropic Sub-Grade (CBR=15%) | 0.25 | 0.87 |
| | Back-Calculated | Estimated from Load | Cross-Anisotropic | Isotropic Sub-Grade (CBR=15%) | 0.33 | 0.60 |

#### 4.8.5.1 HIPAVE

The initial set of deflection results, as calculated by HIPAVE consider the average contact stress, as calculated from known wheel loads and measured tyre contact areas (see Section 4.4.3). This modelling employs a three meter deep sub-grade of elastic modulus 150MPa.

**Table 4.73: HIPAVE deflection results, unloaded truck, measured moduli and estimated contact pressures.**

| Section | Contact Pressure (kPa) | Payload (Tonnes) | Base Modulus (Mpa) | Base-course Modulus Characterisation | Calculated Deflection (mm) | Measured Deflection (mm) |
|---|---|---|---|---|---|---|
| 1 | 311 | 0 | 271 | Static | 1.3 | 1.5 |
| 1 | 311 | 0 | 441 | Resilient | 0.9 | |
| 1 | 311 | 0 | 126 | Back-Calculation | 2.7 | |
| 2 | 297 | 0 | 254 | Static | 1.4 | 2 |
| 2 | 297 | 0 | 338 | Resilient | 1.1 | |
| 2 | 297 | 0 | 246 | Back-Calculation | 1.5 | |
| 3 | 317 | 0 | 255 | Static | 1.4 | 2 |
| 3 | 317 | 0 | 363 | Resilient | 1.05 | |
| 3 | 317 | 0 | 104 | Back-Calculation | 3.1 | |

**Table 4.74: HIPAVE deflection results, loaded truck, measured moduli and estimated contact pressures.**

| Section | Contact Pressure (kPa) | Payload (Tonnes) | Base Modulus (Mpa) | Base-course Modulus Characterisation | Calculated Deflection (mm) | Measured Deflection (mm) |
|---|---|---|---|---|---|---|
| 1 | 620 | 220 | 271 | Static | 3.3 | 2.5 |
| 1 | 620 | 220 | 441 | Resilient | 2.3 | |
| 1 | 620 | 220 | 595 | Back-Calculation | 1.9 | |
| 2 | 607 | 220 | 254 | Static | 3.5 | 4 |
| 2 | 607 | 220 | 338 | Resilient | 2.8 | |
| 2 | 607 | 220 | 1000 | Back-Calculation | 1.3 | |
| 3 | 624 | 220 | 255 | Static | 3.5 | 5 |
| 3 | 624 | 220 | 363 | Resilient | 2.7 | |
| 3 | 624 | 220 | 382 | Back-Calculation | 2.6 | |

The above modelling was then repeated with Barker-Brabston sub-layering of the base-course, which approximates nonlinearity, presented in Table 4.75 and Table 4.76. The modulus of the base-course is dependent on the sub-grade modulus and geometry of sub-layers and therefore does not vary for each section.

**Table 4.75: HIPAVE deflection results, unloaded truck, Barker-Brabston UGM materials and estimated contact pressures.**

| Section | Contact Pressure (kPa) | Payload (Tonnes) | Base Modulus (Mpa) | Calculated Deflection (mm) | Measured Deflection (mm) |
|---|---|---|---|---|---|
| 1 | 311 | 0 | Barker-Brabston Base | 0.7 | 1.2 |
| 1 | 311 | 0 | Barker-Brabston Sub-Base | 1.4 | |
| 2 | 297 | 0 | Barker-Brabston Base | 0.7 | 2 |
| 2 | 297 | 0 | Barker-Brabston Sub-Base | 1.4 | |
| 3 | 317 | 0 | Barker-Brabston Base | 0.7 | 2 |
| 3 | 317 | 0 | Barker-Brabston Sub-Base | 1.4 | |

**Table 4.76: HIPAVE deflection results, loaded truck, Barker-Brabston UGM materials and estimated contact pressures.**

| Section | Contact Pressure (kPa) | Payload (Tonnes) | Base Modulus (Mpa) | Maximum Deflection (mm) | Measured Deflection (mm) |
|---|---|---|---|---|---|
| 1 | 620 | 220 | Barker-Brabston Base | 1.8 | 2.5 |
| 1 | 620 | 220 | Barker-Brabston Sub-Base | 3.4 | |
| 2 | 607 | 220 | Barker-Brabston Base | 1.8 | 4 |
| 2 | 607 | 220 | Barker-Brabston Sub-Base | 3.4 | |
| 3 | 624 | 220 | Barker-Brabston Base | 1.8 | 5 |
| 3 | 624 | 220 | Barker-Brabston Sub-Base | 3.4 | |

#### 4.8.5.2 CIRCLY

Table 4.79 and Table 4.80 present pavement deflection estimates via CIRCLY, with a contact pressure of 890kPa. Each table include deflection estimates considering a two metre thick base-course over a sub-grade of 15% CBR (elastic modulus of 150 MPa). The base-course elastic modulus has been defined by the various methods outlined in Section 4.7.4, Section 4.7.5 and Section 4.8.1. All CIRCLY modelling

(Except for the results in Section 4.8.4) consider the materials to be cross-anisotropic with a ratio of two (vertical modulus divided by horizontal modulus) and without any sub-layering. The latter is due to the Austroads (Jameson, 2012) sub-layering method built into CIRCLY not being developed for heavy wheel loads. Note, deflection results for isotropic characterisation are noted as arising from CIRCLY and HIPAVE as they produce identical models when excluding any sub-layering or anisotropy, except that a load radius is nominated in CIRCLY. This has been found to have a negligible impact the results in this case.

Initial modelling was completed with an infinite sub-grade, and is presented in Table 4.77 for an unloaded truck and Table 4.78 for a loaded truck. Modelling with an infinite sub-grade depth has been included here, as it was utilised for the results generated in Section 4.8.3 and Section 4.8.4. The results can then be compared to modelling presented later, with a three meter deep sub-grade, to provide comment of the effect of this simplification on the modelling.

**Table 4.77: CIRCLY deflection results, unloaded truck, measured moduli, cross-anisotropic materials and estimated contact pressures. Infinite sub-grade.**

| Section | Contact Stress (kPa) | Radius (mm) | Base Modulus (Mpa) | Static/Resilient? | Calculated Deflection (mm) | Measured Deflection (mm) |
|---|---|---|---|---|---|---|
| 1 | 311 | 454 | 271 | Static | 1.02 | 1.5 |
| 1 | 311 | 454 | 441 | Resilient | 0.69 | |
| 2 | 297 | 465 | 254 | Static | 1.03 | 2 |
| 2 | 297 | 465 | 338 | Resilient | 0.84 | |
| 3 | 317 | 450 | 255 | Static | 1.08 | 2 |
| 3 | 317 | 450 | 363 | Resilient | 0.81 | |

**Table 4.78: CIRCLY deflection results, loaded truck, measured moduli, cross-anisotropic materials and estimated contact pressures. Infinite sub-grade.**

| Section | Contact Stress (kPa) | Radius (mm) | Base Modulus (Mpa) | Static/Resilient? | Calculated Deflection (mm) | Measured Deflection (mm) |
|---|---|---|---|---|---|---|
| 1 | 620 | 568 | 271 | Static | 2.55 | 2.5 |
| 1 | 620 | 568 | 441 | Resilient | 1.81 | |
| 2 | 607 | 574 | 254 | Static | 2.7 | 4 |
| 2 | 607 | 574 | 338 | Resilient | 2.17 | |
| 3 | 624 | 566 | 255 | Static | 2.7 | 5 |
| 3 | 624 | 566 | 363 | Resilient | 2.05 | |

As per the finding in Section 4.8.3, CIRCLY and HIPAVE produce identical modelling outputs with equal inputs and with the exclusion of material sub-layering. For this reason, the reader is referred to Section 4.8.5.1 for deflection estimates relating to an isotropic base-course on a three meter deep sub-grade.

**Table 4.79: CIRCLY deflection results, unloaded truck, measured moduli, cross-anisotropic base-course materials and estimated contact pressures.**

| Section | Contact Stress (kPa) | Radius (mm) | Base Modulus (Mpa) | Static/Resilient? | Calculated Deflection (mm) | Measured Deflection (mm) |
|---|---|---|---|---|---|---|
| 1 | 311 | 454 | 271 | Static | 1.25 | 1.5 |
| 1 | 311 | 454 | 441 | Resilient | 0.9 | |
| 1 | 311 | 454 | 126 | Back-Calculation | 2.3 | |
| 2 | 297 | 465 | 254 | Static | 1.3 | 2 |
| 2 | 297 | 465 | 338 | Resilient | 1 | |
| 2 | 297 | 465 | 246 | Back-Calculation | 1.3 | |
| 3 | 317 | 450 | 255 | Static | 1.3 | 2 |
| 3 | 317 | 450 | 363 | Resilient | 1 | |
| 3 | 317 | 450 | 104 | Back-Calculation | 2.8 | |

**Table 4.80: CIRCLY deflection results, loaded truck, measured moduli, cross-anisotropic base-course materials and estimated contact pressures.**

| Section | Contact Stress (kPa) | Radius (mm) | Base Modulus (Mpa) | Static/Resilient? | Calculated Deflection (mm) | Measured Deflection (mm) |
|---|---|---|---|---|---|---|
| 1 | 620 | 568 | 271 | Static | 3.3 | 2.5 |
| 1 | 620 | 568 | 441 | Resilient | 2.3 | |
| 1 | 620 | 568 | 595 | Back-Calculation | 1.9 | |
| 2 | 607 | 574 | 254 | Static | 3.4 | 4 |
| 2 | 607 | 574 | 338 | Resilient | 2.8 | |
| 2 | 607 | 574 | 1000 | Back-Calculation | 1.4 | |
| 3 | 624 | 566 | 255 | Static | 3.4 | 5 |
| 3 | 624 | 566 | 363 | Resilient | 2.6 | |
| 3 | 624 | 566 | 382 | Back-Calculation | 2.5 | |

From the above results, it is clear that a three meter deep sub-grade produces greater deflection estimates (than an infinite sub-grade), that more closely reflect the deflection measurements taken in the current study.

### 4.8.6 Finite Element Analysis

The following sections detail the investigation of FEA for modelling haul road pavements. Generally, as with the results in Section 4.8.3 FEA has produced higher deflection estimates than linear-elastic software and as such appears to produce better estimates of the measured deflections.

#### 4.8.6.1 Pavement Layer Structure Resulting from Nonlinear Modelling

The pavement and sub-grade layer structures that were derived through the iterative process described in Section 3.9.4, and used to determine pavement deflections via FEA are presented below. From comparison of the elastic modulus resulting for the lower sub-grade portions with the consistent 150MPa sub-grade adopted for the axisymmetric modelling, provides some explanation of the lower calculated deflections. The increase in modulus with depth is evidence that the over-burden pressure dominates over that induced by the wheel loading.

**Table 4.81: Derived pavement and sub-grade structure, Section 1 rear axle, unloaded truck.**

| Layer | Thickness (m) | Resilient Modulus (MPa) |
|---|---|---|
| Base | 2 | 267 |
| Sub-Grade 1 | 2 | 225 |
| Sub-Grade 2 | 3 | 255 |
| Sub-Grade 3 | 6 | 310 |
| Sub-Grade 4 | 7 | 396 |

**Table 4.82: Derived pavement and sub-grade structure, Section 1 rear axle, loaded truck.**

| Layer | Thickness (m) | Resilient Modulus (MPa) |
|---|---|---|
| Base | 2 | 393 |
| Sub-Grade 1 | 2 | 304 |
| Sub-Grade 2 | 3 | 310 |
| Sub-Grade 3 | 6 | 341 |
| Sub-Grade 4 | 7 | 420 |

**Table 4.83: Derived pavement and sub-grade structure, Section 2 rear axle, unloaded truck.**

| Layer | Thickness (m) | Resilient Modulus (MPa) |
|---|---|---|
| Base | 2 | 212 |
| Sub-Grade 1 | 2 | 175 |
| Sub-Grade 2 | 3 | 201 |
| Sub-Grade 3 | 6 | 247 |
| Sub-Grade 4 | 7 | 320 |

**Table 4.84: Derived pavement and sub-grade structure, Section 2 rear axle, loaded truck.**

| Layer | Thickness (m) | Resilient Modulus (MPa) |
|---|---|---|
| Base | 2 | 326 |
| Sub-Grade 1 | 2 | 234 |
| Sub-Grade 2 | 3 | 236 |
| Sub-Grade 3 | 6 | 268 |
| Sub-Grade 4 | 7 | 340 |

**Table 4.85: Derived pavement and sub-grade structure, Section 3 rear axle, unloaded truck.**

| Layer | Thickness (m) | Resilient Modulus (MPa) |
|---|---|---|
| Base | 2 | 210 |
| Sub-Grade 1 | 2 | 178 |
| Sub-Grade 2 | 3 | 199 |
| Sub-Grade 3 | 6 | 234 |
| Sub-Grade 4 | 7 | 290 |

**Table 4.86: Derived pavement and sub-grade structure, Section 3 rear axle, loaded truck.**

| Layer | Thickness (m) | Resilient Modulus (MPa) |
|---|---|---|
| Base | 2 | 285 |
| Sub-Grade 1 | 2 | 240 |
| Sub-Grade 2 | 3 | 234 |
| Sub-Grade 3 | 6 | 255 |
| Sub-Grade 4 | 7 | 308 |

#### 4.8.6.2 Deflection Results

Deflection estimates completed with FEA modelling are presented below. Table 4.87 details deflection estimates considering the plane strain condition with a single

wheel gear load. Subsequently, Table 4.88 presents plane-strain modelling, with both wheel gears present on the rear axle of a Komatsu 830E included.

**Table 4.87: Deflection results from FEA modelling (plane-strain model, single dual-wheel gear only).**

| Section | Width of Load (mm) | Contact Pressure (kPa) | Max. Deflection (mm) |
|---|---|---|---|
| 1 | 2380 | 620 | 9.8 |
| 2 | 2281 | 607 | 11.8 |
| 3 | 2181 | 624 | 13.1 |

**Table 4.88: Deflection results from FEA modelling (plane-strain model, rear axle).**

| Section | Width of Load (mm) | Contact Pressure (kPa) | Max. Deflection (mm) |
|---|---|---|---|
| 1 | 2380 | 620 | 11.4 |
| 2 | 2281 | 607 | 13.6 |
| 3 | 2181 | 624 | 15.4 |

Three-dimensional FEA pavement deflection results are presented in Table 4.89. The top half of the table reflects the calculated deflection with a simple linear-elastic sub-grade with an elastic modulus of 150MPa, with the bottom half being a repeat for the analysis with a nonlinear sub-grade applied, as per Table 4.81 through Table 4.86.

**Table 4.89: Summary of three-dimensional FEA modelling, with linear-elastic (150MPa) and nonlinear sub-grades.**

| | | | | | Max. Deflection (mm) Nominal Mesh Size (m) | | |
|---|---|---|---|---|---|---|---|
| Section | Sub-Grade Modulus (MPa) | Payload (Tonnes) | Width of Load (mm) | Contact Pressure (kPa) | 1 | 0.25 | Measured Deflection (mm) |
| 1 | 150 | 0 | 2155 | 311 | 1.2 | | 1.2 |
| 2 | | | 2107 | 297 | 1.3 | | 2 |
| 3 | | | 2181 | 317 | 1.3 | | 1.9 |
| 1 | | 220 | 2380 | 620 | 3.2 | | 2.6 |
| 2 | | | 2281 | 607 | 4.1 | | 3.8 |
| 3 | | | 2181 | 624 | 3.9 | | 5.2 |
| 1 | variable | 0 | 2155 | 311 | 1.4 | | 1.2 |
| 2 | | | 2107 | 297 | 1.6 | | 2 |
| 3 | | | 2181 | 317 | 1.6 | | 1.9 |
| 1 | | 220 | 2380 | 620 | 2.4 | 2.5 | 2.6 |
| 2 | | | 2281 | 607 | 3.4 | 3.4 | 3.8 |
| 3 | | | 2181 | 624 | 3.5 | 3.4 | 5.2 |

### 4.8.7 Comparison of Pavement Curvature

Following a comparison of the maximum deflections predicted by various analysis methods it was considered advantageous to also investigate the calculated pavement curvature. This is a common approach taken in the literature for validation of a modelling technique, which is made possible in this case due to the measurement of curvature in deflection testing. The initial set of results consider curvature in the traditional sense, that is the pavement surface deflection profile commencing at the centre of a rear axle dual-wheel gear and extending longitudinally backwards from the truck.

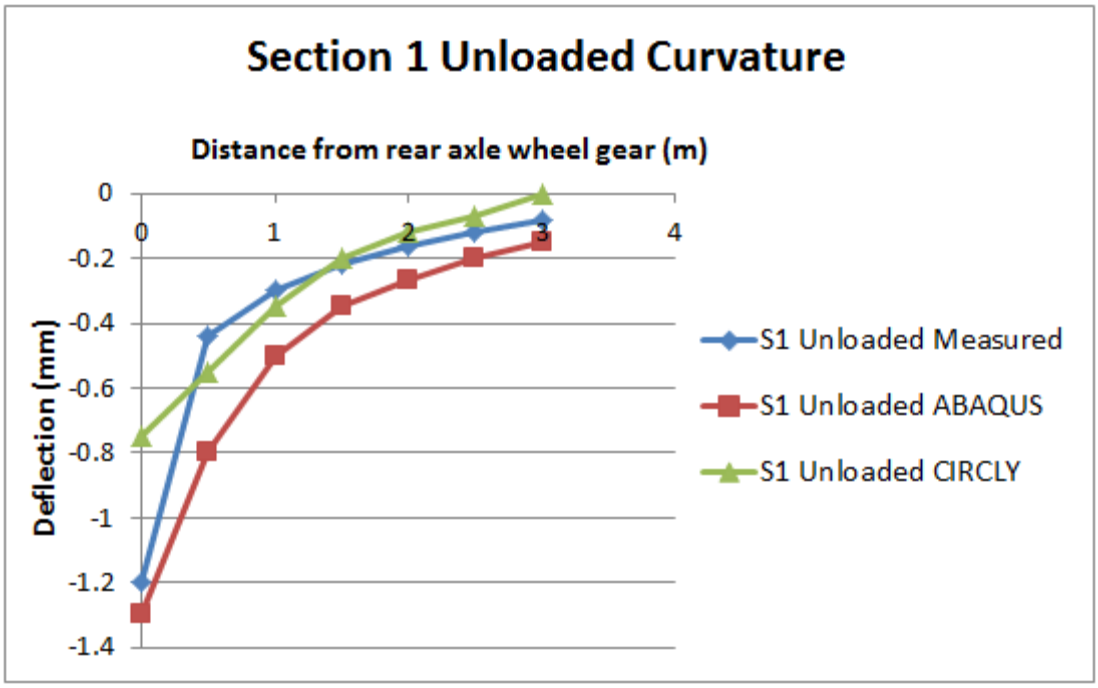


**Figure 4.77: Section 1, measured and predicted curvature (centre of wheel gear backwards) for unloaded truck.**

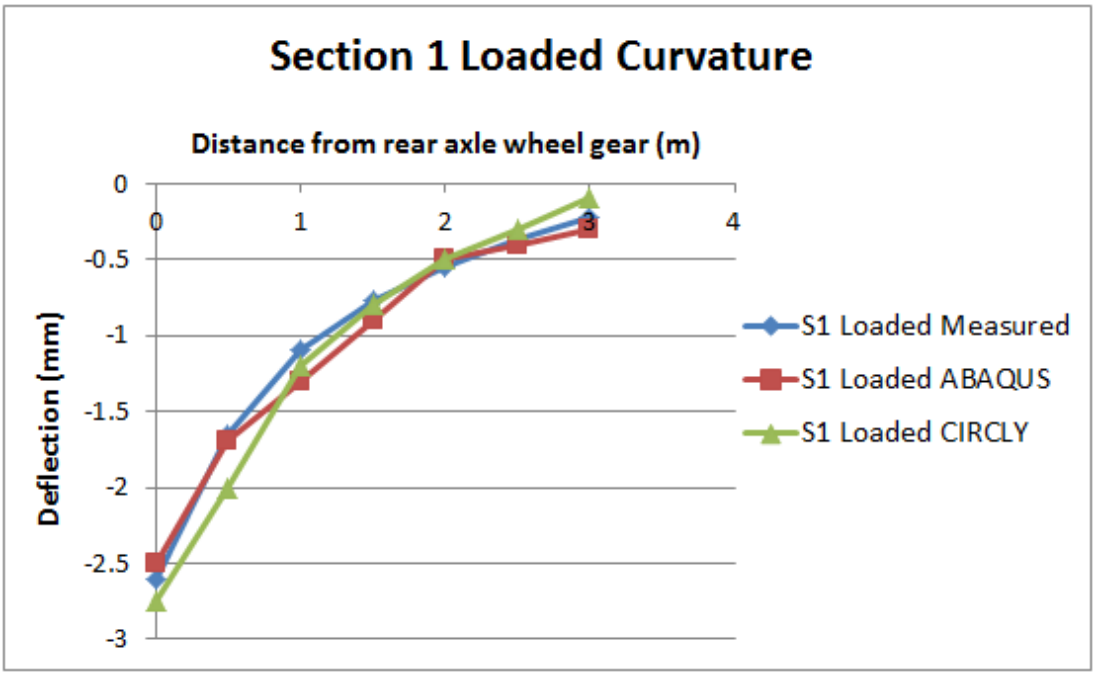


**Figure 4.78: Section 1, measured and predicted curvature (centre of wheel gear backwards) for loaded truck.**

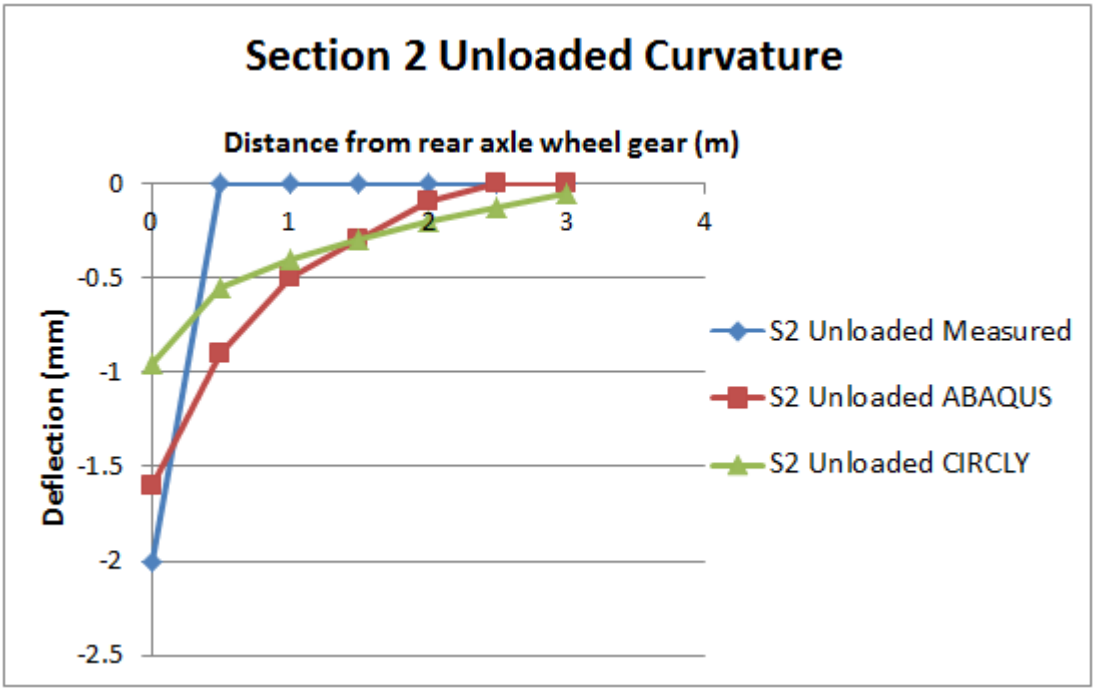


**Figure 4.79: Section 2, measured and predicted curvature (centre of wheel gear backwards) for unloaded truck.**

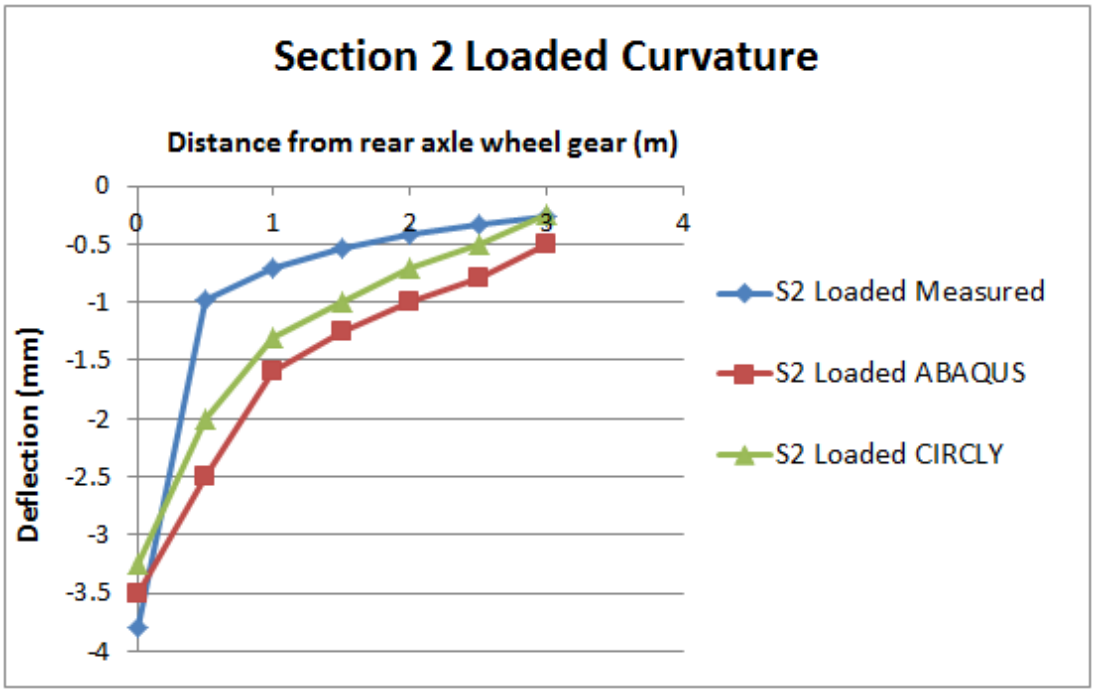


**Figure 4.80: Section 2, measured and predicted curvature (centre of wheel gear backwards) for loaded truck.**

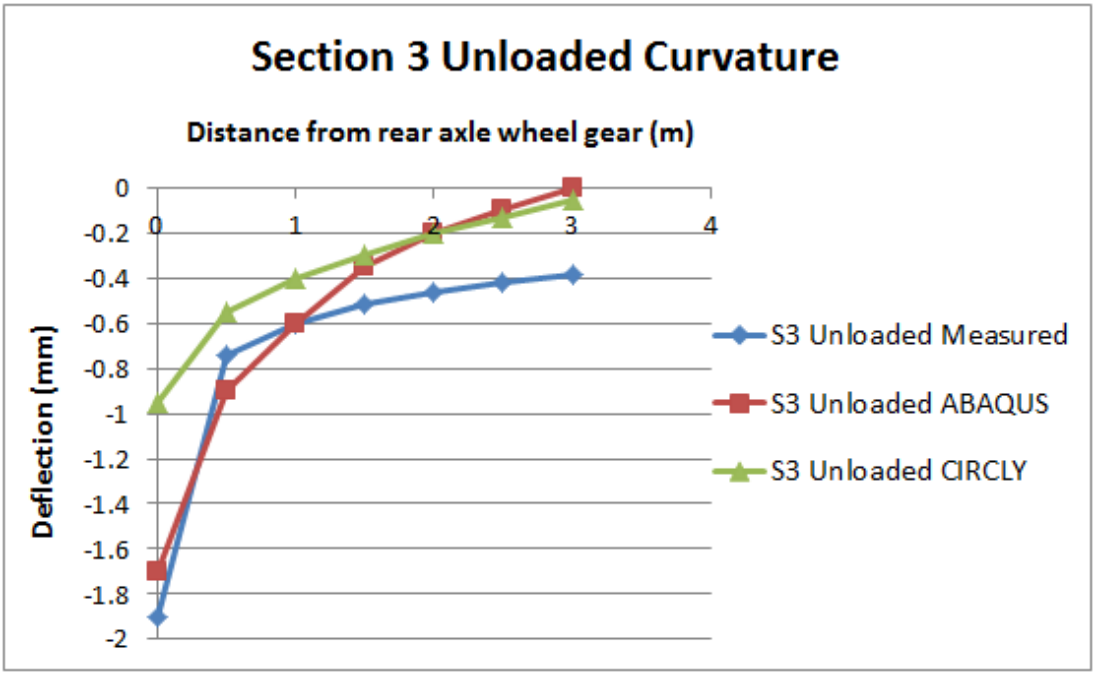


**Figure 4.81: Section 3, measured and predicted curvature (centre of wheel gear backwards) for unloaded truck.**

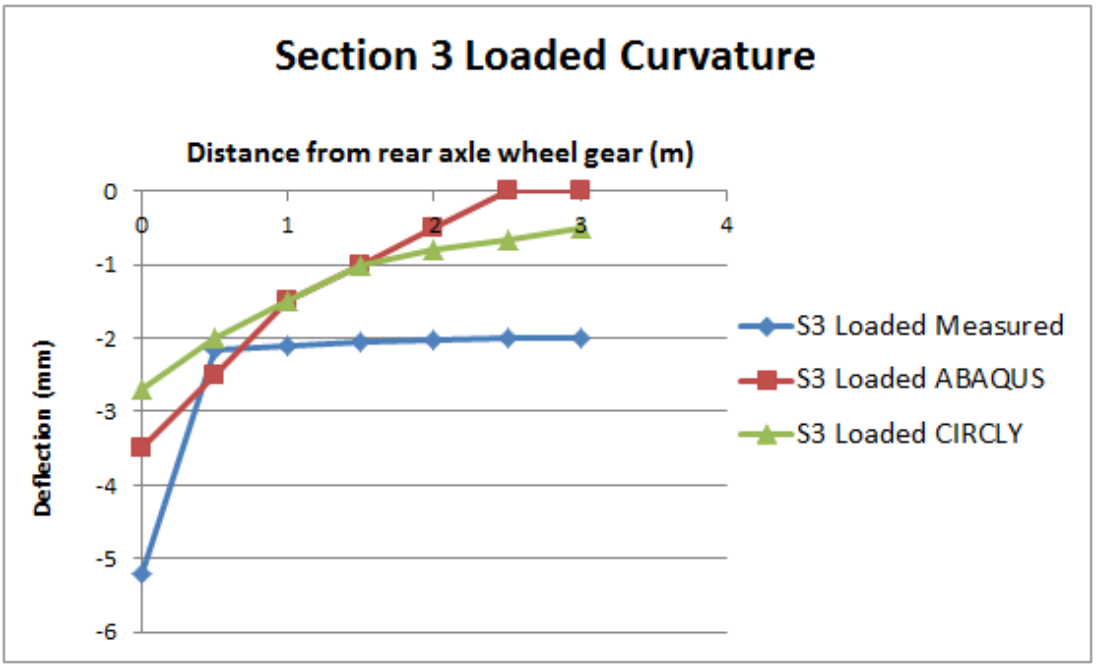


**Figure 4.82: Section 3, measured and predicted curvature (centre of wheel gear backwards) for loaded truck.**

Following modelling of curvature, in the common sense from the centre of load backwards, the deflection profile along the rear axle was also modelled and compared to the measured profile. This comparison provides insight into the ability of both modelling techniques with regard to replicating observations in the field. Secondly, it provides an indication of the degree of wheel interaction modelled by each method.

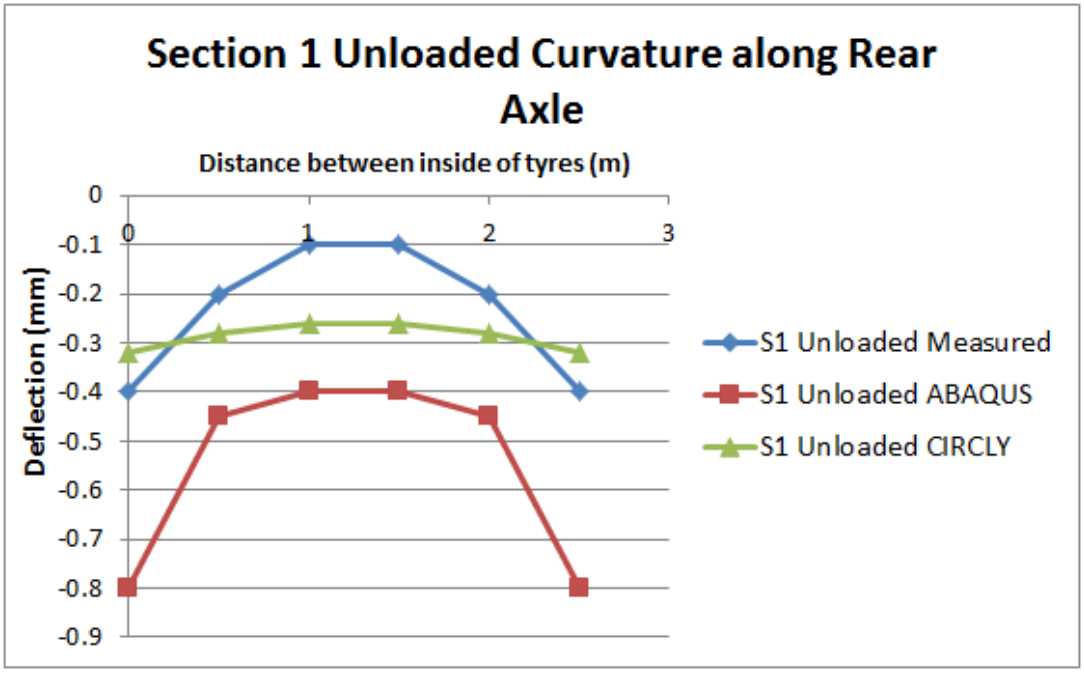


**Figure 4.83: Section 1, predicted curvature along the rear axle (from insides of tyres) for unloaded truck.**

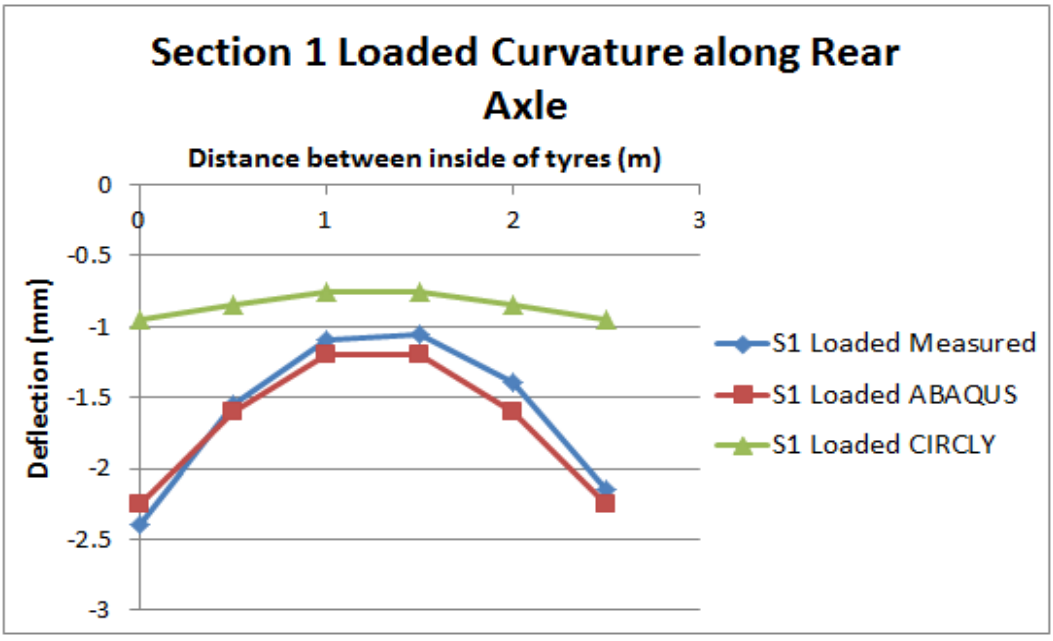


**Figure 4.84: Section 1, predicted curvature along the rear axle (from insides of tyres) for loaded truck.**

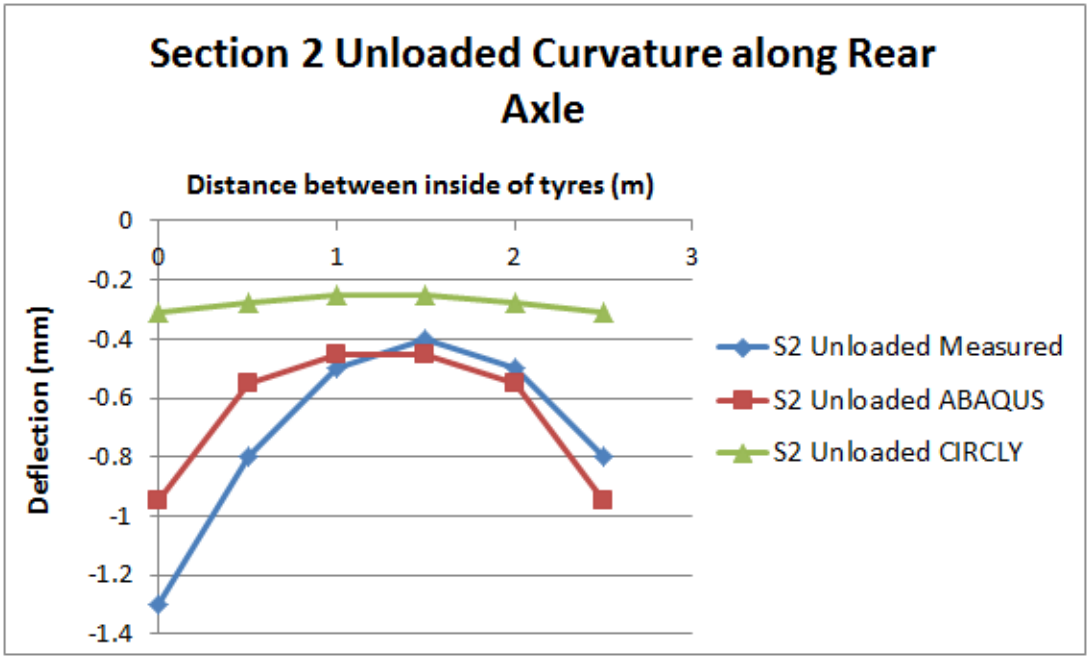


**Figure 4.85: Section 2, predicted curvature along the rear axle (from insides of tyres) for unloaded truck.**

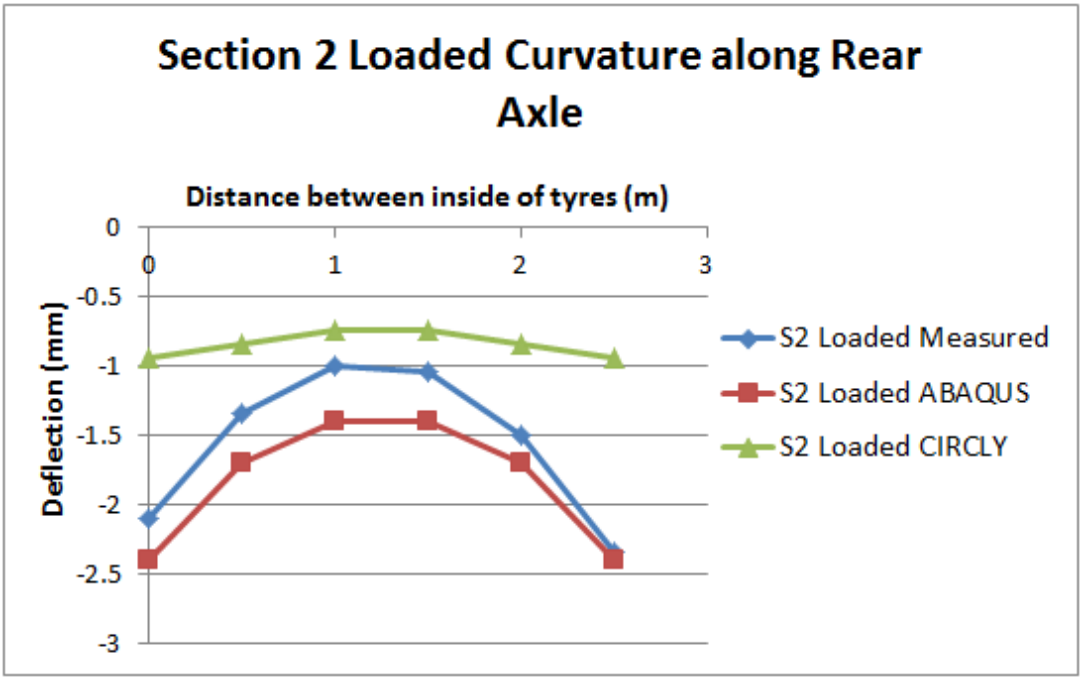


**Figure 4.86: Section 2, predicted curvature along the rear axle (from insides of tyres) for loaded truck.**

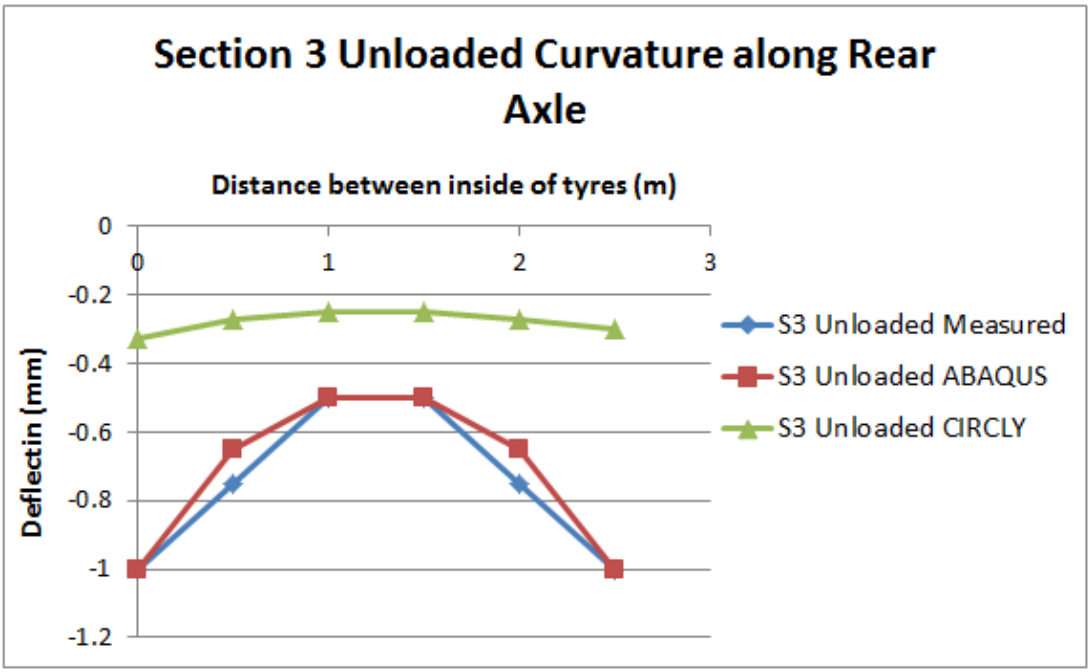


**Figure 4.87: Section 3, predicted curvature along the rear axle (from insides of tyres) for unloaded truck.**

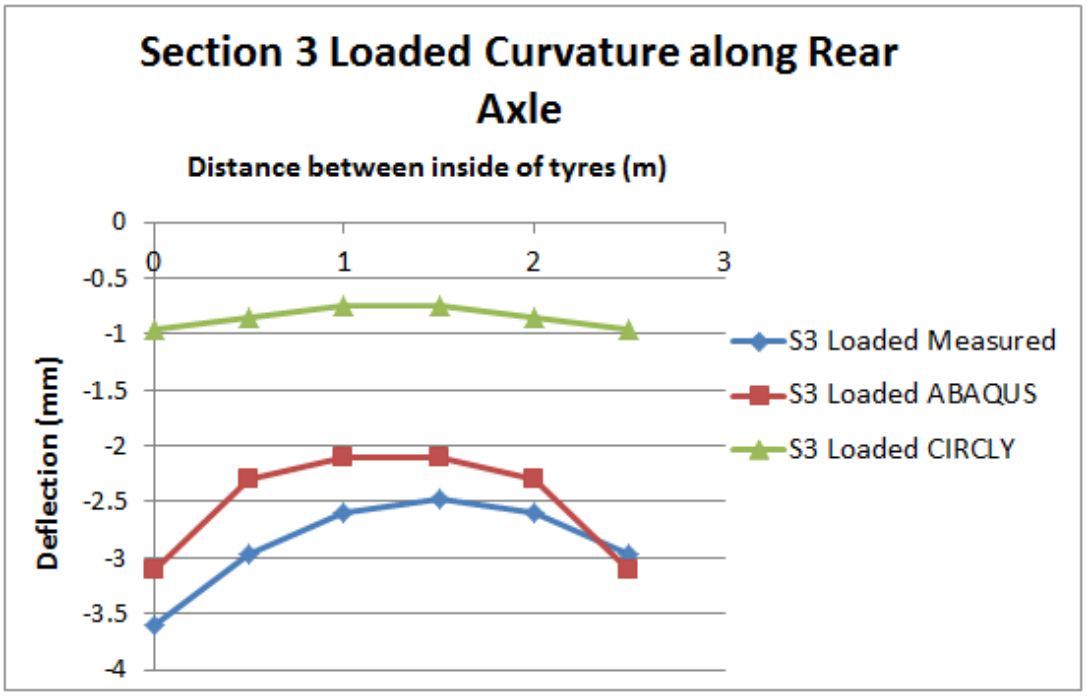


**Figure 4.88: Section 3, predicted curvature along the rear axle (from insides of tyres) for loaded truck.**

### 4.8.8 Modelling of Wheel Load Interaction

The results of wheel interaction modelling with various software packages are presented below. HIPAVE analysis is presented in Figure 4.89. This modelling considers a loaded Komatsu 830E applied to pavement section 1, with a sub-grade elastic modulus of 150MPa and the base-course elastic modulus determined through tri-axial testing with monotonic loading. The results in Figure 4.89 result from a completely isotropic linear-elastic modelling.

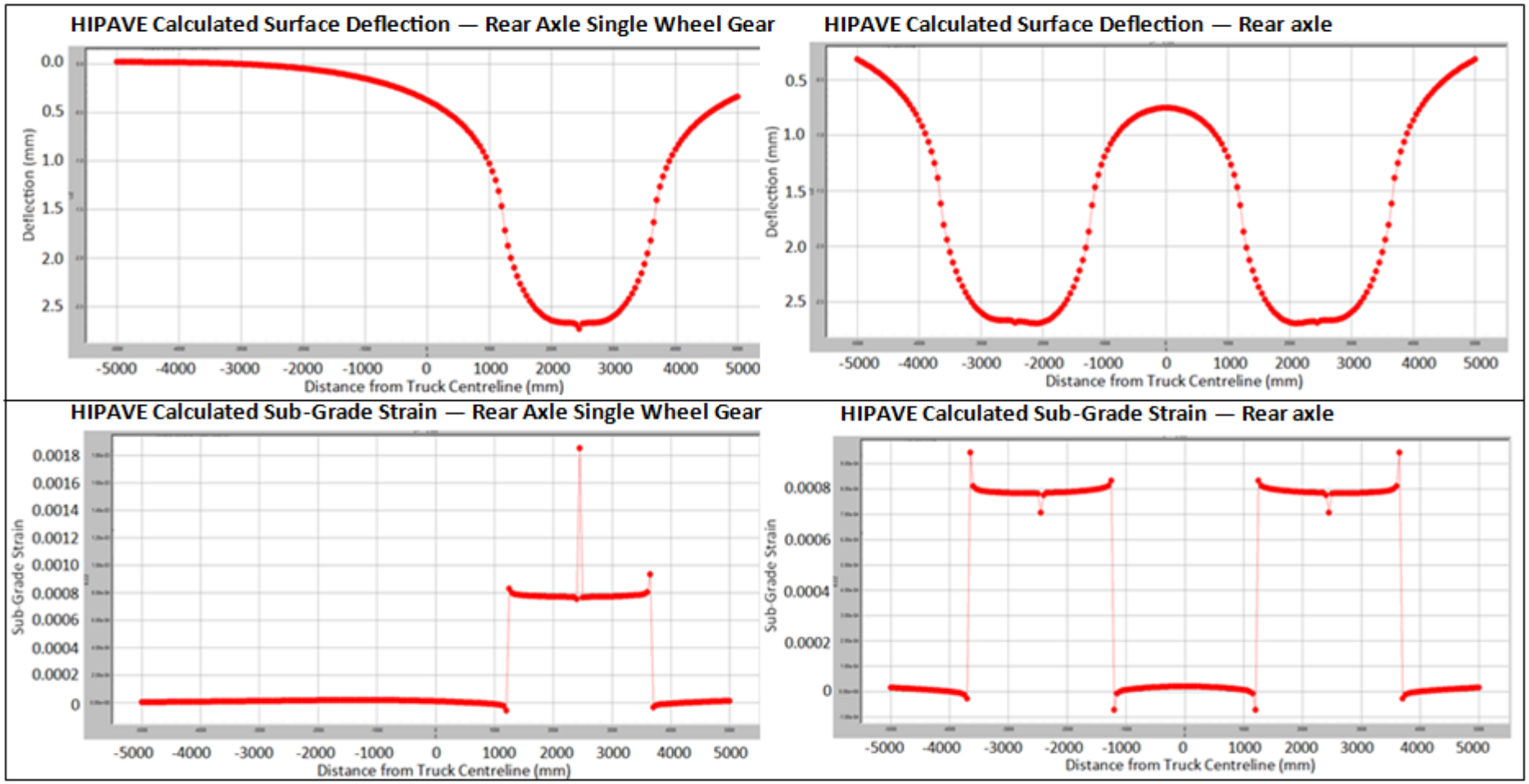


**Figure 4.89: Comparison of pavement surface deflection and sub-grade vertical compressive strain, calculated by HIPAVE (note differences in vertical scale).**

The results of CIRCLY analysis of tyre interaction are presented in the following. This analysis applied the same inputs as above, with the exception of the sub-grade, which was modelled as anisotropic (as opposed to isotropic in HIPAVE). The results in Figure 4.90 result from linear-elastic modelling with a cross-anisotropic base-course and an isotropic sub-grade.

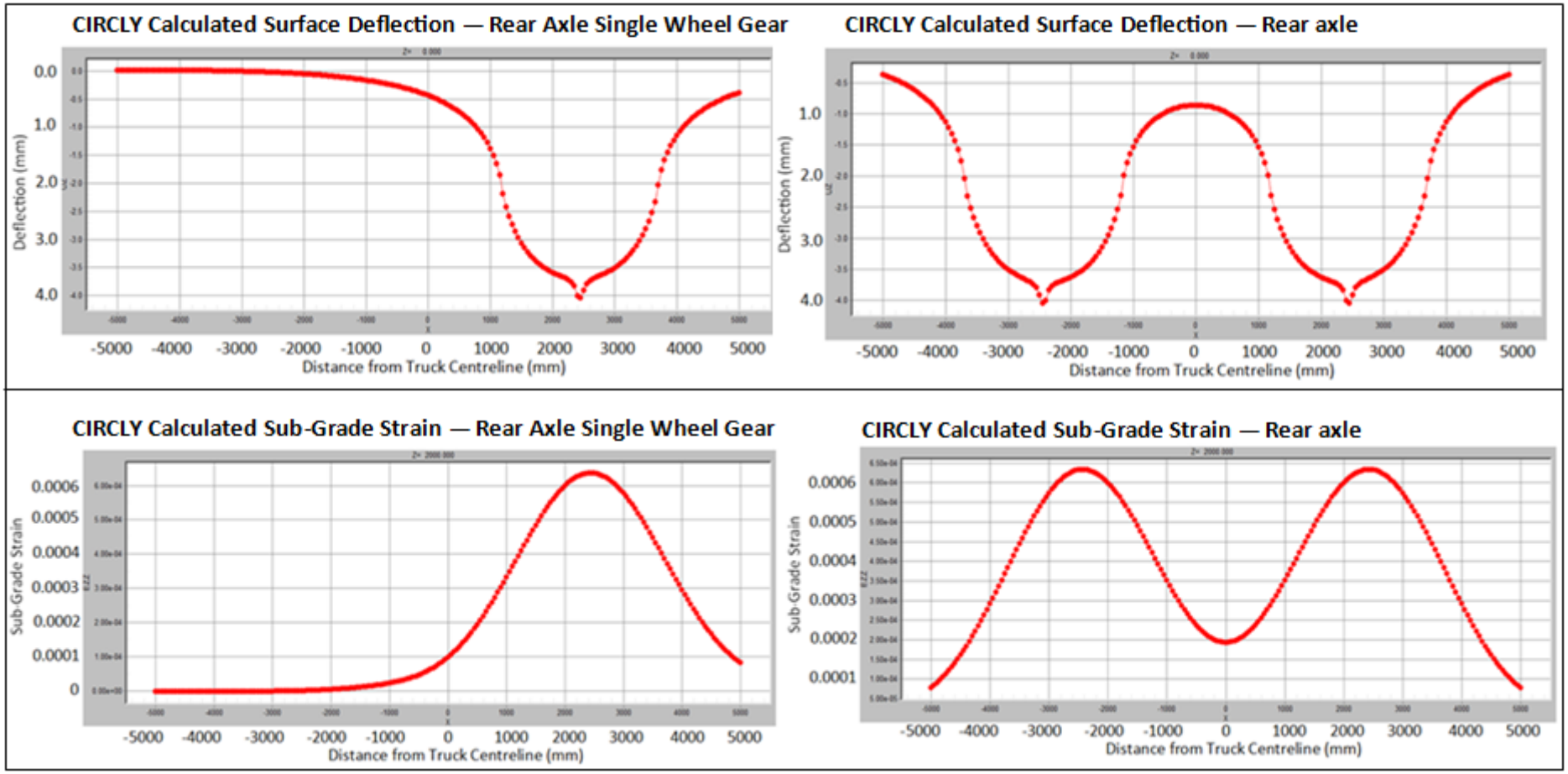


**Figure 4.90: Comparison of pavement surface deflection and sub-grade vertical compressive strain, calculated by CIRCLY.**

Results of pavement surface deflection and sub-grade vertical strain, calculated through three-dimensional nonlinear FEA for each pavement section are presented in Table 4.90. Note that the sub-grade was considered to have a layered structure, as detailed in Section 3.9.4, with the elastic modulus values presented in Section 4.8.6.1. 'Single Wheel Gear' and 'Rear Axle' refer to the wheel loads included in the respective modelling, in order to provide insight into the impact of including multiple wheel loads in the inputs to the FEA modelling.

**Table 4.90: Summary of critical values showing effect of wheel load interaction in FEA modelling of the pavement sections.**

| | | Middle of Rear Axle | | | | | |
|---|---|---|---|---|---|---|---|
| | | Pavement Surface Deflection (mm) | | Sub-Grade Strain (microstrain) | | Critical Sub-Grade Strain (microstrain) | |
| Section | Payload (Tonnes) | Single Wheel Gear | Rear Axle | Single Wheel Gear | Rear Axle | Single Wheel Gear | Rear Axle |
| 1 | 0 | 0.22 | 0.4 | 13 | 24 | 16 | 24 |
| 1 | 220 | 0.9 | 0.9 | 77 | 133 | 123 | 360 |
| 2 | 0 | 0.25 | 0.5 | 27 | 59 | 53 | 61 |
| 2 | 220 | 0.8 | 1.45 | 78 | 152 | 128 | 152 |
| 3 | 0 | 0.25 | 0.45 | 13 | 29 | 18 | 29 |
| 3 | 220 | 0.95 | 1.3 | 81 | 220 | 139 | 272 |

### 4.8.9 Pavement Lifetime Estimates

CBR design curves have been developed with

#### 4.8.9.1 CBR Design Curves

CBR design curves have been generated following the method in Pereira (1977), with used of the updated S77-1 curve presented in White (2007). The first (Figure 4.91) relates to all wheels present on the haul truck being applied separately in the calculation process, the latter (Figure 4.92) considers the rear axle dual-wheel gears as a combined load.

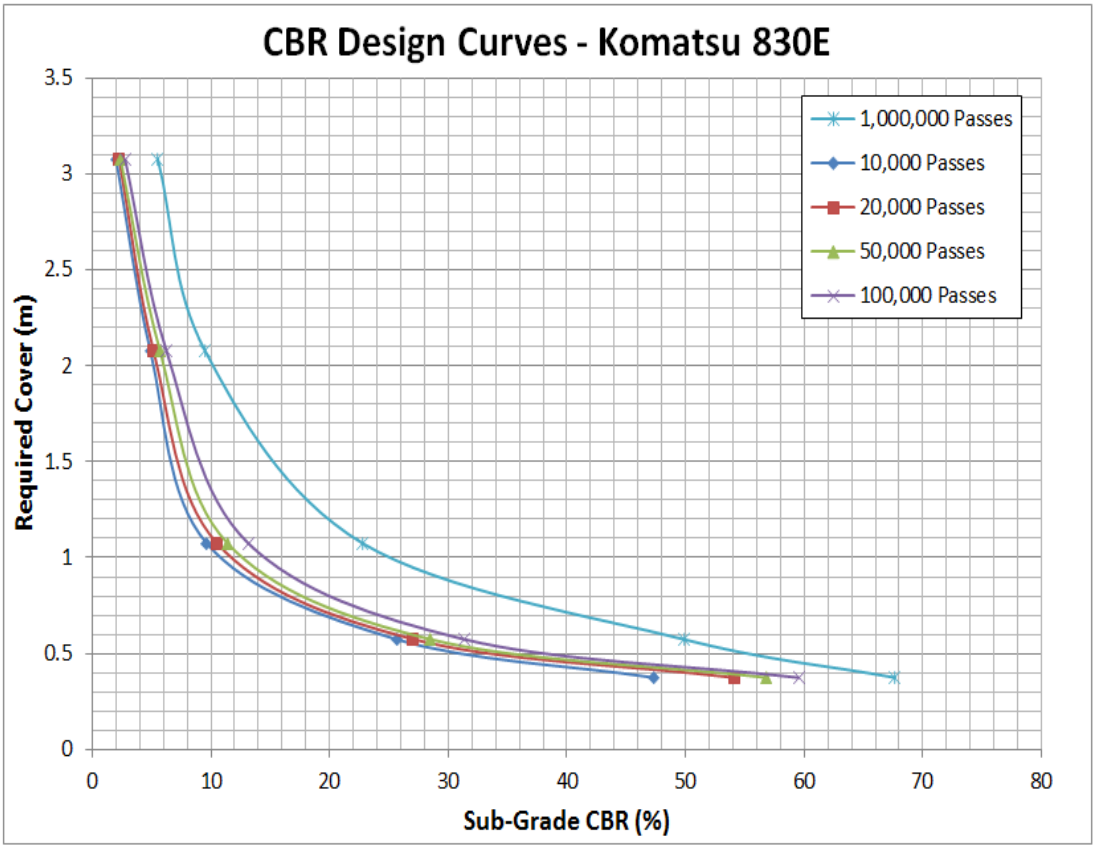


**Figure 4.91: CBR design curves derived with the S77-1 curve (White, 2007) and method in Pereira (1977) with all wheels considered separately in determination of ESWL.**

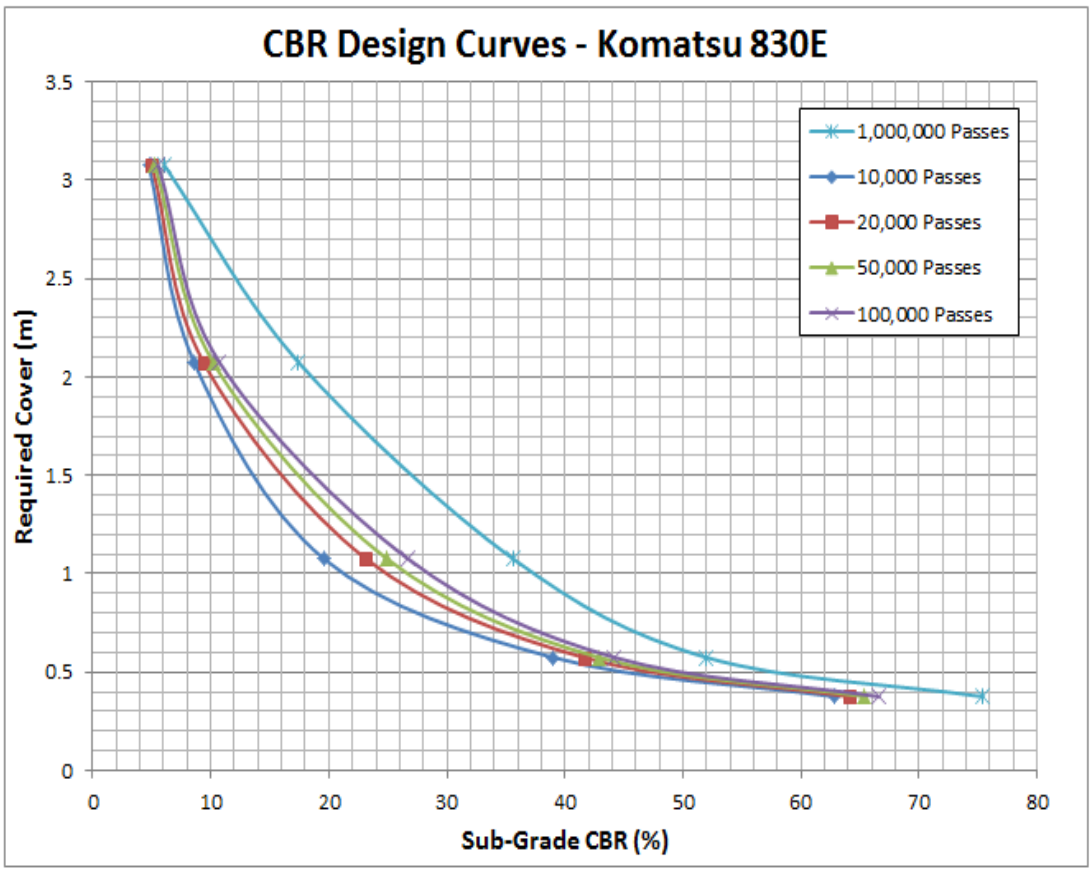


**Figure 4.92: CBR design curves derived with the S77-1 curve (White, 2007) and method in Pereira (1977) with dual wheel gears modelled as a single wheel load in determination of ESWL.**

#### 4.8.9.2 Comparison of Pavement Lifetime Estimates

Pavement lifetime estimates, comparing empirical and mechanistic-empirical design procedures are presented in Table 4.91. Note that for all results below, CIRCLY and HIPAVE results relate to the application of elastic moduli determined through tri-axial testing with monotonic loading, whereas all results from FEA were determined with application of the measured resilient modulus. Selection of moduli types is discussed in Section 5.8.6.

**Table 4.91: Pavement lifetime estimates via various methods, and category of haul road from Thompson et al (2009), considering a haul road with a total of less than 100,000 daily tonnes haul (considering sub-grade strain from ABAQUS).**

| S77-1 Lifetime Estimate | | | CIRCLY Lifetime Estimate | | HIPAVE Lifetime Estimate | | ABAQUS Lifetime Estimate | | |
|---|---|---|---|---|---|---|---|---|---|
| Sub-Grade CBR (%) | Base Thickness (m) | Repetitions | Sub-Grade Strain | Repetitions | Sub-Grade Strain | Repetitions | Sub-Grade Strain | Repetitions | Category |
| 3 | 2.7 | 10,000 | 0.002250 | 28 | 0.001390 | 2,751 | 0.001535 | 1,072 | 2 |
| 5 | 2.3 | 100,000 | 0.002000 | 92 | 0.000725 | 3,093,449 | 0.001295 | 8,007 | 1 |
| 5 | 3.1 | 1,000,000 | 0.001000 | 113,848 | 0.000860 | 535,706 | 0.000915 | 283,447 | 1 |
| 10 | 1.1 | 20,000 | 0.002700 | 0 | 0.001550 | 704 | 0.001980 | 18 | 2 |
| 10 | 1.35 | 100,000 | 0.002250 | 3 | 0.001250 | 17,740 | 0.001555 | 671 | 2 |
| 15 | 0.9 | 50,000 | 0.002200 | 0 | 0.001800 | 12 | 0.001705 | 42 | 2 |
| 15 | 1.5 | 1,000,000 | 0.001400 | 4,393 | 0.001020 | 7,733,538 | 0.001020 | 7,733,538 | 1 |
| 20 | 0.5 | 20,000 | 0.002400 | 13,870 | 0.001600 | 29,255,955,149 | 0.001850 | 159,137,996 | 2 |

Results of pavement lifetime estimates for a loaded Komatsu 830E, arising from empirical and linear-elastic design methods described in Section 3.9.8, are presented in Table 4.92. Pavement lifetime estimates derived through three-dimensional FEA analysis are then presented in Table 4.92. Each pavement section is modelled with a 2m thick base-course, to reflect actual conditions at the time of site testing.

**Table 4.92: Comparison of design pavement lifetime determined for a loaded truck from various methods.**

| Section | Design Method | Sub-Grade Strain | N |
|---|---|---|---|
| 1 | S77-1 | - | >1E+6 |
| | CIRCLY | 0.000680 | 1.11E+11 |
| | HIPAVE | 0.000450 | 1.89E+15 |
| | FEA | 0.000360 | 3.65E+17 |
| 2 | S77-1 | - | >1E+6 |
| | CIRCLY | 0.000730 | 2.07E+10 |
| | HIPAVE | 0.000600 | 2.12E+12 |
| | FEA | 0.000152 | 2.51E+26 |
| 3 | S77-1 | - | >1E+6 |
| | CIRCLY | 0.000207 | 2.07E+10 |
| | HIPAVE | 0.000580 | 4.72E+12 |
| | FEA | 0.000272 | 2.72E+20 |

NOTE: denotes a base of 10 (for example E+6 = 1,000,000)

# 5 Discussion

## 5.1 In-situ Testing Methods

The in-situ testing completed for the project is discussed in the following. The majority of these tests involve utilisation of test-methods that have been largely developed specifically for this study, as discussed in Section 3.5. For the discussion below, it is assumed these methods produce results with the accuracy stated in Section 3.5.

## 5.2 Pavement Texture

Measurement of pavement texture on unsealed pavement surfaces has not been the subject of significant research in the past. The nature of the surface can change rapidly with traffic volume and composition, climatic effects and maintenance works. It is difficult to define texture of an unsealed alignment for the purpose of estimating end-user impacts such as fuel consumption and vehicle wear. For this project it was considered appropriate to include such a measure, as tyre rubber hysteresis (see Section 2.2.2) is suspected of playing a significant role in generation of haul truck rolling resistance. As discussed within Section 3.5.5, the wavelength considered to constitute pavement texture has been adjusted for this project to allow consideration of texture within the extent of a tyre contact patch. Utilising this methodology, the results achieved reflect the observed condition of the pavement on the day of rolling resistance testing.

Section 1 was observed to have a smooth surface, with loose material well swept to the windrows at the side of the pavement. Sections 2 and 3 were both seen to present significantly more texture, with Section 2 dominated by divots and some fixed stoniness, whereas the Section 3 surface was typically dominated by loose stone with a maximum particle size of 50mm (estimated only). These observations are reflected in the texture estimation results, with Section 2 showing the greatest variance in results along its alignment, with Section 3 having the greatest texture.

It is difficult to comment upon these results in comparison to 'typical' or previously-measured texture for haul road surfaces, as to the author's knowledge it has not been attempted in the past. The RDS discussed in Section 3.5.6.3 does take account of some short wavelength roughness effects that may be considered within the range of texture adopted here, but would have a minimal effect on the final score. Despite the lack of precedent, the logical alignment between observation and measured results is considered to provide some assurance of the results attained.

## 5.3 Pavement Roughness

The three pavement sections included in the study differ quite significantly with respect to pavement roughness. To summarise Table 4.3, Section 1 has been shown to have approximately half (Section 2) and a quarter (Section 3) the magnitude of roughness over 0.5, 1 and 5m wavelengths and approximately half the roughness for 10 and 20m wavelengths compared to both of the other sections. Therefore, Section 2 has significantly lower roughness for wavelengths of 0.5, 1 and 5m wavelengths and similar roughness for 10 and 20m wavelengths in comparison to Section 3. Table 4.4 supports these findings, as the variance over a 3m moving average has been used to estimate the IRI for each section and therefore Section 1 is shown to be significantly smoother and Section 3 to be the roughest. More sophisticated methods of defining IRI (namely via laser profilometer) are required in order to comment on the relation between the method utilised here and 'standard' measures of roughness through IRI. Additionally, it has been found that Section 2 consistently has greater variation in roughness between wheel paths than the other two pavement sections.

Figure 2.13 provides a broader context for the pavement condition of the pavement sections considered in this project. Through observation it can be seen that Section 1 fits within the 'maintained unpaved roads' category or even in the rougher extremity of the 'older pavements' category. Note that the longer wavelength roughness shown to be present within the Section 1 alignment means it would likely be considered inadequate as a common sealed pavement. Such roads would be traversed by vehicles at much higher speeds than 30km/h and at these speeds it is likely that the roughness would be shown to be higher if the NAASRA counts method or another method utilising stroke measurements of suspensions was utilised. This comment relates to the quarter car model and IRI, which have been

derived from measurements of suspension stroke. Section 2 and Section 3 are classified as 'rough unpaved roads' which is consistent with the observations of surface condition presented in Section 5.3.1. The right-hand vertical scale within Figure 2.13 suggests normal use of Section 2 and Section 3 would normally be restricted to less than 60km/h. This scale relates to highway type vehicles, however it does appear to correlate well with the observations made during testing.

To provide some insight into the physical characteristics that have led to these results, consider the scoring for the RDS, as presented within Table 4.6, Table 4.7 and discussed in Section 5.3.1. Overall, the subjective information provided via the breakdown of RDS scoring correlates well with the findings via moving averages and IRI. However, the RDS considers wear-related pavement defects and not longitudinal unevenness as a result of sub-standard construction techniques, leading to much higher variation for Section 3, which had considerably more wear-related surface defects.

### 5.3.1 Roughness Defect Score

The RDS methodology has been derived specifically to define the overall impact of wear-related defects on pavement condition and ultimately rolling resistance. As discussed in Section 0, the rolling resistance model derived to utilise the RDS score has not been able to be investigated, this occurred due to the whole rolling resistance function not being available in the literature. Despite this, it was still considered that definition of the RDS provided additional insight to the roughness scoring collected through laser scanning, as it describes the nature of the in-situ pavement defects. From the scoring in Section 4.3.4 it is evident that Section 1 was in a superior condition, with Sections 2 and 3 presenting significantly higher scores. Of interest is the fact that Section 1 likely had experienced the most traffic, with Sections 2 and Section 3 likely experiencing only random traffic during construction of the most recent lift on the waste dump. Section 1 and 2 had been maintenance graded previously, as evidenced by the windrows observed adjacent to them. The nature of traffic in the intervening time to the testing is not known, however it appeared that Section 1 was in quite sound condition as evidenced by Figure 3.10. This is in contrast to Section 3, which had a great deal of stoniness, both fixed and loose. Finally, Sections 2 and 3 had a similar level of corrugations.

This information should be considered somewhat independently of the discussion within Section 5.3, which describes the mean deviation of the pavement surface for

varying wavelengths. This methodology lends itself well to the description of sealed pavements, where surface defects are generally infrequent. However, unsealed pavements are expected to present some surface attrition due to trafficking. It is therefore prudent to describe the surface condition through a qualitative means such as the RDS. It is unfortunate that the research completed to develop the rolling resistance function described by Thompson et al (2003) could not be extended, as such a relation could be highly beneficial for day-to-day mine operations. It is recommended that future research consider the RDS function (or some other qualitative assessment such as estimation of IRI using Table 2.3) and how it may relate to rolling resistance.

## 5.4 Pavement Deflection

Pavement deflection measured within this project is difficult to interpret in the absence of similar measurements being taken previously on unbound haul road pavements previously. It is clear that deflections are greater than would be expected on (stiffer) highway pavements subjected to lighter wheel loads. Discussion of the interpretation of pavement deflections is contained within the remainder of this section and specifically within the discussion arising from pavement modelling in Section 5.8.

### 5.4.1 Pavement Curvature

Significant pavement deflection was found to occur in all sections under both unloaded and loaded haul trucks. When combined with the significant magnitude of maximum deflections discussed in Section 5.4, it is clear that the area and volume of pavement material influenced by the large axle loading is significant. Consider that deflection has not been shown to have decayed at a radius of 2500mm, which is the largest radius considered in back-calculation of pavement modulus (see Section 3.9.1). Transit New Zealand (1998) state that a broad deflection bowl relates to the sub-grade layer possessing relatively lower stiffness, with pronounced deflection near the load centre describing relatively lower stiffness of surface layers. From this general guidance it is difficult to comment on the nature of the pavements considered, other than to say it appears that the sub-grade and upper layers are not significantly stiff with relation to the wheel loading applied. Ultimately, curvature has

been defined to allow back-calculation of pavement surface and layer moduli, which facilitates further analysis and discussion. Section 5.7.3 contains discussion relating to the results of back-calculation of deflection and curvature results, and Section 5.8 discusses the implications of pavement design throughout.

There is some uncertainty with the method adopted to define curvature. The deflection has been defined via the use of a moving average, where raw data that suggests a concave deflection bowl can be effectively smoothed. However, it has been considered that overall a significant relation has been shown for the calculation method presented in Section 3.5.7.3. Ultimately, the method has not been utilised prior and consequently there is limited precedent in utilising measured deflections via terrestrial laser scanner and inputting to software designed for FWD test analysis. Secondly, the ratio of tyre contact pressure to material stiffness may be outside of the material and performance models contained within the software packages available, as they have been developed to analyse typical highway pavements with at least a thin flexible surfacing.

### 5.4.2 Interaction of Deflection between Tyres

The deflection profiles along the rear axle and between the front and rear axle of the haul truck used for site testing have been determined. It is clear from these results that there is some interaction between loads, as can be further attested by the observation of the curvature results discussed in Section 5.4.1. To properly interpret this result one should consider the limitations in the understanding of wheel load interaction presented in Section 2.4.2.1, which highlights that current linear-elastic modelling techniques may be insufficient to analyse pavement response in areas horizontally removed from the tyre contact patch. However if the results in Section 4.4.2 are considered, it is clear that the deflection bowls of adjacent dual-wheel assemblies loads do interact. Although wheel load interaction has been shown to occur, it is unlikely to result in a change in the location of critical sub-grade vertical compressive strain which governs mechanistic pavement thickness design. This contention is supported by the outcomes of various modelling techniques (see Section 5.8.4.4). The only caveat to this statement is if a vehicle wander algorithm was built in to the pavement analysis, as is possible with the use of HIPAVE (Mincad Systems). Such an effect could result due to an increase in cumulative pavement damage occurring as the increased strain at the axle centre being added to the damage caused by strains under the wheel loads with the truck in different lateral

positions. In this case the cumulative damage factor could be influenced by anomalous strains calculated in locations radially removed from the load centres, which in turn could decrease predicted pavement life. Similarly, it may be that negative strains are predicted between wheels and subsequently an erroneous increase in pavement life predicted. This topic is further discussed in Section 5.8 with the benefit of observations from pavement analysis utilising the software noted above.

### 5.4.3 Geometry of Tyre Contact Patches

Measurement of tyre contact patches was completed within this project to assist understanding of the geometry and contact characteristics for pavement modelling purposes. From the results in Table 4.18 it is clear that utilising the measured contact geometry with a constant applied load is inappropriate for modelling. The inaccuracy is somewhat improved by utilisation of the method presented by Hadi et al (2003), however total truck loads are still significantly over estimated. If a uniform contact pressure is assumed, it is shown to approximately double with the application of a load to the truck, for the contact geometry shown in Table 4.19. This finding is very significant for the purpose of pavement modelling and design as pavement strains will be significantly larger for the loaded case. These findings suggest that the tyre carcass stiffness, both vertically and radially, must have a significant impact on the contact stress and geometry for large off-the-road tyres. Further research is recommended to better define this effect for the purpose of pavement modelling. If one considers commonly accepted theory relating to interaction of flexible footings (Knappett et al, 2012) and soil reaction stresses, it is clear that a constant pressure is unlikely to be an accurate approximation for pavements subjected to such large loads and significantly large tyre contact geometry.

The published contact area for a 40.00R57 tyre is 1.039 $m^2$ (goodyearotr.com). Table 4.18 shows the average measured contact area for a loaded tyre was 1.047 $m^2$, therefore it appears the measurements taken were accurate. Corresponding to the published contact area is an inflation pressure for a 40.00R57 tyre carrying greater than 60 tonnes of 700kPa. The mine operator stated that they operated their haul truck tyres at higher than recommended inflation pressures (890kPa when the measurements were taken), which is confirmed by these results.

## 5.5 Rolling Resistance

The following sections discuss the results and analysis of the rolling resistance testing. Data has been analysed at various stages, with three different 'data sets' being discussed. The derivation of each is outlined in Section 3.5.8.2 and summarised below.

Throughout the following discussion, the RRC actually refers to a driving resistance. The results for this study have been derived considering the wheel torque applied to the rear axle of the haul truck used in testing, but consider the gross weight of the entire truck, not simply the vertical force applied to the rear axle. Section 5.5.8 includes further discussion of this simplification and Table 4.44 presents adjusted RRC values that reflect the weight being supported by a single wheel.

### 5.5.1 Derivation of Data Sets, Potential Error and Uncertainty

The derivation of three data sets for analysis of rolling resistance testing was critical to the study. Therefore, a detailed discussion of the impacts and potential errors associated with each step is provided below. Firstly, a summary of how each data set was derived is presented. Note that a test case refers to a discrete set of six tests representing a specific combination of truck speed and load over the three pavement sections with three tests being completed with the truck travelling in each direction. Each data set comprises a mean RRC value for each test case and section.

1. Unscreened data set – mean values of RRC calculated from wheel motor torque measurements sampled at a frequency of 0.04 seconds. The only exclusion within the data is the first and last second of the test, to remove uncertainty with the logging being started and stopped manually at each end of the pavement section.
2. Screened data set – within the six tests representing a test case, any calculated RRC point greater than one standard deviation above the highest test mean value or less than one standard deviation under the minimum test mean value is removed. Also, any point with a rate of change exceeding 0.01356kNm (10 pound-feet) torque is removed.
3. Correlated data set – ANOVA hypothesis testing of equal means is completed with the screened data set. A mean value is then selected from tests that are found to have equal means at a level of significance of 0.05.

Mean truck speed values for each test case are presented in Section 4.5.1. For each test case, the variation of mean truck speed values varies from 3.2 to 4.7%. As discussed in Section 5.5.5, there does not appear to be a significant variation in RRC with truck speed within this study, and consequently this variation is not expected to be the source of significant error. However, note that the identification of a relation between truck speed and RRC is made more difficult due to the poor correlations found between RRC and pavement properties for a loaded truck travelling at 15km/h.

The chi-square test results presented in Section 4.5.2 suggest that the RRC data within the screened data set is generally not normally distributed. To further interrogate this result, observation of histograms of the data suggests that kurtosis is more significant than skewness. This infers that much of the data is centrally located, to the extent that it cannot be considered to be normally distributed. Although this means chi-square testing was largely unsuccessful in proving normality in the data, it does provide some insight into the significant number of test cases that were found to have equal mean values through ANOVA testing (discussed below). An example of the distribution of RRC data within the screened data set was presented in Figure 3.20. Further discussion on hypothesis testing is presented below.

Section 4.5.3 presents the mean RRC for each test case and data set. Also included in each set of results (Table 4.25, Table 4.26 and Table 4.29) are the mean RRC values summarising each test speed and payload. These provide additional insight into the correlation between pavement properties and RRC due to variation in only speed or payload.

As the unscreened data set includes all data from the rolling resistance tests, it is expected to present the estimated total energy requirements for truck motion. This value includes truck and driver response to pavement and any other external input such as wind. However, as wheel motor torque was measured directly, it will exclude accessory power usage and the like. In fact, logging of the central inverter power output during the testing suggests that the truck's wheel motors use approximately 70-90% of total power output. It was considered inappropriate to utilise only the data from the unscreened data set to determine the influence of pavement properties. Hence, further analysis was completed to refine the data, producing the screened data set, as outlined above.

The criteria applied to derive the screened data set are nominal in nature. It was considered appropriate to eliminate data that was too far removed from the population mean for each test case. This was done by comparing mean of each test and the population mean of the six tests comprising each test case. From observation of the pavement sections utilised in testing, somewhat consistent results were expected in the calculated RRC throughout each rolling resistance test. As such, outliers were not anticipated to occur due to any interaction between pavement and truck. Furthermore, very low values represent operating conditions where only minimal power output is required, which is not representative of the truck in hauling conditions. The removal of this data has resulted in a reduction in the mean RRC values between the unscreened and screened data set. This suggests the majority of the data removed were high values expected to have been associated with truck or driver response to any external input (for example, the driver applying additional throttle pressure). In the case of driver response, this could be related to perceived pavement conditions, although the driver was instructed to avoid changes in throttle position as much as possible. In reality, if a highly controlled testing environment could have been developed such exclusions would not be necessary. In fact, continuous monitoring of truck power output, throttle position and location on the pavement section could have allowed rapid changes in RRC to be interpreted to provide greater understanding of the relationship. However, as stated above, these data points are considered to have resulted from some external input to the trucks operating state other than pavement interaction. Less potential error is associated with the removal of data due to rapid changes in wheel torque, as they have been observed to occur throughout the range of wheel torque output measured in this study. As mean values are ultimately used for analysis, this therefore should have a negligible effect in most instances.

The removal of data, as discussed above, in deriving the screened data set typically removed 30-50% of data points contained in the unscreened data set. A greater proportion is attributable to the maximum and minimum limits imposed. This explains the drop in mean RRC values observed between Table 4.25 and Table 4.26. Such a proportion of data exclusion appears quite high, but is considered suitable due to the lack of a set test method and the volume of test data.

Section 3.5.8.2 included a comprehensive discussion of the adoption of mean values from tests found to have equal means from ANOVA testing. Only two test cases rejected the null hypothesis (equal means). The null hypothesis was rejected for half of the test cases, when analysed with Kruskal-Wallis hypothesis testing. The

robustness of ANOVA is considered to be reasonably high for the nature of non-normality (see Section 3.5.8.2) observed in this study, which has been interpreted to have resulted due to kurtosis more so than skewness. In the instance of the alternate hypothesis having to be accepted in ANOVA testing (i.e. the mean of tests is not equal), the mean RRC values from the screened data set were adopted. This is a potential source of error. Minimisation of the error was attempted with comparison of correlations inherent in the correlated data set with those present in the other two data sets. The comparison of data sets is considered necessary, as Table 4.28 shows that eight of the 12 test cases were found to have only two tests with equal means. Although this is not an ideal outcome, it does appear that the tests retained within the correlated data set are quite representative of the population mean of the results within the screened data set, which includes all six tests in each test case.

In deriving the test data for this portion of the study, several potential sources of error and unknowns existed. The first relates to the inclusion of a human element within the testing, that is the haul truck driver. From observation of the driver throughout rolling resistance testing, it must be stated that he was vastly experienced and skilled. Despite this fact, it is expected that driver response is present within the unscreened data set, specifically in the form of 'peaks' in the measured wheel motor and central inverter torque output. It has been considered that such discrete changes in the rate of truck power output could not be in response to a pavement feature only, but more likely due to the driver applying additional throttle to maintain vehicle speed. Although such abnormalities have been removed from the data in the generation of the screened data set, it is acknowledged that further influence of the driver is possible within the bounds set. For example, it can be observed in Table 4.21 that the truck speeds are consistently higher than specified to the driver. This may have resulted from some inconsistency between the truck's speedometer to that logged by the GE Invertex software, however it is thought more likely that it results from an attempt made by the driver to maintain a consistent speed. This has resulted in marginally higher than intended vehicle speeds, fortunately this trend is quite consistent throughout the data.

Other potential errors relate to variation of pavement properties over the length of a pavement section. This study has characterised each pavement section through a mean value for each pavement property. For instance, Table 4.3 and Table 4.4 utilise a mean value of the standard deviation of pavement surface undulation over a set moving average and the variance of pavement surface level over a moving

average wavelength of 3m, respectively. Deflection is characterised similarly, with section one and two having a second testing location added in the case of an unloaded truck to provide some assurance. Ideally, the test method used for the rolling resistance experienced by the truck, would have been of such accuracy that continuous monitoring of the wheel motor torque could be compared to discrete portions of each test section and their inherent pavement properties. This would require additional pavement deflection or pavement stiffness testing. Such an attempt could be made in future research if a rapid test method such as Heavy Weight Deflectometer could first be confirmed to correlate with full-scale haul truck deflection testing. Due to such an experimental methodology not being possible for the current study, mean values for each pavement section have been adopted in the analysis of rolling resistance test data. In the case of deflection, Table 4.8 and Table 4.9 suggest that the test values are quite consistent over each section, however the lack of a second test station within section three means that it may have more inherent error. An attempt to control this unknown was made by selecting pavement sections that are expected to be consistent along their length, not just in appearance but also with regard to previous traffic in constructing the waste dump. Section three was removed from any designated roadway, and therefore was expected to present less pavement stiffness than the other two sections. Mine operations personnel advised the traffic layout has remained consistent for the placement of all lifts on the waste dump. However, such assurances and the heterogeneous nature of mine waste material is not sufficient to conclude that stiffness along each section does not vary, without some testing (such as that suggested above) that can be completed at a higher frequency.

Although characterising sections of pavement with a single roughness (typically IRI) value is typical in the literature, this is an imperfect method in the context of correlating pavement condition to RRC. Such measures can be influenced by shorter portions of significantly higher roughness. Again, an attempt was made to utilise uniform pavement sections, which appears to have been somewhat confirmed by the profiles shown by the graphical outputs in Section 4.3, keeping in mind the pavement was unsealed and constructed without a quality control procedure in place.

Potential sources of error also lie within the analysis of rolling resistance data. The process involved in the generation of the screened data set has been discussed previously, though some uncertainty is also present in the refinement to produce the correlated data set. Firstly, the need for two test samples to have equal means or

represent discrete samples of a single population, as tested by the ANOVA and Kruskal-Wallis hypothesis tests respectively, is not certain. The process for refinement was adopted in an attempt to remove uncertainty remaining within the screened data set, after removal of data outside the bounds set to represent driver and truck response. It is contended that if the data appears to have equivalent mean values then it must be consistent. However, the poor acceptance rate of the null hypothesis in Kruskal-Wallis testing does raise some concern. This has resulted from variation in the distribution of ranks within the test data. Which could be due to a difference in the number of data points in the test samples being tested. Secondly, it may result from variation in the mean RRC value between two (or more) tests. As stated above, there was a significant concentration of data points found to be grouped around the mean. This means that the median of two tests would vary, providing a skew in the distribution of ranks for the data points of two compared tests. Both explanations are cause for concern, which is one of the reasons that the screened data set was adopted for use in analysing RRC data and in the development of regression functions. As a result, this decision was made on the basis that the correlations present between RRC and pavement properties utilising the correlated data set were consistent with those observed in the screened data set.

### 5.5.2 Influence of Pavement Properties and RRC

A process has been undertaken to determine which pavement properties correlate with the RRC values derived for each test case within each data set. As a result, the strongest correlations were utilised to complete a multiple linear regression between RRC, pavement deflection and IRI. Finally, the resulting regression equations were applied to determine the relative impact of deflection and IRI to the case of an unloaded and loaded truck. Statistical analyses have been used throughout in order to provide insight into the level of confidence and error associated with each result.

Most prevalent of all the trends identified by the correlation analysis, was the lack of any correlation being identified between a loaded truck at 15km/h and any pavement property. In fact, an inverse trend was observed in this test case when compared to the others in the study, with Section 1 having the highest RRC and Section 3 the lowest. Although no physical data was captured during the rolling resistance experiments to support the suggestion, it is contended that this may be due to the fact that the truck performs in a very inefficient manner at this low hauling speed. It

is logical that the truck would be designed to operate at peak torque, such that it is most efficient when operating in an 'in-service' condition. From the author's experience within the industry, most hauling is completed at a maximum speed of 30-40 km/h. This suggestion could have implications for haul trucks operating on ramps climbing out of mine pits. Such an operating case is beyond the scope of this study. However, in this instance torque output would likely be much higher than the testing at 15km/h in the present study due to the addition of grade resistance experienced by the truck. Testing completed at 15km/h in such an operating condition would provide much greater insight into the response of the truck to pavement properties, and it is recommended that any conclusion concerning a loaded truck travelling at 15km/h be reserved until such a study is completed.

The correlation coefficients presented in Section 4.5.4 include the statistically significant results (exceeding 0.997, as per Table 3.4) noted in Table 5.1. Each is discussed in detail below.

**Table 5.1: Summary of statistically significant correlations between pavement properties and RRC.**

| Data Set | Relation with RRC | Correlation Coefficient |
|---|---|---|
| Unscreened | Deflection (unloaded), all truck speeds | 0.999 |
| | 5m moving average roughness, unloaded, 15km/h | 0.997 |
| | MPD, unloaded, 15km/h | 0.999 |
| Screened | 1m moving average roughness, loaded, all truck speeds | 0.999 |
| | IRI, unloaded, 30km/h | 0.999 |
| Correlated | 5m moving average roughness, unloaded, 15km/h | 0.999 |
| | IRI, unloaded, 30km/h | 0.997 |

The correlations relating to 15km/h truck speed were found to produce negative coefficients when included in the multiple regression analysis, which is discussed below. As stated in Section 3.5.8.2, such results are considered irrational and are

excluded for this study. Further, the correlation between 5m moving average roughness and an unloaded truck travelling at 15km/h was found to correlate poorly (r=0.516) within the screened data set, and subsequently has not been investigated further. MPD was found to have a negative coefficient within each attempted regression analysis completed following the calculation of correlation coefficients, and was excluded from all subsequent analysis. Further, it was surprising that MPD was not shown to significantly correlate with RRC at 30km/h, as the discussion in Section 2.2.5 suggested a more pronounced influence of texture at higher vehicle speeds. Although a significant correlation coefficient was found for the 1m moving average roughness and a loaded truck, it was only found to be significant in a single data set, and subsequently this was not considered a trend warranting further investigation.

Most significantly, the correlation analysis identified a statistically significant correlation in two of the three data sets between IRI and an unloaded truck at 30km/h. A lower correlation coefficient resulted from analysis of the unscreened data set (0.832). This alludes to the greater error and uncertainty associated with the data prior to any screening. It is contended that greater truck and driver reaction occurs due to shorter wavelength roughness than any other property, which is referred to as ‘wheel hop’ by Mclean et al (1996) in Section 2.2.5. More discussion on this topic is included below.

To this point, no discussion has related to the correlation between RRC and pavement deflection. It is noteworthy that in all test cases deflection produced a correlation coefficient with a level of significance of around 0.1 (r=0.988). Throughout the study, a level of significance of 0.05 was adopted to represent a finding of statistical significance. However, as noted in Section 4.5.4, this case should be considered further. If all test cases are considered for 30km/h alone, a correlation coefficient of 0.82 results, which is statistically significant for a level of significance of 0.05 and a sample size of six (requiring a minimum of r=0.811). Furthermore, if the deflection results are considered to an accuracy of 0.1mm, then a statistically significant correlation coefficient results at a level of significance of 0.05 for all data sets. As was discussed in Section 5.4, an accuracy of only 0.5mm has been possible from the measurement techniques for pavement deflection developed for, and used within this study. It is recommended that future research focus on developing a method of measuring pavement deflection to an accuracy of 0.1mm, as a resolution of 0.5mm represents a significant percentage of the total measured magnitude of deflection. As a result of this fact, it appears that greater

uncertainty may have resulted for the findings of this study, whilst being sufficient to address the research objectives. Therefore, pavement deflection was considered in conjunction with IRI within all subsequent regression analyses.

Lastly, the correlation analysis showed a consistent trend of greater influence of longer wavelength roughness for a truck in the unloaded condition and shorter wavelength roughness in the loaded condition. Unfortunately, the poor correlations that have resulted between a loaded truck and RRC at a speed of 15km/h, mean that these results are excluded from this general statement. It was not possible to further analyse this effect with the size of the data set resulting from the experiments in this study. It is recommended this effect is investigated further in subsequent research.

The findings from the correlation analysis discussed above were then utilised to guide the regression analysis, which is discussed in detail below.

Multiple variable regression results presented in Section 4.5.5 are quite consistent between test cases. The only regression equation that could be considered an outlier from those determined from other data sets, is that derived from the results including all test speeds within the unscreened data set. Potential explanations are discussed below. The coefficients of determination are significant and also consistent for each regression equation. Further, the F-probability, as discussed in Section 3.5.8.2, has been shown in Table 4.34 and Table 4.35 to be less than 0.05 in all cases, meaning only a minimal error should be considered to be present within the regression equations. The F-probability effectively defines the probability that the regression equation cannot adequately predict the independent variable (RRC), which has been observed to be sufficiently small for acceptance throughout. Therefore, it is contended that the outcomes of the regression are suitable for use in subsequent analysis and for estimating the driving resistance (as represented by RRC in this dissertation) of a Komatsu 830E haul truck operating at 30km/h on flat terrain. Further testing with alternate vehicle and operating conditions are recommended in future research, such that these functions can be modified. and verified for other operating conditions and vehicles.

From comparison of the regression results considering all operating speeds and only 30km/h, it is clear that the unscreened data set produces distinctly different correlations to the screened and correlated data sets, which are generally well agreed. The lower coefficient of determination ($r^2$) provides some insight. As the lowest values occur from regression with the unscreened data set, it is concluded

that a larger amount of unexplained error is present. This is logical, as this data set includes all data logged during each test, which includes unforeseen truck and driver response. The aim of screening the data, and then completing hypothesis testing to test equal sample means within the population of each test case, was to remove such error and uncertainty. Further, a greater influence of IRI has been determined for the unscreened data set. This may be explained by the fact that both truck dynamic response and driver response are likely to be more sensitive to IRI than pavement deflection. Vehicle dynamic response is known to be related to pavement roughness and it is suggested that driver response is related to driver comfort, which was the basis of pavement roughness measures, as discussed in Section 2.2.5.

For prediction of total energy requirements, including uncertainties that have not been controlled or monitored within this study, the regression equations from the unscreened data should be applied (see Section 4.5.5). For clarity, Equation 5.1 is reproduced from Table 4.35 below. Whereas, in determining the relative influence of each pavement property on the generation of rolling resistance only, thus referring to an isolated wheel and its respective vertical load, the outcomes of the regression from the screened and correlated data should be observed. The equations and illustrated influence of each property displayed in Section 4.5.6 are closely related for these data sets. However, it is recommended that the regression equation noted for the screened data in Table 4.35 should be used for the prediction of RRC (driving resistance), which is reproduced as Equation 5.2 below. Note that, although a consistent trend has been identified between the equations derived from testing at both speeds and 30km/h in isolation, the uncertainty related to the operating state of a loaded truck moving at 15km/h, as discussed above, is considered too great to recommend use of any data from testing at 15km/h to predict the RRC. Due to the similarities between regression outcomes for both speeds and 30km/h, it is noted that that the equations presented below are potentially quite robust, but should be tested further in future research.

As previously discussed, the RRC as measured in this study actually relates to driving resistance, as the power required to maintain steady state motion of the entire vehicle is considered instead of a single wheel. Therefore, the resistance of a single wheel motor also includes the power required for motion of unpowered wheels. This effect is discussed further in Section 5.5.8 and needs to be remembered when observing any output resulting from either of the equations below.

**Equation 5.1: Regression equation for total haul truck driving resistance.**

$$RRC_{DR} = 0.1682 * Deflection + 0.0663 * IRI$$

Where:

$RRC_{DR}$ is the total driving resistance of the truck

**Equation 5.2: Regression equation for haul truck driving resistance.**

$$RRC = 0.1537 * Deflection + 0.058 * IRI$$

Where:

$RRC$ is the driving resistance of the haul truck, with some uncertainty removed for unforeseen truck and driver response

The derived regression equations were then utilised to estimate the proportion of rolling resistance generated by both deflection and pavement roughness. A clear trend is evident within Table 4.39 and Table 4.43. Firstly, note that in both cases, IRI has approximately twice the influence of deflection for an unloaded truck and approximately equal influence for a loaded truck. The latter is also evident in the regression analysis for the unscreened data at 30km/h only. In concluding which set of results to utilise to state the relative influence of each pavement property it is important to consider the significance of the data contained within each data set.

Table 4.40 and Table 4.43 should be observed with regard to the proportion of rolling resistance generated by each pavement property. It is evident from Table 4.43 that approximately one third of rolling resistance experienced by the haul truck travelling at 30km/h in the unloaded condition was attributable to pavement deflection. The remainder, approximately two-thirds, is attributable to IRI. Furthermore, in the loaded condition, approximately half of the rolling resistance may be attributed to both pavement deflection and IRI. The results shown in Table 4.40 further support this finding, with due consideration of the discussion above

relating to uncertainties included in the unscreened data set. It appears that unexplained error is most prevalent in the unloaded case, where the difference in the influence of deflection and IRI is more pronounced. It is contended that this may be due to the effects relating to unloaded truck response as discussed above. To further support this outcome, the relative influence of each pavement property is shown to be similar, when including the test data with a truck speed of 15km/h, see Table 4.39.

The findings above are somewhat unprecedented in the literature. Jamieson et al (2002) suggest that deflection has the greatest influence on rolling resistance experienced by a small commercial truck operating on an unsealed road. Conversely, Thompson et al (2003) suggest that pavement roughness should be utilised as the sole determinant of haul truck rolling resistance. The HDM-4 model (Zaabar et al, 2010a) noted a significant effect for small changes in deflection on thinly bituminous sealed pavements. As was noted in Section 2.2.4, deflection has not been included in the relation for unsealed pavements within the HDM-4 model due to difficulties measuring unsealed pavement deflections. The results from the current study lie within the (rather broad) bounds of these findings stated in the literature, and are recommended as the basis for further research. Further discussion relating the magnitude of RRC estimated by the functions above, and those included in the literature, is included in Section 5.5.8.

Although these findings have been derived from a limited set of test data, it is contended that the application of full scale testing in this study means that the outcome is quite significant. Note that the research conducted by Jamieson et al (2002) considered a single test on unsealed pavements, Thompson et al (2003) considered a total of 36 test cases with testing of a single truck. Ultimately a regression equation was derived involving RDS and truck velocity as the independent variable that was better than significant at the 0.02 level, with a coefficient of determination of 0.27. The result reported for the present study is considered similar in statistical significance to those noted above, though unfortunately there is little consistency between the experimental approaches taken by each study and therefore it is difficult to recommend which should be given precedence. As alluded to in Section 2.2.1, this is a major issue with previous research relating to the study of rolling resistance experienced by large vehicles.

### 5.5.3 Rolling Resistance and Pavement Texture

Texture and load condition do not appear to have any significant relation when considering variation in RRC. The HDM-4 model and VTI consider that large vehicles (therefore heavier wheel loads) experience greater influence from pavement texture than roughness. This is not supported by the correlation coefficients presented in Section 4.5.4.

### 5.5.4 Rolling Resistance and Road Defect Score (RDS)

Similar to texture, no relation between RDS and RRC has been able to be determined. A lower RDS appears to have successfully predicted the lowest RRC values for Section one. However, the identical RDS values for Sections two and three suggest it is not a sensitive enough measure to provide any significant finding within the current study.

### 5.5.5 Rolling Resistance and Vehicle Speed

The correlation coefficients for all data sets (Table 4.31 through Table 4.33) show a statistically significant trend between the 5m moving average roughness and MPD with RRC for a truck travelling at 15km/h in the unloaded condition. Further, a consistent and statistically significant relation is observed between IRI and RRC for each set of data for an unloaded truck travelling at 30km/h. The combination of the these findings is somewhat difficult to account for in that the significant relations found at 15km/h relate to wavelengths of shorter than 1m (MPD) and 5m, whereas the relation noted for the truck speed of 30km/h relates to a wavelength of 3m (IRI). Therefore, it does not appear that truck speed can be attributed to a change in roughness wavelength most influencing RRC for an unloaded truck.

In general it appears RRC is higher at 15km/h than 30km/h for Section one and two, whereas the opposite is observed in Section 3. As was discussed in Section 5.5.2, it is contended that roughness more significantly influences rolling resistance in the unloaded condition. Roughness, in conjunction with deflection, most significantly influences RRC in the loaded condition. Although difficult to comment on the speed dependence of either roughness or deflection, it does appear that one must result in higher rolling resistance within the bounds of the roughness and deflection values measured for Section two and three. It may be that the short wavelength roughness and texture present on Section three affected a greater energy loss through tyre

hysteresis, however pavement deflection is also significantly higher than the other sections for the loaded condition. Sandberg et al (2011) suggest a speed dependence of pavement texture with truck speed. It is possible that the haul truck energy losses are analogous to this effect in response to pavement roughness. Furthermore, note that the VTI model as reported by Hammarstrom et al (2008) considers rolling resistance due to roughness is affected by velocity, with an increase in RRC resulting from an increase in speed. The lack of research relating pavement deflection and rolling resistance makes it difficult to comment on the likelihood that this effect has occurred in the present study. Perhaps indicative of the two effects alluded to above, Jamieson et al (2002) report that an increase in loose material present at the surface of an unsealed road increased rolling resistance by 25%. The study was completed with a light truck at steady state speeds ranging from 20 to 75 km/h, no comment was made on the relative roughness effect with an increase in speed. This result is thought to correlate much closer to the estimated MPD than IRI in the context of the current study, and therefore is unlikely to represent a suitable answer to the relationship in the variation of RRC with changes in deflection and roughness, as discussed above.

It appears that a significant correlation exists between pavement deflection and RRC at a truck speed of 15km/h. As discussed in Section5.5.2, it is contended that pavement deflection significantly influences rolling resistance at a truck speed of 30km/h. The lack of any correlation identified at 15km/h may be due to the haul truck having been designed to operate most efficiently at hauling speeds, which typically vary from 30-40km/h. However, this cannot be confirmed from the data gathered for the present study.

### 5.5.6 Rolling Resistance and Payload

It is likely that the increase in tyre load, resulting from a larger applied payload, leads to a greater energy loss at the tyre/pavement interface. Rolling resistance experienced as a result of pavement deflection is more adversely impacted by the application of a greater wheel load. This is evidenced by the portion of RRC attributable to deflection significantly increasing with an increase in pavement deflection resulting from the truck being loaded. A greater range of truck payloads should be considered in future research in order to confirm this relation.

### 5.5.7 Rolling Resistance and Pavement Stiffness

A detailed discussion of RRC and pavement deflection was provided in Section 5.5.2. The following section discusses the relation between the pavement stiffness that has been estimated from the testing and RRC. Although closely related, it is important for the topic of pavement design that the two be considered separately.

Table 4.20 provides a summary of pavement structural parameters, both directly measured and back-calculated. It was ultimately concluded that the Evercalc software may not be well suited for back-calculation of pavement stiffness for the magnitude of wheel loading included in the testing for the study (see Section 5.7.3). Consequently, the significantly higher elastic modulus back-calculated for Section 2 presented in Table 4.20 is considered anomalous. Based on measured pavement curvature, it appears that pavement stiffness follows a similar trend to maximum induced deflection, which was discussed in relation to RRC previously. In making a subjective assessment based on the discussion contained within Jamieson et al (2009), it appears that Section 3 may have had limited sub-grade stiffness due to the 'flat' curvature measured (which is well illustrated in Figure 4.42). This perhaps provides some insight in to the relative influence of sub-grade stiffness, as the laboratory testing did not show the resilient modulus to vary significantly between samples taken from each pavement section (see Figure 4.58). This statement must be considered in conjunction with the fact that it ignores the relative in-situ density of the pavement layers, which were not measured as part of the study. It is recommended that any future research consider to what depth the zone of influence of a moving wheel load extends, and whether this significantly impacts the RRC experienced by haul trucks. Overall, observation of pavement stiffness values and measured pavement curvature suggests that RRC is influenced by pavement stiffness in a similar manner to pavement deflection. Pavement deflection is considered to best represent pavement stiffness within this study. As such, future research should better focus on definition of pavement stiffness rather than simply deflection, as no statistically significant correlation was found between any of the pavement stiffness measures included in the present study and RRC.

### 5.5.8 Comparison with Available Models

In considering the comparison of the RRC values and resulting regression models within the current study, the lack of consistency between test methods and regression techniques within the literature (see Section 2.7) must be remembered. Additionally, previously developed RRC regression functions for haul trucks consider the only pavement input as the RDS (Thompson et al, 2003), or have been developed with scaled-down loading (Widodo et al, 2011). Further, IRI (pavement roughness) and MPD (pavement texture) have been defined by non-standard test methods. This complication is further compounded by the fact that there isn't consistency in the methods utilised to define each property for the various models presented within the literature. Measurement of pavement deflection in all models that include deflection is defined by Benkelman beam testing. However, as discussed in Section 3.5.7, this method is not suitable for a large, rigid haul truck and in this case provides further uncertainty as to the adequacy of applying the models included in Section 3.5.8.3. Despite this, testing of the models was completed to provide insight into the comparison of measured magnitudes against past research. Further, this facilitated comment on the functions that appear to hold some promise in being able to accurately estimate haul truck rolling resistance with consideration of pavement properties.

Two models developed for haul trucks have been tested in this project. Table 4.45 presents the results of rolling resistance (RRMIN) as per Thompson et al (2011). From the results here, it is evident that the model over estimated the rolling resistance as the minimum (speed-dependent) RRC is greater than the typical values measured throughout the current project. Further, the results suggest that rolling resistance is relatively immune to changes in pavement roughness, represented by RDS in the model. It is not clear if any payload was applied to the truck during the coast-down testing completed prior to regression of the derived relations. This may not have been considered, as the relationship was developed as a means of benchmarking haul roads to understand the user costs associated with progressive deterioration of the pavement surface. Predictions via the model reported by Widodo et al (2009) are presented in Table 4.46. From these results, it is clear that this method greatly over estimated the RRC for the conditions considered, even with the adjusted RRC values resented in Table 4.44 to consider a single wheel load. This model has been derived from the terramechanics models discussed in Section 2.2.3 and involves quite detailed tyre and load-based inputs. The physical testing from which the model constants were derived did not consider

wheels of similar geometry to that in this project, but rather a small cart towed by a utility vehicle. Furthermore, the variation in contact area due to loading and the inclusion of dual-wheel assemblies should be considered. In producing the estimates in Table 4.46, the total contact area measured (see Section 4.4.3) for the dual wheel assembly was used. Therefore, it appears that at this stage the model is not suitable for predicting rolling resistance experienced by haul trucks. Additionally, it takes account of 'soft soil' effects and not pavement surface characteristics, and therefore appears it is more appropriate for estimating rolling resistance in non-compacted soil conditions. It is possible that this was the focus of the model's development, due to the conditions commonly experienced in Indonesian coal mines, however this is not stated within the literature. Comparison with commonly reported RRC values in Table 2.5 reveals that the measured values are significantly lower than that reported from previous haul road research. Kaufman et al (1977) reported a RRC of 2% for rigid, asphaltic or cement stabilised soil pavements. Other results in Table 2.5 suggest that a value of 2% may be possible with hard, smooth and well maintained pavements, although no values lower than this are reported. Therefore, the results in Table 4.44suggest that the pavements tested for the current were in a good condition, which matches the observations made during the testing. Other potential influences affecting this result are advances in tyre technology since a large portion of the available research was completed. It is possible that higher tyre inflation pressures may have been utilised during the models development. The latter is certainly plausible, with the mine operators increasing tyre pressure in order to lower the threat of punctures on haul roads in a sound condition.

The estimated RRCs utilising the roughness and speed-dependent equation presented by Cenek (1994) provide perhaps the closest fit to the measured results. Note that this model has been derived applying driving resistance, which was the same approach applied in the rolling resistance tests utilised for the current study. However, the truck used in the models development had a mechanical drivetrain, whereas the Komatsu 830E used in testing for the current investigation had an electronic drivetrain. No attempt has been made to correct for this difference. As noted in Section 4.5.7, application of Equation 3.20 shows the predicted results are generally under estimates. The 30km/h show a statistically significant correlation with the correlation coefficient exceeding 0.997 (limit for level of significance of 0.05). For clarity, Figure 5.1 is presented. As can be seen, in all but one case the model under-predicts the measured RRC.  estimate.

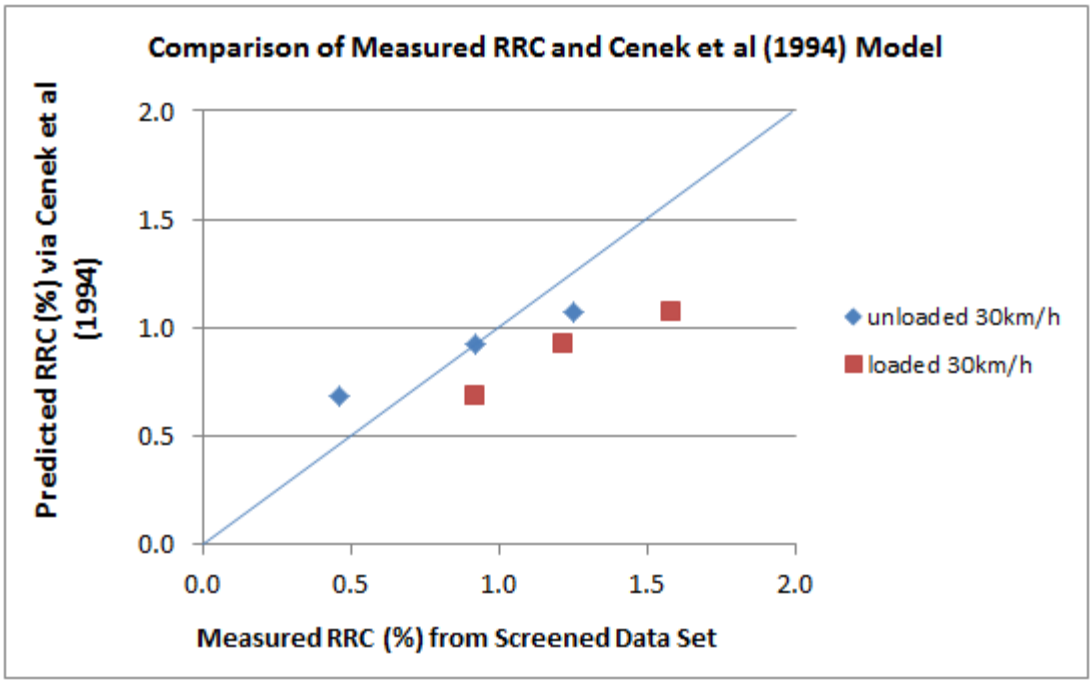


**Figure 5.1: Correlation between measured RRC and that predicted by Cenek et al (1994) model.**

Therefore, it appears that predicting rolling resistance with consideration of roughness and vehicle speed could be quite accurate, however the dependence on speed may cause significant errors in using the model for predicting RRC for the pavements tested. Research completed in New Zealand, subsequent to the derivation of the above model and taking account of pavement Benkelman beam rebound deflection, has proven inappropriate for estimating RRC for haul trucks. This is due to the coefficient applied to truck weight being excessive when applied to haul trucks and consequently resulting the large negative values presented in Table 4.49. As discussed prior, Equation 2.6 and Equation 2.7 include consideration of both rebound deflection and roughness, but were not able to be tested due to the complexity of the required inputs.

The HDM-4 model is based on the ARFCOM model, and has been validated and modified for driving conditions in many countries since being originally developed in Australia. For this project, the basis for inclusion of the model is its extensive application around the world and its ability to be adapted to specific conditions, should it show promise for the estimation of haul truck rolling resistance. Observation of the results in Table 4.50 should be made with consideration of

vehicle parameters having a negligible effect at low speeds, hence the inclusion of only a single table of results. In all cases it can be seen that these estimations are considerably lower than those that have been measured. This may be due to the fact that constants have not been defined (rather stated as being zero) for unsealed pavement texture and deflection. Consequently, the effect of texture and deflection are not accounted for and the estimated values are therefore lower than would otherwise be the case. From the discussion above, the omission of deflection is likely significant. Also note that vehicle-related constants were selected considering rigid trucks with only two axles, rather than the heavier long-haul articulated vehicles also included in the model. These two effects require further investigation, however the model has estimated RRC values with a similar order of magnitude to the measured values. It is possible that with an appropriate inclusion of texture and deflection, this model could provide some benefit in estimating haul truck rolling resistance.

Discussion of the models developed in Europe (ECRPD and VETO) is combined, as the models are very similar with modification to magnitude of constants. The ECRPD model was developed from testing with a 27 tonne truck, with the final results including transmission and drivetrain losses, thus producing driving resistance estimates. This is a potential inaccuracy; however it is not apparent how transmission losses are influenced by the Komatsu 830 haul truck used for testing in this project having an electronic drivetrain and being powered by electric wheel-hub motors, as discussed above. Sandberg et al (2011), in presenting the ECRPD model states that trucks are more sensitive to roughness than texture, with velocity significantly impacting response to both. The velocities in this study appear too low to have a significant effect. However, the estimated RRC values are more significantly impacted by texture, likely due to the fact that only sealed pavements were considered in the model's derivation. The reverse may have been true if the velocity had been able to be increased to highway speeds in the current study, for which the model was derived. Obviously, this is not possible due to the limitations of the vehicle used in the testing. Furthermore, the measured texture depths are likely significantly higher than with the pavements considered in the derivation of the model. Accordingly, estimates are of the correct order of magnitude, but lower than the measured values in all cases. The VETO model estimates even lower values as the velocity dependence for roughness has been removed and the constants reduced. For this reason, it is concluded that the ECRPD model provides a greater promise for use in estimating haul road rolling resistance. However, the lack of the

inclusion of a term to capture the effect of pavement structure in either model means that it appears to hold less promise than that of other models discussed above.

In all cases, it must be noted that all models estimate RRC highest for Section 1 and lowest for Section 3. This is due to the fact that the sections have been found to have consistent relative magnitudes of roughness, texture and deflection. If one of the available models was to have captured all pavement properties simultaneously, it may have provided some further insight into the relative effect of each. Therefore, it is recommended that, of the models tested in this study, the HDM-4 model be investigated in future research.

## 5.6 Fuel Consumption

Fuel consumption estimates have been derived for this study through application of a mechanistic model (HDM-4) and a simplified energy-mass balance model. In both instances, in-built functions used to predict the rolling resistance generated due to pavement condition have been replaced with the RRC from the screened data set. This data set has been applied, as both models include allowances for inefficiencies and auxiliary power requirements. The HDM-4 model does this in a more direct manner through consideration of engine speed and maximum power output. The Department of Resources model applies factors to the power required to overcome grade, air and rolling resistance to allow for inefficiencies and accessory power requirements. It should be noted that the HDM-4 model has not been developed with consideration of haul trucks, and consequently results are taken from extrapolations. This provided the impetus for the attempted validation with a model that has been developed specifically for haul trucks (the Department of Resources model).

As shown in Table 4.53, the HDM-4 model predicts a significant increase in IFC with addition of a payload to the truck. For the RRC values measured in the current study, the model estimates a 67% increase in IFC with the addition of load at 15km/h and a 111% increase at 30km/h. This occurs due to a larger truck mass being applied to the higher RRC values for the loaded truck case. Tan et al (2011) state a relation between changes in rolling resistance to fuel consumption of 3:1 for cars and 4:1 for trucks. The modelling completed for this study suggest a ratio of 1.9:1 results for an unloaded haul truck and 1.3:1 for a loaded truck. This has been

determined from the equation resulting from least-square regression between the RRC and estimated IFC at 30km/h. Therefore, from this result it appears that haul trucks may be more sensitive to changes in rolling resistance than highway vehicles. Further discussion on this topic is contained below.

The Department of Resources model predicts a 183% increase in IFC with the addition of payload at 15km/h and a 258% increase at 30km/h. As this model is linear, and grade and air resistance are considered consistent throughout, any change in RRC results in an equivalent change in IFC. For this reason, further comment on the sensitivity of haul trucks to change in RRC and IFC is not possible from this model's results.

Figure 4.49 shows that a least-square regression between the two models results in a coefficient of determination exceeding 0.99. The coefficient of correlation between the two sets of data is approximately 0.998, which is significant at the 0.05 level. Although this suggests the models are equivalent in predicting changes in IFC with input of RRC, note that for the unloaded case, the HDM-4 model predicts an IFC that is on average 54% higher than the Department of Resources model for the unloaded truck case. The reverse is true for the loaded case, with the Department of Resources predicting an average 9% higher IFC. This difference is attributable to the allowances for mechanical losses and accessory power made by the HDM-4 model, as discussed above. The estimated auxiliary power requirements and mechanical inefficiencies represent a greater portion of power requirements when the RRC is lower (i.e. the unloaded case). At operational speeds (30km/h) it appears the models are quite similar, and consequently it appears general conclusions can be drawn for the results for the IFC values estimated with a truck speed of 30km/h.

Therefore, it appears that haul truck fuel consumption is quite sensitive to the addition of load. In addition, haul truck IFC appears more sensitive to changes in RRC than for cars and commercial trucks. From the discussion in Section 5.5.2, it is clear that rolling resistance experienced by a haul truck at 30km/h appears equally influenced by pavement roughness and deflection, with the latter providing significantly greater influence for the loaded condition compared to the unloaded condition. As a result, it is recommended that haul road pavement design, construction and maintenance include consideration of pavement stiffness in addition to the generation of pavement roughness.

The fuel consumption model, particularly the HDM-4, require calibration for large haul trucks. The Department of Resources model's assumptions relating to

mechanical inefficiencies should also be confirmed. It is recommended that future studies include calibration of such models, preferably in conjunction with the measurement of RRC. This represents the practical link between an understanding of haul truck rolling resistance and a mine owner's profits.

## 5.7 Laboratory Testing

Laboratory testing was focussed on defining strength and stiffness characterisation of the sampled materials to allow comparison of modelled and measured deflections from in-situ testing. Only PSD testing was completed with regard to index testing. Despite this, sufficient information was gathered to allow assessment as per AS 1726. Section 1 and Section 3 were classified as well to poorly graded silty gravel and Section 2 as a sandy gravel. A more detailed discussion of each laboratory test is presented below.

### 5.7.1 Particle Size Distribution

PSD results have been compared to the MRWA recommended grading envelope for lateritic gravels for use within base-course layers in semi-arid and arid areas of Western Australia (MRWA, 2003). Such climatic conditions occur at the majority of mine sites within the state and around Australia. This specification has been developed for pavements intended to be sealed by thin sprayed bituminous wearing courses. Although haul roads are generally unsealed, this specification does represent gravel material that has been observed to present acceptable performance within unbound granular pavements. Table 4.55 suggests the materials are well or poorly graded gravels. Sections 2 and 3 are not sufficiently uniform in grading to be classified as well-graded gravels, as indicated by a coefficient of curvature value below the minimum of one (MRWA, 2003). When assessing the materials in accordance with MRWA selection guidance, the materials were found to be deficient in fines as indicated by the low dust ratio values. All samples included particles in excess of the recommended 37.5mm maximum.

Selection criteria for gravel materials proposed for wearing courses on unsealed pavements generally relate to Atterberg limits, in combination with PSD and specifically fines content. The laboratory testing regime for this project involved a finite quantity of sampled material for testing, with strength and stiffness testing

being prioritised. Subsequently, Atterberg limit tests have not been carried out. Furthermore, this project is focussed on exploration of structural design techniques, and therefore, comment on the suitability of sampled materials for functional pavement performance is beyond the scope of this study.

### 5.7.2 Shear Parameters

Table 4.59 summarises the Mohr-Coloumb shear envelopes for the three materials tested. Figure 4.68 through Figure 4.70 show the Mohr's circle of stress resulting from testing of the samples from each pavement section. It can be seen that the materials present relatively consistent properties, however note that the result for Section 1 should be taken as indicative only, as it is based solely on two stages of tri-axial testing. This was due to the load ring, responsible for measuring the deviatoric force, needing to be replaced and possibly having produced inaccurate results for the first stage of the test. Unfortunately, in an effort to ensure the sample was preserved so that multi-stage testing was successful, the highest confining pressure of 300 kPa was completed first for this sample. It is suspected that the stress history then impacted the results of the testing completed at 100kPa and 200kPa confining pressures. Despite this complication it appears adequate to estimate the shear parameters for Section 1 from the analysis of the two stages that were completed successfully, and based on the similarity with results for the other two sections.

The shear parameters found for these materials suggests they are relatively strong. Austroads do not provide guidance on potential shear parameters for pavement materials within the Guide to Pavement Technology. Presumptive values in an Austroads research paper (Gonzalez et al, 2012) show that based on the internal angle of friction the materials fall between high quality sub-grade material and low quality sub-base material. The South African Pavement Engineering Manual (The South African National Roads Agency, 2013) contains similar guidance on presumptive material parameters. Assessment for compliance to these guidelines provides a similar characterisation of the materials encountered. The materials within this project present a very high value of apparent cohesion, especially considering the materials were not typically dried-back for tri-axial testing (moisture ratios typically in excess of 90% OMC) and thus negative pore pressures within each sample should have been relatively low. The exception to this is the sample from Section 1, which as discussed in Section 3.8.2 was removed from the cell after

the first stage of testing and sealed and stored for approximately four weeks. However, the internal angle of friction characterises the materials as being, at best, analogous to select ferricrete sub-grade. This discussion compares the materials sampled for the project to the national pavement specifications of the South African National Roads Agency and presumptive values published by Austroads. It should not be considered an assessment of the suitability of the materials for use in mine haul road pavements. Rather, it characterises them as typical gravel materials which are, in general, unsuitable for use in base-course layers within sealed roads in Australia and South Africa.

### 5.7.3 Elastic Modulus of Pavement Materials

The pavement and material elastic moduli was tested via three means; back-calculation of deflection/curvature data measured from static wheel loads, multi-stage tri-axial testing and RLTT testing. All methods were described previously in Section 3.8. Discussion of the elastic modulus results from each has been combined below, including a comparison of results derived by each method to provide explanation of the values used within pavement modelling and analysis.

Calculation methods as described in Section 3.9.1.1 have been included to provide insight into the applicability of a simple, and commonly applied, methodology for estimating elastic settlements under shallow footings. This method calculates elastic moduli values similar to the secant modulus (to plastic failure) values contained within Table 4.61. Note that this method considers the pavement and foundation as a single isotropic mass with no allowance for non-linear soil behaviour. This suggests that such values may be appropriate for long-term loading, which is unlikely to be required for haul road pavement design. Section 1 is calculated to have the highest elastic modulus value. This result is contrary to the discussion below relating to laboratory testing with monotonic or static loading. Further, it helps to describe the need for more detailed analysis taking account of pavement surface curvature.

Results from back-analysis of measured deflection bowls with Evercalc software suggest that curvature has a profound effect on the estimation of elastic modulus values. Section 3, with wide and relatively deep deflection bowls, presents the lowest elastic modulus values. Back-analysis of Section 2 (in the case of the truck being subject to a payload) was not possible due to the steep curvature close to the centre of the contact area. The calculation was repeated allowing modulus values as

high as 2000 MPa but a convergence to a solution was not possible. Accordingly, the elastic modulus is stated as greater than 1000 MPa, as it is recommended by Austroads in Gonzalez et al (2012) as the maximum presumptive value for unbound granular material. Discussion of values recommended by Australian road authorities is included below, which suggests this value is well outside that used for commercial pavement designs. Further, comparison with moduli values derived through laboratory testing suggests that these results may be anomalous.

Some uncertainties in relation to the use of Evercalc for back-analysis do exist, especially with regard to inputting such large wheel loads. As discussed within Section 3.9.1.2, modulus values have been calculated with curvature considered to commence from the edge of the equivalent radius of the contact patch (representing a circular contact patch equal in area to the measured contact patch) and also from the centre of the load. The back-calculated moduli values from the edge of the load were found to be exceptionally high and suggest that the Evercalc software may not be appropriate for determination of pavement modulus for the wheel load and pavement type considered. This is further supported by the relatively high RMS values reported for all results, especially in the case of the curvature commencing at the edge of the loaded area. However, in the absence of a specific program being available for back-analysis of pavement deflection with large, static wheel loads, Evercalc has been considered the best available means for analysis of in-situ test data. Furthermore, the in-situ density of the pavements that were subject to deflection testing is unknown. Measurement of this property would have required large water or sand replacement tests, which was judged to be too time consuming within the tight timeframe applied to the project's in-situ testing regime. Such tests would have only extended to less than a metre depth, and so would have provided only a small amount of additional data.

Tri-axial testing commonly used to determine soil elastic moduli employs a constant vertical strain rate and is repeated over several stages, each with a varied confining pressure. As soils exhibit stress-dependent behaviour, a unique stress-strain curve results for each stage of testing. Elastic modulus results from the tri-axial tests (monotonic loading) have shown to be significantly lower than that calculated through back-analysis (static loading). Several explanations are possible, the first being the difference in the load rate employed by the two tests. Furthermore, the result may be related to the level of strain and best explained by observation of both the relative geometry of a tri-axial sample (200mm deep) and the layer thickness designated within back-analysis of pavement curvature data (2m). A 4mm

deflection, if considered consistent throughout a 2m layer considered in Evercalc represents a strain of only 0.2%. Plastic yield, the point used to define tangent elastic modulus from tri-axial testing, can be observed to occur at much larger strains for all tests in Section 3.8.2, and therefore it is reasonable to expect relatively lower elastic modulus estimates. Separating the base-course layer into multiple, thinner layers within the back-analysis may remedy this issue. Unfortunately this was not found to assist in the back-calculation of pavement elastic modulus. Another limitation of the method is that a maximum of only four layers are able to be included in back-calculations completed by the Evercalc software. Consequently, preference was given to better defining soil conditions at depth by employing three layers of sub-grade, as the analysis was observed to be significantly influenced by the pavement foundation structure.

The Section 2 sample had a relatively low elastic modulus determined through tri-axial testing. This may be explained by its low sample relative density of only 86% MDD. It is expected a higher modulus value would have resulted if density was equal to that of the samples tested for the other sections (95-100% MDD). Testing of Section 1 with 300 kPa confining pressure is somewhat anomalous. For this stage of the test a different load ring was utilised for measurement of deviatoric load. As explained previously, following completion of this stage, the sample was removed, sealed and stored for the subsequent testing stages with confining pressures of 100 kPa and 200 kPa. Yield was observed at a higher strain for the 200 kPa confining stress stage, which may be explained by the stress-history effects on the sample and also potential moisture changes. The former is expected to have had a greater influence.

Resilient modulus values found through RLTT testing shows modulus under cyclic loading to be higher than that under static loading. Results between the three sections tested were relatively consistent, with Section 1 having the highest resilient modulus of 441 MPa at a mean normal stress corresponding to deviatoric stress of 890 kPa. Austroads (Jameson, 2008) recommend presumptive values of 150-400 MPa for base quality gravels under thin bituminous surfacing. MRWA advise that moduli shall not exceed these presumptive values, but also state that the maximum mean normal stress to be considered acting on the top sub-layer of granular base-course should not exceed 240 kPa. This emphasises that the higher stress state being considered within unbound granular haul road pavement base-courses should indeed have a significant effect on the design resilient modulus value. If resilient modulus values were taken at 240 kPa mean normal stress results would have been

376, 302 and 277 MPa for Sections 1, 2 and 3 respectively. Although the maximum presumptive value provided by Austroads would no longer be exceeded, it is clear the materials tested are relatively stiff. Therefore it is considered that the 400 MPa upper bound value may be unnecessarily restrictive to haul road pavement analysis, but the maximum mean normal stress should be considered (influenced by wheel contact stress) in selecting maximum values used for haul road pavement design.

The resilient modulus result for Section 2 is likely influenced by a low relative density of 86% MDD. However, the sample had also dried back to 58% OMC. Such an effect, as described in Section 2.5, is likely to increase modulus values and thus the effects of low density may be offset. This result suggests that compaction of similar materials may not be critical for pavement performance if they are allowed to operate in dry conditions.

Back-analysis via Evercalc software has produced the highest elastic modulus results of any method. Tri-axial testing consistently produced the lowest results, with RLTT testing predicting resilient modulus values 1.32 to 1.63 times larger. Note that the confining pressure in the upper pavement layer was likely between the two modified stress regimes used in RLTT testing of 30 to 40 kPa and 150kPa, with deviatoric stress ranging from 500 to 900 kPa. This has meant that some interpolation of results has been used to predict the resilient modulus for the confining stresses shown in Table 4.57. These stress states have been inferred via linear interpolation of tri-axial results in Table 4.60, for a deviatoric stress of 890 kPa. The above assumes that pavement response in all cases is purely elastic. Figure 4.62 through Figure 4.64 suggest that there is an accumulation of permanent strain and therefore an assumption of purely elastic response is perhaps inaccurate. If Table 4.60 and Table 4.61 are compared, it is clear that elastic moduli taken at the failure point are substantially lower. However, consider that this point is that of shear failure, which was not observed at any time during in-situ testing. Ultimately the understanding of unbound granular material permanent deformation and how it relates to changing resilient modulus values is still the subject of ongoing research, as described in Section 2.6.5.

From the various results for elastic modulus, it appears that the resilient modulus values are more appropriate for pavement design in areas of free traffic flow or where intended haulage operating speeds are achieved in the majority of cases. Tri-axial elastic modulus (monotonic loading and tangent modulus to yield) values therefore appear more appropriate for areas of slow moving and stopped vehicles,

such as hard-standings and parking areas. A conservative design approach may be to utilise the tri-axial elastic moduli values for all areas. However, consider that higher values resulted from the back-analysis of deflections resulting from a static load, and therefore in-situ pavement performance (in terms of the elastic modulus mobilised) may be superior to that predicted from the results of laboratory testing. This topic requires further investigation, preferably incorporating pavement moisture variations. Ultimately, such a decision should include consideration of a dynamic load factor to account for vertical body accelerations of haul trucks traversing rough surfaces. Such consideration is beyond the scope of this study.

### 5.7.4 Permanent Deformation Behaviour in Repeated Load Triaxial Testing

Some discussion of the permanent deformation results found through laboratory testing (Section 4.7.4.2) should be included. Considerable accumulation of strain can be observed from approximately sequence 55 of testing (Austroads test method AG:PT/T053). Sequence 57 to 65 in the RLTT test include the only instances of stress ratios (deviatoric:confining stress) that exceed 2.5. Additional deformation from sequence 66 through 72 include the additional stress states added to reflect the large deviatoric stresses present under a haul truck, with a maximum stress ratio of approximately 2. These results suggest that yielding of the material is likely at a stress ratio of 2.5, with subsequent loading resulting in accumulated strain. Sequence 55 involves a confining mean normal stress of 120kPa and a deviatoric (and shear) stress of 300kPa. Due to the consistency of shear parameters found for the three sections, a shear strength of 405kPa results for this stress state. Therefore a shear stress approximately 74% of failure is applied at sequence 55. In the context of the shakedown theory discussed in Section 2.6.5.2, it appears that Range 2 response (plastic creep shakedown, see Figure 2.36) occurs with stress ratios below 2.5 and/or where materials experience a shear stress less than 74% of their yield. The amount of data collected in this study is insufficient to provide further comment on design employing stress ratios or the shakedown theory. It is recommended that it be further investigated in the future.

## 5.8 Pavement Numerical Modelling and Design

The ability of each pavement analysis method to predict the measured response of the haul roads tested in this study is presented in the following. This includes some

discussion of the back-calculation technique employed by the Evercalc software. Secondly, a comparison of the pavement lifetime estimated by each method is made.

### 5.8.1 Back-Calculation of Pavement Modulus

A discussion of the back-calculation of base-course modulus values is contained within Section 5.7.3. This section focusses on the impact of modelling with the modulus values determined. From this discussion, and comparison with laboratory measured values, it appears that the two back-calculation methods provide the upper and lower bound values of base-course modulus. The hand-calculation method provides the lowest estimate in all cases (unloaded/loaded truck for each pavement section). Equation 3.29 is essentially a simplified displacement calculation of the linear-elastic axisymmetric solution presented in Section 2.5.1, which is similar to the technique employed by CIRCLY and HIPAVE. It has been derived from consideration of a semi-infinite, homogenous, isotropic and elastic mass. However, it also relies on influence factors that have been calculated to allow different loading geometries, whereas both CIRCLY and HIPAVE assume circular loading due to the assumption of axisymmetric conditions. It is thought this is the main source of difference, as it can be seen from the results that CIRCLY and HIPAVE also under estimate pavement deflection, which is exacerbated for section three, which has the lowest pavement stiffness.

The use of Evercalc software for the back-calculation of haul road pavement base-course modulus appears inappropriate. Stiffness values predicted by this software typically have resulted in significant under estimates of pavement deflection in the case of a loaded truck. For the unloaded case, base-course modulus results more closely reflect those measured in the laboratory, which suggests the method is better able to consider the wheel loads present in this analysis (41 tonne for a single dual-wheel gear, as considered in the back-analysis). Adoption of a presumptive maximum modulus value appears justified, as the deflection predicted by all methods employing the 1000 MPa maximum value noted in Table 4.64 and Table 4.65 produce gross under estimates of pavement deflection. As discussed above, this value is also noted by Austroads (Gonzalez et al, 2012) as a maximum elastic modulus for unbound granular materials and is therefore recommended to be adopted for haul road design, until more specific research on this parameter is completed.

### 5.8.2 Comparison of Axisymmetric Modelling

Observation of Figure 4.71 and Figure 4.72 suggest that only minor differences result in the predicted deflection profile generated by linear-elastic and FEA modelling, with all inputs held constant. FEA typically predicts a slightly lower deflection at the centre of the wheel load contact area, a trend that in most instances continues to a radius of three metres. Further, it does not appear that the relationship is significantly influenced by base-course modulus. Other than the maximum deflection, the most notable difference in the CIRCLY, HIPAVE and ABAQUS deflected profiles is the deflection at a radius of three metres when the base-course is characterised with the resilient modulus. It is thought that this difference is coincidental and is not indicative of any known difference between the two solution methods.

There are a few possible explanations for the lower pavement deflection calculated by the FEA analysis. Firstly, the FEA model has been reduced in size by assuming a roller boundary condition on the faces sectioning the wheel load. No radial displacement occurs along these faces. Concurrently, it appears that the two methods treat Poisson's ratio differently. CIRCLY and HIPAVE apply Poisson's ratio as presented in Section 2.5.1, whereby pavement strain is calculated with direct input of Poisson's ratio. As is discussed further in Section 5.8.3, the horizontal stress state appears to be more influenced by the anisotropic ratio adopted. FEA calculates the stress state of each element via first calculating the nodal displacements within the selected mesh (that is for each individual element). It is thought that a combination of these two differences provide the explanation for the variation between the two methods. Due to the lateral restraint provided in the FEA analysis, the base-course and sub-grade materials appear to be artificially stiffened, which ultimately reduces the deflection predicted.

Figure 4.71 and Figure 4.72 also provide confirmation that CIRCLY and HIPAVE produce identical results with all analysis inputs constant. Although this is evident from the user and theory manuals published by the software developer, it was thought important to highlight this result, as CIRCLY is used to complete cross-anisotropic modelling in the remainder of the discussion. All HIPAVE modelling employs an isotropic base-course characterisation.

The above results relating to prediction of surface deflection, suggests that linear-elastic modelling could result in conservative design. This will be discussed further below.

### 5.8.3 Comparison of Isotropic and Anisotropic Base-Course Characterisation

Observation of the results in Section 4.8.4 show that the assumption of the pavement base-course as cross-anisotropic leads to greater calculated deflections than with an isotropic characterisation. The predicted curvature beyond one metre from the load centre, which is approximately equivalent to twice the tyre contact radii, are in close agreement. It is contended that in the case of CIRCLY, the cross-anisotropic ratio of two (vertical modulus:horizontal modulus) results in less horizontal stress being transmitted radially from the load. This is evidenced by Figure 4.75 and Figure 4.76, which manifests in CIRCLY predicting shorter pavement lifetimes than HIPAVE in Table 4.91. However, this effect is isolated to the area of pavement near the application of the wheel load. In general, CIRCLY has been shown to under estimate deflection (see Section 4.8.5.2). Further, observation of the results in Section 4.8.7 suggest the measured curvature appears more pronounced near to the wheel load. Such a deflected profile is more evident in modelling utilising a cross-anisotropic base-course material, as in Section 4.8.4. For these reasons, cross-anisotropic base-course characterisation was adopted throughout the remainder of analysis completed by CIRCLY.

### 5.8.4 Deflection and Curvature Estimates

The discussion in Section 5.5.2 suggests that an ability to model haul road pavement structural response is an important factor in determining end-user costs. This is relevant for rolling resistance derived from both pavement roughness and deflection. Roughness is considered to develop as a consequence of structural failure within the theories currently employed, where the critical response is the level of vertical compressive strain at the top of the sub-grade. Calculation of this parameter requires a detailed understanding of response due to loading geometry and material properties. Deflection is dictated by the elastic stiffness of the pavement structure, which is determined by pavement structural analysis. The pavement modelling results discussed in the following section is therefore the practical manifestation of the findings of the study relating to rolling resistance. It is intended that the recommendations arising from this area of the study assist a pavement designer in optimising haul road user costs.

Deflection estimates have been produced via elastic theory, as described in Pereira (1977). This is the method that was used to calculate deflections within the original

derivation of CBR design curves for heavy wheel loads. Subsequent to this analysis, computer software developed by Mincad Systems (CIRCLY and HIPAVE) for mechanistic-empirical and industrial pavement design were trialled. Finally, Finite Element Analysis via ABAQUS CAE 6.10 (Dessault Systemes) was undertaken. There is a degree of consistency observed between the various methods, which is supported by the variances from measured values presented in Section 4.8.

#### 5.8.4.1 Elastic Theory as per US Army Corps

Several adapted variations of the theory presented by Pereira (1977) for estimation of pavement surface deflections have been trialled. Equation 3.30, applies the maximum deflection factor with consideration of all wheels ($F_M$) present on the haul truck. This has been found to better estimate deflections than Equation 3.31. The latter employs the maximum deflection factor for a single wheel load ($F_e$). The ratio between each factor ($F_M/F_e$) was utilised in determining the ESWL. It can be seen in Table 4.67 and Table 4.69 that the maximum deflection factor for multiple wheels is very similar to that for a single wheel when considering the unladen truck, with the ratio increasing to approximately 1.5 for a laden truck. This suggests that wheel interaction occurs when the truck is loaded but is not significant when unladen. Wheel interaction is further discussed in Section 5.8.4.4. The best overall deflection estimates occurred with the dual-wheel assemblies modelled as a single wheel load; with the net area of the two wheel contact areas utilised in conjunction with the pressure arising from a known wheel gear load. This approach has not been suggested by Pereira (1977) and therefore its application in design is not well understood, however it is proposed that more accurate design pavement thicknesses may result. Based on the preceding discussion, it is recommended that the sub-grade failure theory employed by the S77-1 curve be better understood before being superseded by design curves derived utilising only single wheel gears. This recommendation has implications for mechanistic-empirical design utilising the sub-grade failure theory derived from the S77-1 curve by Wardle et al (2001), as discussed in Section 2.5.3. It is recommended by Wardle et al (2007) that for design purposes single wheel gears are modelled, with a check for interaction by also modelling multiple wheel gears.

Despite the above discussion, it should be noted that deflection estimates are relatively poor when wheels on the same gear are considered separately in the model detailed by Pereira (1977). For example, it can be seen in Table 4.71 that a

variance of 41% occurs when analysis was completed with 'average contact pressures' and all six wheels were accounted for separately. This is the approach suggested for use in determination of design CBR curves (Pereira, 1977). Note that the 'average pressures' (known wheel load divided by measured contact area) fall within the range of inflation pressures suggested by tyre manufacturers for a 40.00R57 tyre.

It is clear from observation of Table 4.66 and Table 4.67 that deflection is significantly over estimated when applying inflation pressure as the tyre contact pressure. An extremely high inflation pressure was utilised for the site deflection measurements in this project (890 kPa), which even exceeds the maximum recommended by tyre manufacturers (goodyearotr.com). This inflation pressure has been adopted for haul trucks site wide and was not able to be modified for this study. As may be expected, the contact area was also found to be less than that stated by tyre manufacturers (goodyearotr.com). It appears that in order to replicate the deflections measured in this study, reduction factors of 2/3 for unladen situations and 4/5 for laden cases should be applied to inflation pressures. Currently, the impact of the pressure distribution profile on pavement response is not well understood. From the results of this study, it appears accurate representation of the contact pressure profile may be critical to pavement analysis including large off-the-road- tyres, as alluded to by Austroads (Jameson, 2008).

#### 5.8.4.2 Linear-elastic Modelling

Initial linear-elastic modelling was completed within CIRCLY, with an infinite sub-grade depth (Table 4.77 and Table 4.78), so that comparison can be made with a sub-grade depth of 3m (Table 4.79 and Table 4.80). The shallower sub-grade depth can be observed to result in significantly increased deflections. It appears that the higher deflection values better reflect the measured values (see Table 4.79 and Table 4.80). Additionally, HIPAVE results presented in Table 4.73 and Table 4.74 relate to a 3m deep sub-grade and isotropic base-course characterisation. As suggested in the discussion above, the HIPAVE produces greater under estimates of the measured deflections than CIRCLY. This appears to be attributable to the isotropic characterisation of the base-course. Further, Table 4.72 shows lower variance for modelling completed by CIRCLY with a cross-anisotropic base-course, while the correlation coefficients are similar. Therefore, it is recommended cross-

anisotropic base-course characterisation for linear-elastic modelling be further considered. Such a discussion is contained within Section 5.8.6 and Section 5.9.

Table 4.75 and Table 4.76 present the HIPAVE calculated deflections with the base-course idealised as nonlinear via the Barker-Brabston sub-layering method (see Section 2.6.1). It is evident that the use of base-course materials in the Barker-Brabston model leads to under estimates of deflection, for an unloaded and loaded truck. The use of Barker-Brabston sub-base material produced a reasonable estimate for deflections observed at Section one. This is intuitive as the maximum elastic modulus for Barker-Brabston sub-base materials is 275MPa (White, 2007), which is similar to the elastic modulus of the material sampled from Section one. Due to the significant depth of base-course (2m), the maximum modulus value will be utilised to characterise a significant portion of the pavement. The use of either Barker-Brabston material classes appears to result in under design of the haul roads constructed, where materials similar to those comprising the pavement sections in this study are used.

Single wheel gear modelling has been included in the analysis with a summary of the results presented in Table 4.72. The basis for the inclusion of this analysis is the recommendation by Wardle et al (2003) that modelling include only a single wheel gear, as discussed in Section 2.4.2.1. A large average variance between measured and estimated deflections is evident in Table 4.72 within the HIPAVE analysis with all wheel loads included. This result suggests modelling only single wheel loads may be inappropriate, with the potential to produce under-design. Further discussion of wheel interaction is contained in Section 5.8.4.4.

For the reasons discussed above, the remainder of linear-elastic modelling was completed within CIRCLY, applying a 3m deep sub-grade and cross-anisotropic base-course characterisation.

The curvature results presented in Section 4.8.7 suggest that CIRCLY generally produced under estimates of the measured deflection profiles. This is most pronounced in the prediction of the deflected profile along the rear axle, where significant under-estimations of both maximum deflection and slope of curvature can be observed. It is contended that this is mostly due to the consideration of wheel interaction through the use of super-position within linear-elastic modelling. Section 4.8.8 includes a detailed discussion on this topic. Another potential reason for the underestimates produced by CIRCLY is the lack of material nonlinearity, whereby the increased stress state due to interaction does not result in additional strain being

calculated within the pavement between wheel loads. It appears from the estimates of deflection and curvature produced by linear-elastic solutions that wheel interaction may be critical for modelling of haul roads, and therefore it may be more appropriate to utilise more advanced numerical analysis methods.

#### 5.8.4.3 Finite Element Analysis

It is clear from observation of Table 4.87 and Table 4.88 that plane strain idealisation results in poor deflection estimates, as reported by Ghadimi et al (2013). Therefore, it is recommended that the plane strain models are not utilised for design purposes, including for the estimation of pavement life.

Note that the mesh size adopted throughout the study appears to have negligible impact on the results. Table 4.89 shows that a reduction of the typical mesh size from 1m to 0.25m had a minimal impact on the predicted surface deflections. The 0.25m mesh size was the maximum size applied near the load centre throughout all FEA analysis. The comparison of a 0.25m and 1m dimension refers to the maximum mesh size at any point in the model. Consequently, in order to maintain reasonable calculation times, a typical mesh size of 1m was adopted.

Three-dimensional FEA produced the most accurate pavement surface deflection estimates of any method trialled. Table 4.89 shows accurate estimates for three-dimensional modelling, including wheel loads of an unladen and laden haul truck. The three-dimensional modelling was completed with the benefit of the iterative procedure described in Section 3.9.4 to determine an optimised sub-grade layer structure. Observation of Table 4.89 reveals that a simplified sub-grade structure (resilient modulus of 150MPa throughout) results in relatively less accurate deflection estimates. Perhaps more significantly, these results reveal that the sub-grade structure significantly influences the pavement response. This is predicated on the greater variation of deflection estimates than observed for the modelling discussed above, with a sub-grade structure determined iteratively to take account of stress-dependent effects. These estimates are of greater accuracy (average variance of 20.4%) than the corresponding estimates derived with CIRCLY and HIPAVE (average variance of 25% in Table 4.72), where the static elastic modulus was utilised, which was noted above to produce the most accurate deflection predictions. The average variance for deflections predicted through FEA within Table 4.89 is 17.2%. As a result, it appears that sub-grade structure is influential to

the prediction of haul road pavement response and that FEA is better able to include this effect.

In addition to calculating pavement deflection with much greater accuracy, nonlinear FEA was also able to produce much closer estimates of pavement curvature in comparison to linear-elastic methods. This is evidenced by the deflection profiles presented in Section 4.8.7. It is thought likely that the superior ability of FEA to predict deflected surface profiles, should result in superior estimations of critical pavement response, specifically sub-grade strain. Of note is the closeness of fit between the measured deflection profiles along the rear axle measured and predicted by FEA. From observation of these results, it is contended that the nonlinear FEA has been able to best address the issue of wheel interaction.

One issue that needs to be considered is that material nonlinearity was completed by an iterative process external to the numerical solution method described in Section 2.5.2. AS described in Section 2.5.2, such a model is generally included in the constitutive matrix. This simplification provided benefits in terms of calculation time, however it does mean that the material may not be truly represented in a nonlinear manner. Rather the maximum induced vertical stress state within each sub-grade layer was used to determine the resilient modulus of the layer in the subsequent iteration of the analysis. The relative impact of this approach in comparison to inclusion of a nonlinear constitutive material model is not known. However, it has been shown to produce the best estimates of pavement deflection and curvature in this study. As a result, it is recommended that future investigations further apply nonlinear modelling to haul road pavement analysis.

FEA modelling utilised resilient modulus instead of the elastic modulus values (derived through monotonic tri-axial testing), which were adopted for the other analysis methods discussed above. This appears to have resulted in quite close estimates of the measured pavement response, and therefore is recommended for future investigations of haul roads. Secondly, the use of resilient modulus should produce the most representative critical pavement response for the prediction of pavement life, as it considers transient loads. Where different analysis methods are utilised, other methods for the definition of elastic modulus should be considered, however validation should be made with comparison to measured pavement responses.

#### 5.8.4.4 Modelling of Wheel Load Interaction

As alluded to in the above sections, it appears that wheel load interaction is a key issue in the modelling of haul road pavement response. Deflections via linear-elastic methods typically result in under estimates, whereas nonlinear FEA modelling predictions closely reflect the measured. The main difference arises from the assumption the theory of superposition being suitable to consider load interaction in (axisymmetric) linear-elastic. All reasons for this will be discussed in the following.

The modelling included within the US Army Corps of Engineers method (Pereira, 1977) implies that wheel interactions do occur and may lead to critical strains occurring at depth between adjacent wheel gears. It is inherent within the method adopted to calculate ESWL that deflection from all other wheels fitted to the design vehicle are added to estimate the maximum deflection. This value is then used to calculate the equivalent single wheel load (ESWL) that would produce the estimated maximum deflection. This is quite a significant effect and means that in order to maintain the original pavement model, CBR design curves should not be generated with only a single wheel gear. Rather all wheels present on a haul truck should be included. Further, inclusion of only a single gear would serve to decrease the required cover thickness for a given CBR, as the ESWL calculated with depth would be decreased.

Figure 4.89 presents a comparison of surface deflected profile and sub-grade vertical compressive strain predicted by HIPAVE with half (‘Single Wheel Gear’) and all (‘Rear Axle’) of a Komatsu 830E rear axle included in the modelling. It shows that although surface deflection is approximately doubled at mid-axle (Distance from Truck Centreline=0) with both wheel-gears included, the sub-grade strain remains unaffected. Therefore, in the instance of the pavement modelled (section 1 with the base-course characterised by the static elastic modulus), the predicted pavement lifetime would be unaffected by wheel interaction. The HIPAVE modelling is identical to that of CIRCLY, except the base–course is characterised as isotropic. The above modelling was then repeated with a cross-anisotropic base-course in CIRCLY (all other parameters were the same), with the results presented in Figure 4.90. Again, the pavement surface deflection can be seen to approximately double. However, sub-grade strain can be seen to also double in this case. Consequently, this result may suggest that the inclusion of cross-anisotropy could be critical to the modelling of wheel load interaction within linear-elastic modelling. This further supports the discussion in Section 5.8.3 and is expanded in Section 5.9. Although a significant finding, note that CIRCLY has typically significantly under estimated both measured

deflection and curvature. Additionally, when comparing Figure 4.89 and Figure 4.90 it is evident that the critical (design) sub-grade strain is unaffected by the inclusion of both wheel gears. It is possible, that for certain pavement configurations, this single change in the modelling could alter the predicted pavement life, however from the results of this study it appears unlikely. The impact of cross-anisotropic base-course characterisation on predicted pavement design life is discussed in Section 5.8.6.

A similar comparison of the effect of modelling with a single wheel gear and both wheel gears present on the Komatsu 830E was made with nonlinear FEA modelling. Table 4.90 presents a summary of surface deflection and sub-grade vertical compressive strain. The columns on the right hand side include the critical (design) sub-grade strain, this comparison is made to test if wheel interaction can affect the design outcome. It is evident that the FEA modelling has been significantly influenced by the inclusion of a second wheel gear. Note that the wheel loads from the front axle of the truck were also included in the FEA modelling, but were found to have a negligible effect on the pavement response at locations under the rear axle. Further, it is possible that wheel interaction can produce the critical sub-grade strain at the mid-point of the rear axle, especially in the unloaded truck case. When combined with the relative agreement between FEA calculated and measured surface deflection profiles along the rear axle presented in Section 4.8.7, this suggests that haul road pavement modelling should be completed with nonlinear FEA in order to properly include the effect of wheel interaction.

The reason for the superior treatment of wheel interaction in FEA is thought to be related to the fact that the stress state at a point between two loads is influenced by both wheel loads. This stress state is then used to predict displacements and subsequently strains (see Section 3.9.4). Linear-elastic modelling completed by any of the US Army Corps of Engineers (Pereira, 1977) method, HIPAVE and CIRCLY use superposition to add the calculated pavement response due to each defined wheel load. These models therefore accept the assumption that superposition effectively represents load interaction. Pavement response is also impacted by the radial separation of each load. Secondly, the iterative nature of the nonlinear treatment of materials in FEA modelling may further impact the degree of interaction of stresses due to adjacent wheel loads. In the context of this study, the maximum stress present in each pavement layer was selected to calculate the layer's resilient modulus for the subsequent analysis. This may have resulted in an over-estimation of the wheel load interaction, and it is recommended that future investigations adopt

a nonlinear relation within the material's constitutive matrix in preference to the approach adopted for this study.

It is recommended that haul road pavement structural analysis is completed by numerical methods. This recommendation is in contrast to the comment made by Thompson (2011) that both linear-elastic and numerical methods produce similar results. Further, the recommendation of Wardle et al (2003) to model only a single wheel gear for design of heavy-duty pavements does not appear to extend to haul roads. The above conclusions are primarily based on the vast differences in the relativity of sub-grade strains at the middle of the rear axle and directly below wheel loads when analysis is completed with linear-elastic methods and FEA. As a result of these differences, the final outcome of pavement design may be significantly varied, which is discussed further below.

### 5.8.5 CBR Design Curves

The following discussion relates to the accuracy of the CBR design curves derived through use of the S77-1 method (Pereira, 1977). This assessment is based on the accuracy of the deflections predicted through use of the equations within the S77-1 method for a Komatsu 830E haul truck.

Firstly, it is appropriate to consider the impact of the wheel load used for derivation of design curves. The curves presented in Figure 4.91 have been developed with use of the known wheel loads and the contact pressure published by tyre manufacturer, Goodyear (goodyearotr.com). The measured tyre contact geometry, as presented in Section 4.4.3, results in slightly smaller contact areas of approximately one square metre. Use of this value would produce slightly higher wheel deflection factors, thus increasing ESWL, and the required CBR value for a given cover thickness. Consideration of wheel load and contact area is much simpler than with mechanistic-empirical design, where the contact pressure is a critical input and is quite variable, as discussed in Section 5.8.2. The net result is that, for the tyre pressures observed during testing for the current study, pavement thickness would be under-designed with use of Figure 4.91.

In considering wheel loads and their interaction, note that the S77-1 procedure (Pereira, 1977) for the generation of CBR design curves includes all wheels on the design vehicle. However, modelling a dual assembly as an equivalent single tyre load (average contact pressure over a circular area comprising the net contact area

for two tyres) was also trialled. This idealisation produced the most accurate deflection estimates in this project, which are also very similar to those calculated by HIPAVE and CIRCLY software, see Table 4.71. Figure 4.92 shows the CBR design curves from consideration of dual wheel assemblies as a single tyre contact. Utilising an equivalent single wheel load for the dual wheel assemblies resulted in significantly thicker pavements being required for similar sub-grade CBR values. This arose due to larger ESWL values resulting than when each wheel load was considered separately. The effect extends to a depth of two metres, as the deflection factor is greater when considering the dual wheel loads together. However, it is not recommended this set of curves be used for design purposes. Consequently, all wheel loads have been considered separately in derivation of the design curves presented in Figure 4.91. These curves are recommended for pavement designs with a Komatsu 830E haul truck as the design vehicle. The fact that the method producing the most accurate deflections estimates appears to produce inappropriate design curves, suggests this is currently a knowledge gap that should be addressed in future research.

Finally, the design curves in Figure 4.91 include an additional 75mm allowance, to allow for material equivalencies and ‘standard’ pavement configuration, as discussed within Section 3.9.9.1. This provides a pavement thickness with the minimum cover over a sub-grade of a known CBR value, but considers a P-154 material that has a minimum CBR value of 20%. This is a relatively poor material that would not be suitable for use as sealed base-course or sub-base as per MRWA specifications (MRWA et al, 2003). Consequently, mechanistic design could provide a valuable tool with reductions in pavement thickness possible due to stiffer materials being utilised. For the purpose of short-term roads with rapid construction and less quality control, especially relating to compaction effort, these design curves may be appropriate. However, for long-term roads, some reduction in pavement depth due to stiffer material may be economical if a suitable mechanistic-empirical design procedure was to be found.

### 5.8.6 Comparison of Pavement Lifetime Estimates

From observation of Table 4.91 and Table 4.92 it is clear that the various mechanistic-empirical design methods investigated do not correlate well with the pavement lifetime predicted by the S77-1 method. In all instances CIRCLY under estimated pavement lifetime in comparison to the S77-1 curves. HIPAVE and FEA

calculated strains produce a similar result, except that pavement lifetime is predicted to be significantly longer than that produced with the S77-1 curve for higher sub-grade strengths (CBR 15%). An extrapolation of the sub-grade theory developed by Wardle et al (2001), from the S77-1 curves, has been made with the inclusion of a pavement with a CBR 20% (elastic modulus of 200 MPa). The lifetime predictions for this pavement are consistent with the trend outlined above.

The underestimates produced by CIRCLY are explained by the fact that the sub-grade failure theory was developed for the APSDS software, which employs the same solution method as CIRCLY, but with isotropic pavement materials. As discussed in Section 5.8.3, the effect of the inclusion of an anisotropic base-course is increased deflections. It appears this effect has manifested in an increased critical sub-grade strain for all the pavements tested in the generation of Table 4.91. Note that Figure 4.90 does show that critical sub-grade strain is not affected by anisotropic characterisation of the base-course, this is due to a two metre base-course and 150MPa sub-grade being considered in the calculation of the sub-grade strain in this instance. This is effectively a much stiffer pavement than those tested in the derivation of Table 4.91.

In contrast to the CIRCLY predicted pavement lifetime, HIPAVE has produced results greatly exceeding those from the S77-1 curve. This is a surprising result, as the development and validation of the sub-grade failure theory employed in this study was effectively completed with the same solution method employed by HIPAVE (including isotropic characterisation of materials). It is possible that this is indicative that the theory is being inappropriately extrapolated in utilisation for wheel loads as large as those considered in this study. If this is the case, it is important that future research considers the viability of field trials to extend this method. It is understood that this has been completed for airfield design due to the introduction of larger commercial aircraft, as discussed previously. However, no recommendation to modify the S77-1 curve has been found in the literature.

It appears that the consideration of nonlinear base-course characterisation has a significant impact on predicted pavement lifetime. It is suggested in Section 5.8.4.4 that three-dimensional nonlinear FEA results in increased interaction between wheel loads. Similarly, inclusion of all wheel gears results in an increase in critical sub-grade strain due to load interaction. Table 4.90 suggests that the location of the critical sub-grade strain is the middle of the rear axle (between two wheel gear loads) for an unloaded truck. Further, it appears the interaction is such that the

deflection under each wheel load is increased when the truck is loaded. The net result is that the predicted pavement lifetime is greatly influenced by the degree of wheel interaction in the analysis, with the potential for the critical location being laterally removed from the centres of the wheel loads. This should be considered in haul road pavement design.

The pavement lifetimes predicted by HIPAVE and ABAQUS do show some similarity. HIPAVE ultimately predicts longer pavement lifetime than ABAQUS, and hence represents a less conservative design option. However, the correlation does support the comment of Thompson (2009) that linear-elastic and numerical methods can produce a similar result. From the discussion in Section 5.8.4, it is clear that FEA better predicts the measured pavement response and as a result has been recommended to be for use in pavement design. The lifetime predictions in Table 4.91 further support the use of FEA, as the more conservative design method. CIRCLY presents very short predicted lifetimes, but was shown to under estimate pavement surface deflection in Section 5.8.4.2. As such it appears the cross-anisotropic characterisation of base-course material should be avoided at the current time. It is recommended this is investigated further for haul road design in the future.

## 5.9 Recommended Haul Road Pavement Design Criteria

From the above discussion, it appears that a specific failure theory is needed for haul roads. Thompson (2009) suggests an absolute limit of 2500 microstrain at any point in the pavement for a ‘Category 3’ haul road (see Figure 2.20). This level of strain results in the number of allowable strain repetitions equating to less than a single pass of a haul truck for a sub-grade CBR of 15%, utilising the failure theory developed by Wardle et al (2001). The implication is that the pavement will require maintenance after the passage of every truck in order to avoid adverse operating conditions. The pavement lifetime in Table 4.91 relates to the formation of a 20mm rut and/or unacceptable roughness. The categories of haul road presented by Thompson (2009) include consideration of the level of serviceability (amount of ore hauled along the road daily) with an indication of the regularity of maintenance. It is contended that an unsealed pavement would show a significant level of distress prior to ruts progressing to a depth of 20mm, and thus the application of this failure criteria result in over estimates of pavement life and under estimate the frequency of maintenance presented by Thompson (2009). Table 4.91 includes an indication of

the haul road category according to Thompson (2009), considering the sub-grade strain calculated from FEA. The pavements shown to have higher sub-grade strains in Table 4.91 would be considered 'Category 3' if the road was to be used for haulage of greater than 100,000 tonne a day and accordingly would require frequent maintenance. Consequently, it is not surprising to note that the allowable repetitions resulting from the failure theory reported by Wardle et al (2001) suggest approximately 1,000 and less repetitions until failure. This estimated life does not consider the progression of functional and environmental defects, but essentially serves as the upper bound of time until maintenance is required to avoid a pavement presenting high rolling resistance due to roughness. Note that the inclusion of the CBR 20% sub-grade appears inappropriate as an indicator of maximum time until maintenance, which is logical as it represented an extrapolation of the sub-grade failure theory. Overall, it appears that when considering the sub-grade strains calculated by three-dimensional FEA, the sub-grade failure theories of Wardle et al (2001) and Thompson (2009) align relatively well. It could be possible to use the former to estimate the minimum road maintenance frequency to provide greater insight to design, whilst utilising the latter for the selection of strain and serviceability limits (class of haul road).

With regards to the testing of pavement materials for haul road design, it is recommended that further investigation be completed with a nonlinear relation included in the constitutive matrix in FEA modelling, prior to any further recommendation being made. If the iterative method used in this study is employed, it appears an extended regime of RLTT is most appropriate.

The roads tested for rolling resistance in this study presented a very low calculated sub-grade strain (see Table 4.92). No matter the daily haulage volume, all three roads are classed 'Category 1'. Further, they have been noted as presenting low rolling resistance in Section 4.5.7, which is subjectively predicted by Figure 2.20 due to this classification. Interestingly, the prediction method for rolling resistance presented by Thompson (2011) (Table 4.45) shows reasonable correlation with those measured as part of this study, although over-predictions occur for all three pavement sections. However, the relatively low RDS scores and road classification suggests that the results of this study correlate well with those presented by the various research published by Thompson, which are summarised in Thompson (2011). Therefore, it would appear the results of this research are well aligned with the literature, although the roads tested are typically of a higher serviceability level.

It is recommended that haul roads are designed in accordance with Figure 2.20 (Thompson, 2009). The selection pavement layer orientation may then be manipulated to reduce surface deflection in order to optimise rolling resistance. This action should not be taken at the expense of significantly increasing sub-grade strain, as this is likely to increase the required maintenance frequency in order to avoid increased rolling resistance due to pavement roughness progression. An indication of the maximum maintenance frequency may be estimated using the failure theory presented by Wardle et al (2001). The results of this study suggest that the critical strain should be calculated by nonlinear and three-dimensional FEA. This design practice should be supported by sound functional design and maintenance, both of which are discussed in the literature, to which the reader is referred.

# 6 Conclusions

## 6.1 Thesis Outcomes

Pavement deflection and curvature testing can be successfully completed via the use of terrestrial laser scanning techniques to an accuracy of 0.5mm.

Progressive screening of rolling resistance test data suggests that some truck and driver response influences the total energy consumption of the haul truck. This is evidenced by the reduction in RRC values calculated for the unscreened, screened and correlated data sets derived within this study.

A statistically significant relationship was shown between haul truck rolling resistance and pavement roughness (correlation coefficient exceeding 0.993 for a sample size of three, at a level of significance of 0.05) for an unloaded haul truck travelling at a speed of 30km/h. Pavement roughness was estimated from the measured variance of each pavement section considering a three metre moving average.

A statistically significant relationship (correlation coefficient exceeding 0.811 for a minimum sample size of six at a level of significance of 0.05) has been observed between measured haul truck rolling resistance and pavement deflection.

From analysis of the data determined through rolling resistance and pavement testing, it appears that pavement roughness and deflection most influence rolling resistance. The influence of roughness appears approximately twice that of deflection for an unloaded truck. The influence of roughness and deflection appears approximately equal for a loaded Komatsu 830E haul truck.

No pre-existing relation from the literature was able to accurately predict the rolling resistance experienced by the Komatsu 830E haul truck during rolling resistance tests.

The haul truck rolling resistance coefficient has been shown to be higher for a loaded truck. It is thought that this is due to the greater influence of pavement deflection representing energy loss in the structural response of the pavement. Consequently, the fuel consumption of a Komatsu 830E is expected to increase significantly with the addition of a payload. Modelling within this study suggests an

increase of 67-183% for a truck speed of 15km/h and 111-258% for a truck speed of 30km/h.

From the fuel consumption modelling completed in this study, it has been observed that a 1.9% change in rolling resistance for an unloaded Komatsu 830E haul truck and a 1.3% change for a loaded Komatsu 830E, results in a 1% change in fuel consumption.

Evercalc software does not appear to accurately back-calculate the pavement elastic modulus, based on the root mean square of error typically exceeding 25%. This result is logical if one considers the inaccuracy of methods employing elastic theory in predicting measured pavement deflections.

Where all inputs are consistent in each method, linear-elastic and FEA predict similar pavement deflection and curvature when modelling is completed in the axisymmetric condition. The difference in maximum deflection, located at the centre of the wheel load contact area, did not exceed 0.2mm for the pavement sections modelled in this study. Typically, linear-elastic modelling has been shown to predict slightly higher deflection than FEA.

Anisotropic characterisation of the base-course within CIRCLY produces larger pavement deflections than identical modelling with an isotropic characterisation of the base-course. This has been shown to result in much shorter predicted pavement lifetime or a lower class of road haul road, when assessed with the failure theories of Wardle et al (2001) and Thompson (2009), respectively.

The plane-strain approximation has been shown to poorly predict pavement surface deflected profiles. This agrees with results in the literature and suggests that a plane-strain approximation is inappropriate for haul road pavement design.

Consideration of dual wheel gears as a single wheel load within the procedure for calculating pavement deflection in the process of determining ESWL presented by Pereira (1977) produced better estimates of the measured pavement deflection. As this idealisation violates the original pavement model reported by Pereira (1977), ESWL resulting from this simplification should not be used for the generation of CBR design curves.

An average variance of 41% occurs between measured deflections and deflections calculated via the procedure detailed in Pereira (1977). This is the method included in the procedure for the generation CBR design curves. Therefore, it appears that

haul road design with curves generated from the S77-1 method should not be relied upon for haul road pavement design.

It has been shown that nonlinear three-dimensional FEA better predicts the measured pavement deflections and curvatures than any other method tested. Based on the comparison of measured and predicted pavement surface deflection profiles, it appears that this superior ability is due to FEA better considering wheel load interaction. It appears that the use of super-position with linear-elastic methods under estimates wheel interaction occurring for a Komatsu 830E haul truck on the pavement sections included in the study. Interaction is significant to the extent that the critical sub-grade strain typically occurs under the mid-point of the unloaded truck's rear axle when modelling with nonlinear three-dimensional FEA. Further, the critical sub-grade strain is significantly increased by inclusion of multiple wheel gears within nonlinear three-dimensional FEA. This effect was not observed for any of the linear-elastic methods trialled.

Comparison of the predicted pavement lifetimes via the failure theory of Wardle et al (2001) and the haul road classification presented by Thompson (2009), suggests that more conservative results occur with the strain calculated by nonlinear three-dimensional FEA compared to linear-elastic solutions employing an isotropic characterisation of the base-course. Linear-elastic analysis with the inclusion of an anisotropic base-course is considered inappropriate for haul road modelling at the current time, based on the aforementioned poor correlation between predicted and measured curvature within this study.

The pavement lifetimes predicted by the failure theory of Wardle et al (2001) suggest longer lifetimes than that of the model presented by Thompson (2009). This result shows that the two correlate to some extent, as the latter includes consideration of functional defects for unsealed roads.

None of the mechanistic-empirical pavement design methods trialled correlate well with the pavement lifetimes suggested by design CBR curves generated from the S77-1 curve.

It has been shown that the haul roads tested in this study were very high quality roads via the pavement classification and lifetime predictions determined through nonlinear three-dimensional FEA modelling. Further, the rolling resistance values measured are consistently less than those predicted by the model included in Thompson (2011). Consequently, it is concluded that the results of this study appear

to fit well with the published work of Thompson, which represents the majority of advanced research in the area of haul road pavements.

## 6.2 Thesis Contribution

The relative contribution of pavement roughness and deflection to haul truck rolling resistance has not been defined or, to the knowledge of the author, investigated previously. Further, the finding that pavement deflection appears to have an equal influence on rolling resistance for loaded haul trucks is without precedence in the literature. This finding should present opportunities for cost savings for mine owners in the haulage of waste and ore.

A comparison of the relative ability of closed-form and numerical analysis methods to predict measured haul road pavement response is not available in the literature. Consequently, it is currently uncertain how a haul road pavement is best analysed, and indeed, which pavement response should be interrogated and optimised in the design. These issues have been addressed and a recommended practice for haul road design presented in Section 7.2. The present study focussed on a small number of haul road pavements and a single model of haul truck, and as such a set of recommendations to extend this research is provided in Section 7.1. In combination, this study represents an initiation of more traditional pavement research and design techniques being applied to haul road pavements. The outcomes suggest that the performance of haul road pavements could be optimised with the recommended practice presented below.

# 7 Recommendations

## 7.1 Recommendations for Future Research

Further validation testing of terrestrial laser scanning techniques is required to increase the proven accuracy of the method for measurement of pavement deflection and curvature.

Consideration should be made of an attempt to relate haul road pavement stiffness and rolling resistance in the future. It is recommended that rapid test methods such as heavy weight deflectometer be considered, such that a higher frequency of testing along a pavement section can be completed.

The conclusions reached in the current study relating to rolling resistance and pavement properties, should be tested with an extension to different mine haulage vehicles to test the influence of different vehicle sizes before general conclusions can be made. The regression equations derived within the current study should be tested and revised with the results of such research. If any of the rolling resistance models in the literature are to be investigated for application to haul roads, the HDM-4 model should be considered based on the correlation (correlation coefficient of 0.997 at a level of significance of 0.05) found between its predictions and the measured rolling resistance in this study. This suggests that the method can calculate the relative changes in rolling resistance, but the magnitude of estimates are incorrect. It is thought that this may be able to be corrected with the availability of further test data.

Future research should consider to what depth into the pavement and sub-grade that stresses from haul truck wheel loads extend. This may have a significant influence on pavement design attempting to optimise the rolling resistance of a haul truck considering the influence of pavement deflection found in this study.

Further investigation of the potential for haul road pavement design via application of stress ratios or the shakedown theory should be considered, based on the results of permanent deformation testing completed on samples from the three pavement sections included in this study showing rapidly accumulated strain after experiencing a stress ratio of 2.5.

The inclusion of anisotropic pavement materials within linear-elastic modelling of haul road pavements should be further investigated. Comparison with measured deflection values in the current study suggests it may be inappropriate.

FEA analysis with the inclusion of nonlinear material behaviour via insertion of a nonlinear relation within the material constitutive matrix should be investigated in preference to the iterative approach applied in this study. This investigation should include materials models that have been defined through both monotonic and repeated load triaxial testing, to confirm which test best represents the nonlinear behaviour of the UGM material in the modelling. This could be best achieved through a validation with measurements of full-scale pavement response.

## 7.2 Recommendations for Haul Road Pavement Design

Pavement stiffness should be considered in haul road design in an attempt to reduce rolling resistance. This is recommended on the basis of the significantly larger estimated fuel consumption of a loaded haul truck compared to an unloaded truck found in this study.

Haul road pavement design is best completed via a mechanistic-empirical method. Structural analysis should be completed by nonlinear three-dimensional FEA with application of the failure theory presented by Thompson (2009). Due to wheel load interaction effects, the location of the critical sub-grade strain may not be directly under wheel loads, and as such other locations of the sub-grade should be investigated. Some indication of the maintenance intensity may be gained by also considering the pavement life predicted by the failure theory of Wardle et al (2001). However, this assumes that the pavement functional design is optimised to the extent that it is equivalent to a sealed pavement. As such, the functional design (selection of wearing course materials) should be considered in conjunction with the structural design method suggested above, for which guidance can be found in the literature.

# 8 References

Akritas. M.G. Papadatos. N. 2001. Heteroskedastic one-way ANOVA and lack-of-fit tests.

Arnold, G. D., A. Hughes, D. Robinson, D. (2002). The application of shakedown approach to granular pavement layers.

Arnold, G. K. (2004). Rutting of granular pavements. The University of Nottingham.

ARRB Group. 2011. Roughometer 3. Vermont South, Victoria. Australia.

ASTM. 2009. D1195/D1195M Standard test method for repetitive static plate load tests of soils and flexible pavement components, for use in evaluation and design od airport and highway pavements.

Atkinson, J. H. (2000). Non-linear soil stiffness in routine design. *Geotechnique, 50*(5), 487-508.

Atkinson, T. (1992). Design and layout of haul roads.

Australian Bureau of Statistics. (2013). Western Australia's Energy Consumption. Retrieved 22 September, 2013, from www.abs.gov.au.

Austroads. 2007. Austroads test method AG:AM/T001 Pavement roughness measurement with an inertial laser profilometer.

Austroads. 2008. AG:PT/T250 Modified surface texture depth (pestle method).

Austroads. (2014). About Austroads. Retrieved 22 December, 2014, from www.austroads.com.au.

Austroads. (2007). AG:PT/T053 determination of permanent deformation and resilient modulus characteristics of unbound granular materials under drained conditions.

Barker, W. Brabston, W. (1975). Development of a structural design procedure for flexible airport pavements. Report No. S-75-17. Vicksburg, Mississippi USA: US Army Corps of Engineers, Waterways Experiment Station.

Bekker, M. G. (1956). *Theory of land locomotion. The mechanics of vehicle mobility*: The University of Michigan Press.

Bernstein, R. (2013). Probleme zur experimentellen motorpflugmechanik. *Der Motorwagen*, 9, 199-206.

Beskou, N. D. Theodorakopoulos, D. D. (2011). Dynamic effects of moving loads on road pavements: a review. *Soil Dynamics and Earthquake Engineering, 31*, 547-567.

Bouzidi, R. Coulibaly, L. Jouve, P. (2003). Behaviour of unbound granular materials - part 1: isotropic case. *Computers and Geotechnics, 30*, 185-204.

Bowles. J.E. 1997. Foundation analysis and design, Fifth Edition. The McGram-Hill Companies.

Brito, L. A. T. (2011). *Design methods for low volume roads.* The University of Nottingham.

Britton, M. Hodkiewicz, M. Kefford, A. (2012). Energy efficiency metrics in mine design.

Brown, S. F. (1996). Soil mechanics in pavement engineering. *Geotechnique, 3*, 383-426.

Brown, S. F. (2004). Application of soil mechanics to design and testing of pavement foundations. Paper presented at the 8th Conference on Asphalt Pavements for Southern Africa (CAPSA '04), Sun City, South Africa.

Bureau of Resources and Energy Economics. (2012). Energy in Australia.

Bureau of Resources and Energy Economics. (2012A). *Key facts Australia's Energy Sector.*

Caterpillar. (2007). Caterpillar on-highway truck application and drivetrain spec'ing.

Cenek, P.D. Jamieson, N.J. Ball, G. (1996). Effect of pavement deflection on rolling resistance of commercial vehicle tyres. Paper presented at the 3rd International Symposium on Pavement Surface Characteristics, Christchurch, New Zealand.

Chen .W.F. El-Metwally S.E.E. 2011. Understanding structural engineering from theory to practice. CRC Press.

Cheung. Y.K. Chan. H.C. 2002. Reinforced Concrete Deep Beams. CRC Press.

Civil Aviation Safety Authority. (2013). Manual of Standards Part 139 – Aerodromes. Version 1.11, November 2013. Australian Government, Canberra ACT.

Chatti, K. Zaabar, I. (2012). Estimating the effects of pavement condition on vehicle operating costs. Washington D.C. USA: National Cooperative Highway Research Program. Michigan State University.

Chen, W. T. (1971). Computation of stress and displacements in a layered elastic medium'. *International Journal of Engineering Science, 9*, 775-800.

Clark, S. (1981). *Mechanics of pneumatic tyres*.

Collins, I. F. (2000). Geomechanical analysis of unbound pavements based on shakedown theory. *Journal of Geotechnical and Geoenvironmental Engineering, 126*(1), 50-59.

Crossley, C.P. Kibiwot, V.N. Reynolds, A.J. Rickson, R.J. (2001). Rut formation and rolling resistance on earth roads. *Journal of Agricultural Engineering Research, 78*(1), 99-107.

Czaplicki. J.M. 2014. Statistics for mining engineering. Taylor & Francis Group, London, UK.

Dawson, A. Kolisoja, P. (2004). Permanent Deformation Roadex 2 Northern Periphery.

Dawson, A. Kolisoja, P. Vuorimies, N. (2008). Understanding low-volume pavement response to heavy traffic loading: Roadex 3 Northern Periphery.

de Carteret, R. Jameson, G. (2009). Review of the relationship to predict sub-grade modulus from CBR Sydney, NSW 2000 Australia: Austroads.

de la Vergne, J. N. (2003). *Hard rock miners handbook and rules of thumb* (3 ed.). North Bay, Ontario Canada. Tempe, Arizona USA: McIntosh Engineering.

Department of Resources, Energy and Tourism. (2010). Energy efficiency opportunities - energy mass balance: mining. Barton, ACT.

Department of Resources, Energy and Tourism. (2012). Analyses of diesel use for mine haul and transport operations.

Desai. C.S. Zaman. M. 2014. Advanced geotechnical engineering. Soil-structure interaction using computer and material models. CRC Press. Taylor & Francis Group. Boca Raton, Florida. USA.

Descornett, G. (1990). Road surface influence on tire rolling resistance.

Dessault Systemmes. 2011. ABAQUS CAE 6.10 [Computer software].

Dickson Gibbons. J. Chakraborti. S. 2003. Nonparametric statistical inference, Fourth Edition. Marcel Dekker, Inc. 270 Madison Avenue, New York, USA.

Douglas, R. A. Valsangkar, A. J. (1992). Unpaved geosynthetic-built access roads: stiffness rather than rut depth as the key design criterion. *Geotextiles and Geomechanics, 11*, 45-59.

Douglas, R. A. Valsangkar, A. J. (1997). Heavy load, low tire pressure rutting of unbound granular pavements. *Journal of Transportation Engineering, 123*(5), 357-363.

Dynatest. http://www.dynatest.com/equipment/structural/hwd.aspx. Accessed on 24 July 2015.

Ekblad, J. (2008). Statistical evaluation of resilient models characterizing coarse granular materials. *Materials and Structures, 41*, 509-525.

Evans, L. R. Harris, J. R. MacIsaac, J. D. (2009). NHTSA Tire fuel efficiency consumer information program development: Phase 1 - Evaluation of

laboratory test protocols. East Liberty, Ohio USA: National Highway Traffic Safety Administration.

Federal Aviation Administration. (1995). Advisory circular 150/5320-6D airport pavement design and evaluation (cancelled). U.S. Department of Transport, Washington D.C.

Feir. B.J. Toothaker. L.E. 1974. The anova f-test versus the Kriuskal-Wallis test: A robustness study. Presented at the Annual Meeting of the American Educational Research Association (59th) Chicago, Illinois, USA, 1974.

Fervers, C. W. (2004). Improved FEM simulation model for tire-soil interaction. *Journal of Terramechanics, 41*(2-3), 87-100.

Foster, C. R. Ahlvin, R. G. (1954). Stress and deflections induced by a uniform non-circular load. *Highway Research Board, 33*.

Frost, M. W. (2004). Cyclic triaxial test in clay subgrades for analytical pavement design. *Journal of Transportation Engineering, 130*(3), 378-386.

Gee-Clough, D. (1977). The Bekker theory of rolling resistance amended to take account of skid and deep sinkage. *Journal of Terramechanics, 14*(3), 183-187.

Gee-Clough, D. (1980). Selection of tyre sizes for agricultural vehicles *Journal of Agricultural Engineering Research, 25*, 261-278.

Geosciences Australia. Accessed 30 August, 2013, from www.ga.gov.au.

Ghadimi. B. 2015. Numerical modelling for flexible pavements materials applying advanced finite element approach to develop mechanistic-empirical design procedure. Thesis presented for degree of Doctor of Philosophy, Curtin University School of Civil and Mechanical Engineering.

Ghadimi, B. Asadi, H. Nikraz, H. Leek, C. (2013). Effects of geometrical parameters on numerical modelling of pavement granular material. 2013 Airfield and Highway Pavement Conference: Sustainable and Efficient Pavements, Jun 9 2013, pp. 1291-1303. Los Angeles, CA, USA. American Society of Civil Engineers.

Gidel, G. Breysse, D. Hornynch, P. Chauvin, J. Denis, A. (2001). A new approach for investigating the permanent deformation behaviour of unbound granular material using the repeated load triaxial apparatus. *Bulletin Des Laboratiores Des Ponts Et Chaussees, 233*, 5-21.

Gillespie, T. (1992). *Everything you always wanted to know about the IRI, but were afraid to ask!* Paper presented at the Road Profile Users Group Meeting, Lincoln, Nebraska USA.

Glass. G.V. Peckham. P.D. Sanders. J.R. 1972. Consequences of failure to meet assumptions underlying the fixed effects analyses of variance and covariance. Review of Educational Research, vol. 42, No. 3 pp 237-288.

Gonzalez. A. Saleh. M.F. Ali. A. 2007. Evaluating nonlinear models for unbound granular materials in accelerated test facility. Transportation Research Record, No. 1990 pp 141-149.

Gonzalez, A. Bodin, D. Jameson, G. Oesar, M. Vuong, B. (2012). Development of a non-linear finite element pavement response to load model. Sydney, NSW 2000 Australia: Austroads.

Graham. A. 2013. Statistics. A complete introduction. Hodder & Stoughton Ltd, 338 Euston Road, London, UK.

Grahn, M. (1991). Prediction of sinkage and rolling resistance for off-road vehicles considering penetration velocity. *Journal of Terramechanics, 28*(4), 339-347.

Greene, D. L. 2006. Reducing greenhouse gas emissions from transportation. A presentation to the Legislative Commission on Global Climate Change.Raleigh, North Carolina USA.

Greenwood, I. D. Bennett, C. R. (2003). HDM-4 fuel consumption modelling.

Grujicic, M. Marvi, H. Arakere, G. Haque, I. . (2010). A finite element analysis of pneumatic-tire/sand interactions during off-road vehicle travel. *Multidiscipline Modelling in Materials and Structures, 6*(2), 284-308.

Hadi, M. Bodhinayake, B. C. (2003). Non-linear finite element analysis of flexible pavements. *Advances in Engineering Software, 34*, 657-662.

Hambleton, J. P. Drescher, A. (2009). Modeling wheel induced rutting in soils: Indentation *Journal of Terramechanics, 46*, 35-47.

Hammarstrom. U. Karlsson. R. Sorensen. H. 2008. Road surface effects on rolling resistance – coastdown measurements with uncertainty analysis in focus. Deliverable D5(a). ECRPD project. VTI, Sweden.

Hammarstrom, U. Erikkson, J. Karisson, R. Yahya, M. (2012). Rolling resistance model, fuel consumption model and the traffic energy saving potential from changed road surface conditions: The Swedish Transport Administration.

Hamory. G. 2015. Western Australian pavements in colonial times 1829 to 1860. Australian Geomechanics Vol. 50. No. 1 pp 3-14.

Hetherington, J. G. Littleton, I. (1978). The rolling resistance of towed, rigid wheels in sand. *Journal of Terramechanics, 15*(2), 95-105.

Holman, P. (2006). Caterpillar haul road design and management. St. Charles, Illinois USA: Big Iron University.

International Organisation for Standardisation. (2009). ISO 28580: Passenger car, truck and bus tyres - methods of measuring rolling resistance - single point test and correlation of measurement results. Geneva, Switzerland.

iWitnessPRO. http://www.iwitnessphoto.com/products/iwitnesspro.html accessed on 16 December 2013.

Jackson, R. Willis, J. Arnold, M. Palmer, C. (2011). Synthesis of the effects of pavement properties on tire rolling resistance: National Centre for Asphalt Technology.

Jameson, G. (2008). AGPT02/08 Guide to pavement technology part 2: pavement structural design. Sydney, NSW 2000 Australia: Austroads.

Jameson, G. (2008A). Technical basis of Austroads guide to pavement technology part 2: pavement structural design: Austroads.

Jameson, G. Shackleton, M. (2009). AGPT05/09 Austroads guide to pavement technology part 5: Pavement evaluation and treatment design. Sydney, NSW 2000 Australia: Austroads.

Jamieson, N. J. Cenek, P. D. (1999). Effect of pavement construction on the fuel consumption of trucks Opus Central Laboratories.

Karg, C. Haegeman, W. (2009). Elasto-plastic long-term behaviour of granular soils: experimental investigation. *Soil Dynamics and Earthquake Engineering, 29*, 155-172.

Kaufman, W. W. Ault, J. C. (1977). Design of surface mine haulage roads - a manual. Pittsburgh, Pennsylvania USA: United States Department of the Interior. Bureau of Mines.

Kecojevic, V. Komljenovic, D. (2010). Haul truck fuel efficiency and CO2 emission under various engine load conditions. *Mining Engineering, 62*(12), 44-48.

Khan. A. Rayner. G.D. 2003. Robustness to non-normality of common tests for the many-sample location problem. Journal of Applied Mathematics and Decision Sciences, 7(4), pp 187-206.

Kim, D. Kim, J. R. (2007). Resilient behaviour of compacted subgrade soils under the repeated triaxial test. *Construction and Building Materials, 21*, 1470-1479.

Kim, M. (2007). Three-dimensional finite element analysis of flexible pavements considering nonlinear pavement foundation behaviour. University of Illinois at Urbana-Champaign.

Kim, M. Tutumluer, E. (2010). Validation of a three-dimensional finite element model using airfield pavement multiple wheel load responses *Road Materials and Pavement Design, 11*(2), 387-408.

Kim, S. (2004). Determination of aggregate physical properties and its effect on cross-anisotropic behaviour of unbound aggregate materials. Texas A&M University.

Knappett, J. A. Craig, R. F. (2012). *Craig's soil mechanics* (8 ed).Spon Press. Abingdon, Oxfordshire, England.

Komandi, G. (1999). An evaluation of the concept of rolling resistance. *Journal of Terramechanics, 36*, 156-166.

Komatsu. (2006). Komatsu 830E-AC electric drive truck.

Komatsu. (2007). Komatsu 930E-4 electric drive truck.

Komatsu. http://www.komatsu.com.au/AboutKomatsu/Technology/Pages/AHS.aspx accessed on 25 July 2015.

Komzsik, L. 2009. What every engineer should know about computational techniques of finite element analysis. Second Edition. CRC Press.

LaClair, T. J. (2006). Rolling resistance. *The Pneumatic Tyre*: National Highway Traffic Safety Administration.

Lambert, J. P. Fleming, P. R. Frost, M. W. (2008). The assessment of coarse granular materials for performance based pavement foundation design. *International Journal of Pavement Engineering, 9*(3), 203-214.

Lee, T. (2010). Development and validation of rolling resistance based haul road management. Purdue University.

Leica Geosystems. 2014. Cyclone 8.1.3 [Computer software].

Lekarp, F. (1999). Resilient and permanent deformation behaviour of unbound aggregates under repeated loading. Stockholm, Sweden: Royal Institute of Technology, Division of Highway Engineering.

Lekarp, F. Dawson, A. (1998). Modelling permanent deformation behaviour of unbound granular materials. *Construction and Building Materials, 12*(1), 9-18.

Lekarp, F. Isacsson, U. Dawson, A. (2000). State of the art 1: resilient response of unbound aggregates. *Journal of Transportation Engineering, 126*(1), 66-75.

Lekarp, F. Isacsson, U. Dawson, A. (2000A). State of the art 2: permanent strain response of unbound aggregates. *Journal of Transportation Engineering, 126*(1), 76-83.

Lenngren, C. A. (2009). Using falling weight deflectometer data for new construction interactive design *Bearing Capacity of Roads, Railways and Airfields*.

Lenngren, C. A. Faldner, L. . (2010). *Fuel cost considerations regarding truck rolling resistance on different pavement types*. Paper presented at the 11th International Symposium on Concrete Roads, Seville, Spain.

Li, Y. Corder, G.D. McLellan, B.C. (2011). Transport in the minerals industry - Contributions to greenhouse gas emissions and potential for mitigation. *Minerals Engineering, 24*, 1430-1439.

Li, Y. Liu, W. Y. Frimpong, S. (2012). Effect of ambient air temperature on stress, deformation and temperature of dump truck tyre. *Engineering Failure Analysis, 23*, 55-62.

Lin, Y. Hwang, S. (2004). Temperature prediction of rolling tyres by computer simulation. *Mathematics and Computers in Simulation, 67*, 235-249.

Lindly, J. Townsend, J. T. Elsayed, A. (1995). How top-size affects the resilient modulus of roadway base materials. *Engineering Journal of University of Qatar, 8*, 127-138.

LLoyd, B. (2003). Asset management of roads. Paper presented at the 26th Australasian Transport Research Forum, Wellington, New Zealand.

Main Roads Western Australia. (2001). Pavement deflection and curvature: Benkelman beam test.

Main Roads Western Australia. (2003). A guide to the selection and use of naturally occurring materials as base and subbase in roads in Western Australia.

Main Roads Western Australia. (2011). Test method WA 100.1-2011. Sampling procedures for soil and manufactured granular materials.

Main Roads Western Australia (2012). Specification 501 pavements.

Main Roads Western Australia (2013). Engineering Road Note 9. Procedure for the design of road pavements.

Mclean, J. Foley, G. (1998). Road surface characteristics and condition: effects on road users: Australian Roads Research Board.

Mclean, J. Ramsay, E. (1996). Interpretations of road profile - roughness data: Review and research needs. Vermont South, Victoria 3133 Australia: Australian Roads Research Board.

Micceri. T. 1989. The unicorn, the normal curve, and other improbable creatures. Psychological Bulletin, 1989, Vol. 105, No. 1 pp 156-166.

Michelin. (2000). Earthmover & industrial tire reference. Greenville, South Carolina USA.

Mincad Systems. (2009). APSDS 5.0 [Computer software]. Melbourne, Australia.

Mincad Systems. (2009A). HIPAVE user manual. Richmond South, Victoria 3121 Australia.

Mincad Systems. (2012).CIRCLY 5.1 [Computer software]. Melbourne, Australia.

Mincad Systems. (2012A). CIRCLY 5 user manual. Richmond South, Victoria 3121 Australia.

Mincad Systems. (2012B).HIPAVE 5.0 [Computer software]. Melbourne, Australia.

Mincad Systems Pty Ltd. (2014). CIRCLY theory and background manual – Draft 1. Richmond South, Victoria 3121 Australia.

MIRIAM. (2013). Models for Rolling Resistance in Road Infrastructure Asset Management Systems. (2013). Retrieved 13 June, 2013, from miriam-co2.net.

Muir-Wood, D. (1990). *Soil behaviour and critical state soil mechanics*: Cambridge University Press.

National Cooperative Highway Research Program (NCHRP). 2004. Guide for mechanistic-empirical design of new and rehabilitated pavement structures. Transportation Research Board. USA.

Nguyen, A. D. (2007). *Lower bound shakedown analysis of pavements by using the interior point method.*

Nielsen, L. Sandberg, T. . (2002). A new model for rolling resistance of pneumatic tyres. *Society of Automotive Engineers*.

Nikraz. H.R. 1998. Highway and Traffic Engineering 468. Pavement Design. Course Notes. Curtin University of Technology

Norgate, T. Haque, N. (2009). Energy and greenhouse gas impacts of mining and mineral processing operations. *Journal of Cleaner Production*.

Norgate, T. Jahanshahi, S. (2011). Reducing the greenhouse gas footprint of primary metal production: Where should the focus be? *Minerals Engineering*.

Onafeko, O. (1969). Analysis of the rolling resistance losses of wheels operating on deformable terrain *Journal of Agricultural Engineering Research, 14*(2), 176-182.

Oxford Dictionaries. (2014). Retrieved 22 December, 2014, from www.oxforddictionaries.com.

Pereira, A. T. (1977). Instruction report S-77-1. Procedures for the development of CBR design curves. Washington, D.C.: U.S. Army Engineer Waterways Experiment Station.

Picoux, B. Ayadi, A. E. Petit, C. (2009). Dynamic response of a flexible pavement submitted by impulsive loading. *Soil Dynamics and Earthquake Engineering, 29*, 845-854.

Pillai, S. P. (2004). Effect of tyre overload and inflation pressure on rolling loss (resistance) and fuel consumption of automobile and truck/bus tyres. *Indian Journal of Engineering & Materials Sciences, 11*, 406-412.

Plackett, C. W. (1985). A review of force prediction methods for off-road wheels. *Journal of Agricultural Engineering Research, 31*, 1-29.

Rao, C. S. (1991). Finite element method for structural design of heavy duty granular pavements. *Computers & Structures, 40*(5), 1223-1233.

Rodway, B. Wardle, L.J. Wickham, G. (1999). Interaction between wheels and wheel groups of new large aircraft. Paper presented at the Airport Technology Transfer Conference, Atlantic City, USA.

Sahoo, U. C. R., K. S. (2010). Effect of non-linearity in granular layer on critical pavement responses of low volume roads. *International Journal of Pavement Research and Technology, 3*(6).

Sandberg, U. (2010). Pavements providing low rolling resistance. Paper presented at the International Sustainable Pavements Workshop, Airlie Centre, Warrenton, Virginia USA.

Sandberg, U. Haider, M. Conter, M. Goubert, L. Gergiers, A. Glaeser, K. Schwalbe, G. Zoller, M. Boujard, O. Hammarstrom, U. Karlsson, R. Ejsmont, J. A. Wang, T. Harvey, J. T. (2011). Rolling resistance – basic information and state-of-the-art on measurement methods: VTI.

Santero, N. J. Masanet, E. Horvath, A. (2011). Life-cycle assessment of pavements part 2: Filling the research gaps. *Resources, Conservation and Recycling, 55*, 810-818.

Schmidt, B. Ullidtz, P. Eilskov Jensen, B. (2009). Road pavements and fuel consumption.

Schmidt, B. Ullidtz, P. Anderson, J. B. Nielsen, O. J. (2010). The energy-saving road - a technical report. Energy savings in road transport as a function of the functional and structural properties of roads: Danish Road Directorate.

Schuring, D. (1963). Mechanics of rigid wheels.

Seed, H. B. Mitry, F. G. Monismith, C. L. Chan, C. K. (1967). *Prediction of flexible pavement deflections from laboratory repeated load tests*. Washington, DC, USA: Highway Research Board.

Shastri, S. S. Kemper, S. F. Sonigra, T. R. Hill, T. R. Beales, J. (2012). Australia's mining thirst - GTL solution. Perth, Western Australia 6004.: GHD.

Siripun, K. Nikraz, H. Jitsangiam, P. (2011). Mechanical behaviour of unbound granular road base materials under repeated cyclic loads. *International Journal of Pavement Research and Technology, 4*(1), 56-66.

Sitkei, G. (1966). The bulldozing resistance of towed rigid wheels in loose sand. *Journal of Terramechanics*.

Spiegel. M.R. 2011. Schaum's easy outlines. Statistics, second edition. McGraw-Hill Companies, Inc.

Staffell, I. (2011). The energy and fuel data sheet. Birmingham, UK: University of Birmingham.

Stamatis. D.H. 2012. Essential statistical concepts for the quality professional. Taylor and Francis Group, Boca Raton FL, USA.

Standards Australia. (1993). AS 1726 geotechnical site investigations.

Standards Australia. (1997). AS 1289.5.3.5 methods of testing soils for engineering purposes. Method 5.3.5: soil compaction and density tests - determination of the field dry density of a soil - water replacement method.

Standards Australia. (1998). AS 1289.6.4.1 methods of testing soils for engineering purposes. Method 6.4.1: soil strength and consolidation tests - determination of compressive strength of a soil - compressive strength of a specimen tested in undrained triaxial compression without measurement of pore water pressure.

Standards Australia. (2003). AS 1289 methods of testing soils for engineering purposes. Method 5.1.1: Soil compaction and density tests - Determination of the dry density/moisture content relation of a soil using standard compactive effort.

Standards Australia. (2007). 1289.5.4.1 methods of testing soils for engineering purposes. Methods 5.4.1: Soil compaction and density test – Dry density ratio, moisture variation and moisture ratio.

Standards Australia. (2007A). AS 1289.5.8.1 methods of testing soils for engineering purposes. Method 5.8.1: soil compaction and density tests - determination of field density and field moisture content of a soil using a nuclear surface moisture-density gauge - direct transmission mode.

Standards Australia. (2007B). AS 1906.1 retroflective materials and devices for road traffic control purposes – part 1: retroflective sheeting.

Standards Australia. (2009). AS 1289.3.6.1 methods of testing soils for engineering purposes. Method 3.6.1: soil classification tests - determination of the particle size distribution of a soil - standard method of analysis by sieving.

Sukumaran, B. (2004). *Three dimensional finite element modelling of flexible pavements*. Paper presented at the 2004 FAA Worldwide Airport Technology Transfer Conference, Atlantic City, New Jersey, USA.

Sukumaran, B. Kyatham, V. (2004). Suitability of using California bearing ratio test to predict resilient modulus. Paper presented at the Federal Aviation Administration Technology Transfer Conference.

Taborek, J. J. (1957). *Mechanics of vehicles*: Penton.

Tan, F. Thoresen, T. Lloyd, B. (2011). Update of vehicle/road relationships underpinning road user costs and externality costs - literature review: Sydney, NSW 2000 Australia: Austroads.

Tannant, D. D. Regensburg, B. (2001). Guidelines for mine haul road design. Kelowna, British Columbia Canada: University of British Columbia.

The South African National Roads Agency. (2013). South African pavement engineering manual. Chapter 10. Pavement Design.

Theyse, H. L. (1997). Mechanistic-empirical modelling of the permanent deformation of unbound pavement layers.

Thompson, R. J. (2009). Design, construction and maintenance of haul roads *SME Mining Engineering Handbook*.

Thompson, R.J. (2011). Mine haul road design, construction and maintenance management. Available as e-book: http://ebooks.edocumentonline.com/miningroads_curtin_2011/, accessed 07 July 2015.

Thompson, R. J. Visser, A. T. (1997). A mechanistic structural design procedure for surface mine haul roads. *International Journal of Mining, Reclamation and Environment, 11*, 121-128.

Thompson, R. Visser, A. (2003). Mine haul road maintenance management systems. *The Journal of the South African Institute of Mining and Metallurgy*.

Thompson, R. Visser, A. Heyns, P. (2004). Integrating real-time mine haul road maintenance management with mine-wide asset location and communication systems. Paper presented at the 6th International Conference on Managing Pavements.

Thoresen, T. Roper, R. (1996). Review and enhancement of vehicle operating cost models: assessment of non urban evaluation models Australian Roads Research Board.

Tonkovich, A. Li, Z. DiCecco, S. Altenhof, W. Banting, R. Hu, H. (2012). Experimental observations of tyre deformation characteristics on heavy mining vehicles under static and quasi-static loading. *Journal of Terramechanics, 49*, 215-231.

Transit New Zealand (1998). Pavement deflection measurement and interpretation for the design of rehabilitation treatments.

Transportation Research Board. (2006). TRB Special report 286. Tires and passenger vehicle fuel economy Transport Research Board.

Turnbull, W.J. Ahlvin, R.G. 1957. Mathematical expression of the CBR relationships. Proceedings 4th International Conference on Soil Mechanics and Foundation Engineering vol. 2. Pp. 178. London.

Tutumluer, E. (1995). Predicting behaviour of flexible pavements with granular bases. Georgia Institute of Technology.

Tutumluer. E. Thompson, M.R. 1997. Granular base moduli for mechanistic pavement design. Proceedings of the ASCE Airfield Pavement Conference pp 33-47, ASCE, Seattle, Washington.

University of New England, School of Psychology. http://webstat.une.edu.au/unit_materials/c6_common_statistical_tests/test_signif_pearson.html, accessed on the 23 July, 2015.

Venkataraman, P. (2007). Effect of nitrogen filling on tire rolling resistance and vehicle fuel economy. Clemson University.

Vishay Precision Group. 2011. P3 Strain indicator and recorder.

Vosselman. G. Maas. H. 2010. Airborne and terrestrial laser scanning. Whittles Publishing. Dunbeath, Caithness KW6 6EY, Scotland, UK.

Vuong, B. Jameson, G. Sharp, K. (2008). AGPT04A/08 Guide to pavement technology part 4A: granular base and subbase materials. Sydney, NSW 2000 Australia: Austroads.

Wardle, L. (1999). APSDS 4.0 – airport pavement structural design system users manual. Richmond, Victoria Australia: Mincad Systems Pty Ltd.

Wardle, L. Rodway, B. Rickards, I. (2001). Calibration of advanced flexible aircraft pavement design method to S77-1 method. Proceedings Advancing Airfield Pavements. American Society of Civil Engineers 2001 Airfield Pavement Specialty Conference, Illinois, USA, 192-201.

Wardle, L. (2010). CIRCLY and mechanistic pavement design: the past, present and towards the future.

Wardle, L. J. Rickards, I. Hudson, K. (2005). HIPAVE - a mechanistic design tool for heavy-duty industrial pavements. Paper presented at the AAPA 2005 Pavements Industry Conference, Surfers Paradise, Queensland Australia.

Wardle, L. Rickards, I. Lancaster, J. (2006). HIPAVE – A tool to assist in the mechanistic empirical pavement of heavy duty industrial flexible pavements. Paper presented at the 10th International Conference of Asphalt Pavements (ISAP), Quebec, Canada.

Wardle, L. Rickards, I. Lancaster, J. Tighe, S. (2007). Heavy duty industrial pavement design guide revision 1.035: Mincad Systems Pty Ltd.

Wardle, L. Rodway, B. (2010). Advanced design of flexible aircraft pavements. Paper presented at the 24th ARRB Conference, Melbourne, Australia.

Wardle, L. Youdale, G. Rodway, B. (2003). Current issues for mechanistic pavement design.

Washington Department of Transport. (2005). Evercalc 5.0 [Computer software].

Werkmeister, S. Dawson, A. R. Wellner, F. (2004). Pavement design model for unbound granular materials. *Journal of Transportation Engineering, 130*(5), 665-674.

White, G. W. (2007). An investigation of the Australian layered elastic tool for flexible aircraft pavement thickness design. Queensland University of Technology.

Widodo, N. P. Kramabibrata, S. Wicaksana, Y. Wattimena, R. K. Hermawan, F. Nardono. (2009). A preliminary field-study to determine rolling resistance in surface coal mines. Paper presented at the International Symposium on Earth Science and Technology.

Widodo, N. P. Kramabibrata, S. Wicaksana, Y. Wattimena, R. K. Hermawan, F. (2009A). Rolling resistance study of gravelly sand material on laboratory scale.

Wong, J. Y. (2010). *Terramechanics and off-road vehicle engineering* (2 ed.).

Xia, K. (2011). Finite element modelling of tire/terrain interaction: Application to predicting soil compaction and tire mobility. *Journal of Terramechanics, 48*(2), 113-123.

ycharts.com. Accessed on 08 July 2015. ycharts.com/indicators/iron_ore_spot_price_any_origin

Yong, R. N. Eiyo, F. (1990). Road surface roughness and tyre performance. *Journal of Terramechanics, 27*(3), 219-239.

Youdale, G. P. (1984). Review of limiting subgrade strain criterion: NAASRA.

Zaabar, I. Chatti, K. (2010). Calibration of the HDM-4 models for estimating the effect of pavement roughness on fuel consumption for U.S. conditions. *Transport Research Record*, 105-116.

# Appendix A – Example Estimate of Energy Consumed in Load and Haul Cycle

**Table A.0.1: Example estimate of energy consumed in average hauling loading/unloading cycle (Department of Resources, Energy and Tourism, 2010).**

| Parameter | Description | Value | Units |
|---|---|---|---|
| Gross machine operating weight | Maximum operating weight (Manufacturer specifications) | 317.50 | t |
| Vehicle weight | = Chassis Weight + Body Weight + Liner + sideboards + tail extension<br>= 102.3t + 27t + 11.5t | 140.8 | t |
| Load | | 175.00 | t |
| Loading capacity | Manufacturer specifications, struck | 73.00 | $m^3$ |
| Gross vehicle weight (GVW) | = Vehicle Weight + (Loading Capacity x Density)<br>= 141t + ($73m^3$ x $2.4t/m^3$) | 316.00 | t |
| Weight on rear axle (loaded), $W_{rl}$ | = 67% of GVW (Manufacturer specifications) | 211.72 | t |
| Weight on rear axle (unloaded), $W_{ru}$ | = 53% of GVW (Manufacturer specifications) | 167.48 | t |
| Rolling resistance | Tabulated value, whereby 10 kg/t equals 1%. Assume a relatively smooth, maintained and watered dirt road | 3.5% | |
| Traction coefficient | Firm earth, tabulated | 0.55 | |
| Percentage gradient | = Rise / Length<br>= 72/1600 | 4.5% | |
| Effective gradient | = Actual Percentage Grade + Rolling Resistance | 8% | |
| Angle of ascent (θ) | $\tan^{-1}$ (percentage gradient ) | 4.57 | degrees |
| Hauling time | Time taken to transport the load to the dumping point, determined from speed and distance | 360 | secs |
| Loading time | Time taken for the excavator to load the truck | 90 | secs |
| Manoeuvring and dumping time | Time taken to position the truck and unload | 27 | secs |
| Return time (empty) | Time taken to transport the load to the dumping point, determined from speed and distance | 138 | secs |
| Cycle time | = Hauling + Loading + Manoeuvring and Dumping + Return Time | 615 | secs |
| Power required | = GVW × Effective Gradient | 25.28 | t |
| Rimpull (R) | See Figure 5 and notes for explanation of this step | 25.28 | t |
| Usable rimpull ($R_{eff}$) | $R \times W_{rl}[\%] \times \cos\theta$, where θ is the angle of the slope from the horizontal | 16.88 | t |
| Usable power | = $W_{rl}$ ×Traction Coefficient | 116.45 | t |
| Torque at wheels | = Rimpull × gravity × wheel radius | 281.28 | kNm |

**Table A.0.2: Example estimate of energy consumed in hauling loading/unloading cycle continued (Department of Resources, Energy and Tourism, 2010).**

| Parameter | Description | Value | Units |
|---|---|---|---|
| Velocity | From gradeability graph (see Figure 5) | 16 | km/hr |
| Power required | Formula 5.1, p. 122 | 654.27 | kW |
| Wheel rotations/ second | Vehicle velocity [m/s]/[π×wheel outside diameter] | 0.416 | radians/ second |
| Power from wheel torque | 2πω × (Torque at Wheels [kNm]) | 735.38 | kW |
| Power from rimpull | $= v[km/hr] \times \frac{1000}{3600}[\frac{m/s}{km/h}] \times R \times 1000\left[\frac{kg}{t}\right] \times g\left[\frac{m}{s^2}\right] \times \frac{1}{1000}\left[\frac{kW}{W}\right]$ | 735.38 | kW |
| Engine output power | Power from rimpull/0.95, assuming 95% transmission efficiency | 774.08 | kW |
| Fuel input power, $P_f$ | Power/0.25, assuming 25% efficiency at wheels | 2941.51 | kW |
| Fuel input per second | Assuming a calorific value of 38.6MJ/L, Fuel Input $= \frac{P_f\left[\frac{kJ}{s}\right]}{38.6[MJ/L] \times 1000[\frac{kJ}{MJ}]}$ | 0.076 | L diesel/s |
| Fuel consumption (loaded cycle) | Fuel Input Per Second × Haul Cycle Time | 27.434 | L diesel |
| Fuel consumption (loading) | Fuel Input Per Second ×Loading Cycle Time | 3.060 | L diesel |
| Fuel consumption (dumping) | Fuel Input Per Second ×Dumping Cycle Time | 2.058 | L diesel |
| Fuel consumption (unloaded return) | Recalculated model using gradeability curve, with an effective gradient of 2% (rolling resistance reduces effective gradient on descent) rimpull of 1.9 t, velocity of 44 km/h | 2.02 | L diesel |
| Fuel consumption, total cycle | Sum of fuel consumption over the four cycles | 34.57 | L diesel |
| Fuel tank capacity | | 3222.00 | L diesel |
| Number of cycles per tank | Fuel Tank Capacity/Fuel Consumption per Cycle | 93.12 | cycles |
| Aero resistance | $= \frac{1}{2} C_d \rho A v^3 \times \frac{1}{1000}\left[\frac{kW}{W}\right]$ | 2.24 | kW |
| KPI: L/t | | 0.2 | L/tonne |
| KPI: L/100km | | 2160.6 | L/100km |
| KPI: L/100km per tonne of GVW | | 6.84 | L/100km/ tonne of GVW |

# Appendix B – Terrestrial Laser Scanner Assurance Test Report

## B1.0 Aim

The purpose of this testing regime is to test the accuracy of surface deflection measurement by means of terrestrial laser scanning technology.

## B2.0 Procedure

A testing rig was setup consisting of ply-board simply supported at opposite ends and in the centre (see Figure B.1). The centre support was packed at progressive increments of 3, 6, 12 and 19mm. Atop the ply-board was a temporary pavement marker, which had been customised to include a 2mm Class 2 retro-reflective strip in accordance with AS 1906 (Standards Australia, 2007B) and a 24mm black ‘dot’. The strip is used to highlight a known point in the Cyclone software, which is used to perform the analysis of the laser scanning data. The dots were to provide a point of contrast on the white markers, which can then be designated as points of interest within processing for photogrammetric analysis techniques, which were ultimately not used.

**Figure B.1: Test surface setup.**

Following testing, analysis was completed to determine the deflection in each case. Registration of the scanworlds (original and deflected) was completed by Leica

Cloudworks Cyclone software. For laser scanning the class 2 retro-reflective strips were compared to measurements taken directly at the surface (which was covered in a fine sand to provide texture similar (see Figure B.2) to that anticipated on unsealed haul road pavements, the intended location of full scale testing).

**Figure B.2: Fine sand placed on test surface.**

## B3.0 Results

Table B.0.1 depicts the terrestrial laser scanning results via means of measuring to the reflective strip mounted on temporary pavement marker. Table B.0.2 presents the same results, measured between registered scanworlds at the surface, along the 'crest' of the deflected profile.

**Table B.0.1: Surface movement measured at the temporary pavement marker Class 2 retroreflective strip.**

| Registered Scanworlds | | Actual Vertical Movement (mm) | Average Measured Movement (mm) |
|---|---|---|---|
| 1 | 2 | 3 | 3.6 |
| 1 | 3 | 6 | 6.1 |
| 1 | 4 | 12 | 12.2 |
| 1 | 5 | 19 | 19.8 |

**Table B.0.2: Surface movement measured as the difference by surface level between scanworlds.**

| Registered Scanworlds | | Actual Vertical Movement (mm) | Average Measured Movement (mm) |
|---|---|---|---|
| 1 | 2 | 3 | 3.0 |
| 1 | 3 | 6 | 5.9 |
| 1 | 4 | 12 | 12.6 |
| 1 | 5 | 19 | 19.0 |

## B4.0 Discussion

In both cases measurement of surface displacement is on average within 1mm of the known movement of the surface.

Measuring the displacement of the surface between the two scans appears to provide a more accurate means of testing pavement deflection. However in some circumstances such as rough pavement surface texture and due to occlusion near adjacent objects this approach may be difficult and hence measuring the displacement of the retro-reflective strips on the pavement markers may prove more viable.

## B5.0 Conclusion

Measurement shall be taken at the displacement between pavement surfaces in preference to displacement to of the retro-reflective strips. However the later should always be checked as a means of quality control and may be used in the absence of satisfactory data being observed between the displacement of the pavement surface.

The accuracy of vertical displacement measurement from a 10 meter range is likely within 0.5mm.